GPO PRICE $ _____

CSFTI PRICE(S) $ _____

Hard copy (HC) 3.00

Microfiche (MF) .65

ff 653 July 65

ROCKETDYNE
A DIVISION OF NORTH AMERICAN ROCKWELL CORPORATION
6633 CANOGA AVENUE CANOGA PARK, CALIFORNIA 91304

R-7450-1

J-2 ENGINE PERFORMANCE ANALYSIS
FLIGHT AS-501 (APOLLO 4)
S-II AND S-IVB STAGES

Contract NAS8-19
Exhibit A, Para. A.3.a

PREPARED BY

Rocketdyne Engineering
Canoga Park, California

APPROVED BY

P. D. Castenholz
J-2 Program Manager

NO. OF PAGES 302 & xviii **REVISIONS** DATE 17 May 1968

DATE	REV. BY	PAGES AFFECTED	REMARKS

FORM R18-G REV. 9-67

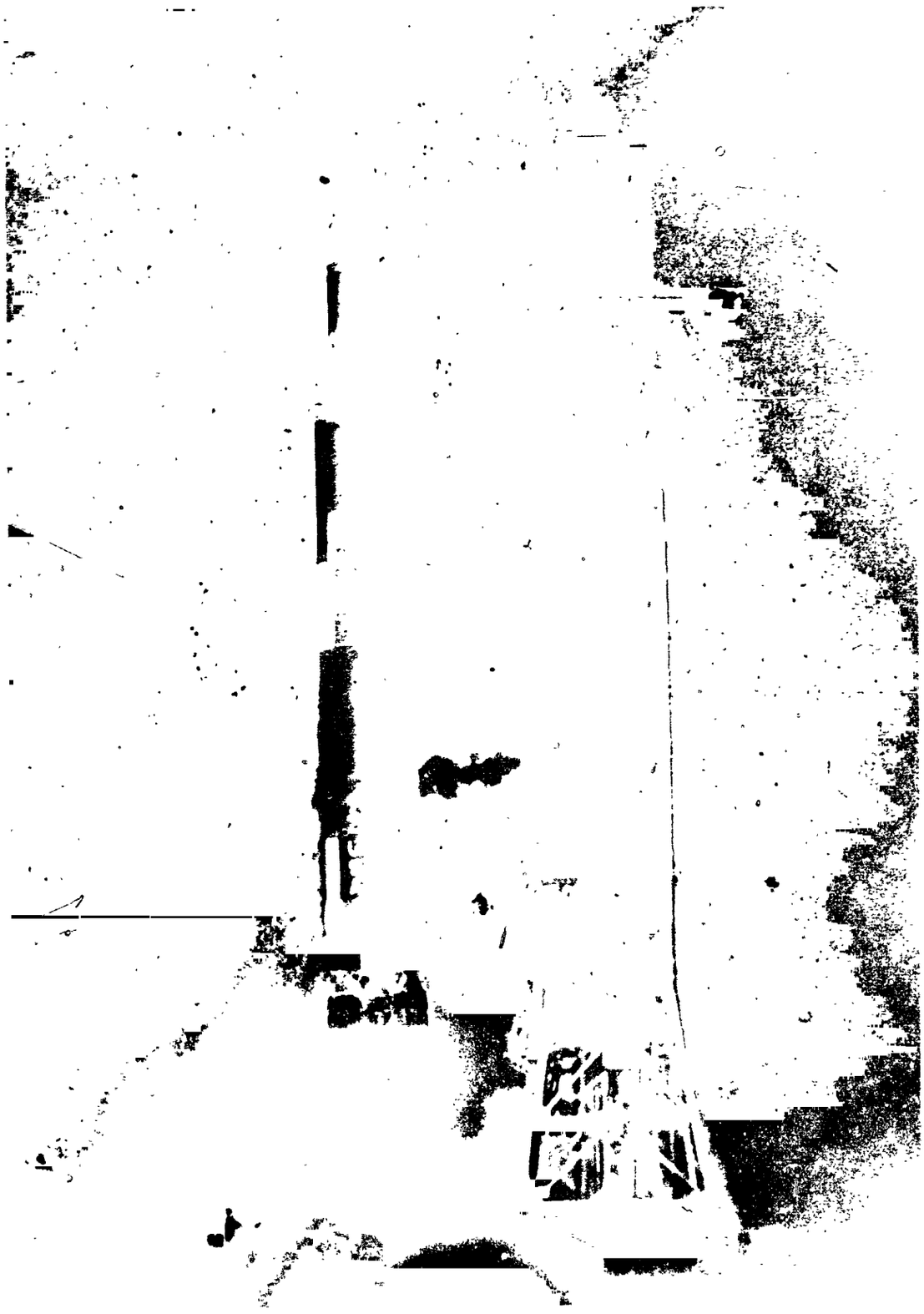

1DC14-11/9/67-C1E

Frontispiece. Flight AS-501 Liftoff

FOREWORD

This J-2 Engine Flight Report, "J-2 Engine Performance Analysis of Flight AS-501 (Apollo 4), S-II and S-IVB Stages," R-7450-1, was prepared by Rocketdyne, a Division of North American Rockwell Corporation.

ABSTRACT

This report presents the flight performance results of J-2 engines J2026, J2028, J2030, J2035, and J2043 in the S-II stage, and J-2 engine J2031 in the S-IVB stage of the AS-501 (Apollo 4) Saturn V flight vehicle. Included are the engine start transients, mainstage performance, and cutoff transients for the S-II and S-IVB stages, as well as the environmental conditions during the orbital coast period between the initial start and restart of the J-2 engine in the S-IVB stage.

CONTENTS

ILLUSTRATIONS

TABLES

INTRODUCTION

The AS-501 (Apollo 4) vehicle was successfully launched at 7:00 AM (EST) on 9 November 1967 from Launch Complex 39A in the Merritt Island Launch Area (MILA) at Kennedy Space Center (KSC).

FLIGHT DESCRIPTION

The AS-501 (Apollo 4) was an unmanned Apollo test with primary objectives of demonstrating the structural integrity of the Saturn V launch vehicle and satisfactory command module lunar return re-entry performance

The vehicle was launched on an azimuth of 90 degrees along a firing azimuth of 72 degrees east of true north. The S-IC, S-II, and S-IVB stages performed satisfactorily to insert the S-IVB/instrument unit (IU), and command/service module (CSM) into a earth near-circular parking orbit of approximately 120 miles.

The pre-ignition sequencing for the S-IVB stage second burn was initiated near the end of the second revolution as the vehicle passed over the continental United States. At the start of the third revolution, as the vehicle passed north of the KSC area, the S-IVB was re-ignited. The S-IVB second burn, which simulated a translunar injection, was controlled to yield an apogee ellipse altitude of approximately 10,350 miles, which will intersect the earth on its re-entry phase. After cutoff of the S-IVB second burn, the S-IVB/IU and CSM coasted for 10 minutes prior to separation. During this time, the vehicle had a fixed attitude relative to the sun for thermal considerations. The S-IVB/IU was then separated from the CSM. Following this period of active life, the S-IVB/IU entered a dormant and controlled phase.

VEHICLE DESCRIPTION

The AS-501 flight vehicle is composed of eight major separable items (Fig. 1):

First Stage (S-IC)
Second Stage (S-II)
Third Stage (S-IVB)
Instrument Unit (IU)
Lunar Module (LM)
Apollo Service Module (SM)
Apollo Command Module (CM)
Launch Escape System (LES)

STAGE DESCRIPTION USING J-2 ENGINES

The second stage, S-II (Fig. 2) contains five J-2 engines to provide its propulsion. The five engines are located in the stage as indicated in Fig. 3 .

The engine serial number and its location in the stage are as follows:

Engine Location	Engine Serial Number
Engine No. 1	J2026
Engine No. 2	J2043
Engine No. 3	J2030
Engine No. 4	J2035
Engine No. 5	J2028

The third-stage S-IVB (Fig. 4) contains one J-2 engine to provide its propulsion. The serial number of this engine is J2031.

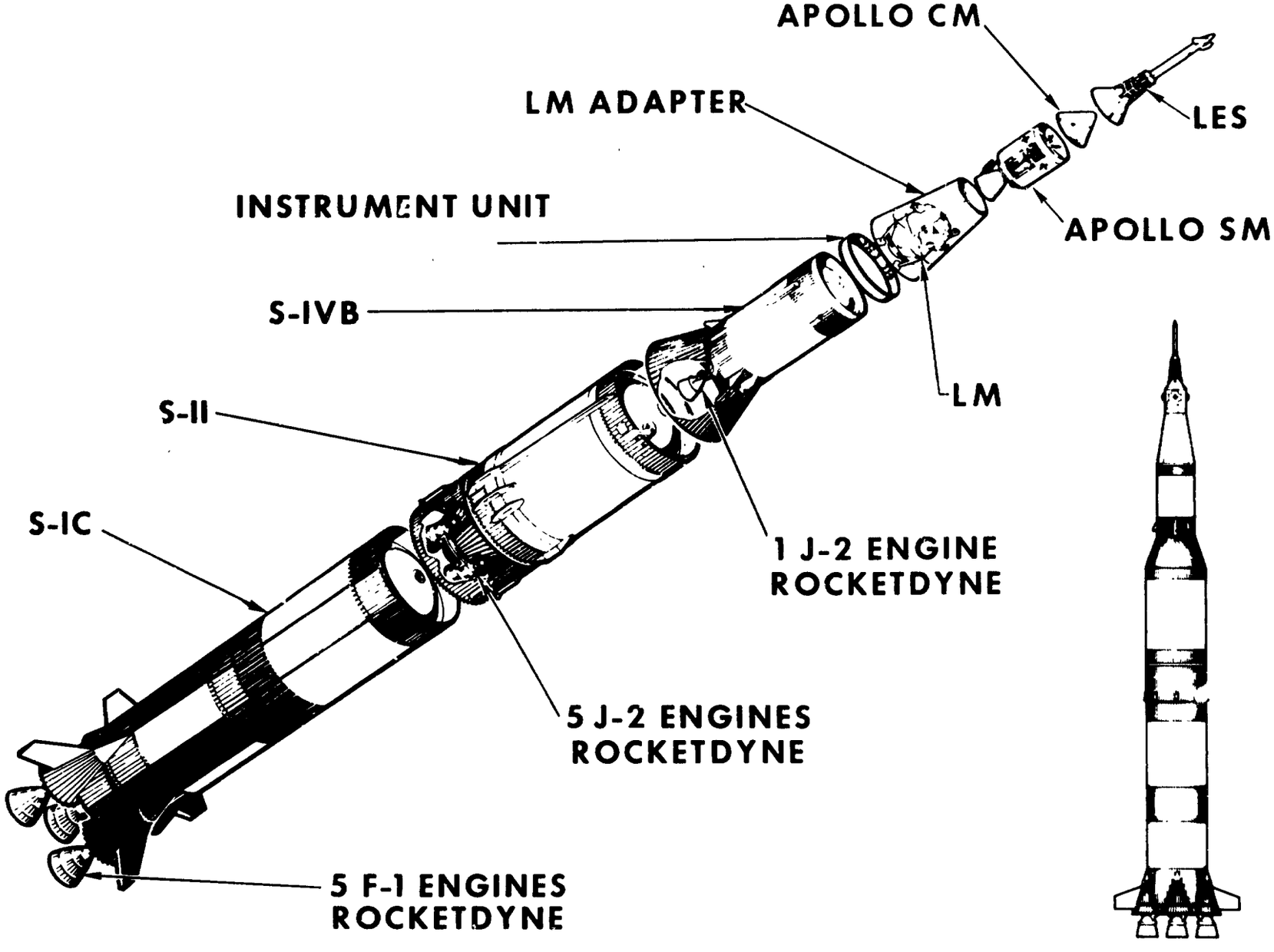

Figure 1. Saturn V/Apollo Vehicle

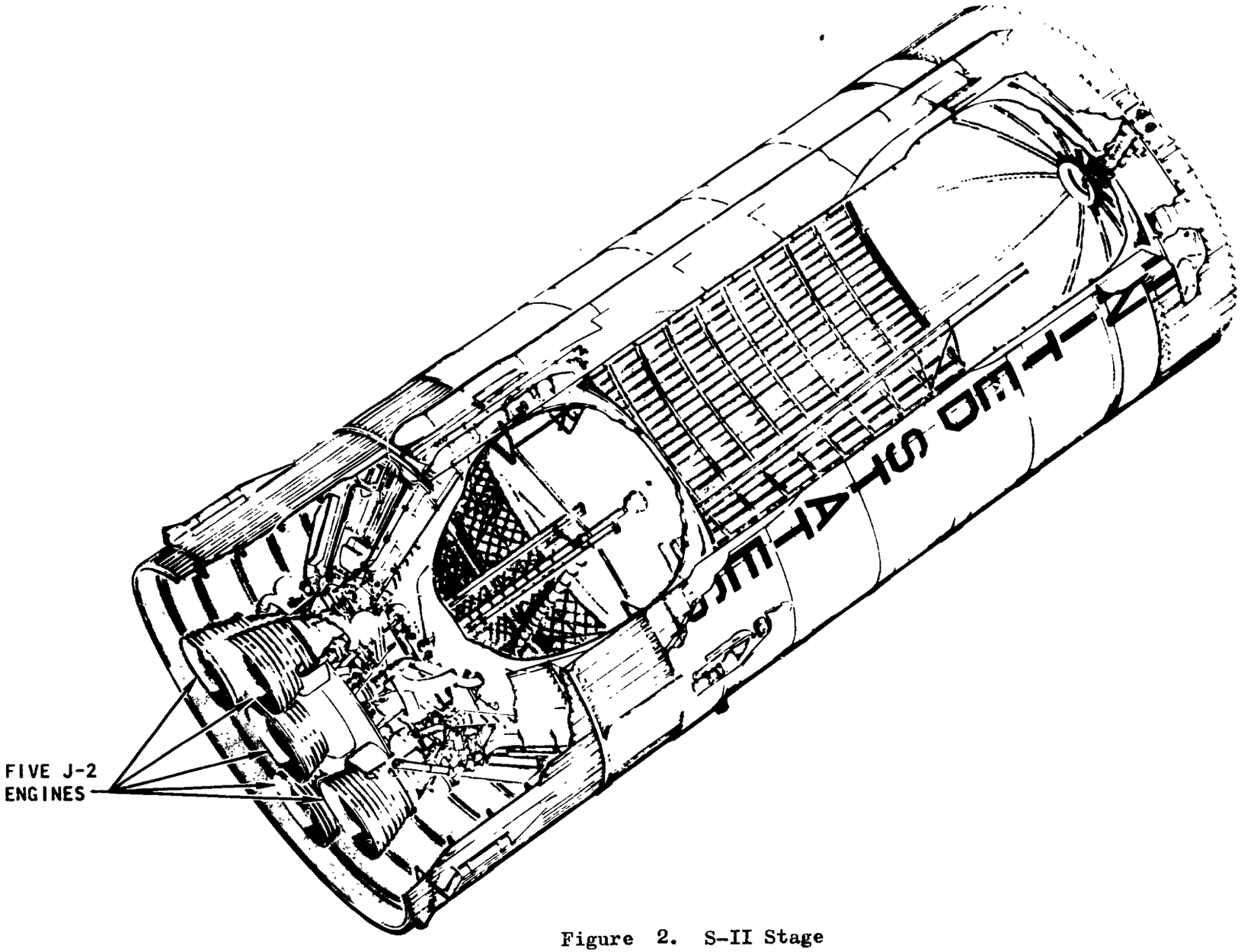

Figure 2. S-II Stage

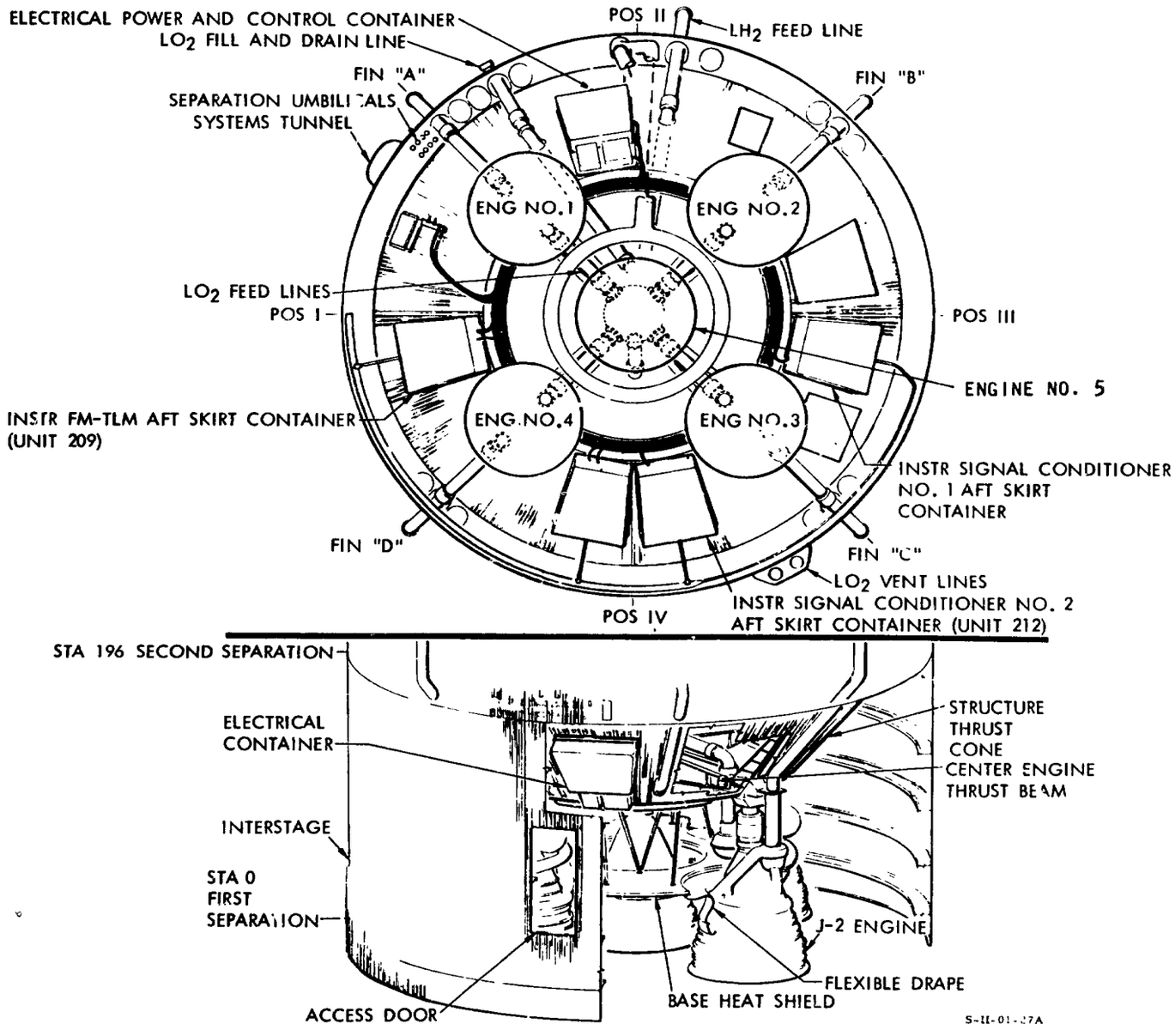

Figure 3. S-II General Arrangement, Aft Skirt

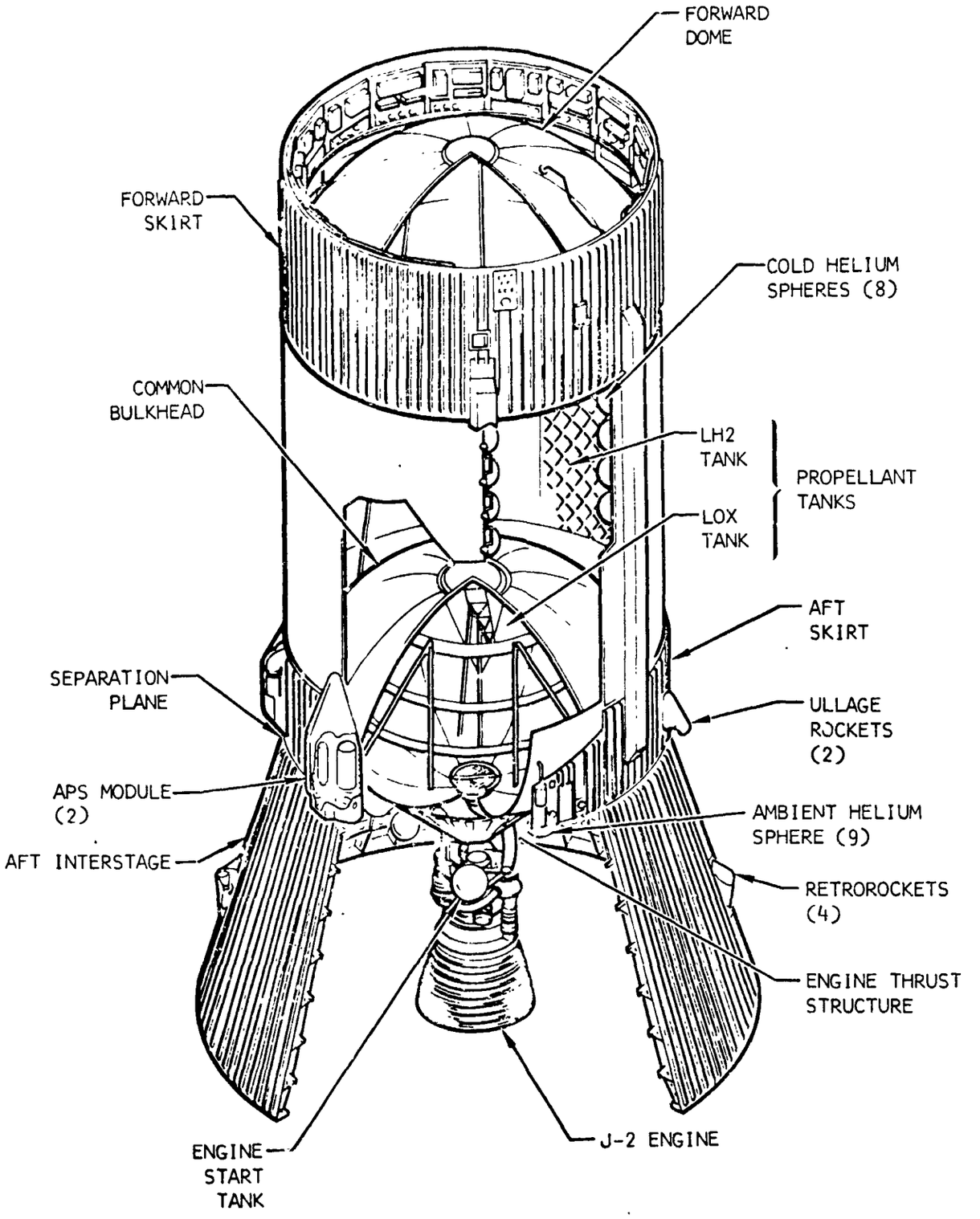

Figure 4. S-IVB-501 Stage Cutaway

REPORT CONTENTS

This report presents the flight performance results of the five J-2 engines in the S-II stage and the single J-2 engine in the S-IVB stage of the AS-501 vehicle. Included in the results are the engine start start transients, mainstage performance, and cutoff transients for the S-II and S-IVB stages, as well as the environmental conditions during the orbital coast period between the initial start and restart of the J-2 engine in the S-IVB stage.

SUMMARY

Performance of the J-2 engines on both the S-II and S-IVB stages of the Saturn V AS-501 vehicle was satisfactory in all phases of flight operation.

During the flight, the oxidizer heat exchanger on engine J2035 (S-II stage, engine No. 4) appeared to be obstructed because of low flow compared to the other engines on the S-II stage. The remaining heat exchangers satisfactorily adjusted to the higher demand that was placed on them, even though the demand, near the end of the stage operation, was above the engine model specification limits.

A momentary high helium consumption noted on engine J-2043 (S-II No. 2) was believed to be due to improper purge valve operation caused by contamination.

During the S-II stage operation, no temperature limits were exceeded as a result of base heating temperatures, and were less severe than expected. The S-IVB environmental conditions were either close to that predicted or less severe than that predicted.

Mainstage thrust, specific impulse, and mixture ratio performance were well within the expected operating range on all engines of both stages.

CONCLUSIONS

The following conclusions can be made from the flight evaluation of AS-501:

1. The J-2 engine can satisfactorily restart after a two-orbit coast.
2. The engine mainstage performance was satisfactory in all respects, and measured engine parameters were in good agreement with those predicted.
3. The effect of the thermal environment was not as severe as expected, and was well within the capability of the engine operating limits.
4. Orbital temperatures were as expected; however, the ullage rocket heating rates were negligible.

RECOMMENDATIONS

The results of the AS-501 flight evaluation indicate that, while engine operation was quite satisfactory, these recommendations can be made:

1. Install a filter in the oxidizer inlet line to the heat exchanger to prevent foreign particles from entering the heat exchanger.
2. Install a filter in the helium inlet line to the pressure-actuated purge control valve to prevent foreign particles from lodging in the valve, subsequently preventing the proper seating of the valve.
3. Insulate the start tank and helium tank temperature transducers from external effects to provide better temperature data in orbit.
4. Conduct a laboratory test program to define the start tank vent and relief valve operating characteristics. This, together with item 3, will provide three methods of temperature determination of the start tank and helium tank during flight.
5. Provide for a higher telemetry-sampling rate for the fuel pump discharge pressure, oxidizer pump discharge pressure, and MOV position potentiometer.
6. Increase engine vibration measurement calibration range to prevent overdriving the amplifier output during engine operation. Recommended calibration ranges are: dome, 100 g rms; oxidizer ring, 150 g rms; fuel pump, 200 g rms.

PRELAUNCH AND LAUNCH HISTORY

ENGINE ACCEPTANCE TESTS

Table 1 is a summary of the acceptance tests of the engines on the S-II and S-IVB stages.

TABLE 1

ENGINE ACCEPTANCE TEST HISTORY

Engine S/N	Engine Starts	Accumulative Time, seconds	Final Test Date, 1965	Delivery Date, 1965
J2026	4	659.5	15 June	24 June
J2043	4	736.3	18 October	16 November
J2030	4	454.4	13 July	4 August
J2035	3	359.3	4 August	24 August
J2028	8	624.1	1 July	8 July
J2031	3	358.5	15 July	23 September

AS-DELIVERED ENGINE CONFIGURATION

The engine configuration (modification number designation), as delivered to NASA, is as follows:

J2026 MD 3x5 11x13 20x23x25 28x32x34 38x40 47x49 51x53 60x64x68 70x72x76 80x82x84x86 87x97x99x101x106x111x116 118x122 124x127x130 132x134x138 142x153

J2028 MD 3x5 11x13 20x23x25 28x32x34 38x40 51x53 60x64x68 70x72x76 80x82x84x86 87x97x99x101x106x111x116 118x122 124x127x130x134x138 144x153

J2030 MD 3x5 11x13 20x23x25 28x32x34 38x40 51x53 60x64x68 70x72x76 80x82x84x86 87x97x99x101x106 107x111x116 118x122 124x127x130 132x134x138 143x153

J2031 MD 3x5 11x13 20x23x25 28x32x34 38x40 51x53 61x64x68 70x72x76 80x82x84x86 88x97x99x101x106 107x116 118x122 123x127x130 132x134x138 143x153

J2035 MD 3x5 11x13 20x23x25 28x32x34 38x40 51x53 61x64x68 70x72x76 80x82x84x86 88x97x99x101x106 108x116 118x122 123x127x130 132x134x138 144x152 153x158

J2043 MD 3x5 11x13 20x23x25 28x30x32x34 38x40 51x53 61x64x68 70x72x76 80x82x84x86x88x97x99x101x106 108x116 118x122 123x130 132x134x137 144x149x152 153x155x158x161x173x179

STAGE ACCEPTANCE TESTS

The engines, following stage installation, completed the following acceptance tests (Table 2):

TABLE 2

STAGE ACCEPTANCE TEST HISTORY

Engine S/N	Position	Cumulative Starts*	Cumulative Time, seconds	Final Test Date, 1966
J2026	1	6	1403.0	30 December
J2043	2	6	1475.6	30 December
J2030	3	6	1193.6	30 December
J2035	4	5	1098.9	30 December
J2028	5	10	1363.5	30 December
J2031		6	858.0	26 May

*Does not include stage static test No. A20010, which was terminated prior to mainstage signal because of ASI ignition detector short

ENGINE SERVICING RECORD

The following is a summary of significant engine problems encountered during the accomplishment of engine checkouts, modifications, and inspections

Engine Contamination Inspection

EFIR J2-20 was generated and accomplished on all S-II-1 engines following the discovery of contaminates in the stage oxidizer tank. The engine oxidizer systems were opened to allow inspection of critical components, i.e., the oxidizer turbopump, main injector, and gas generator injector. No serious contamination was found.

ASI No. 1 Spark Trace Anomaly

Data from an oscilloscope test of engine J2030 spark systems on the S-II stage revealed a negative pulse at the start of every positive spark pip on No. 1 ASI spark igniter. The ECA package was replaced. Subsequent investigations revealed that the ECA in question was satisfactory and that the noted condition was associated with the ground support equipment. Cognizant Rocketdyne personnel at KSC were alerted of the situation.

Spark Igniter Cables Pressure Test

Five of the twenty engine spark igniter cables on the S-II stage were pressure tested in compliance with ECP J2-538; the pressurizing tubes on the remaining igniter cables were too short to allow the test to be performed. Two igniter cables on engine J2026 were found de-pressurized; further tests of these cables revealed one with a leak, which was replaced. All spark igniter cables were subsequently fitted with Schrader valves and pressure tested, except for engine J2043 G-1 spark cable, which appeared to have a

pressurization tube restriction Subsequent analysis determined that the condition noted would not adversely affect spark igniter performance and was dispositioned acceptable for flight.

Electrical Connector Corrosion Inspection

Corrosion was noted on connector P1 of engine J2030 during ECA package replacement and prompted an inspection of eight selected connectors from each engine position on the S-II stage However, inspection of these connectors yielded no defects.

Engine Valve Timing Difficulties

The initial engine sequence accomplished on the S-II stage at KSC revealed four out of five main oxidizer valves ramp times out of specification limits, and two engines with marginal gas generator oxidizer poppet opening delay times. Subsequent attempts to retime these valves were seriously hampered by lack of precision instruments to determine actual size of orifices removed and installed. The problem was finally alleviated by use of pre-sized orifices.

Customer Connect Line Leakage

Leak checks performed on the S-II center engine (J2028) revealed a leak at the fuel bleed line customer connection. Initial attempts to correct the leakage, first by seal replacement and then by hand lapping the flange sealing surfaces, were unsuccessful. Measurements of the stage-supplied mating flange showed the seal bleed hole to be incompatible with the Naflex

seal design (also stage-supplied). A satisfactory joint was finally effected by careful and accurate position of the seal. As an immediate solution to this problem, the North American Rockwell Corporation Space Division has initiated steps to incorporate a new seal design.

Significant Engine Hardware Replacements (Post-Delivery)

Electrical Control Assembly. All engines on the S-II stage received ECA replacements prior to stage static testing to change STDV delay timer from 0.064 to 1.0 second. In addition, the engine J2030 ECA was changed again at KSC because of indication of a spark exciter failure which was subsequently determined to be caused by faulty KSC monitoring equipment.

Oxidizer Turbopump. Inspection after stage static testing revealed turbine wheel cracking on engines J2028, J2030, and J2043, which necessitated oxidizer turbopump replacement on these engines.

Main Oxidizer Valve. A detonation in the actuator of the MOV on engine J2026 resulted in removal, inspection, and reinstallation (per EFIR J2-26) of the MOV on all engines. In addition, the engine J2026 MOV was replaced again because of helicoil insert problem.

Pneumatic Regulators. All regulators were replaced with new assemblies (per ECP J2-602) to resolve a life-cycle controversy.

Additional Major Problems (Post-Delivery)

No significant major problems were encountered during post-delivery testing with engine J2031. Oxidizer turbopump cavitation was experienced just prior

to shutdown on the final S-II static stage test, which was programmed for a oxidizer low-level cutoff. Engine J2035 encountered the most severe cavitation.

Because of high fill rates during oxidizer tanking, the antivortex baffling in the S-II stage oxidizer tank sump was damaged severely, resulting in contamination with aluminum particles. Oxidizer pump disassembly was required on all five engines. All but one small piece of aluminum was finally recovered.

CHECKOUT HISTORY

The S-IVB stage for vehicle AS-501 arrived at Kennedy Space Center (KSC) from the Sacramento Test Center (STC) on 14 August 1966. The S-II-1 stage arrived at KSC from Mississippi Test Facility (MTF) on 21 January 1967.

Both stages were subjected to routine post transportation, receiving inspection and checkouts in the vehicle assembly building (VAB). Concurrent with these tests, stage and engine modifications were conducted.

A preliminary erection of the AS-501 launch vehicle was accomplished in the VAB on 1 November 1966, utilizing a spacer instead of the S-II stage to permit advanced checkouts of the launch vehicle integrated systems. The mating of all flight stages was accomplished later in the week of 23 February 1967.

On 27 May 1967, the launch vehicle was de-mated for an integrity inspection of the internal welds of the S-II stage fuel and oxidizer tanks. While this inspection was being accomplished, engine modifications on both S-II and S-IVB stages continued. The following significant engine tasks were started and/or completed during this period: remove, inspect, and clean main oxidizer valves (EFIR J2-26); remove and inspect helium regulator assemblies (ECP J2-602); and install redundant start tank and helium tank flight instrumentation (ECP J2-594). Other scheduled engine tasks also were conducted during this time period.

Following erection of the launch vehicle to the mobile launcher, the vehicle was transported to launch pad 39A on 26 August 1967. Launch vehicle integrated tests and checkouts begun immediately and were carried on concurrently with engine modifications. The engine oxidizer pump primary seal drain line modification (ECP J2-620) was satisfactorily accomplished on both S-II and S-IVB stages, except for burst diaphragms that were added following countdown demonstration test (CDDT). All scheduled engine tasks were completed on time.

COUNTDOWN DEMONSTRATION TEST

The CDDT milestone was successfully achieved on 13 October 1967, after numerous holds and cancellations because of procedural lags, ground equipment malfunctions, and computer problems. However, difficulties and problems were generally expected because the facilities, procedures, and vehicle were being tested for the first time as an integral unit. With the exception of the oxidizer tank baffle problem on the S-II stage, which was discovered following CDDT, data from the test demonstrated that the AS-501 launch vehicle and launch support equipment to be compatible and operational. Following CDDT, entry into the S-II oxidizer tank (to replace defective low-level sensors) revealed that the antivortex baffling in the oxidizer tank sump had failed. A search was initiated that recovered all of the broken baffle material except for the equivalent of three small pieces. A decision was made to inspect the oxidizer systems of all five engines on the second stage; only one of the missing pieces was located (in the volute passage of engine No. 5, J2028). Following repair of the oxidizer tank baffle, a decision was reached to proceed with the launch.

FLIGHT READINESS TEST

The flight readiness test (FRT) was successfully accomplished on 26 October 1967, with no major problems.

ENGINE FLIGHT CONFIGURATION

The J-2 engines utilized on the AS-501 launch vehicle conformed to Engine Model Specification R-2158bs, dated 7 February 1966, and the engine configuration for the applicable S-II and S-IVB stages is documented in the Saturn J-2 Configuration, Identification, and Status Report of R-5788, dated 1 November 1967.

The engine configuration, as flown, is as follows:

J2026 3x5 11x13 20x23x25 28x32x34 38x40 47x49 51x53 60x64x68 70x72x76
80x82x84x86 87x91x97x99x101x106x111x116 118x122 124x127x130
132x134x138 143x148 149x151x153x155x157 158x161x168x176
178x180x188x190x202x205x218 219x221x224x226 227x230x234
236x240x244x246 247x251x256 257x259x276x278x284x289x291x295x299

J2028 3x5 11x13 20x23x25 28x32x34 38x40 51x53 60x64x68 70x72x76
80x82x84x86 87x91x97x99x101x106x111x116 118x122 124x127x130
132x134x138 144x149x151x153x155 158x161x165x168x176
178x190x198x202x205x218 219x221x225 227x230x234 236x238x240x244x246
248x252x256 257x259x276x278x284x289x291x295x299

J2030 3x5 11x13 20x23x25 28x32x34 38x40 51x53 60x64x68 70x72x76
80x82x84x86 87x91x97x99x101x106 107x111x116 118x122 124x127x130
132x134x138 143x148 149x151x153x155x157 158x161x168x176
178x180x188x190x202x205x218 219x221x224x226 227x230x234
236x240x244x246 247x251x256 257x259x256
257x259x276x278x284x289x291x295x299

J2031 3x5 11x13 20x23x25 28x32x34 38x40 51x53 61x64x68 70x72x76
80x82x84x86 88x97x99 101x105 107x116 118x122 123x127x130
134x138 143x148 151x153x155x158x160 161x163x168x176x180x183
184x188x191x200x213 215x217 219x223x227x230 231x238x241
242x244x249x260x265 267x269x271 272x275 276x285x288x291x299x301

J2035 3x5 11x13 20x23x25 28x32x34 38x40 51x53 61x64x68 70x72x76
80x82x84x86 88x97x99x101x106 108x116 118x122 123x127x130 132x134x138
144x148 149x151x153x155x158x161x168x176 177x188x190x202x205x218
219x221x224x226 227x230x234 236x238x240x246 248x251x256
257x259x269x276x278x289x291x295x299

J2043 3x5 11x13 20x23x25 28x30x32x34 38x40 51x53 61x64x68 70x72x76
80x82x84x86 88x97x99x101x106 108x116 118x122x130 132x134x137
144x148x149x151x153x155x158x161x168x173x176 177x179
180x188x190x202x205x218 219x221x224x226 227x230x234 236x240x244x246
247x251x256 257x259x276x278x284x289x291x295x299

LAUNCH AND FLIGHT DESCRIPTION

The AS-501 (Apollo 4) vehicle is the first flight in the Saturn V Program and the fourth flight of the Apollo Program. As an integral part of the vehicle, the S-II and S-IVB stages had associated flight test objectives which are included herein.

Mission

The objective of the Apollo-Saturn V Program is to land men and scientific equipment on the surface of the moon for the purpose of manned exploration of the lunar surface in the vicinity of the landing site, and to return the men to earth safely. The program consists of a series of research and development (R&D) test flights in which the primary objective is to flight test and qualify the AS-501 space vehicle.

AS-501 is the first flight vehicle of the Saturn V series. The basic purpose of the unmanned AS-501 mission is to develop the Saturn V launch vehicle and the Apollo command and service modules for future manned flights.

Mission Objectives

Primary objectives are those that are mandatory; therefore, malfunctions of launch vehicle systems, ground support equipment, or instrumentation that would result in failure to achieve these objectives will be cause to hold or cancel the mission until the malfunction has been eliminated. The following paragraphs define primary objectives as extracted from NASA directives.

The primary objectives listed below were obtained from National Aeronautics and Space Administration, "Apollo Flight Mission Assignments" (Office of Manned Space Flight, Apollo Program), M-D MA 500-11, SE 010-000-1, 14 November 1966, Washington, D.C.

1. Demonstrate the structural and thermal integrity and compatibility of the launch vehicle and spacecraft; confirm launch loads and dynamic characteristics
2. Demonstrate separation of:
   a. S-II from S-IC (dual plane)
   b. S-IVB from S-II
3. Verify operation of the following subsystems:
   a. Launch vehicle: propulsion (including S-IVB restart), guidance and control, and electrical system
   b. Spacecraft: command module heat shield (adequacy of block II design for entry at lunar return conditions) and selected subsystems
4. Evaluate performance of the space vehicle emergency detection system in an open-loop configuration
5. Demonstrate mission support facilities and operations required for launch, mission conduct, and CM recovery

The primary objectives listed below were obtained from NASA "SA-501 Launch Vehicle Mission Directive," revision A, Change 1, 29 June 1967, George C. Marshall Space Flight Center, Huntsville, Alabama:

1. Determine in-flight launch vehicle internal environment
2. Verify prelaunch and launch support equipment compatibility with launch and spacecraft systems
3. Demonstrate the S-IC stage propulsion system, and determine in-flight system performance parameters
4. Demonstrate the S-II stage propulsion system, including: programmed mixture ratio shift and the propellant management system, and determine in-flight performance parameters
5. Demonstrate the S-IVB stage propulsion system including the propellant management systems, and determine in-flight system performance parameters.
6. Demonstrate the launch vehicle guidance and control system during S-IC, S-II, and S-IVB powered flight, achieve guidance cutoff, and evaluate system accuracy
7. Demonstrate launch vehicle sequencing system
8. Demonstrate compatibility of the launch vehicle and spacecraft
9. Demonstrate the capability of the S-IVB auxiliary propulsion system during S IVB powered flight and orbital coast periods to maintain attitude control and perform required maneuvers
10. Demonstrate the adequacy of the S-IVB continuous vent system while in earth orbit
11. Demonstrate the S-IVB stage restart capability

The primary objectives listed below were obtained from NASA "Program Support Requirements" (Office of Manned Space Flight, Apollo-Saturn V) Washington, D.C., dated 19 September 1966:

1. Launch environmental input from the Saturn V/spacecraft lunar module adapter (SIA) to the simulated LM

2. Determine the force inputs to the simulated LM from the SLA at the spacecraft attachment structure during launch

3. Obtain data on the acoustic and thermal environment of the SLA-simulated LM interface location during launch

4. Determine the overall simulated LM vehicle linear acceleration response to the launch environment

5. Obtain data on the vibratory response of the simulated LM during launch at selected locations in the descent stage

6. Obtain data on the temperature of the simulated LM skin during launch

Secondary Objectives. Secondary objectives are those that are desirable but not mandatory. Malfunctions that may result in failure to attain these objectives may be cause to hold, but not cancel, the countdown as indicated in the Launch Mission Rules Document. The following paragraphs define secondary objectives as extracted from NASA directives.

The secondary objectives listed below were obtained from NASA "SA-501 Launch Vehicle Mission Directive," Revision A, Change 1, 29 June 1967.

1. Determine launch vehicle powered flight external environment

2. Determine attenuation effects of exhaust flames on RF radiating and receiving systems during main engine, retro, and ullage motor firings

The secondary objectives listed below were obtained from NASA "Program Support Requirements," (Office of Manned Space Flight, Apollo-Saturn V) Washington, D.C., dated 19 September 1966:

1. Evaluate launch vehicle internal environment

2. Confirm IU/S-IVB in-flight thermal conditioning system

3. Determine CSM radiation shielding effectiveness and demonstrate operational radiation monitoring instrumentation

4. Demonstrate satisfactory operation of CSM communication subsystem using the block II type VHF and S-band omni antenna

5. Demonstrate satisfactory CSM subsystems performance in the space environment before and after separation from S-IVB and during entry

LAUNCH

The launch vehicle countdown was executed essentially as planned, with no unscheduled holds. Liftoff occurred at 7:00 AM EST on 9 November 1967. Preliminary evaluation of flight results indicated that all phases of powered flight were satisfactory, including inserting the payload into earth-parking orbit.

The S-IVB restart milestone was achieved at 10:09 AM EST as planned, following the second earth orbit. The engine in the S-IVB stage performed satisfactorily during the second burn, and all restart mission objectives were attained. Re-entry and subsequent recovery of the command module was successfully accomplished at approximately 3:30 PM EST on the same day.

The significant event times of AS-501 are shown in Table 3 .

TABLE 3

SIGNIFICANT EVENT TIMES

Event	Range Time, seconds	
	Actual	Predicted
First Motion	-0.48	--
Liftoff Signal (IU)	0.265	--
Start Yaw Maneuver	1.3	--
Start Pitch and Roll	11.7	10.5
S-IC Inboard Engine Cutoff (IECO)	135.5	135.0
S-IC Outboard Engine Cutoff (OECO)	150.8	151.9
S-II Ullage Motor Ignition	151.2	152.4
S-IC Retro Motor Ignition	151.4	152.6
S-IC/S-II Separation	151.4	152.7
S-II Engines Start Command	152.2	153.3
S-II Second Plane Separation	181.4	182.6
Jettison Launch Escape Tower	187.1	188.3
Jettison S-II Aft Cameras	189.8	191.0
Initiation of Iterative Guidance Mode (IGM)	190.2	191.9
S-II Engine Cutoff	519.8	516.3
S-IVB Ullage Motor Ignition	520.4	517.0
S-II Retro Motor Ignition	520.5	517.1
S-II/S-IVB Separation	520.5	517.2
S-IVB Engine Start Command	520.7	517.3
S-IVB Ullage Case Jettison	532.5	529.1
S-IVB First Guidance Cutoff	665.6	656.0
Insertion Into Parking Orbit	675.6	666.0
S-IVB Restart Preparations (Time Base 6)	11,159.6	11,158.5
S-IVB Restart Command	11,486.6	11,484.5
S-IVB Second Guidance Cutoff Signal	11,786.3	11,799.4
Waiting Orbit Injection	11,796.3	11,809.4
S-IVB/CSM Separation	12,386.5	12,399.4

S-II STAGE ENGINE OPERATION

THERMAL ENVIRONMENT

Prelaunch

The prelaunch sequence from initiation of tanking to liftoff was normal. The propellant tanking was accomplished in the following sequence:

1. S-IC fuel on board prior to start of countdown
2. S-IVB oxidizer loading
3. S-II oxidizer loading
4. S-IC oxidizer loading
5. Oxidizer replenishing of all stages
6. S-II fuel loading
7. S-IVB fuel loading

The significant temperatures prior to liftoff, which were a result of the thermal environment and engine preconditioning during this period, were as follows:

1.	Engine compartment gas temperature, F	-35
2.	MOV body temperature, F	-75
3.	MOV closing control line temperature, F	-20
4.	Electrical control assembly temperature, F	+70 to +80
5.	Thrust chamber jacket temperature, F	-250 to -278

Oxidizer was down to the MOV for approximately 4 hours. The warmer GN_2 boattail purge in the S-II stage accounted for the warmer engine thermal environment as compared with the S-IVB stage. The boattail purge was initiated just prior to propellant tanking.

Boost Phase

The boost phase for the S-II stage extends from liftoff of the vehicle to separation of the S-IC/S-II stages. The S-II stage interstage environment, encountered throughout the boost phase, was below those predicted (Fig. 5). The primary effect of the environment can be seen by considering thrust chamber heating rates during boost.

The thrust chamber jacket temperatures at liftoff were satisfactory; however, they were on the low side of the predicted range. The five engines ranged from -250 to -278 F. Warmup rates exceeded those predicted, which resulted in actual rises of 42 to 65 F, as compared to a predicted rise of 38 F. The high warmup rate experienced during the first 70 to 80 seconds after liftoff, together with the low chill, resulted in nominal conditions at engine start (Fig. 6).

The MOV temperatures were not as cold as expected. At engine start, the MOV closing control line temperature on the center engine was -45 F, as compared to a predicted range of -100 to +50 F. However, the MOV body temperature on the center engine was -65 F, as compared to a predicted range of -130 to -235 F (Fig. 7). The warmer than predicted temperatures are attributed to the relatively warm environment experienced during pre-launch chilldown and the boost phase.

The stage environmental and component temperatures prior to liftoff are shown in Table 4 .

TABLE 4

ENVIRONMENTAL AND COMPONENT TEMPERATURES PRIOR TO LIFTOFF

Parameter	Expected or Allowable Temperature Range, F	Data Temperature Range, F
Environmental Gas	-100 to 60	-40 to 20
Thrust Chamber Jacket	-300 to -200	-280 to -250
Electrical Control Assembly	-65 to 140	70 to 80
Primary Instrumentation Package	-65 to 140	15 to 40
Auxiliary Instrumentation Package	-65 to 140	0 to 25

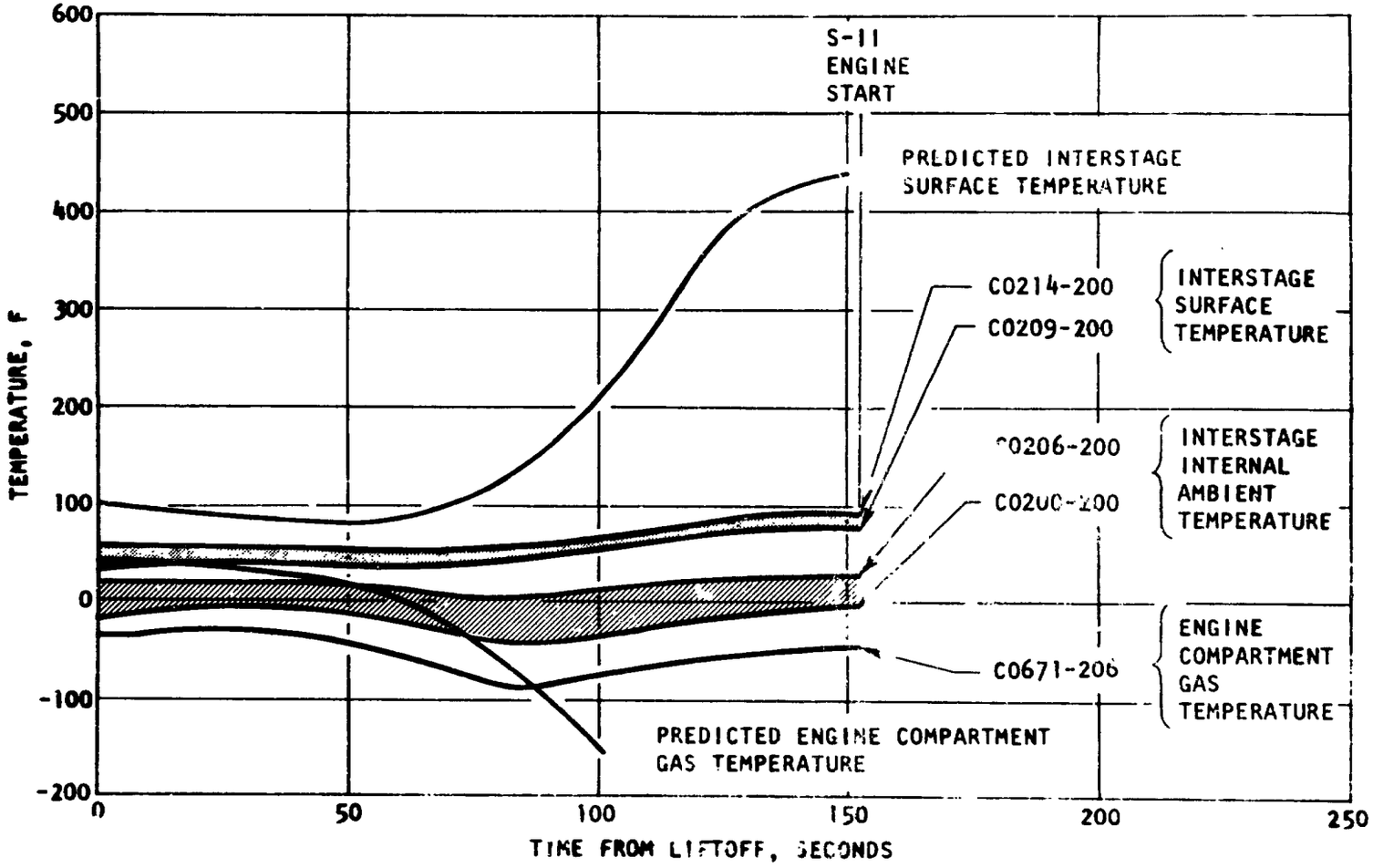

Figure 5. Interstage Environmental Temperature During Boost, S-II Aft

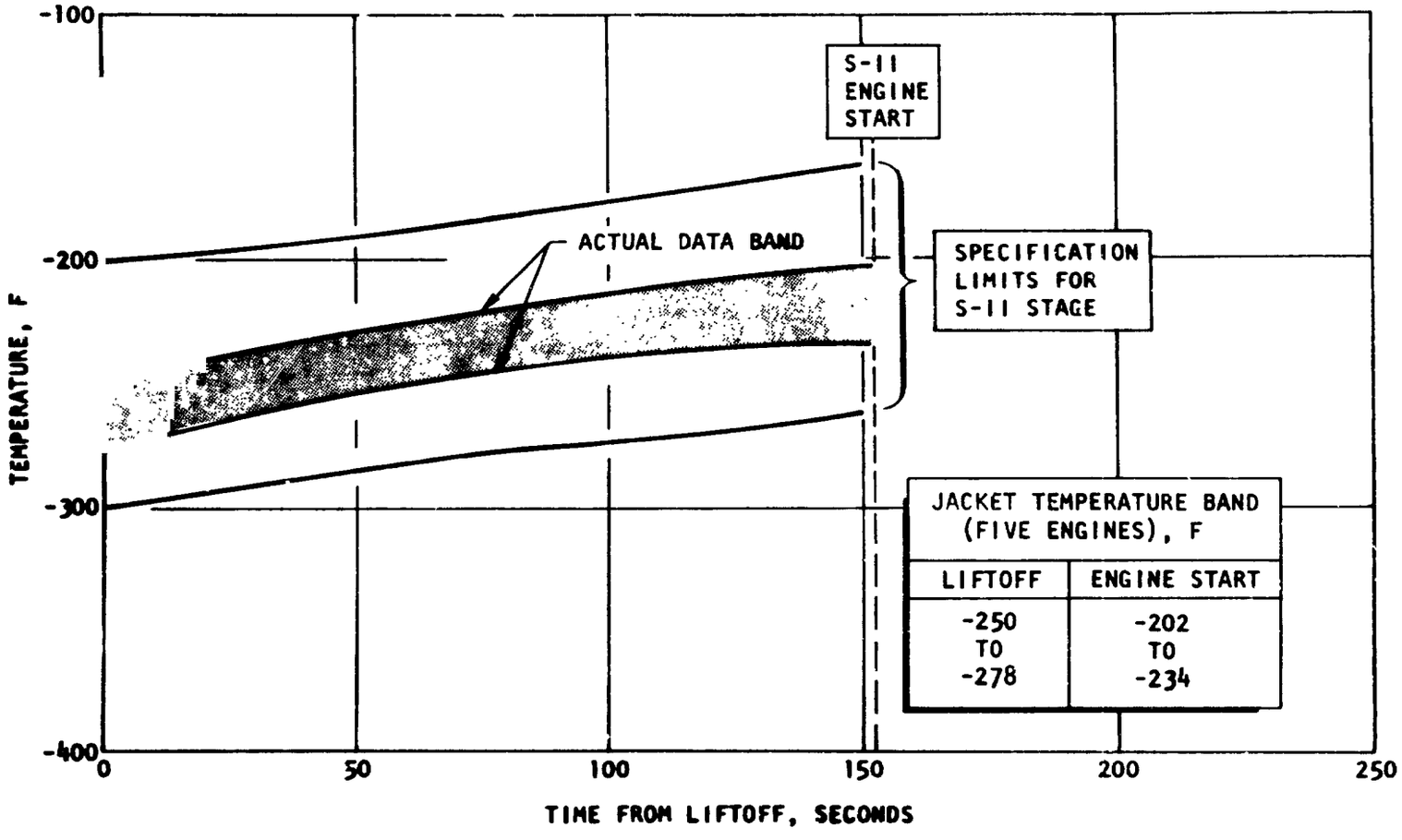

Figure 6. Thrust Chamber Jacket Heatup During Boost, S-II

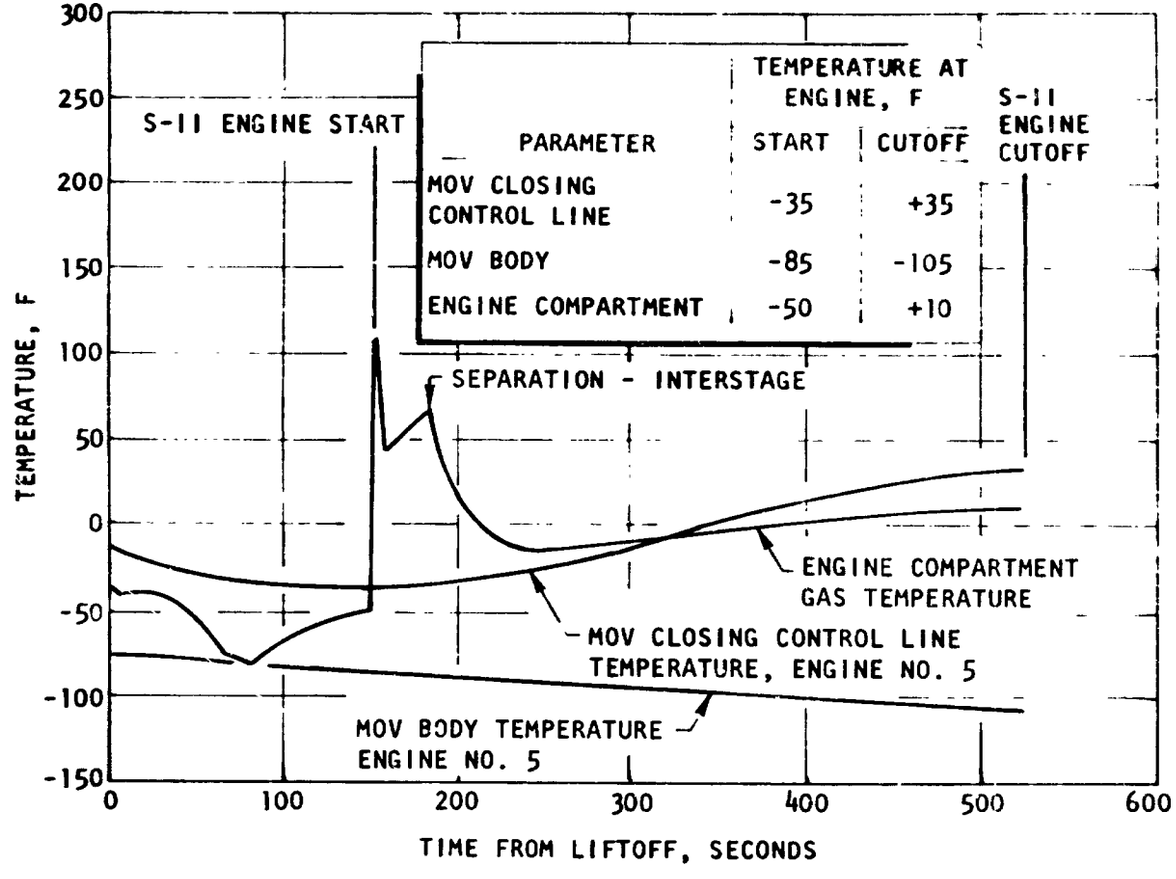

Figure 7. S-II MOV Environment During Boost Phase and Engine Operation

Separation

The S-IC/S-II separation occurred 151.2 seconds after liftoff. S-II stage engine start command occurred 0.8 second after separation.

The system for separating the S-IC/S-II stages uses a dual-plane separation mode. First-plane separation occurs at S-II stage station 0, and second-plane separation occurs at S-II stage station 196. The first-plane separation sequence is preceded by ignition of eight ullage motors, producing a nominal thrust of 188,000 pounds for a duration of 3.7 seconds. Ullage motor ignition occurs when the thrust of the S-IC stage decays to approximately 10 percent. First plane separation starts at this time, which is followed by ignition of the eight S-IC retrorockets, producing a nominal thrust of 866,000 pounds for a duration of 0.67 seconds.

The S-II engines are ignited after first-plane separation while the ullage motors are still at full thrust. The second plane separation occurs 30 seconds after S-II stage engine ignition (181.4 seconds after liftoff).

During the initial 30-second portion of the S-II stage flight, the heat transfer coefficients were based on the predicted hot-gas recovery temperature of 3100 F (MR at 5.5) and 2876 F (MR at 4.7). No comparison of the recovery temperatures could be made between the predicted and measured temperatures on the base heat shield because the gas recovery temperature was below the transducer range (1500 F minimum). It is postulated that the predicted gas recovery temperature of 3100 F (MR at 5.5) and 2876 (MR at 4.7) used in calculating the heat transfer coefficients may have been overestimated.

The heating rates measured on the S-II stage surfaces were generally below the predicted design values. This was also true of the convective heating rates measured on the aft face of the base heat shield.

Base heating temperatures (aft and forward base heat shield) are presented in Fig. 8 and 9. The actual measurements were considerably lower than those predicted. This was probably caused by the high design heating rate predictions and high gas recovery temperature

The S-II stage J-2 engine component temperatures during ergine operation are shown in Table 5.

TABLE 5

J-2 ENGINE COMPONENT TEMPERATURES
DURING OPERATION

Parameter	Temperature to Which Operation Verified, F	Data Temperature Range, F
Electrical Control Assembly (ECA) (all engines)	140	75 to 85
Primary Instrumentation Package (all engines)	140	15 to 40
Auxiliary Instrumentation Package (all engines)	140	10 to 30
Hatband No. 5 (center engine)	600	-90 to 50
Gimbal Actuator Housing (outboard engine)	500	40 to 60
ECA Support Rod (outboard engine)	150	0 to 20
Helium Regulator (outboard engine)	140	15 to 30
Hatband No. 1 (outboard engine)	500	-70 to 40
Hatband No. 7 (outboard engine)	500	-70 (constant)
Armored Harness (outboard engine)	600 (for 5 minutes)	-50 to 250*

*250 F reached 30 seconds after ignition, and decreased thereafter when interstage was jettisoned

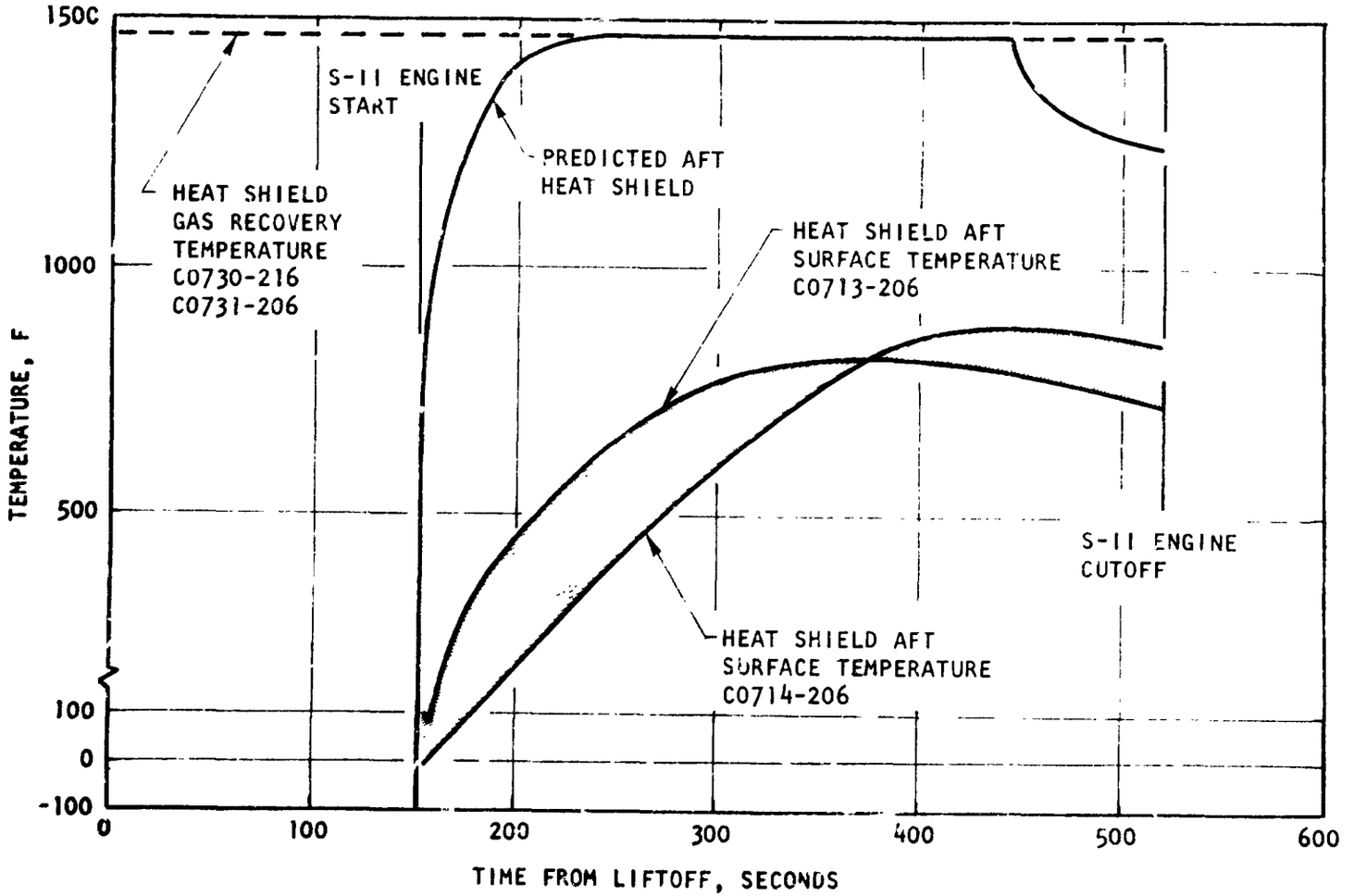

Figure 8. S-II Base Heat Shield Temperature During Engine Operation

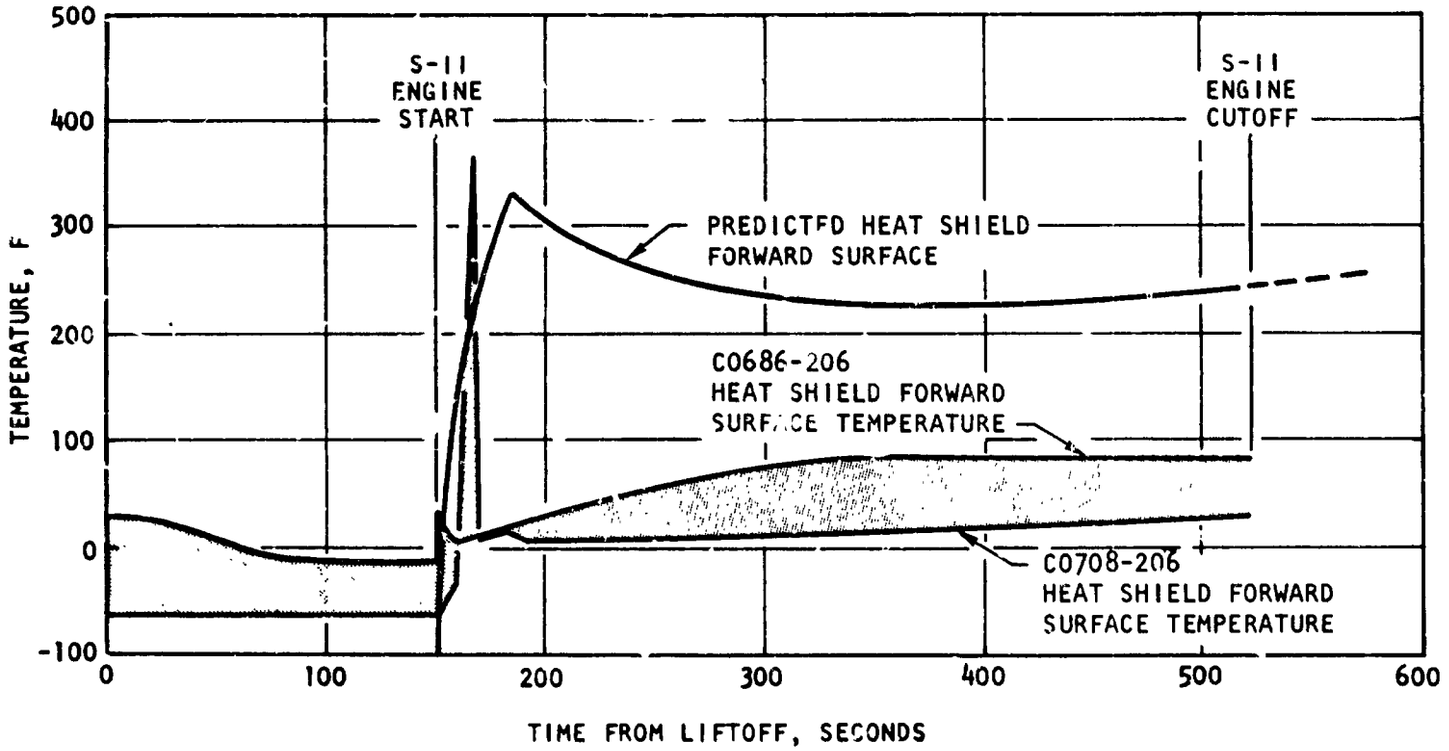

Figure 9. S-II Basic Heat Shield Temperature During Engine Operation

START TRANSIENTS

The start transient performance of the S-II stage engines were satisfactory and within engine model specification limits.

The following ECP modifications affecting start operation were incorporated on all engines:

ECP J2-455--delayed gas generator timing to minimize excessive gas generator temperature spikes and flow reversal

ECP J2-513--retiming of nontemperature-compensated main oxidizer valve; second-stage delay and travel compatible with predicted thermal environment

ECP J2-575--installation of 0.150-inch orifice in the oxidizer ASI supply line to ensure satisfactory ASI operating temperatures

Table 6 shows engine start conditions for S-II flight and the most comparative S-II test (test 028B) conducted at AEDC. From the table, engine J2052 initial conditions on test 028B were indicative of a faster start than the S-II flight engines. Actually, engine J2052 did exhibit the fastest power buildup, with engine No. 4 representing the maximum flight buildup and engine No. 3 the minimum. Review of sea level acceptance testing records indicate the same maximum/minimum engine start characteristics.

Figure 10 compares oxidizer pump outlet pressure transients, S-II flight envelope versus engine J2052 (test 028B). The AEDC test had a significantly higher pressure potential at gas generator ignition, resulting in a faster buildup and a higher percentage of steady-state overshoot. The faster power buildup experienced on test 028B was primarily caused by a 50 F warmer engine exhaust system temperature and a 50 F colder start tank gas temperature that resulted in increased spin-gas energy. The increased spin-gas energy passing through the oxidizer turbine caused engine J2052 spin speed to exceed the S-II flight engines, as shown in Fig. 11.

TABLE 6

ENGINE CONDITIONS AT ENGINE START

Parameter	AEDC Test 1554-028B (J2052)	S-II Flight
Start Tank Pressure, psia	1306	1290 to 1346
Start Tank Temperature, F	-312	-245 to -262
Fuel Pump Inlet Temperature, F	-421.8	-421
Fuel Pump Inlet Pressure, psia	35.6	32
Oxidizer Pump Inlet Temperature, F	-295.5	-296
Oxidizer Pump Inlet Pressure, psia	37.4	34.5
Thrust Chamber Skin Temperature, F	-169	-210 to -230
Fuel Lead, seconds	1.0	1.0
Mean Exhaust System Temperature, F	15	-40
MOV Closing Actuator Temperature, F	-146	-60 to -85
PU Valve Position	Null	Null

Fuel pump spin speed is primarily dependant on start tank pressure, is only slightly affected by start tank gas temperature, and is virtually independant of turbine exhaust system temperature. The higher start tank pressure levels experienced on the flight engines compared to engine J2052, test 028B, resulted in higher fuel pump spin speeds, as shown in Fig 12 .

Figure 13 compares main oxidizer valve opening characteristics. The warmer than expected bouttail environment resulted in short plateau (14-degree open) times on all the flight engines. Engine J2052 exhibited similar MOV first position times on AEDC test 028B, the MOV being replaced prior to test series 028 with a nominal friction valve compared to the abnormally high friction valve used for previous S-II testing. Flight data indicate below normal valve friction on the flight engines, which also contribute to the short plateau times.

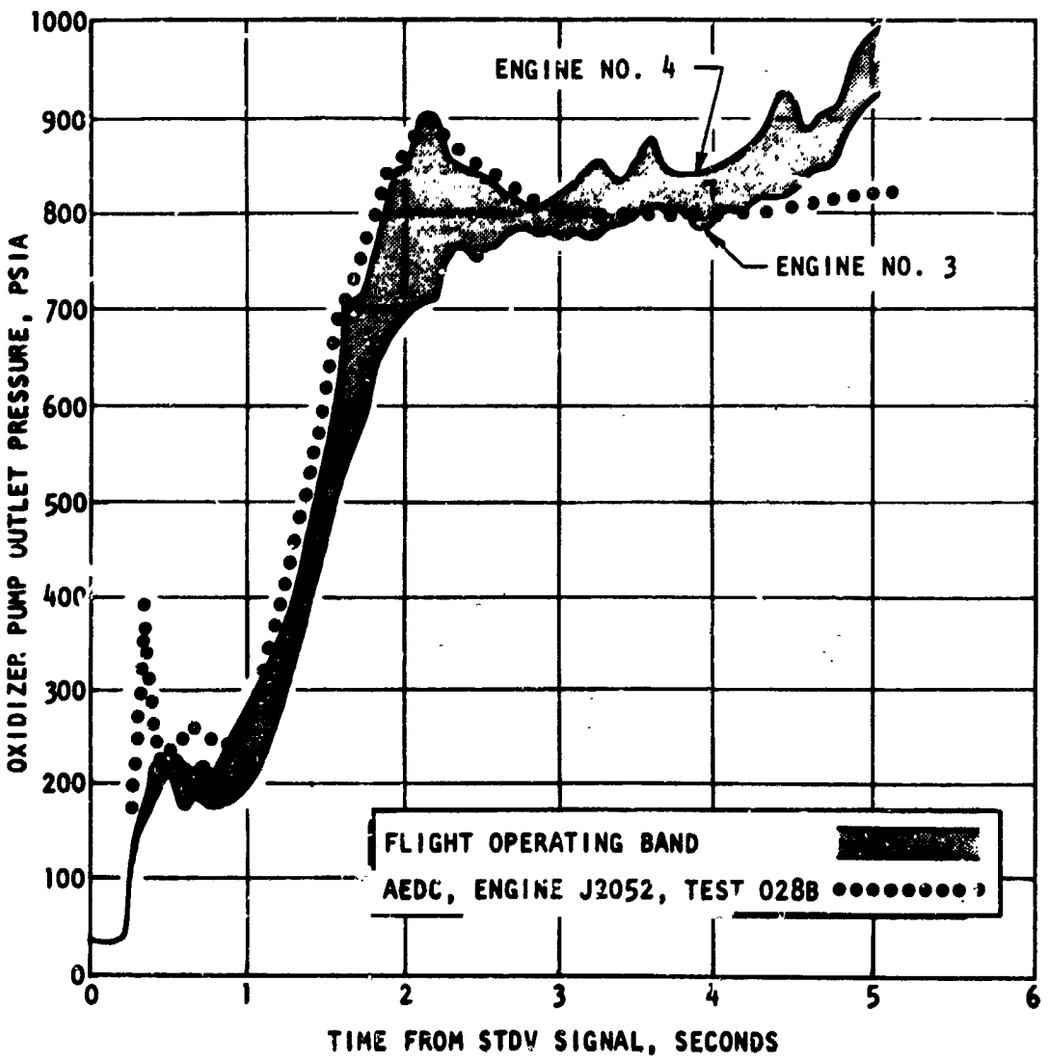

Figure 10. Oxidizer Pump Outlet Pressure During Start Transient

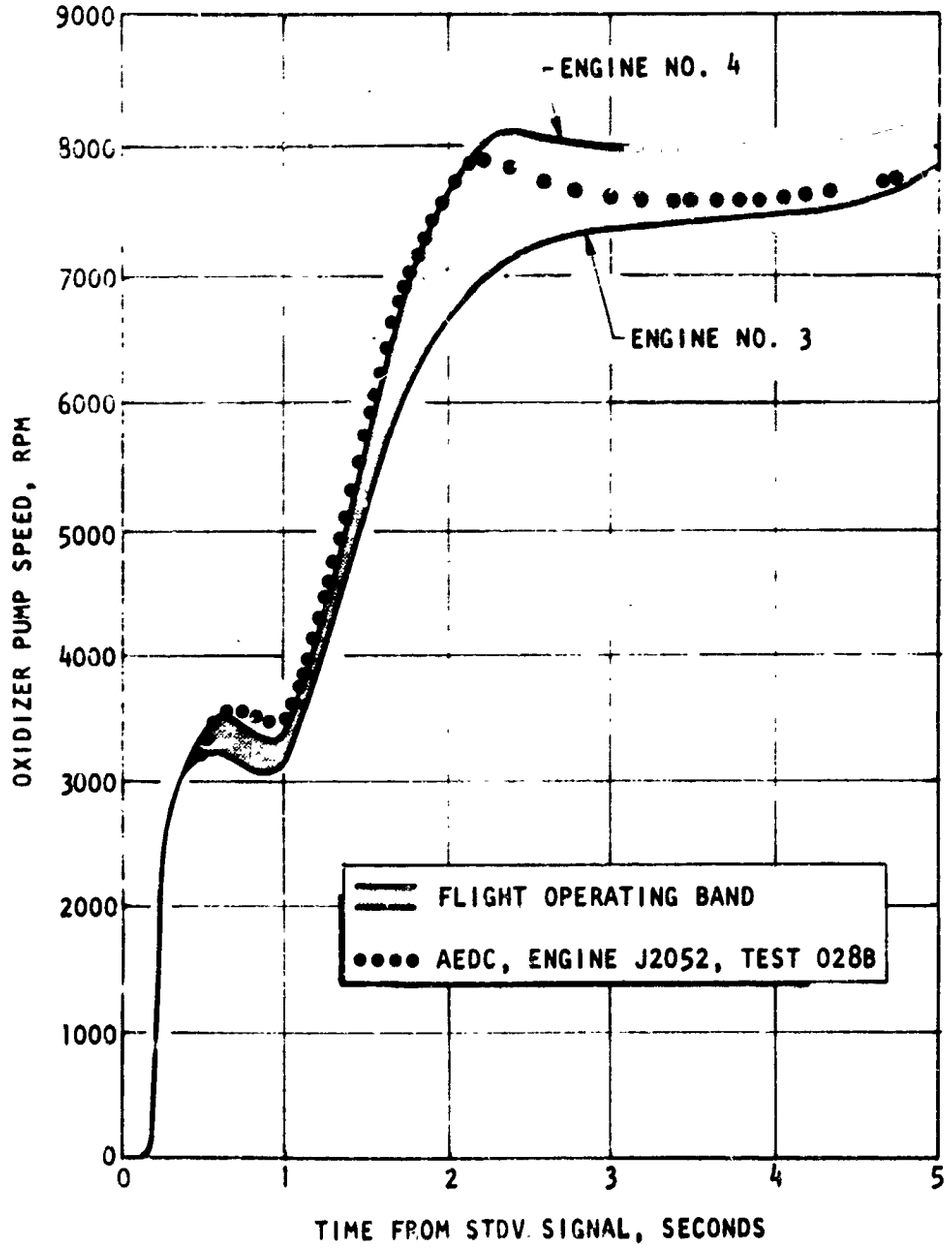

Figure 11. Oxidizer Pump Speed During Start Transient

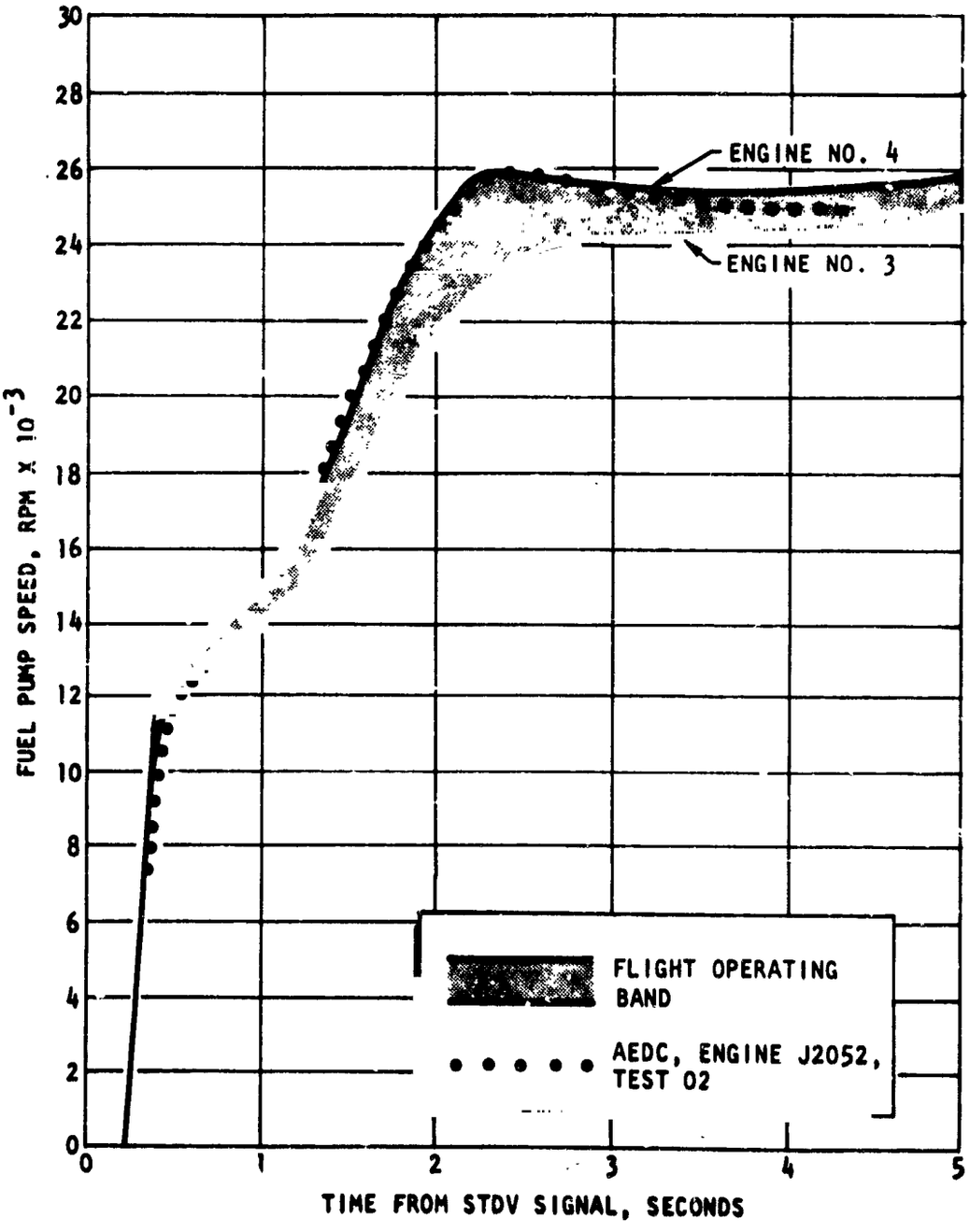

Figure 12. Fuel Pump Speed During Start Transient

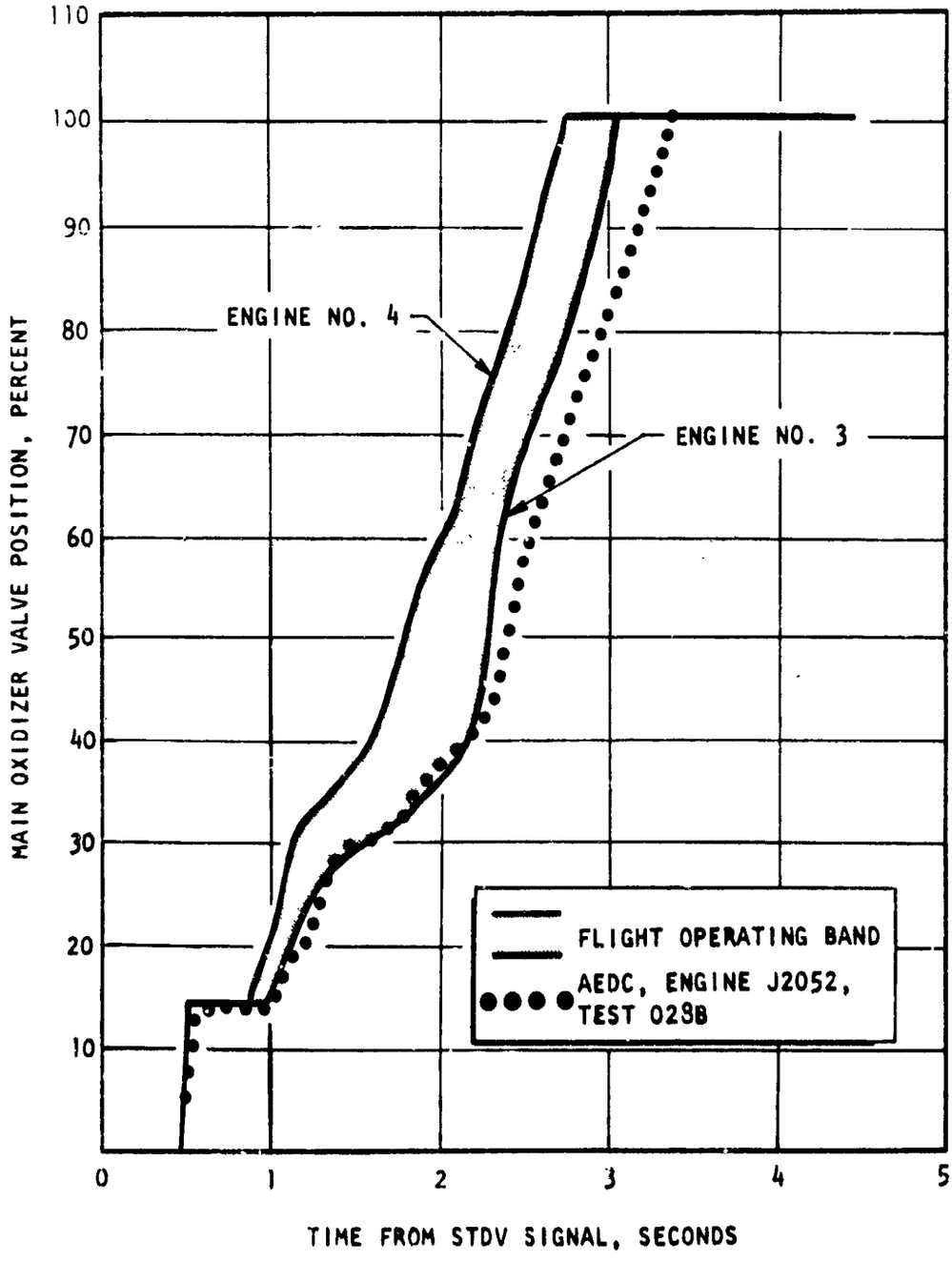

Figure 13. Main Oxidizer Valve Opening Transient

Table 7 compares main oxidizer valve sequence and engine hot-fire opening times experienced at AEDC with the flight engines. The main oxidizer valves used in the flight engines, and for the 16 S-II series tests conducted at AEDC, were the nonthermal-compensating type, timed to the sequence ramp limits of ECP J2-513 (1390 ±40 milliseconds). Although flight MOV opening times were within AEDC test limits (Table 7), the first position delay times approached the minimum satisfactory operational limit of 450 milliseconds.

The reduction of MOV plateau and ramp time decreases fuel pump stall margin during the start transient. The faster MOV opening causes a higher oxidizer flow and, consequently, faster main chamber pressure buildup. Fuel system resistance is increased because of the higher chamber pressure, resulting in an increase in fuel pump head and a commensurate decrease in fuel flow, i.e., reduced stall margin.

Figure 14 compares fuel pump head versus flow plots for the flight and AEDC S-II series test limits. Adequate stall margin was indicated from flight data, even with the adverse effects of reduced MOV first position times.

The fast MOV opening characteristics exhibited during flight operation tend to reduce gas generator power buildup and its associated overshoot temperature transient. Oxidizer pump discharge pressure and, therefore, gas generator oxidizer injection pressure, are reduced when the MOV opens rapidly (leaves the 14-degree plateau position) corresponding to a higher main thrust chamber oxidizer flow.

Extrapolation of AEDC testing results in Fig. 15(fuel turbine inlet temperature profile limits) with test C23B forming a conservative upper boundary. The limits of Fig.15 are indicative of satisfactory gas generator transient performance, and are far below a detrimental value.

The second thrust chamber fuel leak chilldown proved adequate during flight operation, as shown in Fig. 16. Flight performance approximated AEDC testing with the same driving force (approximately 32-psia fuel pump inlet pressure). Thrust chamber resistance, proportional to thrust chamber

TABLE 7

MAIN OXIDIZER VALVE OPENING CHARACTERISTICS

Engine	Sequence*		Flight-AEDC Testing		Opening Control Line Temperature, F	Closing Control Actuator Temperature, F
	Delay, milliseconds	Ramp, milliseconds	Delay, milliseconds	Ramp, milliseconds		
J2026	497	1401	540	1850	-30**	-60**
J2043	494	1417	495	1930		
J2030	485	1362	510	1785		
J2035	490	1395	510	2060		
J2028	492	1372	510	1910	-35	-85
J2052						
Minimum	472	1325	505	1920		-127
Maximum	516	1454	870	2700		-234
Test 028B	496	1440	505	2325		-146

*Limits per ECP 513: delay = 465 ±75 milliseconds; ramp = 1390 ±40 milliseconds

**Flight measurements failed; values extrapolated from countdown demonstration test

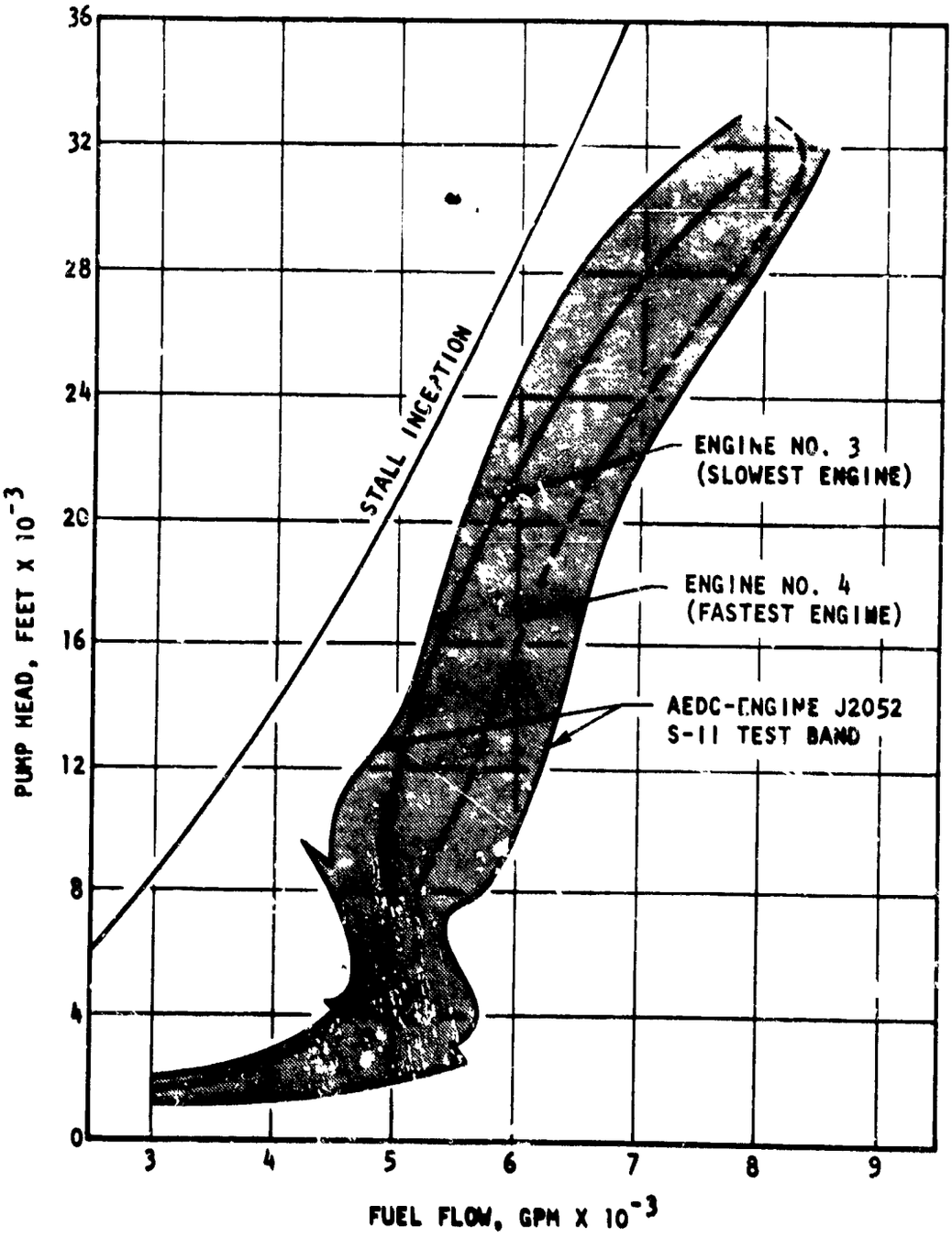

Figure 14. Fuel Pump Head vs Flow Start Transient

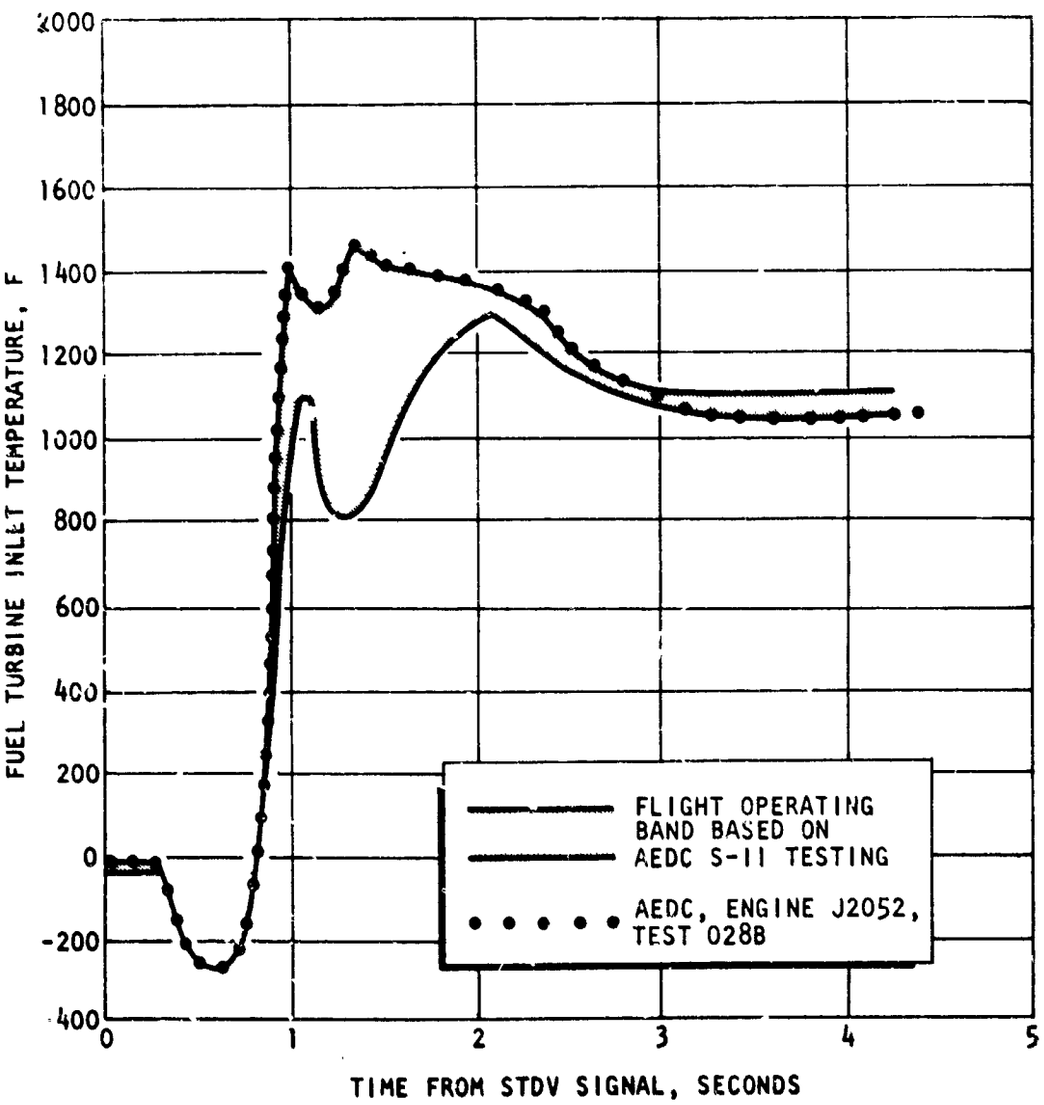

Figure 15. Fuel Turbine Inlet Temperature During Start Transient

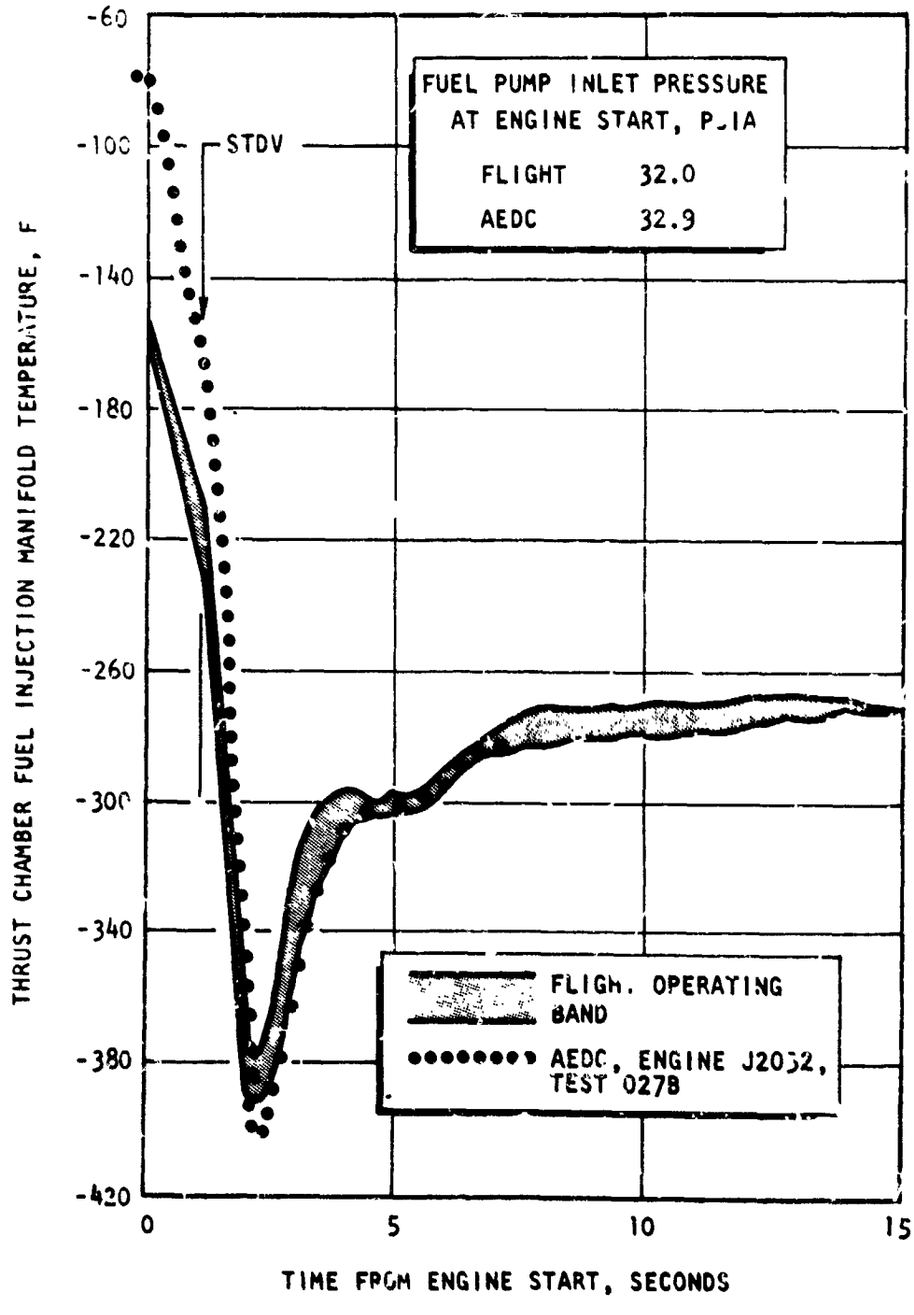

Figure 16. Main Fuel Injection Temperature During Start Transients

temperature, was still high after the second fuel lead, thereby maintaining a desirably high ASI fuel feed pressure. The oxidizer feed system, as discussed in the S-IVB section, does not chill down until after 1 second of fuel lead; therefore, relatively low ASI oxidizer flow was evident prior to spindown. Because pump inlet conditions and engine power buildup were normal, in addition to the above operational characteristics, ASI transient operation appeared to be completely satisfactory.

PROPELLANT INLET CONDITIONS

The engine inlet propellant conditions for all five engines were within specified limits at liftoff and at engine start command (T+152.2 seconds).

Oxidizer NPSH was well above the required 26-feet minimum (Table 8), with an average value of 65 feet at liftoff and 43 feet at engine start command. Fuel NPSH also was satisfactory (Table 8), with an average value of 740 feet at liftoff and 377 feet at engine start command, well above the required 150-feet minimum. Engine No. 2 was excluded from the averages because of an erroneous fuel pump inlet temperature (XC664-202) of -418.9 F at liftoff and -419 F at engine start command. These temperatures were approximately 2 F high when compared with other inlet temperatures. Analysis showed the problem to be caused by a stage instrumentation anomaly and that, by biasing the fuel inlet temperature, the fuel NPSH for this engine was determined to be close to the average.

Oxidizer pump inlet pressure (Fig. 17) behavior, through engine start command, was as expected. The large pressure drop is the result of reduced vehicle acceleration after S-1C outboard engine cutoff (OECO). Oxidizer pump inlet pressures prior to OECO had exceeded the maximum calibration range (50 psia) of the inlet pressure transducers. A calculated value of 77.1 psia at 4.17 g was obtained at S-1C inboard engine cutoff (IECO, T+135.5 seconds) and 74 psia at 3.89 g was computed at OECO.

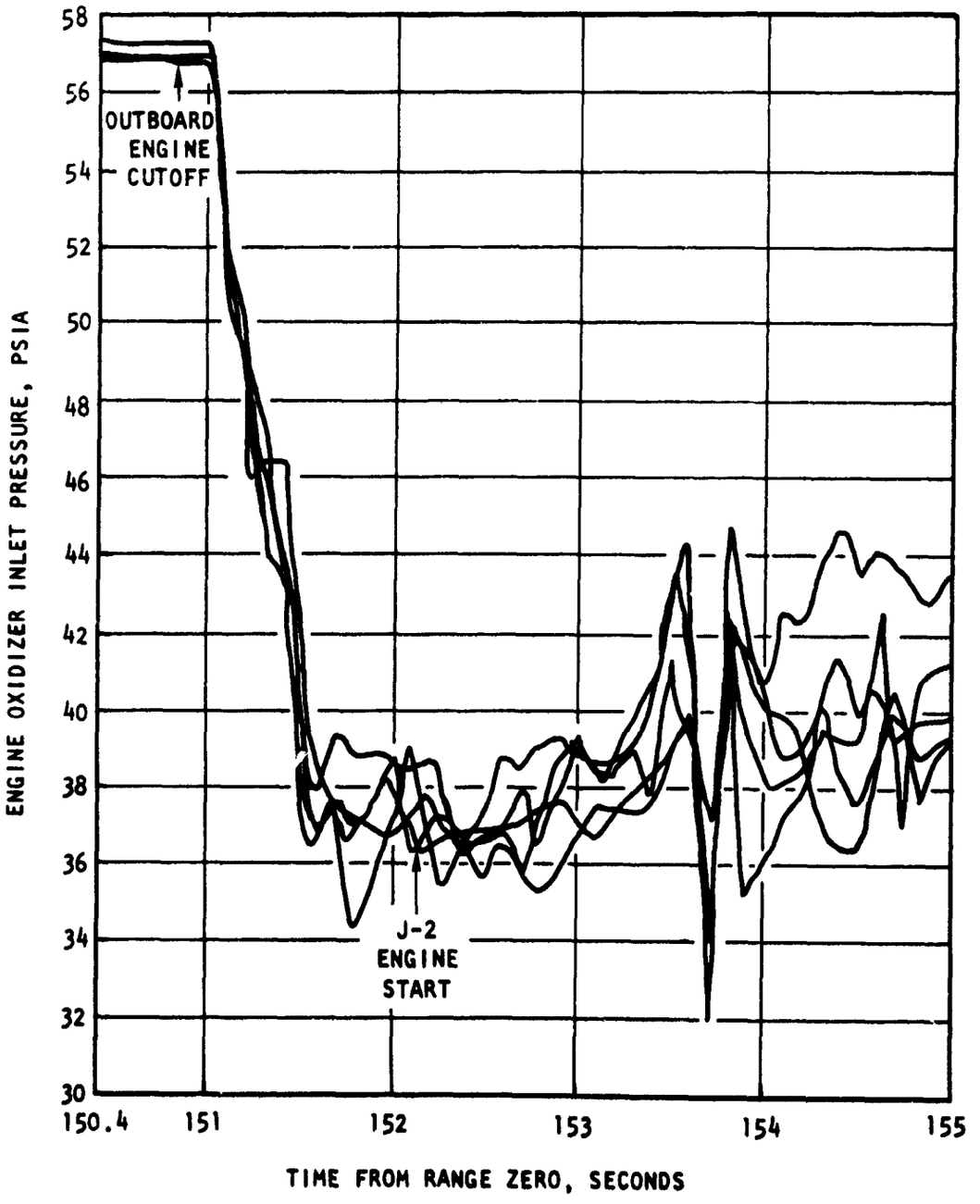

Figure 17. Oxidizer Pump Inlet Pressure During Start Transient

TABLE 8

OXIDIZER AND FUEL LIFTOFF AND ENGINE START NPSH

Engine No.	Liftoff	Engine Start
Oxidizer (26-feet minimum)		
1	65.8	41.3
2	62.9	42.9
3	65.2	44.9
4	64.0	44.8
5	67.5	41.3
Fuel (150-feet minimum)		
1	760	404
2*	481	183
3	794	445
4	710	328
5	692	331

*Erroneous NPSH because of instrumentation anomaly

Figure 18 illustrates the adequency of oxidizer pump inlet pressures and temperatures at engine start command as compared to the engine model specification start limits. The oxidizer pump discharge subcooled requirement (3 F) at engine start command was satisfactorily attained. An average subcooled value of 13 F was achieved (Fig. 19), utilizing the oxidizer helium injection system.

The fuel pump inlet pressures (Fig. 20) exhibited normal behavior during vehicle acceleration changes occurring at S-1C OECO. A portion of the pressure loss, approximately 8 psi, was the result of the stage fuel recirculation pumps being sequenced off at T+150.9 seconds. The remaining

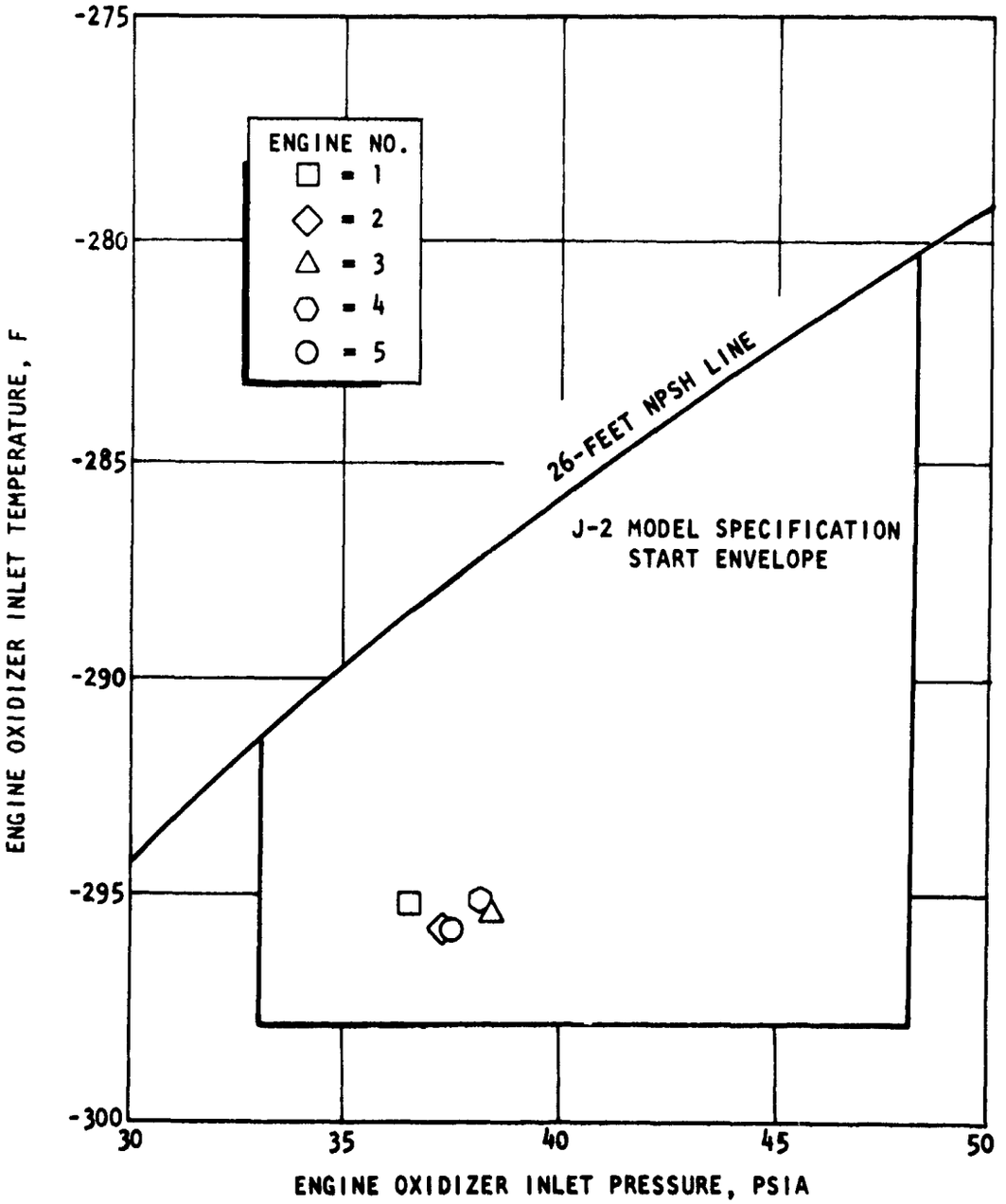

Figure 18. Oxidizer Inlet Pressure and Temperature at Engine Start

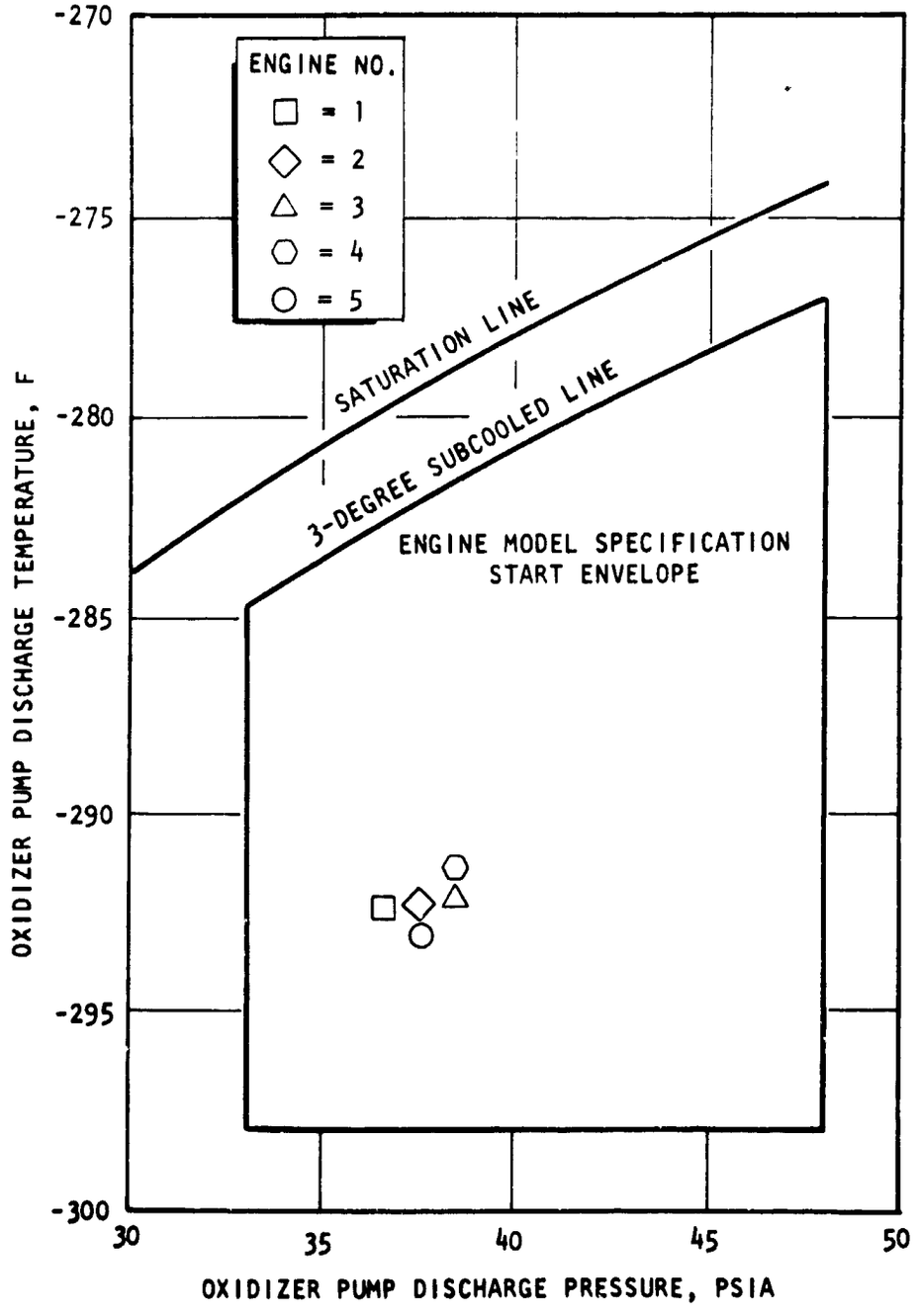

Figure 19. Oxidizer Pump Discharge Degrees Subcooled

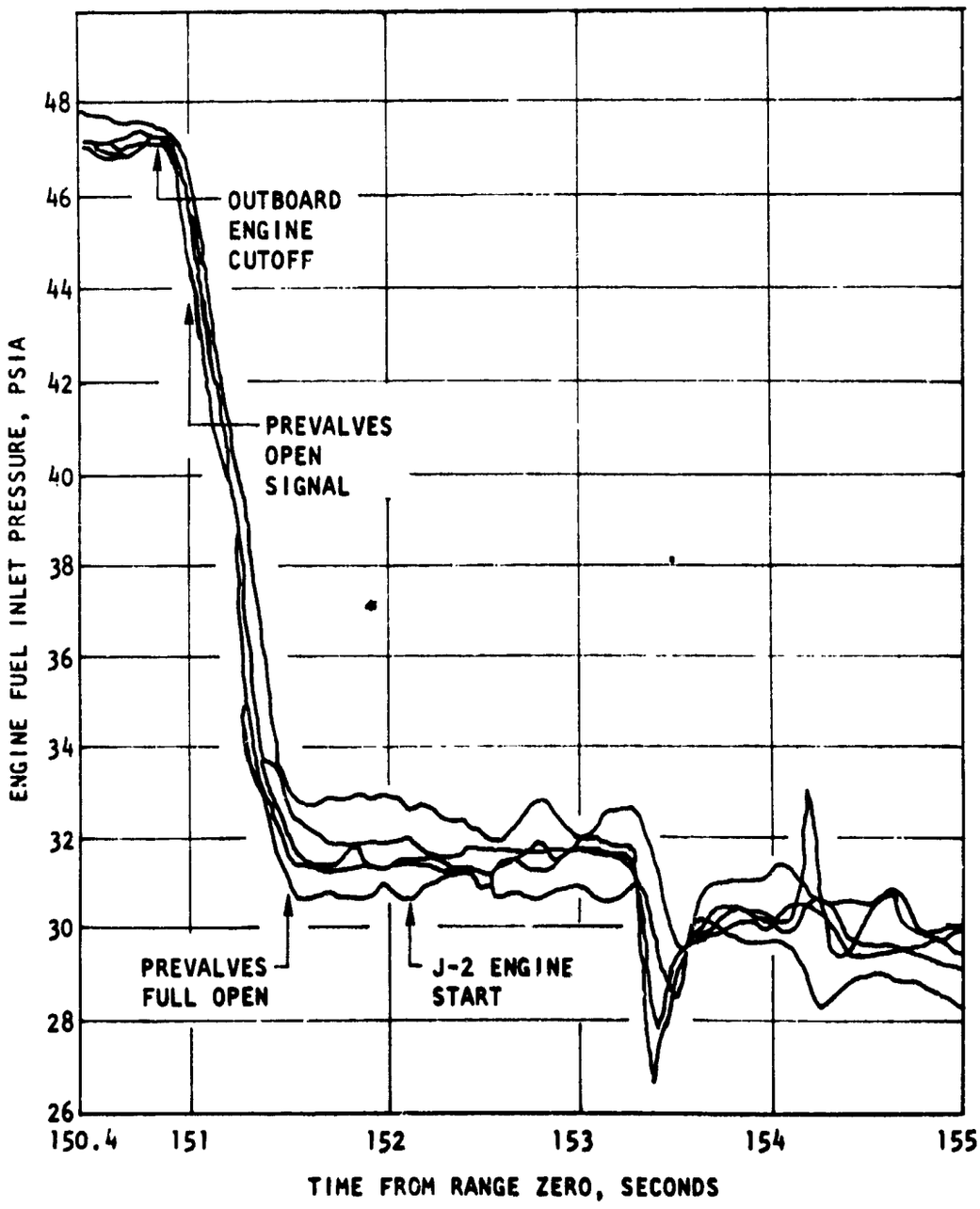

Figure 20. Fuel Pump Inlet Pressure During Start Transients

pressure drop was caused by vehicle acceleration changes. The signal to sequence off the fuel recirculation pumps also sequenced open the stage fuel prevalves and sequenced off the oxidizer tank helium injection system. Fuel pump inlet pressures at S-1C IECO were approximately 47.3 psia, which decayed to 46.0 psia before recovery to values indicated in Fig. 20.

Figure 21 illustrates the engine model specification start requirements for engine fuel pump inlet pressures and temperatures at engine start command. One engine (No. 202) was outside the grouping as a result of the temperature measurement problem. By biasing this temperature, a value of -421.2 was obtained.

Figure 22 compares a cross plot of fuel and oxidizer engine inlet pressures at engine start command with the engine model specification start envelope and the predicated value for all engines. The predicted fuel pump inlet pressure differs from the actual average value by approximately 1.5 psi. This has been attributed to a 1.5-psi decay in the fuel tank ullage pressure at engine start command because of higher than predicted fuel level agitation which cooled the ullage gas temperature and, thereby, lowered the pressure. Oxidizer tank ullage pressure at liftoff had decayed to the minimal limit of 39 psia at liftoff. This has been attributed to an oxidizer tank ullage heat loss to the fuel tank. Recommendations are being considered to: (1) evacuate the common bulkhead to reduce heat loss, or (2) reduce the oxidizer tank ullage pressure limit from 39 to 36.5 psia.

A summary of the propellant inlet parameters is presented in Table 9. The oxidizer bleed valve and fuel pump bearing temperature parameters on two engines (No. 4 and 5) were not recorded because the instrumentation channels were utilized for monitoring MOV actuator and closing control line temperatures on these engines.

Figure 23 depicts fuel pump interstage pressures for all five engines. The pressures, which are indicative of fuel pump performance, were satisfactory. The spikes noted at the beginning and end of engine mainstage

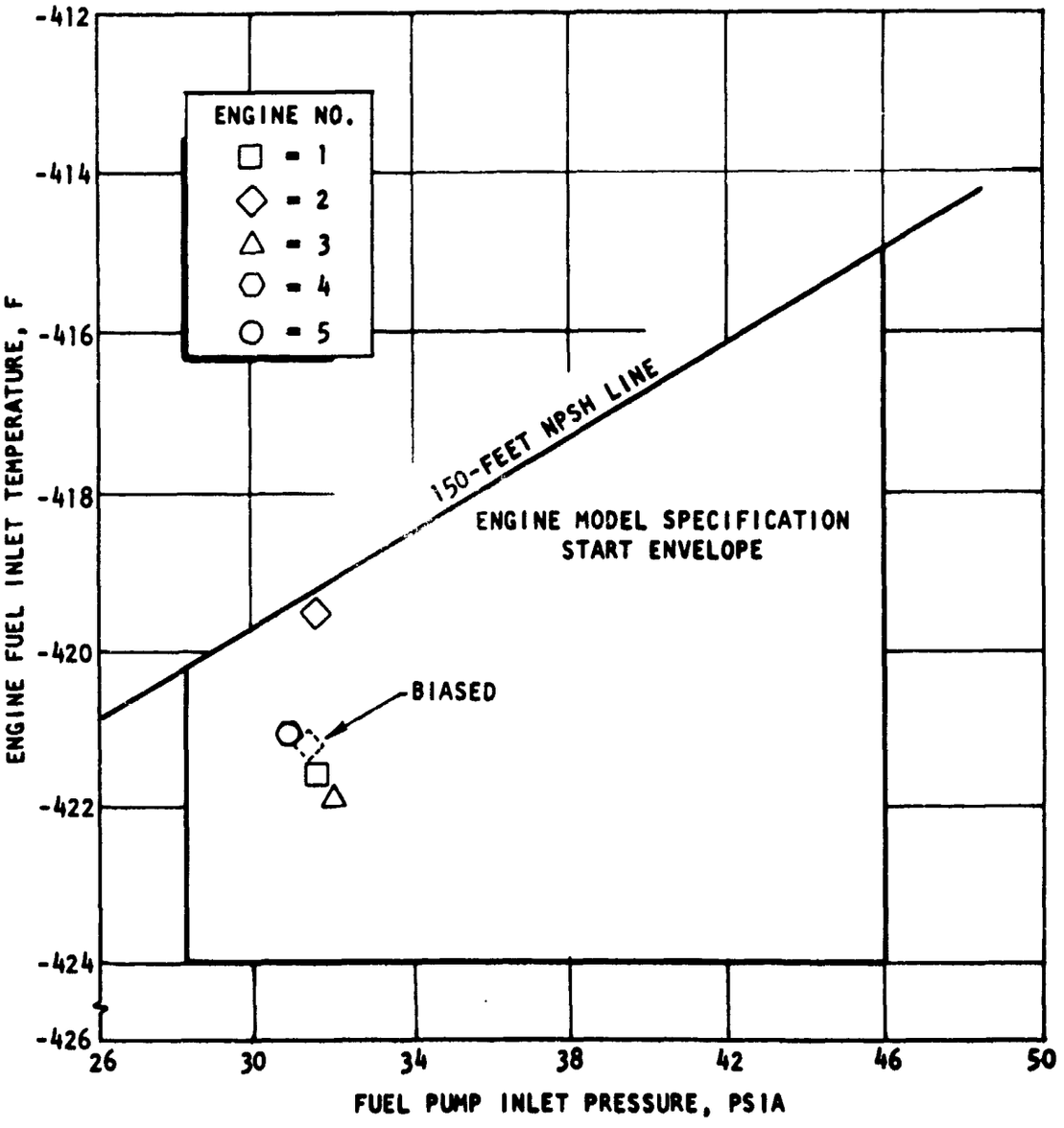

Figure 21. Fuel Inlet Pressure and Temperature at Engine Start

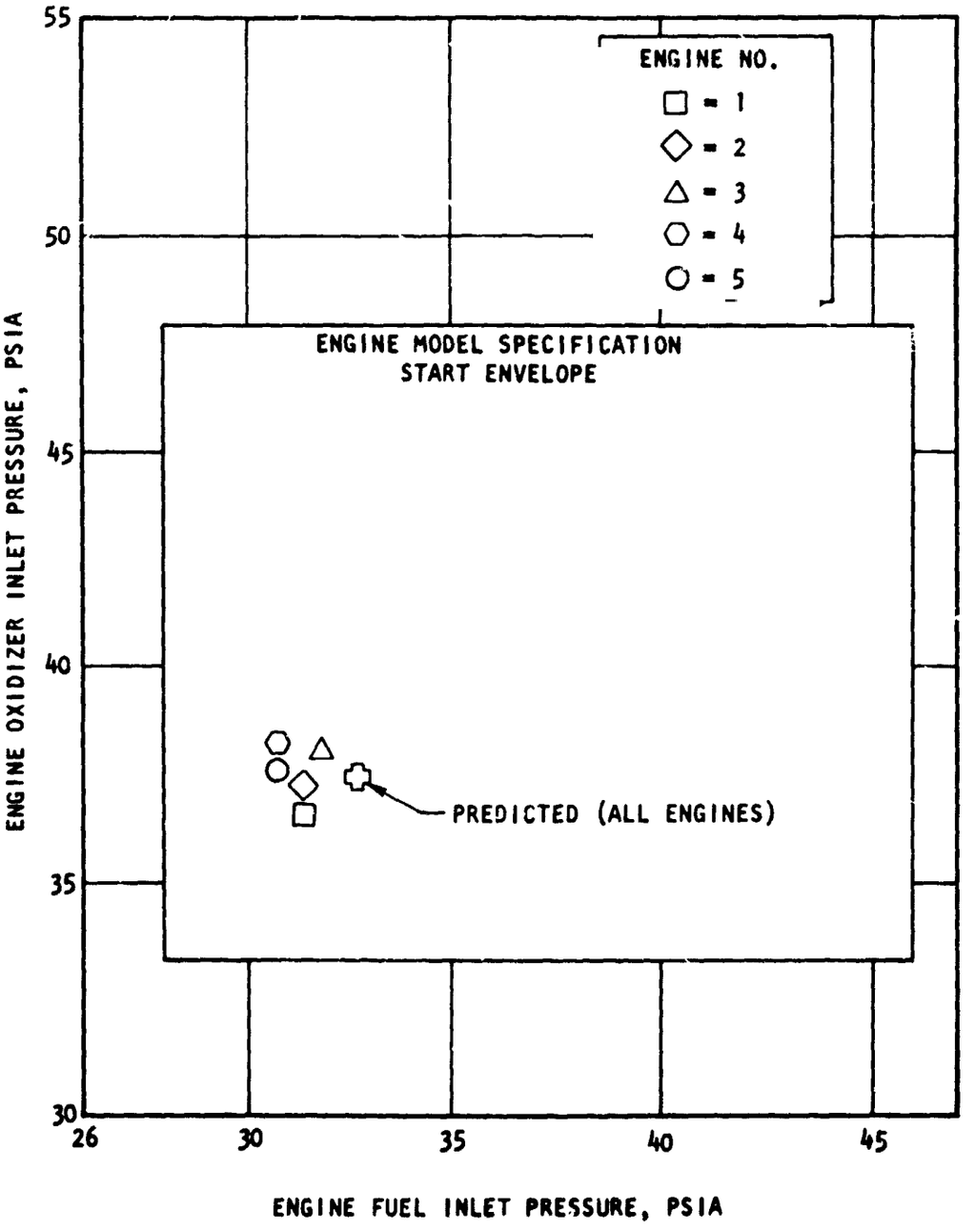

Figure 22. Engine Fuel and Oxidizer Inlet Pressure Start Limits

TABLE 9

STAGE PROPELLIANT SYSTEM PARAMETERS

Parameter	Liftoff						Engine Start					
	Expected or Allowable	(Engine No.)					Expected or Allowable	(Engine No.)				
		1	2	3	4	5		1	2	3	4	5
Fuel Tank Ullage Pressure, psia (VXD252-219)	31 to 34	32.3	32.3	32.3	32.3	32.3	28 to 36	30.3	30.3	30.3	30.3	30.3
Fuel Tank Ullage Pressure, psia (VXD253-219)	31 to 34	31.9	31.9	31.9	31.9	31.9	28 to 36	30.9	30.9	30.9	30.9	30.9
Fuel Tank Liquid Temperature, F (G763-218)	—	-422.3	-422.3	-422.3	-422.3	-422.3	—	-422.1	-422.1	-422.1	-422.1	-422.1
GG Fuel Valve Inlet Temperature, F (C008)	—	-419.5	-420.0	-419.5	-417.0	-419.5	—	-420.4	-516.5	-411.2	-417.5	-416.7
Fuel Inlet Pressure, psia (XD092)	—	42.5	42.0	42.5	42.7	41.8	28 to 46	31.5	31.4	31.8	30.7	30.8
Fuel Inlet Temperature, F (XC664)	-420 minimum	-421.4	-418.9	-421.9	-420.9	-420.95	Fig. 21	-421.5	-419.4	-421.9	-421.0	-421.0
Oxidizer Tank Ullage Pressure, psia (VXD258-206)	39 to 43	39 2	39 2	39.2	39.2	39.2	33 to 41	34.3	34.3	34.3	34.3	34.3
Oxidizer Pump Discharge Temperature, F (C002)	-286 minimum	-290.0	-292.9	-289	-289.5	-290 4	Fig. 19	-292.4	-292.3	-292.0	-291.5	-293
Oxidizer Pump Inlet Temperature, F (XC663)	DNA	-295.5	-294.5	-294.7	-294.5	-295 5	Fig. 18	-295.5	-296.0	-295.5	-295.5	-296
Oxidizer Inlet Pressure, psia (XDG91)		48.5	48.2	49.2	48.7	49.3	33 to 48	36.5	37.3	38.3	38.2	37.5
Oxidizer Bleed Valve Temperature, F (C009)		-287	-288.2	-288				-291.5	-287.5	-288.5		
Oxidizer Tank Liquid Temperature, F (C0758)		-296.25	-296.25	-296.25	-296.25	-296.25		-296.2	-296.2	-296.2	-296.2	-296.2
Fuel Pump Bearing Temperature, F (C0756)		-409	-410.1	-405.75				-413.4	-413.2	-414.5		
Oxidizer Pump Bearing Cooldown Temperature, F (C0757)		-286.5	-285.0	-285.1	-286.5	-286.5		-288.5	-287.4	-288	-288	-289

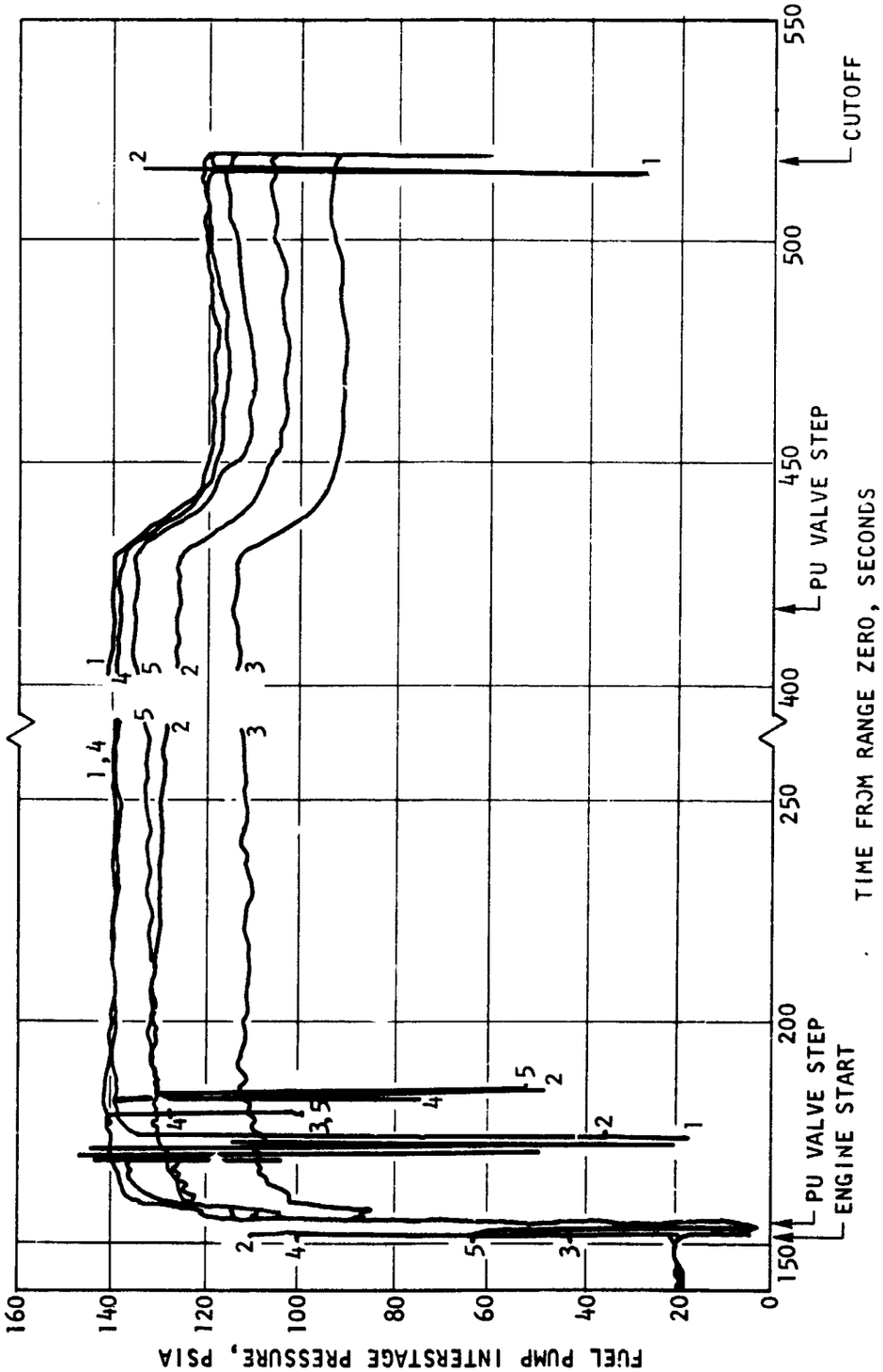

Figure 23. Fuel Pump Interstage Pressure During Engine Start Transient

operation occurred simultaneously on different engine groupings, as noted. Investigation of pertinent engine and fuel pump parameters failed to disclose the cause or effect of these spikes. The spikes are presently being investigated as instrumentation anomalies.

START TANK SYSTEM

Start tank prelaunch and engine start requirements were met on all engines (Fig. 24 and 25). After engine start, the systems functioned as expected, with the tanks refilling and warming up at a rate of approximately 2 F/min. Engine No. 1 reached a maximum pressure of 1465 psia with no apparent vent and relief valve operation. In-house tests on this valve indicated a cracking pressure of 1460 psig. Because the difference is in instrumentation accuracy, valve operation is considered satisfactory. The start tank vent and relief valve on engine No. 5 did not relieve, and the tank pressure reached 1450 psia. Although in-house tests indicated a cracking pressure of 1380 psig, the pressure of 1450 psia is within the maximum allowable cracking pressure of 1500 psig. Therefore, the valve is considered satisfactory.

HELIUM TANK SYSTEM

Helium tank pressures and temperatures at engine start were satisfactory, and are shown in Fig. 26. Following engine start, helium consumption was as expected on all engines except engine No. 2. Excessive helium usage was experienced on this engine during the start transient. The helium loss abruptly stopped approximately 5 seconds after mainstage signal, and the helium usage throughout the remainder of the flight was commensurate with that of the other engines. The additional helium loss was approximately 100 psi/sec, as shown in Fig. 27, and closely approximates the helium usage required for the oxidizer purge system.

Failure of the purge control valve to complete its closing cycle during the engine start transient because of a contaminant particle between the

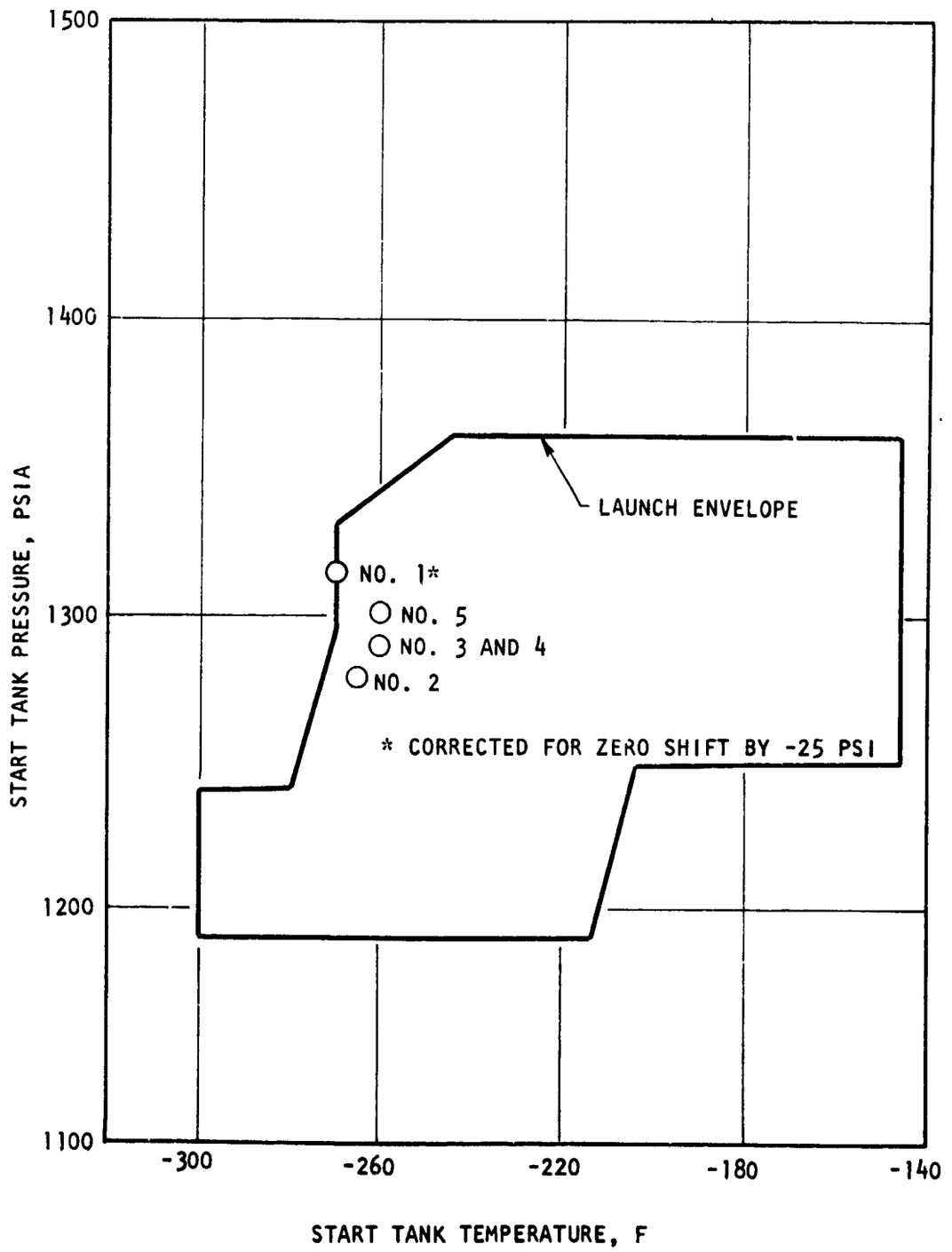

Figure 24. Start Tank Condition (Liftoff -8.9 seconds)

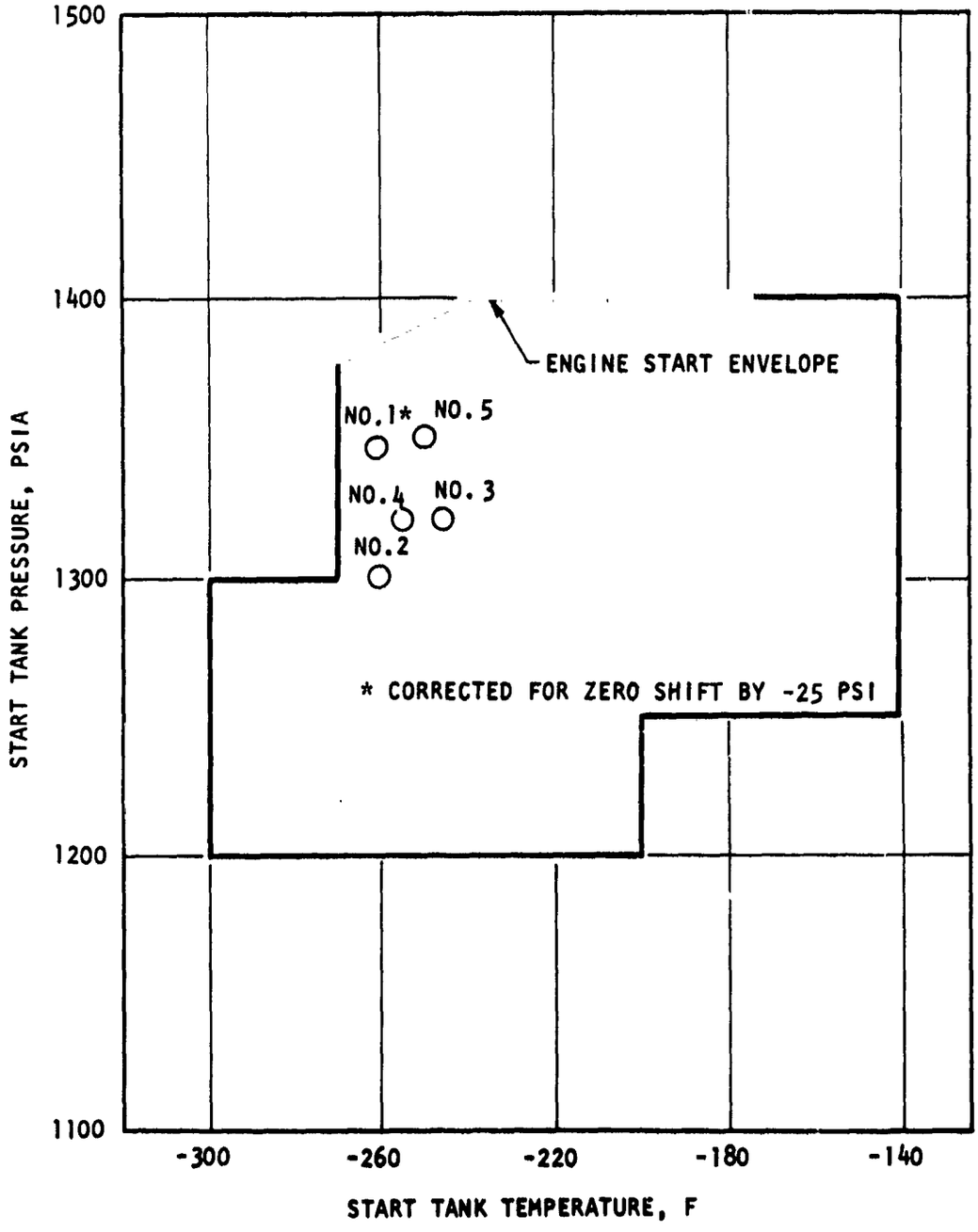

Figure 25. Start Tank Condition at Engine Start

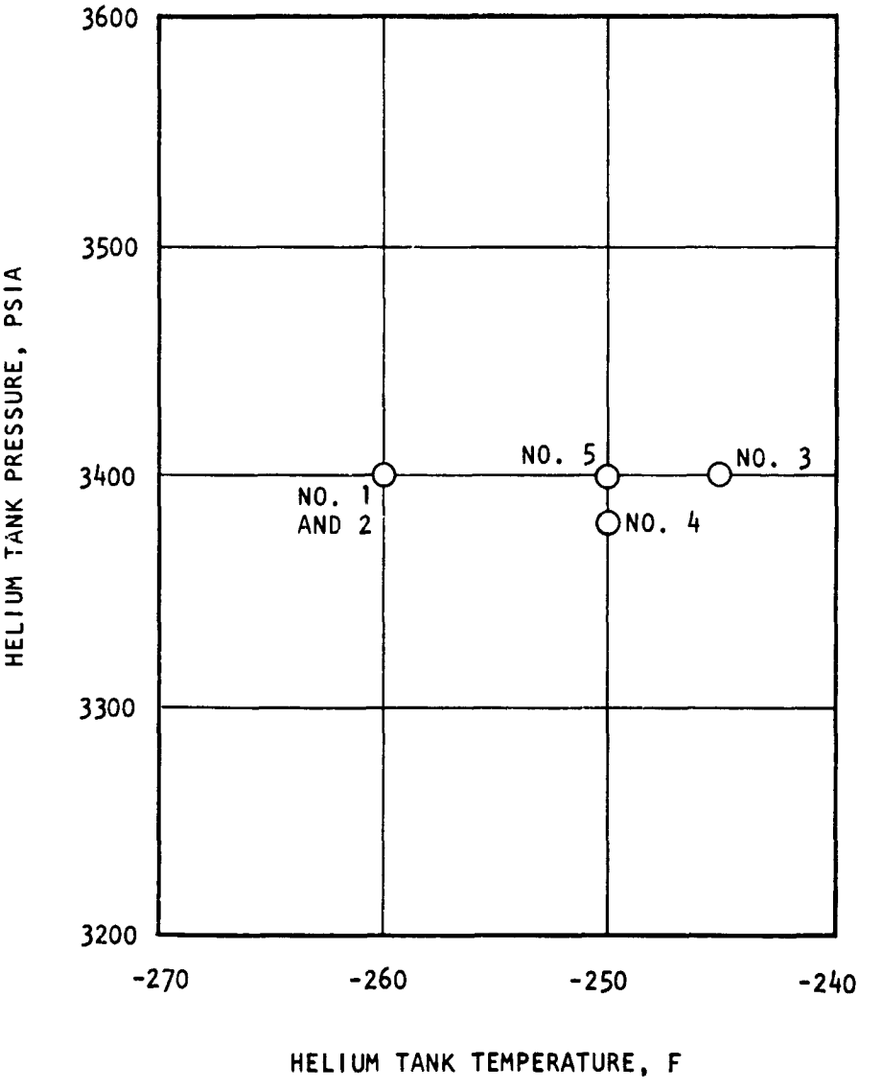

Figure 26. Helium Tank Condition at Engine Start

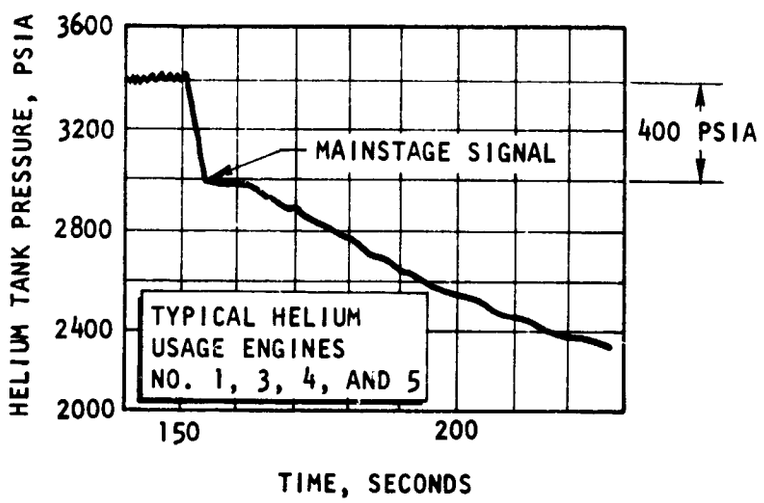

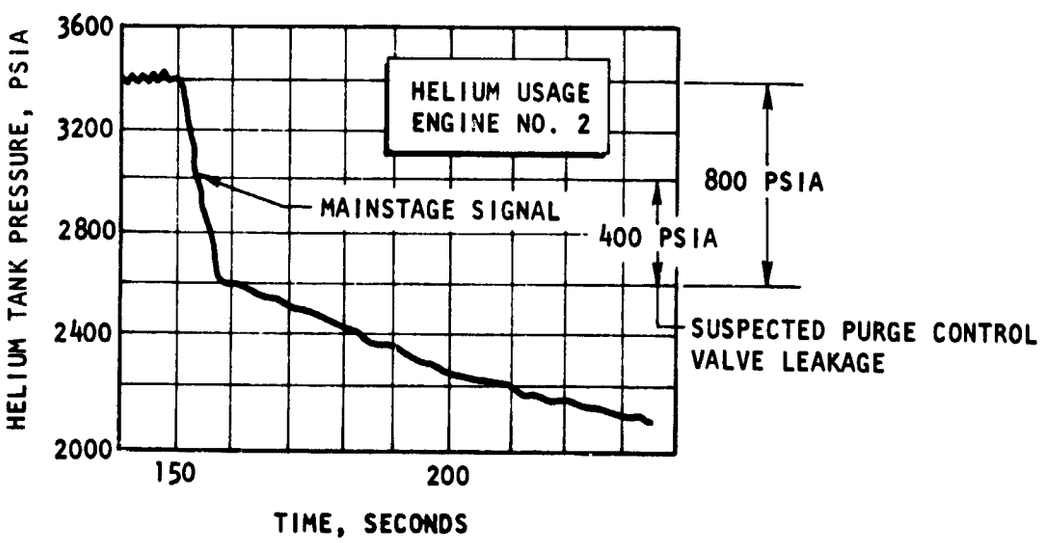

Figure 27. Comparison of Helium Usage During Engine Start

shaft and bore, or because of galling between these two members, was suspected as the cause of the helium loss. As corrective action, ECP J2-470 (replacement of the purge control valve with a similar valve incorporating an inlet filter), which was installed on production engines J2083 and subs, was re-issued as ECP J2-470R1 to provide kits for all delivered engines.

Following analysis of the AS-501 flight data, an investigative program was conducted by Rocketdyne through bench and engine simulator testing that verified that the abnormal helium loss was caused by the purge control valve poppet sticking in mid-stroke or slowly traveling through the maximum flow range for a period of approximately 4 seconds after mainstage signal. The probable cause of the poppet sticking was galling of the shaft and bore or a foreign particle becoming lodged between the two. Although the actual failure was not duplicated, sufficient testing of the pneumatic system was completed to eliminate any other suspect component, and to demonstrate that the purge control valve could cause the helium loss. A complete analysis of the purge control valve history revealed no instance of leakage of this magnitude, and a 10,000-cycle endurance test on the purge control valve failed to produce any valve malfunction, although the poppet shaft and mating bore were found to be heavily galled upon completion of the endurance test.

In addition to the incorporation of ECP J2-470R1 (the purge control valve with the filtered inlet), R&D engine tests are in progress to determine if the vent port on the purge control valve can be capped. If engine tests indicate that this feature can be satisfactorily incorporated, this helium leak path will be positively eliminated.

The engine helium regulators performed satisfactorily throughout engine operation. However, two instrumentation anomalies were evident. Regulator outlet pressure on engine No. 3 incurred a zero shift of +30 psia during the start transient, and data dropouts of up to 45 seconds were experienced on engine No. 5.

THRUST INCREASE

The flight buildup curves are shown in Fig. 28, together with an envelope predicted from AEDC testing and the allowable thrust increase envelope.

All the thrust increase curves are within the allowable buildup envelope. The curves agree well with the envelope predicted from AEDC testing.

MAINSTAGE PERFORMANCE

The engine steady-state performance during the flight has been evaluated and is summarized in Table 10 for the S-II vehicle. Included in this table for comparison are the respective values obtained during engine and vehicle acceptance demonstrations. The values predicted for the flight are based on engine acceptance tests and any significant preflight hardware changes. In general, flight performance agreed with the predictions.

In the following part of this section, a general discussion of data reduction and evaluation procedures is presented. Also included is a detailed evaluation of the performance of each engine. In addition, the results of Rocketdyne's flight reconstruction model are presented. The mainstage operating characteristics were reconstructed for all engines on the S-II vehicle using measured engine interface conditions and PU valve position.

Data Reduction and Evaluation

Evaluation of the engine mainstage performance was made using data obtained from the S-II stage contractor. These data were recorded on magnetic tape at a frequency of 10 samples per second.

The data were processed by using Rocketdyne's digital computer steady-state data reduction program (PT641). This program corrects performance to standard altitude conditions so that comparisons may be made between engine

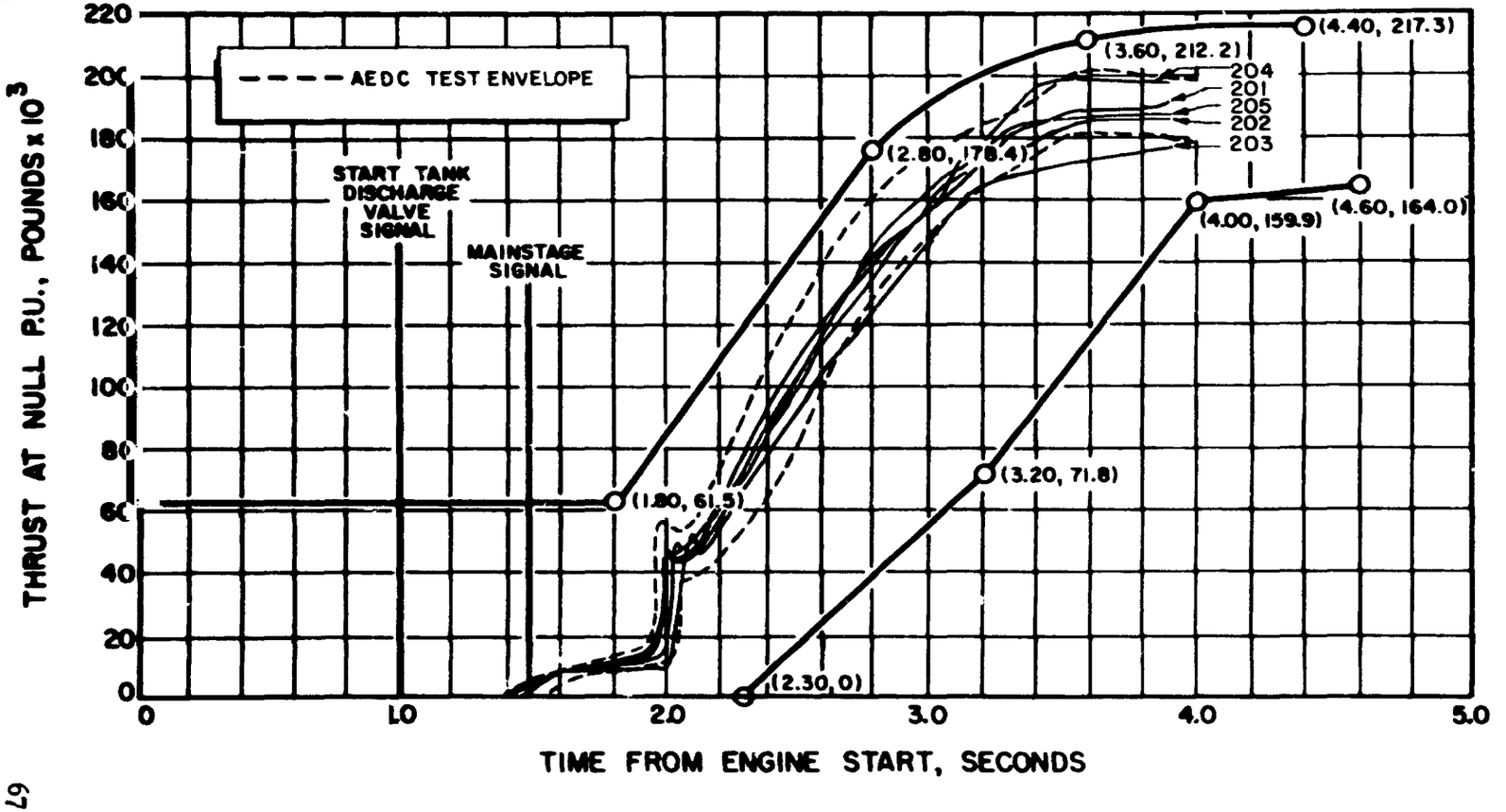

Figure 28. S-II Thrust Increase

TABLE 10

MAINSTAGE PERFORMANCE

Engine No.	Engine S/N	Parameter	Standard Altitude Conditions				Actual Conditions
			Engine Acceptance	Vehicle Acceptance	Predicted Flight (Tag Values)	Flight	Flight
1	J2026	Thrust, pounds	228,766	231,276	228,766	230,251	232,233
		Mixture Ratio	5.526	5.545	5.526	5.591	5.662
		Specific Impulse, seconds	425.4	425.3	425.4	424.9	424.3
2	J2043	Thrust, pounds	226,371	227,516	223,266	223,049	224,996
		Mixture Ratio	5.587	5.549	5.496	5.473	5.545
		Specific Impulse, seconds	423.9	424.4	424.6	425.0	424.4
3	J2030	Thrust, pounds	223,656	225,831	223,656	222,506	225,060
		Mixture Ratio	5.437	5.389	5.437	5.364	5.407
		Specific Impulse, seconds	425.6	426.1	425.6	426.2	425.9
4	J2035	Thrust, pounds	225,108	226,006	225,108	225,716	227,709
		Mixture Ratio	5.553	5.482	5.553	5.512	5.556
		Specific Impulse, seconds	421.2	421.9	421.2	421.6	421.3
5	J2028	Thrust, pounds	226,273	221,775	223,753	221,033	224,203
		Mixture Ratio	5.498	5.478	5.408	5.465	5.504
		Specific Impulse, seconds	423.2	423.3	423.9	423.3	423.1

All performances given at 60 seconds from STDV signal.

Standard altitude conditions:

Oxidizer Pump Inlet Pressure, psia	39.0
Oxidizer Pump Inlet Density, lb/ft^3	70.79
Fuel Pump Inlet Pressure, psia	30.0
Fuel Pump Inlet Density, lb/ft^3	4.40
Fuel Tank Pressurization Tapoff Flowrate, lb/sec	0.80
Oxidizer Heat Exchanger Flowrate, lb/sec	1.80
Auxiliary Pump Power, horsepower	15
Ambient Pressure, psia	0.0

and vehicle acceptance and the flight. These standard conditions include the external engine variables influencing engine performance (engine inlet pressures and temperatures, auxiliary brake horsepower extraction, oxidizer heat exchanger flowrate, and hydrogen tapoff flowrate

A few general techniques have been used in reducing the data to obtain more repeatable results. All flowmeter and pump speeds were counted from the high-frequency oscillograph. In this way, any noise or data dropout could be immediately detected and an accounting made. Also, all of the pressure measurements sensing ambient pressure pre-engine start were "zero shift" corrected by noting the differential between the measurement and ambient pressure just prior to engine ignition.

Flight thrust and chamber pressure were calculated using specific impulse and thrust coefficients as determined from engine acceptance testing. The calculated main chamber pressure was consistantly higher than the measured. This supports evidence from the three S-II vehicles static tested to date at MTF that an approximate 5-psi main chamber bias exists in the FM telemetry systems.

A problem area exists with respect to the fuel pump inlet and discharge temperature measurements. Half-bridges were used on the vehicle that do not compensate for system wire resistance. At the very low cryogenic temperatures of liquid hydrogen, wire resistance is significant in a temperature-bulb measurement. Based on MTF static testing, where a full-bridge static stage inlet temperature measurement is made in addition to the half-bridge telemetry measurement, a correction factor of -1.5 degrees was determined. This factor was incorporated into the data reduction coefficients by the S-II stage contractor. Fuel pump discharge temperature corrections are presently being evaluated.

Engine Performance

The following are individual discussions of performance for the respective engines of the S-II vehicle. Accompanying the remarks for each engine is

a table summarizing significant performance parameters during engine and vehicle acceptance and for the flight. The predicted flight performance values are based on engine acceptance testing and are adjusted for hardware changes, as applicable.

J2026 (Engine No. 1). Table 11 presents a comparison of engine J2026 performance. Predicted flight performance values are the same as engine acceptance values because there were no significant hardware changes pre-flight that would affect mainstage performance. The flight thrust agrees well with the predicted value, but mixture ratio was higher than predicted. During engine acceptance testing, the mixture ratio varied test-to-test from 5.47 to 5.58. This mixture ratio variation was attributed to shifting in operating position of the fuel pump balance piston system, which affects fuel pump efficiency. The flight mixture ratio agrees well with the 5.58 mixture ratio observed on the last engine acceptance test.

J2043 (Engine No. 2). Table 12 summarizes significant performance parameters for engine J2043. The predicted flight performance was based on engine acceptance data, with compensation for expected performance changes resulting from hardware changes made following vehicle acceptance. Hardware changes influencing mainstage performance included the oxidizer turbopump and the oxidizer turbine bypass nozzle. Component test data of the turbopump indicated negligible differences with respect to the original assembly. However, because of uncertainties in oxidizer turbopump replacement and the already higher than nominal mixture ratio, the engine was recalibrated with an oxidizer turbine bypass nozzle change to preclude the possibility of high performance. Flight performance was essentially as predicted.

J2030 (Engine No. 3). Table 13 summarizes significant performance parameters for engine J2030. An oxidizer turbopump change, made following vehicle acceptance, was accounted for in making the flight predictions.

TABLE 11

MAINSTAGE PERFORMANCE, ENGINE J2026(NO.1)

	Standard Altitude Conditions				Actual Conditions
	Engine Acceptance	Vehicle Acceptance	Predicted Flight (Tag Values)	Flight	Flight
Engine Performance					
Mixture Ratio	5.526	5.545	5.526	5.591	5.662
Thrust Chamber Pressure, psia	776.3	783.9	776.3	781.1	787.0
Thrust (vehicle and flight from chamber pressure), pounds	228,766	231,276	228,766	230,251	232,233
Specific Impulse, seconds	425.4	425.3	425.4	424.9	424.3
Engine Oxidizer Flow, lb/sec	455.40	460.67	455 40	459.69	465.22
Engine Fuel Flow, lb/sec	82.42	83.08	82.42	82.22	82.16
Fuel Tapoff Flow, lb/sec	0.8	0.8	0.8	0.8	0.90
Oxidizer Heat Exchanger Flow, lb/sec	1.80	1.80	1.80	1.80	1.50
Fuel Turbopump Performance					
Pump Inlet Pressure (total), psia	30.0	30.0	30.0	30.0	43.2
Pump Inlet Density, lb/ft^3	4.40	4.40	4.40	4.40	4.37
Pump Discharge Pressure (total), psia	1248.7	1262.0	1248.7	1252.3	1258.7
Pump Speed, rpm	27,217.4	27,302.5	27,217 4	27,096 6	27,277.0
Pump Head, feet	38,258.4	38,660.9	38,258.4	38,365.1	38,819.0
Pump Flow, gpm	8488.5	8556.1	8488.5	8468.6	8536.8
Turbine Inlet Temperature, F	1174.4	1216.5	1174.4	1200.7	1221.4
Turbine Inlet Pressure (total), psia	655.9	667.9	655.9	657.3	662.1

psia	1248.7	1262.0	1248.7	1252.3	1258.7
Pump Speed, rpm	27,217.4	27,302.5	27,217 4	27,096 6	27,277.0
Pump Head, feet	38,258.4	38,660.9	38,258.4	38,365.1	38,819.0
Pump Flow, gpm	8488.5	8556.1	8488.5	8468.6	8536.8
Turbine Inlet Temperature, F	1174.4	1216.5	1174.4	1200.7	1221.4
Turbine Inlet Pressure (total), psia	655.9	667.9	655.9	657.3	662.1
Oxidizer Turbopump Performance					
Pump Inlet Pressure (total), psia	39.0	39.0	39.0	39.0	43.2
Pump Inlet Density, lb/ft^3	70.79	70.79	70.79	70.79	4.41
Pump Discharge Pressure (total), psia	1106.8	1127.4	1106.8	1117.6	1130.2
Pump Speed, rpm	8724.4	8859.5	8724.4	8787.1	8810.0
Pump Head, feet	2169.4	2210.6	2169.4	2187.1	2194.4
Pump Flow, gpm	2946.5	2980.0	2946.5	2973.9	2993.5
Turbine Inlet Temperature, F	765.0	819.4	765.0	778.6	793.8
Turbine Inlet Pressure (total), psia	89.2	92.4	89.2	90.6	91.2
Turbine Outlet Temperature, F	605.4	660.0	605.4	623.2	636.7
Auxiliary Pump Power, horsepower	15.0	15.0	15.0	15.0	5.0
Gas Generator Performance					
Oxidizer Weight Flow, lb/sec	3.40	3.49	3.40	3.42	3.46
Fuel Weight Flow, lb/sec	3.68	3.67	3.68	3.64	3.63
Gas Generator Chamber Pressure, psia	685.2	697.8	685.2	686.6	691.6

TABLE 12

MAINSTAGE PERFORMANCE, ENGINE J20043(NO.2)

	Standard Altitude Conditions				Actual Conditions
	Engine Acceptance	Vehicle Acceptance	Predicted Flight (Tag Values)	Flight	Flight
Engine Performance					
Mixture Ratio	5.587	5.549	5.496	5.473	5.545
Thrust Chamber Pressure, psia	764.6	767.8	754.9	754.7	760.5
Thrust (vehicle and flight from chamber pressure), pounds	226,371	227,516	223,266	223,049	224,996
Specific Impulse, seconds	423.9	424.4	424.6	425.0	424.4
Engine Oxidizer Flow, lb/sec	452.95	454.26	445.44	443.76	449.17
Engine Fuel Flow, lb/sec	81.07	81.86	82.40	81.08	81.01
Fuel Tapoff Flow, lb/sec	0.8	0.8	0.8	0.8	1.20
Oxidizer Heat Exchanger Flow, lb/sec	1.8	1.8	1.8	1.8	0.90
Fuel Turbopump Performance					
Pump Inlet Pressure (total), psia	30.0	30.0	30.0	30.0	30.5
Pump Inlet Density, lb/ft^3	4.40	4.40	4.40	4.40	4.37
Pump Discharge Pressure (total), psia	1207.9	1228.3	1220.2	1205.8	1212.0
Pump Speed, rpm	25,880.3	26,033.3	26,844	25,781.4	25,961.0
Pump Head, feet	37,017.1	37,639.1	36,684.3	36,953.7	37,402.7
Pump Flow, gpm	8351.3	8431.6	8337.9	8552.2	8419.1
Turbine Inlet Temperature, F	1221.2	1244.1	1201.8	1222.5	1243.1
Turbine Inlet Pressure (total), psia	609.3	623.0	601.6	606.2	610.5
Oxidizer Turbopump Performance					

psia	1207.9	1228 3	1220.2	1205.8	1212.0
Pump Speed, rpm	25,880 3	26,033.3	26,844	25,781 4	25,961.0
Pump Head, feet	37,017.1	37,639.1	36,684.3	36,953.7	37,402.7
Pump Flow, gpm	8351.3	8431.6	8337.9	8552.2	8419.1
Turbine Inlet Temperature, F	1221.2	1244.1	1201.8	1222.5	1243.1
Turbine Inlet Pressure (total), psia	609.3	623.0	601.6	606.2	610.5
Oxidizer Turbopump Performance					
Pump Inlet Pressure (total), psia	39.0	39.0	39.0	39.0	43.2
Pump Inlet Density, lb/ft^3	70.79	70.79	70.79	70.79	71.11
Pump Discharge Pressure (total), psia	1094.9	1111.6	1073.5	1066.6	1078 7
Pump Speed, rpm	8613.1	8695.4	8512.0	8446.5	8468.0
Pump Head, feet	2144.5	2178.1	2101.8	2082.2	2089.1
Pump Flow, gpm	2931.0	2939.4	2879.7	2872.8	2890.6
Turbine Inlet Temperature, F	795.8	813.5	778.7	783.0	797.8
Turbine Inlet Pressure (total), psia	86.4	88.3	82.95	85.8	86.4
Turbine Outlet Temperature, F	640.3	659.8	626.0	630.9	644.2
Auxiliary Pump Power, horsepower	15.0	15 0	15.0	15.0	5.0
Gas Generator Performance					
Oxidizer Weight Flow, lb/sec	3.34	3.43	3.29	3.32	3.36
Fuel Weight Flow, lb/sec	3.51	3.55	3.50	3.48	3.48
Gas Generator Chamber Pressure, psia	638.1	653.4	631.3	635.8	640.4

TABLE 13

MAINSTAGE PERFORMANCE, ENGINE J2030 (NO. 3)

	Standard Altitude Conditions				Actual Conditions
	Engine Acceptance	Vehicle Acceptance	Predicted Flight (Tag Values)	Flight	Flight
Engine Performance					
Mixture Ratio	5.437	5.389	5.437	5.364	5.407
Thrust Chamber Pressure, psia	756.7	763.9	756.7	754.2	762.4
Thrust (vehicle and flight from chamber pressure), pounds	223,656	225,831	223,656	222,506	225,060
Specific Impulse, seconds	425.6	426.1	425.6	426.2	425.9
Engine Oxidizer Flow, lb/sec	443.90	447.08	443.90	440.03	445.94
Engine Fuel Flow, lb/sec	81.65	82.97	81.65	82.03	82.48
Fuel Tapoff Flow, lb/sec	0.80	0.80	0.80	0.80	0.60
Oxidizer Heat Exchanger Flow, lb/sec	1.80	1.80	1.80	1.80	1.50
Fuel Turbopump Performance					
Pump Inlet Pressure (total), psia	30.0	30.0	30.0	30.0	30.9
Pump Inlet Density, lb/ft^3	4.40	4.40	4.40	4.40	4.38
Pump Discharge Pressure (total), psia	1187.7	1220.6	1187.7	1213.5	1223.7
Pump Speed, rpm	26,532.0	26,792.2	26,532.0	26,548.3	26,720.0
Pump Head, feet	36,403.5	37,405.7	36,403.5	37,188.6	37,626.1
Pump Flow, gpm	8410.2	8545.0	8410.8	8449.4	8512.1
Turbine Inlet Temperature, F	1181.5	1229.0	1181.5	1205.2	1224.2
Turbine Inlet Pressure (total), psia	653.5	673.8	653.5	657.1	664.2
Oxidizer Turbopump Performance					
Pump Inlet Pressure (total), psia	30.0	30.0	30.0	30.0	30.0

Pump Inlet Density, lb/ft	4.40	4.40	4 40	4.40	4.38
Pump Discharge Pressure (total), psia	1187.7	1220.6	1187.7	1213.5	1223.7
Pump Speed, rpm	26,532.0	26,792.2	26,532.0	26,548.3	26,720.0
Pump Head, feet	36,403.5	37,405.7	36,403.5	37,188.6	37,626.1
Pump Flow, gpm	8410.2	8545.0	8410.8	8449.4	8512.1
Turbine Inlet Temperature, F	1181.5	1229.0	1181.5	1205.2	1224.2
Turbine Inlet Pressure (total), psia	653.5	673.8	653.5	657.1	664.2
Oxidizer Turbopump Performance					
Pump Inlet Pressure (total), psia	39.0	39.0	39.0	39.0	43.7
Pump Inlet Density, lb/ft^3	70.79	70.79	70.79	70.79	71.12
Pump Discharge Pressure (total), psia	1055.8	1106.4	1055.8	1062.8	1077.9
Pump Speed, rpm	8517.7	8626.6	8517.7	8423.9	8456.0
Pump Head, feet	2063.4	2164.6	2063.4	2076.3	2088.0
Pump Flow, gpm	2873.6	2893.8	2873.6	2849.1	2871.8
Turbine Inlet Temperature, F	776.8	787.8	776.8	767.7	781.4
Turbine Inlet Pressure (total), psia	82.7	83.3	82.7	83.0	83.8
Turbine Outlet Temperature, F	614.8	628.2	614.8	587.8	599.6
Auxiliary Pump Power, horsepower	15.0	15.0	15.0	15.0	5.0
Gas Generator Performance					
Oxidizer Weight Flow, lb/sec	3.17	3.29	3.17	3.20	3.24
Fuel Weight Flow, lb/sec	3.41	3.44	3.41	3.40	3.40
Gas Generator Chamber Pressure, psia	679.0	700.1	679.0	683.3	690.1

Comparison of component data from turbopump acceptance demonstration tests indicated negligible effect on mainstage performance for the turbopump change and, consequently, predicted flight values are the same as engine acceptance. However, actual flight performance came in lower than predicted by -1100 pounds and -0.073 mixture ratio units. The flight values of thrust and mixture ratio indicate the oxidizer turbine nozzle area of the replacement turbopump to be significantly larger than the original turbine nozzle.

J2035 (Engine No. 4). Table 14 presents a comparison of engine J2035 performance. Predicted flight performance values are the same as engine acceptance values because no major hardware changes were made. Thrust was as predicted, and mixture ratio was -0.04 mixture ratio units lower than engine acceptance.

J2028 (Engine No. 5). Table 15 summarizes the performance of engine J2028. Predicted flight performance was based on engine acceptance values with compensation made for an expected performance shift because of an oxidizer turbopump change following vehicle acceptance. Component test data of the replacement turbopump indicated it would lower the overall thrust and mixture ratio of the engine by -2633 pounds and -0.088 mixture ratio units.

The flight mixture ratio was similar to that observed during engine acceptance and vehicle acceptance, indicating that the performance change resulting from the oxidizer turbopump replacement was less than expected. The flight thrust agreed with the thrust determined from vehicle acceptance, which was lower than that during engine acceptance because of shifts in the gas generator oxidizer system resistance.

During the PU cutback, a PU system resistance shift occurred causing a thrust shift of approximately -3000 pounds. This is shown in Fig. 29 at 448 seconds (range time).

TABLE 14

MAINSTAGE PERFORMANCE, ENGINE J2035 (NO.4)

	Standard Altitude Conditions				Actual Conditions
	Engine Acceptance	Vehicle Acceptance	Predicted Flight (Tag Values)	Flight	Flight
Engine Performance					
Mixture Ratio	5.553	5.482	5.553	5.512	5.556
Thrust Chamber Pressure, psia	767.2	769.7	767.2	769.2	775.5
Thrust (vehicle and flight from chamber pressure), pounds	225,108	226,006	225,108	225,716	227,709
Specific Impulse, seconds	421.2	421.9	421.2	421.6	421.3
Engine Oxidizer Flow, lb/sec	452.87	453.00	452.87	453.16	458 07
Engine Fuel Flow, lb/sec	81.56	82.63	81.56	82.21	82.45
Fuel Tapoff Flow, lb/sec	0.80	0.80	0.80	0.80	0.60
Oxidizer Heat Exchanger Flow, lb/sec	1.80	1.80	1.80	1.80	0.60
Fuel Turbopump Performance					
Pump Inlet Pressure (total), psia	30.0	30.0	30.0	30.0	30.2
Pump Inlet Density, lb/ft^3	4.40	4.40	4.40	4.40	4.37
Pump Discharge Pressure (total), psia	1209.2	1244.8	1209.2	1219.1	1226.1
Pump Speed, rpm	26,401.2	26,536.7	26,401.2	26,563 5	26,719 0
Pump Head, feet	37,056.4	38,139.8	37,056.4	37,357.8	37,775.4
Pump Flow, gpm	8406.3	8510.5	8406.3	8468.0	8521.5
Turbine Inlet Temperature, F	1191.9	1232.8	1191.9	1210.4	1228.0
Turbine Inlet Pressure (total), psia	88.03	87.6	88.03	628.4	633.0
Oxidizer Turbopump Performance					

psia	1209.2	1244.8	1209.2	1219.1	1226.1
Pump Speed, rpm	26,401.2	26,536.7	26,401.2	26,563 5	26,719 0
Pump Head, feet	37,056.4	38,139.8	37,056.4	37,357.8	[illegible]775.4
Pump Flow, gpm	8406.3	8510.5	8406.3	8468.0	8521.5
Turbine Inlet Temperature, F	1191.9	1232.8	1191.9	1210.4	1228.0
Turbine Inlet Pressure (total), psia	88.03	87.6	88.03	628.4	633.0
Oxidizer Turbopump Performance					
Pump Inlet Pressure (total), psia	39.0	39.0	39.0	39.0	43.4
Pump Inlet Density, lb/ft^3	70.79	70.79	70.79	70.79	71.09
Pump Discharge Pressure (total), psia	1076.3	1109.4	1076.3	1088.1	1100.0
Pump Speed, rpm	8642.8	8717.1	8642.8	8662.8	8680.0
Pump Head, feet	2105.1	2171.2	2105.1	2129.6	2136.2
Pump Flow, gpm	2930.5	2931.4	2930.5	2932.4	2943.9
Turbine Inlet Temperature, F	770.4	778.5	770.4	778.6	791.3
Turbine Inlet Pressure (total), psia	86.9	86.4	86.9	87.9	88.5
Turbine Outlet Temperature, F	667.3	648.4	667.3	624.1	635.9
Auxiliary Pump Power, horsepower	15.0	15.0	15.0	15.0	5.0
Gas Generator Performance					
Oxidizer Weight Flow, lb/sec	3.25	3.30	3.25	3.29	3.33
Fuel Weight Flow, lb/sec	3.47	3.44	3.47	3 48	3.48
Gas Generator Chamber Pressure, psia	649.2	655.1	649.2	656.7	661.5

FOLDOUT FRAME - 2

TABLE 15

MAINSTAGE PERFORMANCE, ENGINE J2028 (NO.5)

	Standard Altitude Conditions				Actual Conditions
	Engine Acceptance	Vehicle Acceptance	Predicted Flight (Tag Values)	Flight	Flight
Engine Performance					
Mixture Ratio	5.498	5.478	5.408	5.465	5.504
Thrust Chamber Pressure, psia	778.3	762.8	770.8	760.9	771.3
Thrust (vehicle and flight from chamber pressure), pounds	226,273	221,775	223,753	221,033	224,203
Specific Impulse, seconds	423.2	423.3	423.9	423.3	423.1
Engine Oxidizer Flow, lb/sec	452.40	443.09	445.44	441.35	448.42
Engine Fuel Flow, lb/sec	82.28	80.88	82.40	80.76	81.47
Fuel Tapoff Flow, lb/sec	0.8	0.8	0.8	0.8	0.0
Oxidizer Heat Exchanger Flow, lb/sec	1.8	1.8	1.8	1.8	1.52
Fuel Turbopump Performance					
Pump Inlet Pressure (total), psia	30.0	30.0	30.0	30.0	29.1
Pump Inlet Density, lb/ft^3	4.40	4.40	4.40	4.40	4.37
Pump Discharge Pressure (total), psia	1226.3	1214.3	1220.2	1179.0	1190.2
Pump Speed, rpm	26,868.3	26,521.9	26,844.0	26,524.0	26,755.0
Pump Head, feet	37,575.5	37,211.7	37,394.7	36,137.8	36,830.7
Pump Flow, gpm	8475.7	8332.1	8486.8	8320.1	8387.1
Turbine Inlet Temperature, F	1219.5	1193.5	1199.2	1176.8	1203.5
Turbine Inlet Pressure (total), psia	654.7	641.9	648.6	637.6	645.0
Oxidizer Turbopump Performance					
Pump Inlet Pressure (total), psia	30.0	30.0	30.0		

Pump Discharge Pressure (total), psia	1226.3	1214.3	1220.2	1179.0	1190.2
Pump Speed, rpm	26,868.3	26,521.9	26,844.0	26,524.0	26,755.0
Pump Head, feet	37,575.5	37,211.7	37,394.7	36,137.8	36,830.7
Pump Flow, gpm	8475.7	8332.1	8486.8	8320.1	8387.1
Turbine Inlet Temperature, F	1219.5	1193.5	1199.2	1176.8	1203.5
Turbine Inlet Pressure (total), psia	654.7	641.9	648.6	637.6	645.0
Oxidizer Turbopump Performance					
Pump Inlet Pressure (total), psia	39.0	39.0	39.0	39.0	44.4
Pump Inlet Density, lb/ft^3	70.79	70.79	70.79	70.79	71.10
Pump Discharge Pressure (total), psia	1090.9	1086.2	1073.5	1062.1	1081.0
Pump Speed, rpm	8700.5	8627.2	8617.0	8540.5	8588.0
Pump Head, feet	2157.9	2128.0	2102.5	2077.1	2095.5
Pump Flow, gpm	2927.6	2868.5	2883.4	2857.4	2888.3
Turbine Inlet Temperature, F	800.6	774.9	780.9	752.6	772.1
Turbine Inlet Pressure (total), psia	86.8	83.1	82.81	82.0	83.0
Turbine Outlet Temperature, F	639.7	622.2	624.1	605.8	623.0
Auxiliary Pump Power, horsepower	15.0	15.0	15.0	15.0	0.0
Gas Generator Performance					
Oxidizer Weight Flow, lb/sec	3.40	3.31	3.36	3.28	3.33
Fuel Weight Flow, lb/sec	3.57	3.54	3.57	3.54	3.54
Gas Generator Chamber Pressure, psia	683.4	670.0	677.1	665.6	673.3

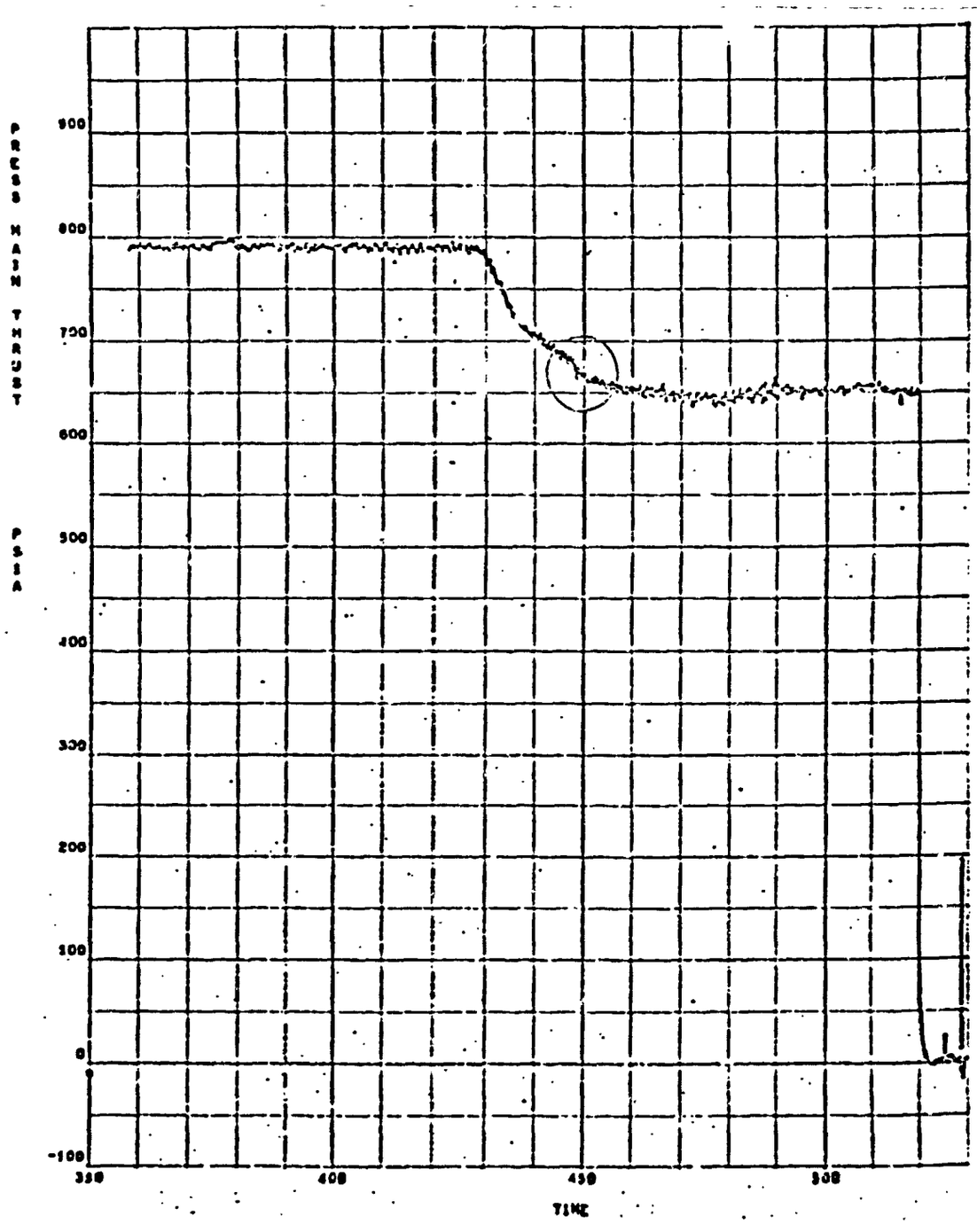

Figure 29. Thrust Shift From PU Resistance Shift

Flight Reconstruction

The mainstage operating characteristics have been reconstructed for the flight engines. The following parameters were reconstructed and compared to the actual values; engine mixture ratio, main thrust chamber pressure, oxidizer and fuel flowrates, oxidizer and fuel pump speeds, oxidizer and fuel pump discharge pressures, and gas generator chamber pressure. In general, the reconstructed performance agreed well with the actual flight performance.

The flight reconstruction was performed using linear influence coefficients to extrapolate the predicted tag values (Table 11 through 14) to actual flight using engine inlet conditions, pressurization flows, power extraction, and PU valve positions. The independent parameters used from the telemetry data are shown in Fig. 30 through 50, and include the following:

Figures 30 through 34	Engine oxidizer inlet temperatures
Figures 35 through 39	Engine fuel inlet temperatures
Figures 40 through 44	Engine oxidizer inlet pressures
Figures 45 through 49	Engine fuel inlet pressures
Figure 50	Heat exchanger oxidizer flowrates

In addition, the following assumptions were made. The engine fuel inlet temperature on engine No. 2 appeared to be biased by approximately 2 degrees, so an average of the other three outboard engines was used. The oxidizer turbopump auxiliary power was assumed to be a constant 4 horsepower for all engines except engine No. 5, which has no extraction pump. Fuel tank pressurization flowrate was assumed to be a constant 0.7 lb/sec, with a step to 1.35 lb/sec at 406 seconds (range time), except for engine No. 5, which had no tapoff.

To make the PU valve position compatible with the flight reconstruction program, the PU valve angles (Fig. 51 through 55) were converted to voltage ratio. The voltage ratios were used to compute the mixture ratio change for the PU excursion using curves of mixture ratio versus voltage ratio

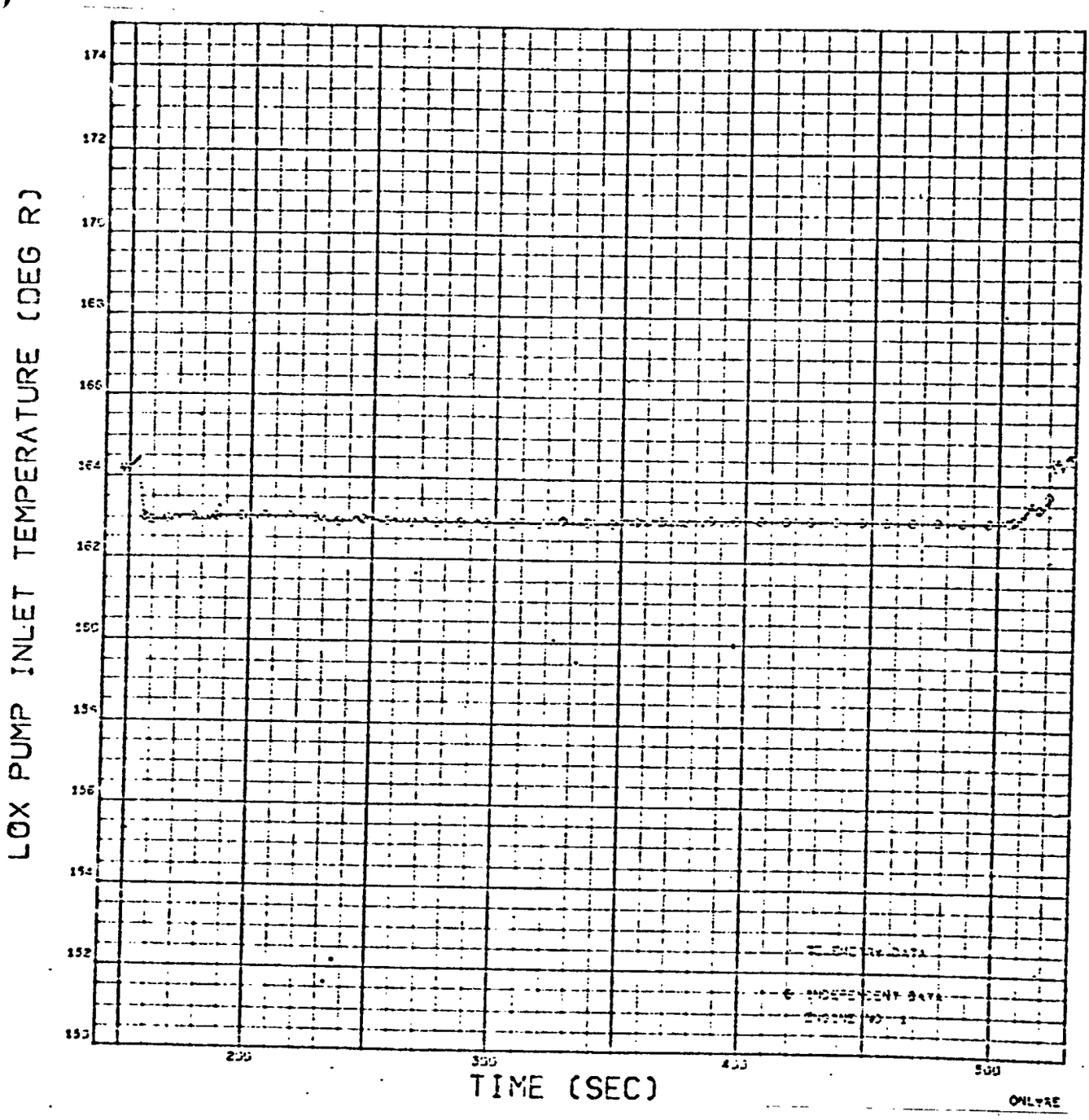

Figure 30. Engine No. 1 Oxidizer Pump Inlet Temperature

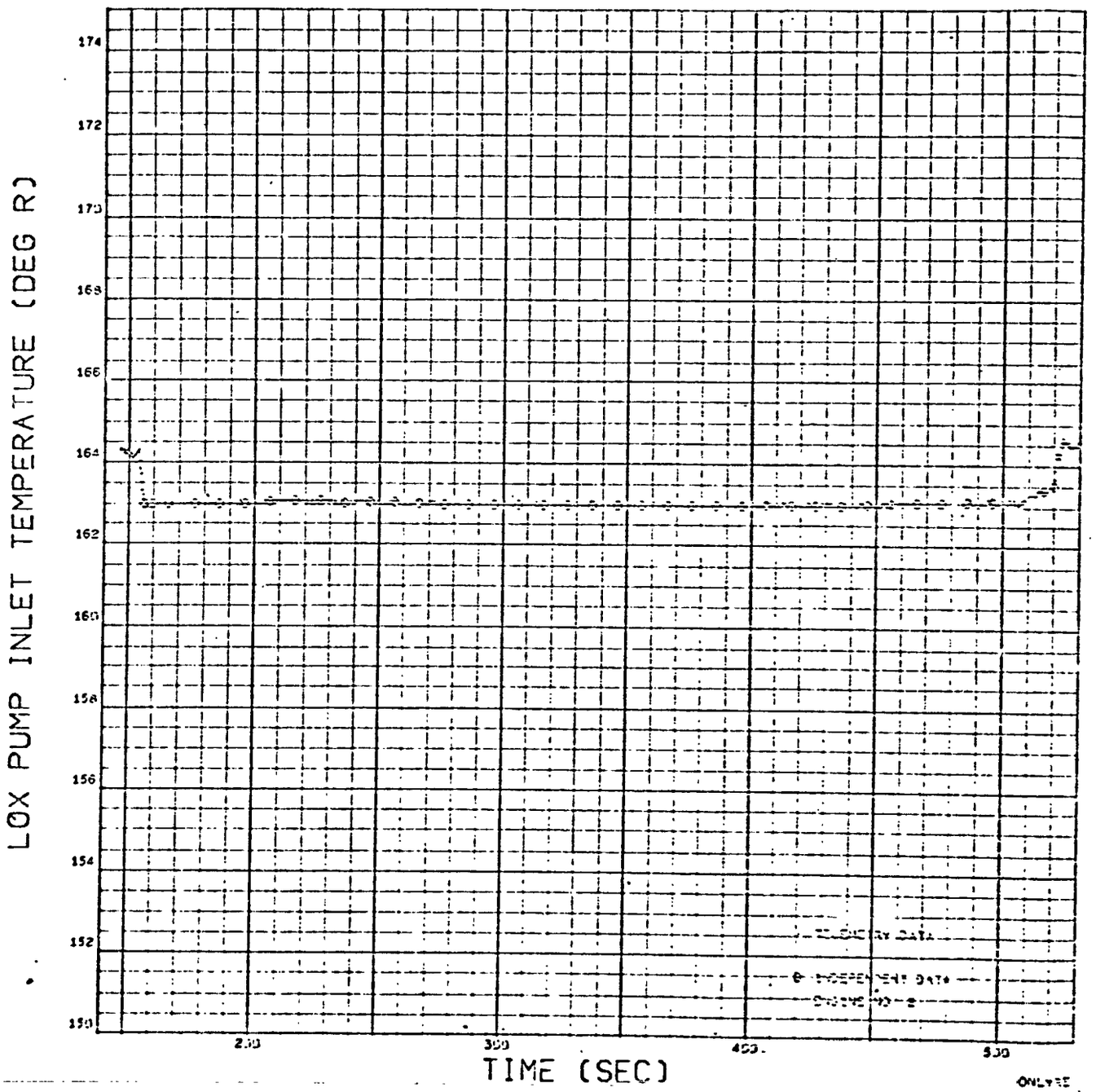

Figure 31. Engine No. 2 Oxidizer Pump Inlet Temperature

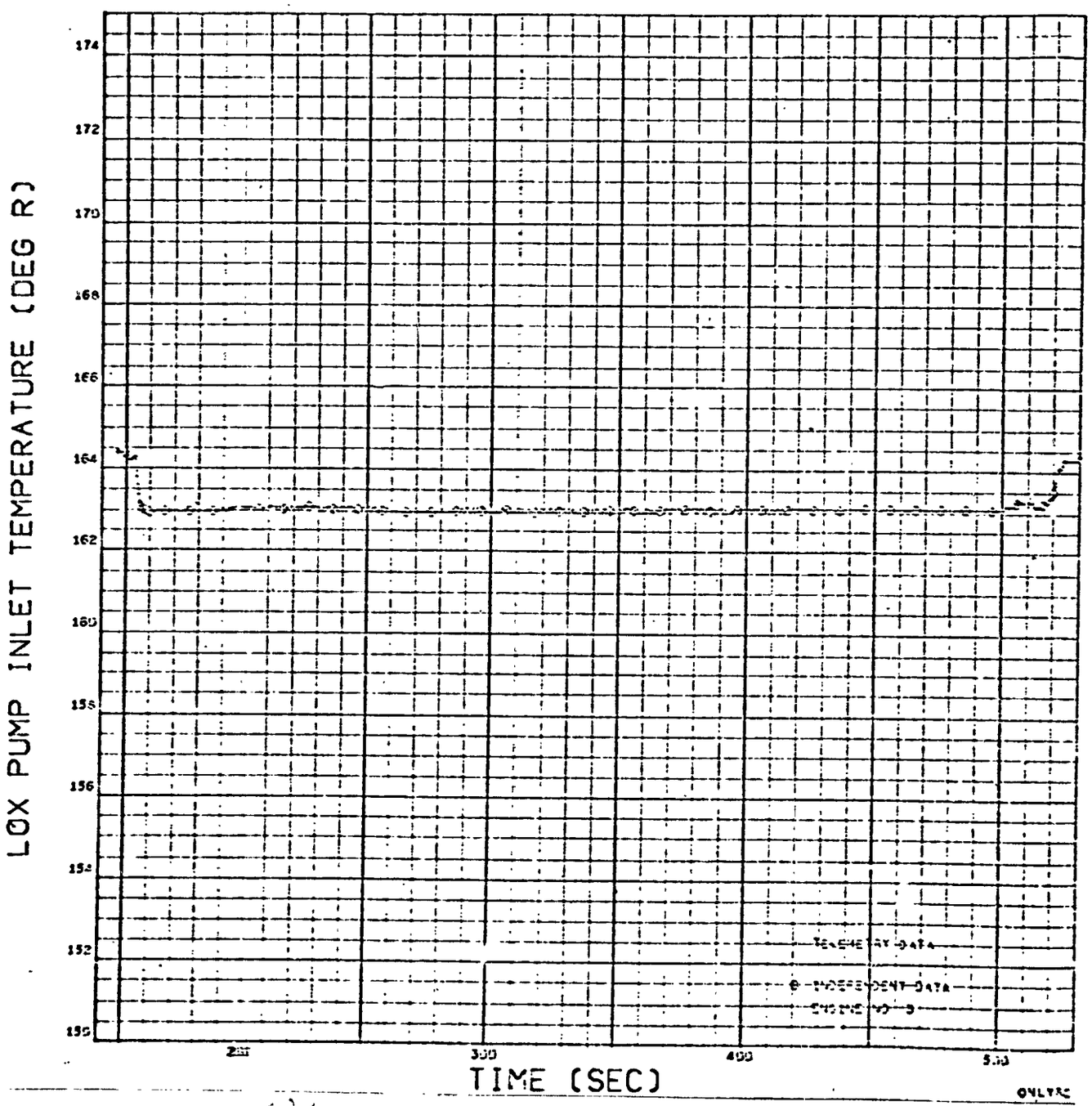

Figure 32. Engine No. 3 Oxidizer Pump Inlet Temperature

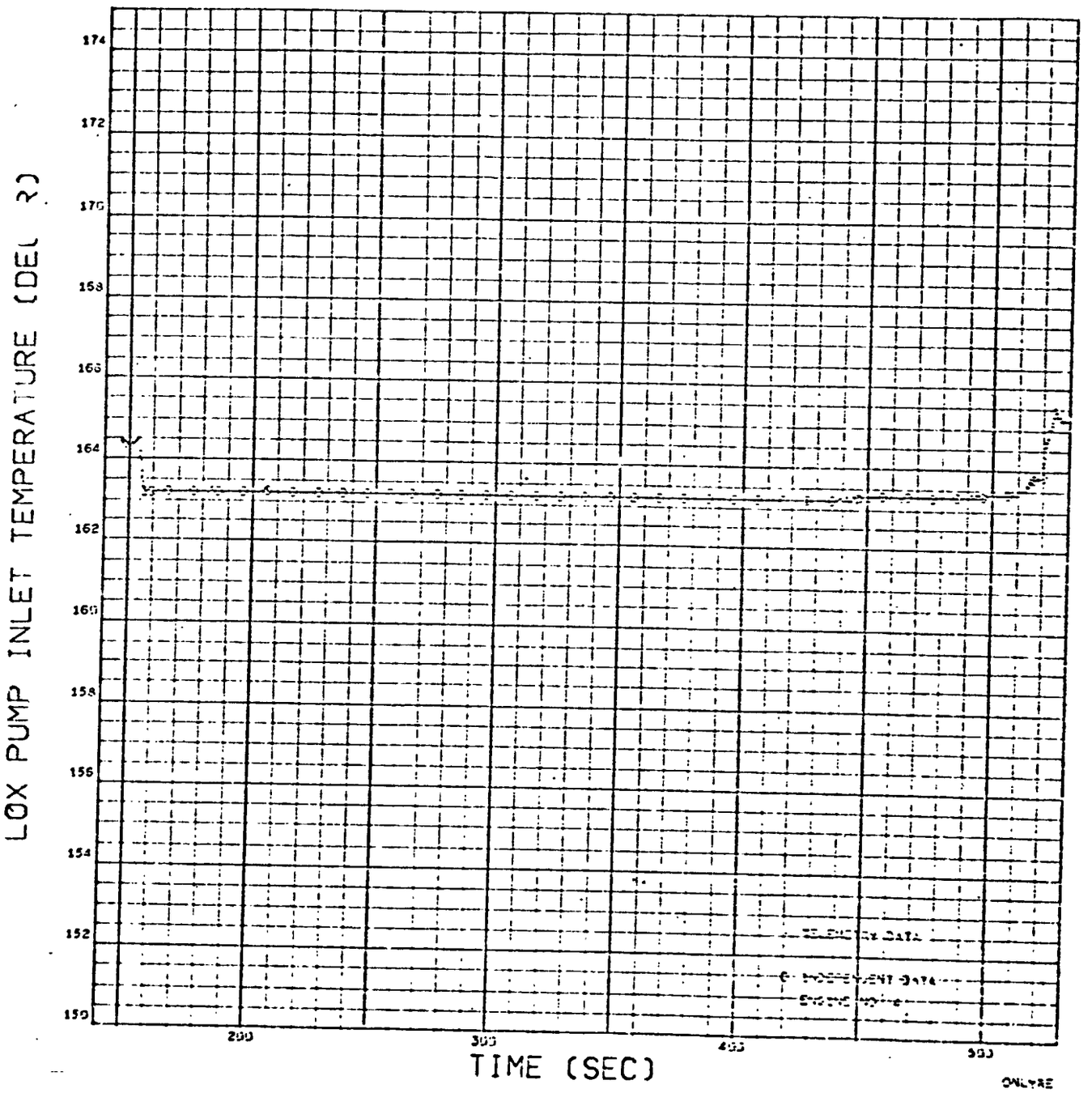

Figure 33. Engine No. 4 Oxidizer Pump Inlet Temperature

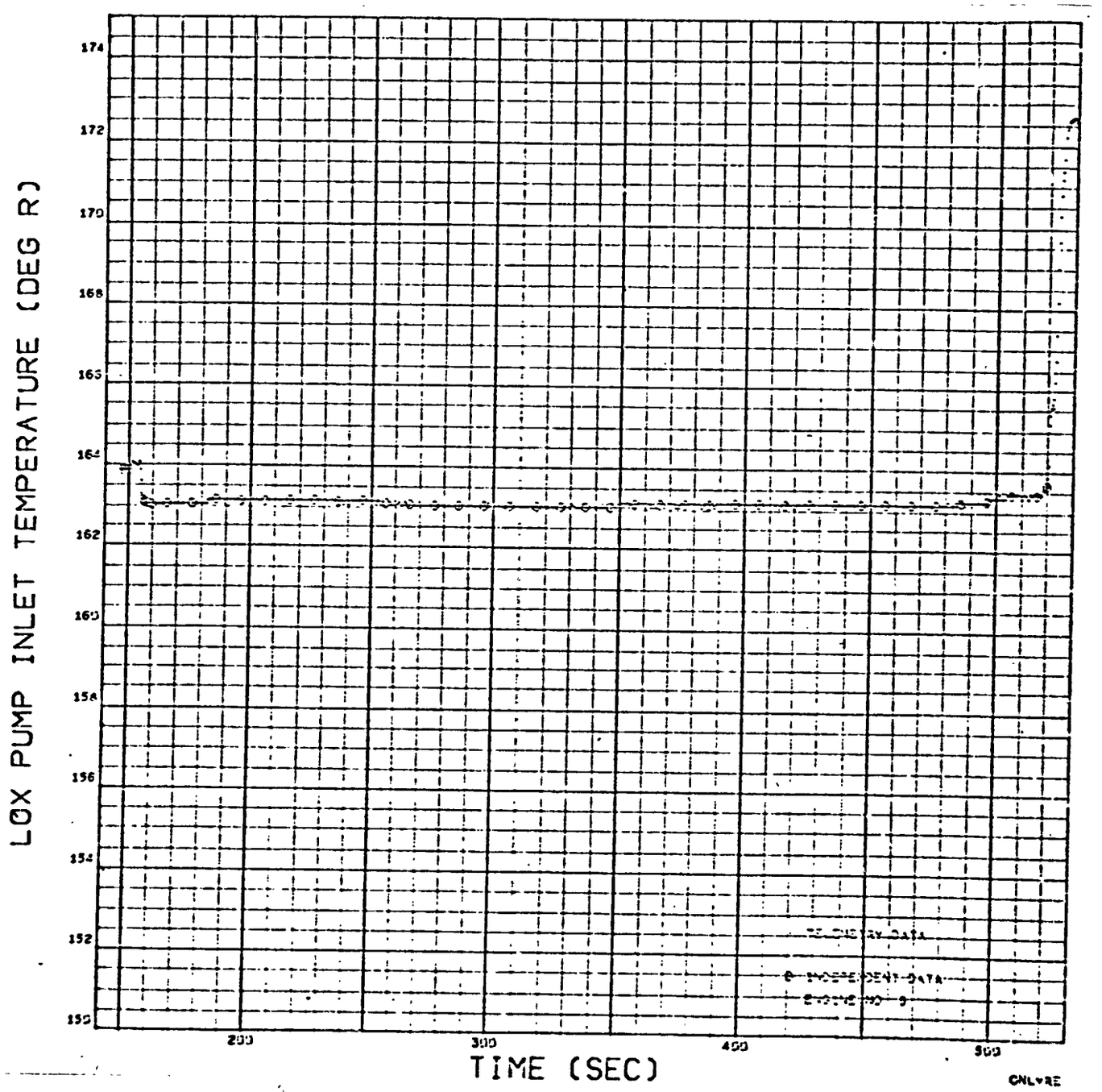

Figure 34. Engine No. 5 Oxidizer Pump Inlet Temperature

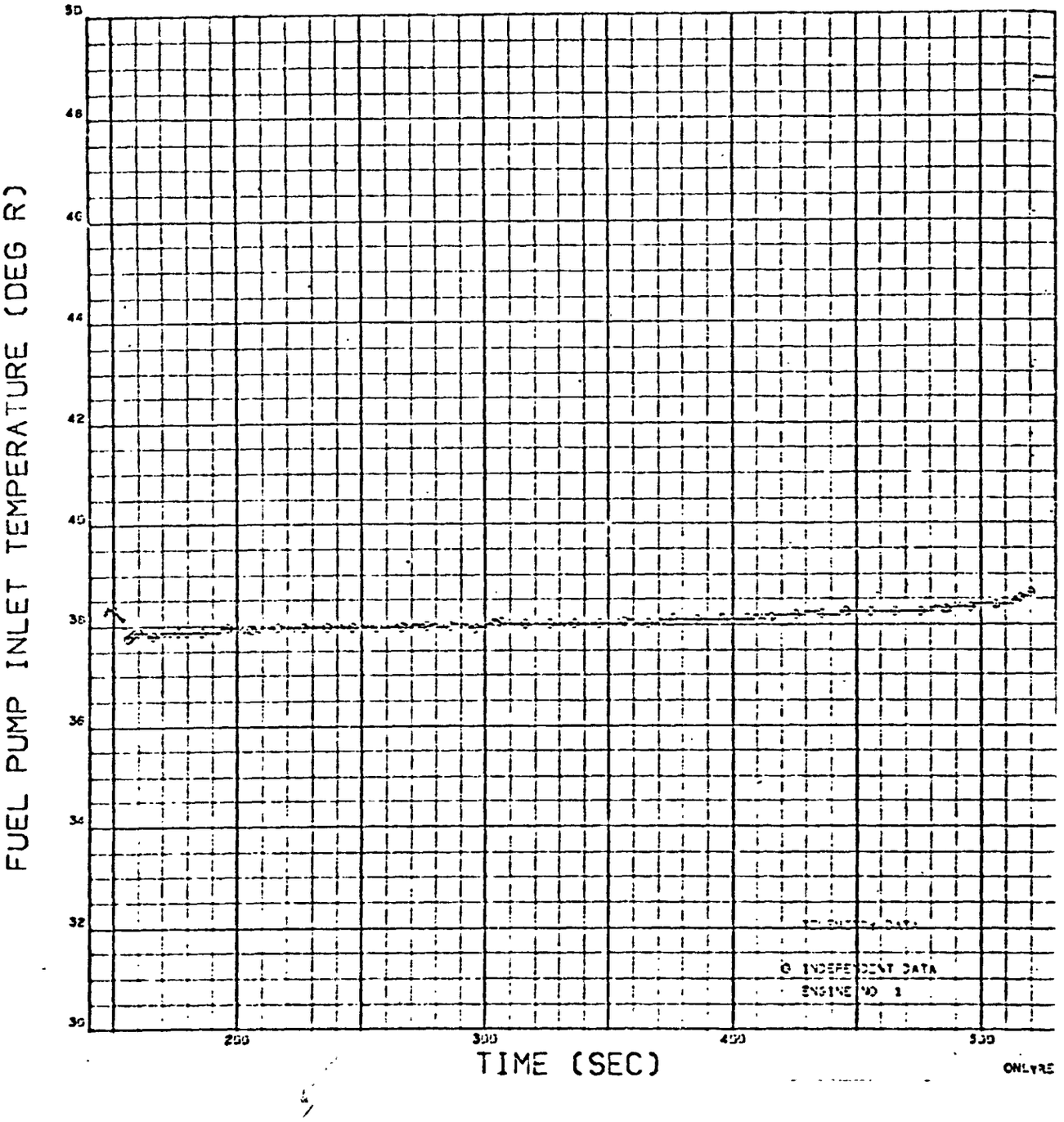

Figure 35. Engine No. 1 Fuel Pump Inlet Temperature

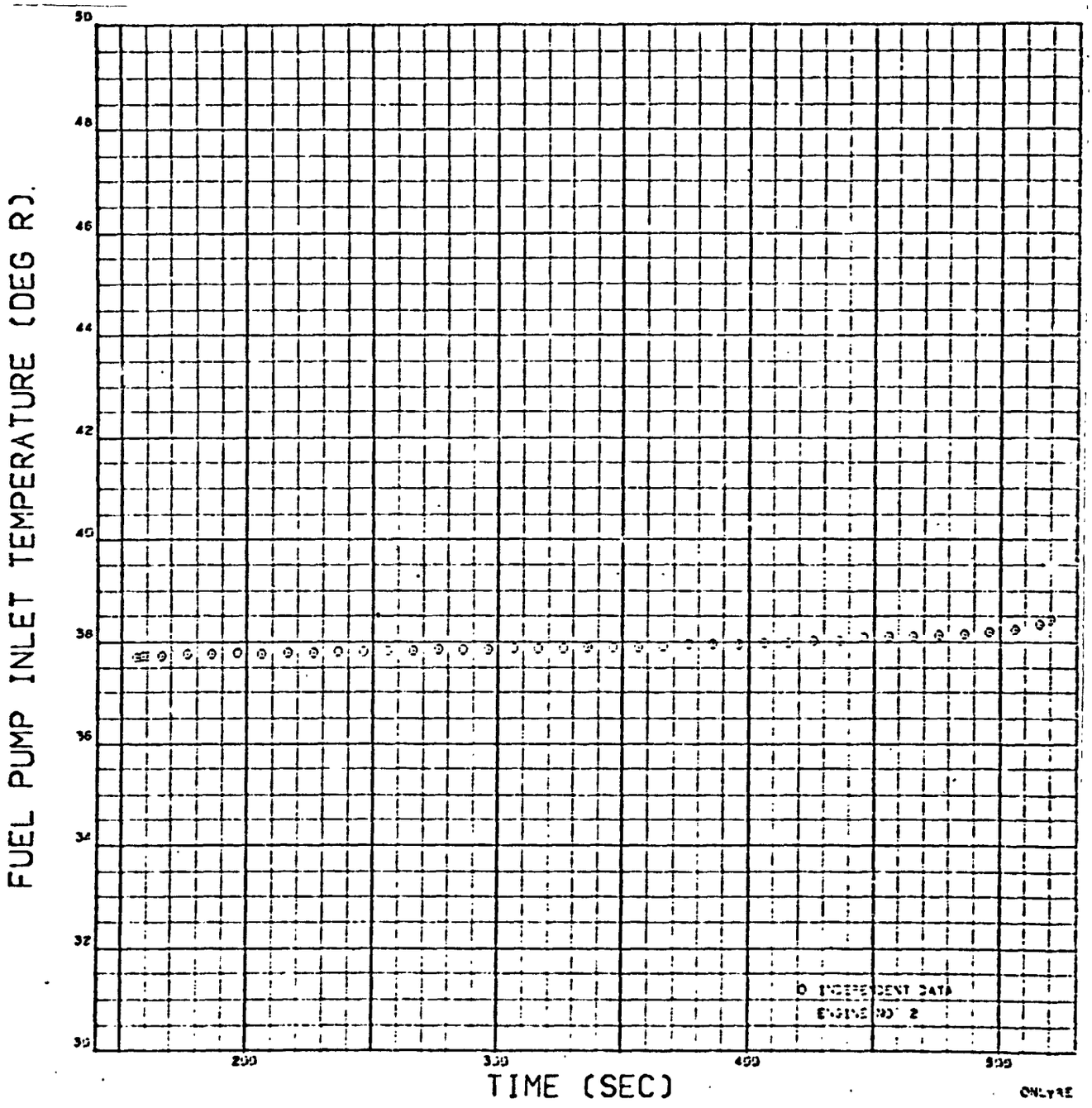

Figure 36. Engine No. 2 Fuel Pump Inlet Temperature

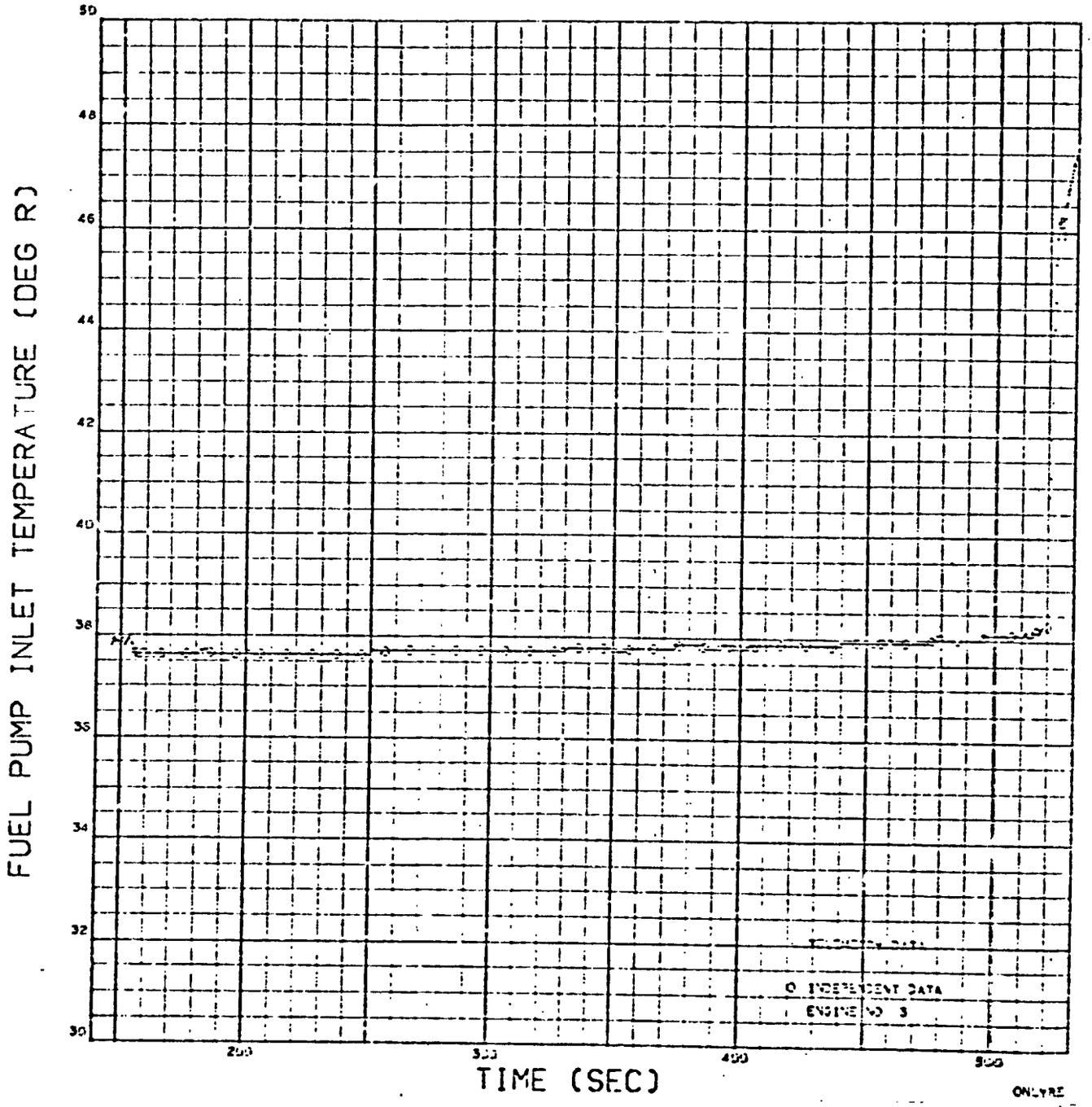

Figure 37. Engine No. 3 Fuel Pump Inlet Temperature

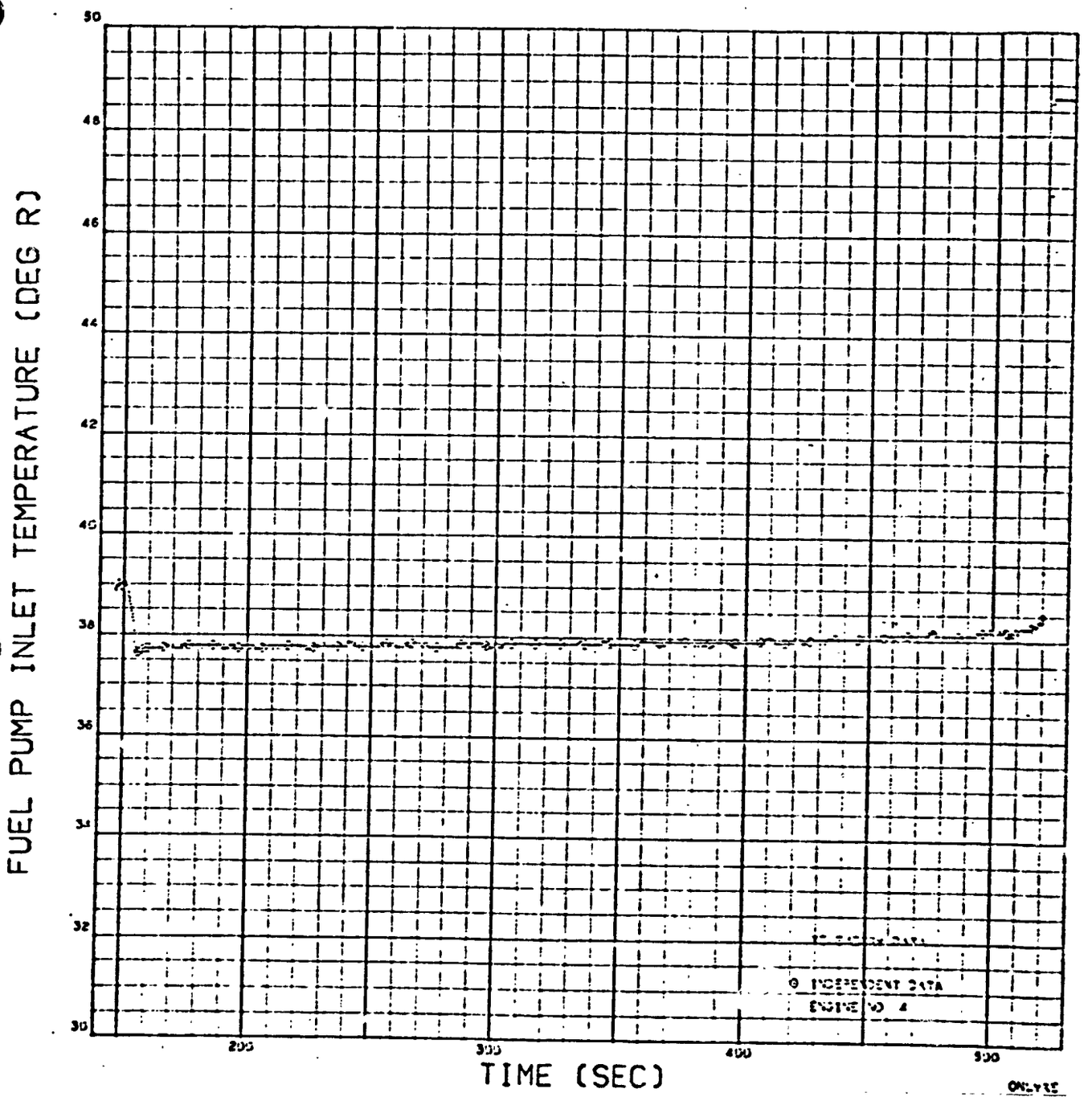

Figure 38. Engine No. 4 Fuel Pump Inlet Temperature

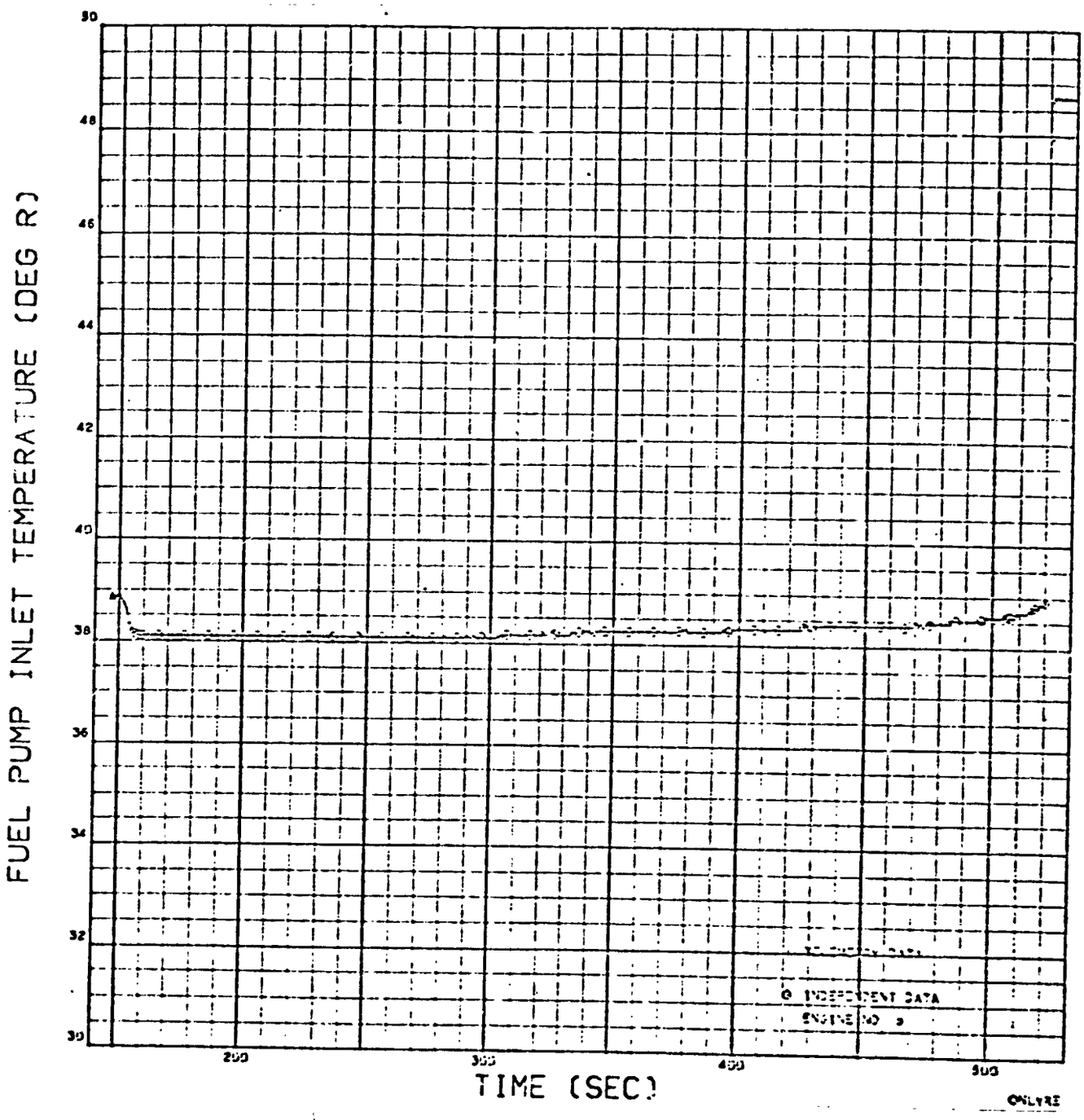

Figure 39. Engine No. 5 Fuel Pump Inlet Temperature

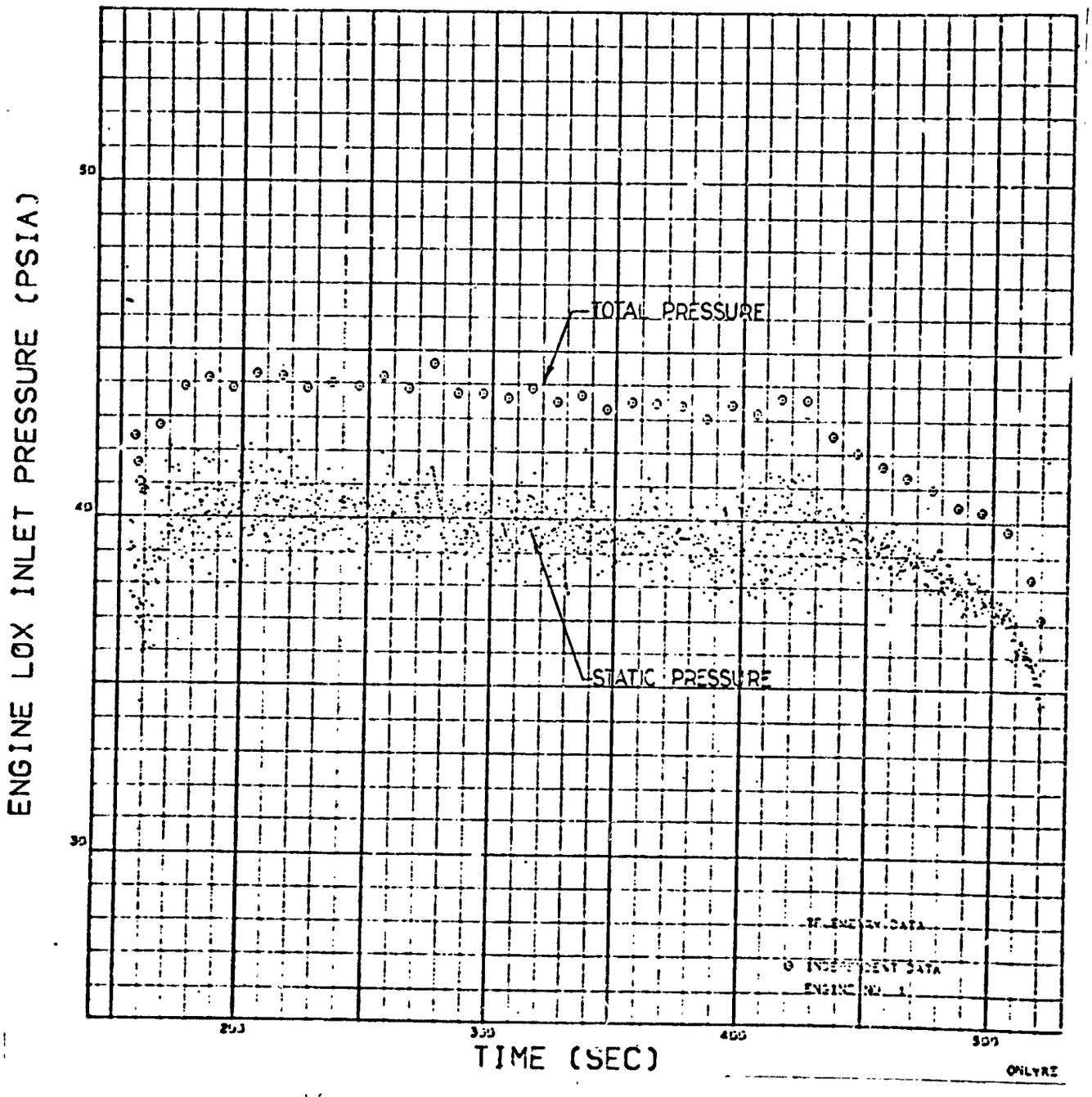

Figure 40. Engine No. 1 Oxidizer Inlet Pressure

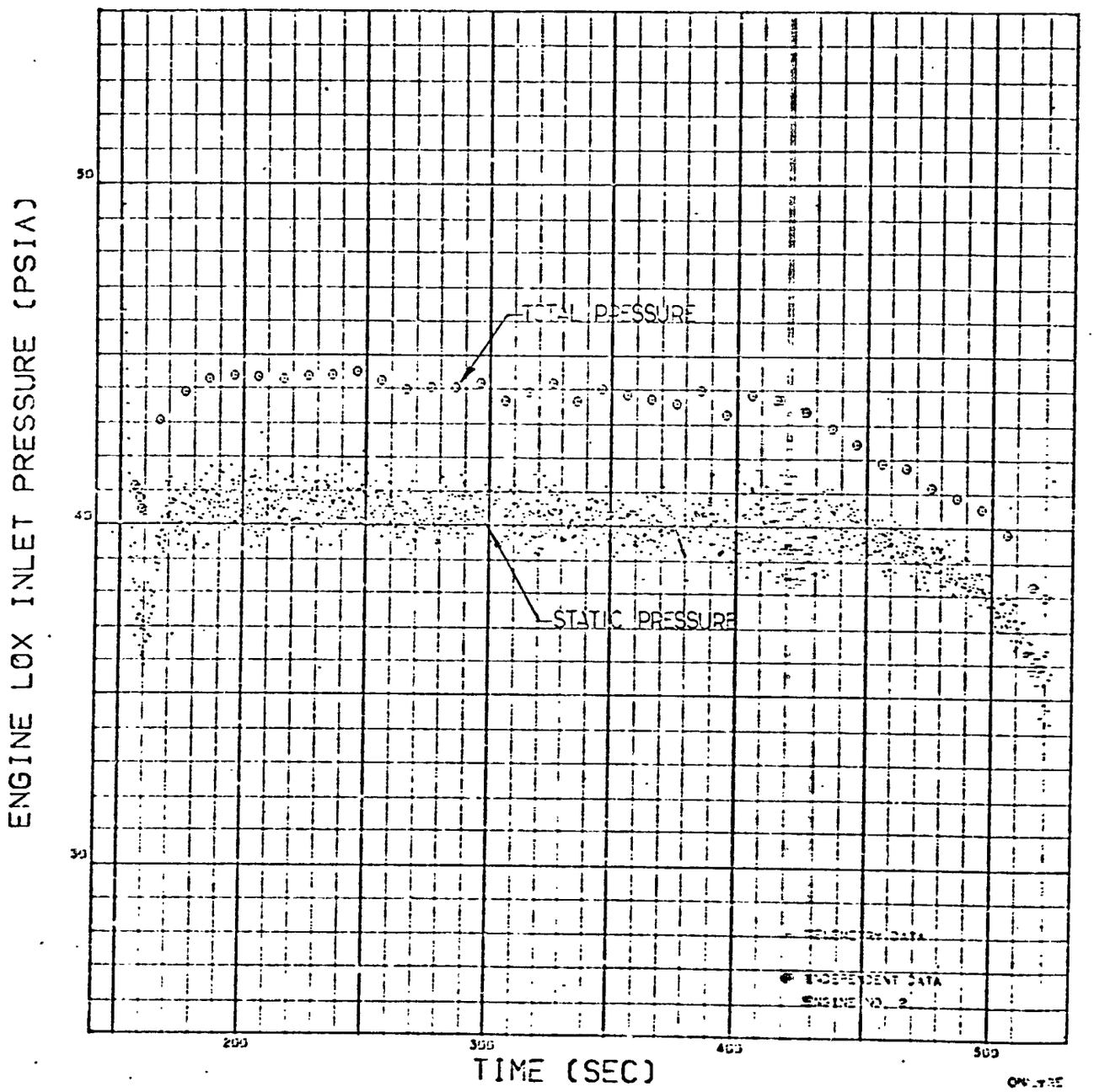

Figure 41. Engine No. 2 Oxidizer Inlet Pressure

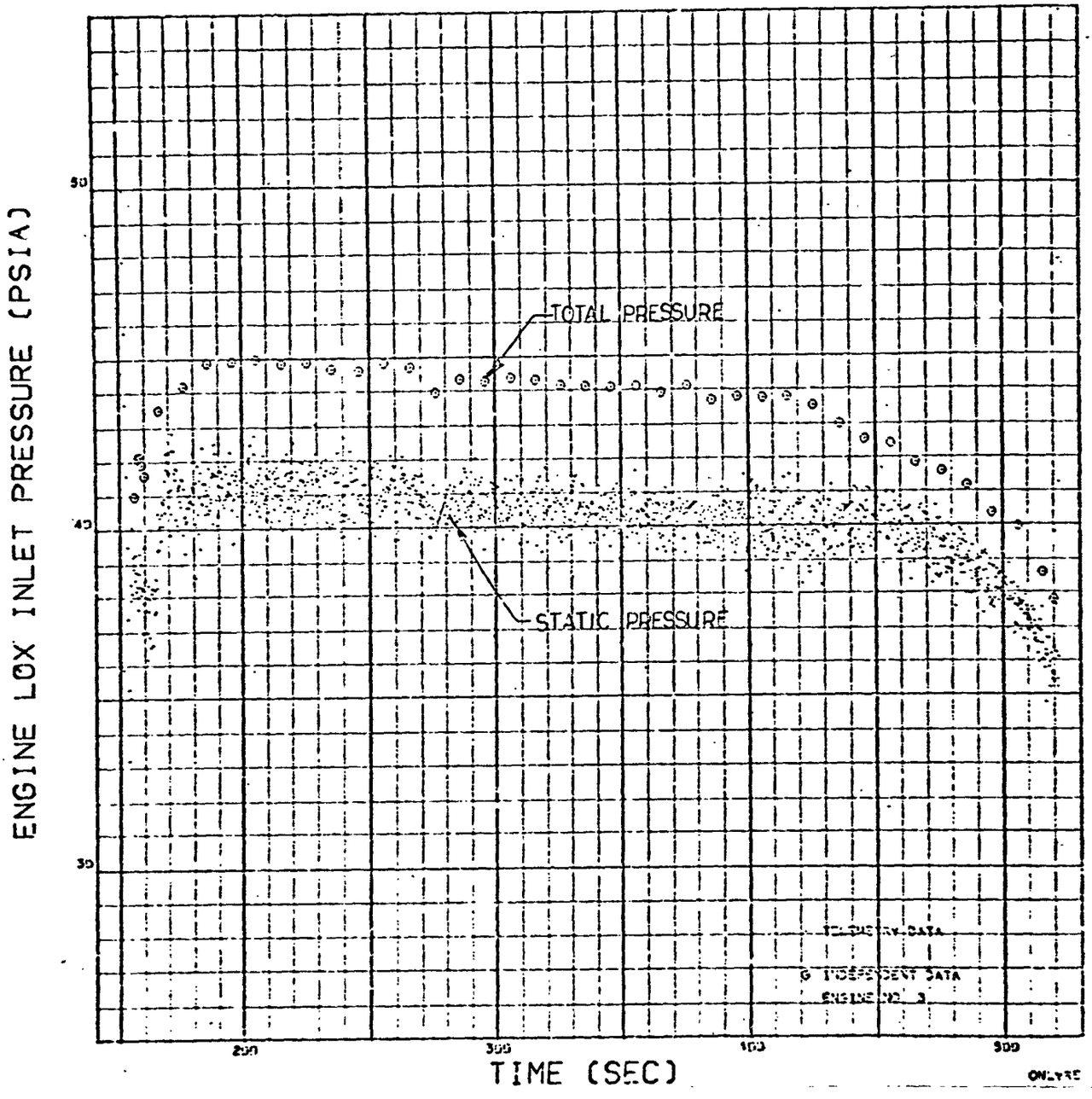

Figure 42. Engine No. 3 Oxidizer Inlet Pressure

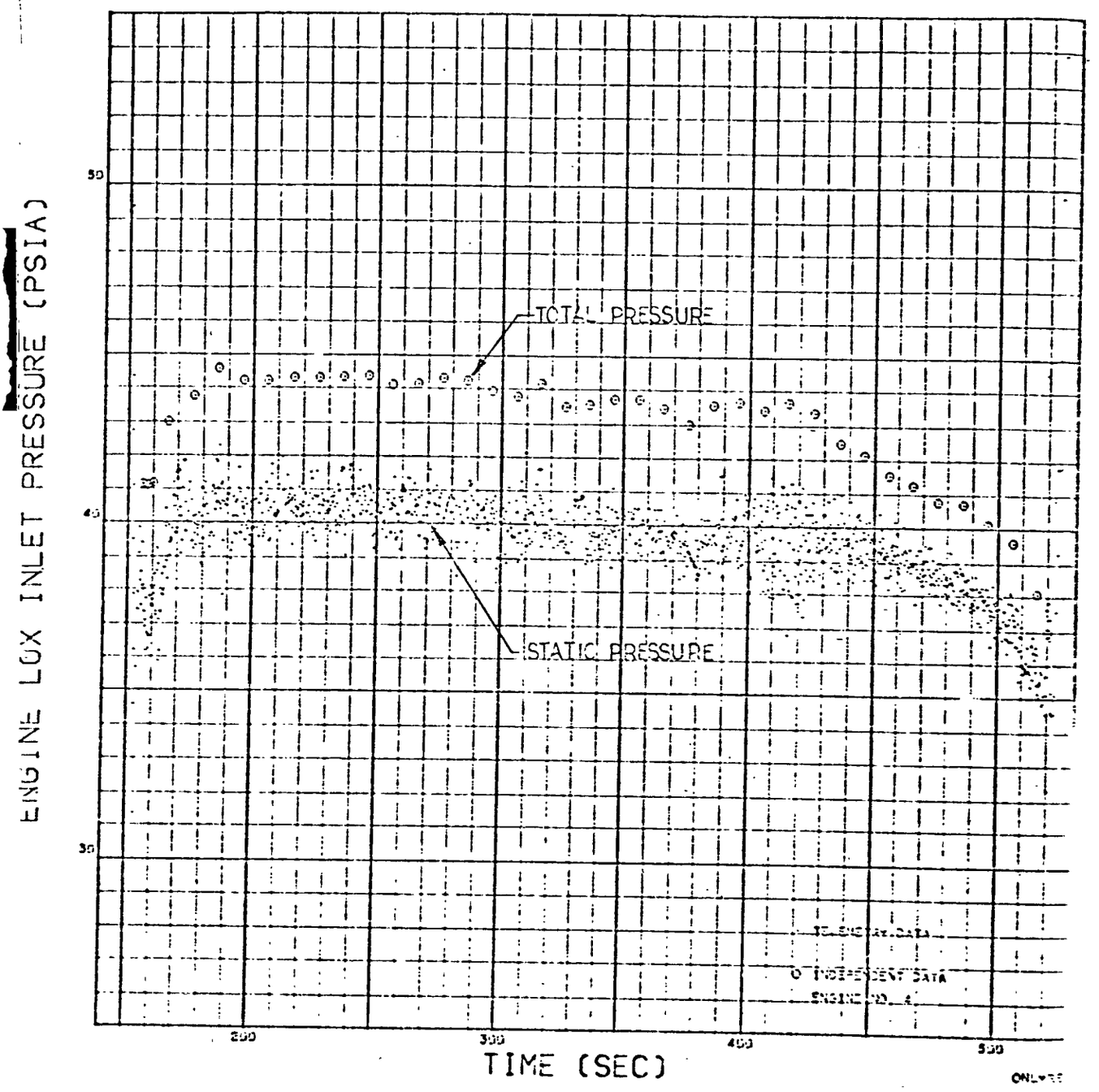

Figure 43. Engine No. 4 Oxidizer Inlet Pressure

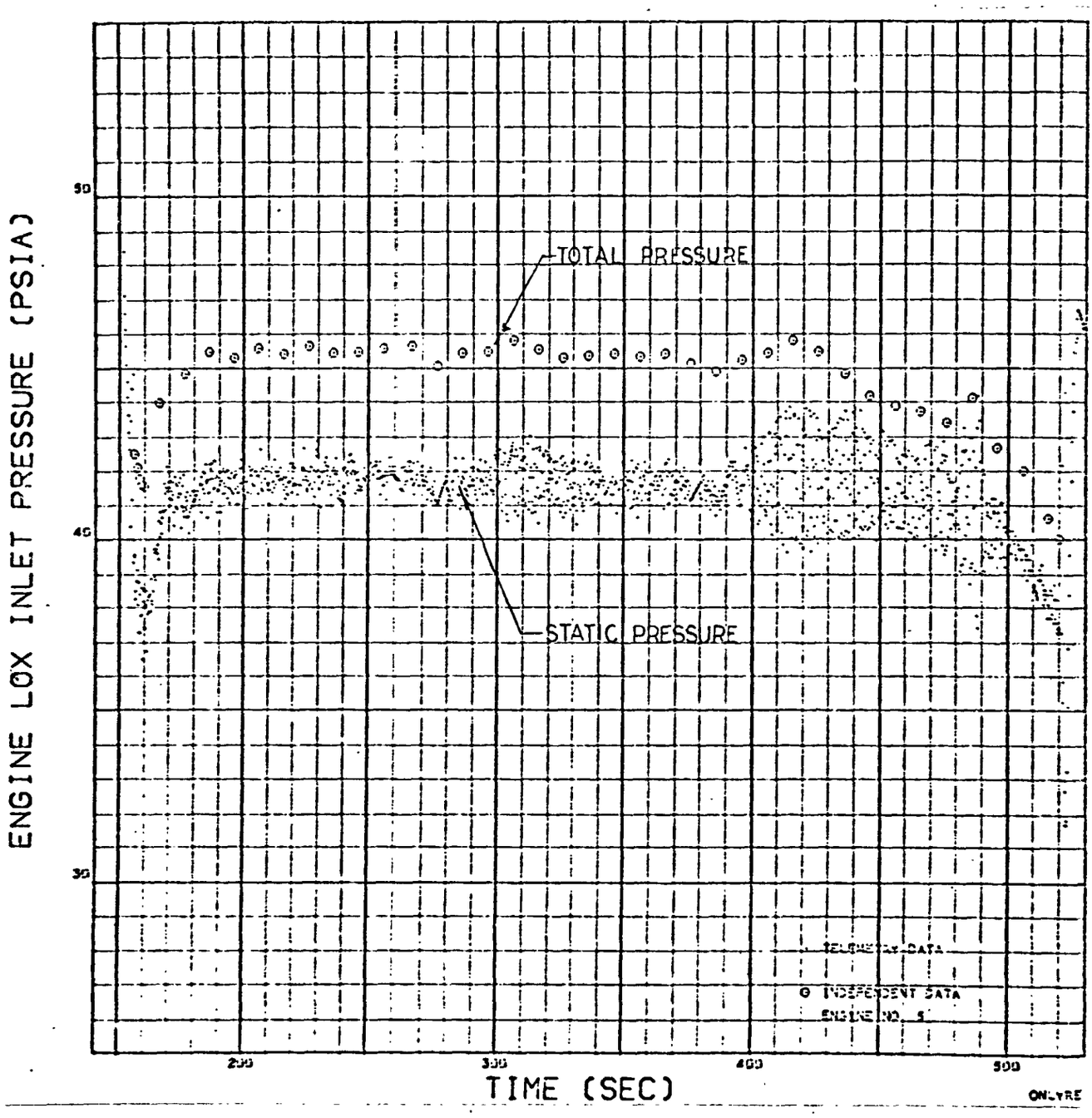

Figure 44. Engine No. 5 Oxidizer Inlet Pressure

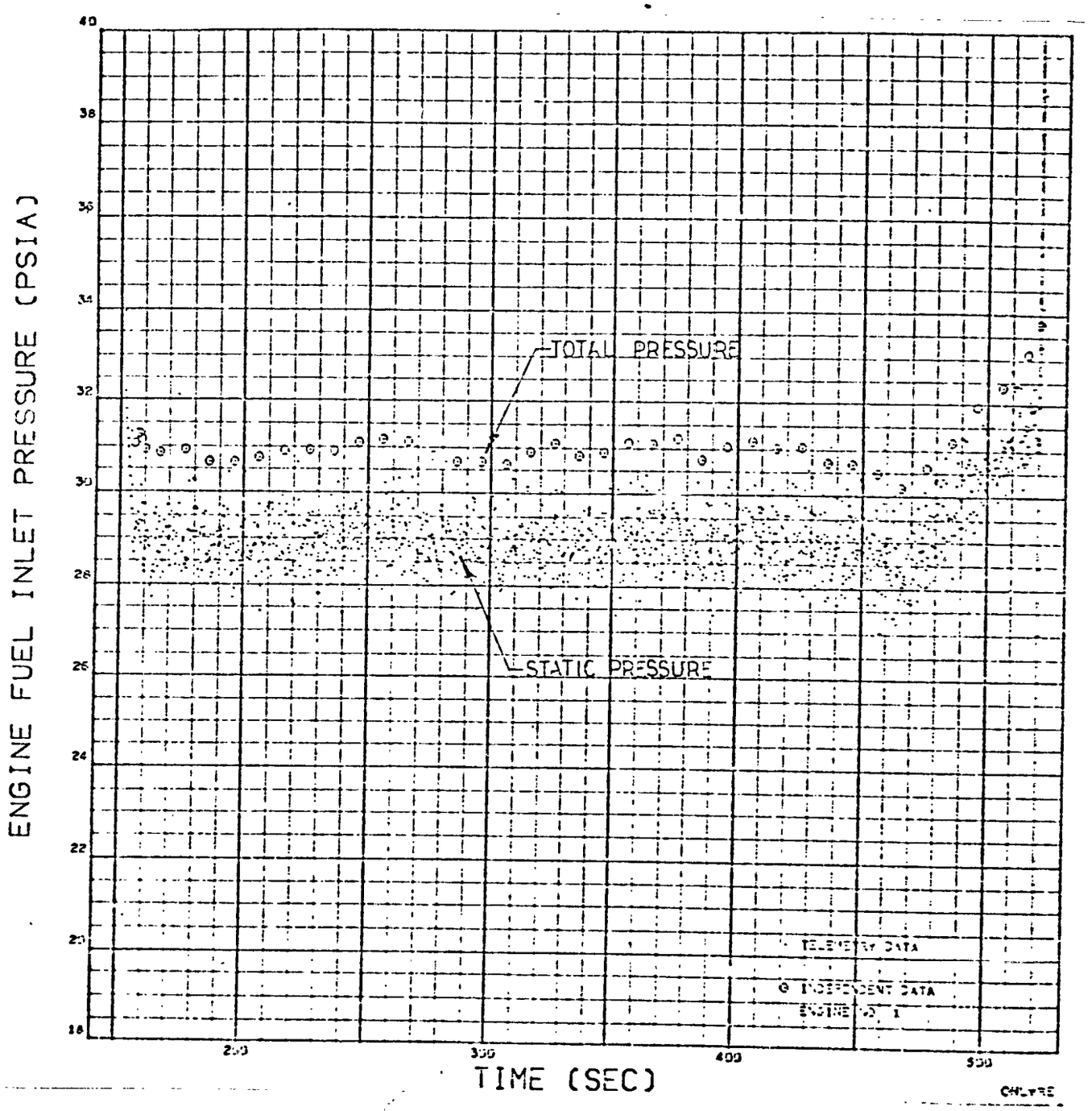

Figure 45. Engine No. 1 Fuel Inlet Pressure

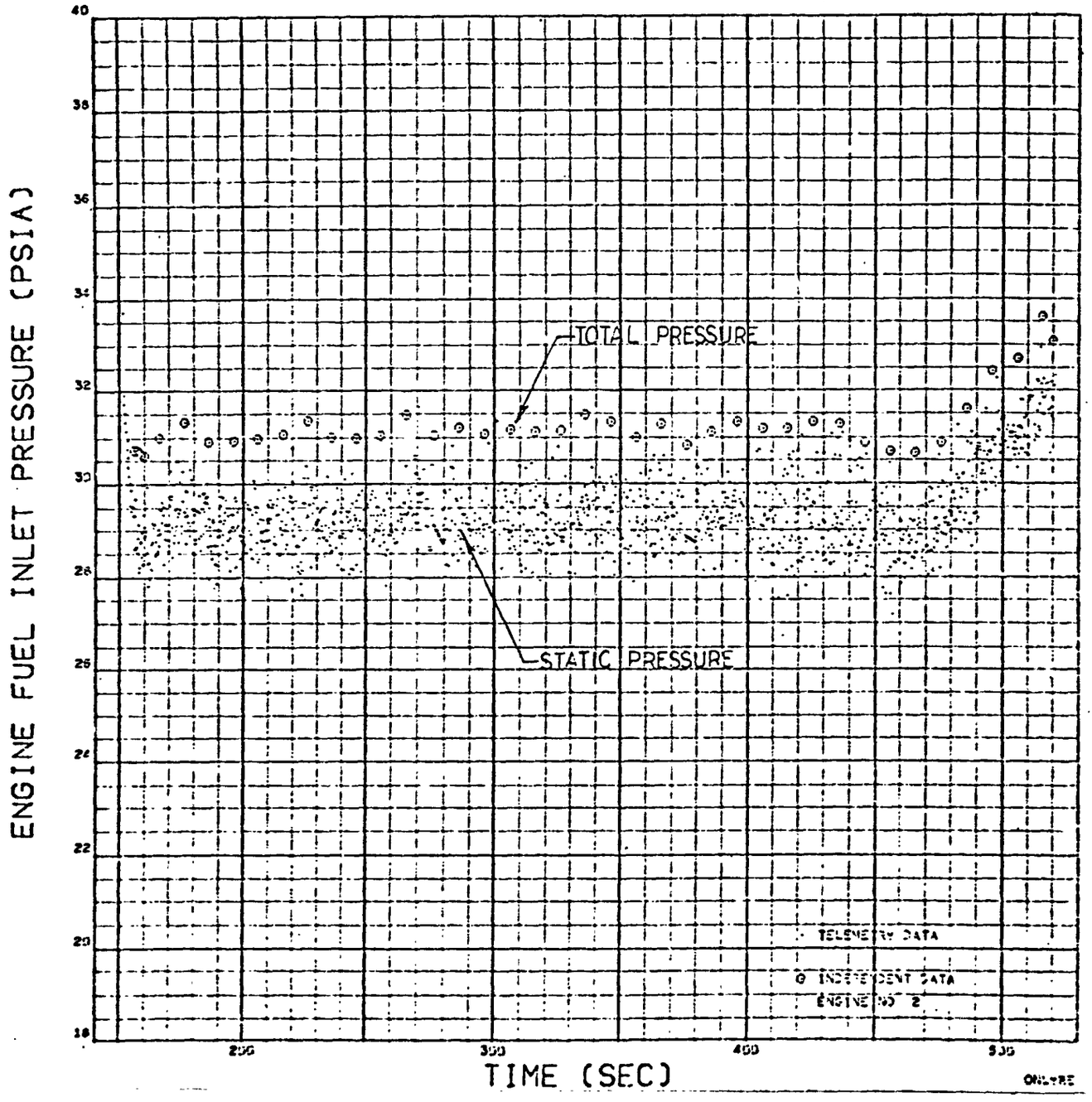

Figure 46. Engine No. 2 Fuel Inlet Pressure

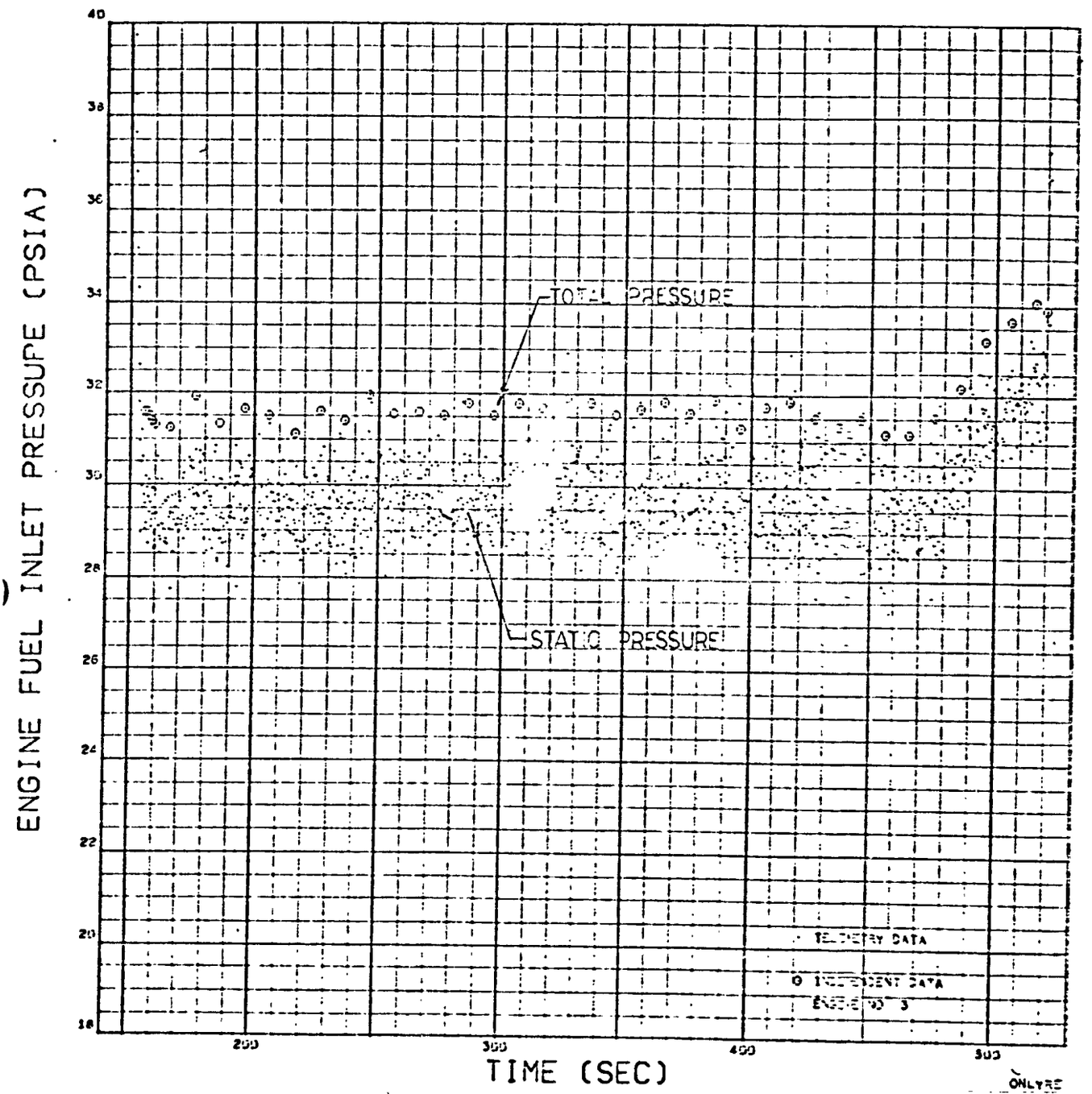

Figure 47. Engine No. 3 Fuel Inlet Pressure

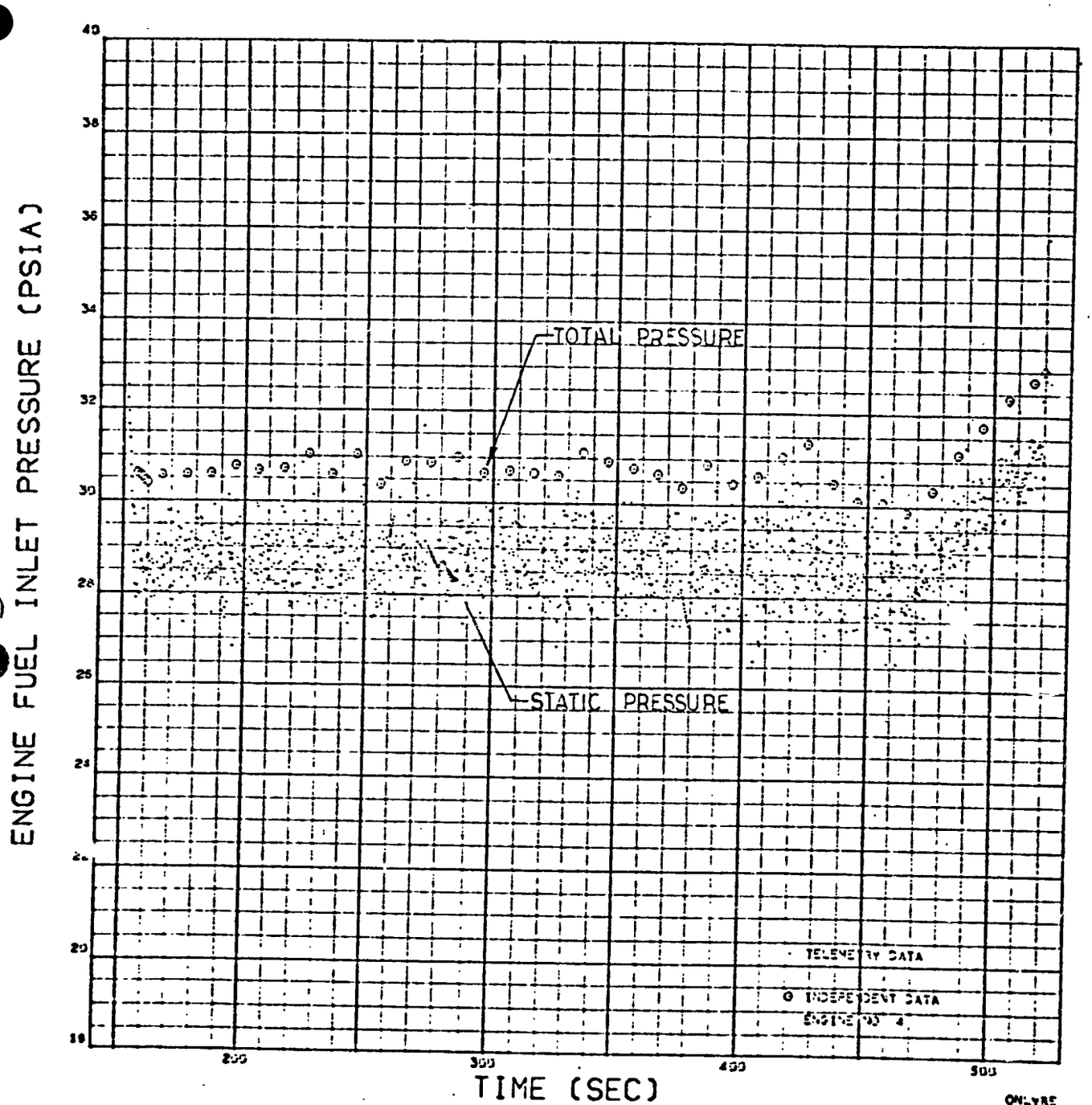

Figure 48. Engine No. 4 Fuel Inlet Pressure

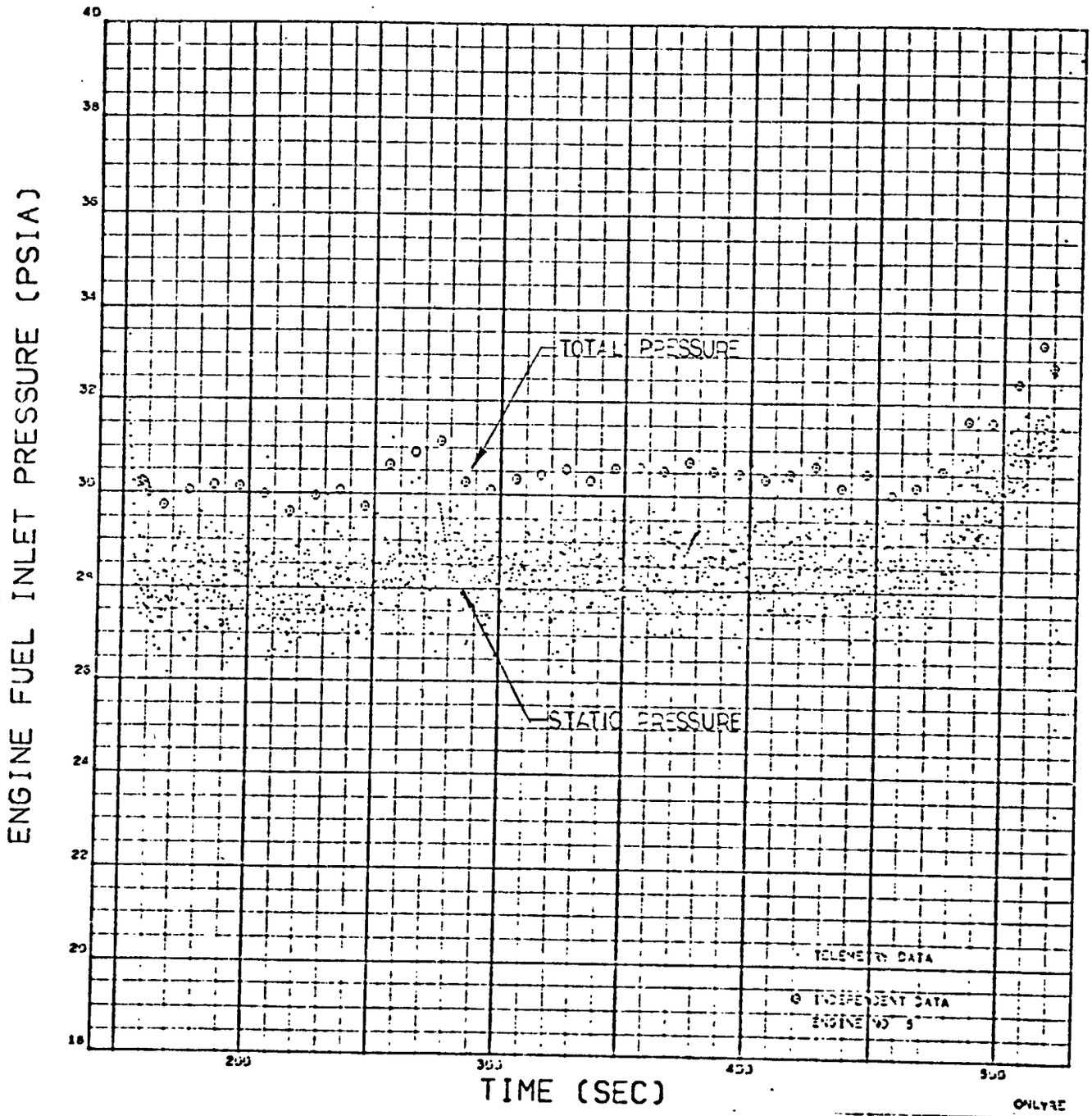

Figure 49. Engine No. 5 Fuel Inlet Pressure

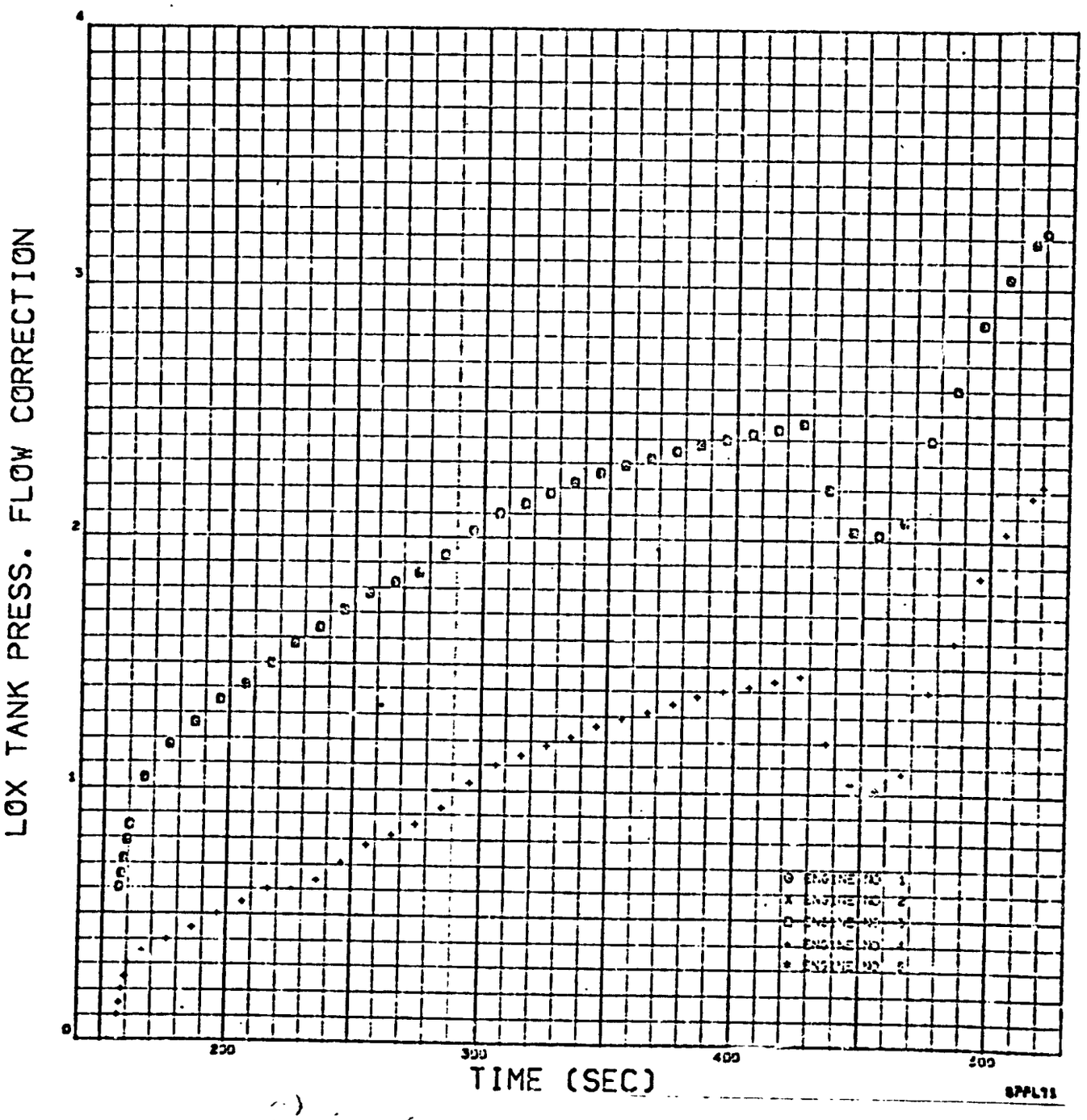

Figure 50. Oxidizer Tank Pressurization Flow for All Engines

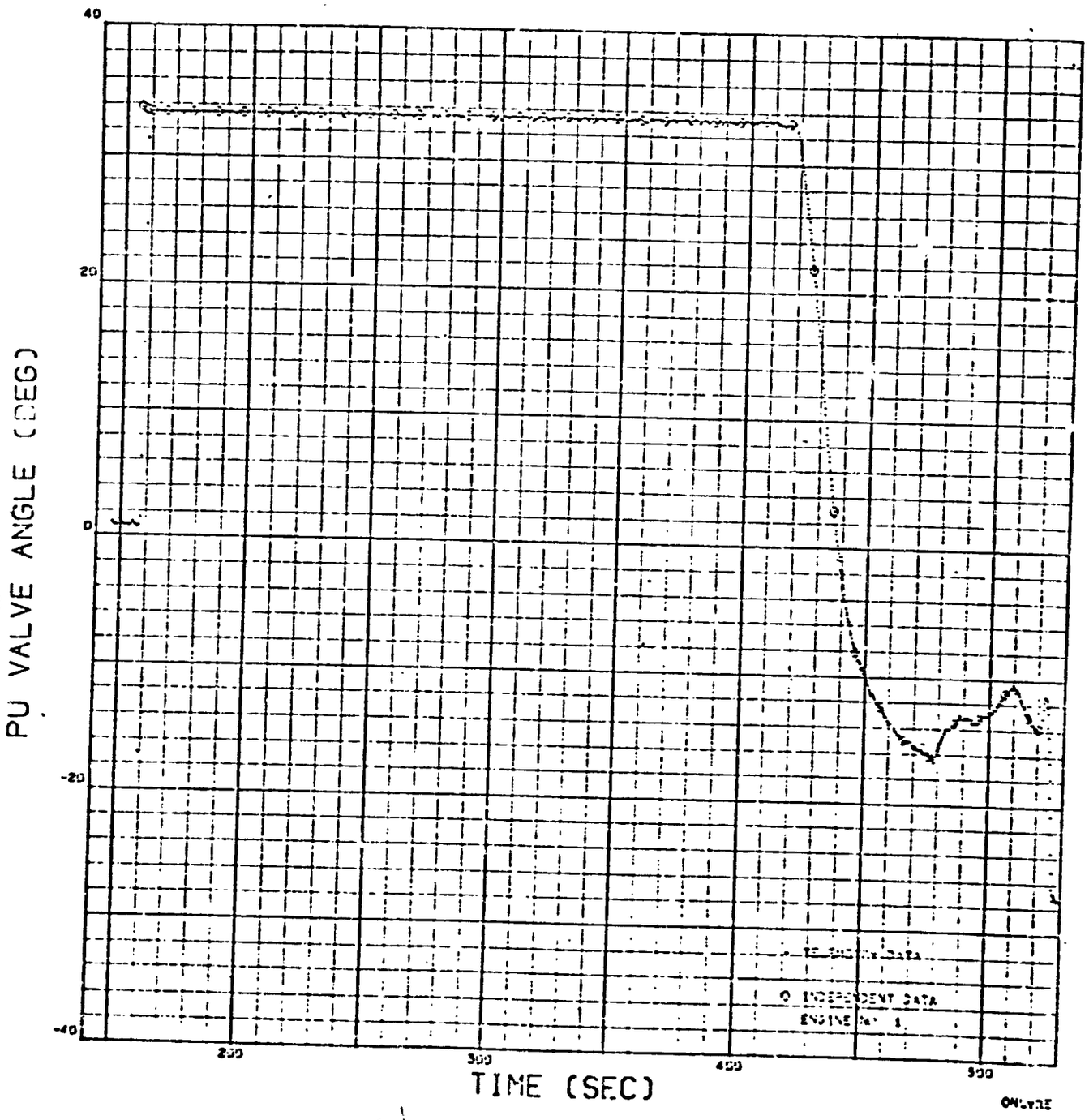

Figure 51. Engine No. 1 PU Valve Angle

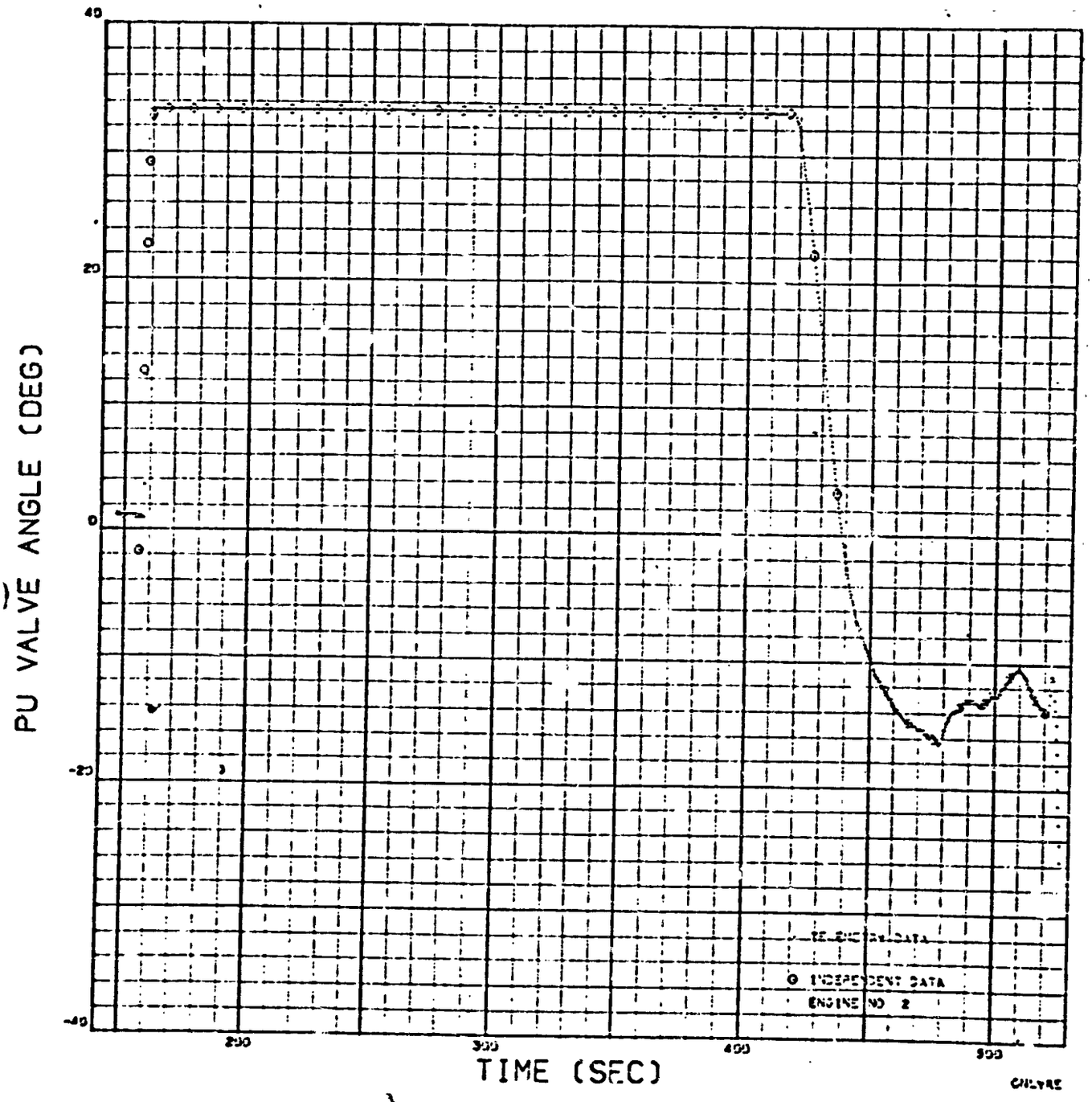

Figure 52. Engine No. 2 PU Valve Angle

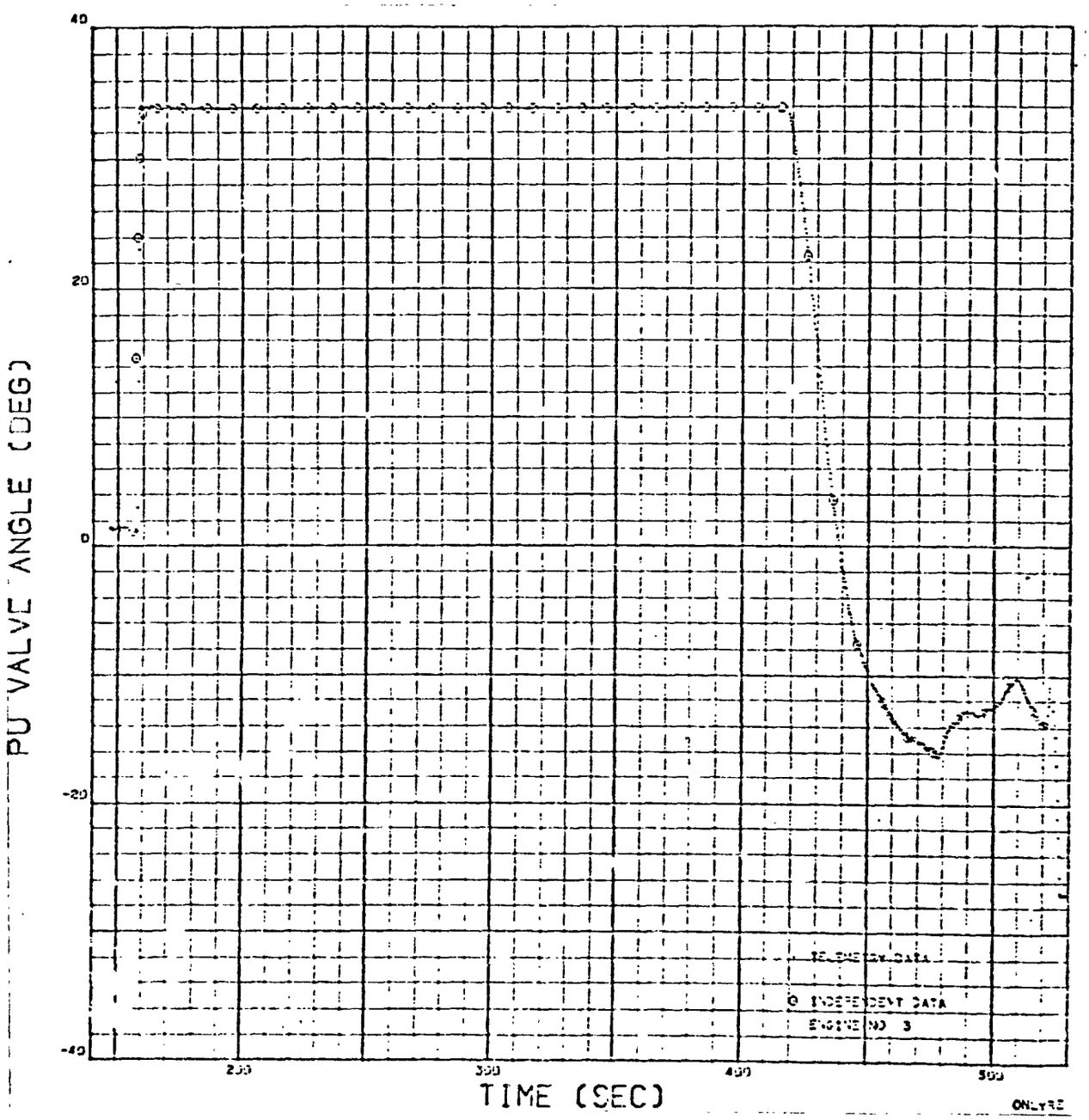

Figure 53. Engine No. 3 PU Valve Angle

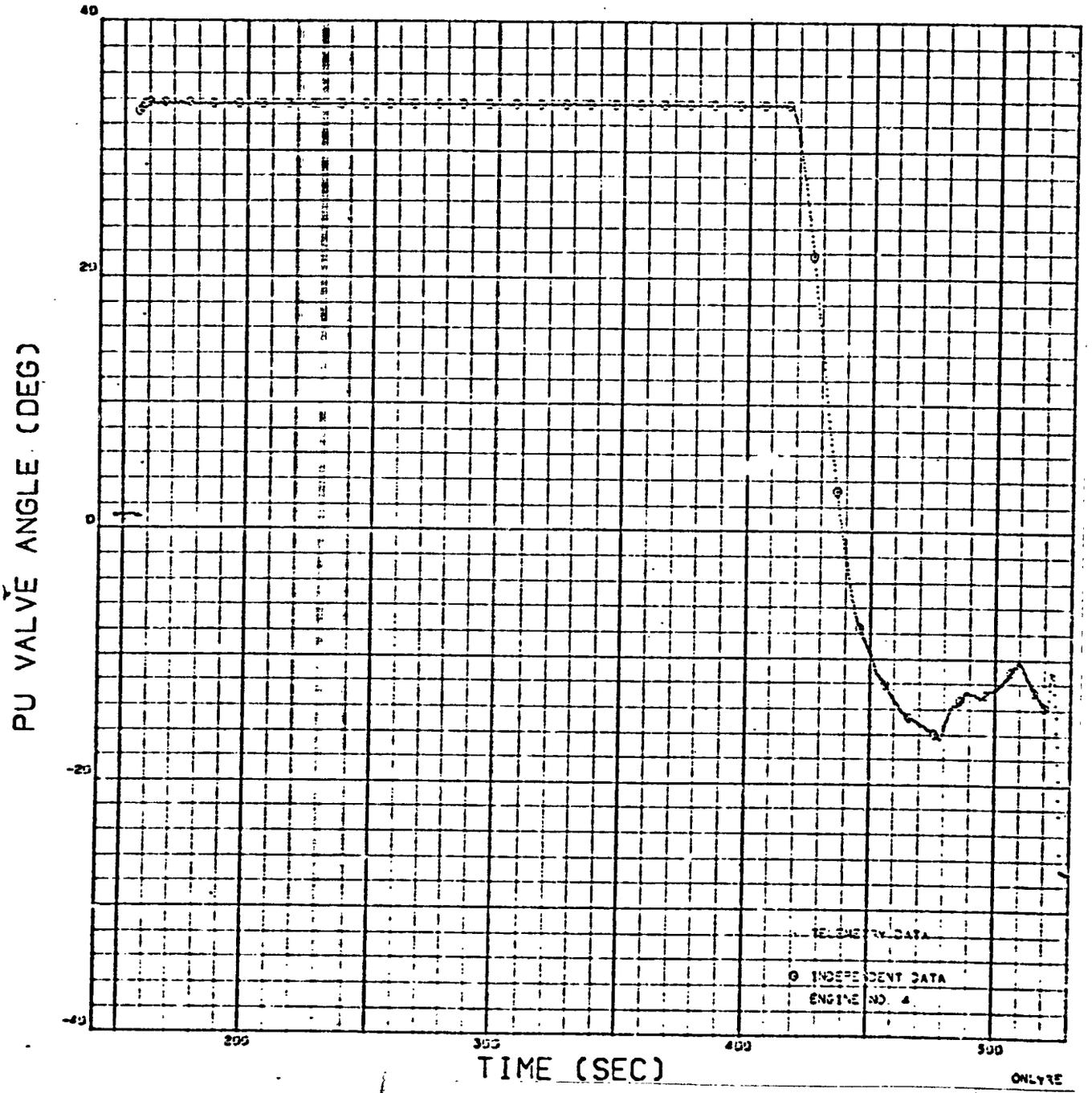

Figure 54. Engine No. 4 PU Valve Angle

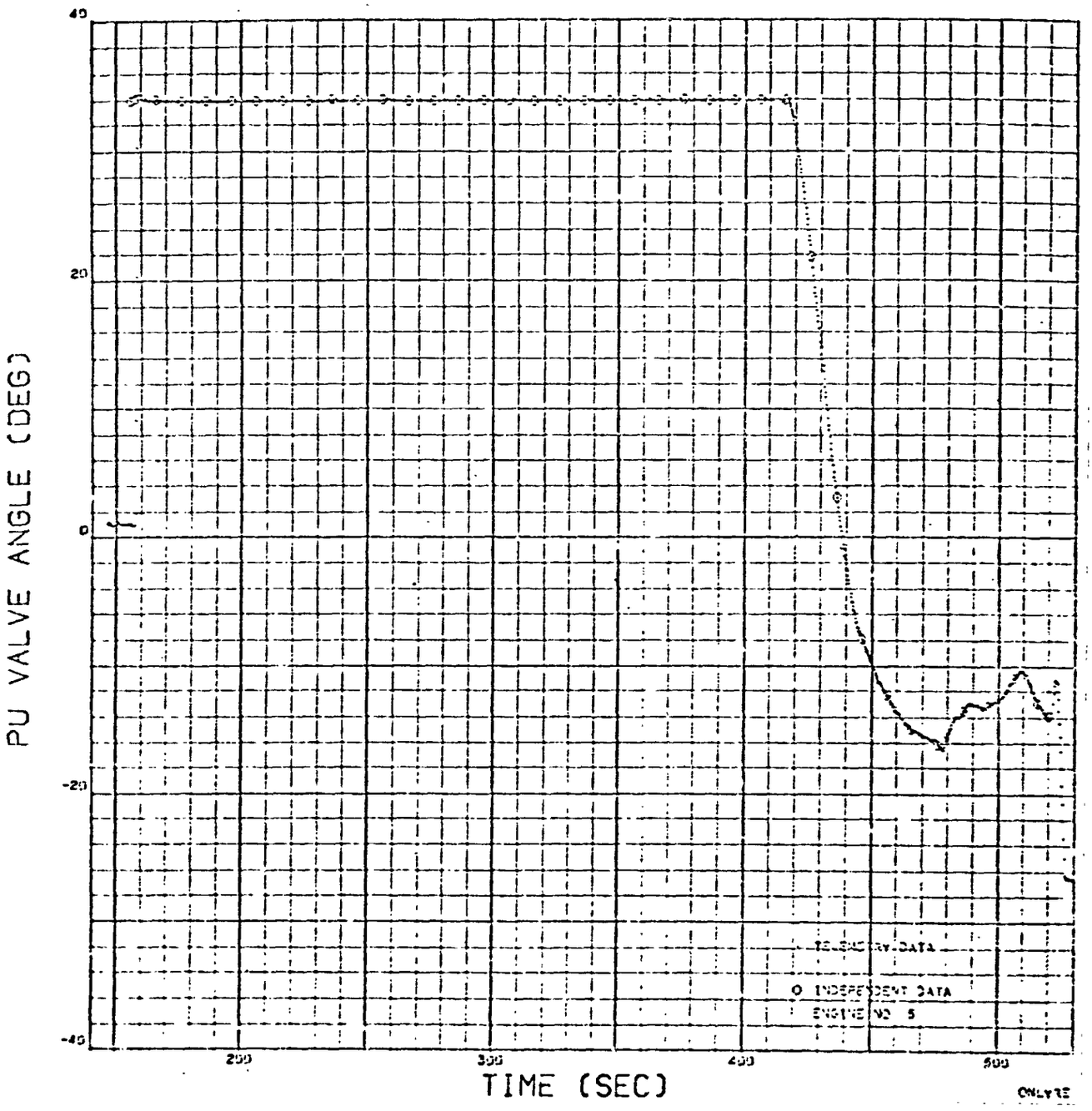

Figure 55. Engine No. 5 PU Valve Angle

from engine acceptance (Fig. 56 through 60). These mixture ratio changes were input to the reconstruction program using the appropriate PU control setting.

Reconstruction of the following parameters are presented in Fig. 61 through 114.

Figures 61 through 65	Engine thrust
Figures 66 through 70	Engine specific impulse
Figures 71 through 75	Engine mixture ratio
Figures 76 through 80	Main thrust chamber pressure
Figures 81 through 85	Engine oxidizer flowrate
Figures 86 through 89	Engine fuel flowrate
Figures 90 through 94	Oxidizer pump speed
Figures 95 through 99	Fuel pump speed
Figures 100 through 104	Oxidizer pump discharge pressure
Figures 105 through 109	Fuel pump discharge pressure
Figures 110 through 114	Gas generator chamber pressure

Actual measured flight performance also is shown for all parameters except thrust and specific impulse. The flows and mixture ratio are based on original telemetry, tape data and, therefore, do not agree exactly with values from Tables 10 through 13, which are based on oscillograph flows.

On engines No. 2 and No. 4, data scatter in the oxidizer flow measurement resulted in the calculation of an erroneously high mixture ratio at 176 seconds (range time).

The engines operated for approximately 270 seconds with the PU valve closed. During this period, the reconstructed performance matched the actual performance quite well. Primarily, differences between reconstructed and actual values were attributed to the uncertainties in the predicted tage values caused by the preflight hardware changes, as discussed previously.

Curves of mixture ratio versus voltage ratio (Fig. 56 through 60) show that the flight PU excursion was as predicted except for engines No. 3 and No. 5. On these engines, the mixture ratio change for a given voltage ratio was slightly greater than during engine acceptance. This is reflected also in other parameters such as chamber pressure, flows, pump speeds, and pump discharge pressures, all of which show a greater than predicted change during PU excursion. In the cases of engines No. 3 and No. 5, major hardware changes were made prior to the flight which could influence the PU excursion. On No. 3, the oxidizer turbopump was changed, and on No. 5, both the oxidizer turbopump and PU valve were replaced

The flight mixture ratio excursion for engine No. 4 was as predicted (Fig. 59), but most of the other parameters changed less than predicted by the reconstruction. This seems to be characteristic of this engine, as also observed during engine acceptance.

Figures 71 through 75 show a slight decrease in mixture ratio during the first 250 seconds of engine operation. This trend is the result of fuel turbine warmup and, has been incorporated in the flight reconstruction model. Figures 95 through 99 show that, during this same time period, the fuel pump speed increased 200 to 300 rpm. This trend in pump speed has not been completely simulated by the reconstruction model.

Table 16 presents reconstructed average thrust, mixture ratio, and specific impulse for the region of maximum PU operation, starting at 90-percent thrust (156.5 to 426 seconds), the region from PU cutback plus 50 seconds to cutoff signal (576 to 520 seconds), and the region from 90-percent thrust to cutoff signal (156.5 to 520 seconds).

TABLE 16

RECONSTRUCTED AVERAGE ENGINE PERFORMANCE

	Average Thrust, pounds	Average Mixture Ratio	Average Specific Impulse, seconds	Average Flowrate, lb/sec
High Mixture Ratio Region (156 to 426 seconds)				
Engine 1	229,369	5.5087	425.59	521.98
Engine 2	222,772	5.4516	424.98	524.07
Engine 3	223,612	5.3975	425.95	524.98
Engine 4	225,568	5.5302	421.43	535.20
Engine 5	225,493	5.3677	424.33	531.35
Average	225,362.8	5.45114	424.46	527.52
50 Seconds After Mixture Ratio Cutback to Cutoff Signal (476 to 520 seconds)				
Engine 1	192,195	4.7660	430.16	445.52
Engine 2	183,097	4.6554	429.78	424.43
Engine 3	186,018	4.6442	430.54	430.51
Engine 4	185,730	4.7307	426.28	435.12
Engine 5	189,140	4.5980	429.08	439.56
Average	187.236	4.67886	429.17	435.03
From 156 Seconds to Cutoff Signal (156 to 520 seconds)				
Engine 1	22[illegible] 063	5.3390	426.65	505.11
Engine 2	21[illegible],964	5.2711	426.07	501.90
Engine 3	215,284	5.2270	427.00	504.01
Engine 4	216,715	5.3488	422.54	512.92
Engine 5	217,354	5.1943	425.40	510.80
Average	216,876	5.27604	425.53	506.95

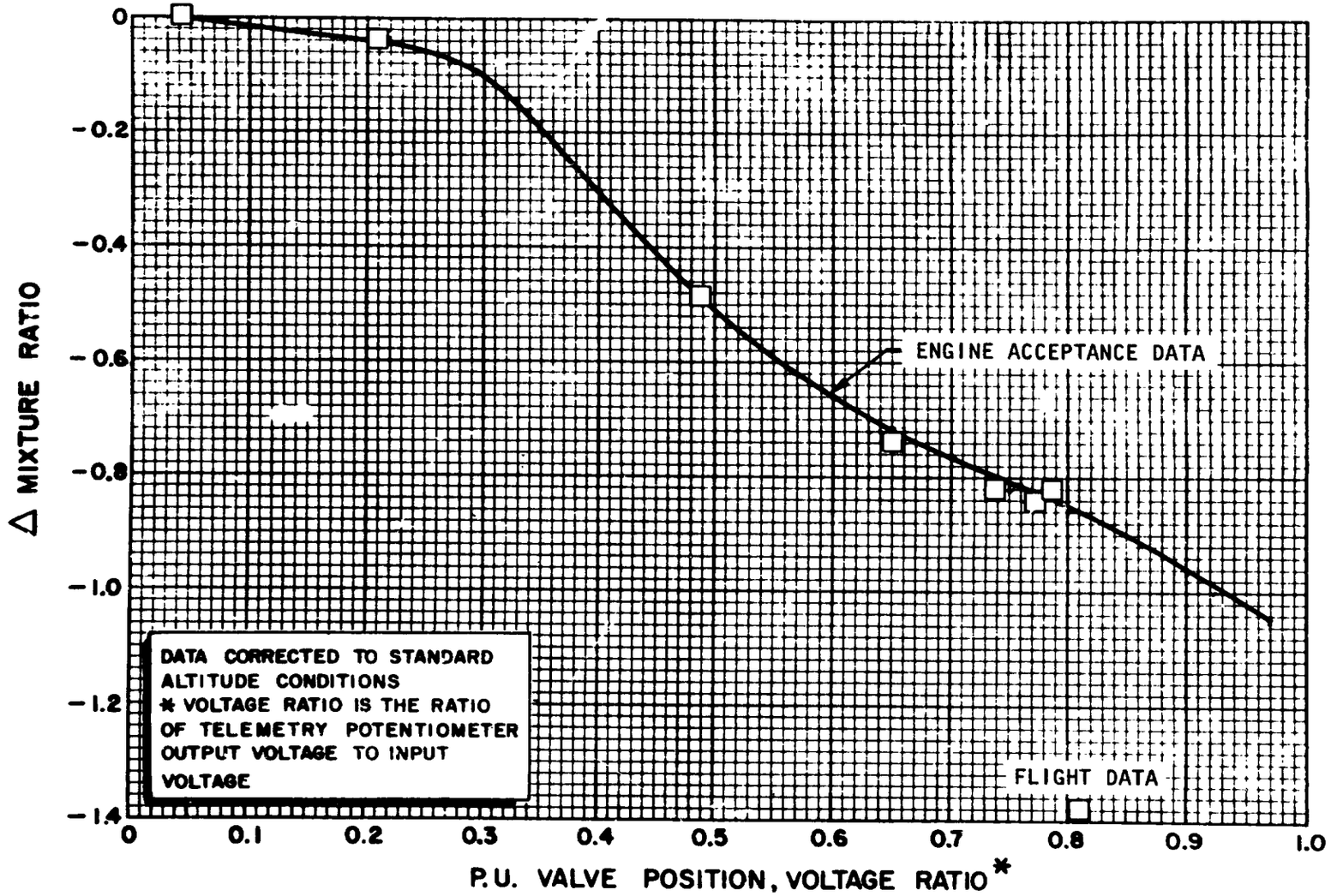

R-7450-1

Figure 56. Mixture Ratio Differential vs Propellant Utilization Voltage Ratio, Engine No. 1

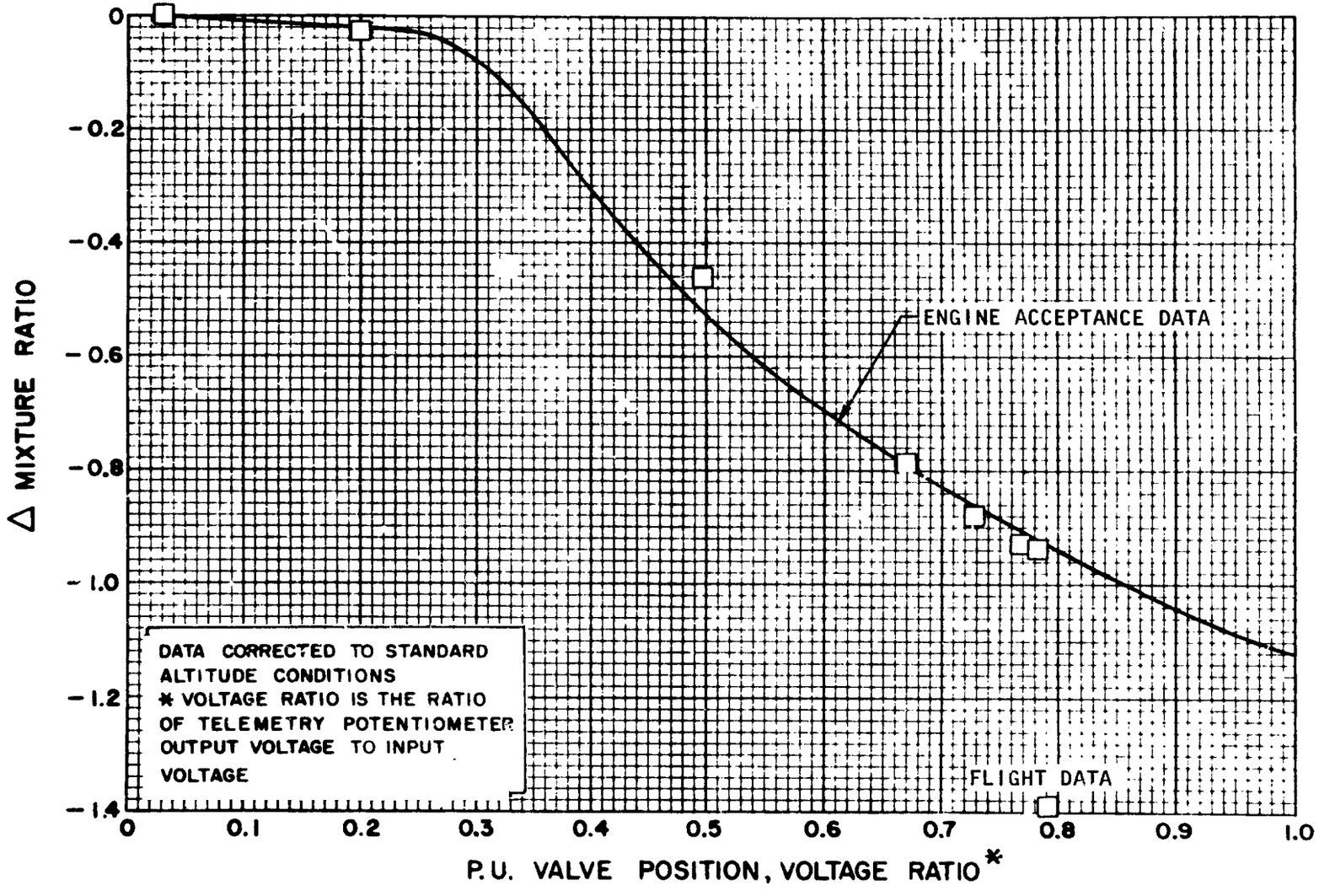

Figure 57. Mixture Ratio Differential vs Propellant Utilization Voltage Ratio, Engine No. 2

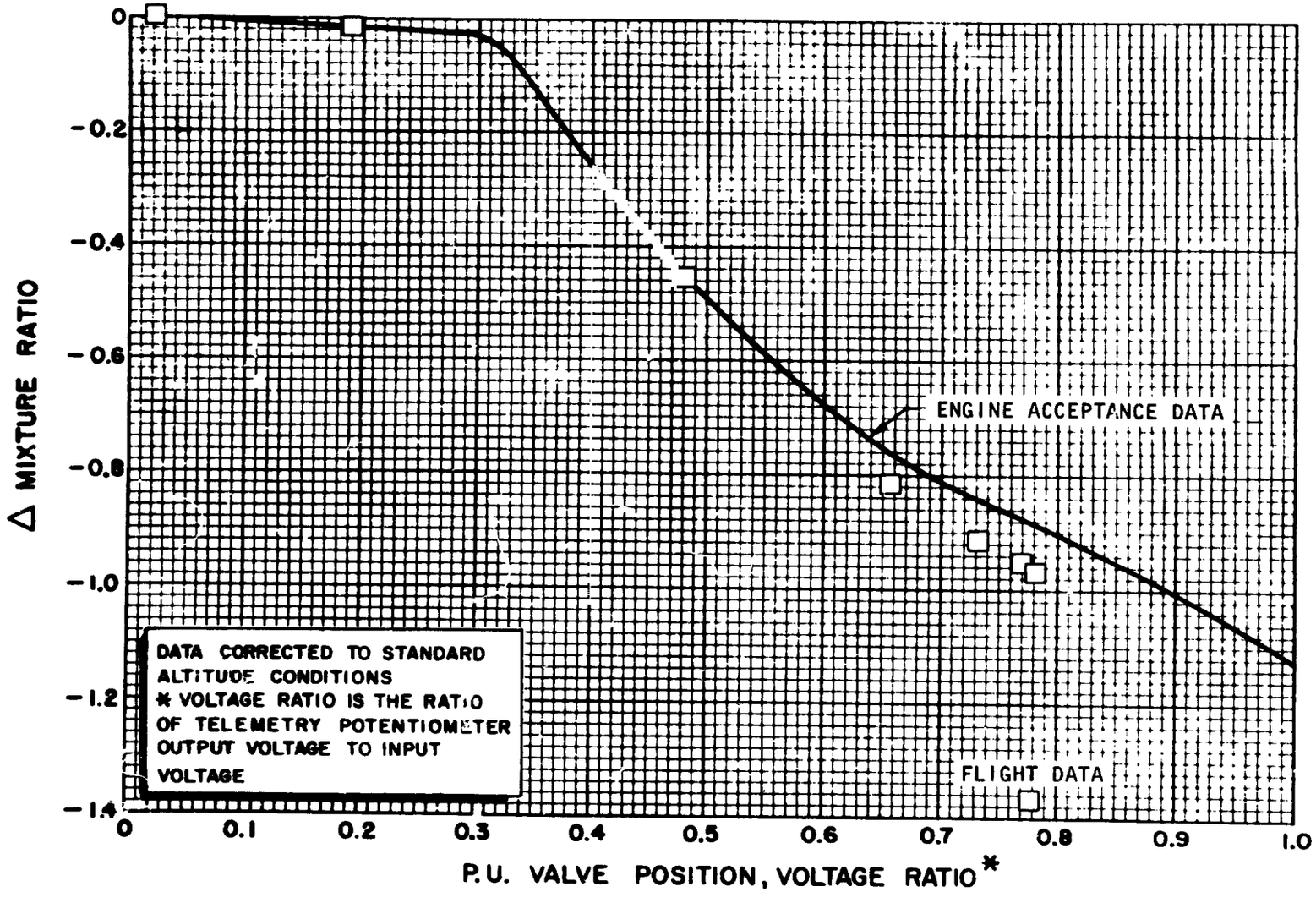

Figure 58. Mixture Ratio Differential vs Propellant Utilization Voltage Ratio, Engine No. 3

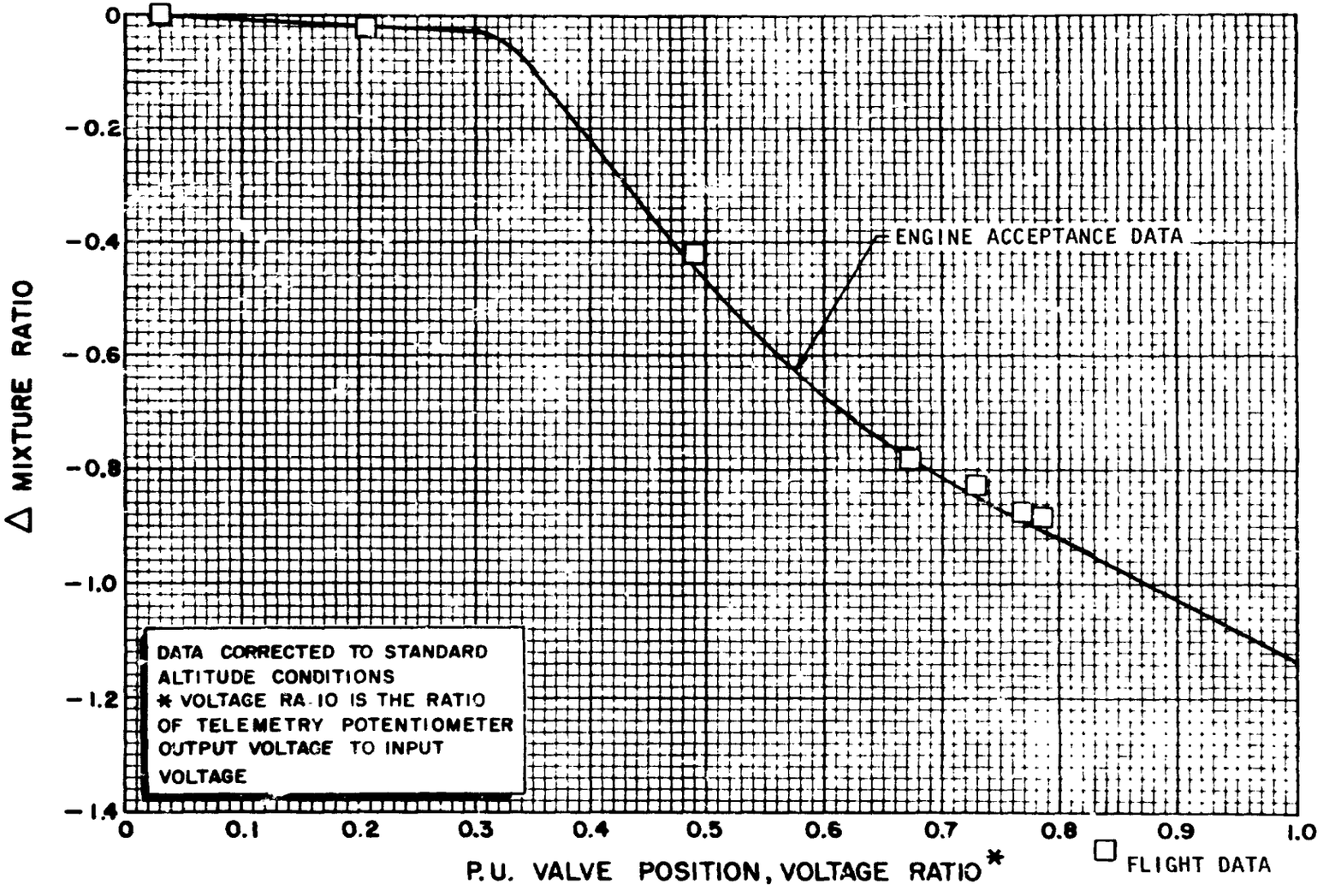

Figure 59. Mixture Ratio Differential vs Propellant Utilization Voltage Ratio, Engine No. 4

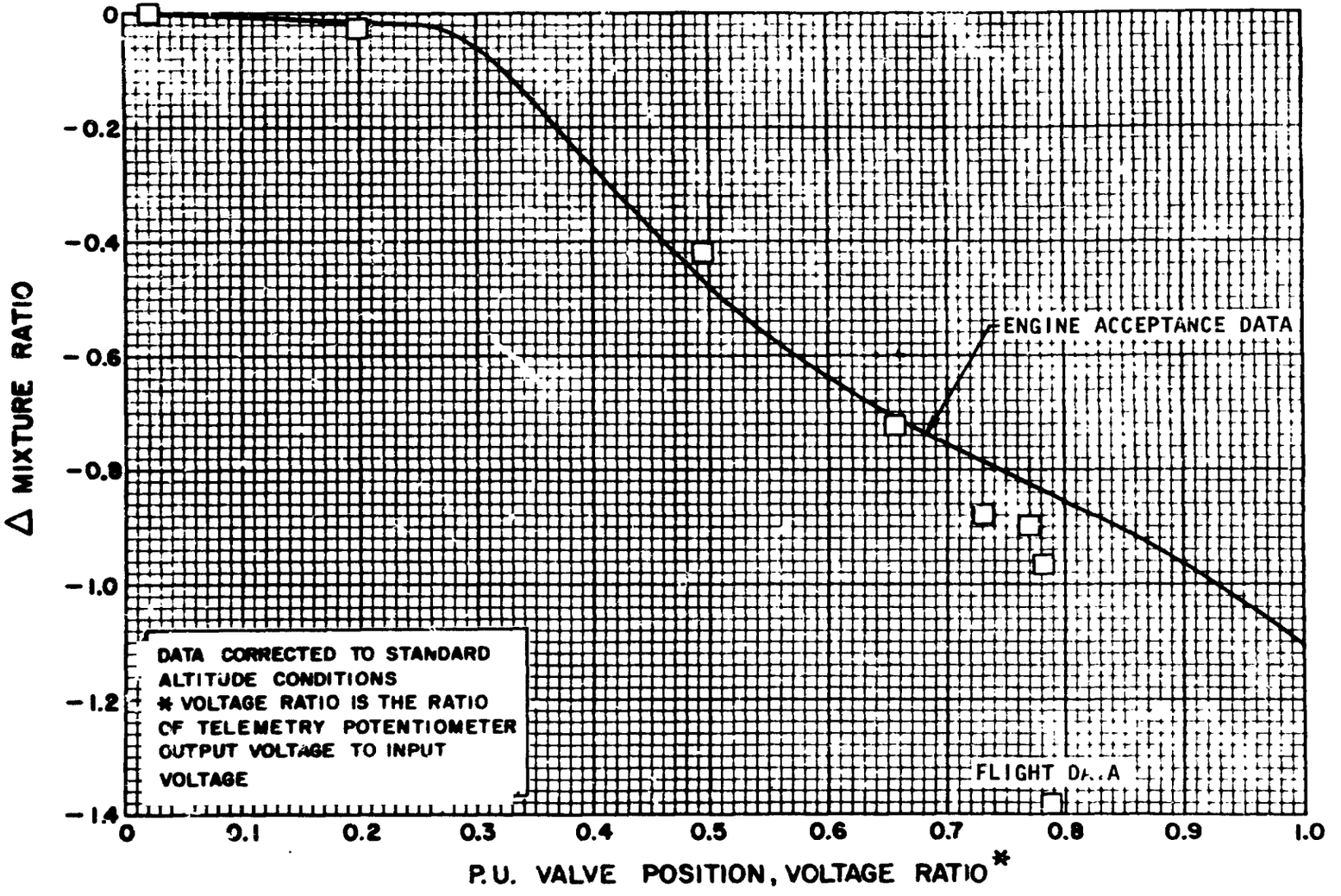

Figure 60. Mixture Ratio Differential vs Propellant Utilization Voltage Ratio, Engine No. 5

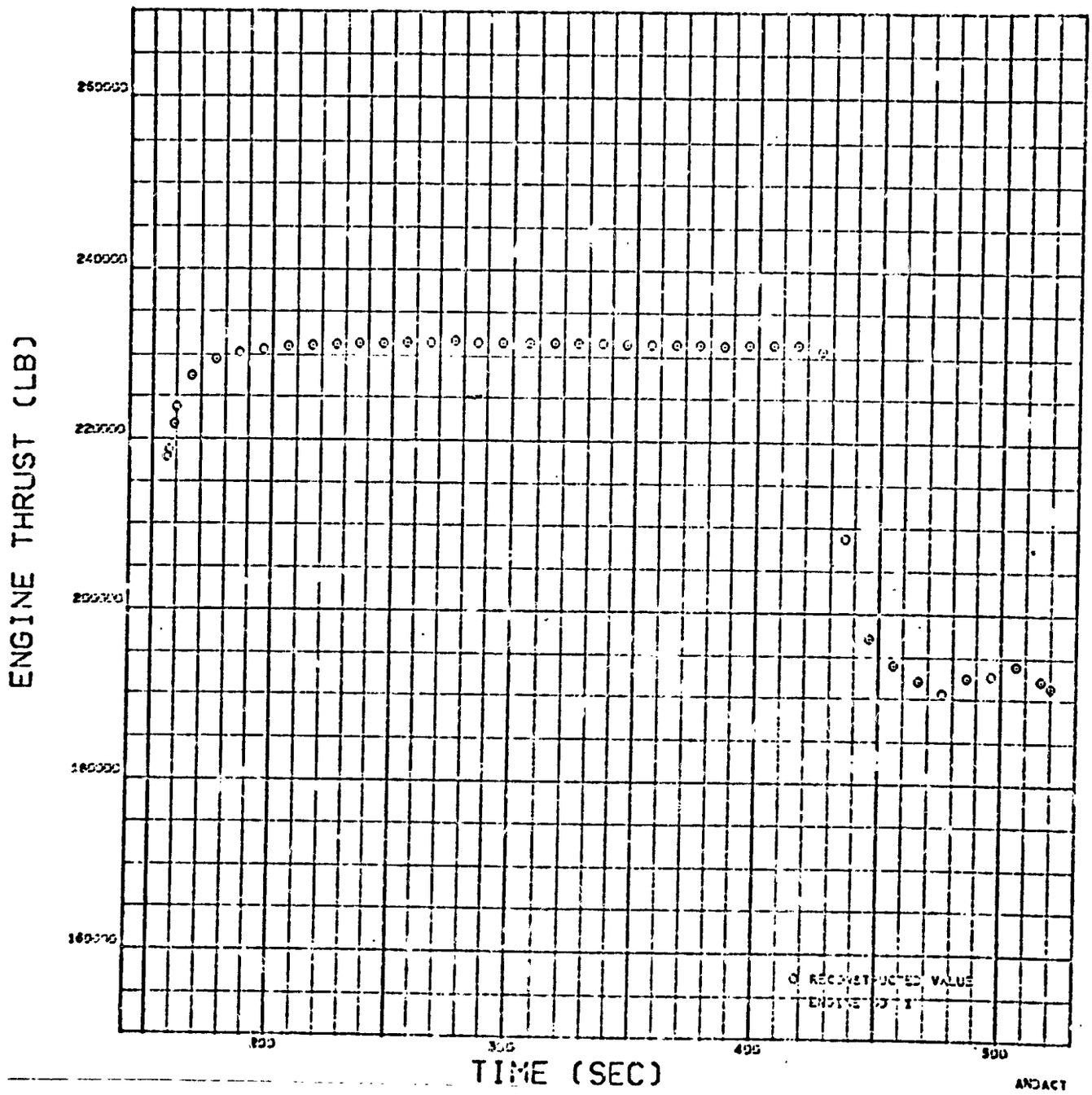

Figure 61. Engine No. 1 Thrust

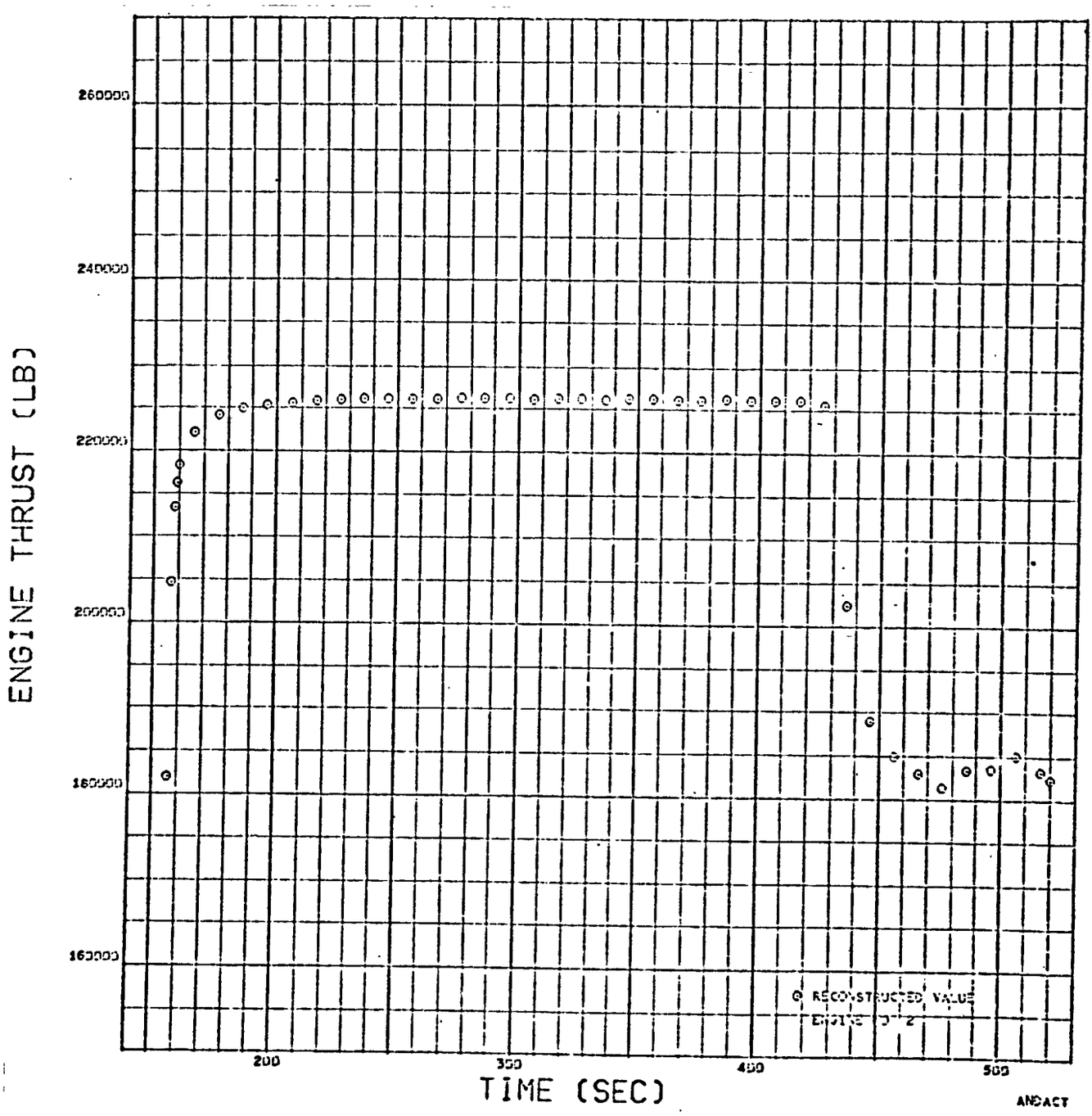

Figure 62. Engine No. 2 Thrust

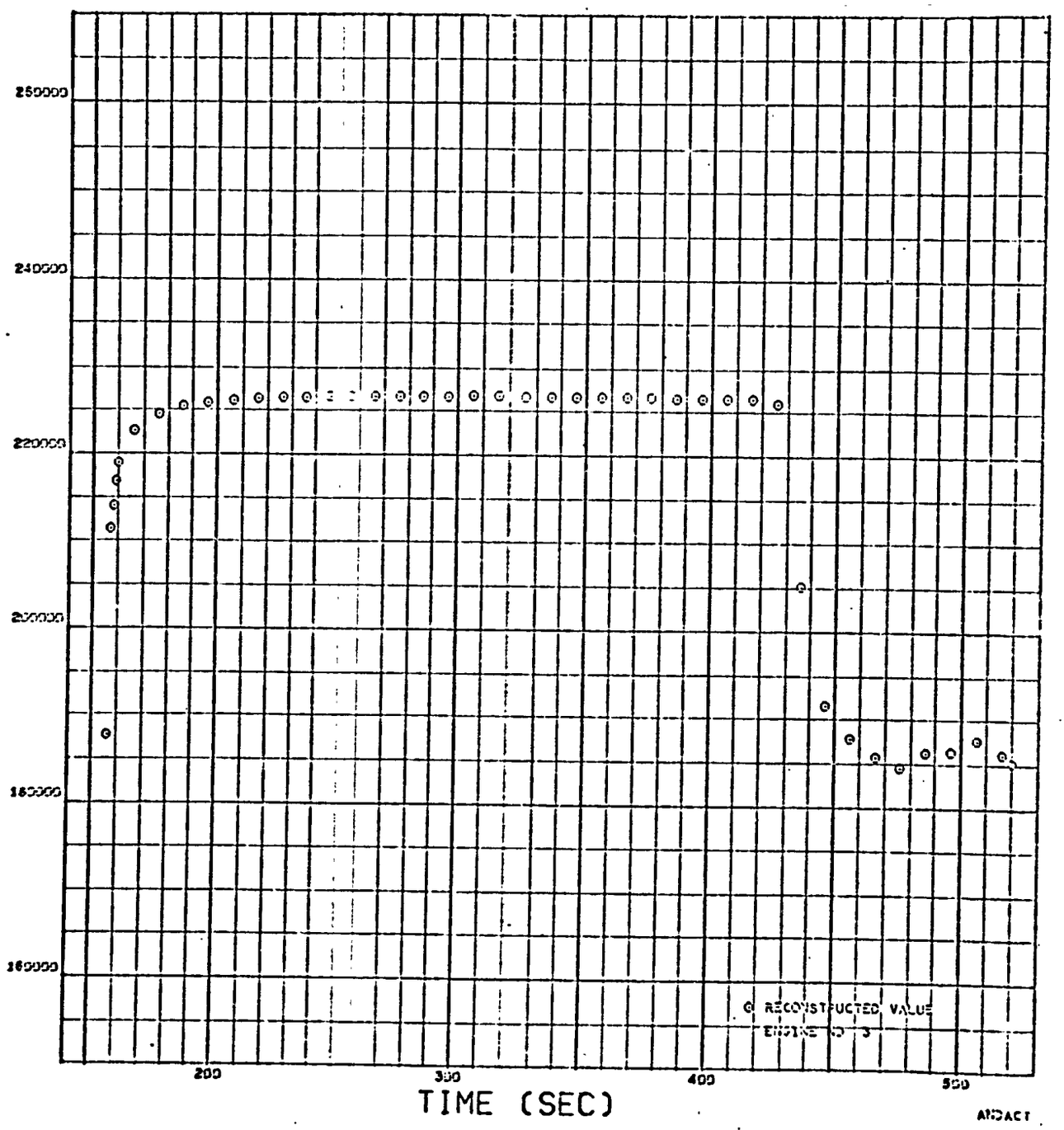

Figure 63. Engine No. 3 Thrust

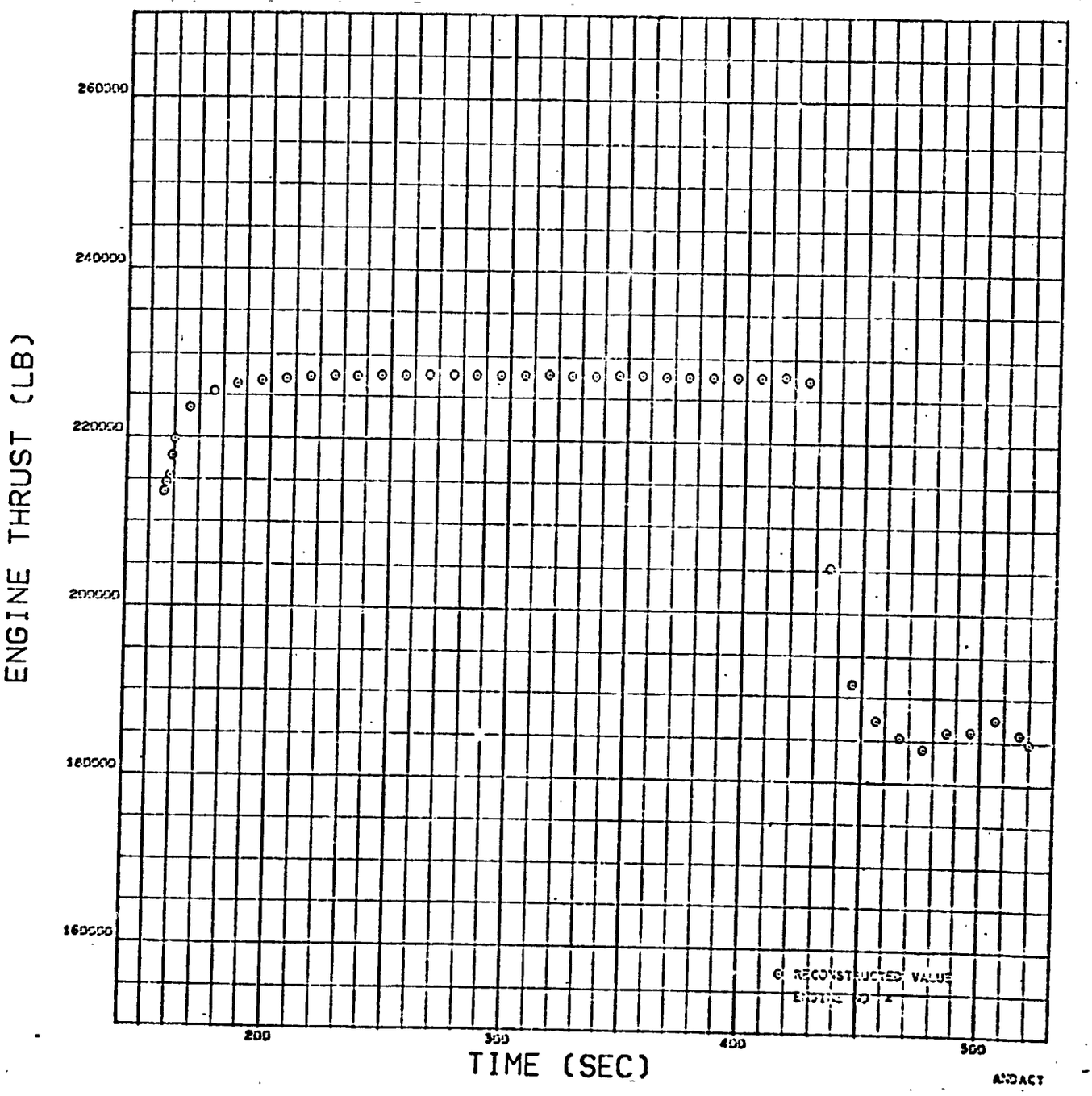

Figure 64. Engine No. 4 Thrust

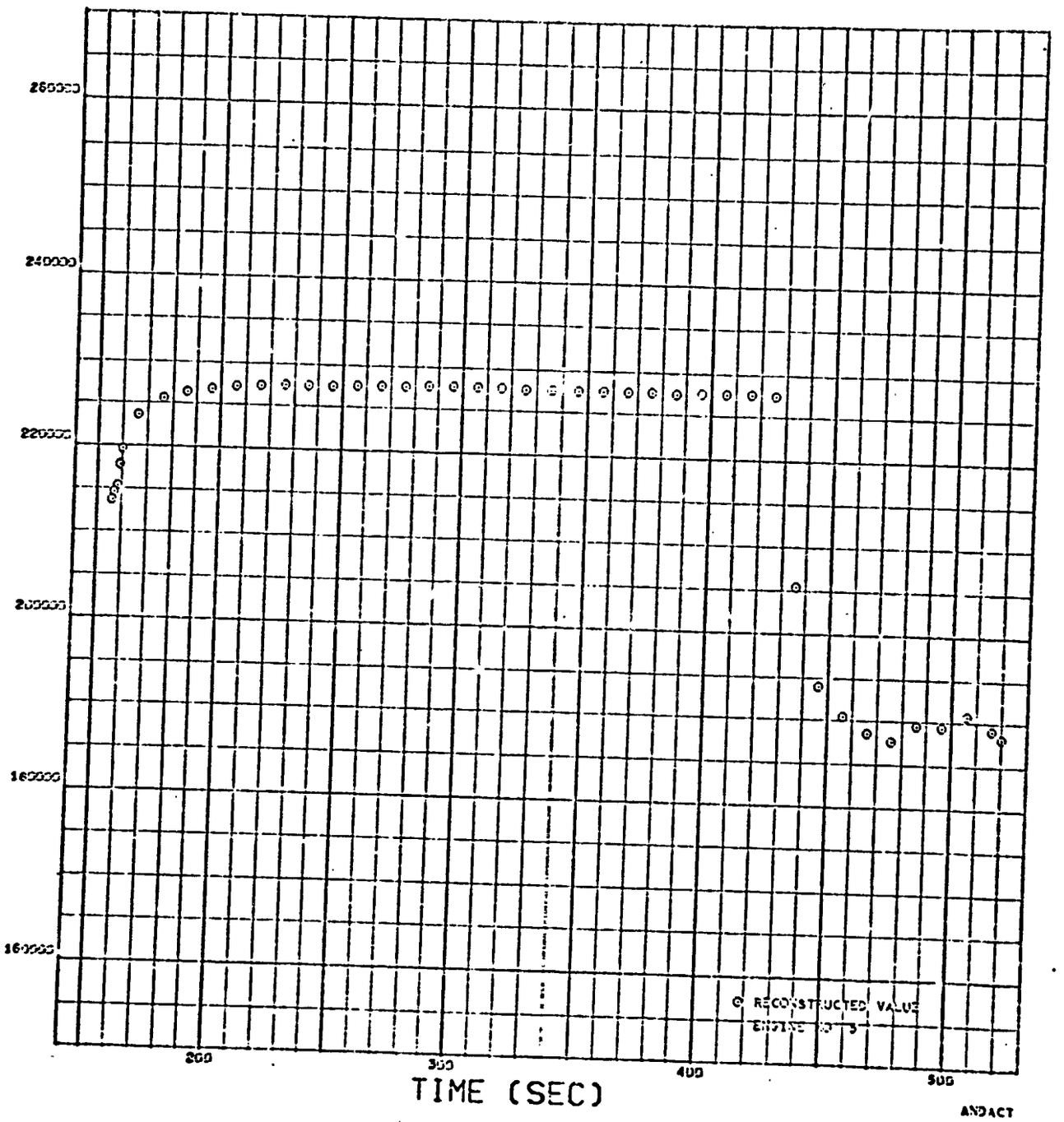

Figure 65. Engine No. 5 Thrust

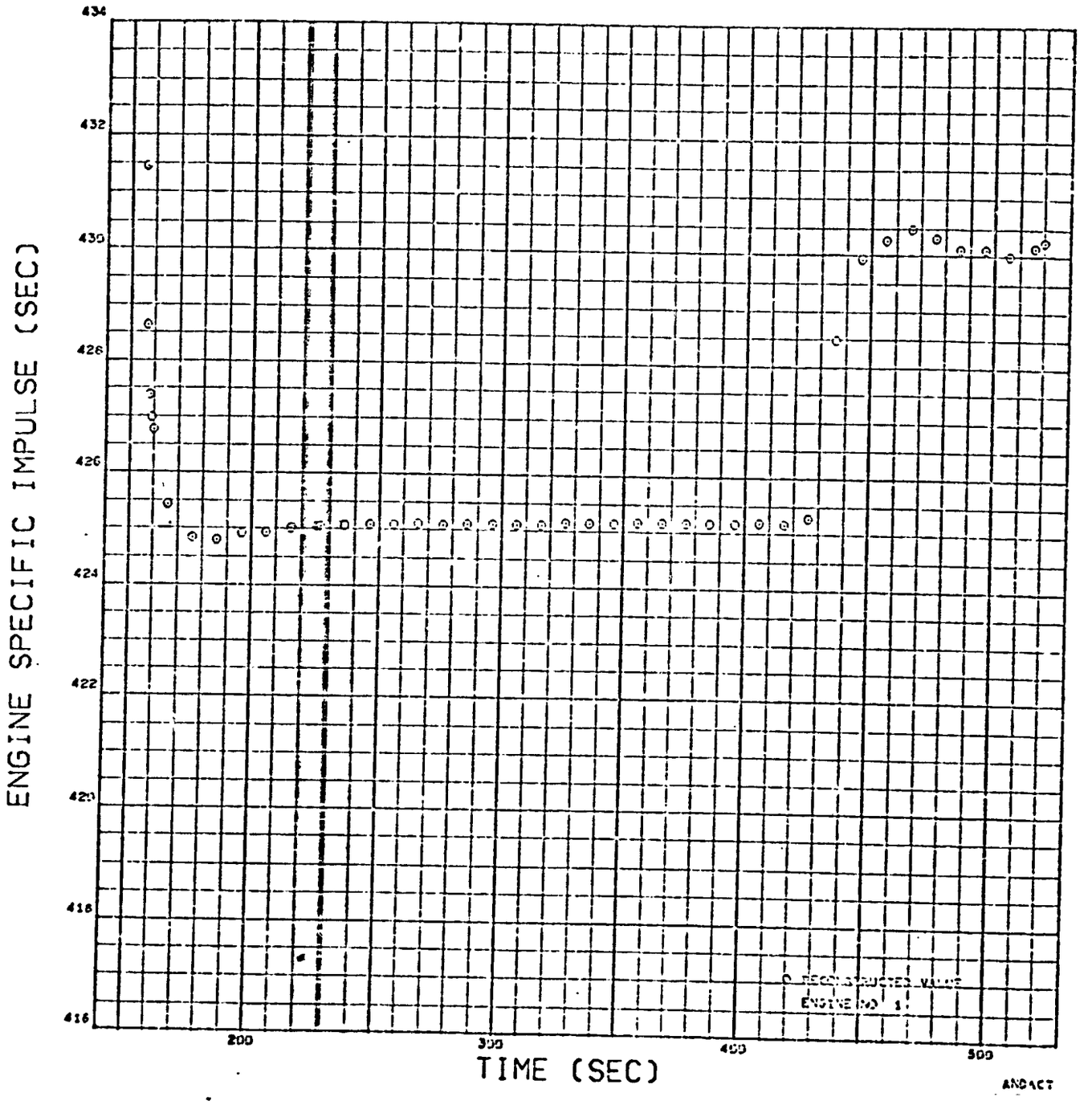

Figure 66. Engine No. 1 Specific Impulse

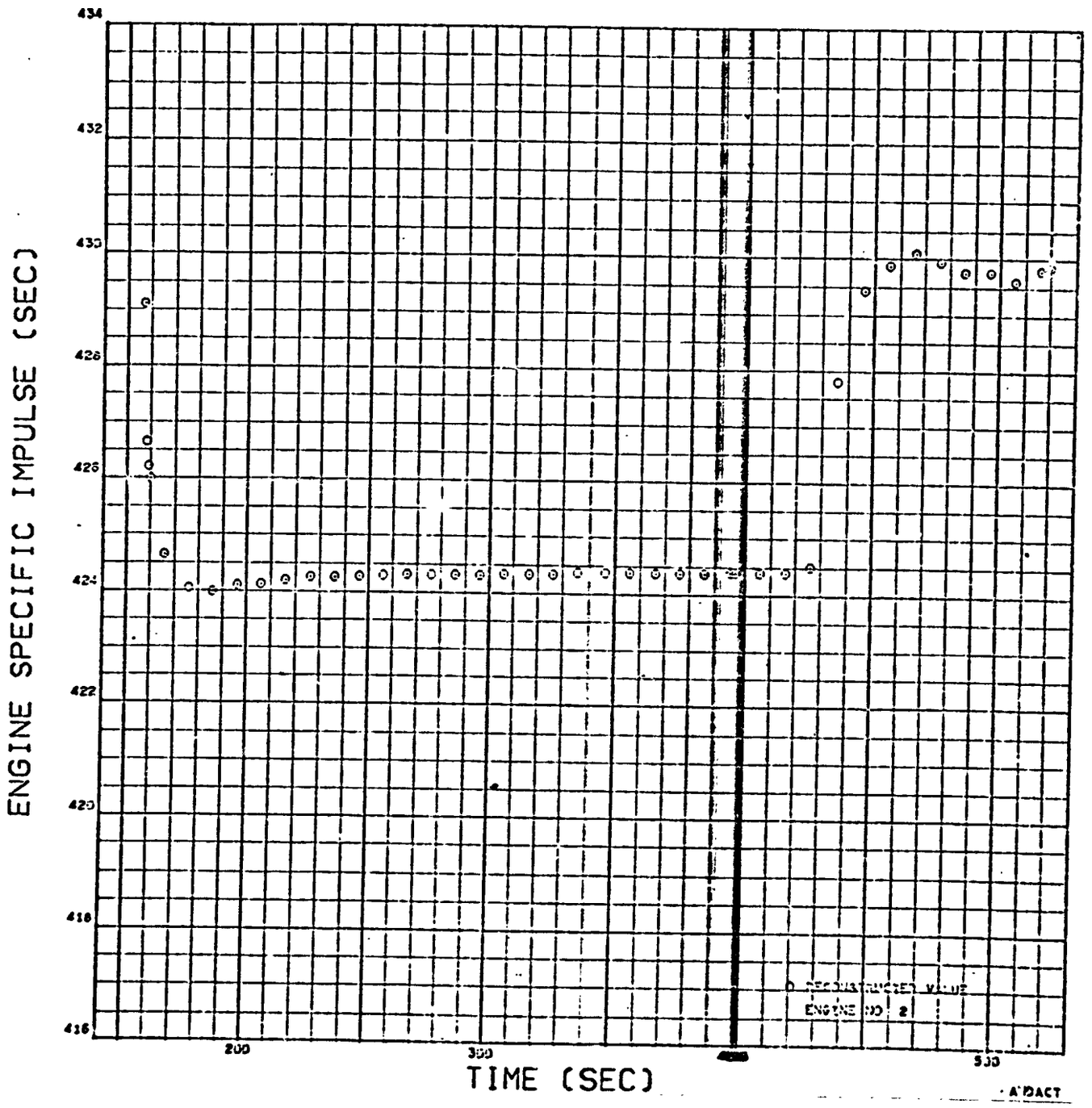

Figure 67. Engine No. 2 Specific Impulse

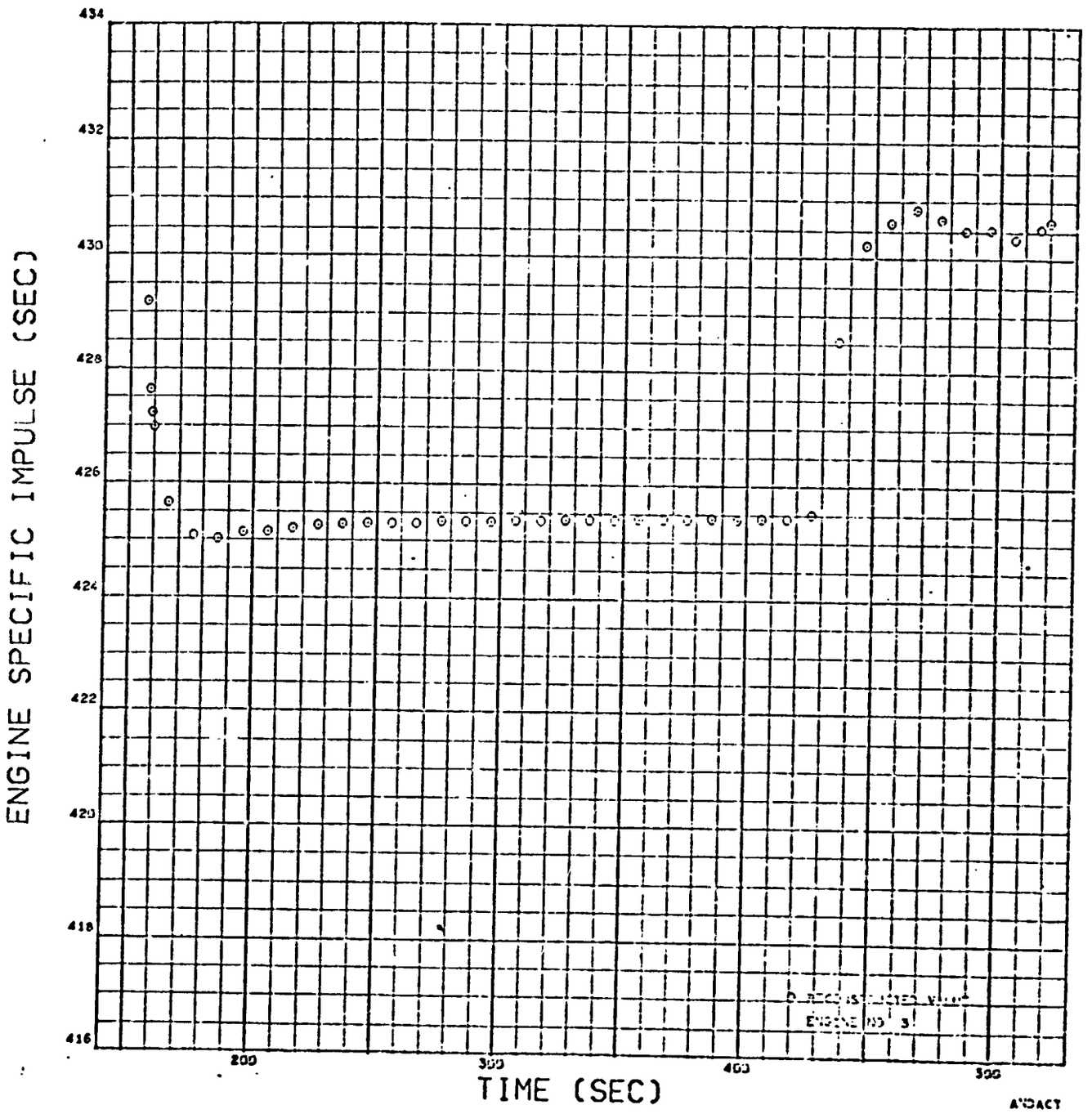

Figure 68. Engine No. 3 Specific Impulse

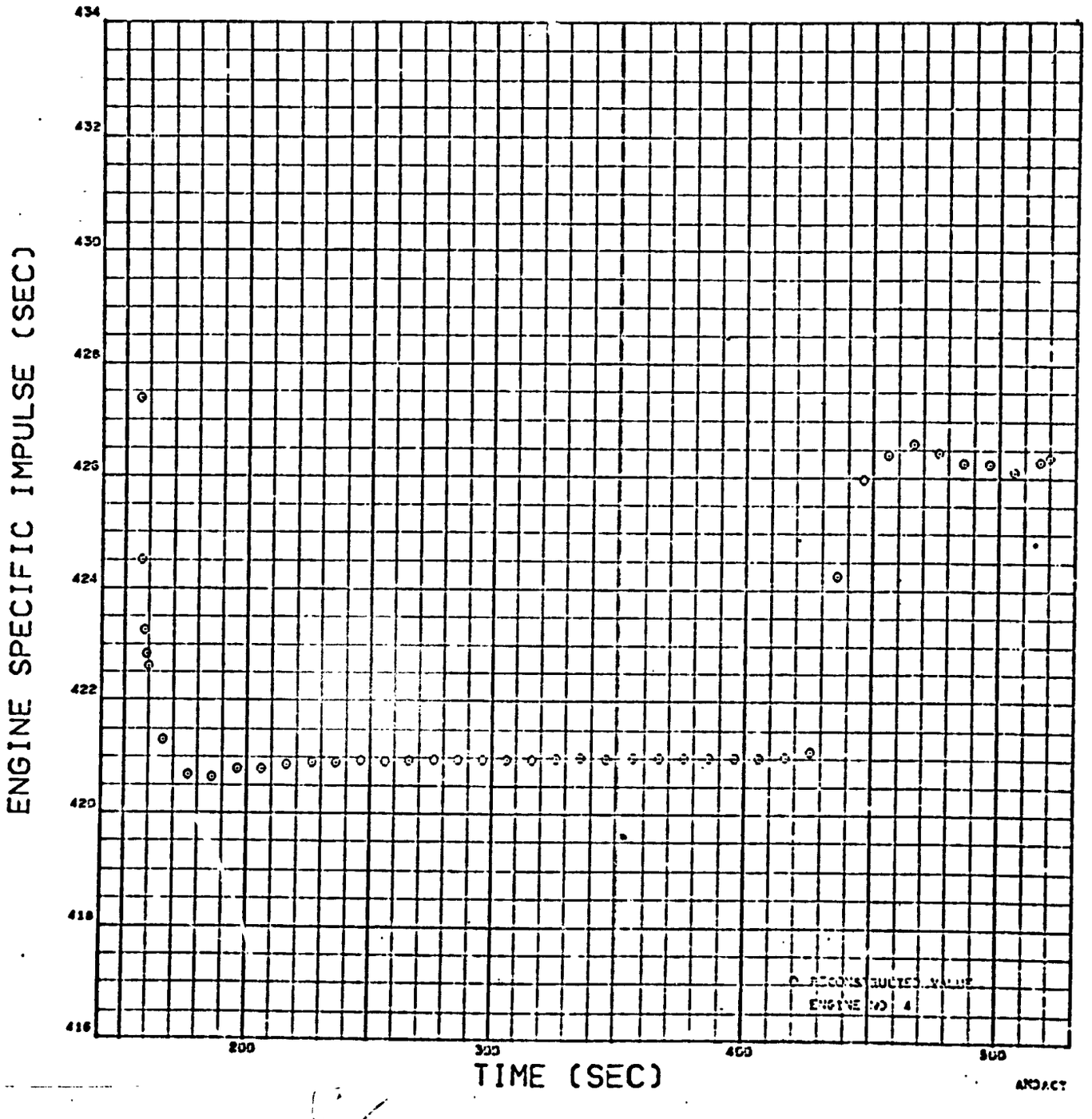

Figure 69. Engine No. 4 Specific Impulse

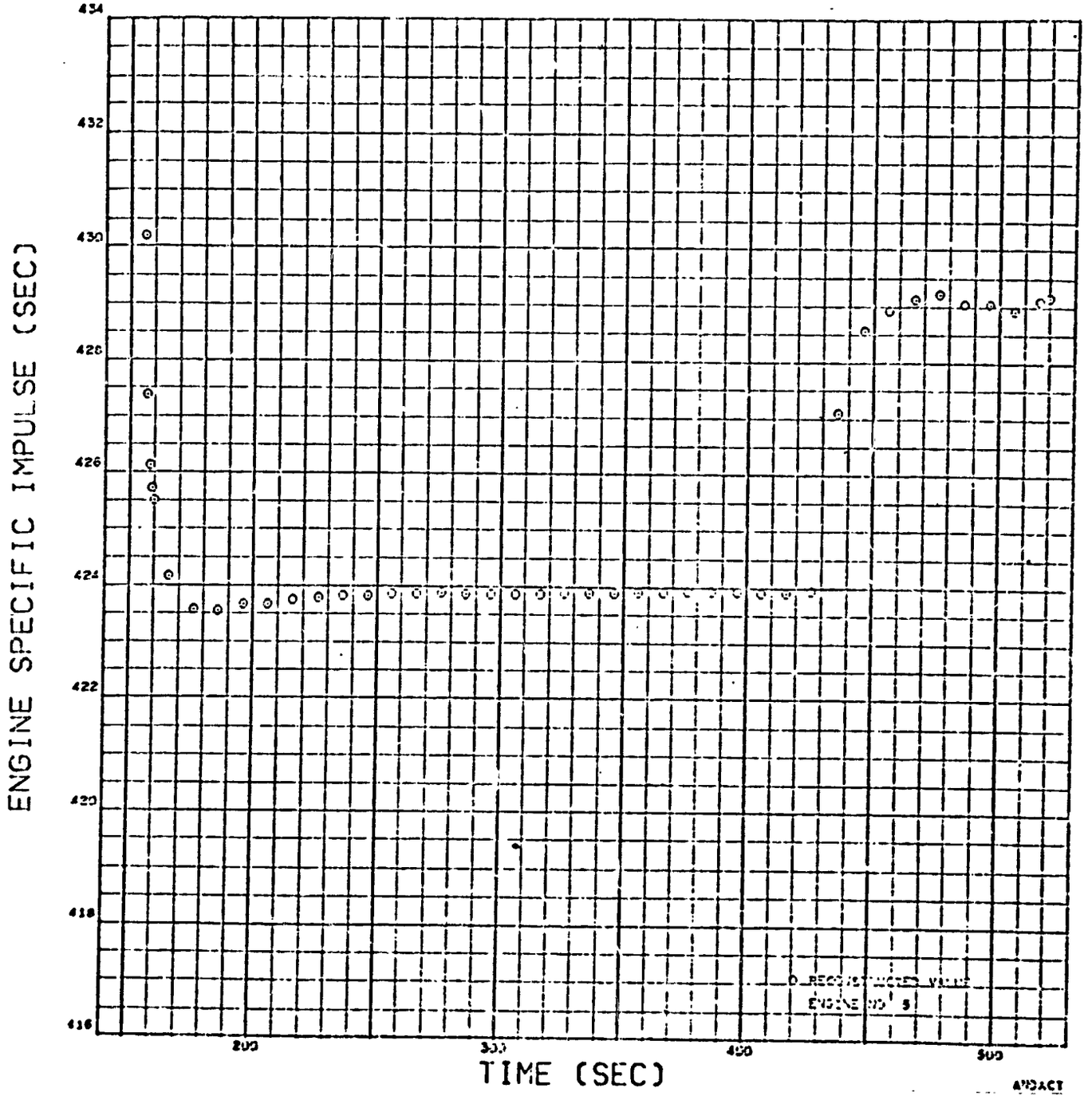

Figure 70. Engine No. 5 Specific Impulse

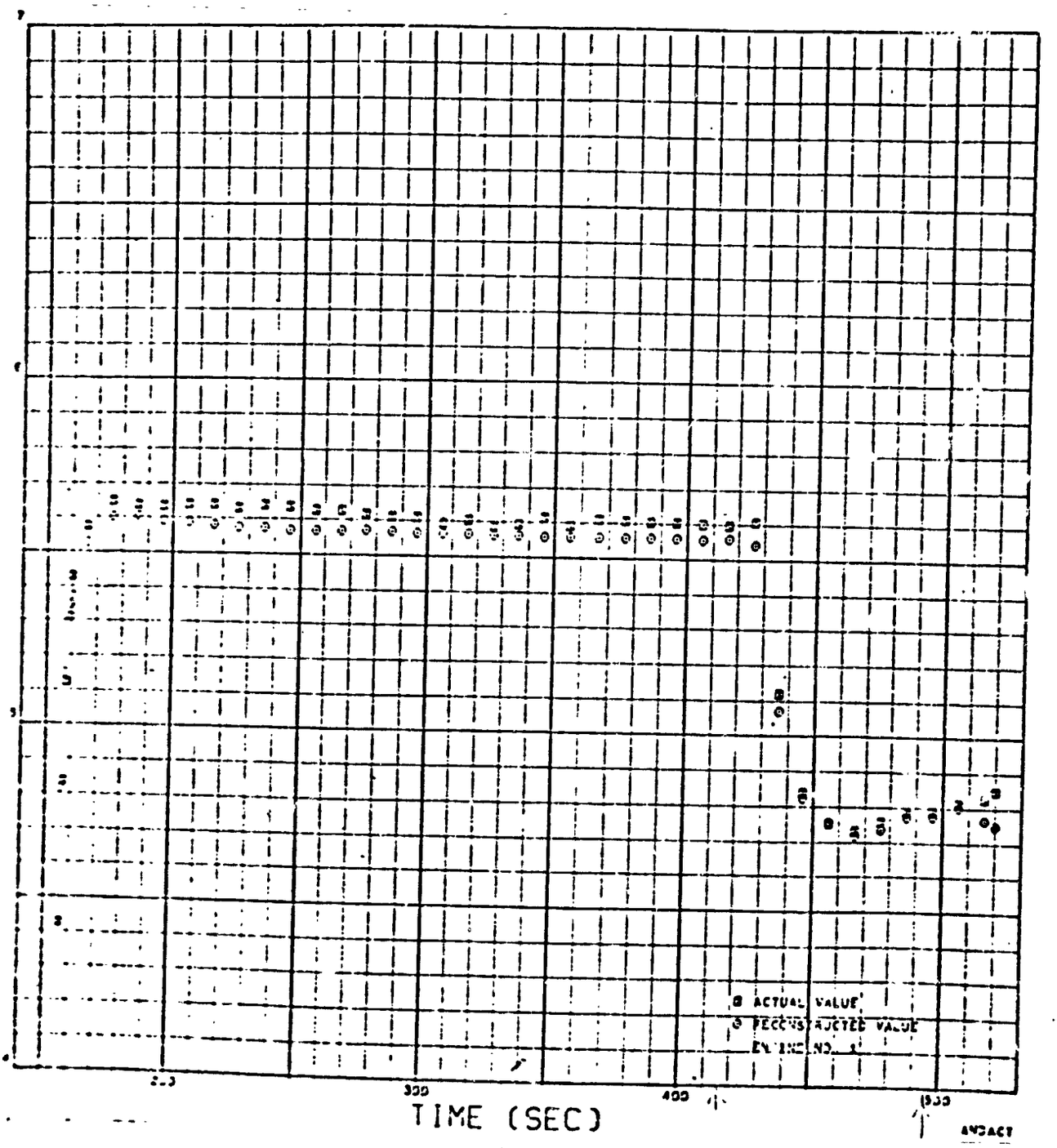

Figure 71. Engine No. 1 Mixture Ratio

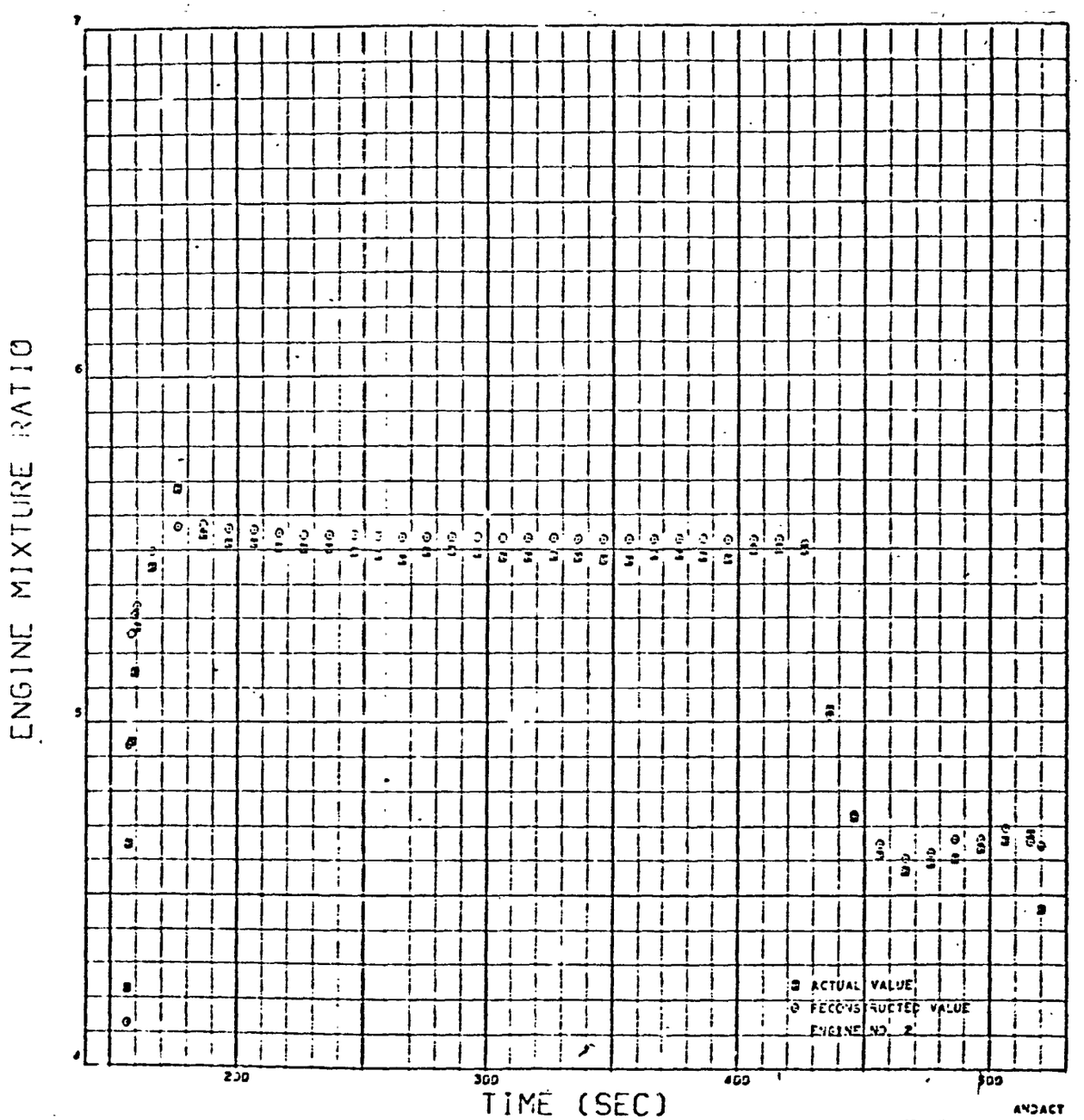

Figure 72. Engine No. 2 Mixture Ratio

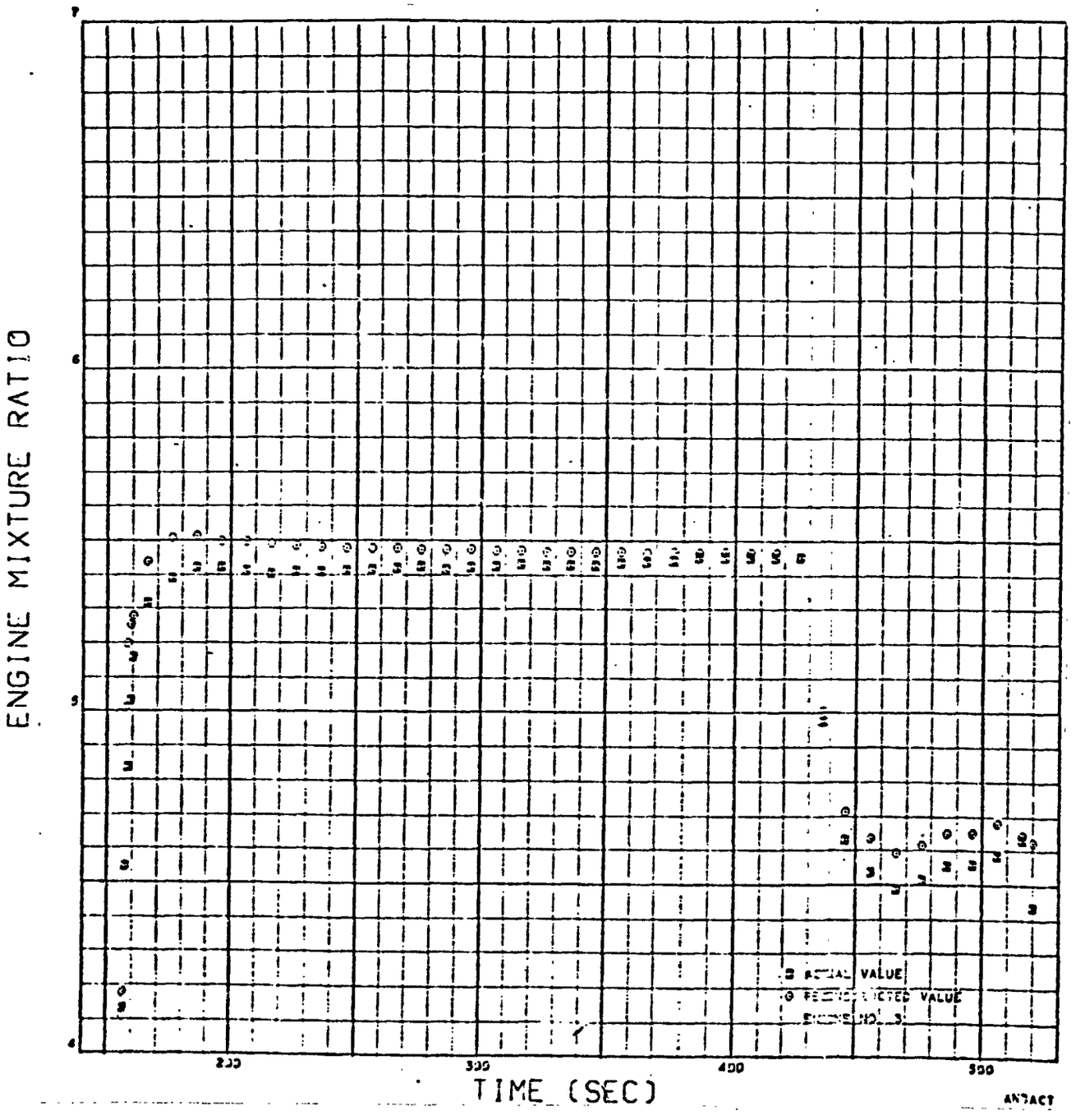

Figure 73. Engine No. 3 Mixture Ratio

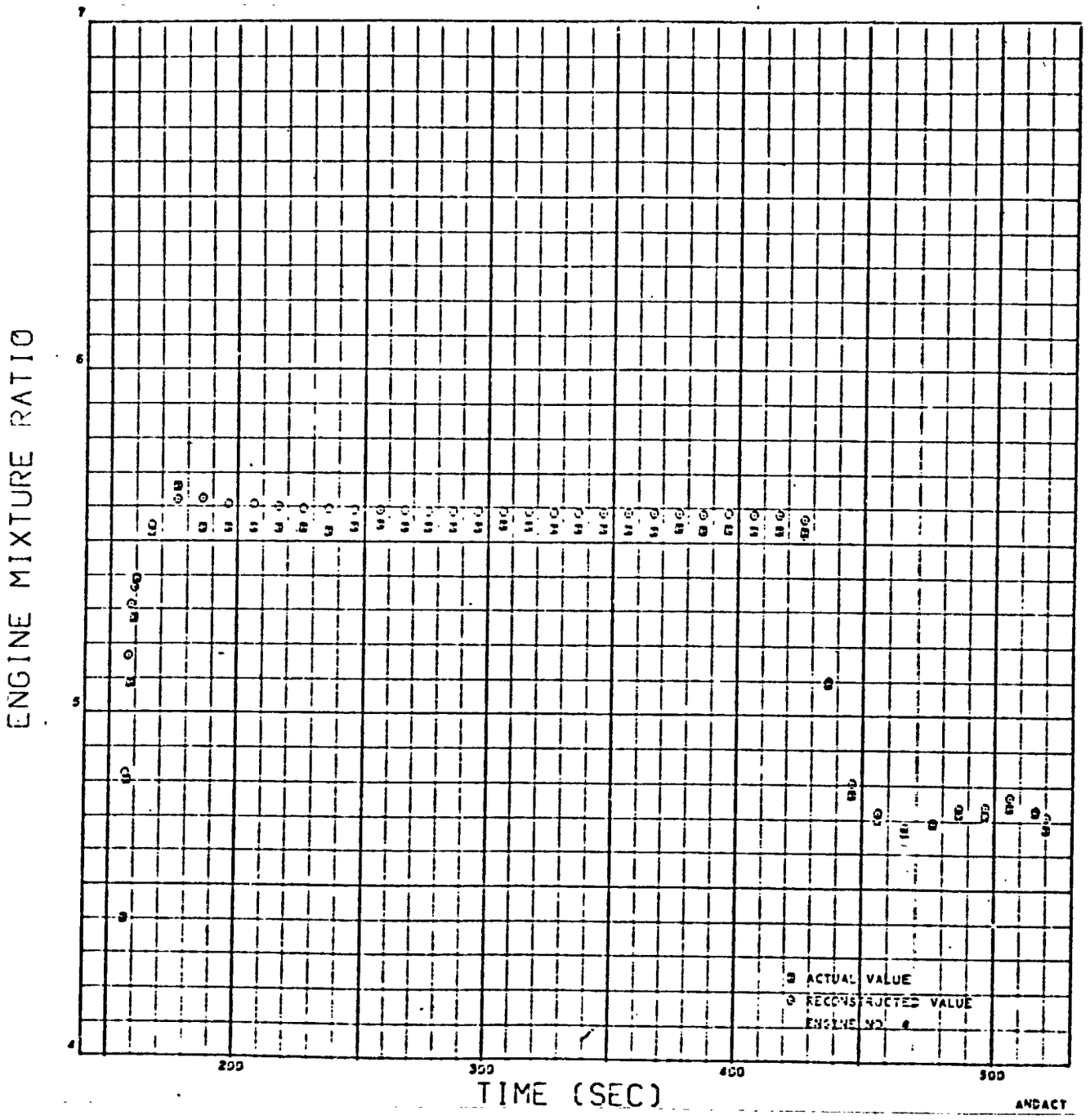

Figure 74. Engine No. 4 Mixture Ratio

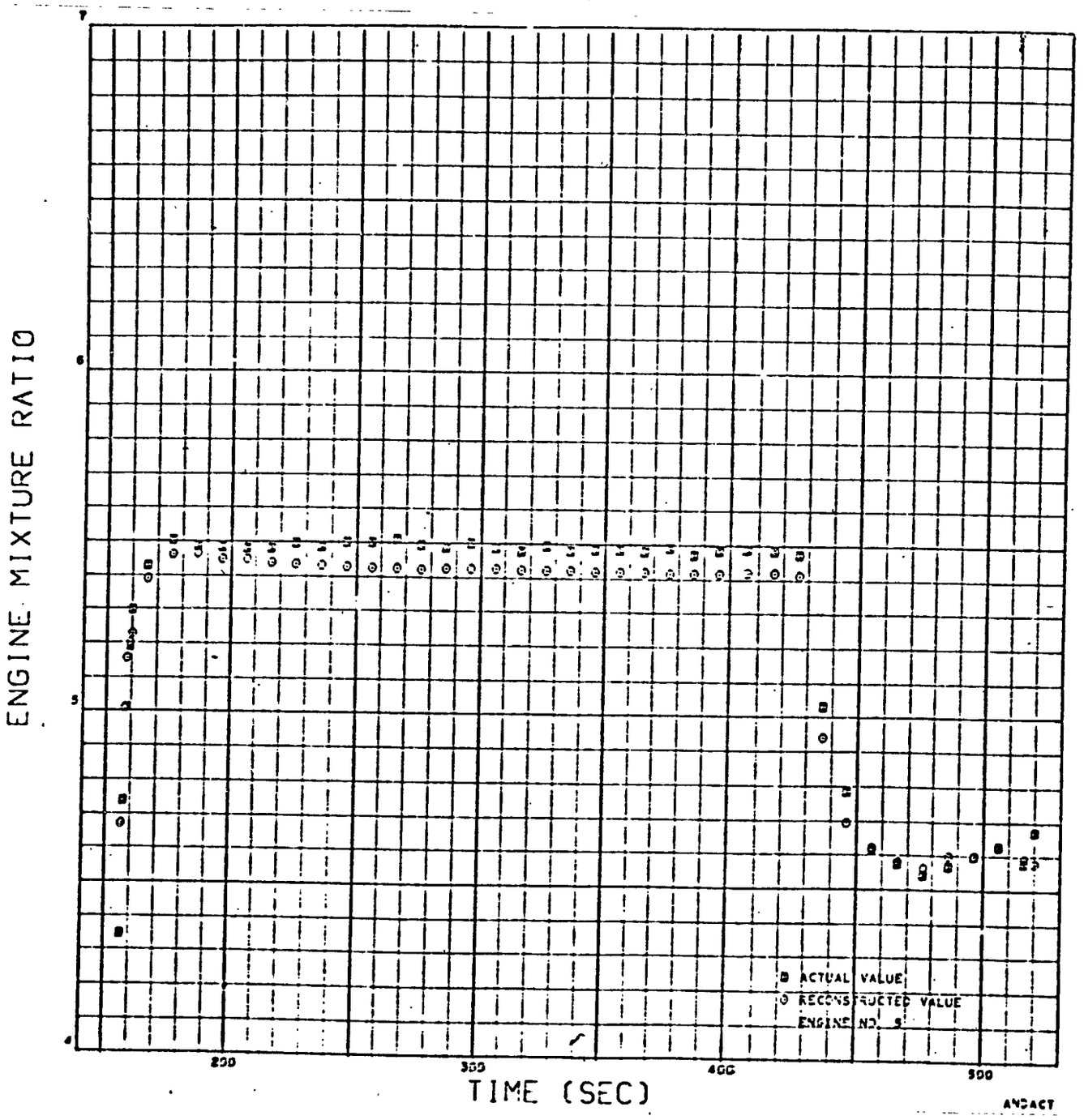

Figure 75. Engine No. 5 Mixture Ratio

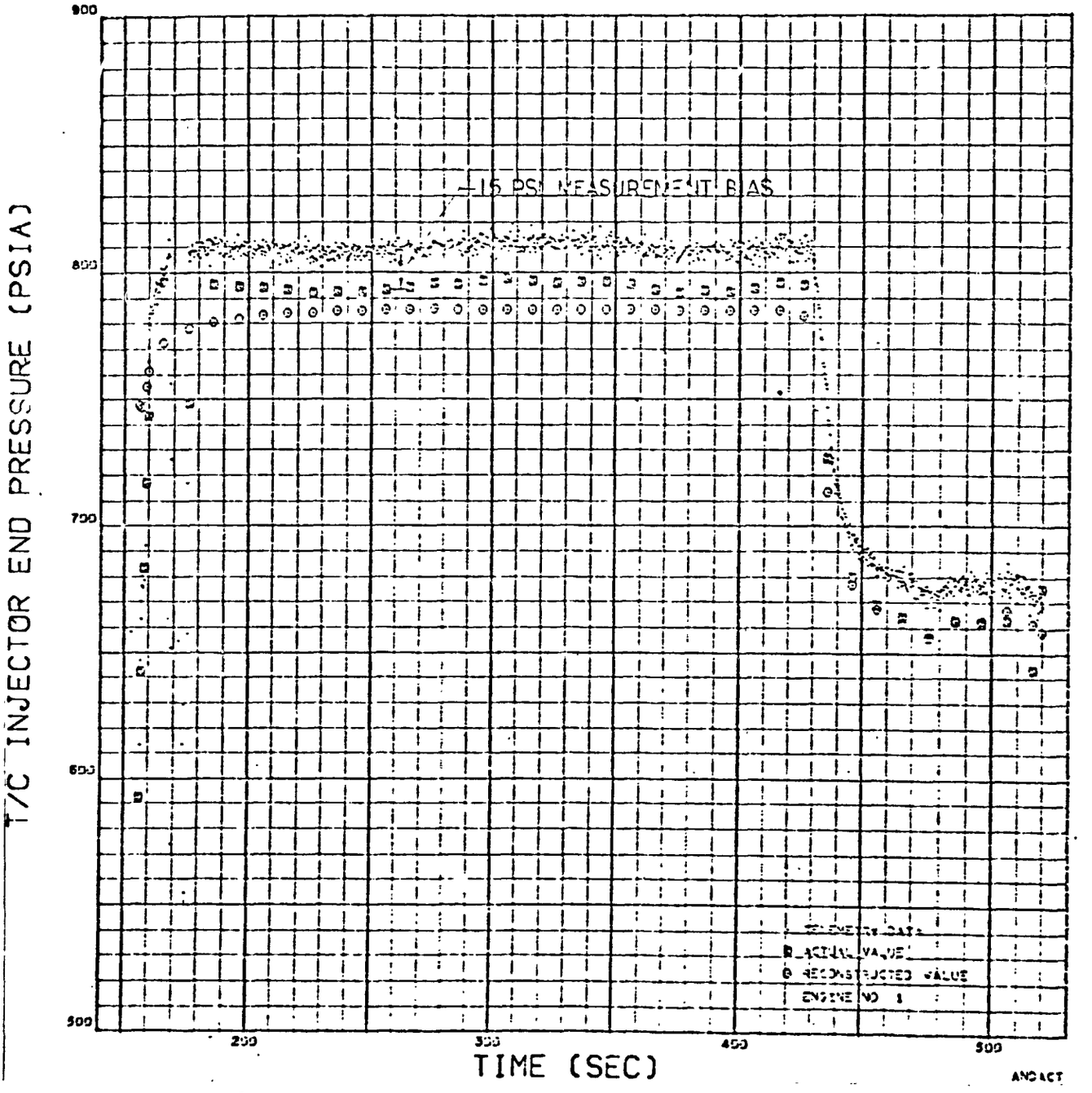

Figure 76. Engine No. 1 Thrust Chamber Injector End Pressure

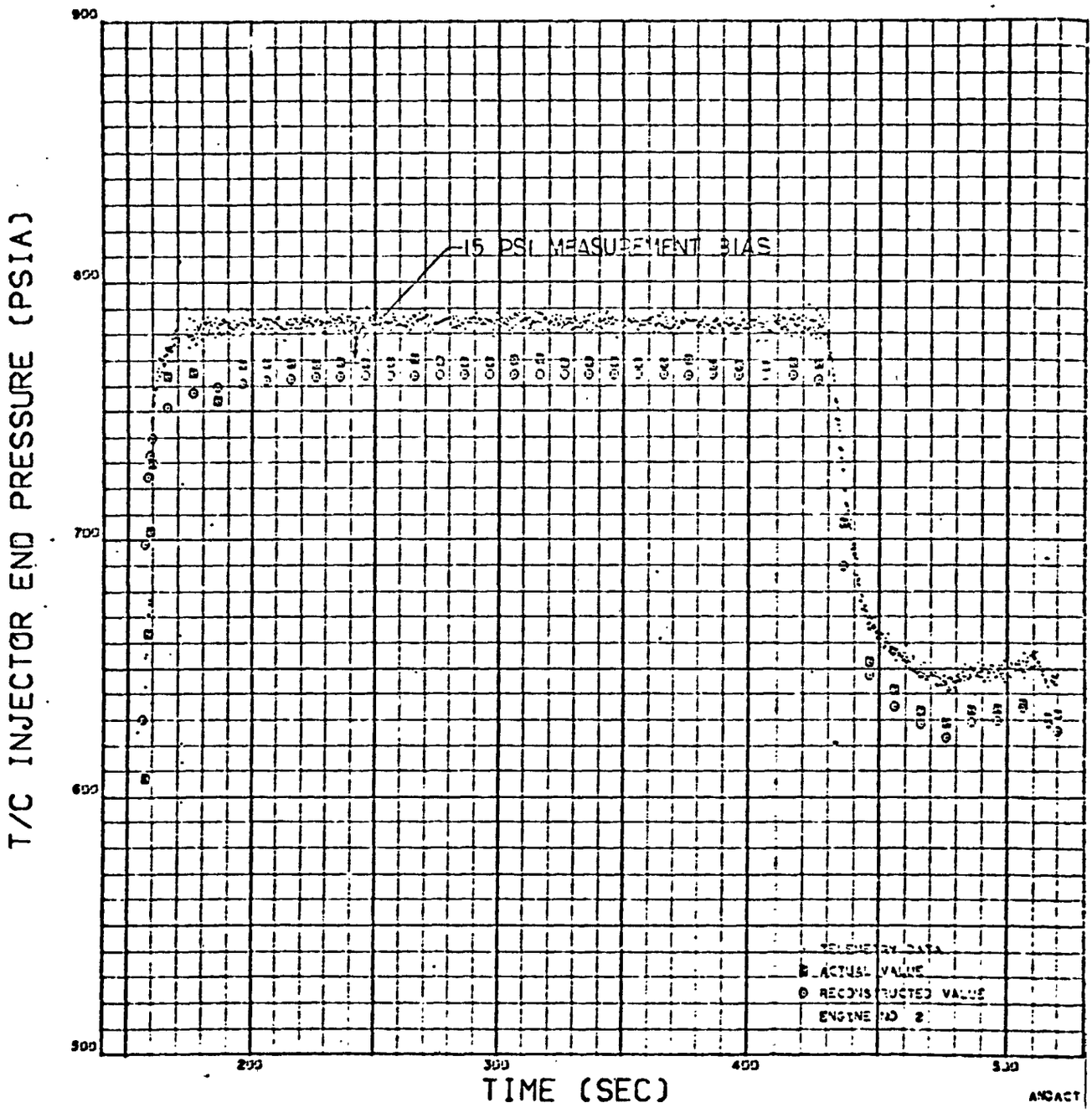

Figure 77. Engine No. 2 Thrust Chamber Injector End Pressure

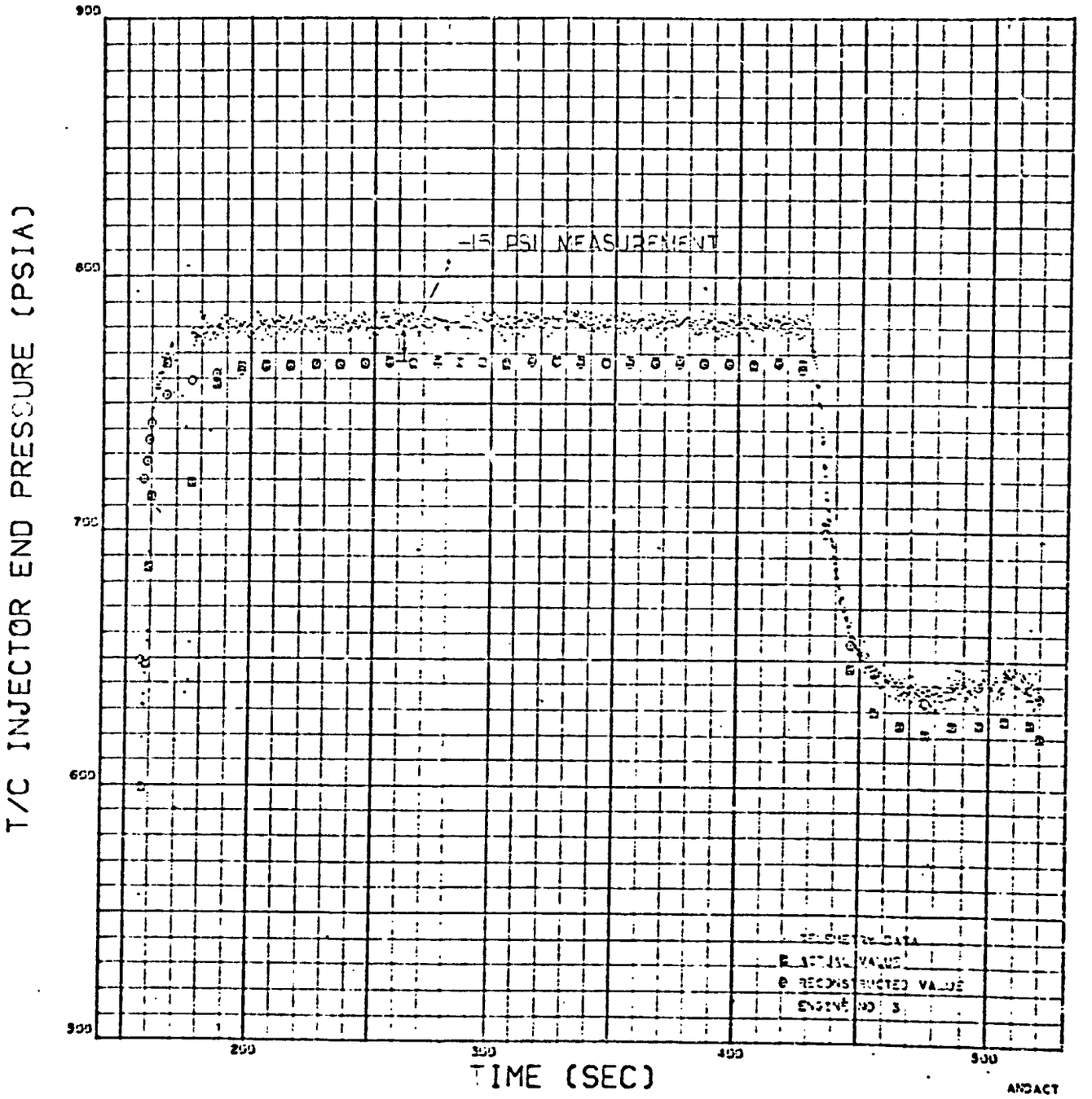

Figure 78. Engine No. 3 Thrust Chamber Injector End Pressure

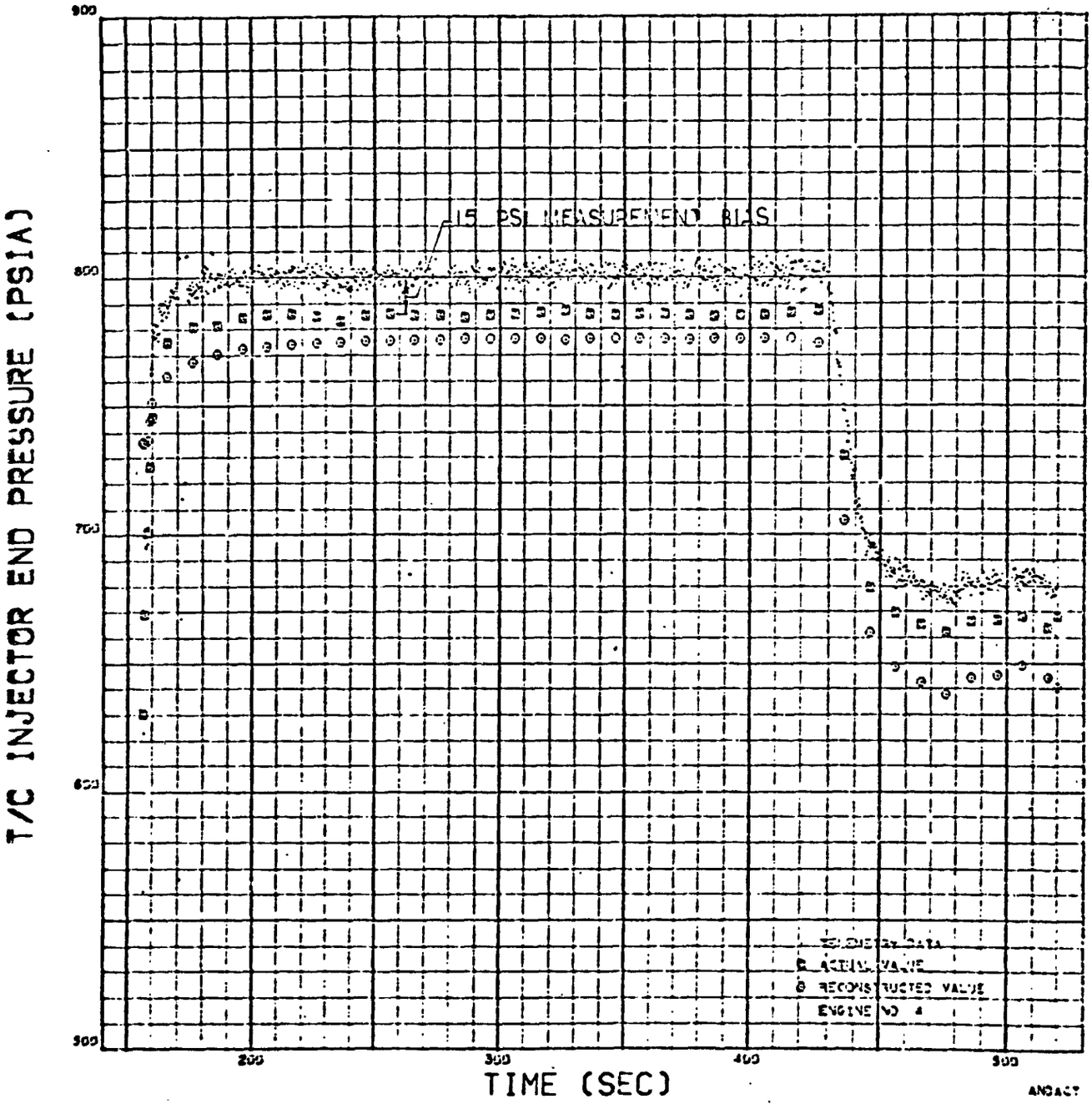

Figure 79. Engine No. 4 Thrust Chamber Injector End Pressure

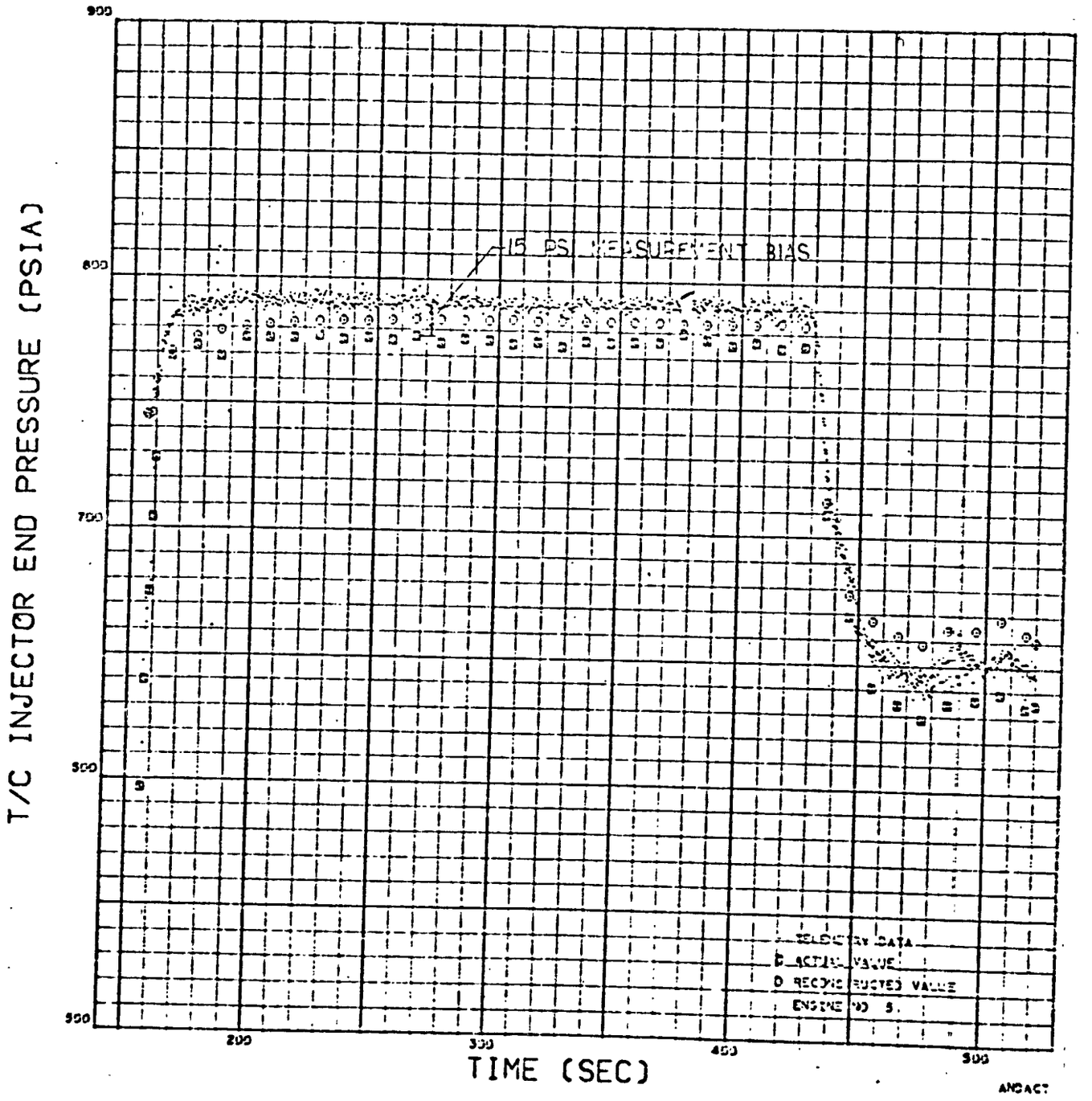

Figure 80. Engine No. 5 Thrust Chamber Injector End Pressure

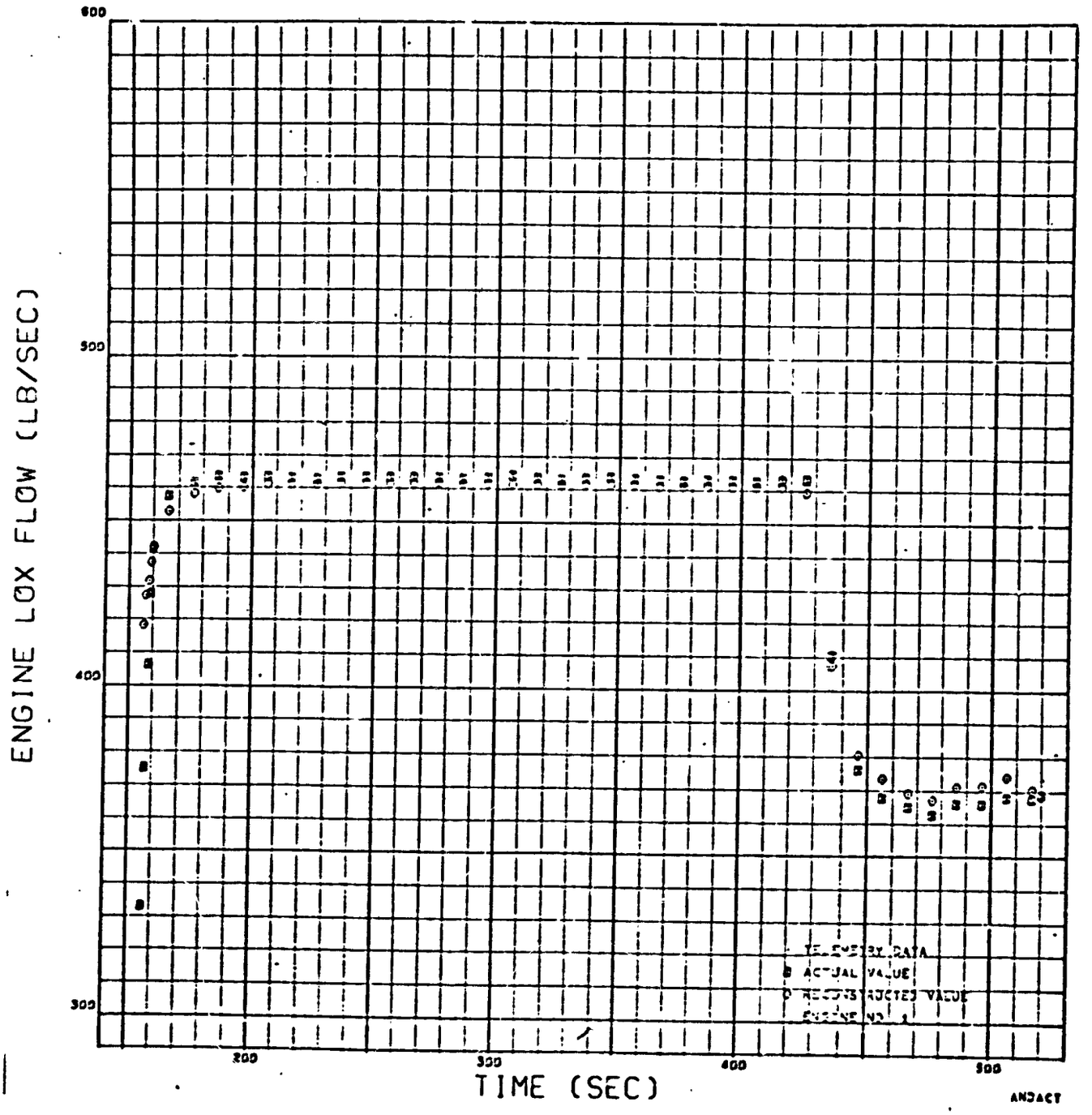

Figure 81. Engine No. 1 Oxidizer Flowrate

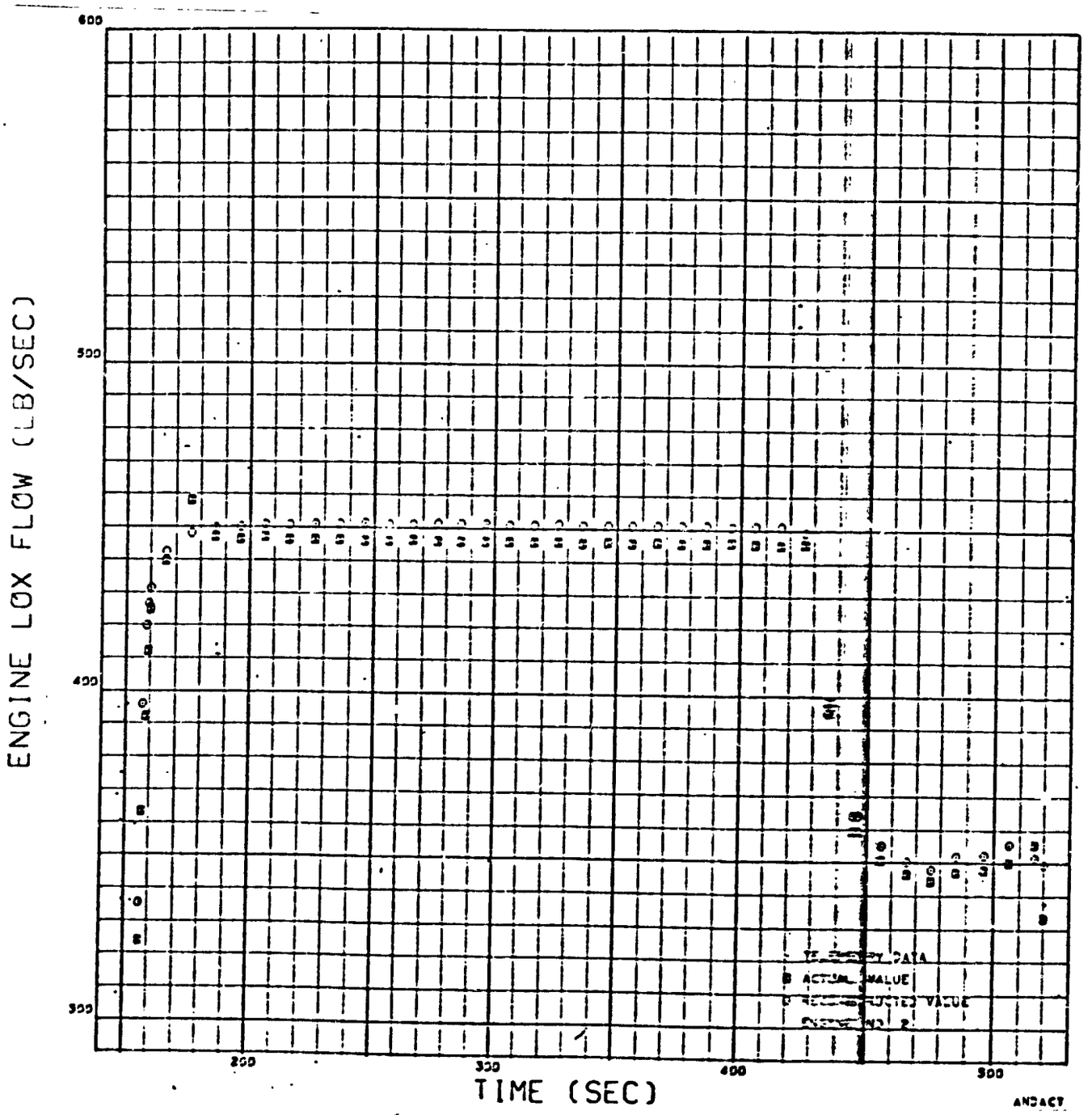

Figure 82. Engine No. 2 Oxidizer Flowrate

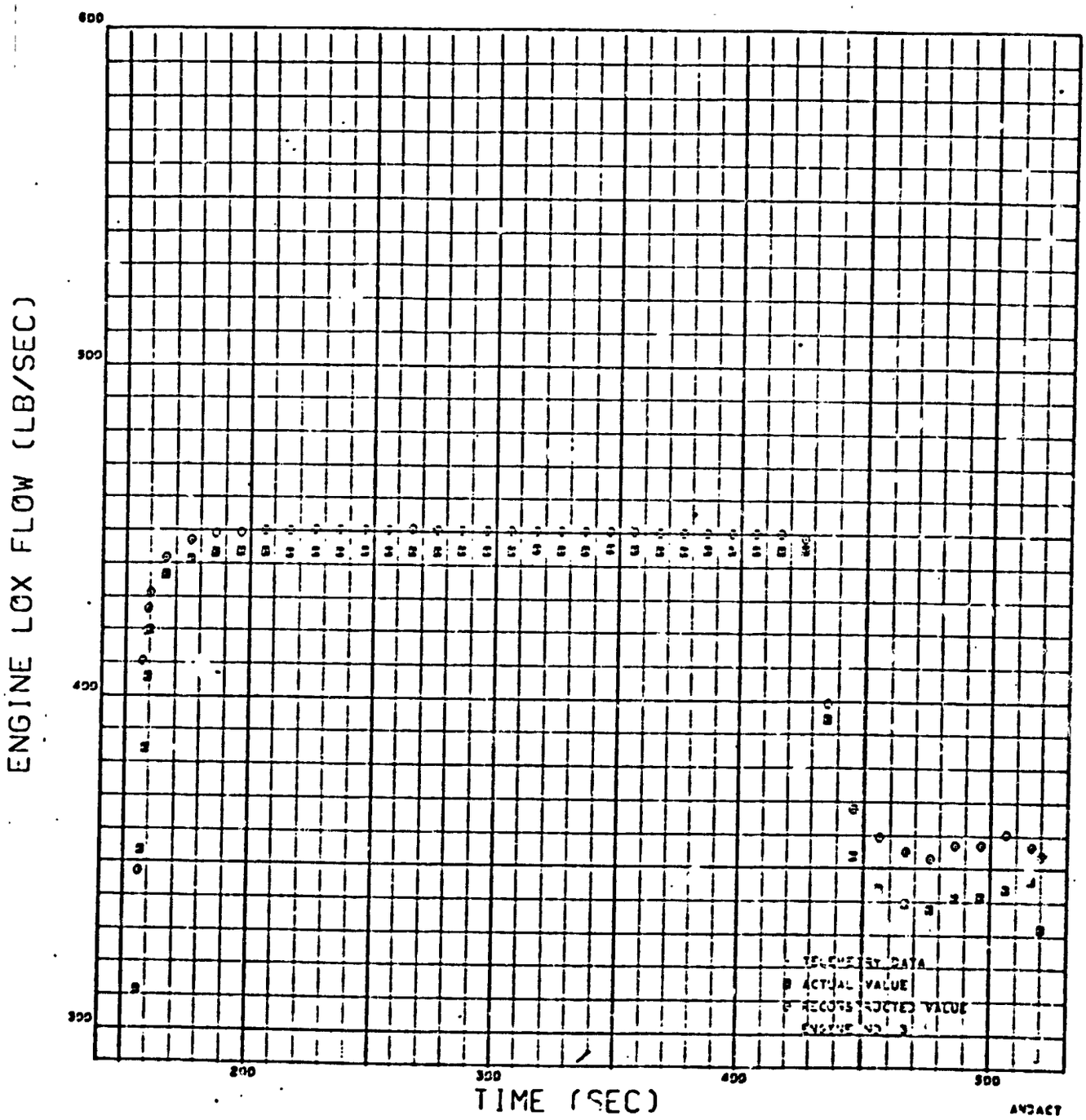

Figure 83. Engine No. 3 Oxidizer Flowrate

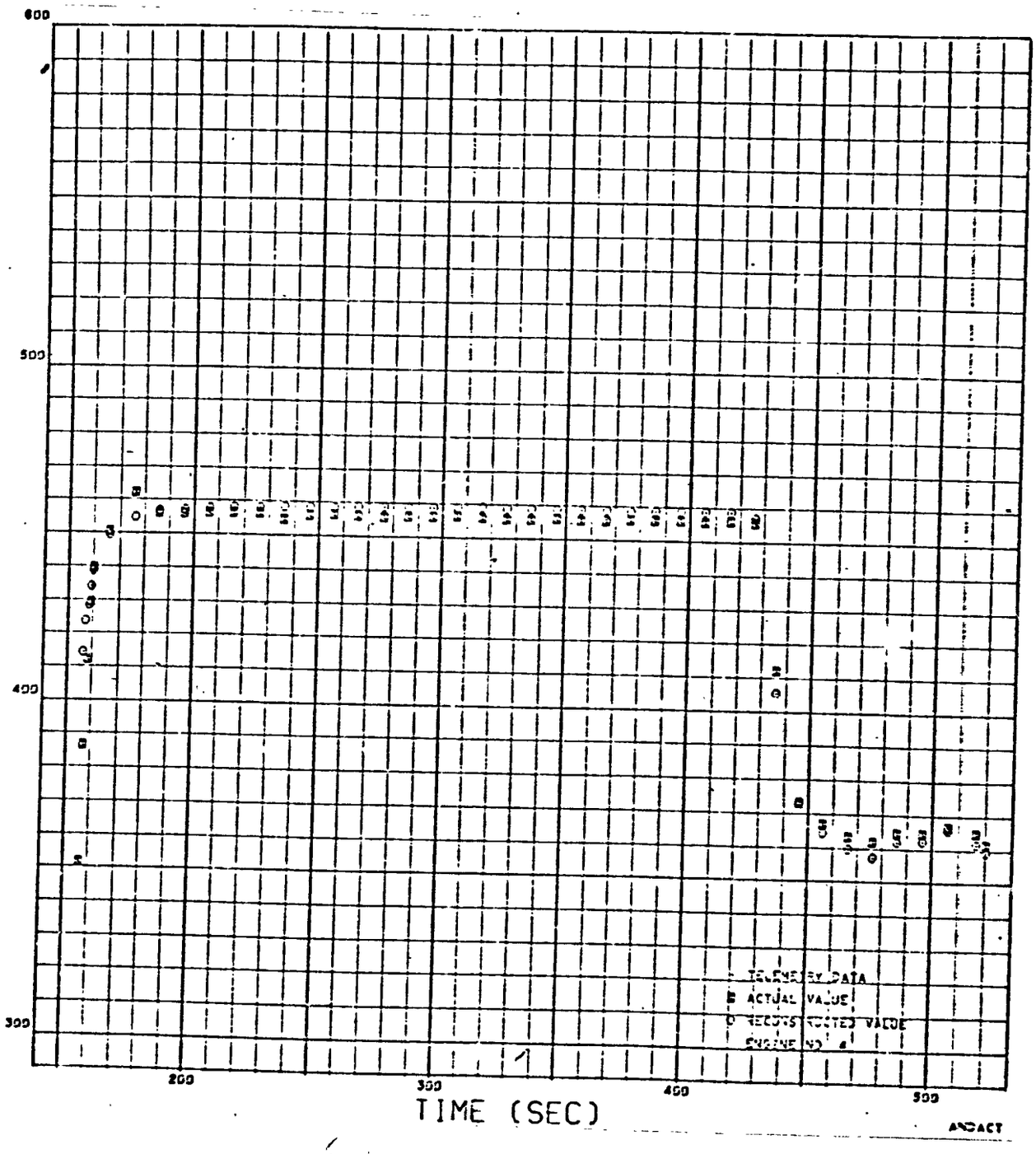

Figure 84. Engine No. 4 Oxidizer Flowrate

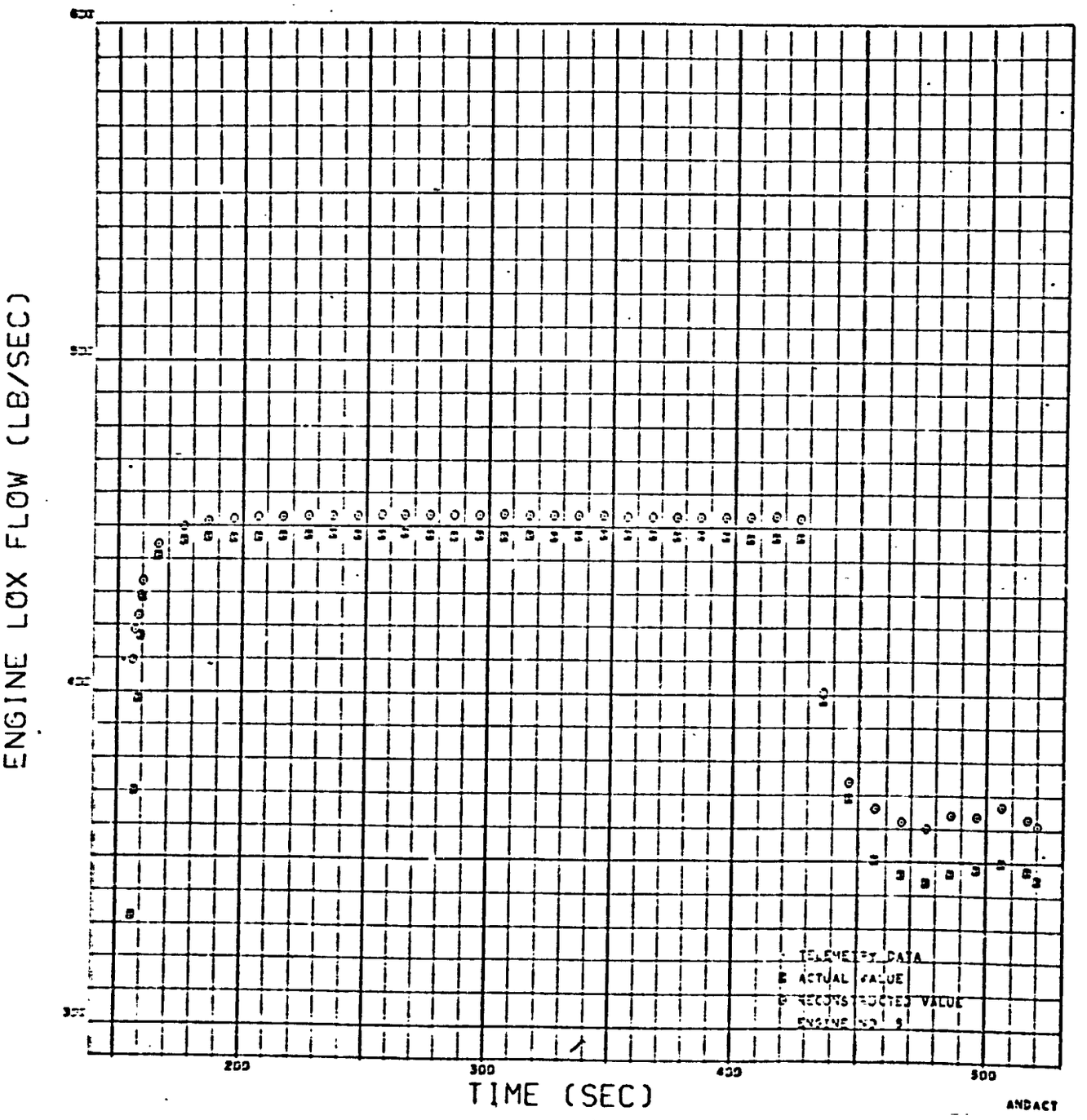

Figure 85. Engine No. 5 Oxidizer Flowrate

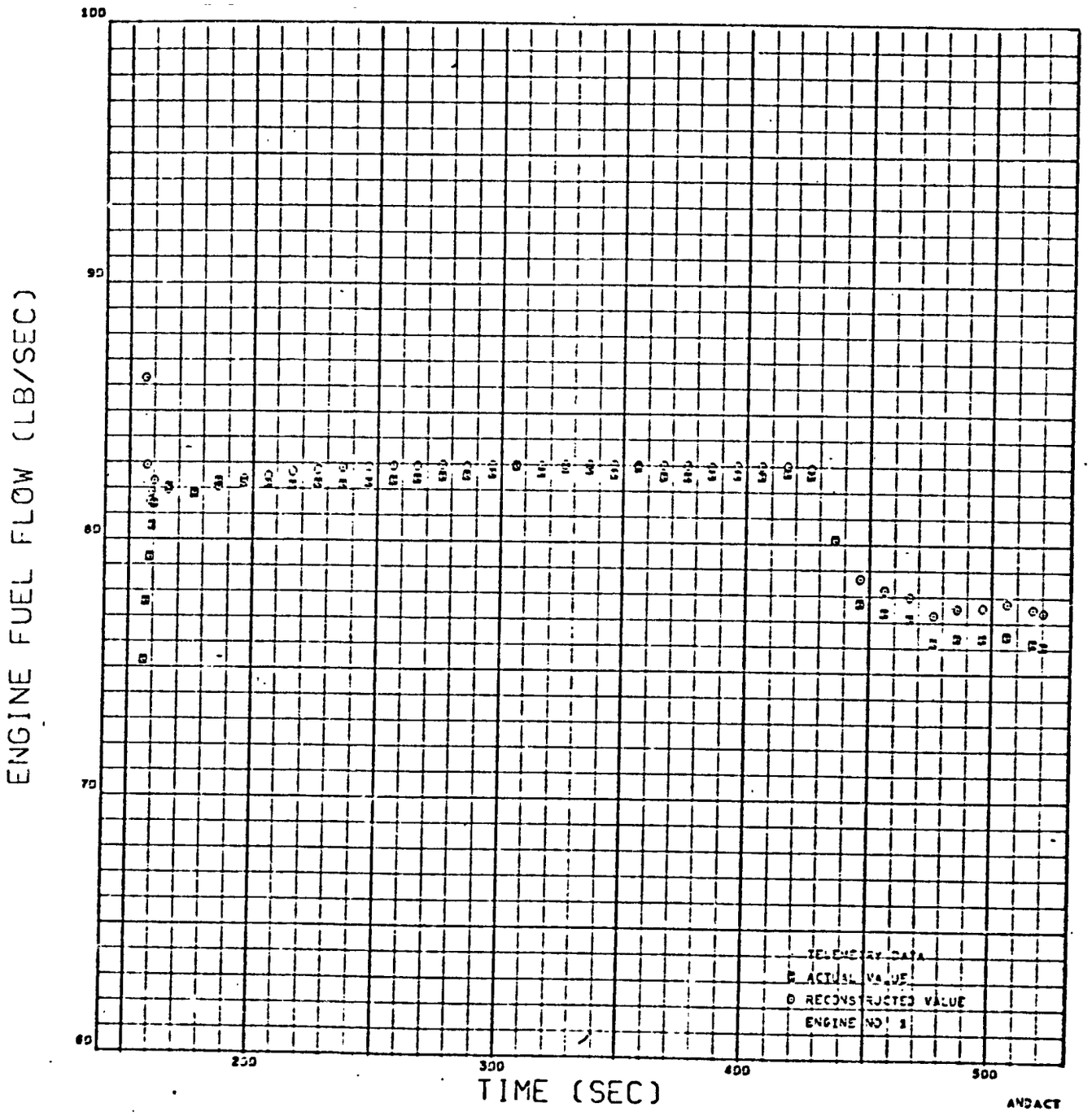

Figure 86. Engine No. 1 Fuel Flowrate

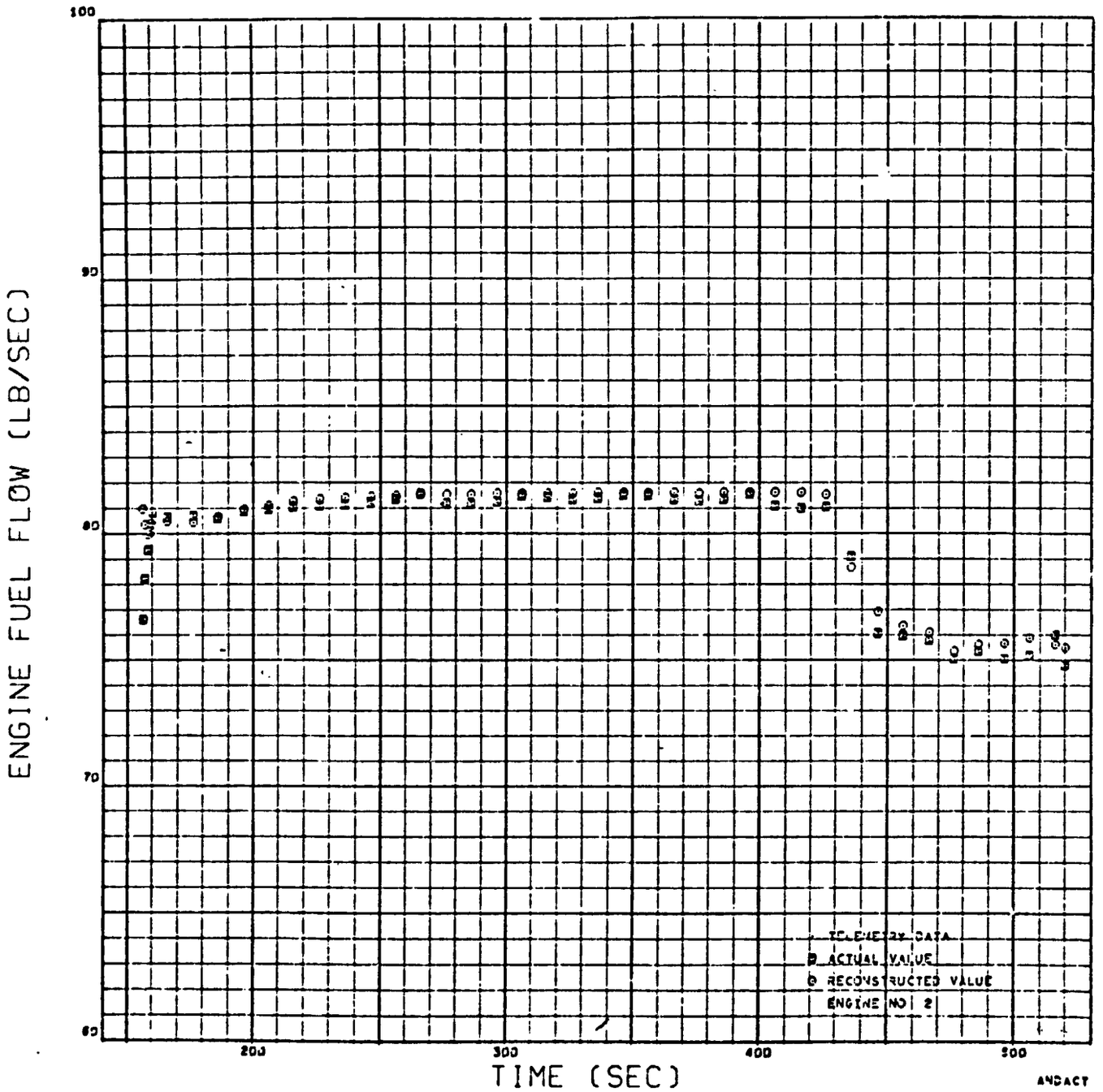

Figure 86A. Engine No. 2 Fuel Flowrate

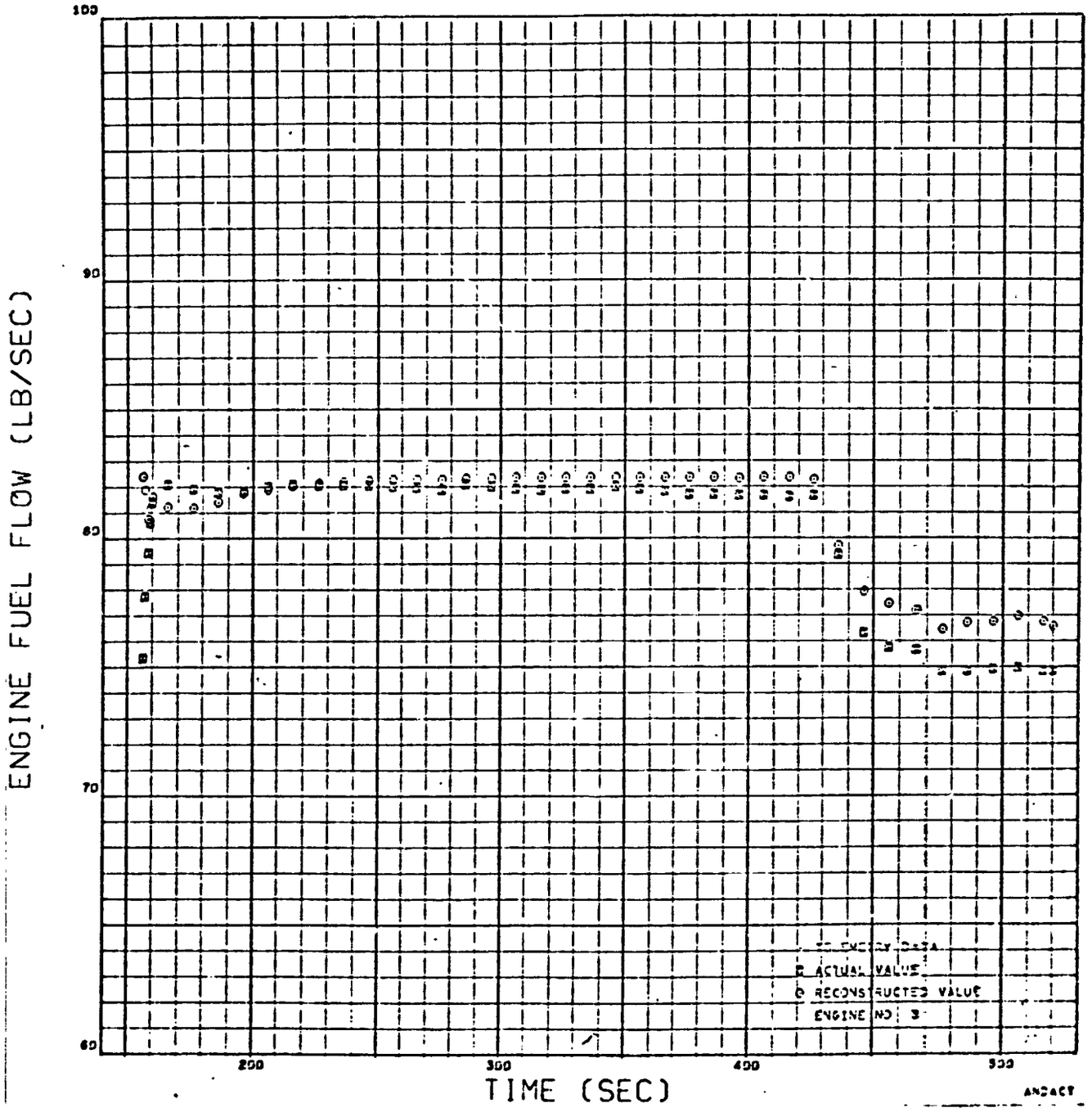

Figure 87. Engine No. 3 Fuel Flowrate

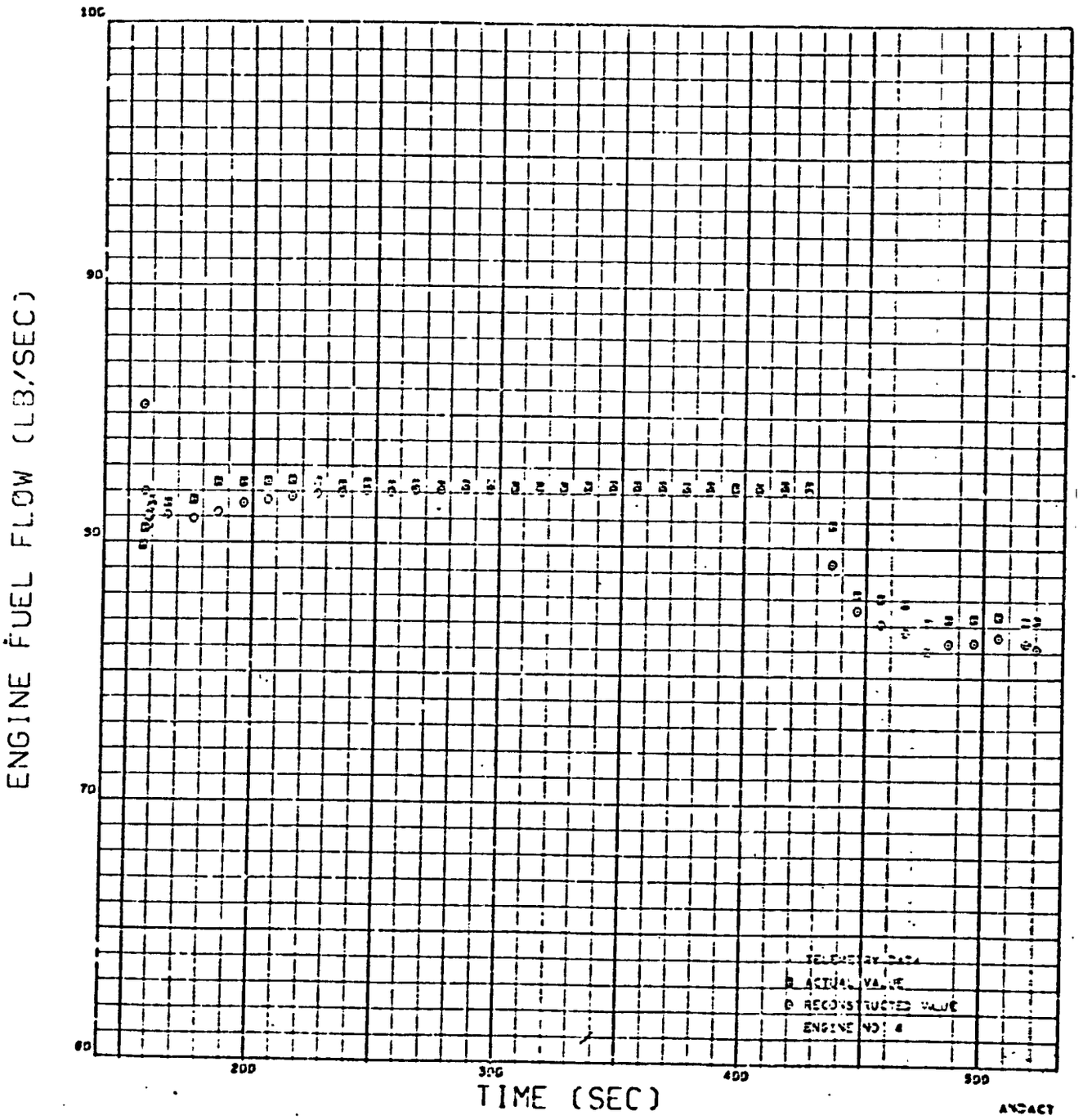

Figure 88. Engine No. 4 Fuel Flowrate

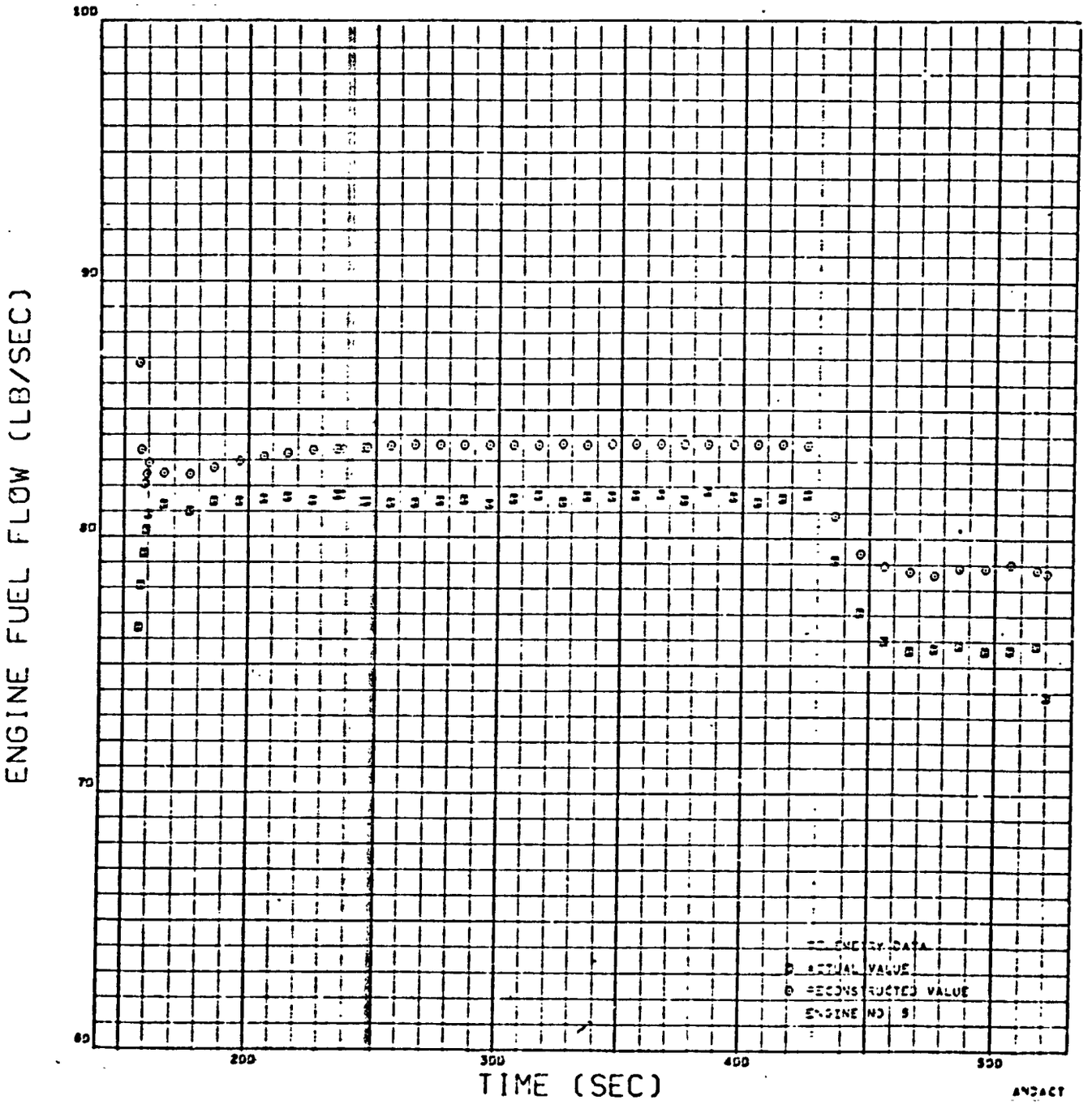

Figure 89. Engine No. 5 Fuel Flowrate

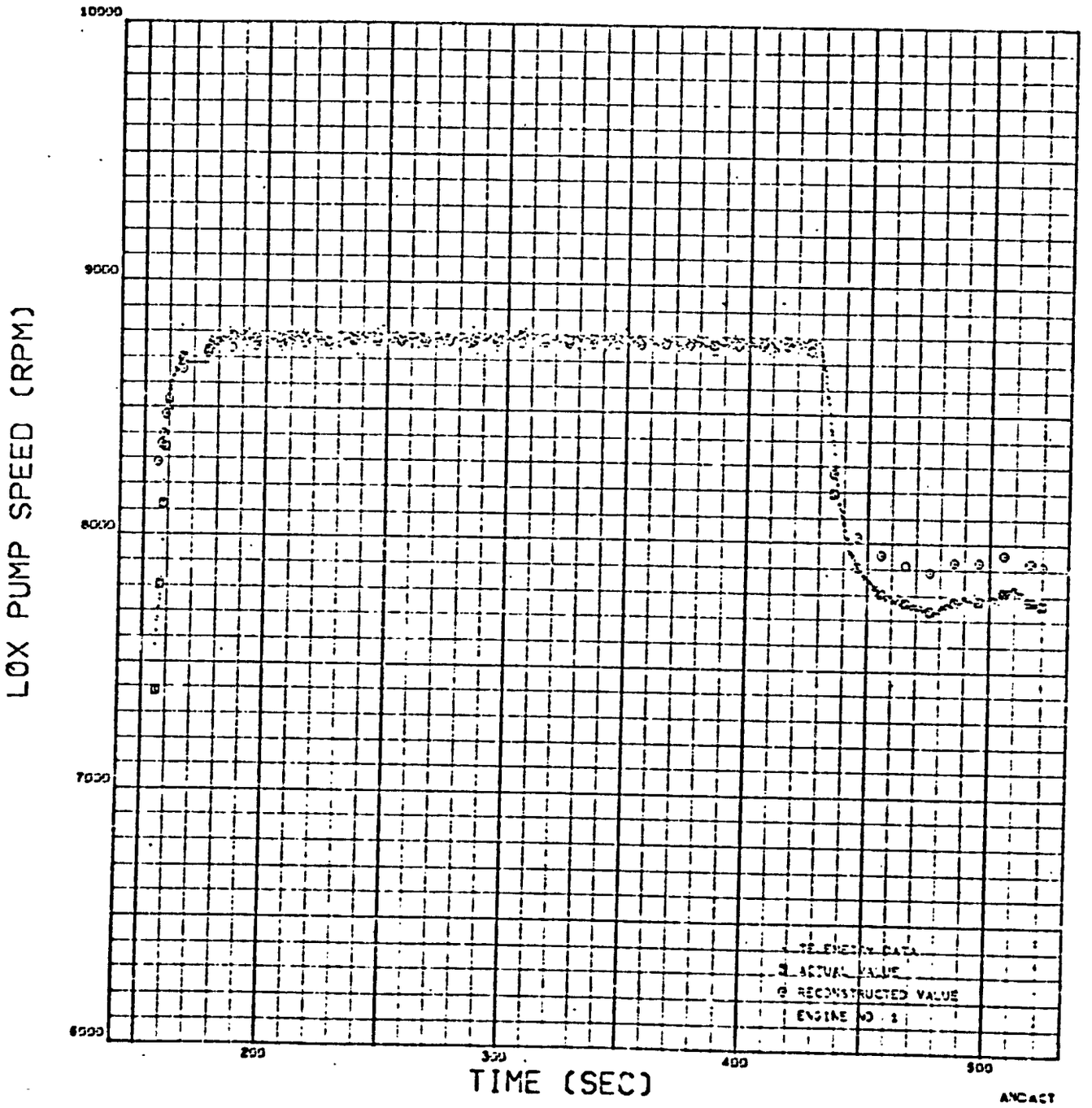

Figure 90. Engine No. 1 Oxidizer Pump Speed

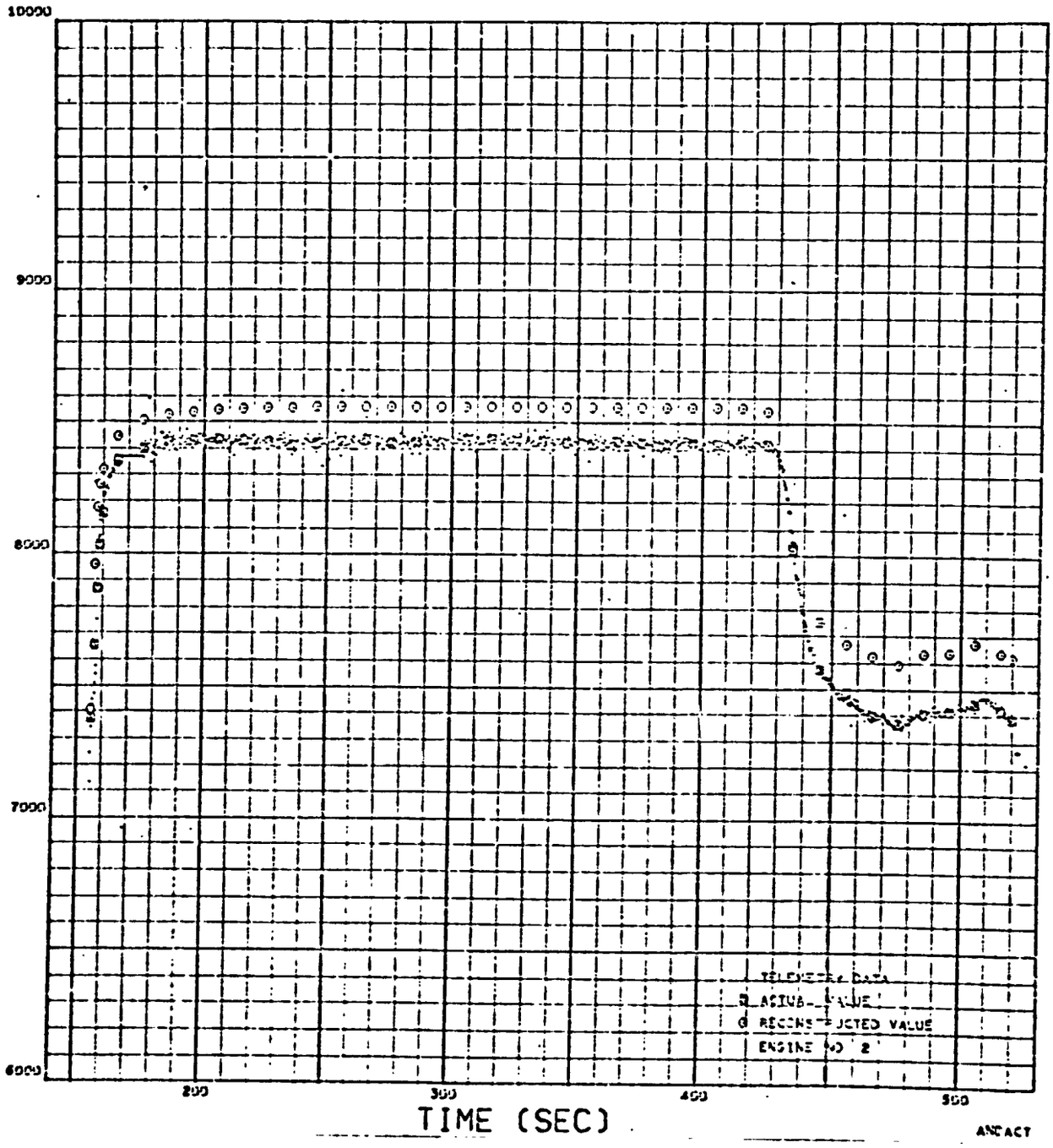

Figure 91. Engine No. 2 Oxidizer Pump Speed

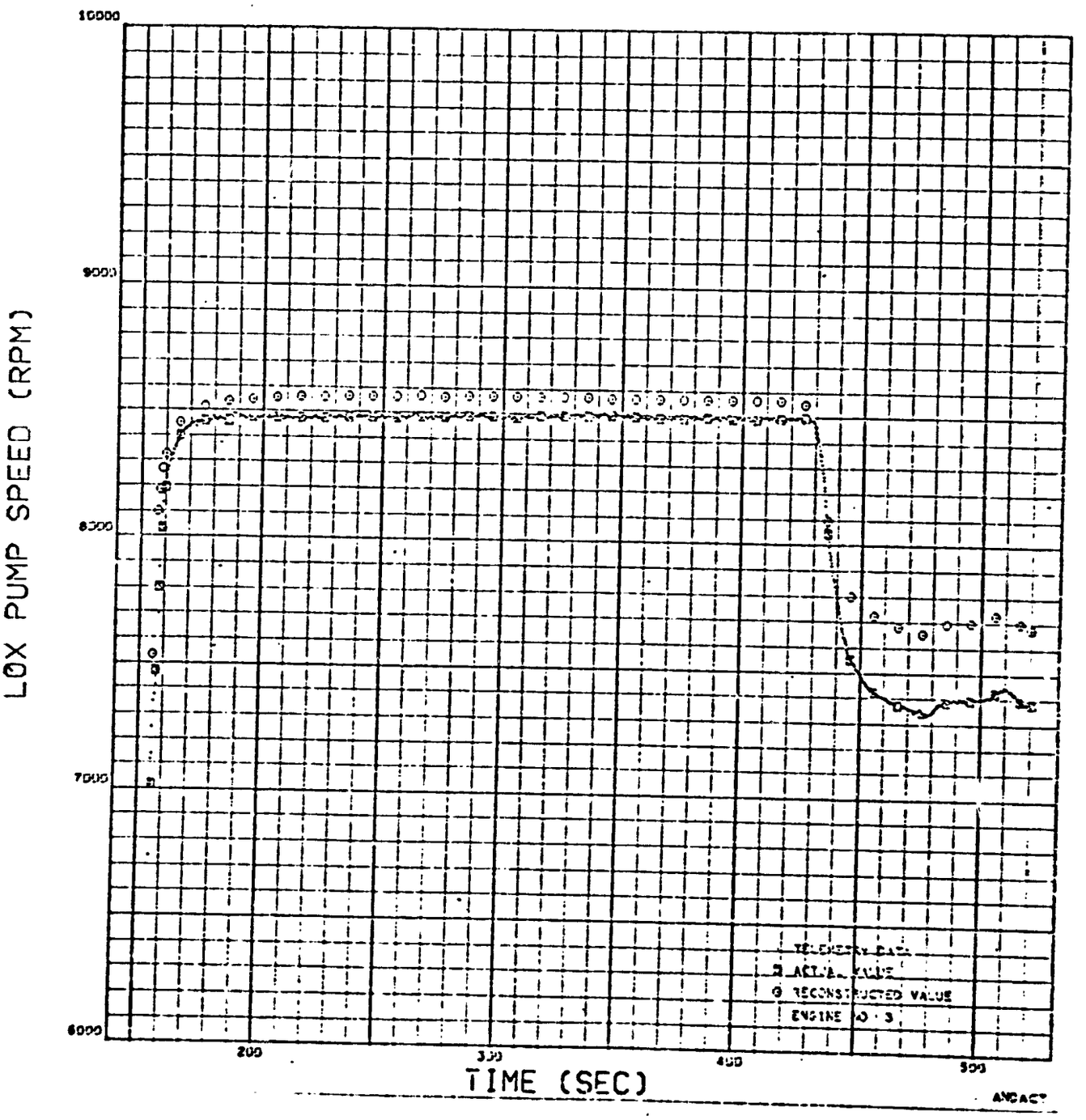

Figure 92. Engine No. 3 Oxidizer Pump Speed

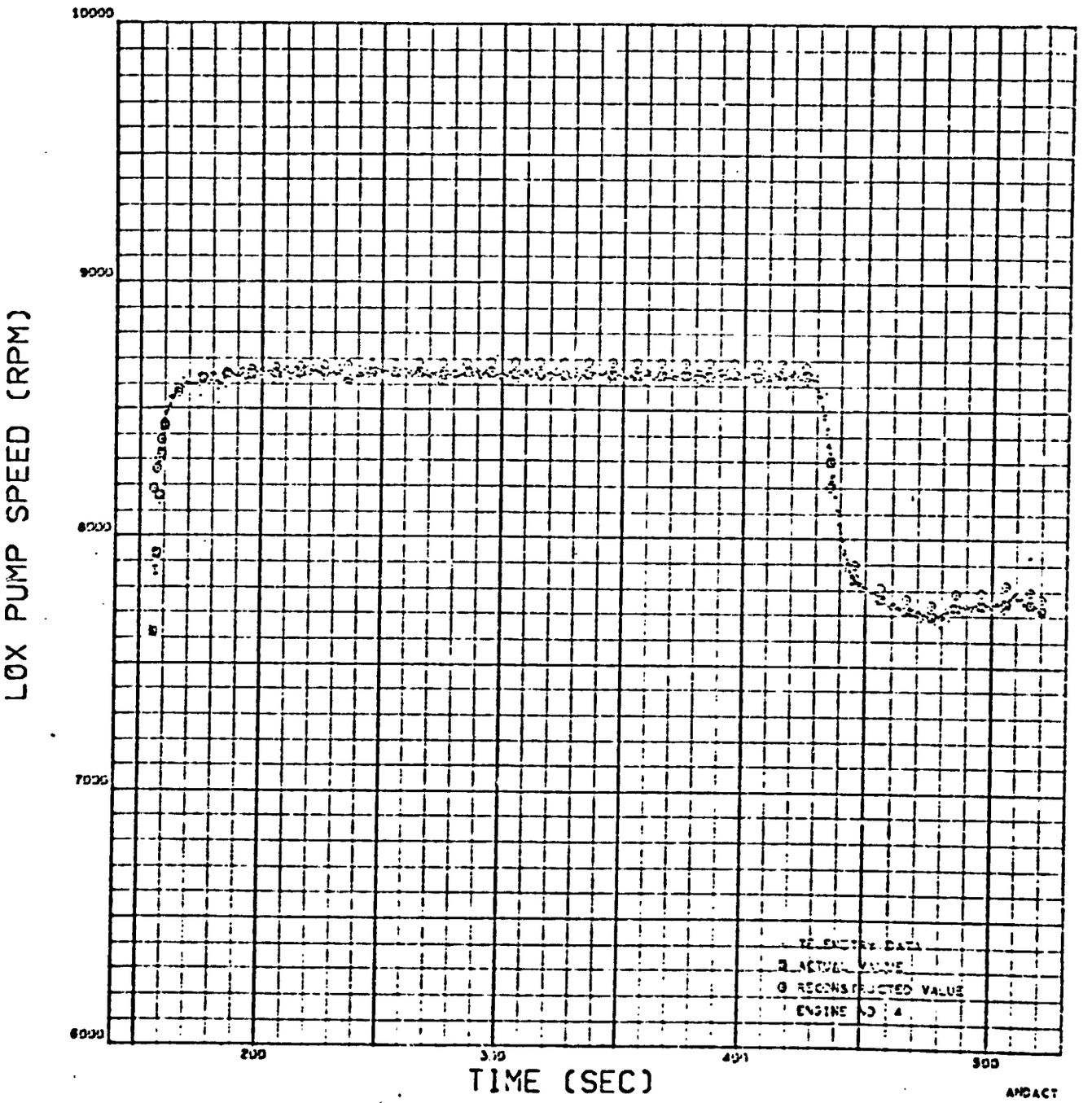

Figure 93. Engine No. 4 Oxidizer Pump Speed

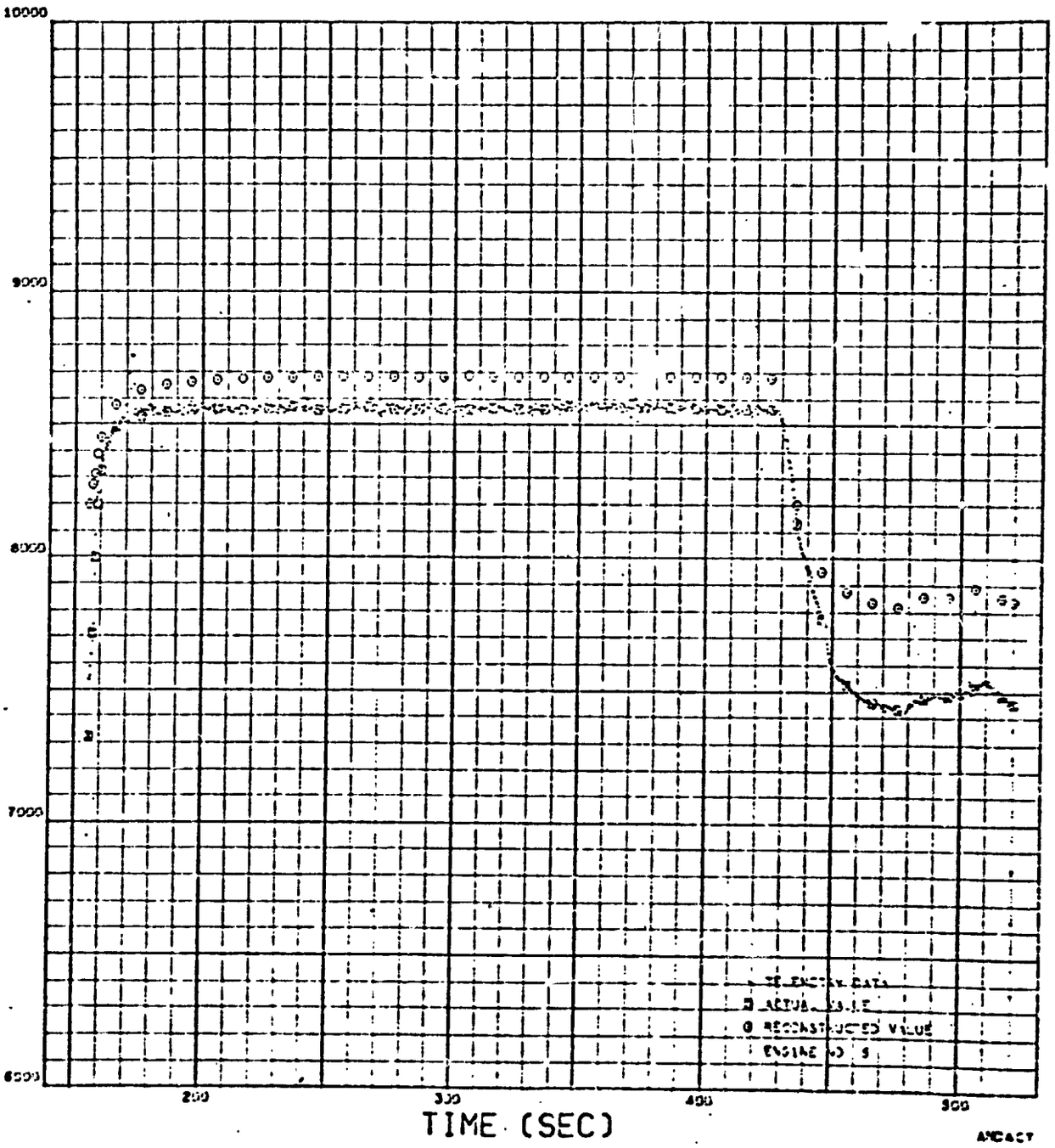

Figure 94. Engine No. 5 Oxidizer Pump Speed

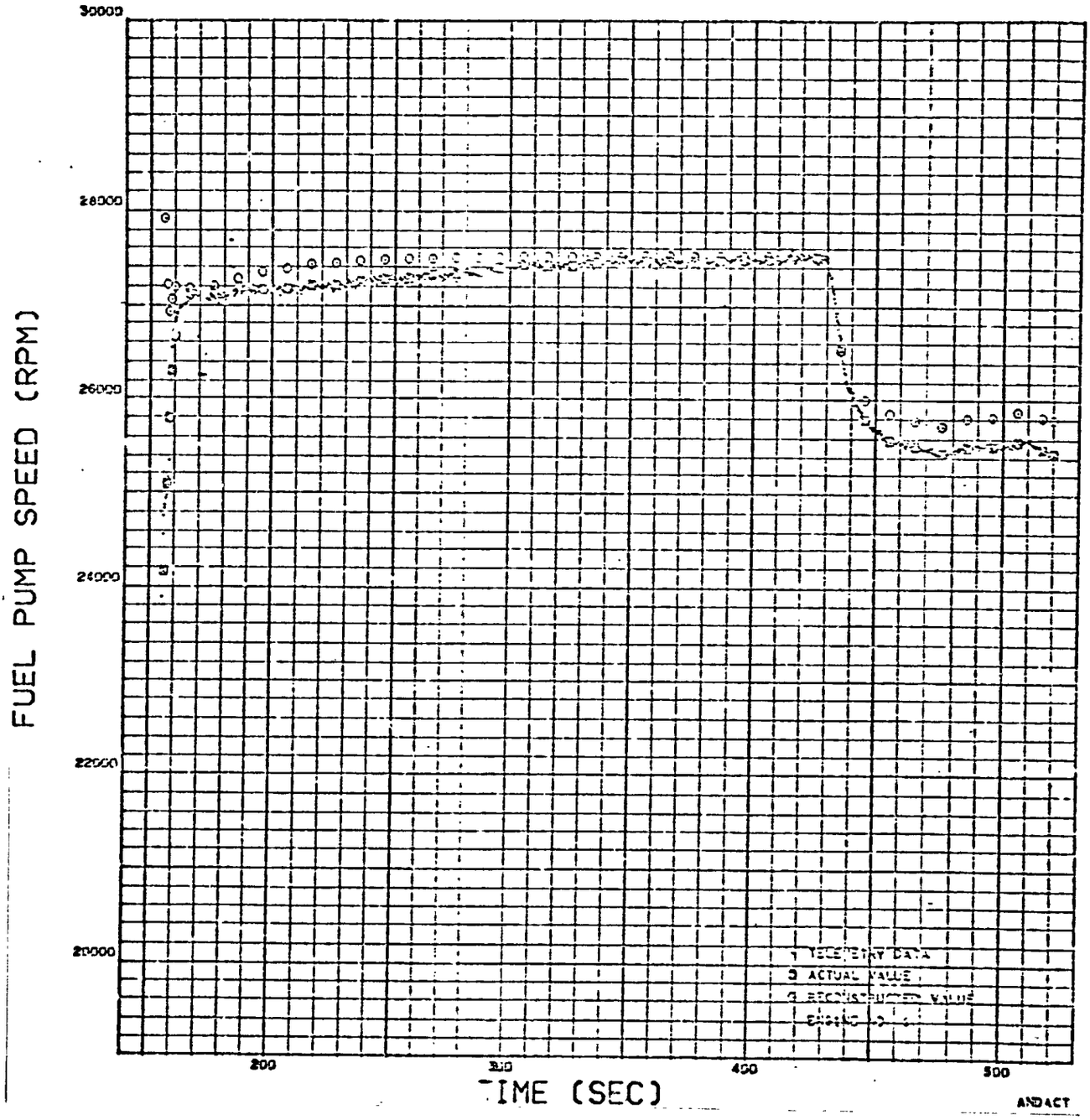

Figure 95. Engine No. 1 Fuel Pump Speed

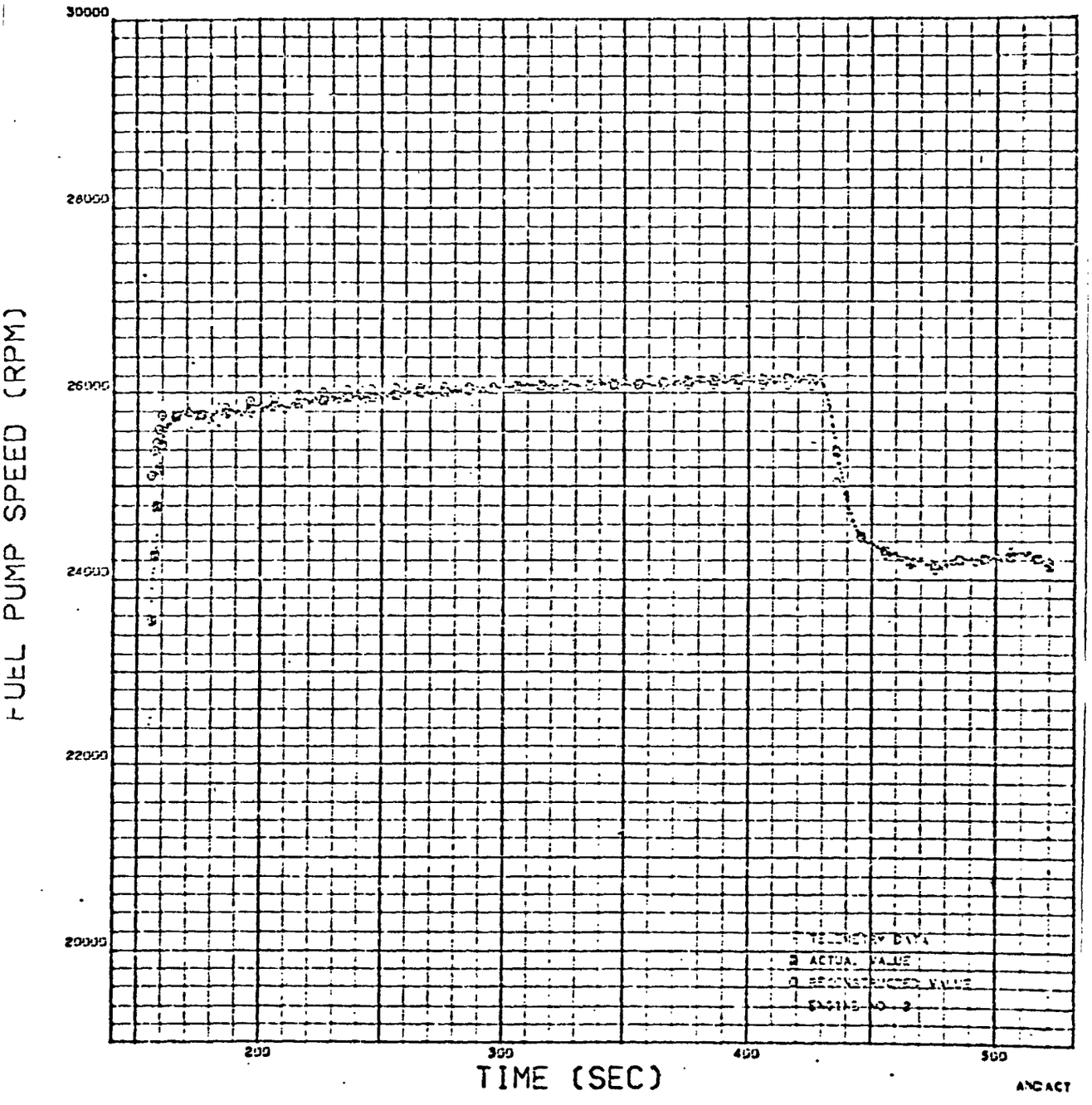

Figure 96. Engine No. 2 Fuel Pump Speed

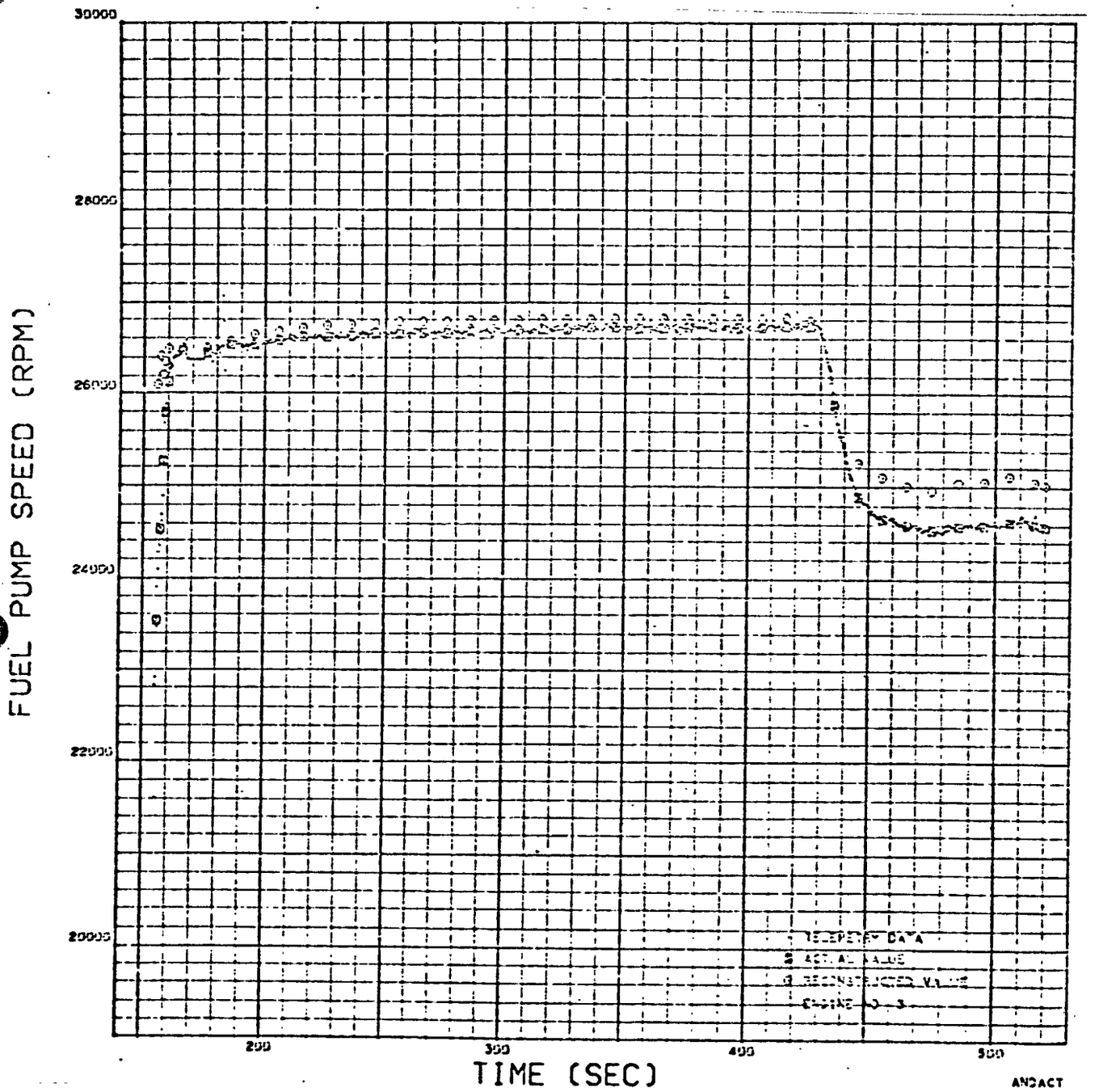

Figure 97. Engine No. 3 Fuel Pump Speed

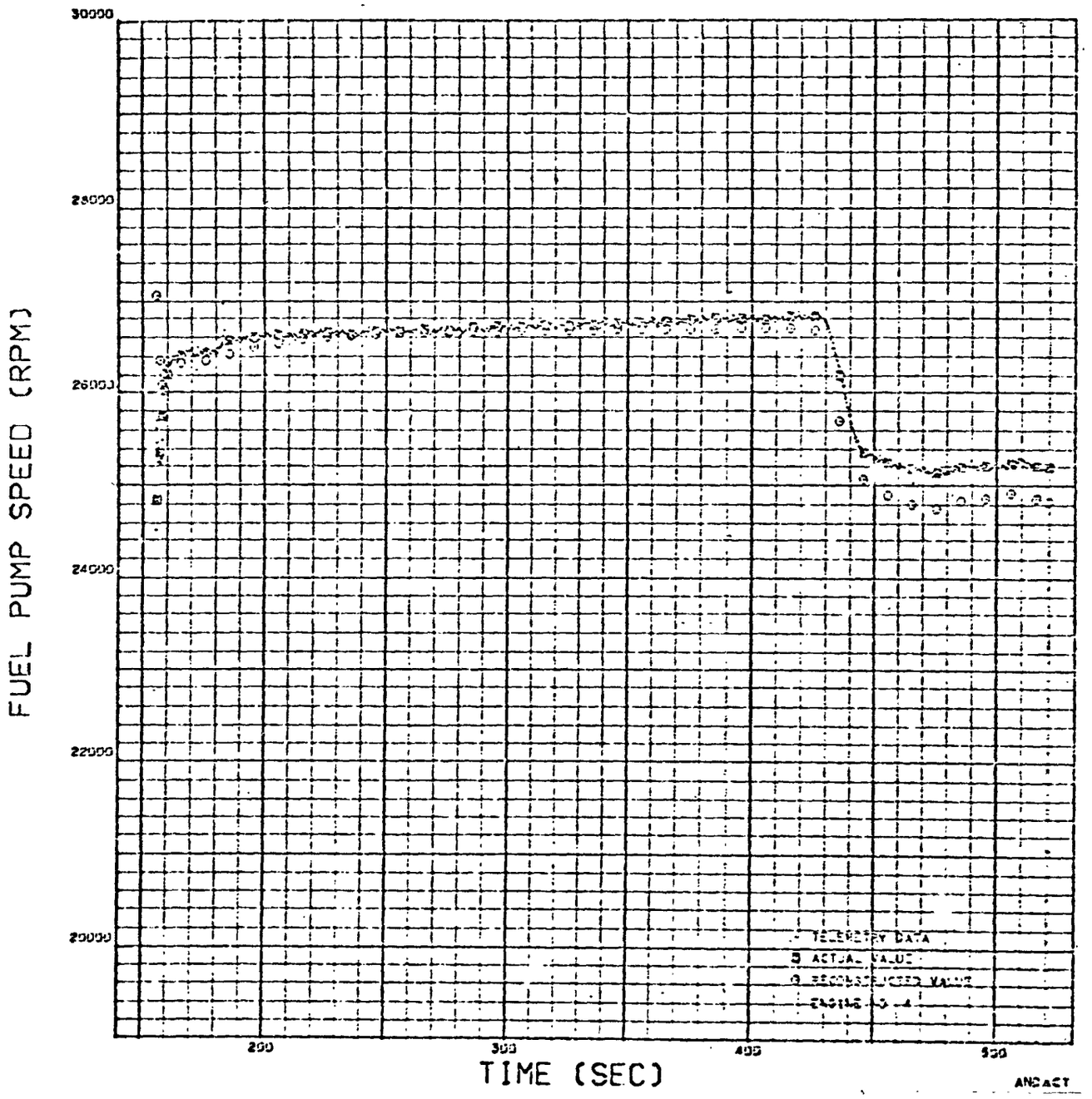

Figure 98. Engine No. 4 Fuel Pump Speed

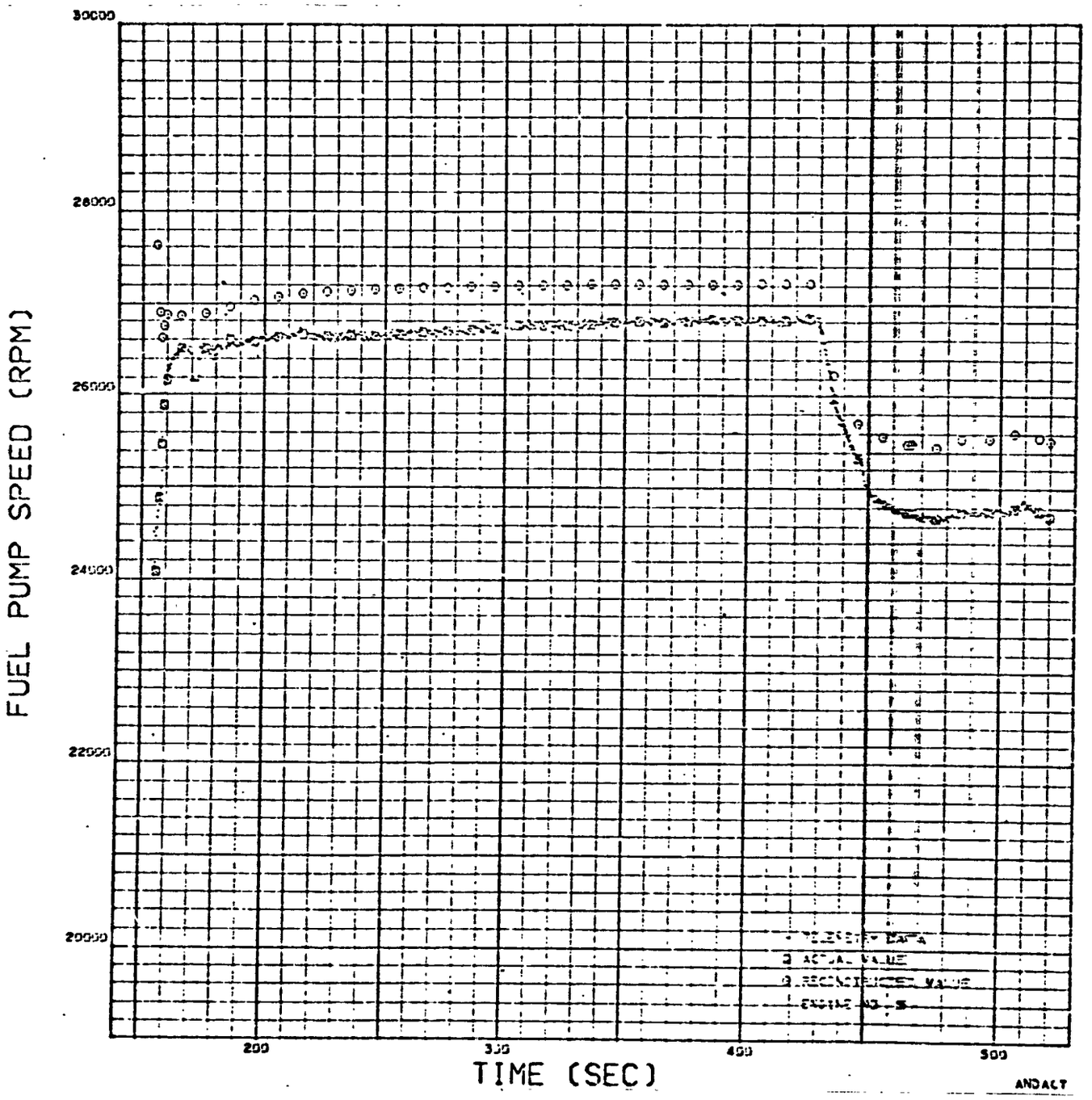

Figure 99. Engine No. 5 Fuel Pump Speed

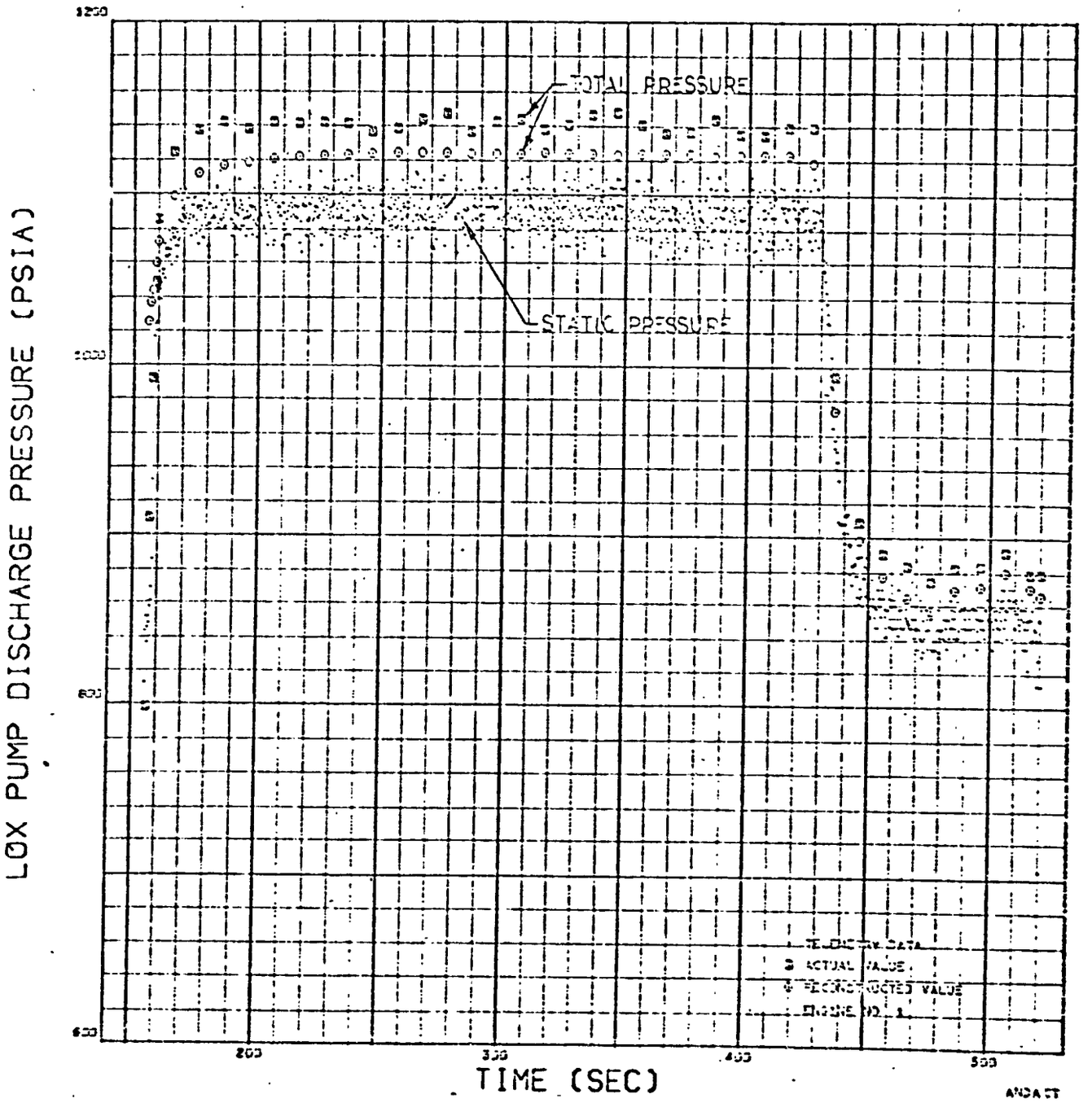

Figure 100. Engine No. 1 Oxidizer Pump Discharge Pressure

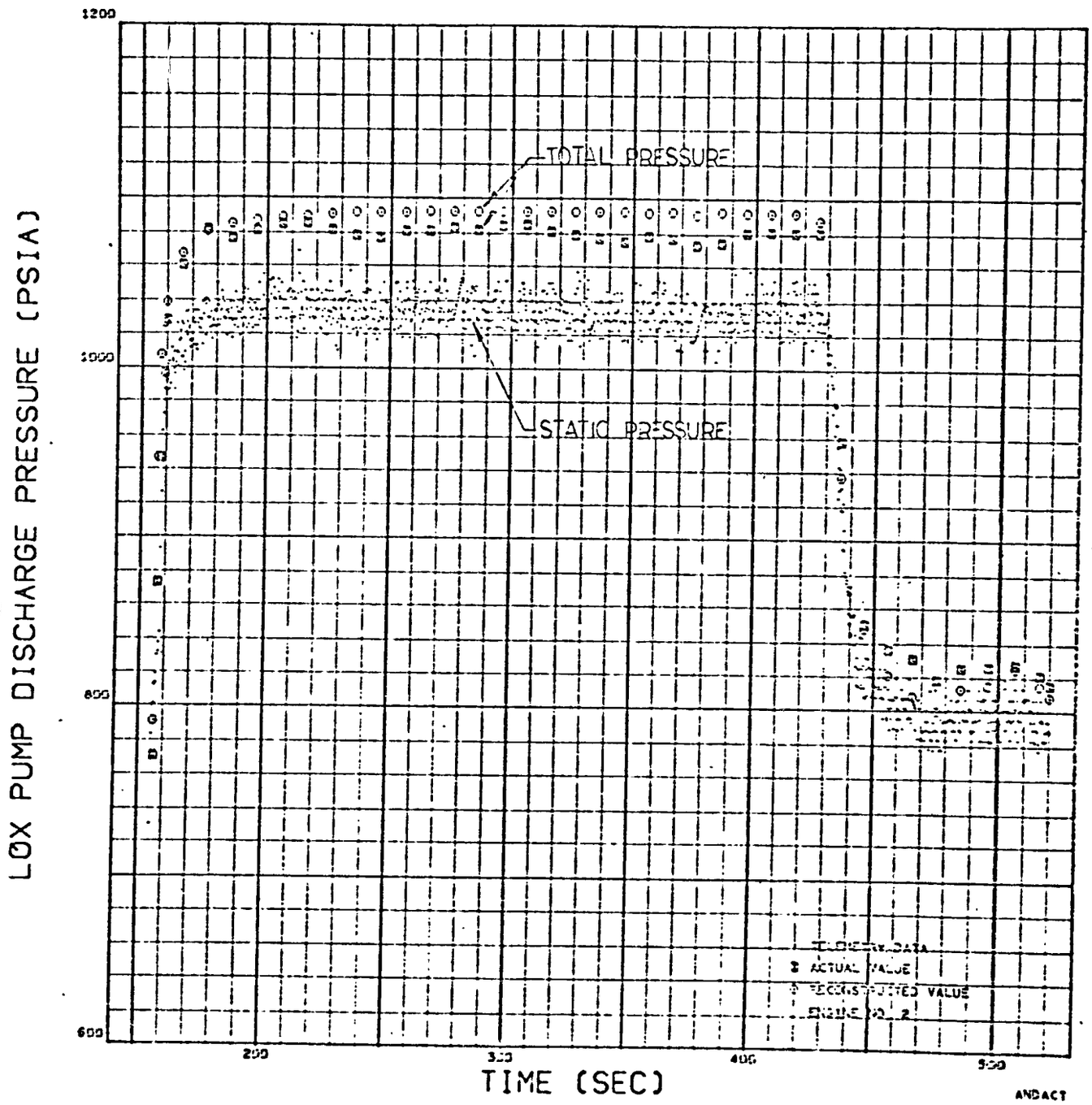

Figure 101. Engine No. 2 Oxidizer Pump Discharge Pressure

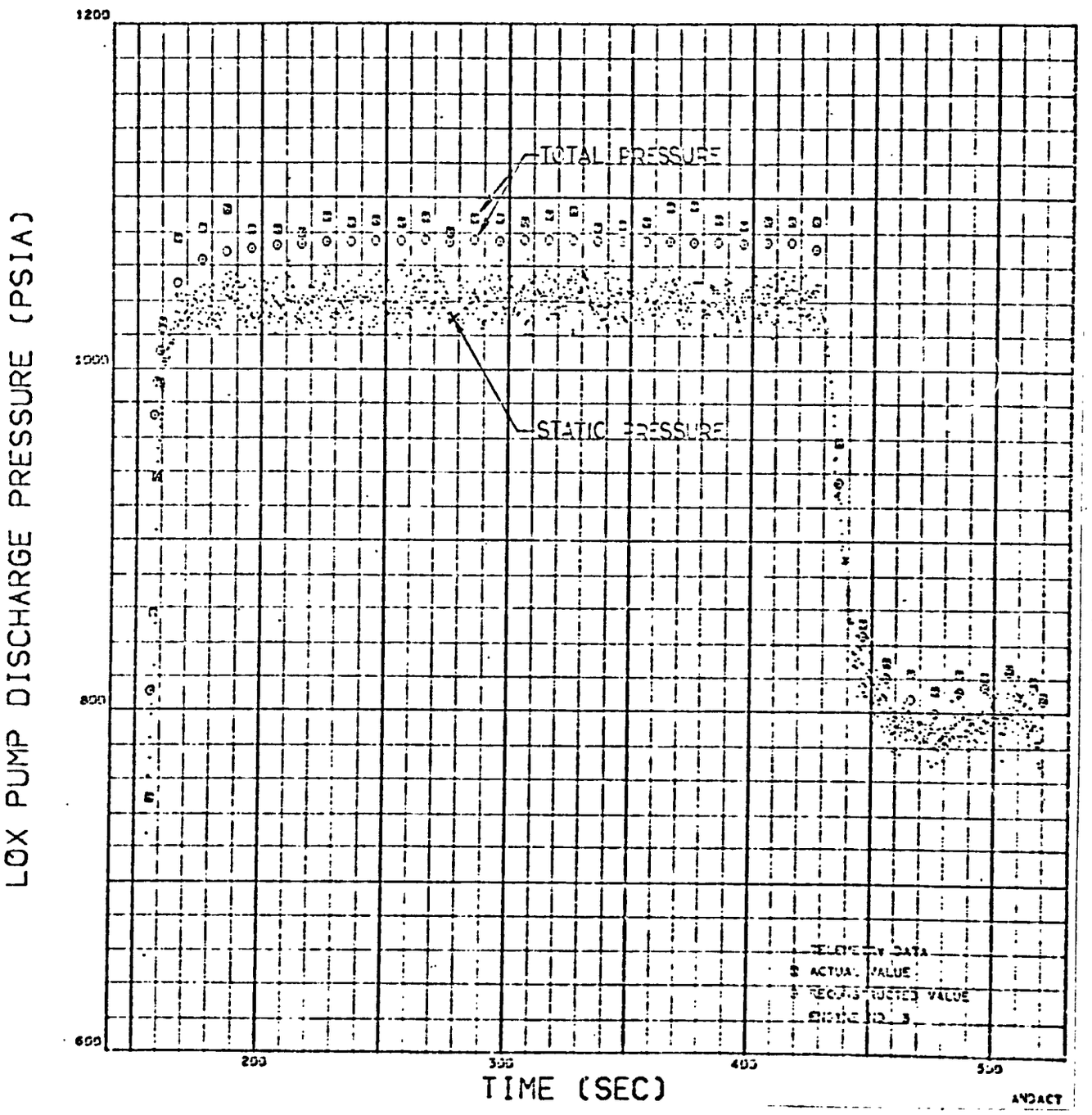

Figure 102. Engine No. 3 Oxidizer Pump Discharge Pressure

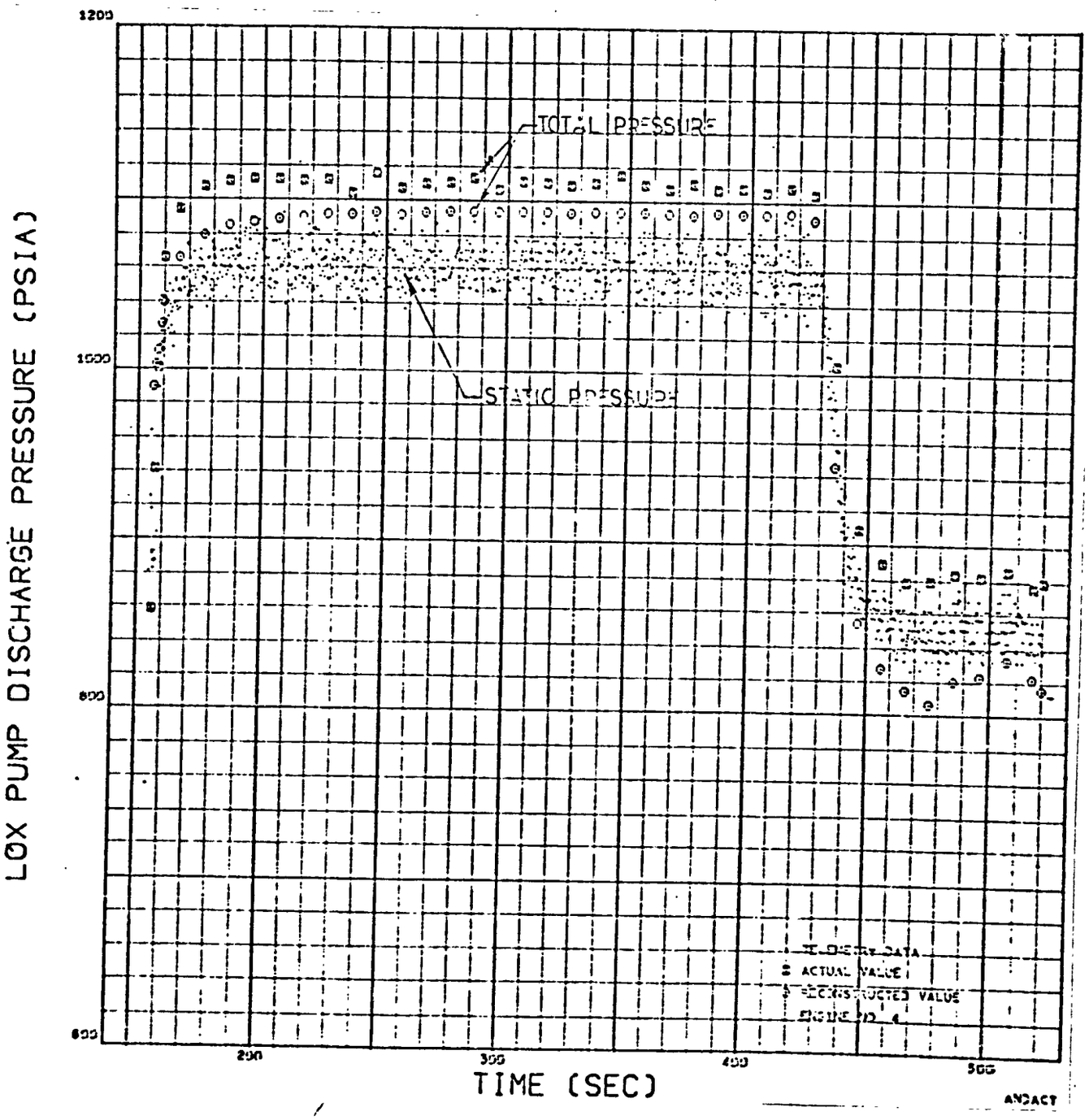

Figure 103. Engine No. 4 Oxidizer Pump Discharge Pressure

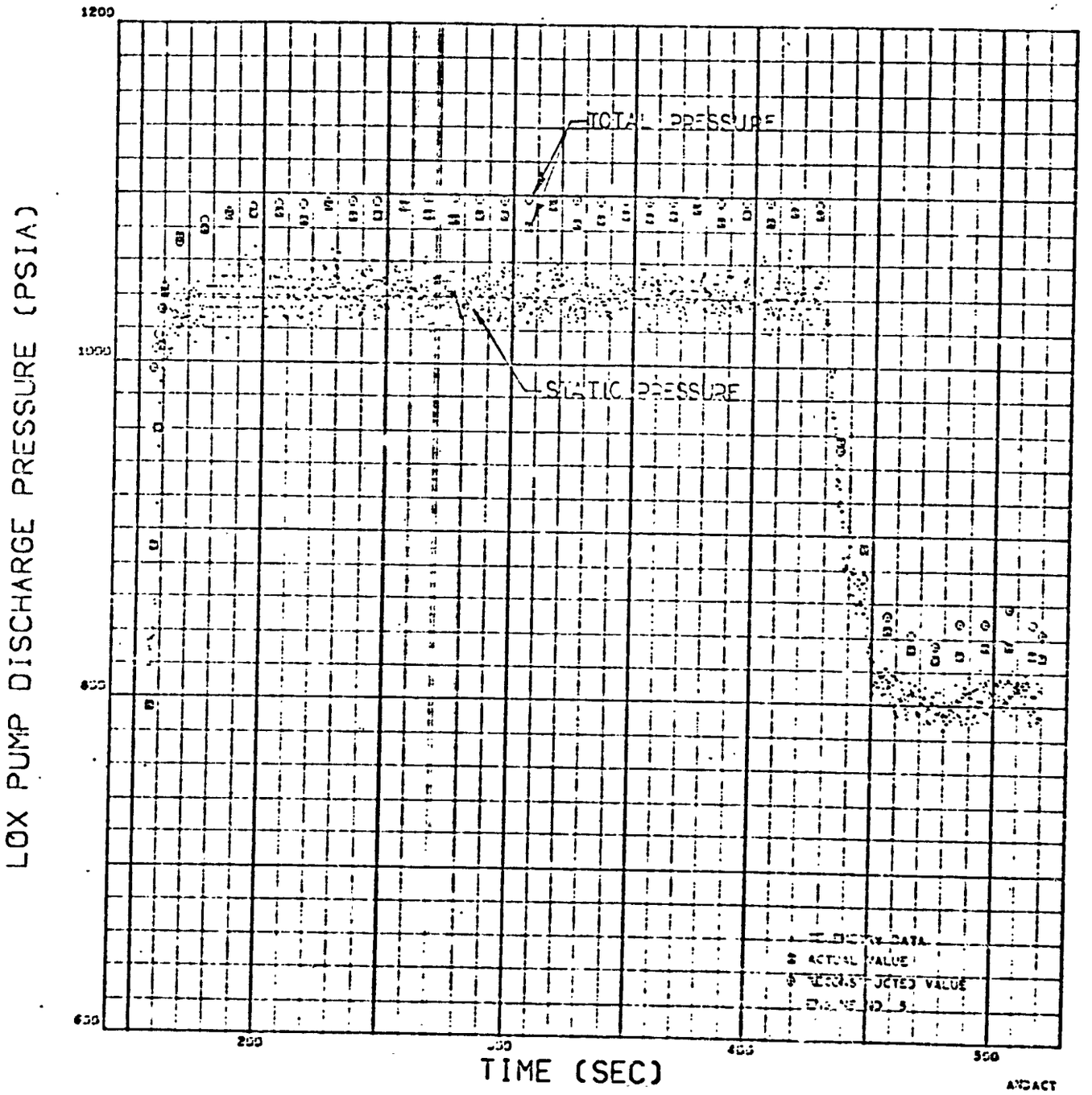

Figure 104. Engine No. 5 Oxidizer Pump Discharge Pressure

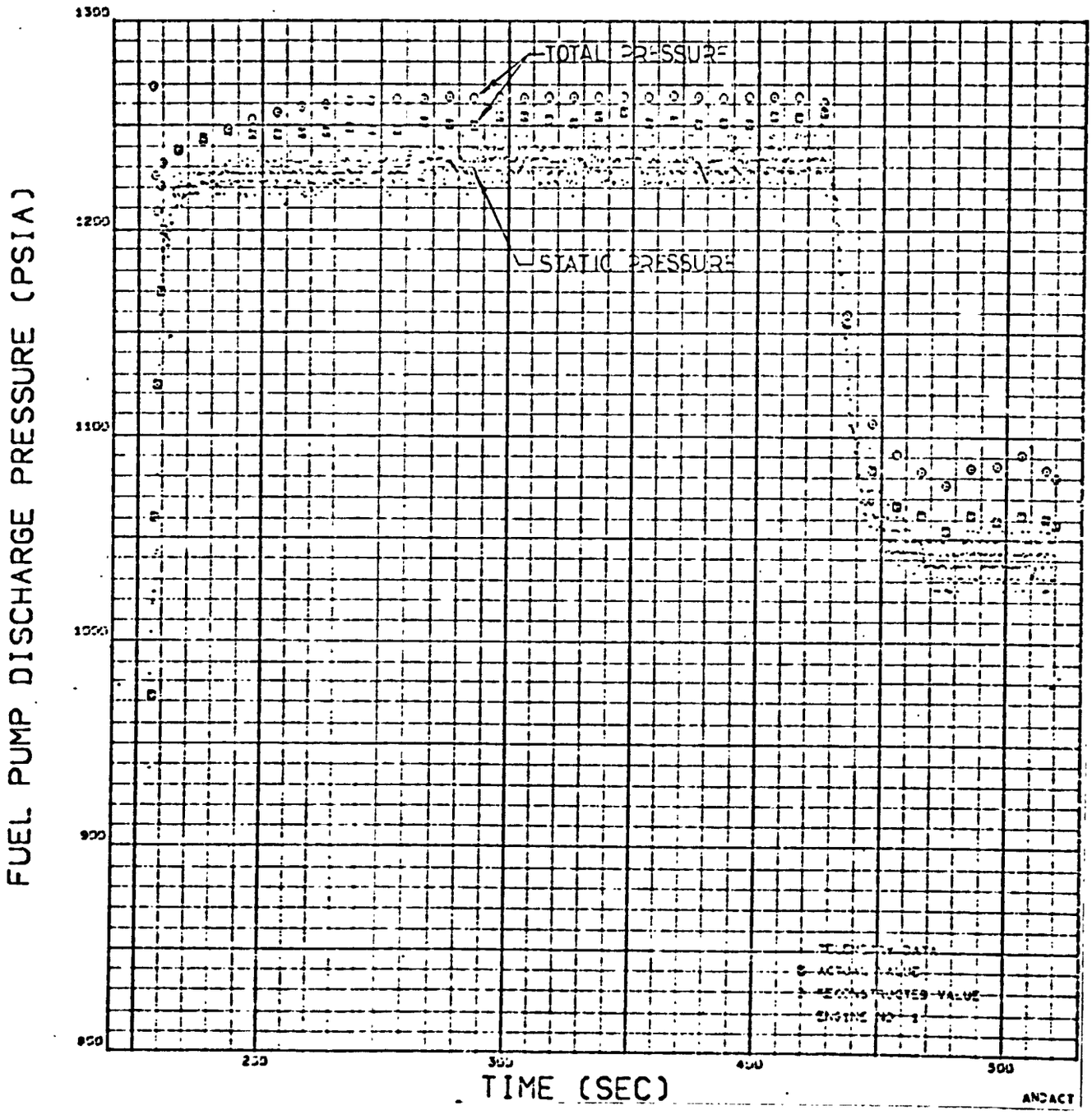

Figure 105. Engine No. 1 Fuel Pump Discharge Pressure

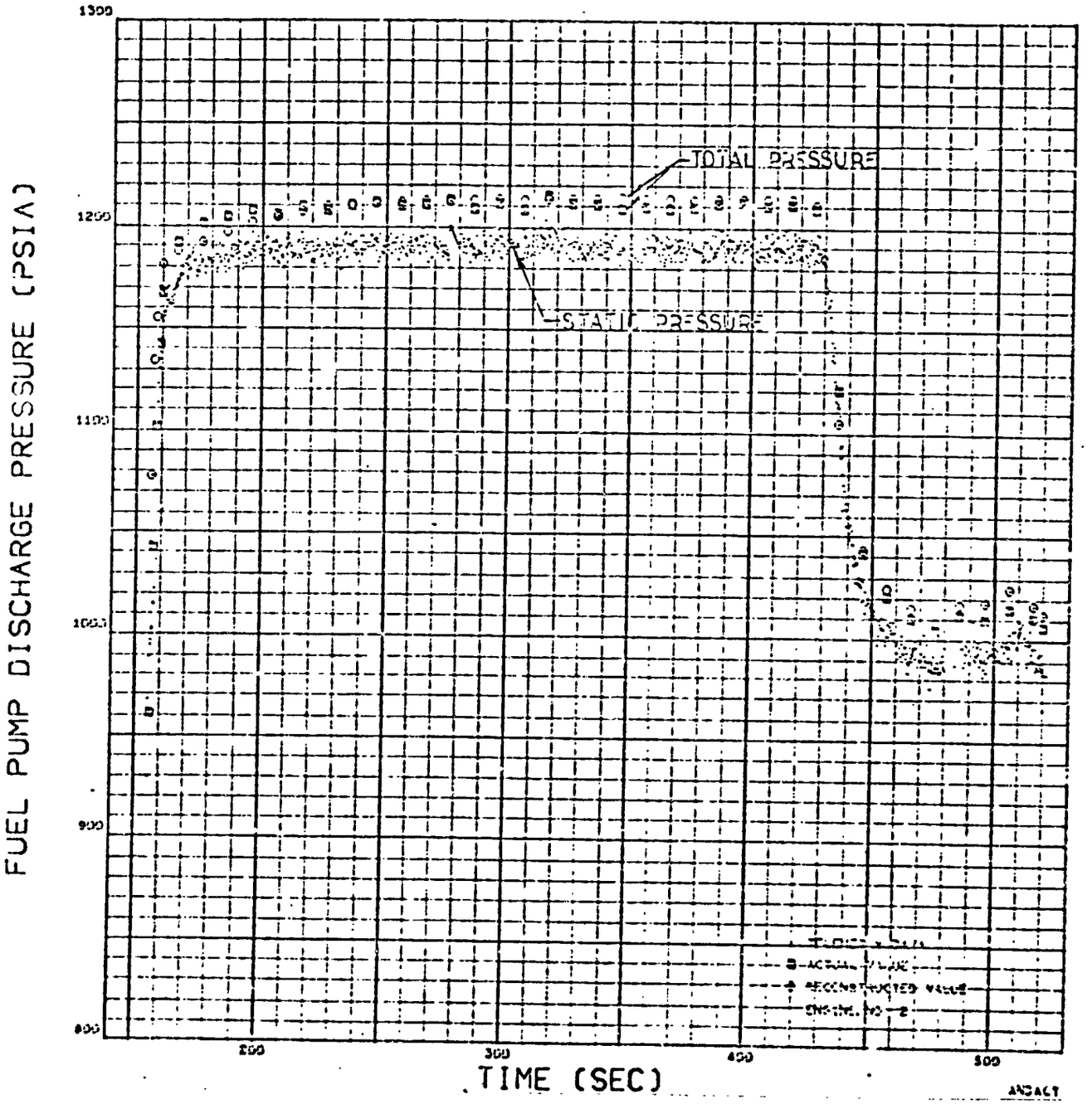

Figure 106. Engine No. 2 Fuel Pump Discharge Pressure

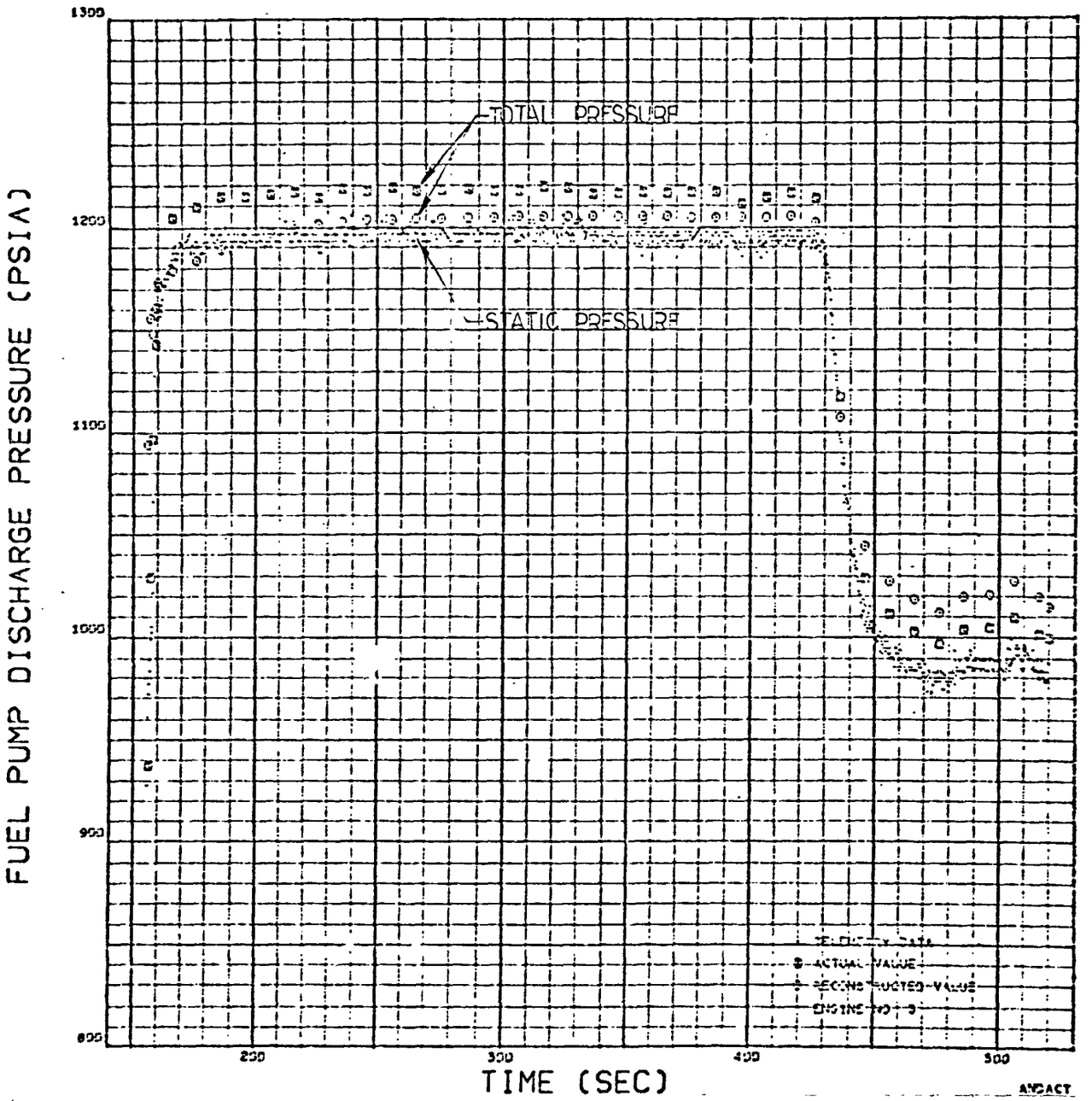

Figure 107. Engine No. 3 Fuel Pump Discharge Pressure

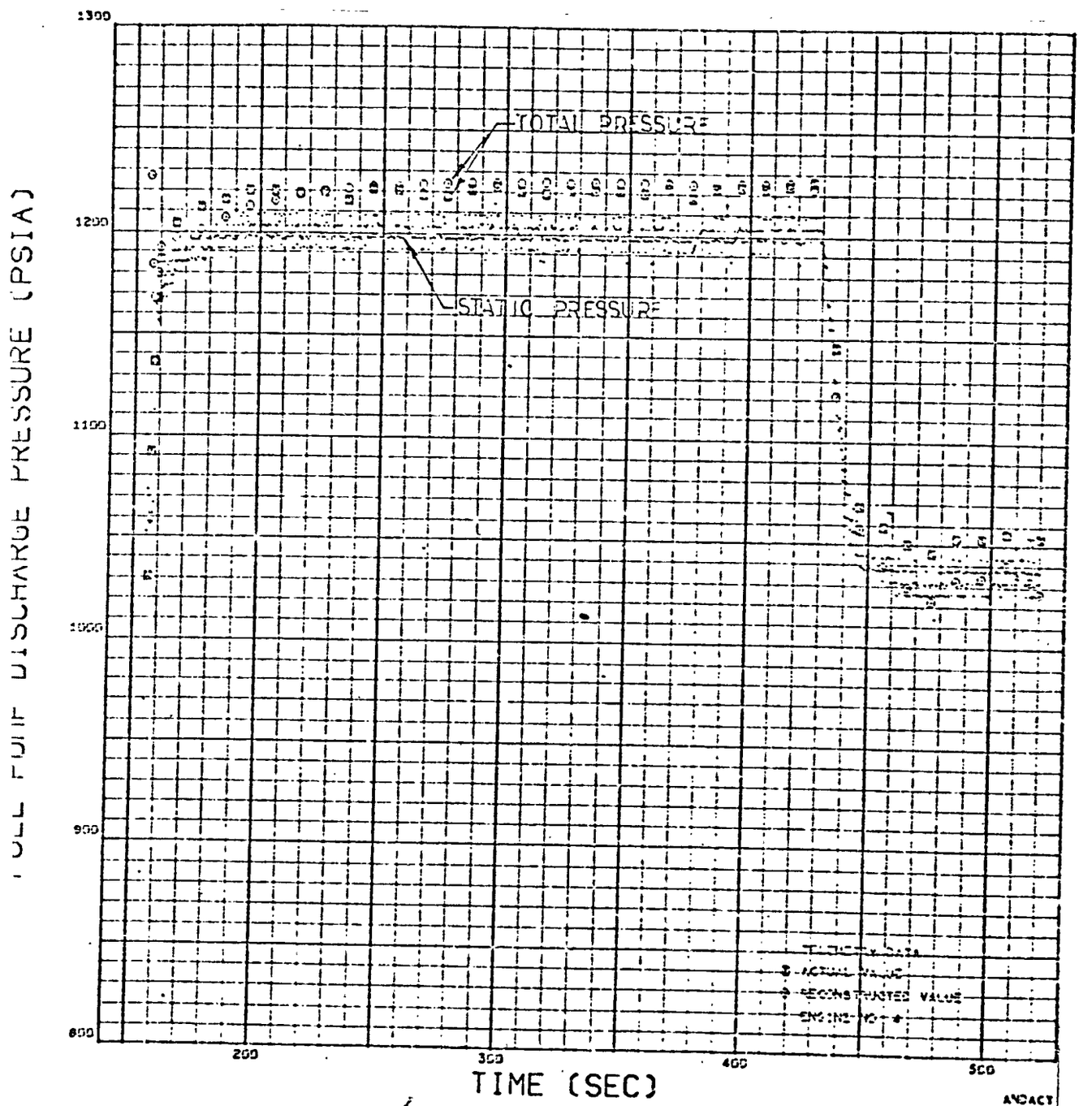

Figure 108. Engine No. 4 Fuel Pump Discharge Pressure

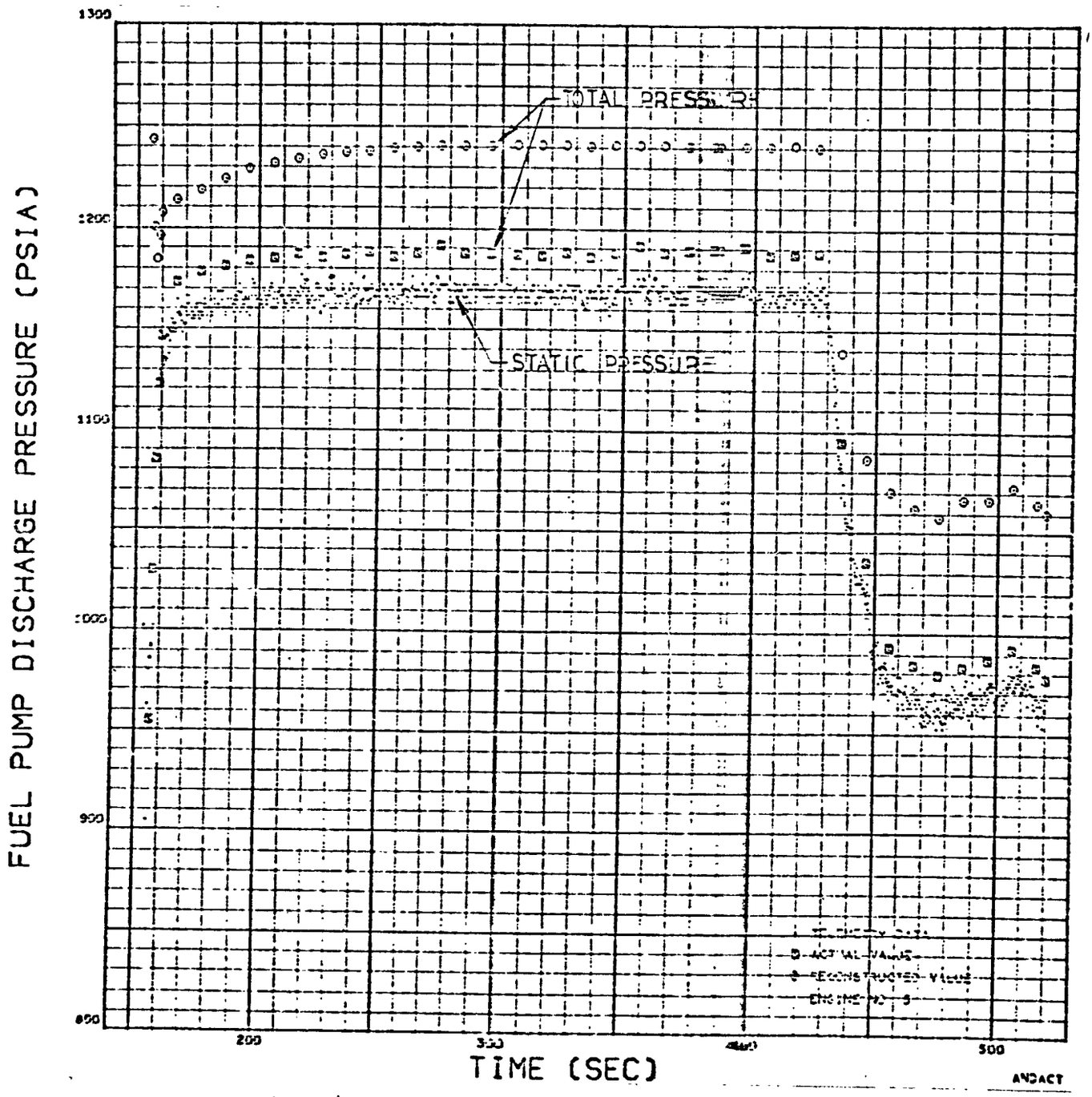

Figure 109. Engine No. 5 Fuel Pump Discharge Pressure

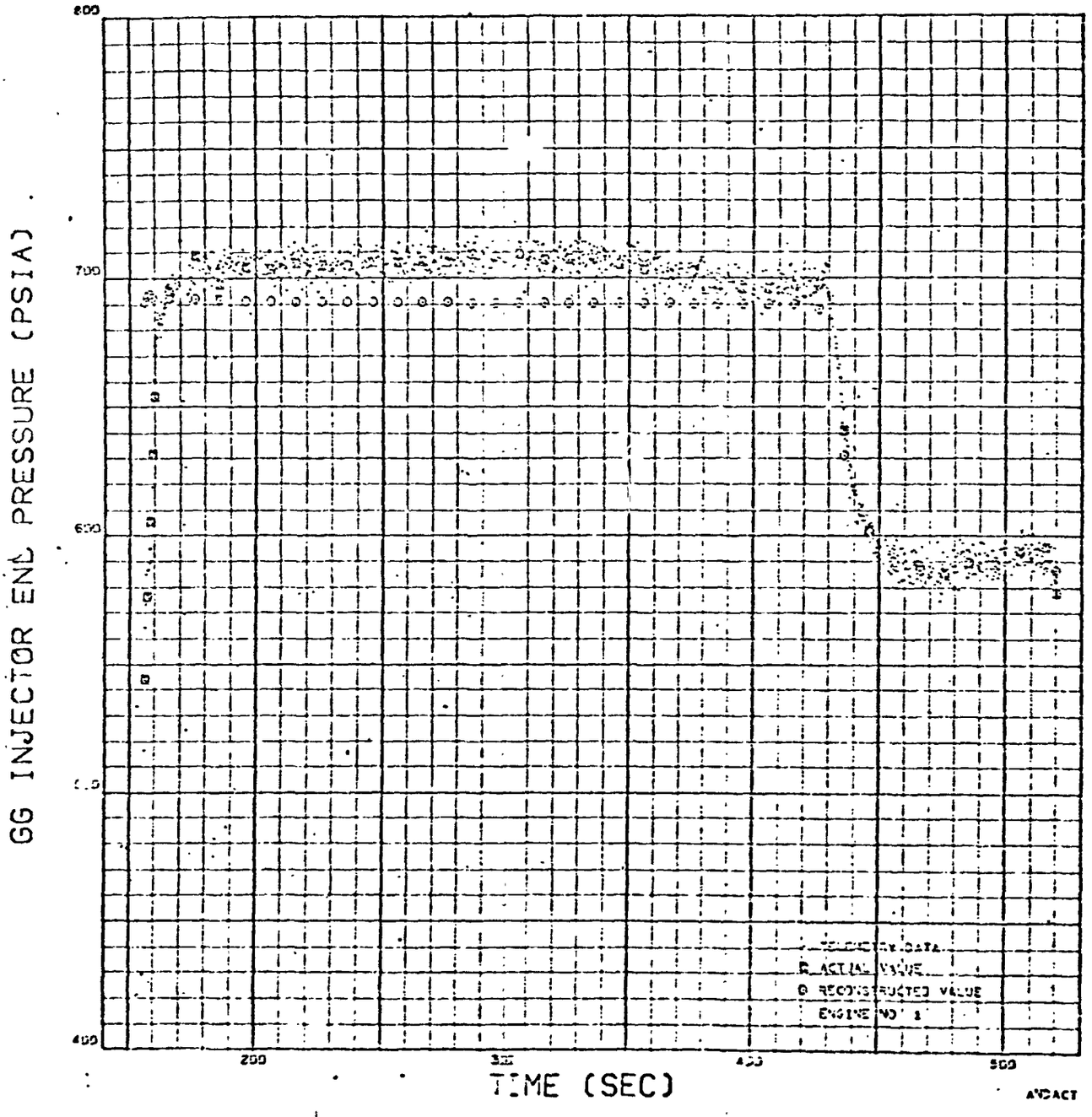

Figure 110. Engine No. 1 Gas Generator Injector End Pressure

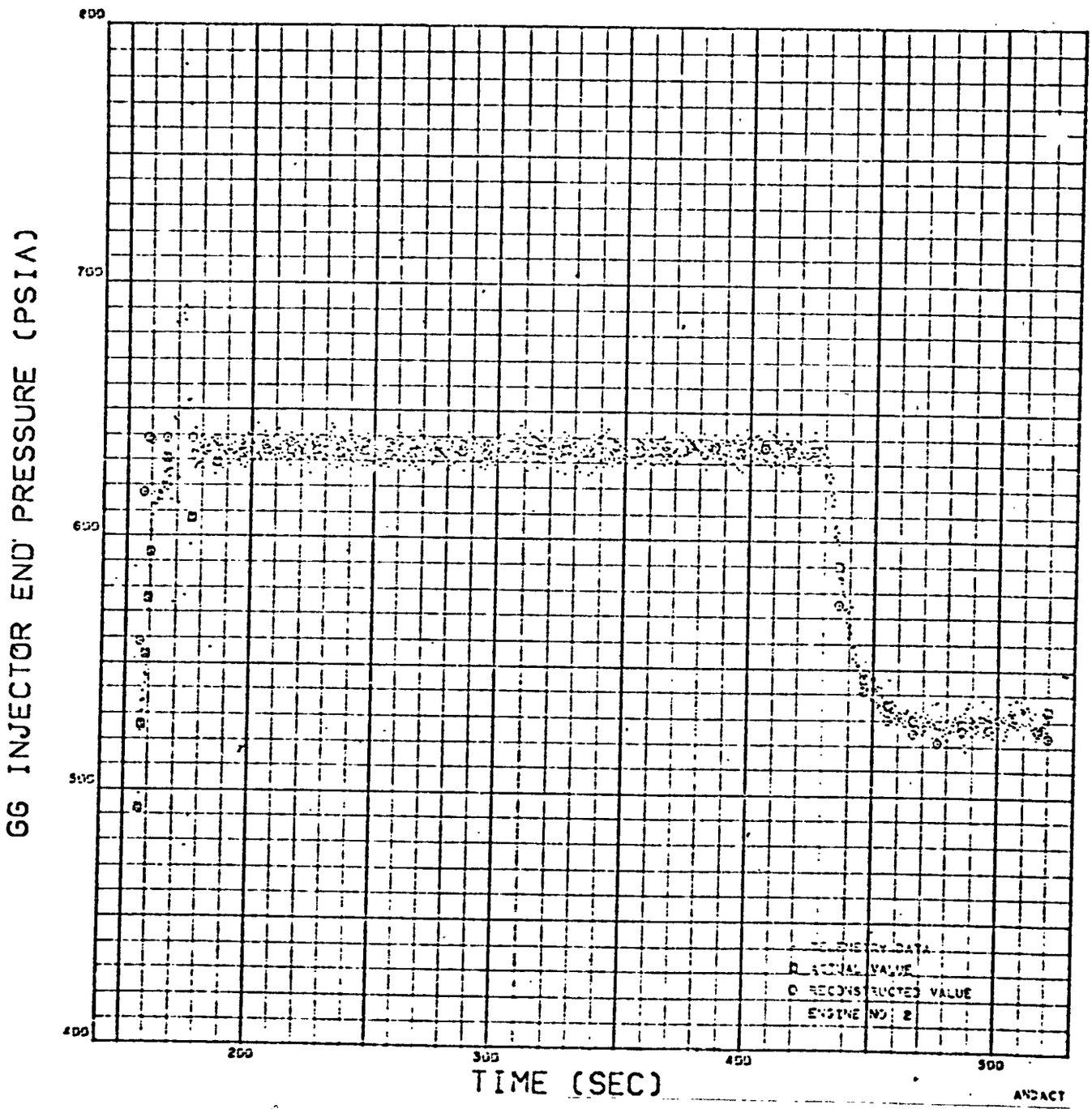

Figure 111. Engine No. 2 Gas Generator Injector End Pressure

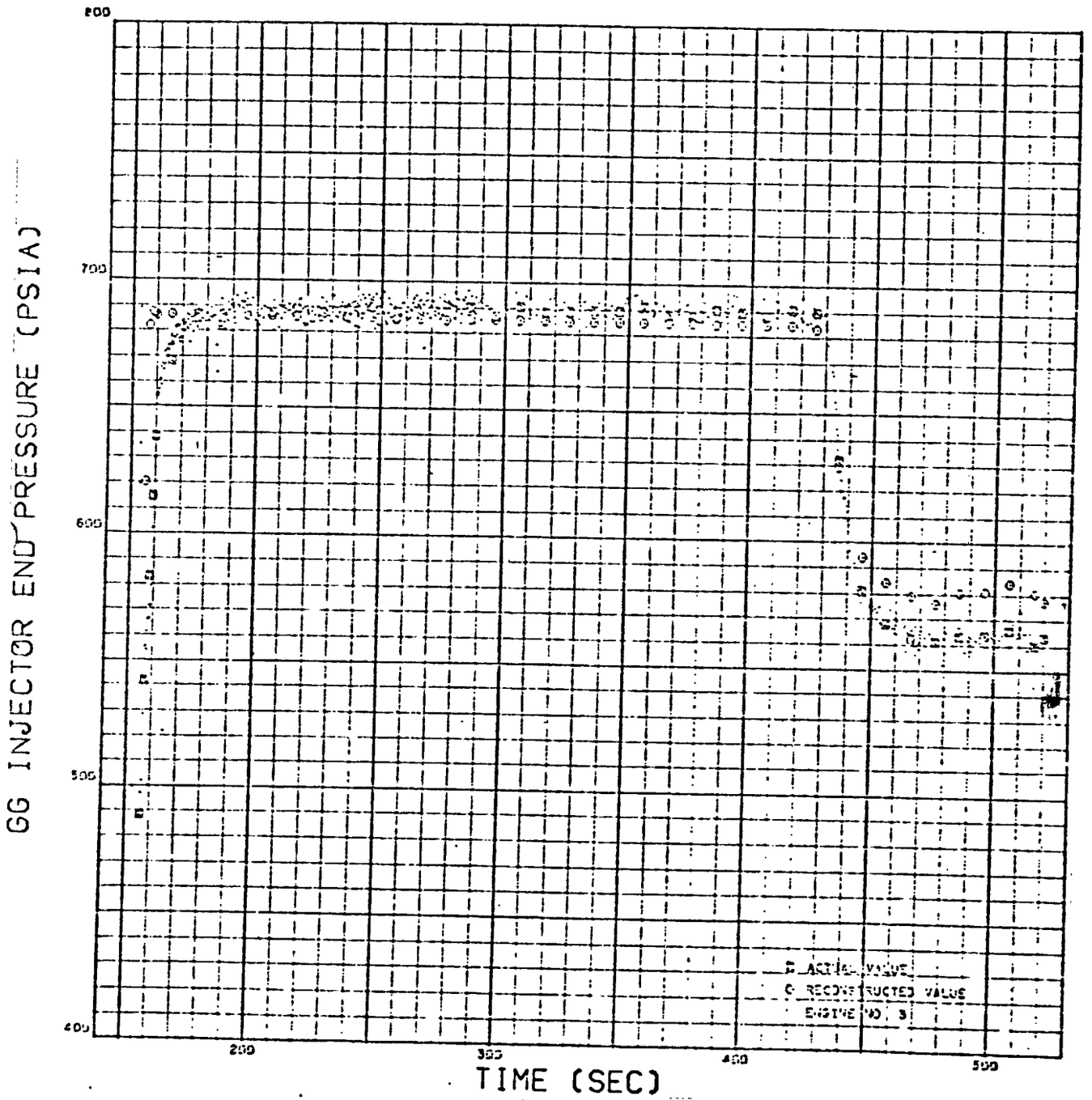

Figure 112. Engine No. 3 Gas Generator Injector End Pressure

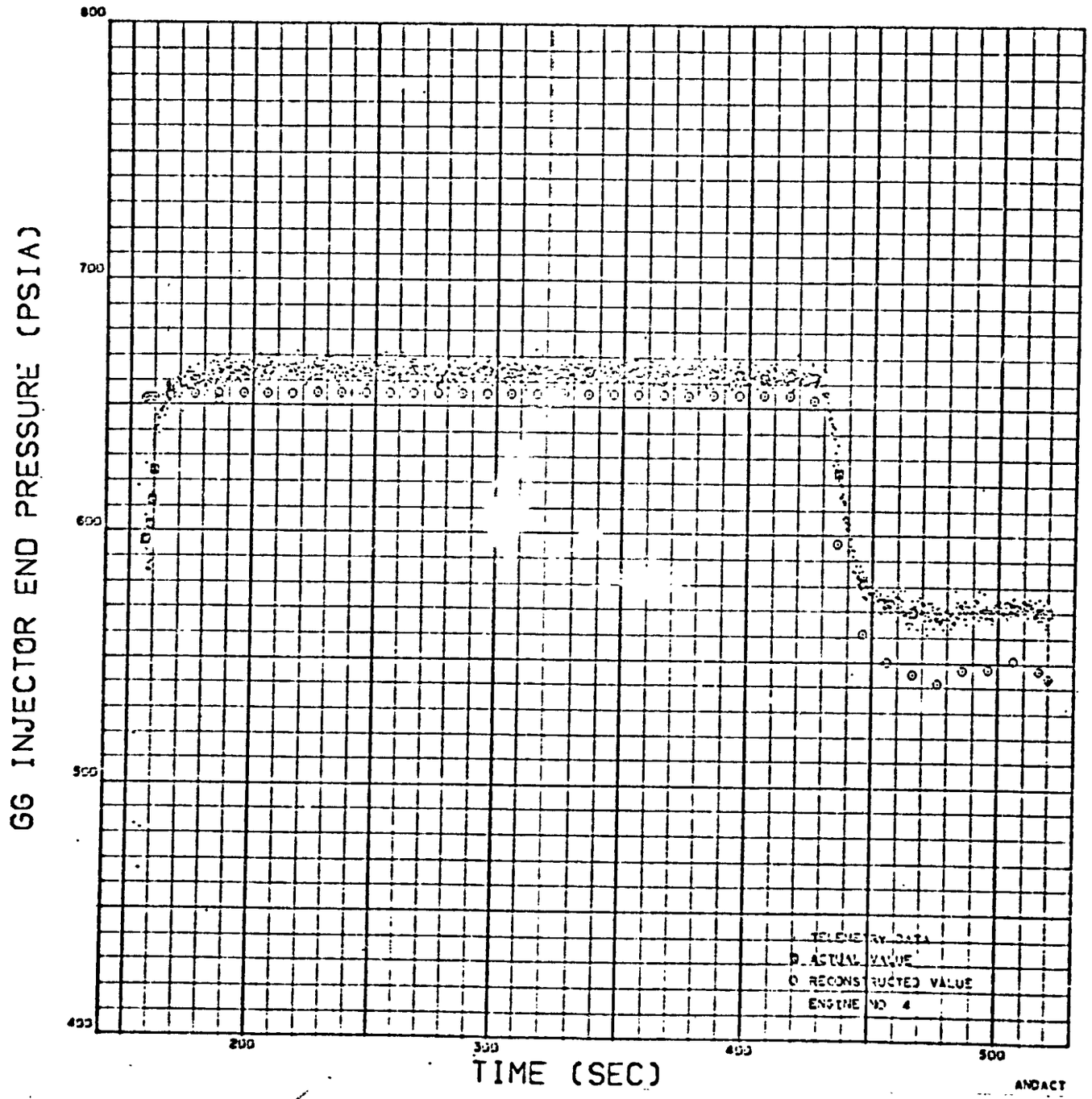

Figure 113. Engine No. 4 Gas Generator Injector End Pressure

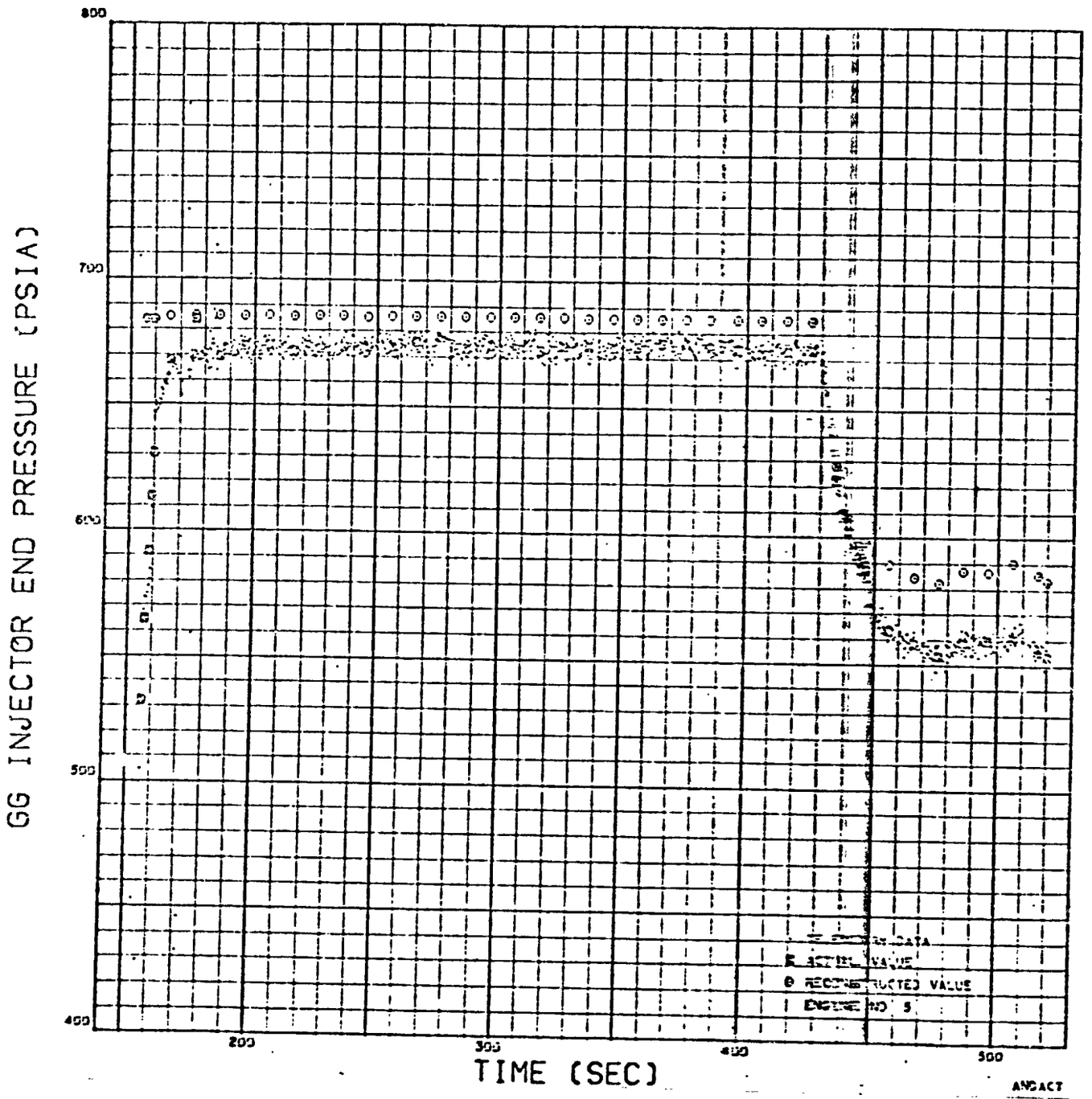

Figure 114. Engine No. 5 Gas Generator Injector End Pressure

TANK PRESSURIZATION PERFORMANCE

The fuel tank pressurization performance is presented in Fig. 115 and 116. The values are within the expected operating bands and consistent with the data seen on vehicle acceptance.

The oxidizer tank pressurization system performance changed between vehicle acceptance testing and the flight. The heat exchanger outlet temperatures and pressurization manifold pressure are presented in Fig. 117 and 118. Individual engine heat exchanger flowrates were not measured on the flight so it was necessary to estimate the flow. The flow was estimated from an operating line based on engine and vehicle acceptance data of heat exchanger outlet temperature as a function of flowrate. This was used to compare vehicle acceptance and flight heat exchanger temperature and pressure for the PU valve fully closed and open (Fig. 119 through 121). Heat exchanger performance was nominal during vehicle acceptance testing. During flight AS-501, the heat exchanger system on engine No. 4 appeared to be obstructed as its flow was low relative to the other engines. This is shown also by the decreased manifold pressure (increased resistance) for flight as compared to vehicle acceptance at the maximum PU level where essentially identical average engine performance and heat exchanger flow exist (Fig. 121).

An analysis based on the tank pressurization volumetric requirements showed that this obstruction in one heat exchanger forced the others to operate at a higher mass flowrate than during static testing. During minimum PU operation near cutoff, a mass flowrate was reached where the heat exchanger system volumetric output was no longer capable of meeting the tank requirement. After this occurred, the oxidizer tank pressure decayed (Fig. 122). The flowrate through the heat exchangers continued to be increased in an attempt to control ullage pressure until the maximum regulator setting was reached. At this high flow, the pressurant was at a saturated vapor condition (Fig. 120). (The exact flowrate could not be determined by use of temperature when this saturated condition was reached.)

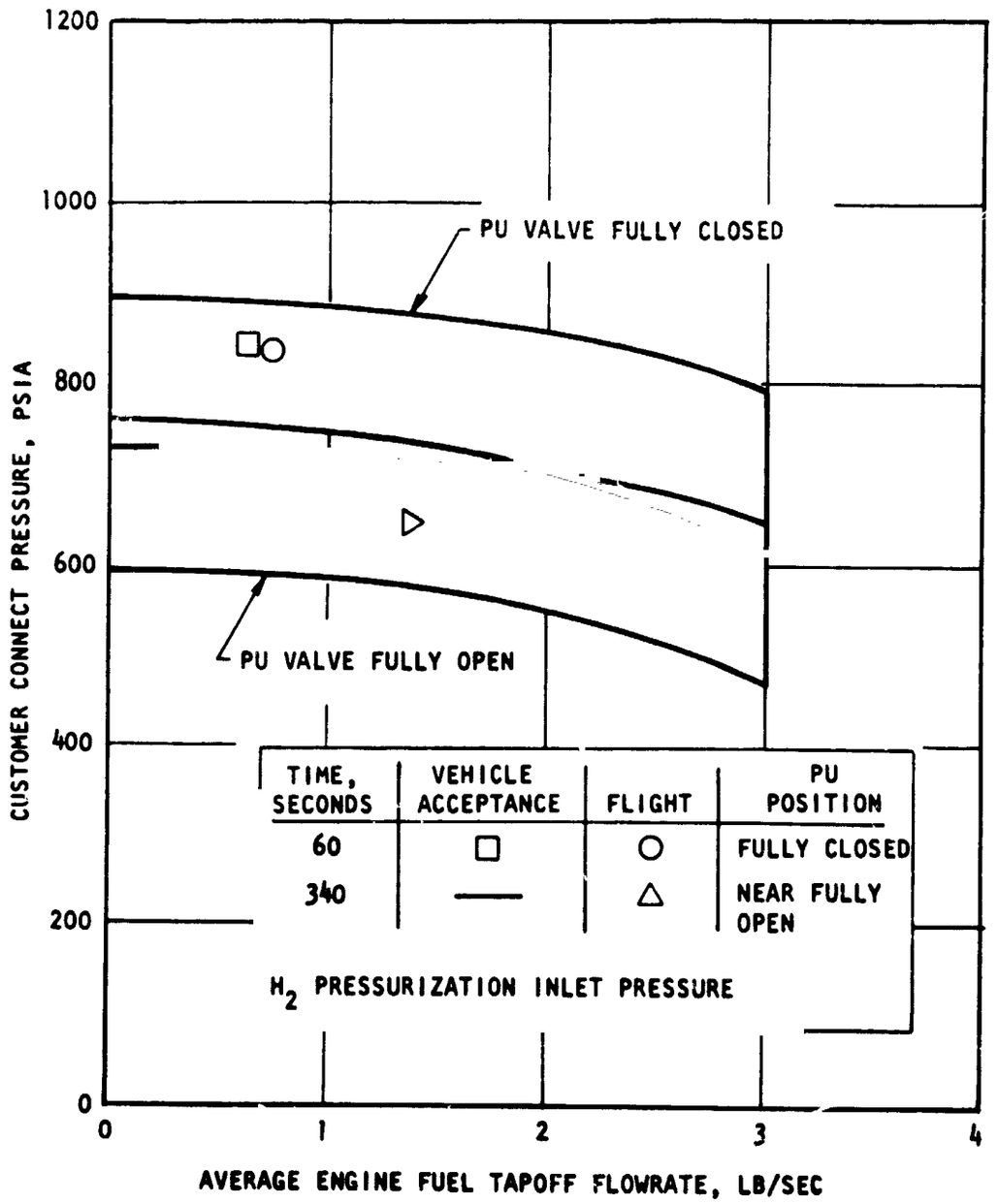

Figure 115. Fuel Tank Pressurization Operating Band

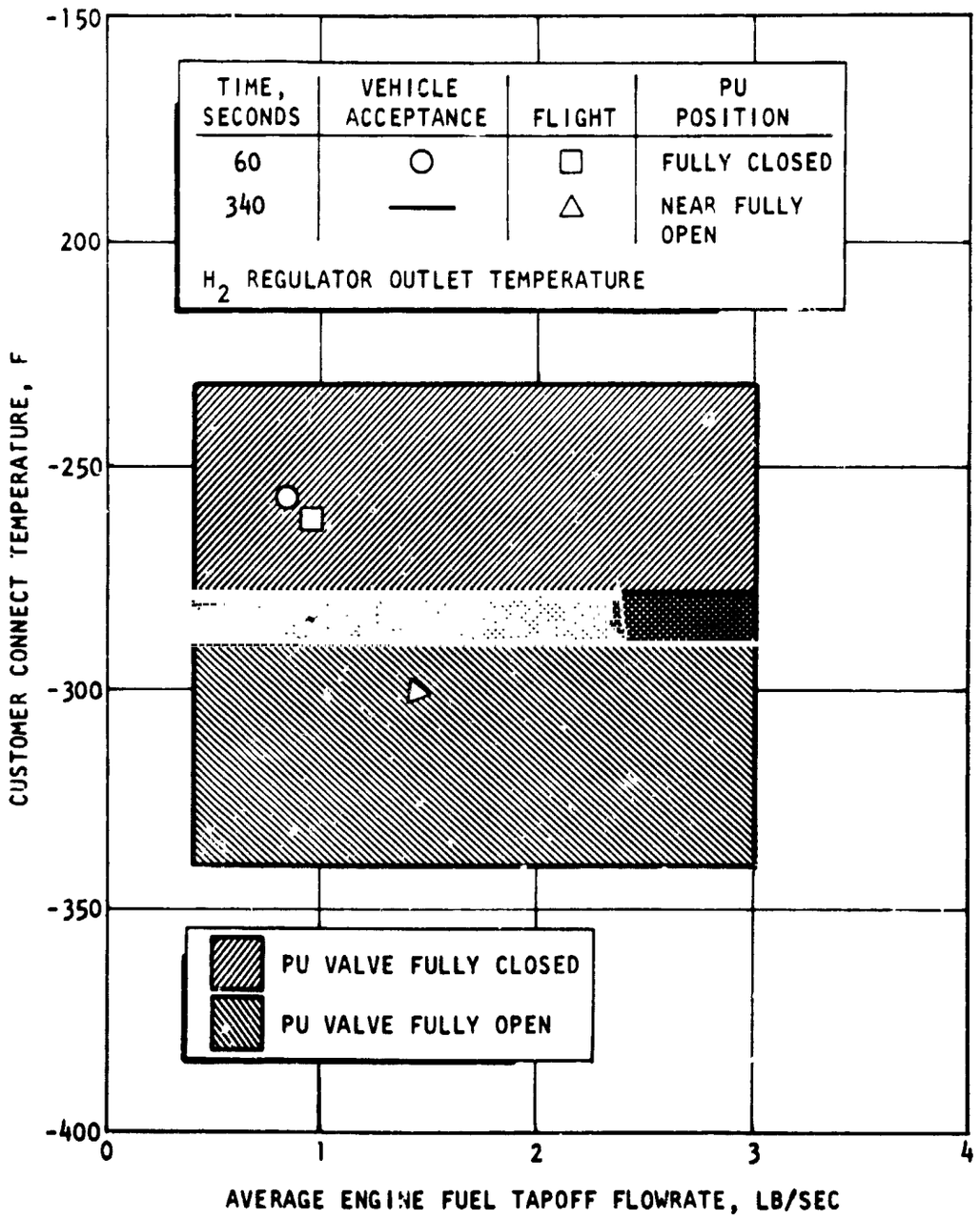

Figure 116. Fuel Tank Pressurization Operating Band

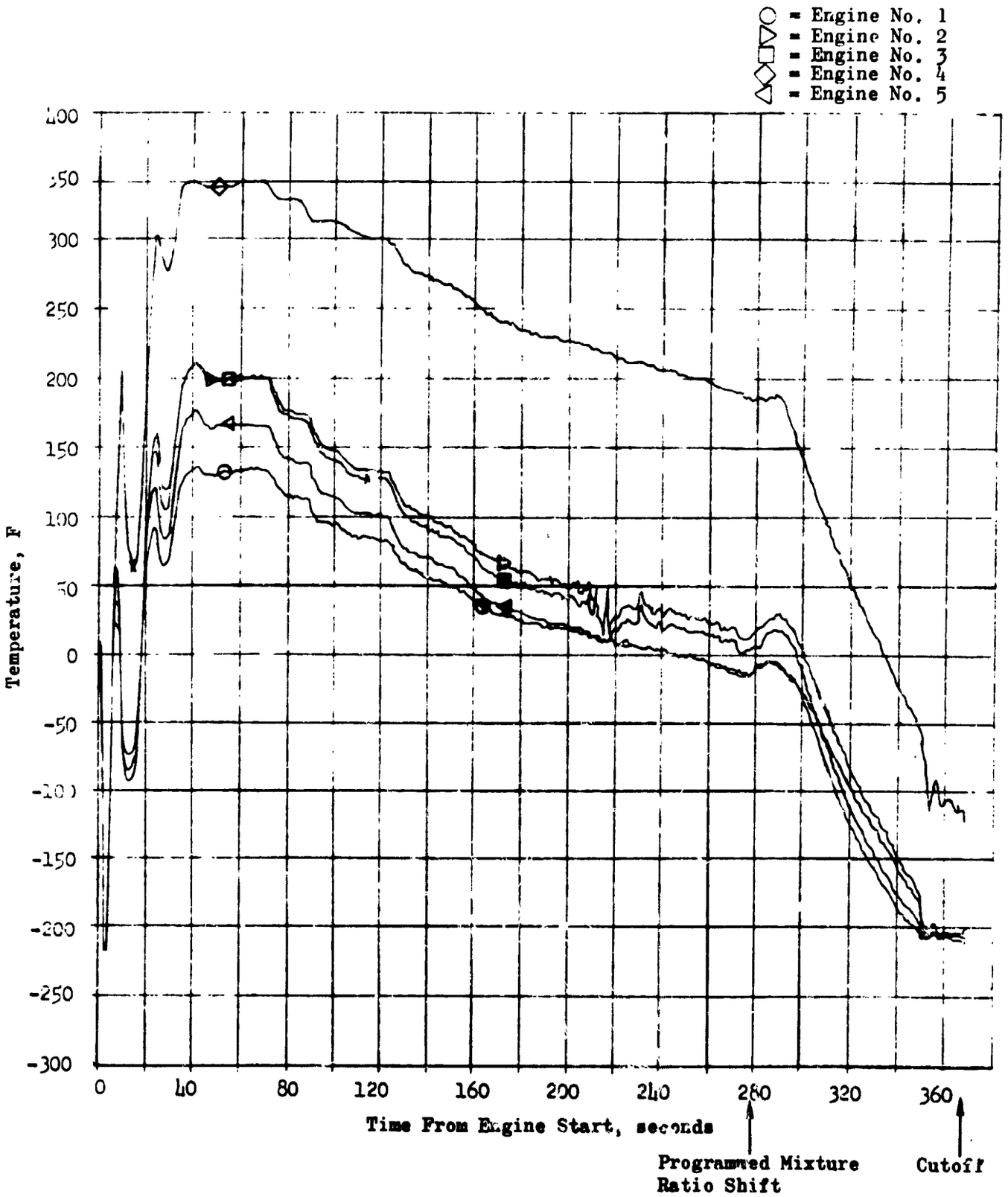

Figure 117. Oxidizer Heat Exchanger Outlet Temperature

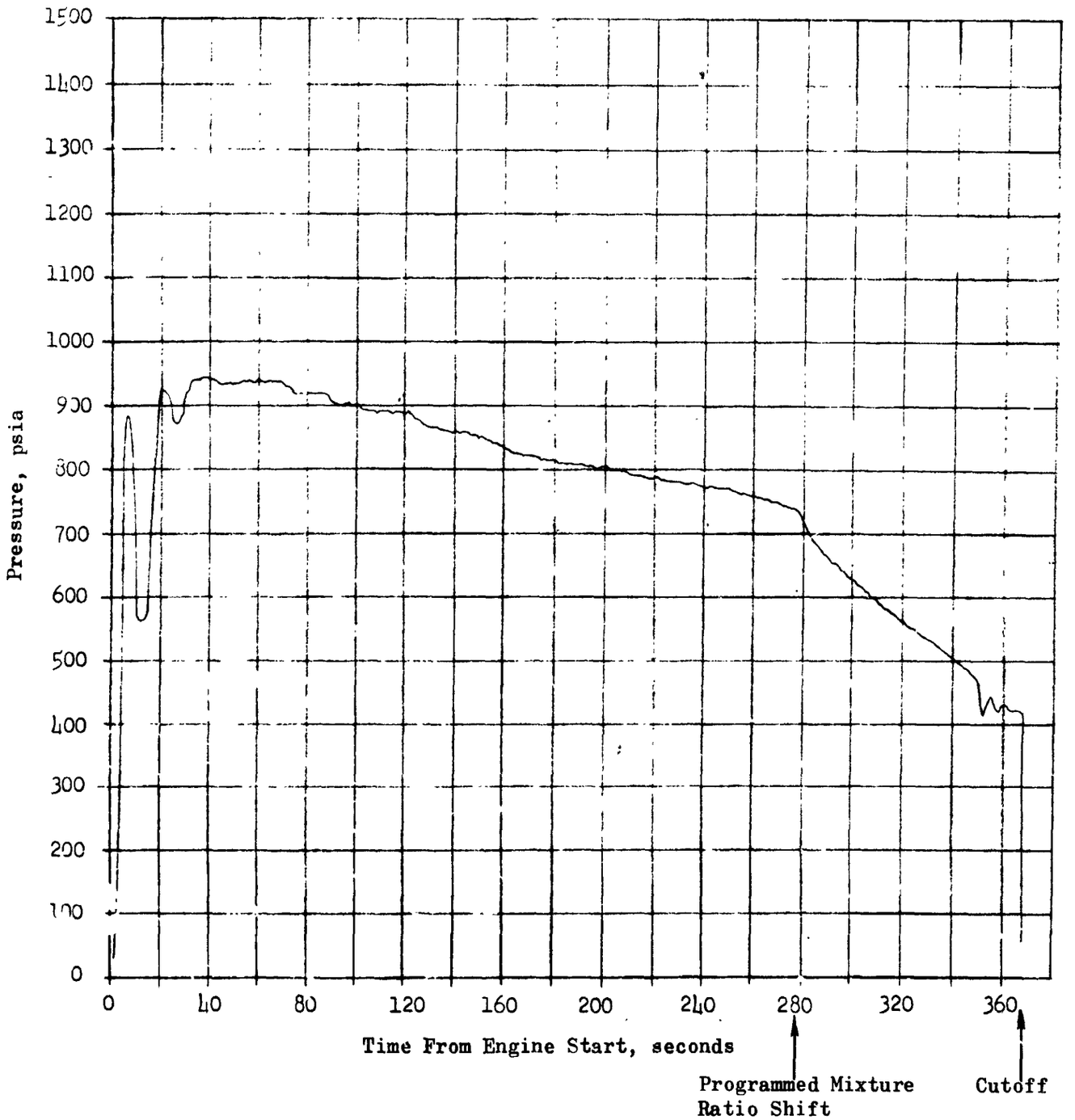

Figure 118. Oxidizer Tank Pressurization Manifold Pressure

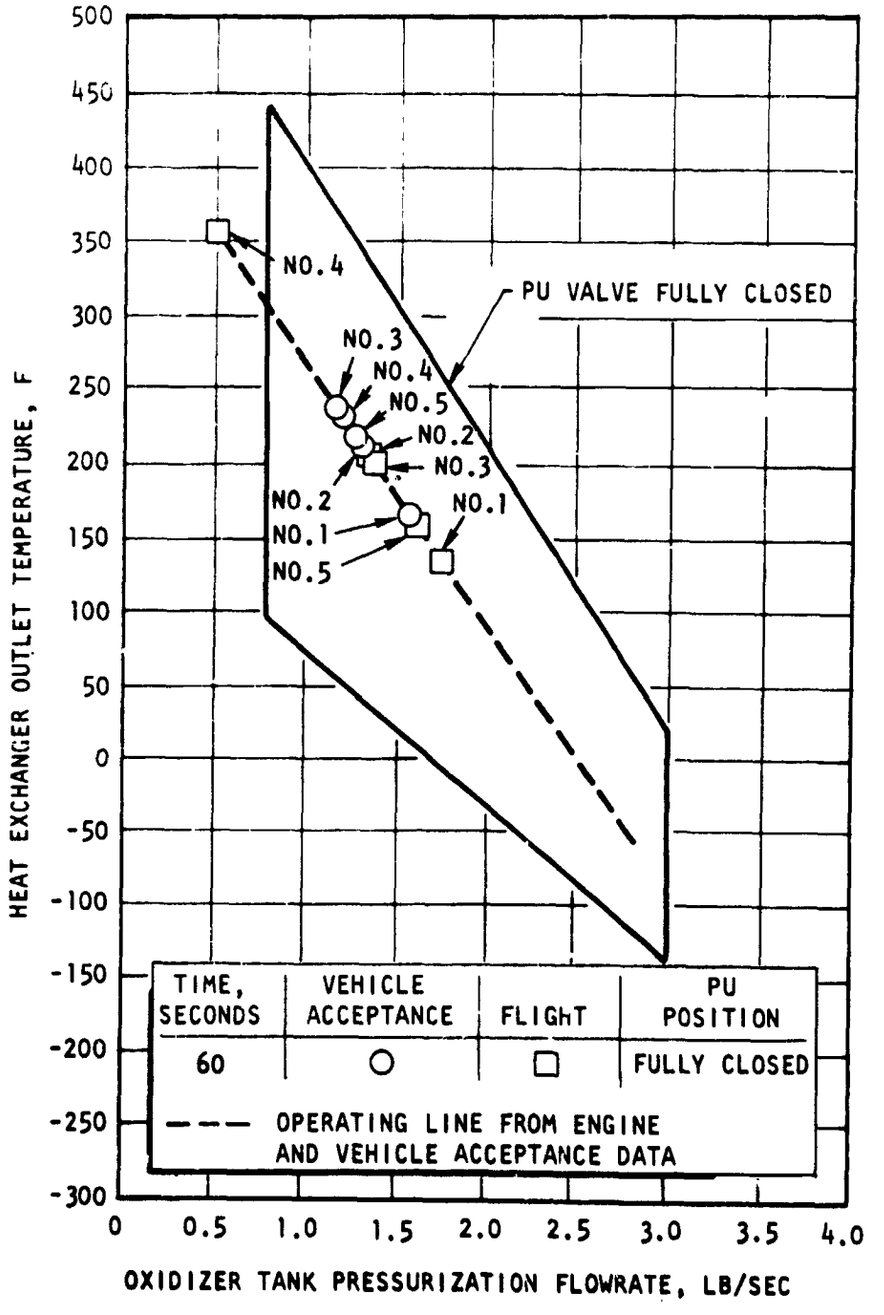

Figure 119. Oxidizer Heat Exchanger Operating Band

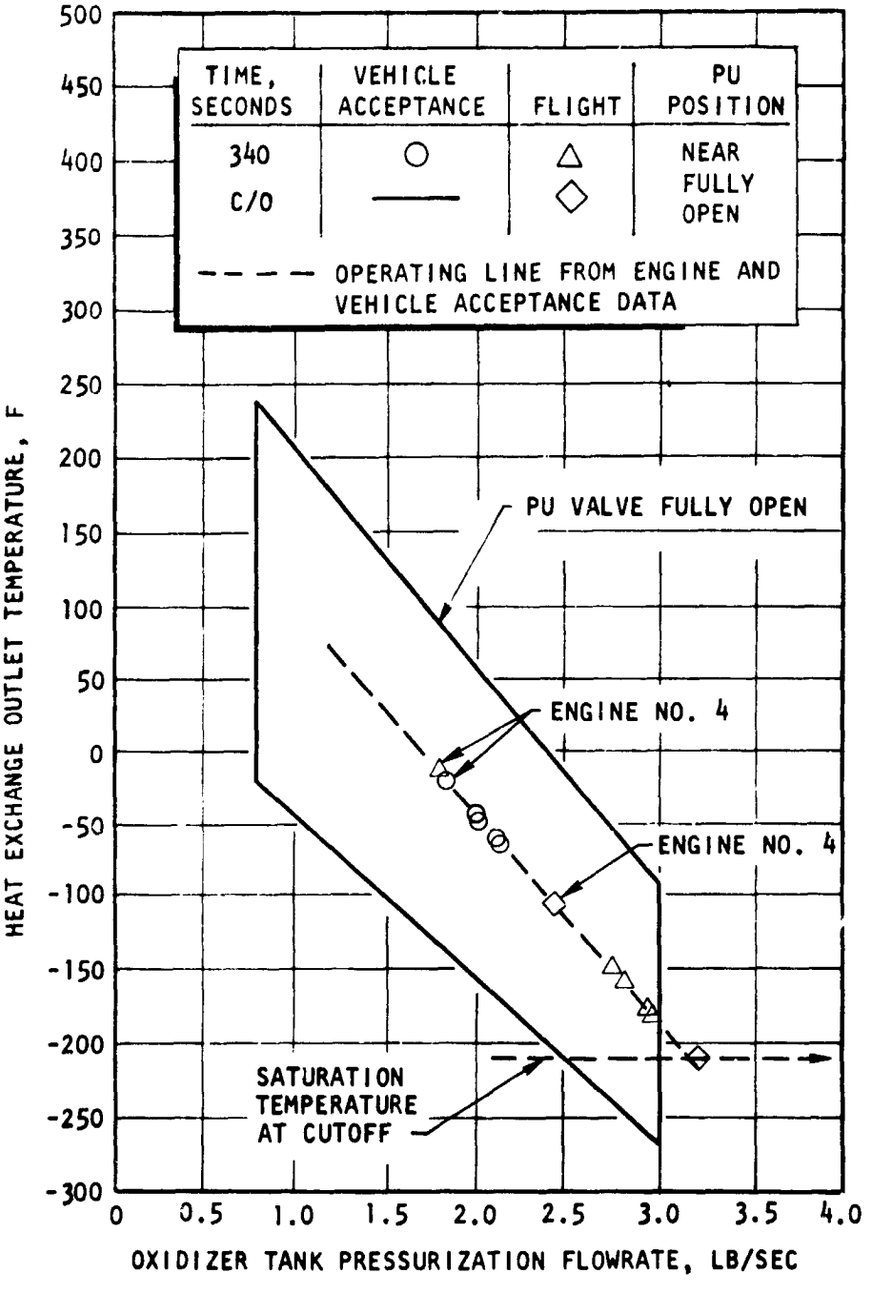

Figure 120. Oxidizer Heat Exchanger Operating Band

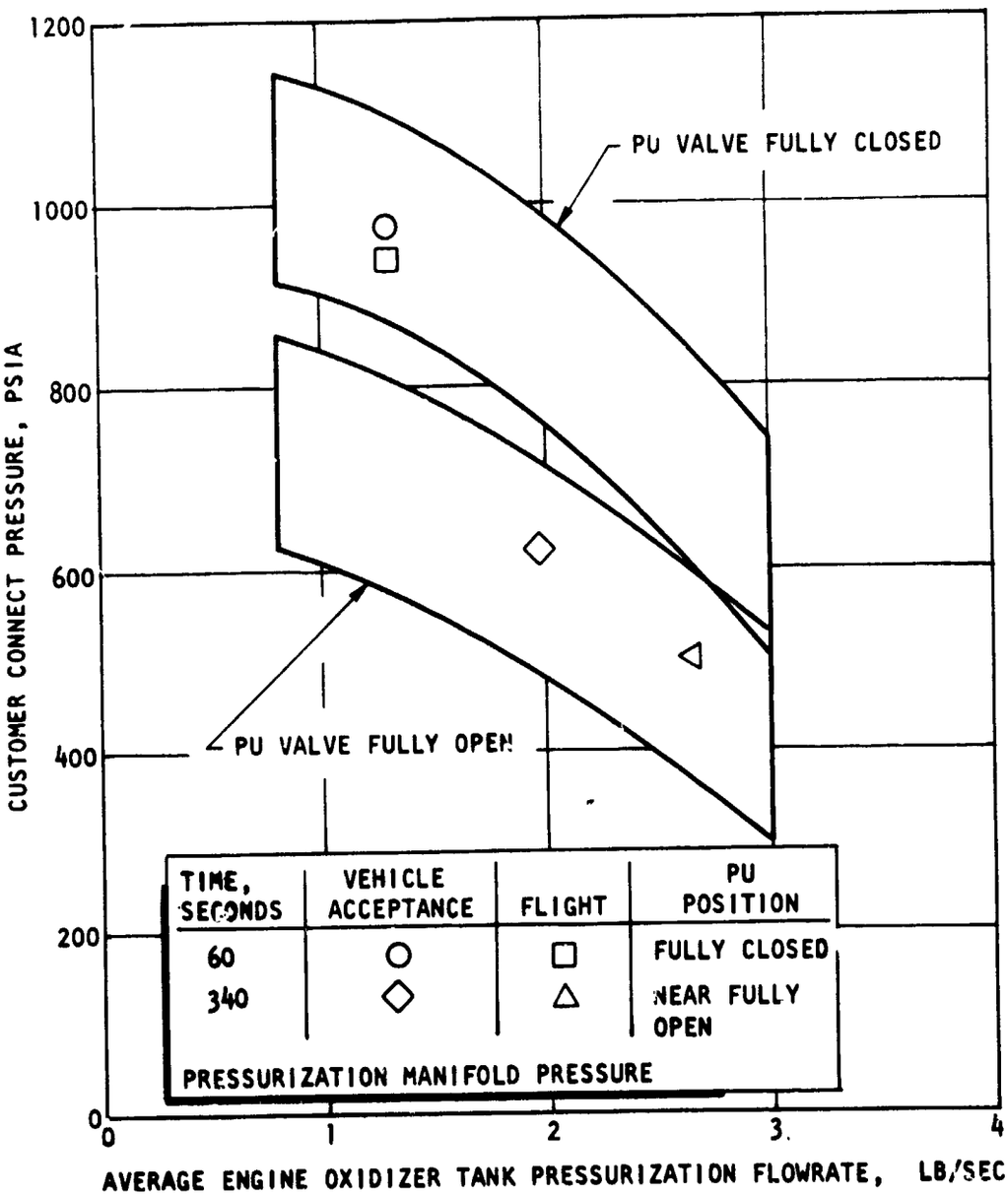

Figure 121. Oxidizer Heat Exchanger Operating Band

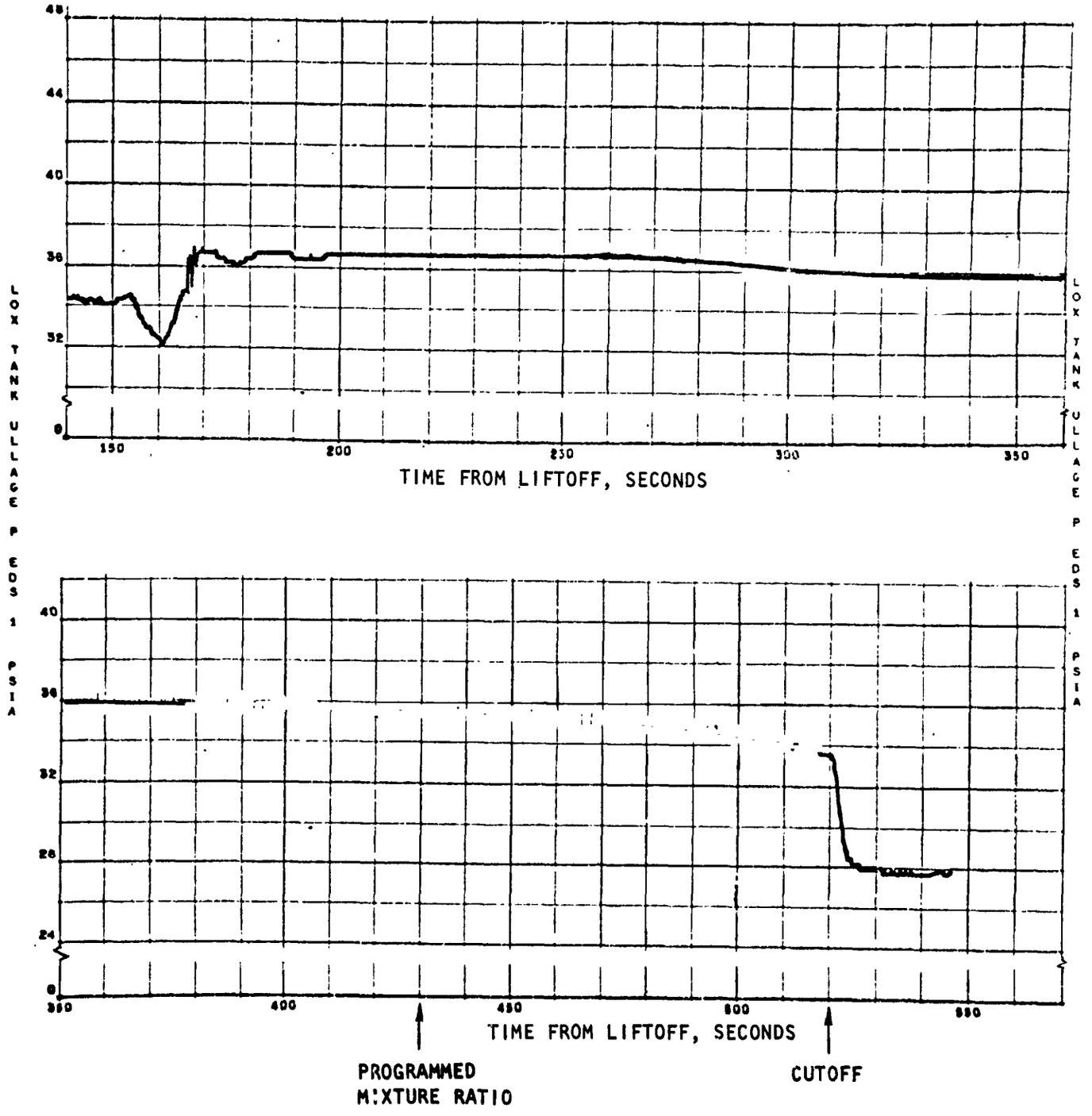

Figure 122. Oxidizer Tank Ullage Pressure

To prevent a reoccurrence of this problem, a heat exchanger filter is being designed to be inserted into the oxidizer supply line. This filter is a wire-mesh configuration that is designed to prevent particles from plugging the heat exchanger and, at the same time, have an insignificant pressure drop.

THRUST DECREASE

The thrust decrease summaries for the S-II stage engines are shown in Table 17.

The actual cutoff impulse values from the flight are about the same as those from engine acceptance tests. This is due to the increase in impulse due to the lower main oxidizer valve actuator temperature on the flight being compensated for by the decrease in impulse due to the lower thrust at cutoff on the flight.

The engine model specification limits on cutoff impulse to 5 percent of rated thrust are 30,000 to 50,000 lb-sec. When the impulse is taken to zero thrust, these limits become 36,400 to 56,400 lb-sec. All flight cutoff impulse values at standard conditions meet the specification requirements. The times from cutoff signal to 5 percent of rated thrust also met the specification requirement (0.800 second maximum).

The thrust decrease traces from the flight are shown in Fig. 123, together with the envelope from engine acceptance testing.

The main oxidizer valve actuator temperature at cutoff was -105 F for the inboard engine. The temperature measurement for the outboard engine failed to record prior to flight. A decision was made not to replace the transducer.

FOLDOUT FRAME 1

TABLE 17

ALTITUDE CUTOFF IMPULSE

Engine No.	1		2	
Engine S/N	J2026		J2043	
Parameter	Engine Acceptance	Flight	Engine Acceptance	Flight
Actual Cutoff Impulse, lb-sec	45,748	39,510	42,213	40,025
Cutoff Impulse at Standard Conditions,* lb-sec	43,790	37,860	42,213	38,518
Time to 5 Percent of Rated Thrust, seconds	0.367	0.380	0.334	0.360
Thrust at Cutoff, pounds	202,340	189,500	200,949	183,900
MOV Actuator Temperature, F	-46**	-105**	0**	-105**
MOV Delay Time, seconds	0.087	0.071	0.076	0.061
MOV Travel Temperature, F	0.173	0.180	0.164	0.180

*Standard conditions: Null PU valve position; main oxidizer valve act of 0 F; standard inlet conditions, pressurizati and auxiliary power extraction

**Assumed, not measured on this engine

FOLDOUT FRAME 2

TABLE 17

ALTITUDE CUTOFF IMPULSE TO ZERO THRUST

	2		3		4		5	
	J2043		J2030		J2035		J2028	
	Engine Acceptance	Flight	Engine Acceptance	Flight	Engine Acceptance	Flight	Engine Acceptance	Flight
	42,213	40,025	44,657	40,310	44,045	44,575	42,626	41,922
	42,213	38,518	44,657	39,200	44,045	43,322	42,626	41,389
	0.334	0.360	0.336	0.310	0.300	0.340	0.345	0.370
0	200,949	183,900	194,989	177,700	204,015	191,400	200,915	178,700
	0**	-105**	0**	-105**	0**	-105**	0**	-105
	0.076	0.061	0.082	0.061	0.087	0.081	0.076	0.091
	0.164	0.180	0.177	0.190	0.170	0.210	0.162	0.190

main oxidizer valve actuator temperature
conditions, pressurization flowrates,
raction

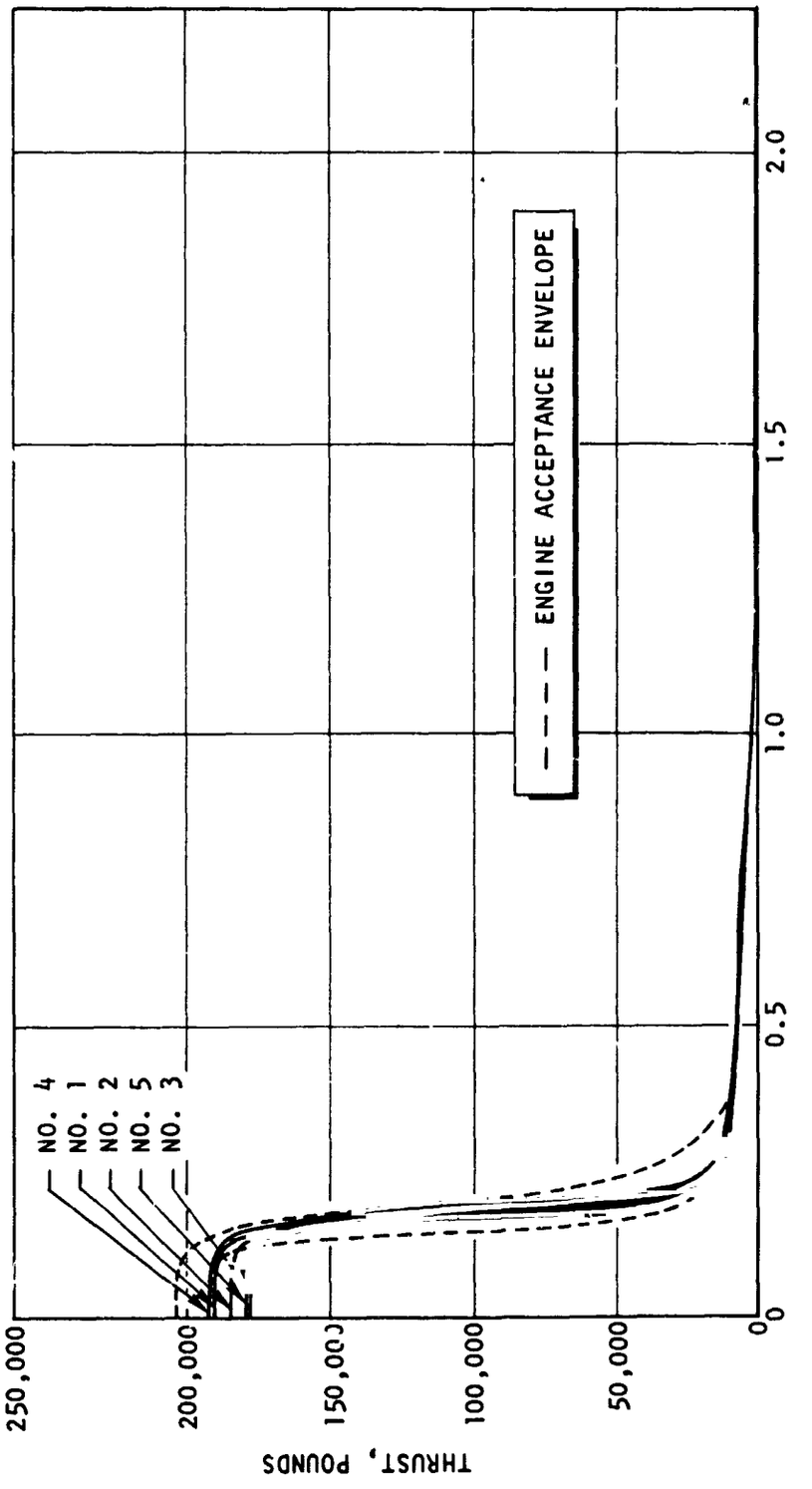

Figure 123. S-II Thrust Decrease Transient

ELECTRICAL SYSTEM

The battery voltages of the S-II stage are presented in Table 18. All battery voltages appear normal. Although the S-II stage does not measure ECA control bus and ignition bus voltages, it can be assumed that engine voltage limits (Table 19) were met satisfactorily during the mission. No problems are evident in the engine electrical system.

TABLE 18

S-II BATTERY VOLTAGES

Measurement No.	Measurement Name	Liftoff	Engine Start	Second Plane Separation	Engine Cutoff
M020-207	Main d-c bus voltage	30.2	29.5	29.5	30.0
M125-207	Ignition d-c bus voltage	26.5	30	*	*

*Battery jettisoned

TABLE 19

ENGINE VOLTAGE LIMITS

Control Power	22 to 31 d-c
Ignition Power	24 to 31 d-c

ENGINE GIMBAL DATA

The engine actuation system on the stage performed satisfactorily during flight, with no significant anomalies noted. The data below indicate the peak actuator loads and maximum gimbal displacement incurred during the boost phase.

Engine No.	Actuator Position	Peak Actuator Loads*, pounds	Maximum Gimbal Displacement**, degrees
1	Pitch	+5,200	-0.9
	Yaw	-5,200	-1.0
2	Pitch	-4,875	±0.75
	Yaw	-4,550	+0.25
3	Pitch	-7,800	+1.0
	Yaw	-5,850	-0.75
4	Pitch	-10,400	+1.1
	Yaw	+3,900	-1.3

*Actuator loads: (-) tension; (+) compression
**Gimbal displacement: (-) actuator retract; (+) actuator extend

There are no problems evident in the engine gimbal data.

VIBRATION ANALYSIS

Analysis of the J-2 engine vibration data, supplied by the MSFC facility, from the S-II stage of the AS-501 flight produced limited valid results. The S-II stage engine cluster data were considered valid during the S-II stage operation, but the validity was limited to the oxidizer pump measurement only during maximum performance for the engine cluster operation. The remainder of the S-II stage engine operation vibration data were questionable, based on the frequency spectra analyses that presented unrealistically similar flat response characteristics for the three engine locations.

Start transient evaluation was seriously impaired by the overranging of the vibration measurements which were scaled for the lower mainstage vibration levels. The engine vibration data, as supplied by MSFC, from the S-II stage during the AS-501 vehicle flight, were analyzed for overall instrumentation performance and response characteristics. A total of 16 engine associated measurements were recorded: the engine dome, oxidizer pump and fuel pump for each engine, plus one gimbal pad measurement. All engine measurements appeared operative during their respective stage operation.

The engine vibration data were recorded on a continuous basis. The MSFC facility provided oscillogram playback and power spectral density (PSD) analysis of the vibration measurements during the S-IC stage and S-II stage operation. The majority of these data during engine operation were questionable. Three S-II stage operation time intervals were sampled for PSD analysis at flight times of 156, 165, and 171 seconds from liftoff (engine cluster ignition occurred at 153.1 seconds). The time interval of 171 seconds has been invalidated (because of telemetry system noise) by the MSFC evaluation group. With the exception of the cluster engines: oxidizer pump data sample at 165 seconds, the vibration data during engine operation were characterized by a questionable flat amplitude response level versus frequency which was similar for the three engine locations. In contrast to these results, static test data produced distinct frequency response characteristics associated with the engine dome and with each turbopump location. The possible validity of the oxidizer pump vibration measurement at 165 seconds was attributed to the lower vibration environment associated with PU change from nominal to maximum engine performance by reducing the oxidizer pump recirculation flow.

As vibration levels exceeded approximately 7 g rms, the data became questionable. A cause of this data condition may be the use of relatively low calibration levels of 35 g rms as compared with the 150 to 200 g rms range used for engine static tests. Although the 35 g rms calibration value is applicable for engine data for 50 to 3000 Hz, the telemetry transmission

bandwidth, the accelerometer, and airborne charge amplifier were operating wideband, 10 to 20,000 Hz, which required the higher measurement range to prevent the high-frequency harmonics from overdriving the amplifier output. The remaining PSD analyses of the S-II stage measurements were made during S-1C stage operation sampled at four time intervals: 1 second (liftoff), 21 seconds, 67 seconds (Mach 1), and 86 seconds (max Q). The maximum levels occurred at liftoff with values ranging from 0.5 to 1.3 g rms, as listed in Table 17.

The MSFC oscillogram oxidizer pump data indicated that the engine cluster performance changed from nominal to maximum at 157.5 seconds, flight time, and that performance again changed at approximately 430 seconds, a decrease from maximum for propellant utilization. (A 0.10-second transient was evident on the stage vibration measurements at 181 seconds, which was attributed to the interstage separation event.) The engine cluster cutoff occurred at 519.5 seconds as referenced to the mainstage vibration level decrease. Following cutoff, transient activity was indicated on all measurements at 520.6 and at 525.0 seconds, but was not conclusively determined to be data or telemetry system noise.

The S-II stage engine cluster's nominal main propellant ignition occurred at 153.1 seconds from liftoff. The peak levels from the MSFC data were 20 to 30 g peak to peak at the engine dome. The high-speed data exhibited a distorted or a shifted effect on these same measurements. The peak activity on all engine measurements occurred 0.5 seconds later and was concluded to be the oxidizer dome prime transient. The levels and durations of this transient could not be definitely determined from the overdriven characteristic. The total duration also included the additional time for amplifier recovery. By utilizing the pump measurements which had the least severe levels, a rough estimate of the durations ranged from 0.050 to 0.200 second for the five-engine cluster. The high-speed data playback verified the priming time initiation of 153.6 seconds, but the duration and apparent interaction of the measurements produced questionable levels.

#4

Engine Start Transients

The engine start transient vibration data were analyzed for determination of levels and duration during the ignition and transition into mainstage periods. These data from the MSFC oscillograms and additional high-speed oscillograms had overdriven or questionable portions during the S-II stage engine start that prevented conclusive results. Direct comparison of the flight transient data levels with static test results was limited by the telemetry system frequency recording bandwidth of 50 to 3000 Hz. The major energy content of static test transient data (recorded 10- to 10,000-Hz bandwidth) is in the 2000- to 6000-Hz frequency range.

Analysis of the S-II stage engine vibration data resulted in the following:

1. The maximum J-2 engine vibrationlevel during the S-1C stage operation occurred at liftoff with a value of 1.3 g rms.
2. The majority of the S-II stage engine vibration data during the engine cluster operation were determined to be invalid. This result was attributed to use of the low calibration range for the airborne amplifiers which were operated wideband from 10 to 20,000 Hz. This wideband system passed the higher frequency harmonics that caused overdriven or limited amplifier outputs to be fed to the telemetry transmission system.

BOATTAIL LEAKAGE

The oxidizer pump seal leakage into the boattail of the S-II stage was alleviated by means of a burst diaphragm assembly installed near the exit of the oxidizer pump primary seal cavity drain line, thus forcing the oxygen to be routed through the overboard drain line. The burst diaphragms, one each on the respective engine, withstood the static leakage during the S-IC boost phase, and the pressure in the oxidizer pump primary seal cavities ranged from 0.5 psia on engine No. 4 to 3 psia on engine No. 2.

Performance of the diaphragms during the powered flight of the S-II stage is presented below.

Engine S/N	Engine No.	Diaphragm Pressure		Mean Primary Seal Cavity Pressure	
		Time From Engine Start, seconds	Pressure At Break, psia	During Maximum PU, psia	During Nominal PU, psia
J2026	1	12	22	10 to 15	9 to 13
J2043	2	26	22	8 to 12	8 to 9
J2030	3	8	21	12 to 20	12 to 17
J2035	4	5	16-1/4	7-1/2 to 11	12 to 16*
J2028	5	268	19	14 to 18	6 to 8

*Pressure rise attributed to increased turbopump leakage

Insufficient volumetric flow resulted in the burst diaphragm on engine J2028 being able to survive two-thirds of the S-II flight duration; the diaphragm ultimately ruptured, with the cavity pressure remaining low.

The burst diaphragms have performed as expected, and representative plots are depicted in Fig. 124 and 125. The combined engine leakage rate during propellant tanking operation was very low, and the gas analyzer registered 0.24 percent concentration of oxygen as compared against a redline of 3 percent concentration.

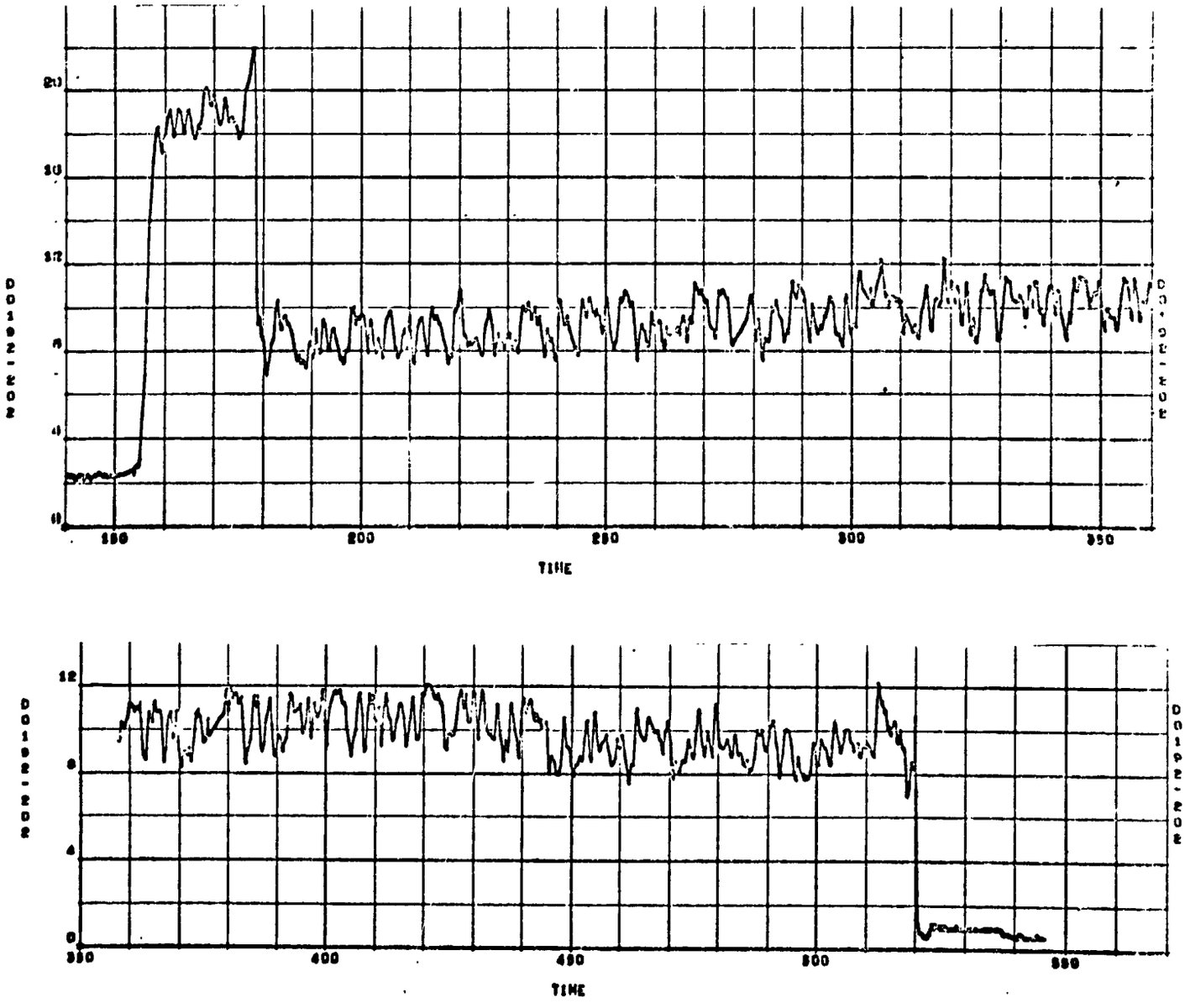

Figure 124. Performance of Burst Diaphragm on Engine No. 2 (S-II Stage)

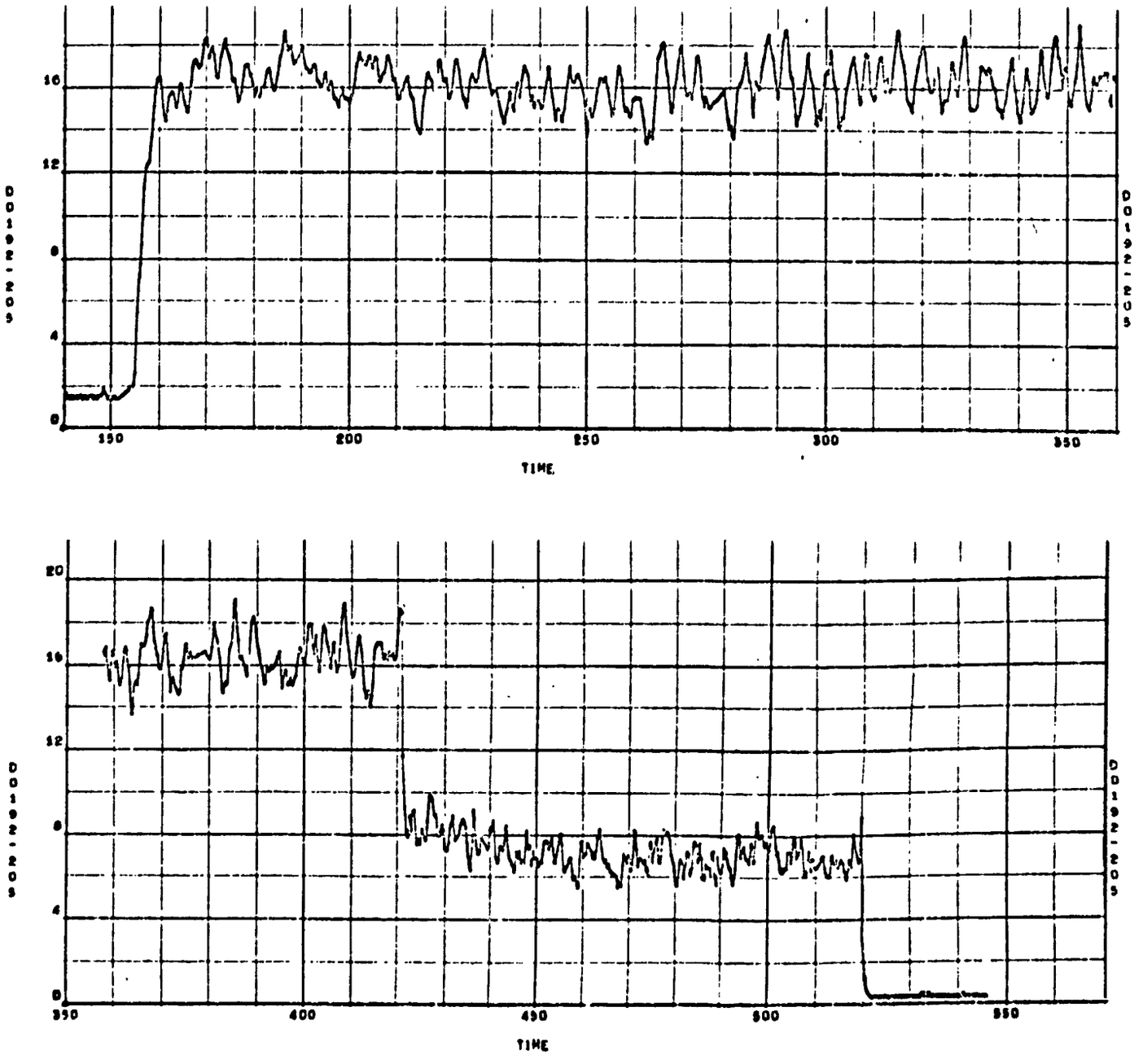

Figure 125. Performance of Burst Diaphragm on Engine No 5 (S-II Stage)

THERMAL ENVIRONMENT

Prelaunch

The prelaunch sequence from initiation of tanking to liftoff was normal. The propellant tanking was accomplished in the following sequence:

1. S-IC fuel on board prior to start of countdown
2. S-IVB oxidizer loading
3. S-II oxidizer loading
4. S-IC oxidizer loading
5. Oxidizer replenishing of all stages
6. S-II fuel loading
7. S-IVB fuel loading

The significant temperatures prior to liftoff, which were a result of the thermal environment and engine preconditioning during this period, were as follows:

1.	Engine area ambient temperature, F	-70
2.	MOV actuator temperature, F	-130
3.	MOV closing control line temperature, F	-85
4.	Electrical control assembly temperature, F	+20
5.	Thrust chamber jacket temperature, F	-245

Oxidizer was down to the MOV for approximately 4 hours. The warmer GN_2 boattail purge in the S-II stage accounted for the warmer engine thermal environment as compared with the S-IVB stage. The boattail purge was initiated just prior to propellant tanking.

Boost Phase

The boost phase covers the period from liftoff of the vehicle to separation of the S-IVB stage from the expended S-II stage.

The S-IVB interstage environment experienced during boost in flight AS-501 was below those predicted (Fig. 126), but was similar to that of flight AS-202 (Ref. R-6750-3) for the same period of boost (150 seconds). The aft interstage skin temperature profile was similar to that predicted, but peaked at a lower value, +165 F, instead of +425 F (Fig. 126).

The thrust chamber jacket temperature at liftoff was within the predicted band of -160 to -280 F (Fig. 127). Rate of thrust chamber jacket warmup was less than predicted, primarily because of colder than predicted aft interstage skin temperature (Fig. 126), which resulted in a reduced contribution from radiation during the final boost phase. The low chill (-250 F at liftoff), together with a lower than predicted aft interstage skin temperature, resulted in the jacket temperature being out of the predicted band of -80 to -180 F at engine start (-200 F at engine start). The thrust chamber nozzle exit heatup rate during boost was similar to that of thrust chamber jacket heatup rate. As with the thrust chamber jacket temperature (Fig. 127), the thrust chamber nozzle exit temperatures (C0385 and C0386) were also out of the predicted band at engine start (Fig. 128).

The MOV temperature in the S-IVB stage was slightly colder than in the S-II stage at liftoff, and was probably caused by the warmer GN_2 boattail purge in the S-II stage. However, the MOV temperatures were similar to that experienced on the AS-202 and AS-203 flights at liftoff (Ref. R-6750-3 and R-6750-2), and within the predicted band at engine start (Fig. 129). The MOV closing control line temperature was -78 F, as compared to the predicted band of -20 to -100 F. The MOV actuator temperature was -145 F, as compared to the predicted band of -140 to -250 F. Figure 129 depicts the two MOV measurements and engine area ambient temperature during boost and J-2 engine operation. The rise in temperatures at J-2 engine start

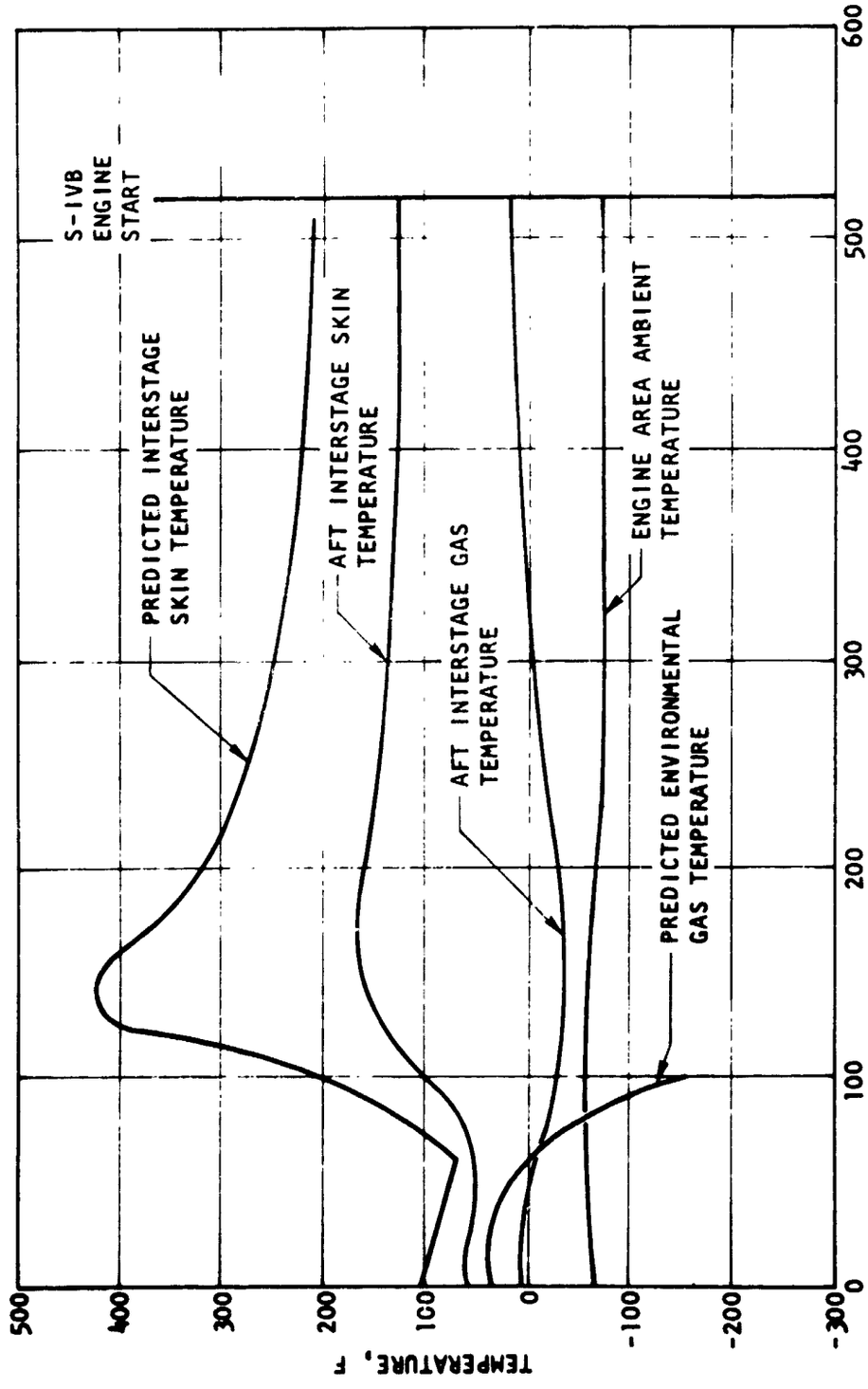

Figure 126. S-IVB Aft Interstage Environment Temperature During Boost

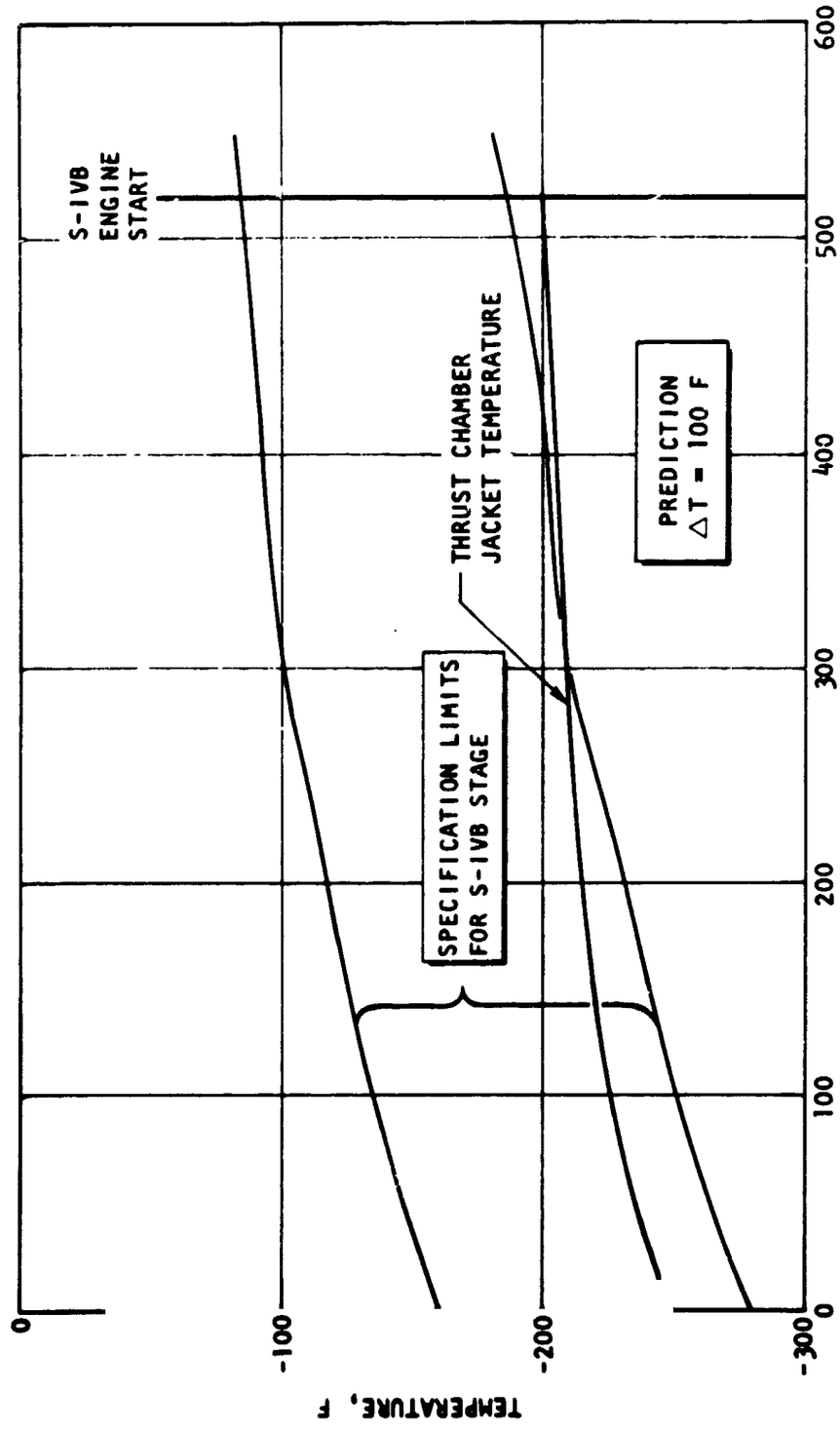

Figure 127. Thrust Chamber Jacket Heatup During Boost

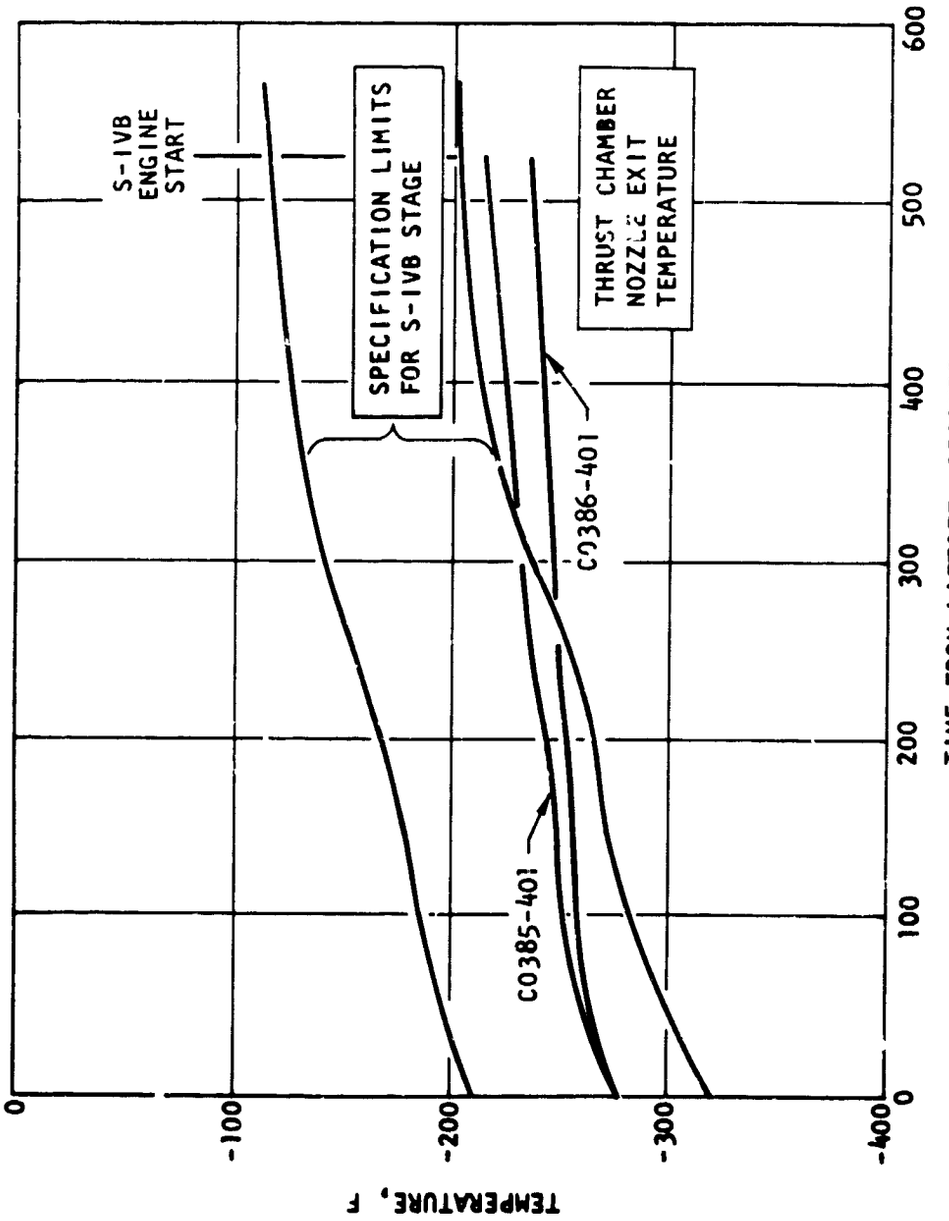

Figure 128. Thrust Chamber Nozzle Exit Heatup During Boost

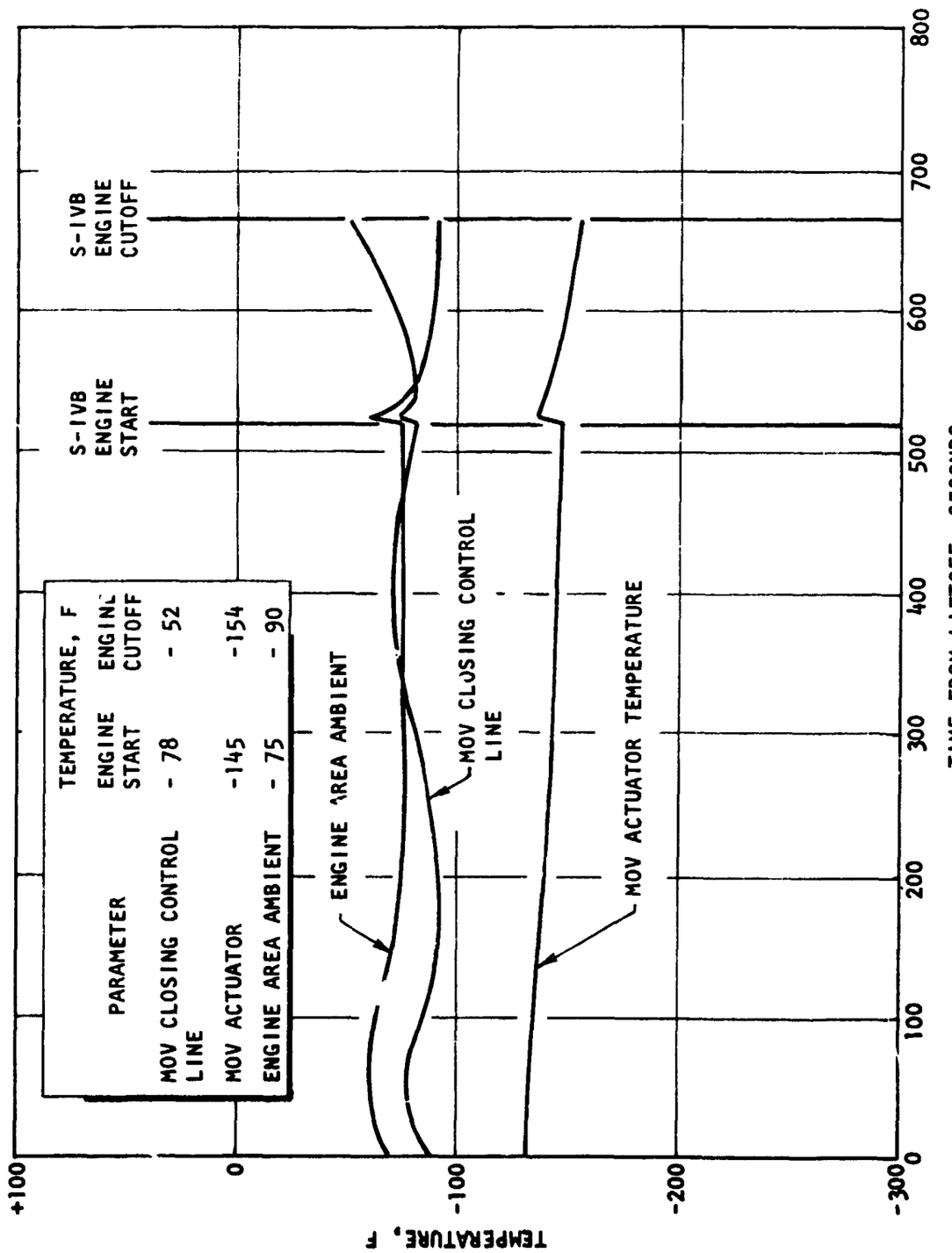

Figure 129. MOV Environment During Boost and Engine Operation

(Fig. 129) is caused by the retromotor exhaust plume (retrofire and separation). The significance of the MOV environment is discussed in the Transient section.

Separation

The S-II/S-IVB separation command occurred 520.5 seconds after liftoff. The S-IVB stage engine ignition occurred 0.2 second after separation command.

The separation of the S-II/S-IVB stages is preceded by ignition of two 3400-pound-thrust ullage motors. The nominal burn time of the ullage motor is 3.9 seconds. Separation command occurs 0.1 second after ullage motor ignition followed by ignition of four 35,700-pound-thrust retromotors. The retromotors burn for a duration of 1.5 seconds. The S-IVB stage engine start command occurred at 520.7 seconds after liftoff (0.2 second after separation command). Separation was completed at 521.5 seconds after liftoff. The heat flux experienced by two calorimeters (C2000 and C2004) was approximately 40 percent less than that predicted in the J-2 engine model specification.

The two calorimeters were provided to measure the heat flux from the TE-29 retromotor exhaust plume at the thrust chamber exit plane. The C2000 calorimeter was located along the retromotor centerline projection onto the J-2 engine and experienced a maximum heat flux of 0.38 Btu/ft^2-sec as compared to the model specification value of 0.6 Btu/ft^2-sec during retromotor firing.

The MOV actuator housing temperature (C2003) and MOV closing control line temperature experienced a rise of approximately 10 F as the engine passed through the retrorocket plume impingement. The engine area ambient temperature (C0010) indicated a rise of approximately 15 F. Figure 129 depicts these measurements during boost and J-2 engine operation. These

temperature rises are comparable to that experienced on flight AS-202 (Ref. R-6750-3) and AS-203 (Ref. R-6750-2).

Orbital Coast

An orbit is defined as one (approximately 90 minutes) revolution around the earth. One of the primary mission objectives was to demonstrate the S-IVB stage engine restart capability. S-IVB stage engine restart was accomplished after a coast period of two orbits, 11,486 seconds after liftoff.

The thrust chamber jacket and nozzle temperatures during the orbital coast period are shown in Fig. 130. The thrust chamber nozzle analytical prediction represents the mean bulk temperature for the insulation portion of the thrust chamber nozzle having a thermally controlled (clean) insulated surface and no effect from the firing of ullage motors at S-IVB stage first-burn engine cutoff. It is apparent that the measured data are close to the predicted temperature profile. Comparison of thrust chamber temperatures between the expected range and actual measurements on flights AS-501 and AS-203 for one orbit is presented in Table 20. The ullage motor operation at S-IVB stage first burn cutoff (88 seconds duration) and at the S-IVB stage engine restart (327 seconds duration) appears to have negligible effect on the thrust chamber heatup.

TABLE 20

THRUST CHAMBER TEMPERATURES DURING PARKING ORBIT

Flight	Expected Temperature Range Subsequent to One Orbit, F	Actual Temperature Data Subsequent to One Orbit, F
AS-501	-80 to 0 (clean) 0 to 105 (dirty)	-120 to -20
AS-203	-80 to 0 (clean) 20 to 125 (dirty)	-80 to -20

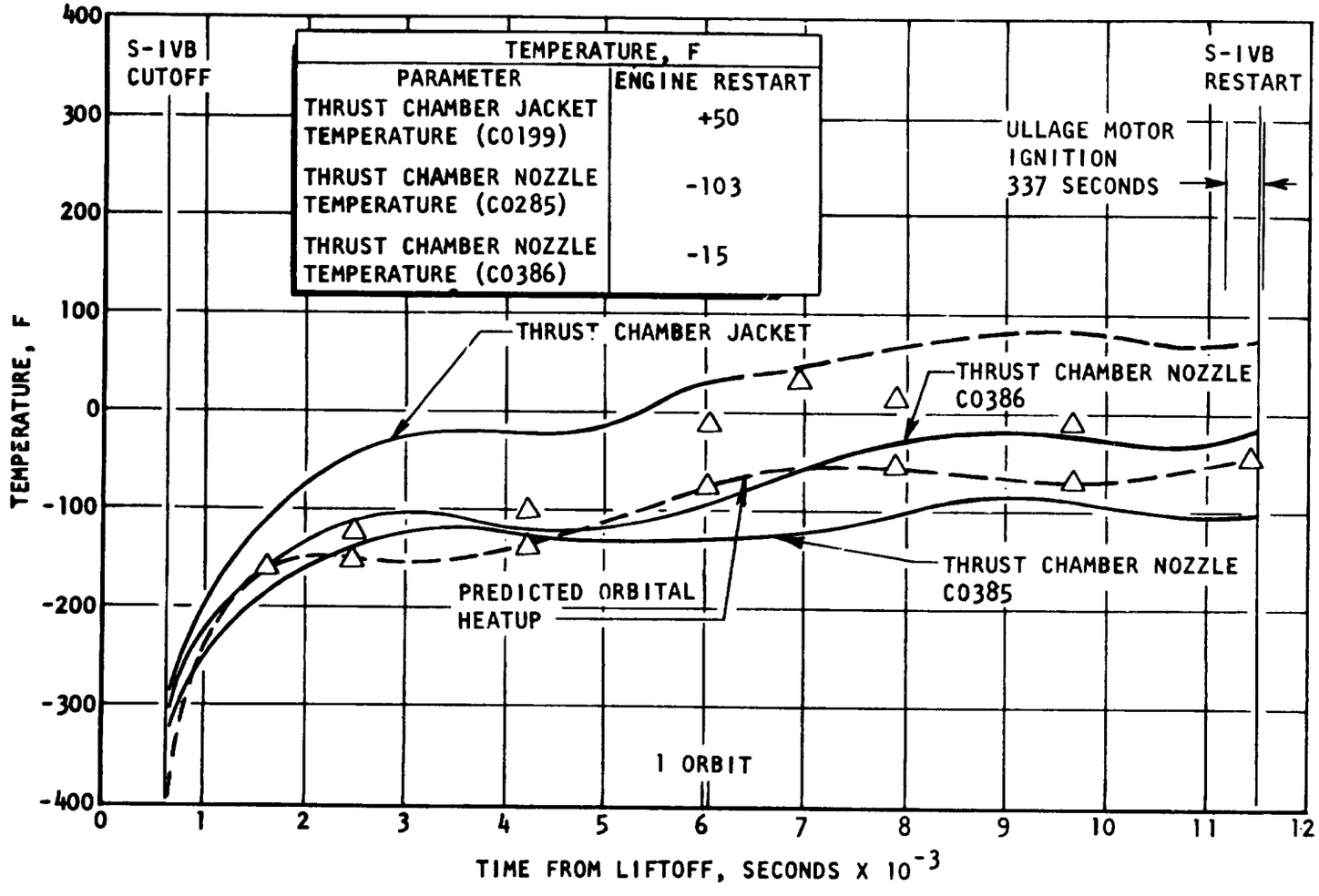

Figure 130. Orbital Heatup of Thrust Chamber Jacket and Nozzle Temperatures

The effect on engine chilldown as a result of the thrust chamber temperatures and fuel lead of 8 seconds at S-IVB stage engine restart is discussed elsewhere in this report.

The MOV temperature environment indicated no apparent response to the ullage motor plume inpingement at restart. No appreciable temperature change was experienced from liftoff to second burn cutoff (Fig. 131). As expected, a slight temperature rise was experienced at S-II/S-IVB separation (Fig.).

Fuel turbine and oxidizer turbine inlet transducer measurements correlated well with that measured on Flight AS-203 (Ref. R-6750-2). Figure 132 depicts the actual fuel turbine and oxidizer turbine inlet temperature measurements experienced on flight AS-501. As postulated in AS-203 report (Ref. R-6750-2), fuel turbine and oxidizer turbine temperature transducer measurements do not represent the crossover duct skin temperatures. Figure 132 also compares the actual turbine and crossover duct temperature measurements during the coast period to the fuel and oxidizer turbine inlet temperatures.

The predicted and actual crossover duct surface temperatures during AS-501 orbital coast are depicted in Fig. 133. These compare very favorably with the predicted curve. The crossover duct on AS-501 was painted black with an emissivity of 0.9.

The crossover duct temperature at the end of the second orbit (at S-IVB restart) was indicating 0 F; which is well within the predicted temperature band (Fig. 133). The exhaust system temperature influence to engine start transients is discussed in the Start Transients section of this report.

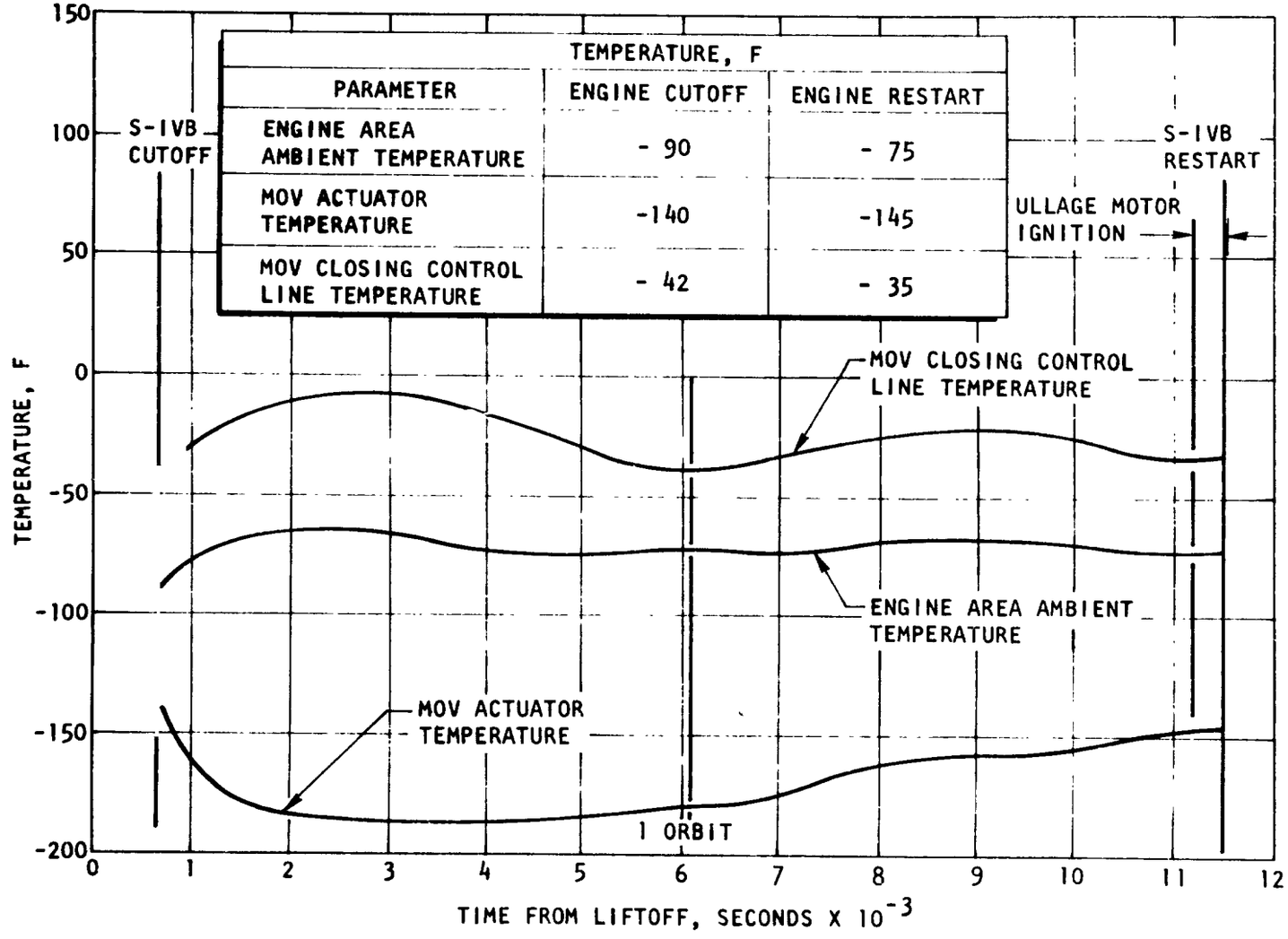

Figure 131. MOV Environment Temperature During Coast

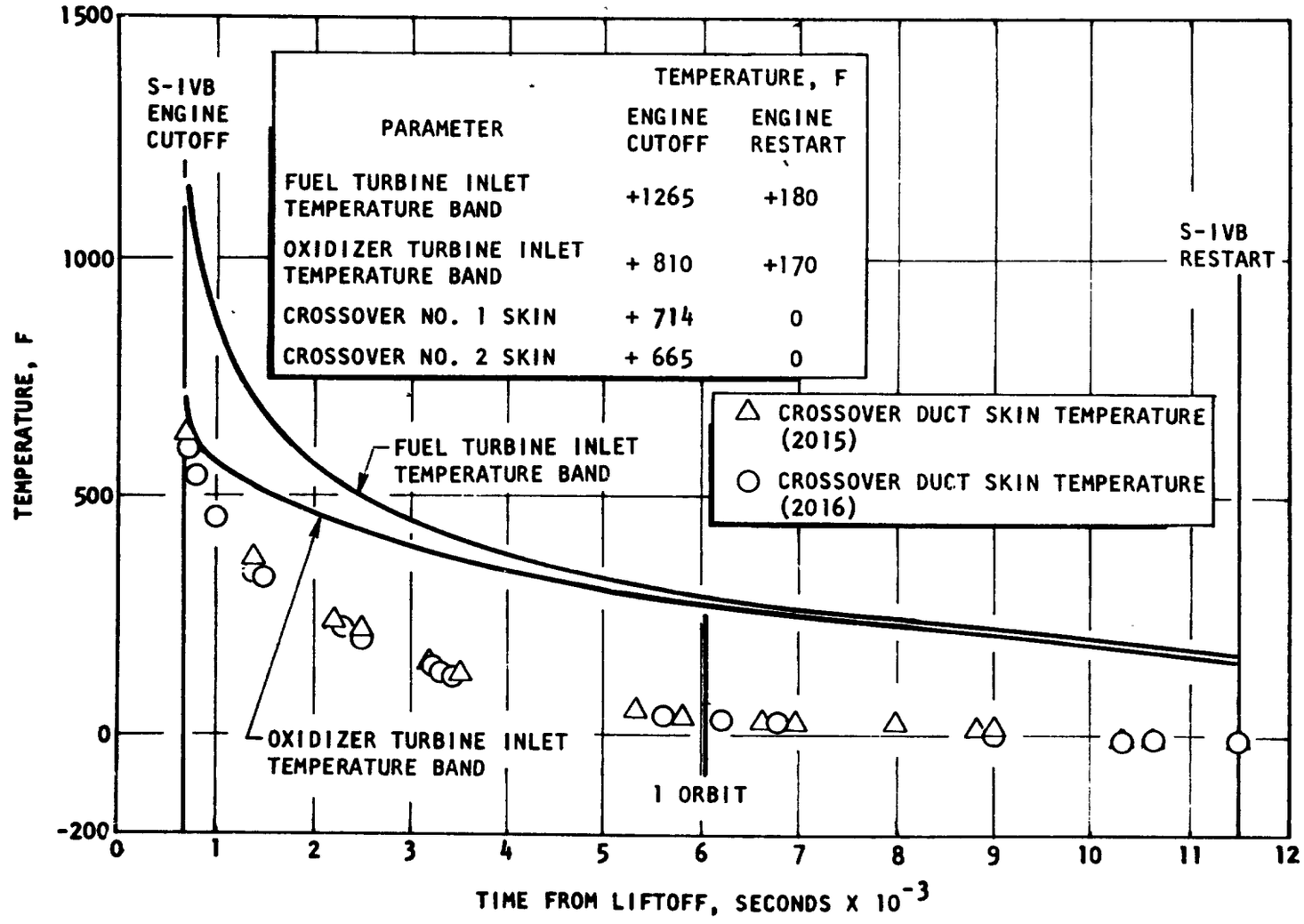

Figure 132. Exhaust System Temperatures During Coast

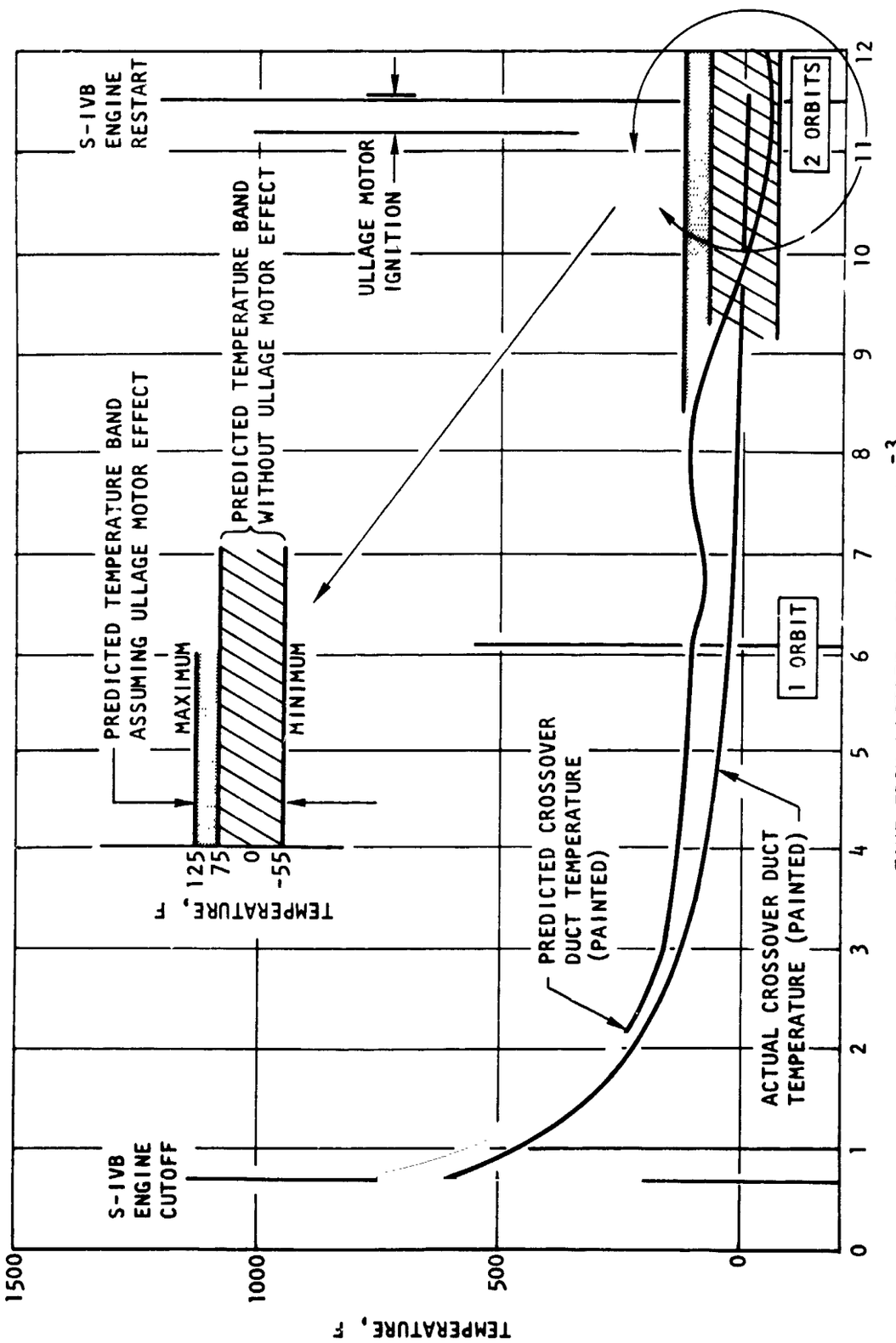

Figure 133. Crossover Duct Temperature During Coast

START TRANSIENTS

Initial Start

Engine J2031 flight transient performance during the first and second engine operations was within model specification limits. Engine operation was also within S-IVB verification testing limits at AEDC on engine J2052. Engine changes that significantly affect start transient performance were incorporated after engine J2031 acceptance, preventing a meaningful comparison of engine acceptance testing and flight. These modifications were as follows:

1. ECP J2-455; delayed gas generator valve timing, to minimize excessive gas generator temperature spikes and flow reversal
2. ECP J2-458; incorporate necessary restart requirements
3. ECP J2-505; thermostatically orificed main oxidizer valve, to prevent variations in valve opening times resulting from temperature changes
4. ECP J2-513R1; reduce MOV opening timing, to be comensurate with optimum start performance
5. ECP J2-590; paint exhaust system with high-emissivity black paint, to affect faster cooldown in space prior to restart
6. ECP J2-598; installation of a smaller diameter ASI oxidizer orifice, to prevent excessive ASI temperature transients during engine start
7. Specially calibrated start tank vent and relief valve, to adequately control tank energy during orbital coast
8. Engine restart with PU valve in the full-open position, to compensate for excessive oxidizer pump transient operation

Table 21 compares start conditions of the S-IVB flight first burn with AEDC (engine J2052) test 1554-026A, the test that most closely resembles

TABLE 21

COMPARISON OF FLIGHT VS AEDC START CONDITIONS

Engine Conditions at S-IVB First Start		
Parameter	AEDC Test No. 1554-026A (J2052)	S-IVB Flight First Start (J2031)
Start Tank Pressure, psia	1317	1275
Start Tank Temperature, F	-173	-193
Fuel Pump Inlet Temperature, F	-421.4	-421.8
Fuel Pump Inlet Pressure, psia	35.4	42.5
Oxidizer Pump Inlet Temperature, F	-293.7	-294
Oxidizer Pump Inlet Pressure, psia	40	40
Thrust Chamber Skin Temperature, F	-173	-200
Fuel Lead Time, seconds	3	3
Mean Exhaust System Temperature, F	-45	-39
MOV Closing Actuator Temperature, F	-69	-145
PU Valve Position	Null	Null

the flight. Although start conditions were quite similar, it appears that the flight would have the more severe start transients. However, J2052 in test 026A exhibited the more severe start characteristics (oxidizer pump spin speed and MOV opening time) as evidenced in Table 22 and Fig. 134 and 135.

Several items aid in explaining the transient performance differences. J2052 had a smaller oxidizer turbine nozzle area than engine J2031, which contributed to a higher oxidizer pump spin speed. Engine J2052 also had a considerably higher main oxidizer valve internal friction which resulted in a much longer plateau (14-degree position) time on test 026A. The extended MOV first position on AEDC test 026A (Fig. 135) resulted in increased gas generator power which in turn caused the rapid power buildup of the oxidizer turbopump (Fig. 134). These differences do not invalidate comparison of the two engines, rather they make AEDC testing conservative estimates of the AS-501, S-IVB flight performance.

AEDC testing indicates that the ASI oxidizer injection temperature approaches a constant (liquid) value within 1 second after engine start. Thus, until spindown is initiated, ASI combustion temperature is a function of thrust chamber and ASI fuel line resistances controlling fuel flow. ASI fuel flow decreases as thrust chamber resistance decreases, represented by main fuel injection temperature. AEDC and flight operation exhibited similar fuel lead characteristics with the same pump inlet characteristics (Fig. 136). At the termination of the 3-second fuel lead, the fuel injection temperature was close to a liquid condition which is more than adequate for satisfactory main thrust chamber operation but adversely affects (high mixture ratio) initial ASI operation. The smaller ASI oxidizer feed system orifice incorporated on engines J2031 and J2052 by ECP J2-598 minimized the effects of reduced fuel flow resulting from low thrust chamber resistance.

Figure 137 presents the S-IVB first start fuel turbine inlet temperature profile extrapolated from applicable AEDC testing.

TABLE 22

COMPARISON OF FLIGHT VS AEDC TEST TRANSIENTS

Engine Start Performance S-IVB First Start		
Parameter	AEDC Test 1554-026A	S-IVB Flight First Start
Main Oxidizer Valve		
Second-Stage Opening Delay, milliseconds	830	450
Ramp, milliseconds	1850	1900
Gas Generator Overtemperature		
Initial Spike, F	1954	*
Overshoot, F	1608	*
Oxidizer Turbine Speed		
Spinup, rpm	3257	3150
Decay, rpm	2964	3000
Chamber Buildup to 550 psia, milliseconds	2.00	2.00

*Not measured in flight

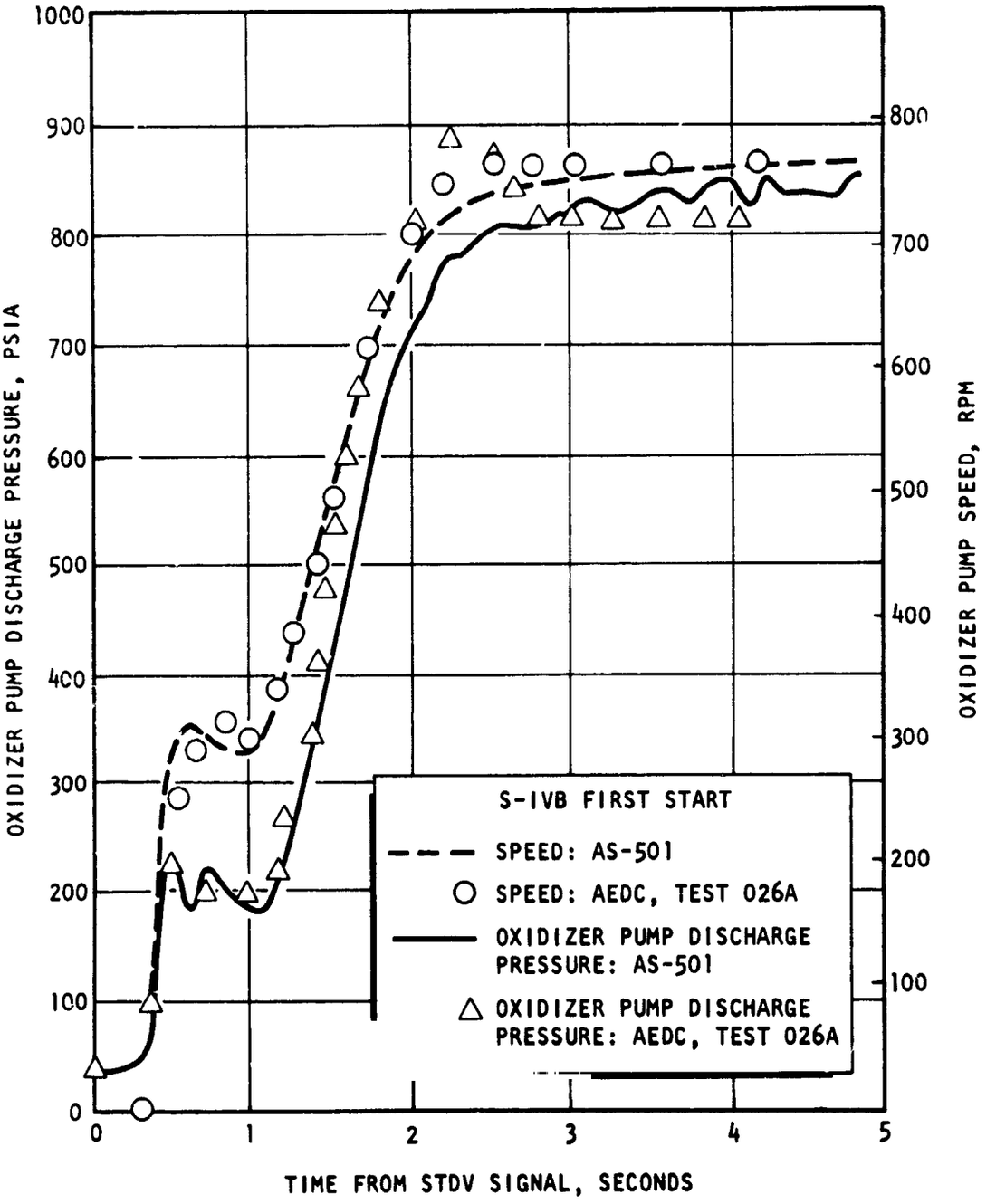

Figure 134. Oxidizer Pump Speed and Discharge Pressure During Start Transient

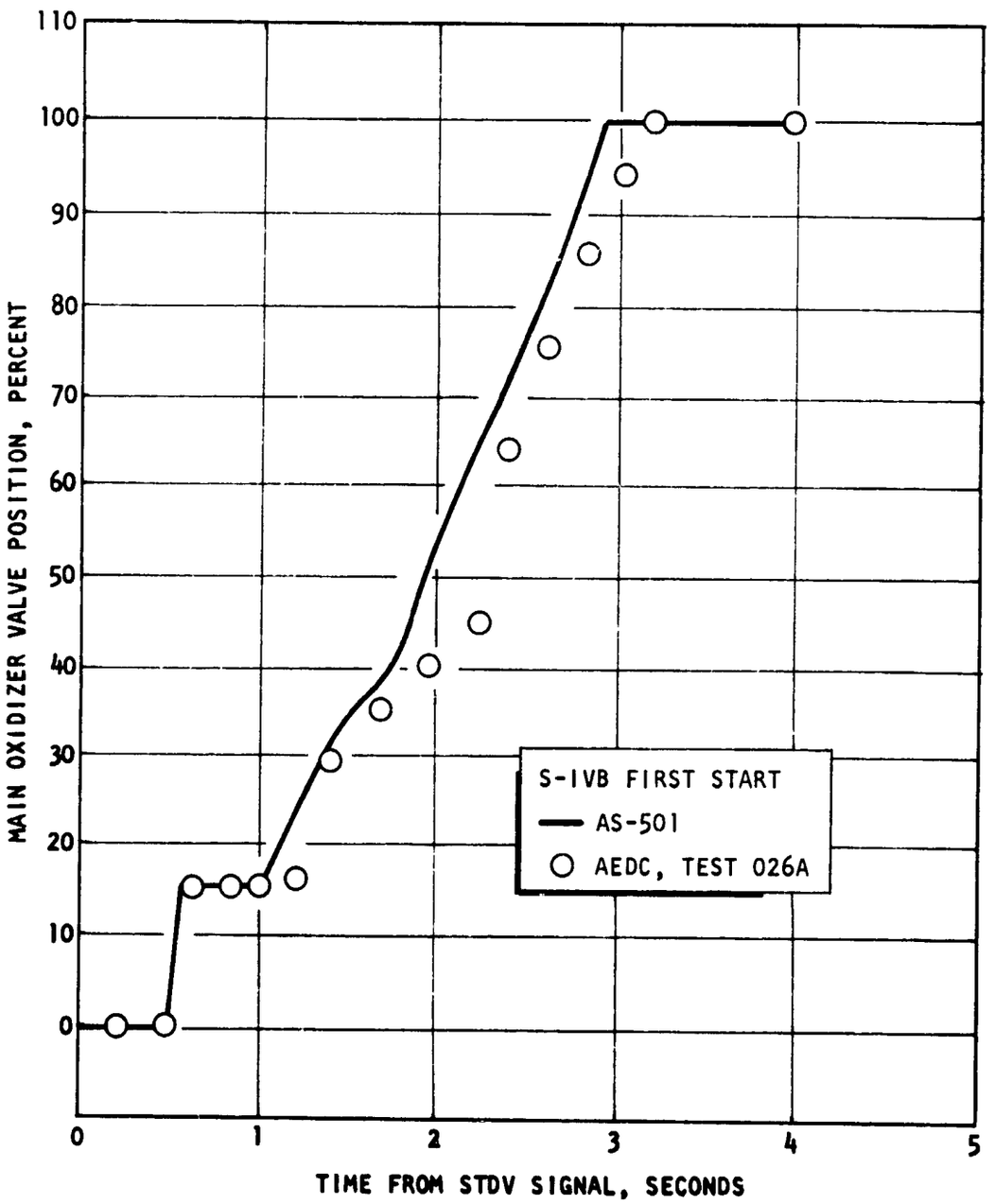

Figure 135. MOV Position During Start Transient

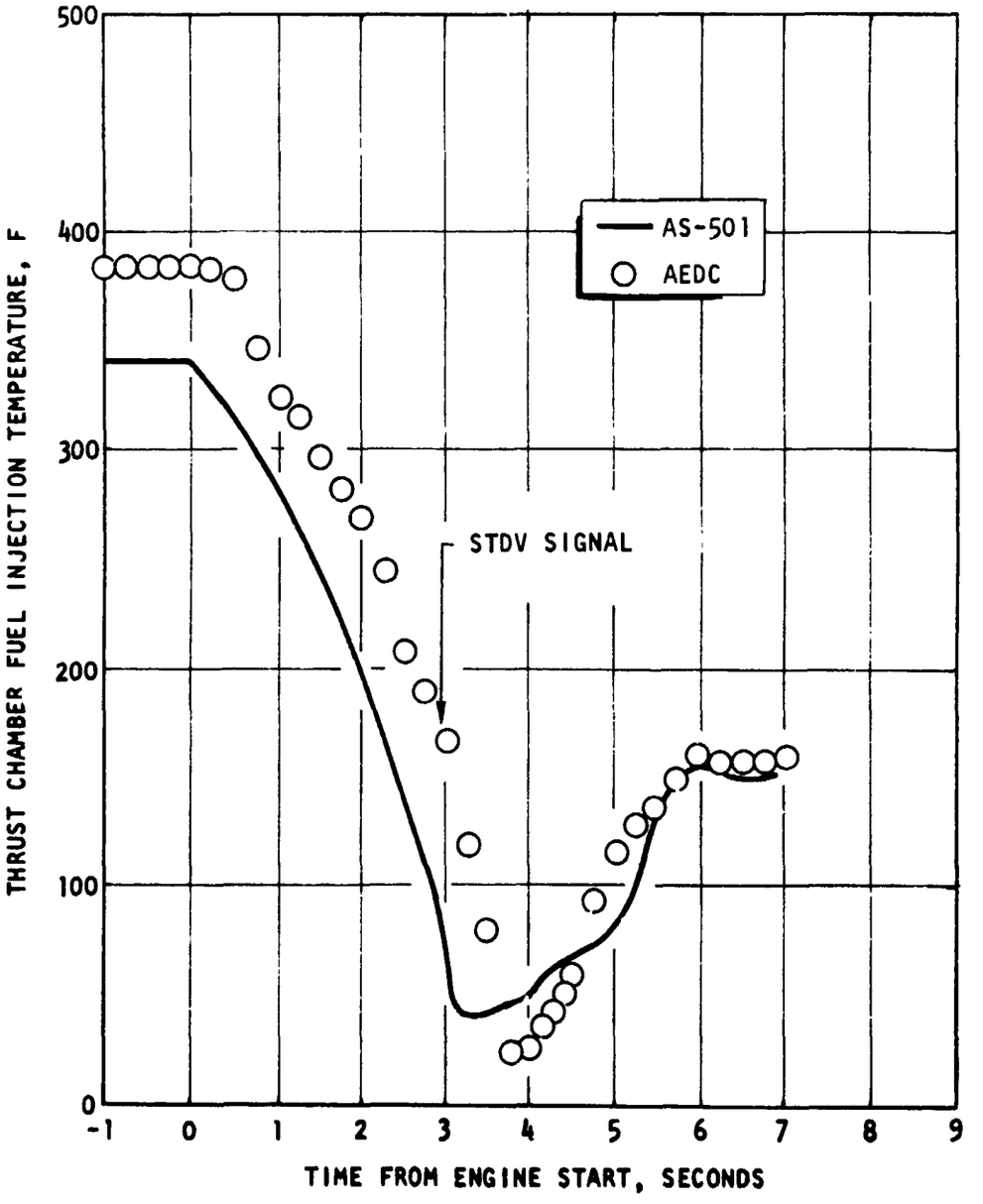

Figure 136. Thrust Chamber Fuel Injection Temperature During Start Transient

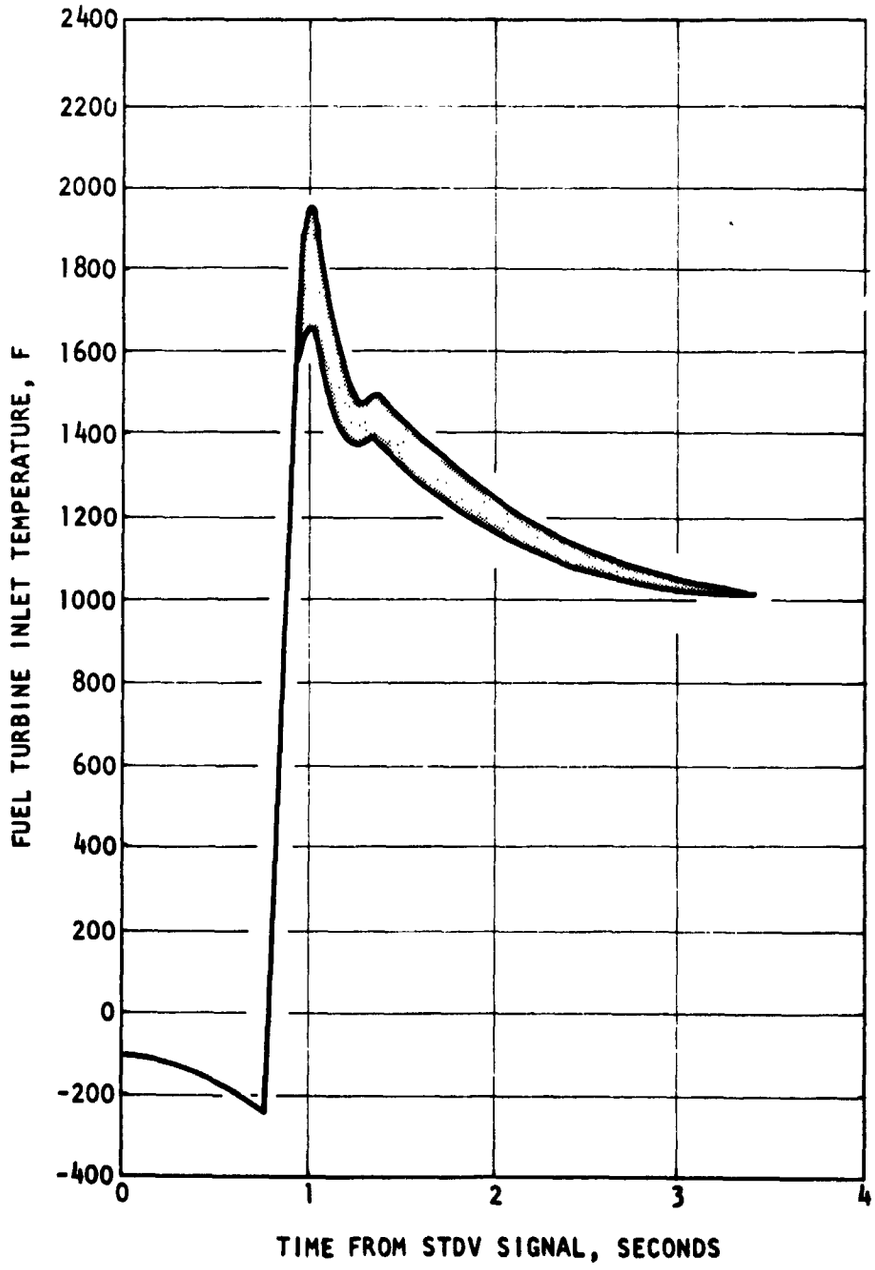

Figure 137. S-IVB First Start Fuel Turbine Inlet Temperature During First Start Transient Extrapolated From AEDC Testing

Figure 138 shows the adequate stall margin exhibited on both S-IVB flight starts versus AEDC test experience limits.

Restart

The S-IVB restart transient operation was as expected. Figure 139 depicts restart oxidizer pump speed and discharge pressure, and Fig. 140 compares oxidizer pump discharge pressure on the first and second starts. The increased oxidizer pump performance during the second start was primarily a result of the elevated prestart mean exhaust system temperature, 110 F versus -39 F on the first start, and slightly higher start tank energy.

The mean exhaust system temperature prior to restart was lower than the predicted maximum of 215 F which is equivalent to approximately 160 rpm less oxidizer turbine spin speed. The beneficial reduction in exhaust system temperature can be attributed to the use of the high-emissivity black paint per ECP J2-590, the particular orientation of the AS-501/S-IVB stage, and the lesser effect of ullage motor impingement. Although start tank energy (1285 psia/-212 F) for restart was higher than for the first burn, it was still a minimum value because of the use of the specially calibrated vent and relief valve.

The effects of elevated exhaust system temperature and start tank energy on transient performance were reduced by restarting with the PU valve in the full-open position, approximately 225-rpm oxidizer pump spin speed reduction.

Figure 141 compares the thermal-compensating main oxidizer valve opening characteristics on the first and second starts with sequence tests conducted at KSC. The oxidizer valve trace on the restart operation exhibited a slightly longer plateau time and the effects of a higher initial engine power buildup. Comparison of KSC sequence time with flight times indicates this particular valve overcompensated for the -150 F closing control actuator temperature as evidenced in Fig. 141, the delay time to the beginning of ramp was slightly shorter in flight.

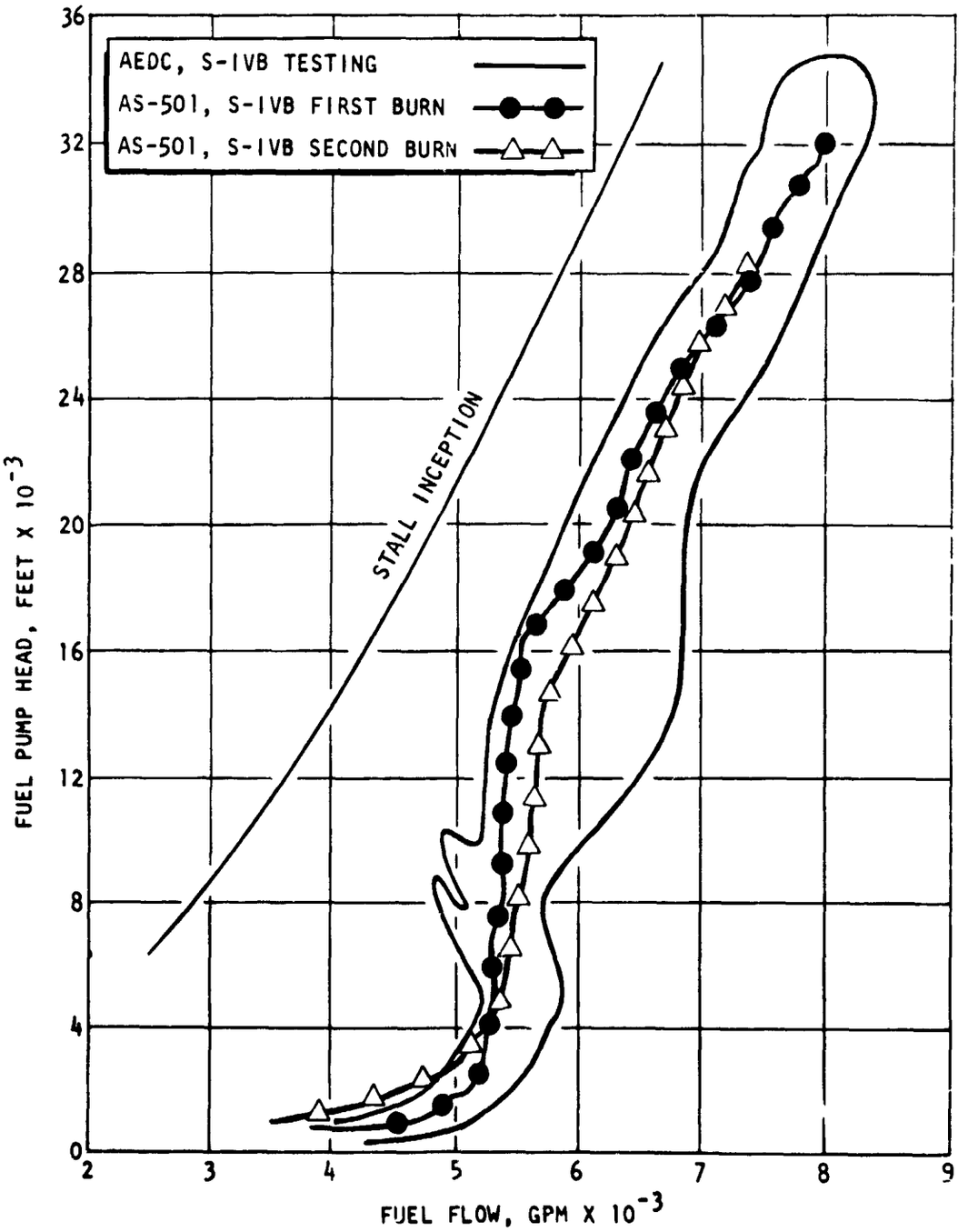

Figure 138. Fuel Pump H-Q Curve During Start Transient

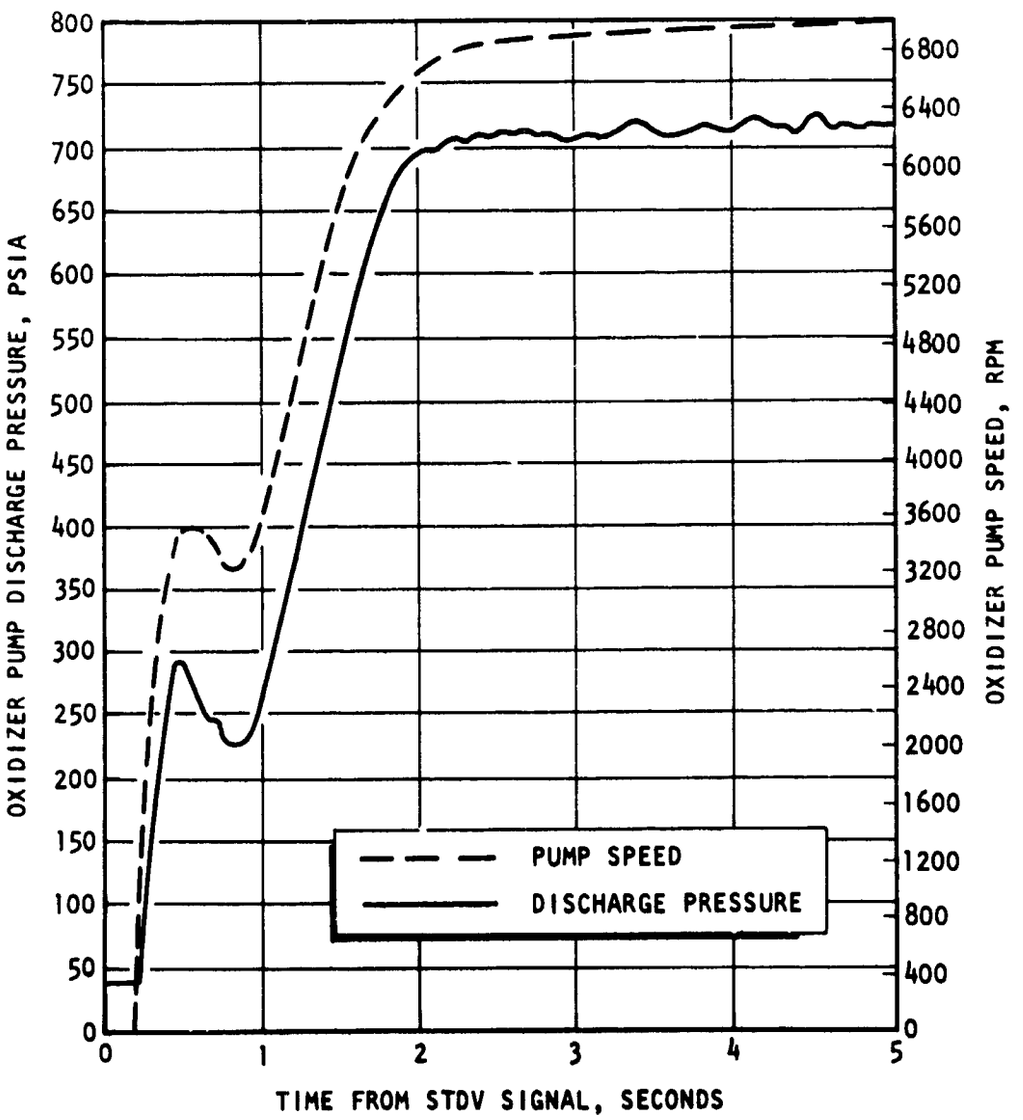

Figure 139. Oxidizer Pump Speed and Discharge Pressure During Start Transient

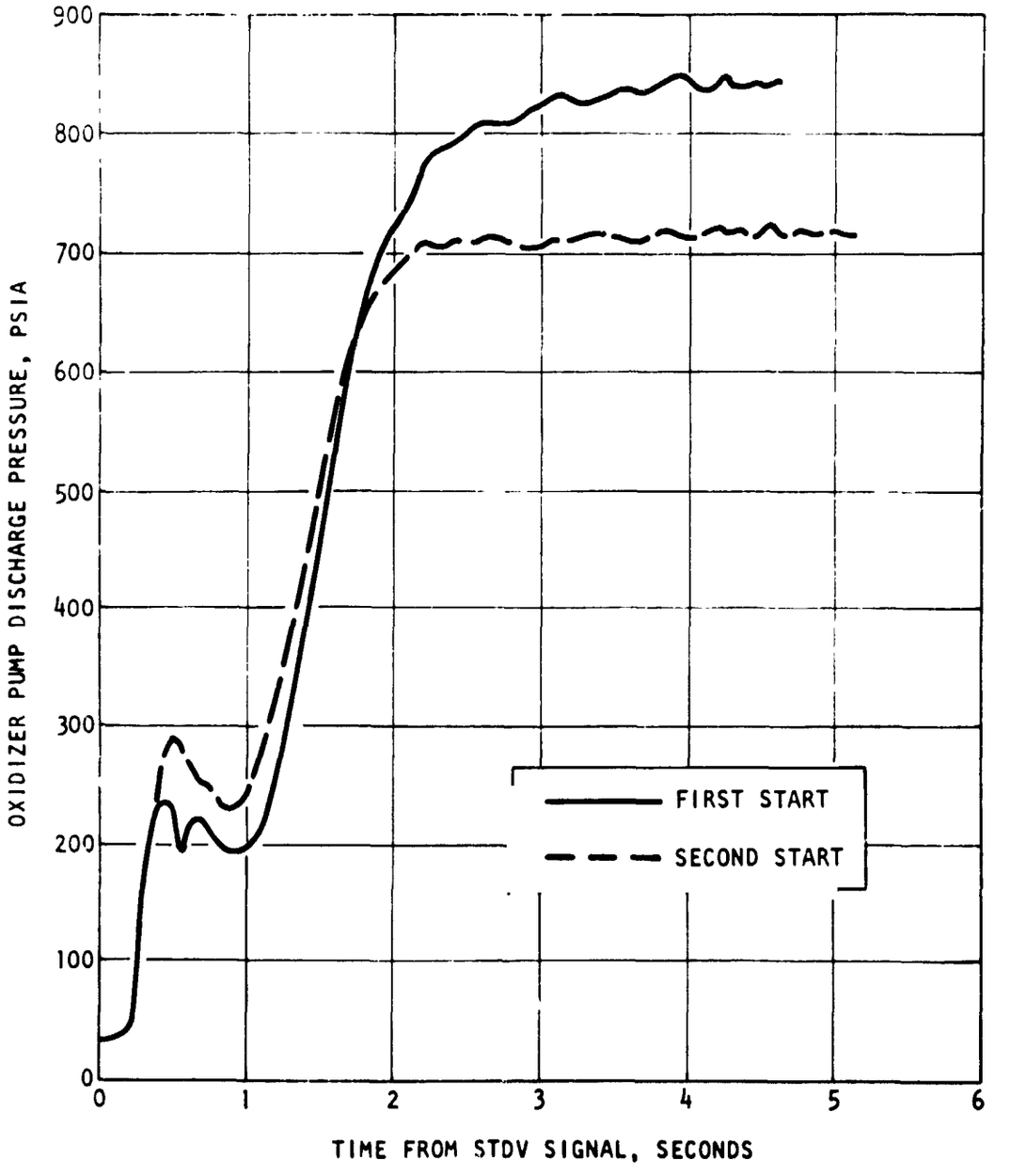

Figure 140. Oxidizer Pump Discharge Pressure During Start Transient

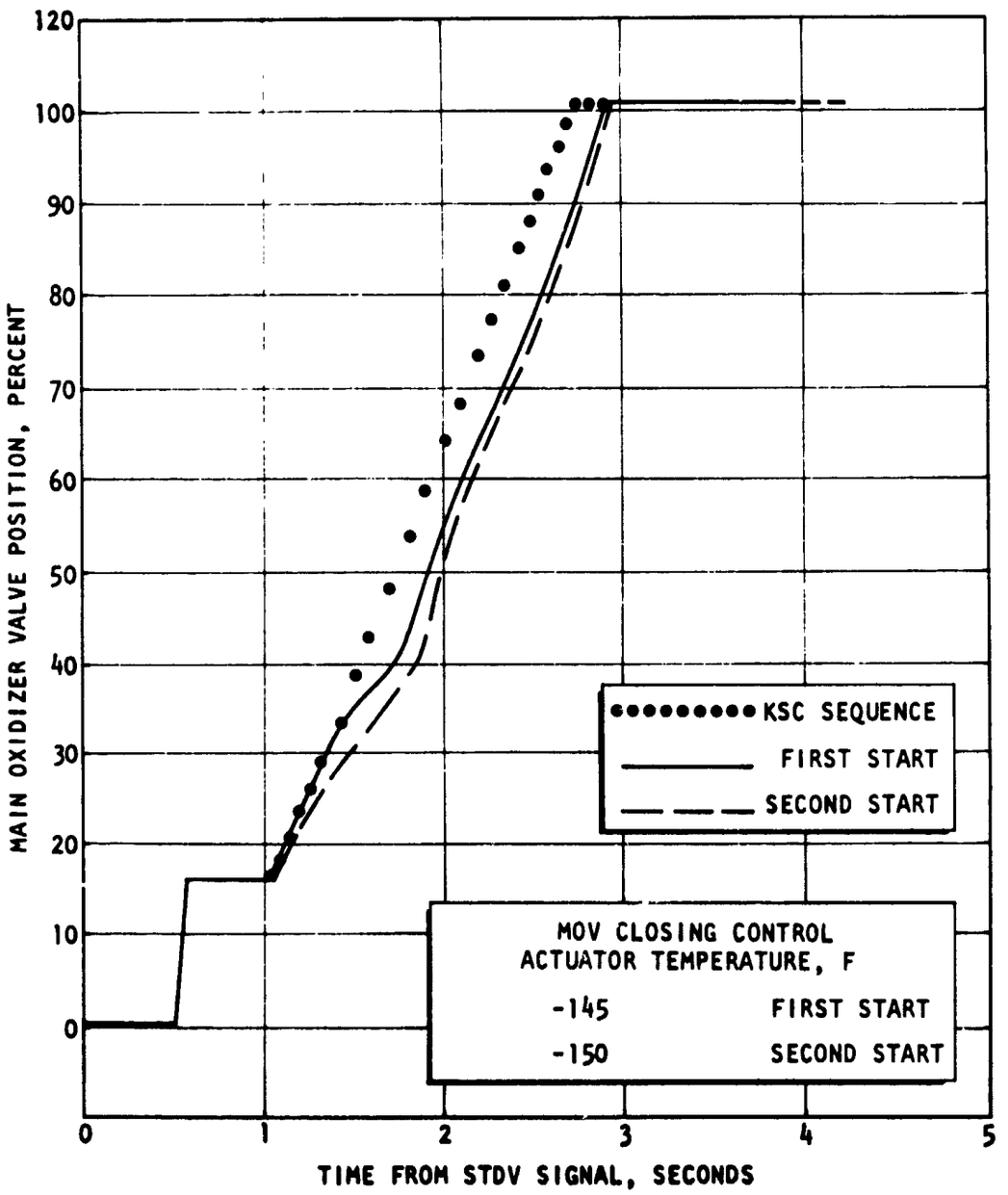

Figure 141. MOV Opening Characteristic Comparison

Figure 142 shows the proportional effect of fuel pump inlet pressure on thrust chamber chilldown during the fuel lead phase of transient operation. Again, satisfactory ASI operation as well as adequate thrust chamber conditioning was achieved during prestart.

Figure 143 is an extrapolation of applicable AEDC testing for the restart fuel turbine inlet temperature transient.

Engine testing has shown that the initial temperature spike is normally not detrimental to fuel turbine performance efficiency because of the low flow rates and initially cold hardware. Overshoot GG temperature spikes (the second temperature spike) will adversely affect fuel turbine efficiency when above 2150 F. As noted in Fig. 137 and 144, this threshold temperature was not exceeded during the first or second starts.

PROPELLANT INLET CONDITIONS

The engine inlet propellant conditions at liftoff, engine start command (ESC) for the first burn (T+520.7 seconds), and ESC for the restart (T+11486.6 seconds) were within specified limits with one exception which will be discussed in a subsequent paragraph.

The engine oxidizer NPSH (Table 23) at liftoff, S-IVB ESC first burn, and restart were satisfactory with all values well above the 26 foot minimum.

Engine fuel NPSH (Table 27) at liftoff and S-IVB ESC first burn was well above the 150 foot minimum. At S-IVB ESC restart, it was approximately 101 feet. This was the result of fuel tank ullage pressure being 3.1 psi below the minimum predicted value of 31 psia at ESC. The unexpected ullage pressure loss has been attributed as either an ullage pressurant diffuser malfunction or a gaseous hydrogen bubble formation in conjunction with the premature termination of fuel tank ullage repressurization that occurred at the end of the second orbit. An erroneous continuous tank vent pressure indication precipitated a mission rule procedure that called

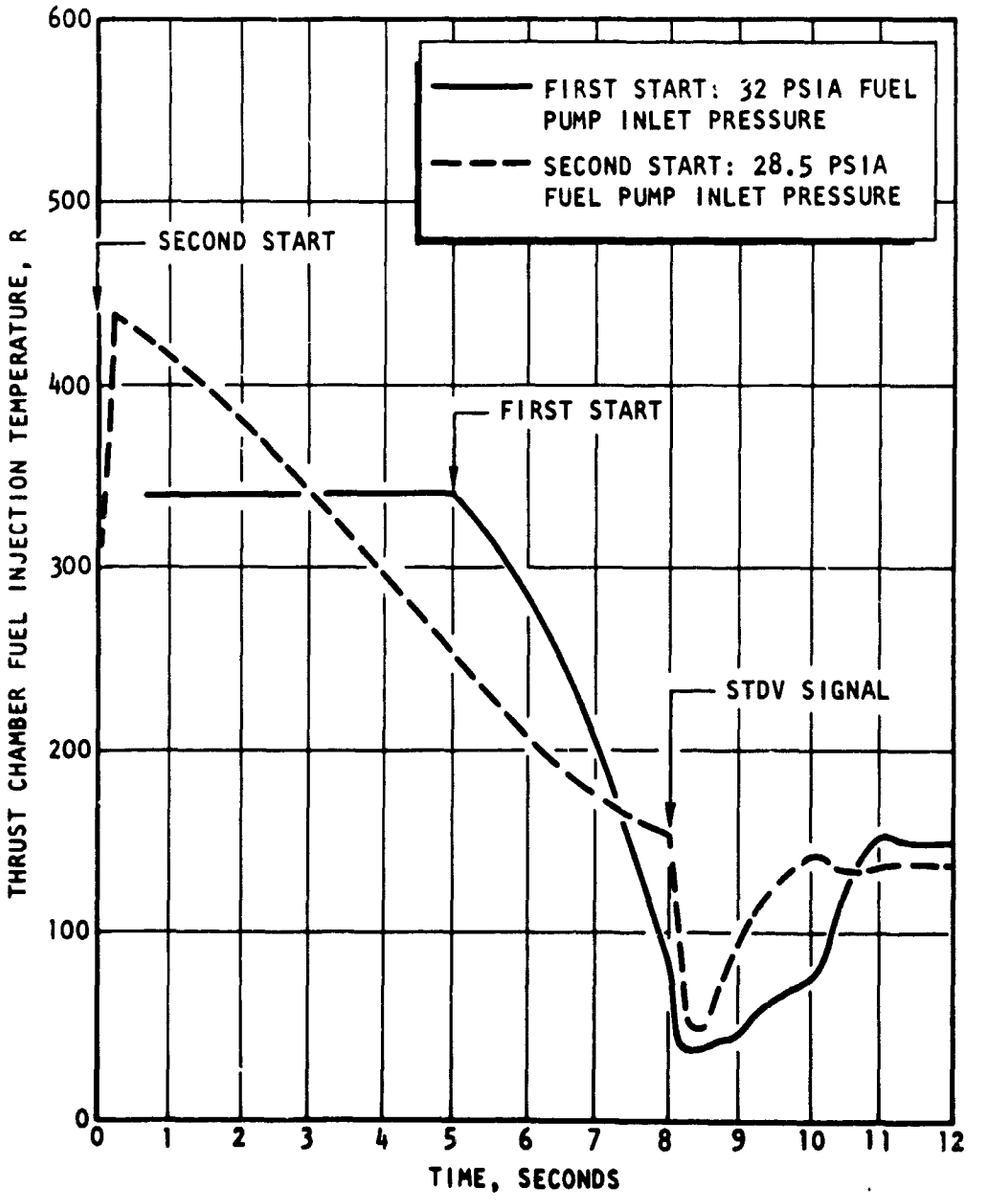

Figure 142. Fuel Injection Manifold Temperature During Start Transient

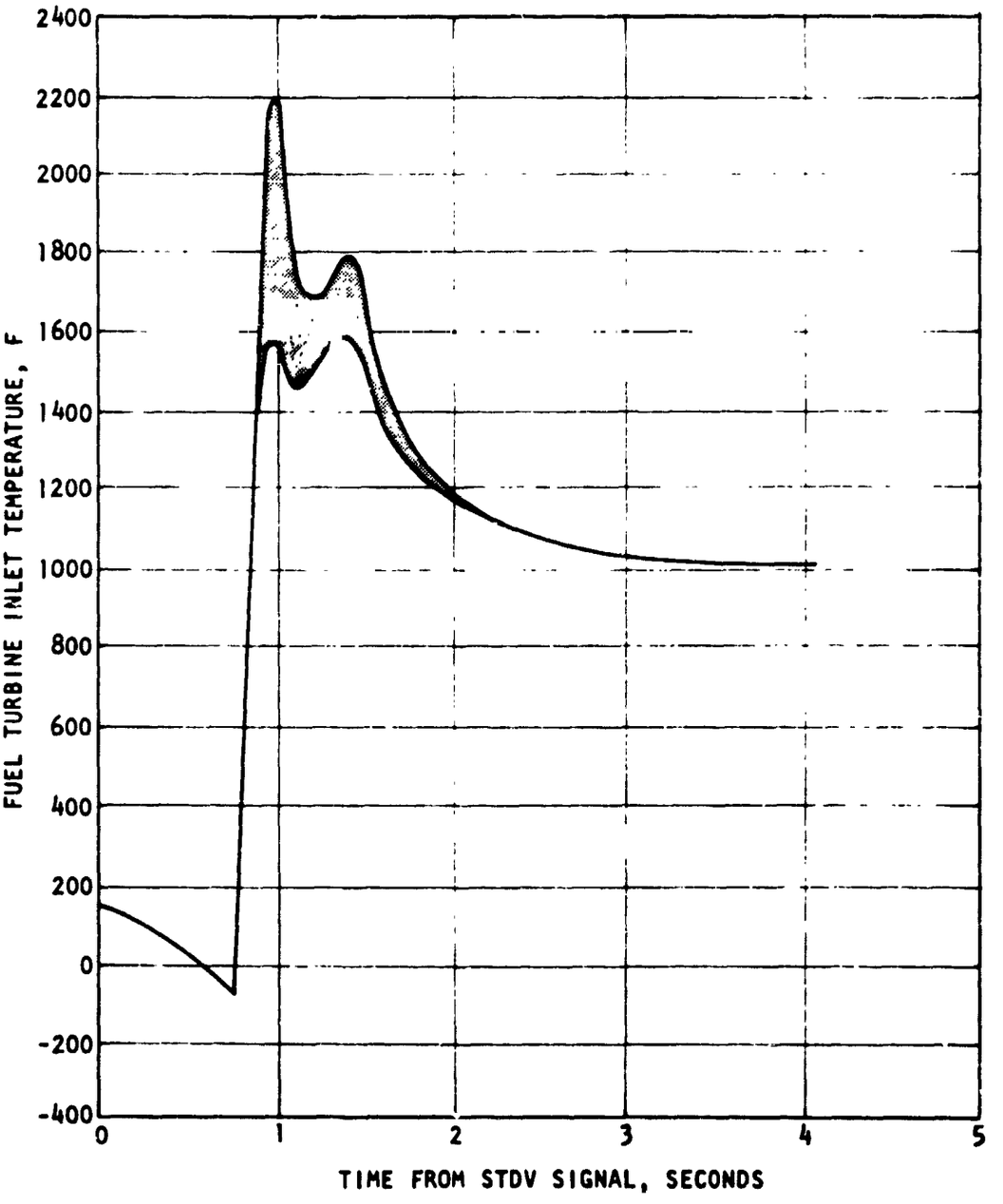

Figure 143. Fuel Turbine Inlet Temperature During Second Start Transient Extrapolated From AEDC Testing

TABLE 23

ENGINE INLET NPSH

	Liftoff	Engine Start (First Burn)	Engine Start (Restart)
Oxidizer (26 foot minimum)	88.4	45.6	51.0
Fuel (150 foot minimum)	814	790	101*

*At STDV signal, the NPSH was 283 feet.

for the sequencing off and on of the fuel tank repressurization system. Unfortunately the "sequence on" function was inadvertently omitted. However, at the completion of the 8-second fuel lead, the fuel inlet temperature had decreased sufficiently to produce a fuel NPSH of 283 feet, a value assuring a safe engine start.

The engine oxidizer inlet pressure profile (Fig. 144) during vehicle acceleration changes occurring from S-II cutoff (T+519.8 seconds) through S-IVB ESC was as expected. The initial pressure drop noted after S-II cutoff was the result of vehicle acceleration changes having a marked effect on the greater density of the oxidizer. At chilldown pump-off sequence (T+520.3 seconds), an additional pressure decay of approximately 9 psi was experienced. Just after ESC, a small pressure surge was noted. The surge was a hydraulic hammer effect produced by the initial opening of the prevalve which permitted tank pressure-fed oxidizer to rapidly pressurize the engine oxidizer feed system which was at a reduced pressure. The reduced pressure was caused by the opening of the engine ASI oxidizer valve at ESC, prior to the actual opening of the stage prevalve.

Figure 145 illustrates the oxidizer pump inlet pressure changes that occurred prior to and during S-IVB ESC restart. The entire pressure loss of 9 psi was attributed to the opening of the prevalve at T+11475.8

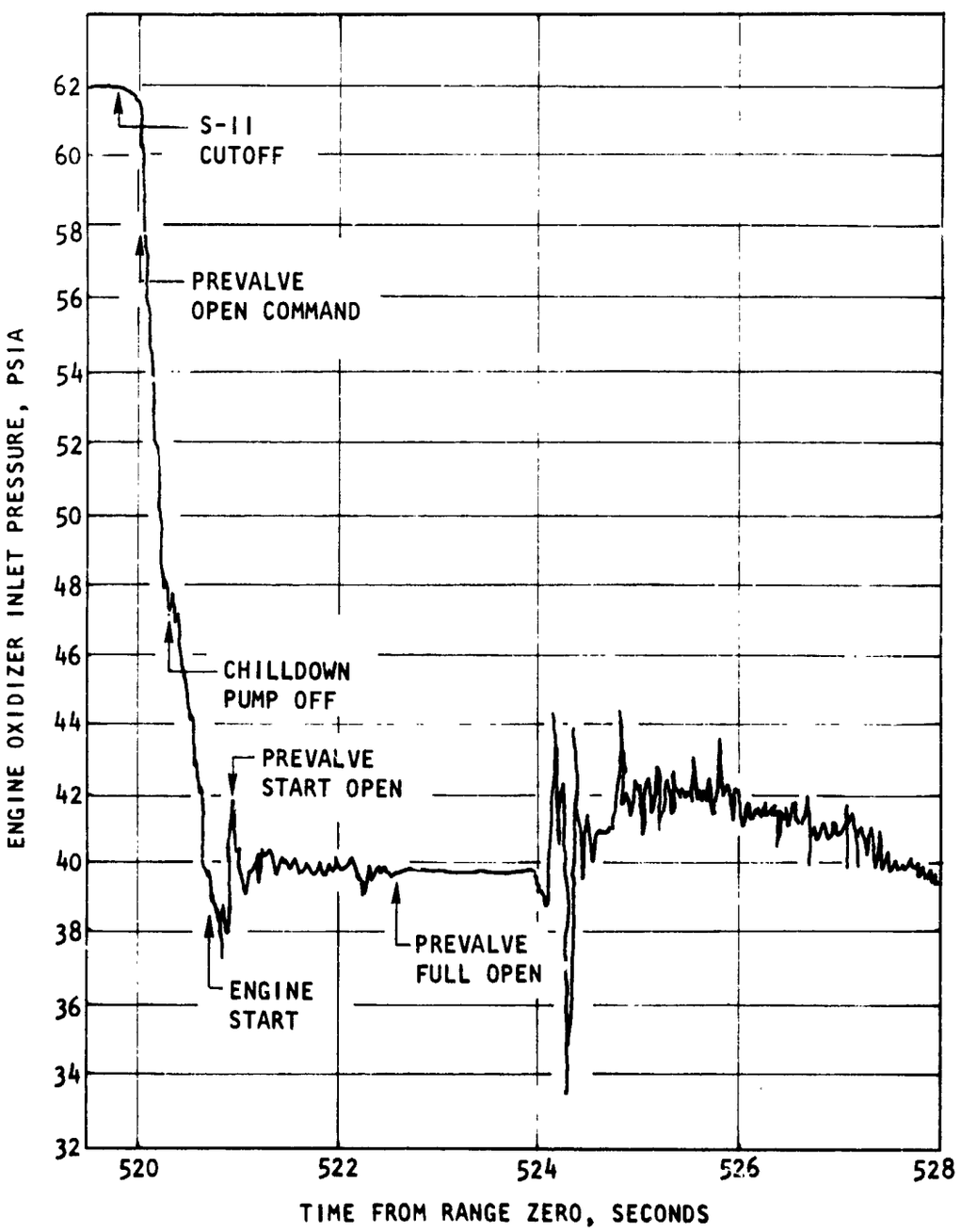

Figure 144. Oxidizer Inlet Pressure During First Start Transient

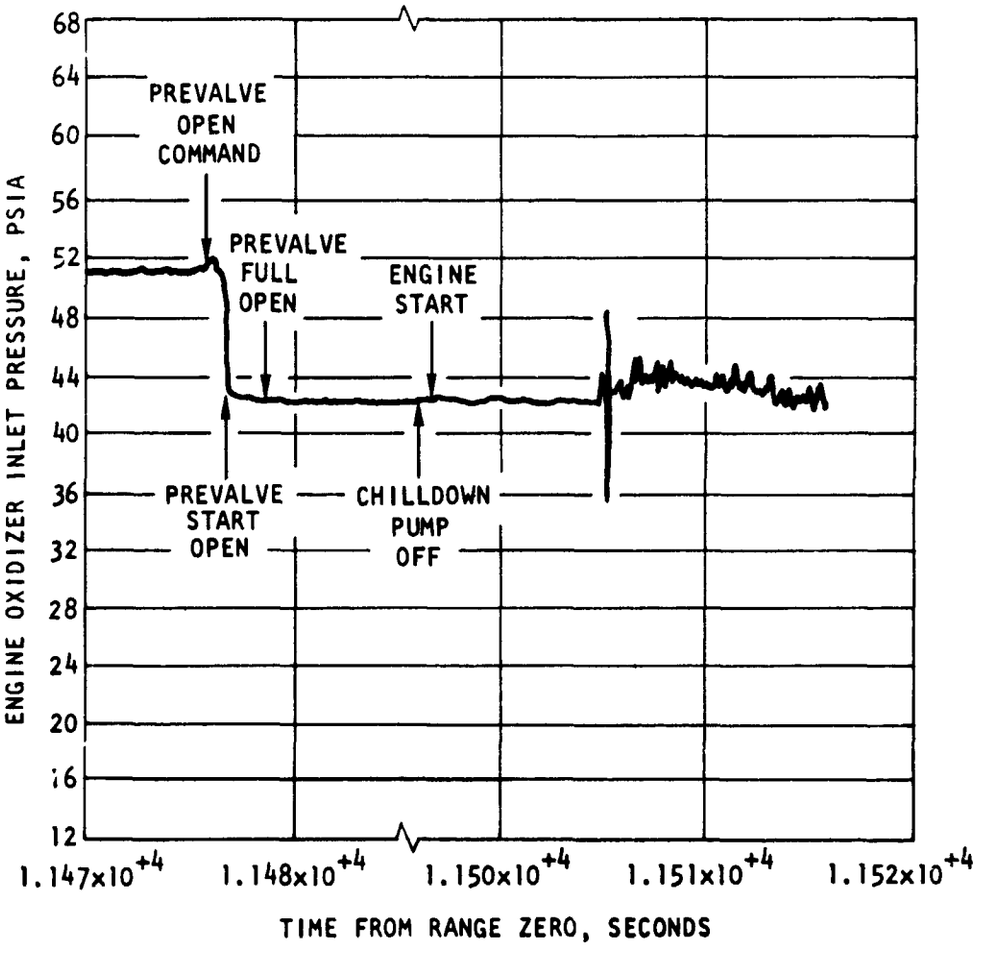

Figure 145. Oxidizer Inlet Pressure During Second Start Transient

seconds which effectively terminated oxidizer chilldown. The chilldown pump was sequenced off at T+11486.0 seconds.

The engine model specification oxidizer pump inlet start envelope (Fig. 146) was met satisfactorily for both S-IVB starts.

The oxidizer chilldown system performed efficiently for both S-IVB engine starts as evidenced (Fig. 147) by the 14.5 F subcooled temperature achieved prior to the first burn and the 15.8 F subcooled value obtained prior to restart. A minimum oxidizer pump discharge subcooled temperature of 3 F is required prior to engine start.

Figure 148 illustrates engine fuel inlet pressure behavior from S-II cut-off through S-IVB ESC. The pressure decay prior to ESC was caused by vehicle acceleration changes. Shortly after ESC, an initial opening of the prevalve caused a loss of chilldown pump head of approximately 7.5 psi. The pressure surge occurring at this time was caused by hydraulic hammer that came as a result of a rapid pressurizing of the engine fuel feed system which had been at a reduced pressure. The reduced pressure was caused by the initiation of the 8-second fuel lead at ESC which opened the main fuel valve while the stage prevalve was still closed.

A satisfactory fuel pump inlet pressure behavior prior to and through S-IVB ESC restart is shown in Fig. 149. Once again the opening of the prevalve caused a loss of chilldown pump head of 6 psi.

Figure 150 shows data points of engine fuel inlet pressure versus engine fuel inlet temperature as compared to the engine model specification start envelope. The values for S-IVB restart are outside the envelope as a result of the fuel tank repressurization problem discussed previously.

A cross plot of engine oxidizer and fuel inlet pressures for both S-IVB starts as compared to predicted values and the J-2 Model Specification start envelope is shown in Fig. 151. The reason for the large engine fuel

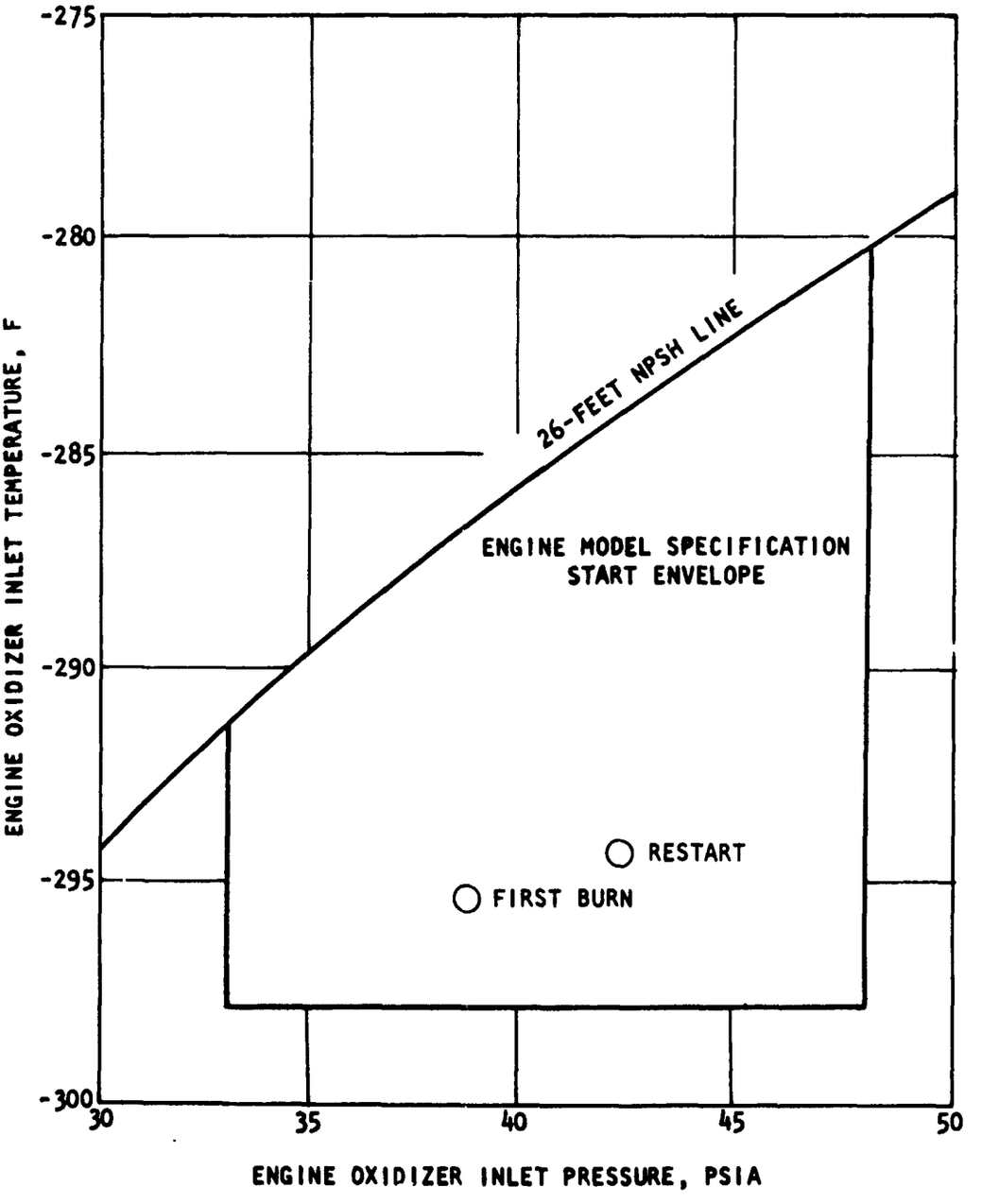

Figure 146. Oxidizer Inlet Pressure and Temperature at Engine Start

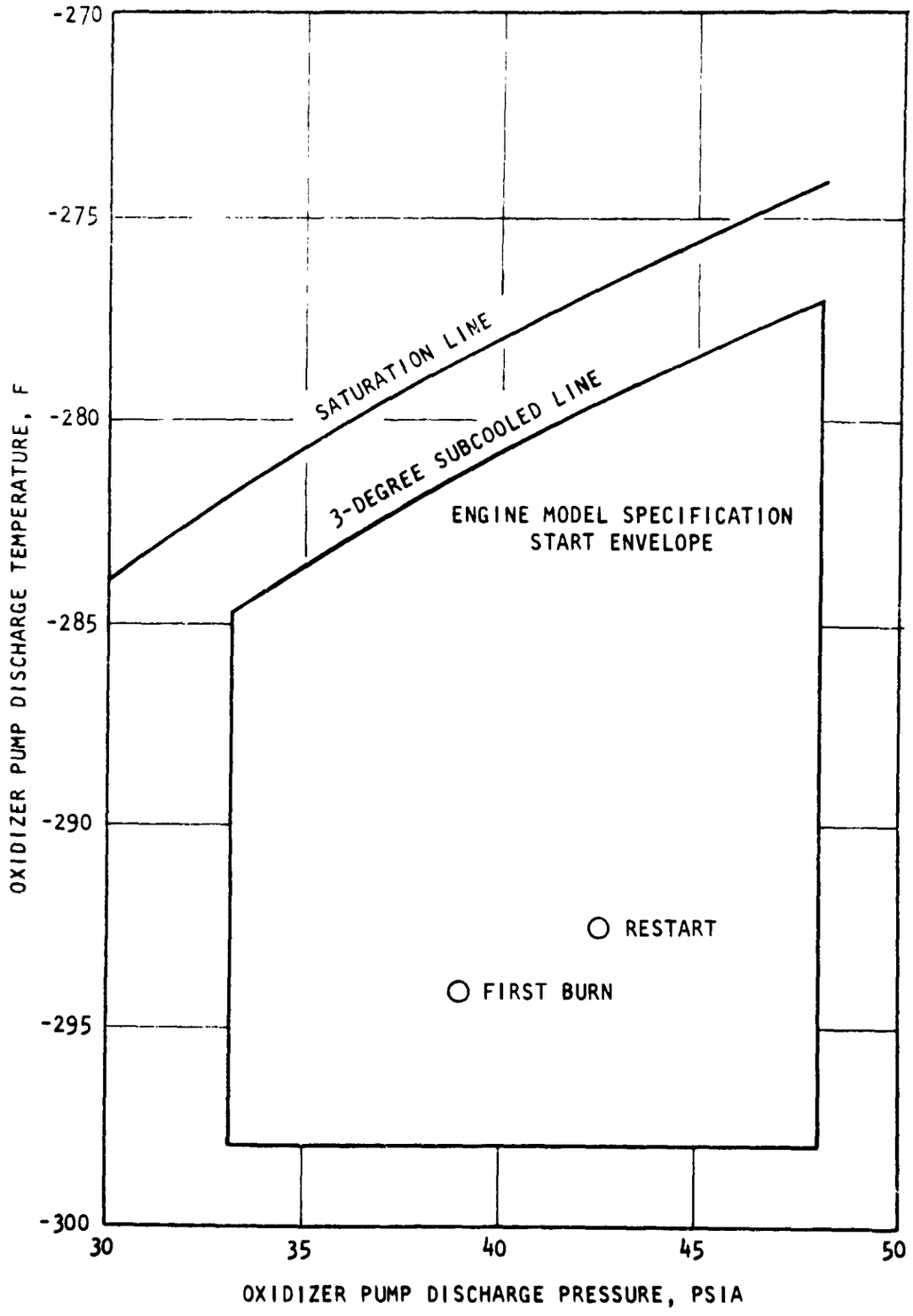

Figure 147. Oxidizer Pump Discharge Degrees Subcooled

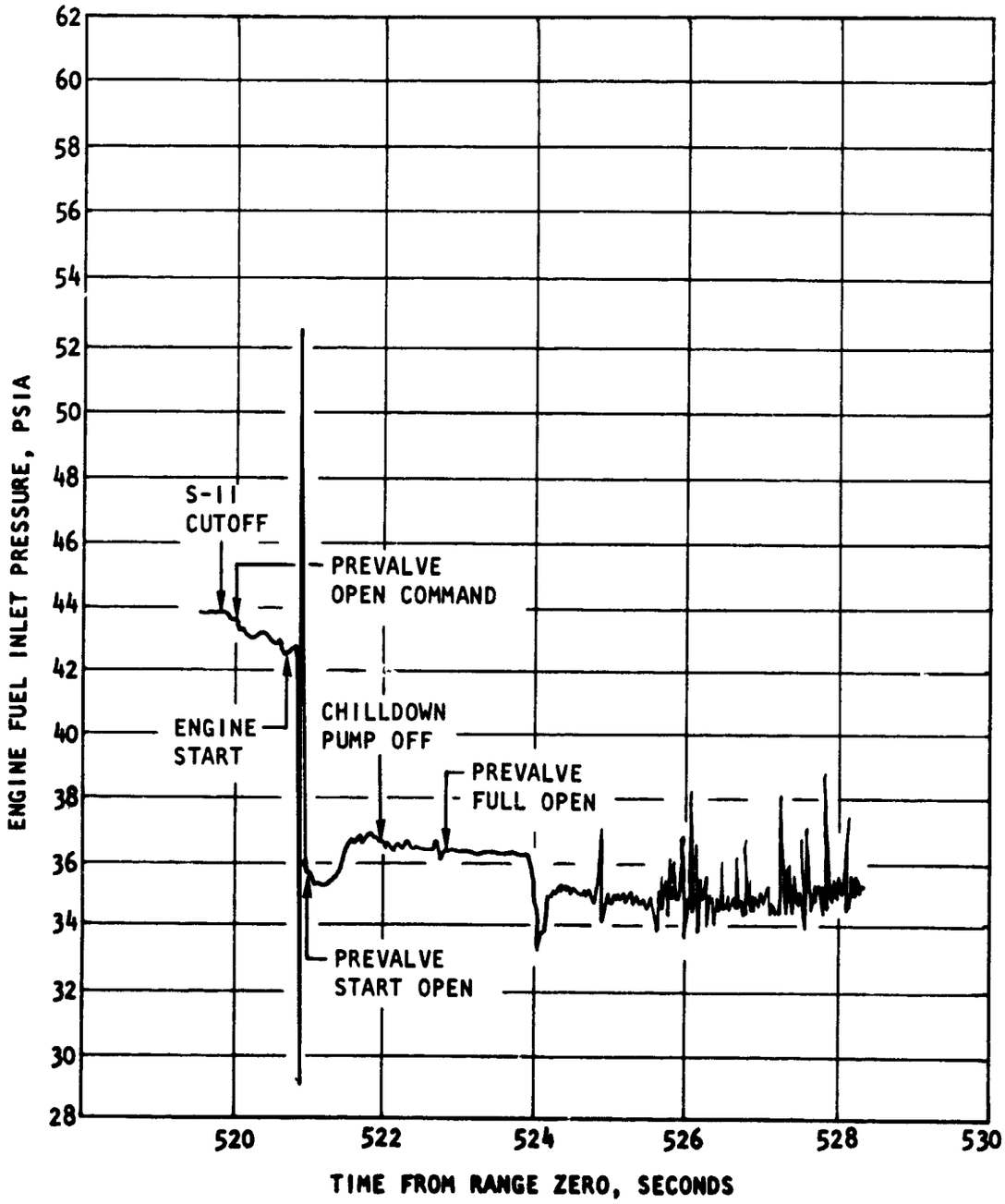

Figure 148. Fuel Pump Inlet Pressure During First Start Transient

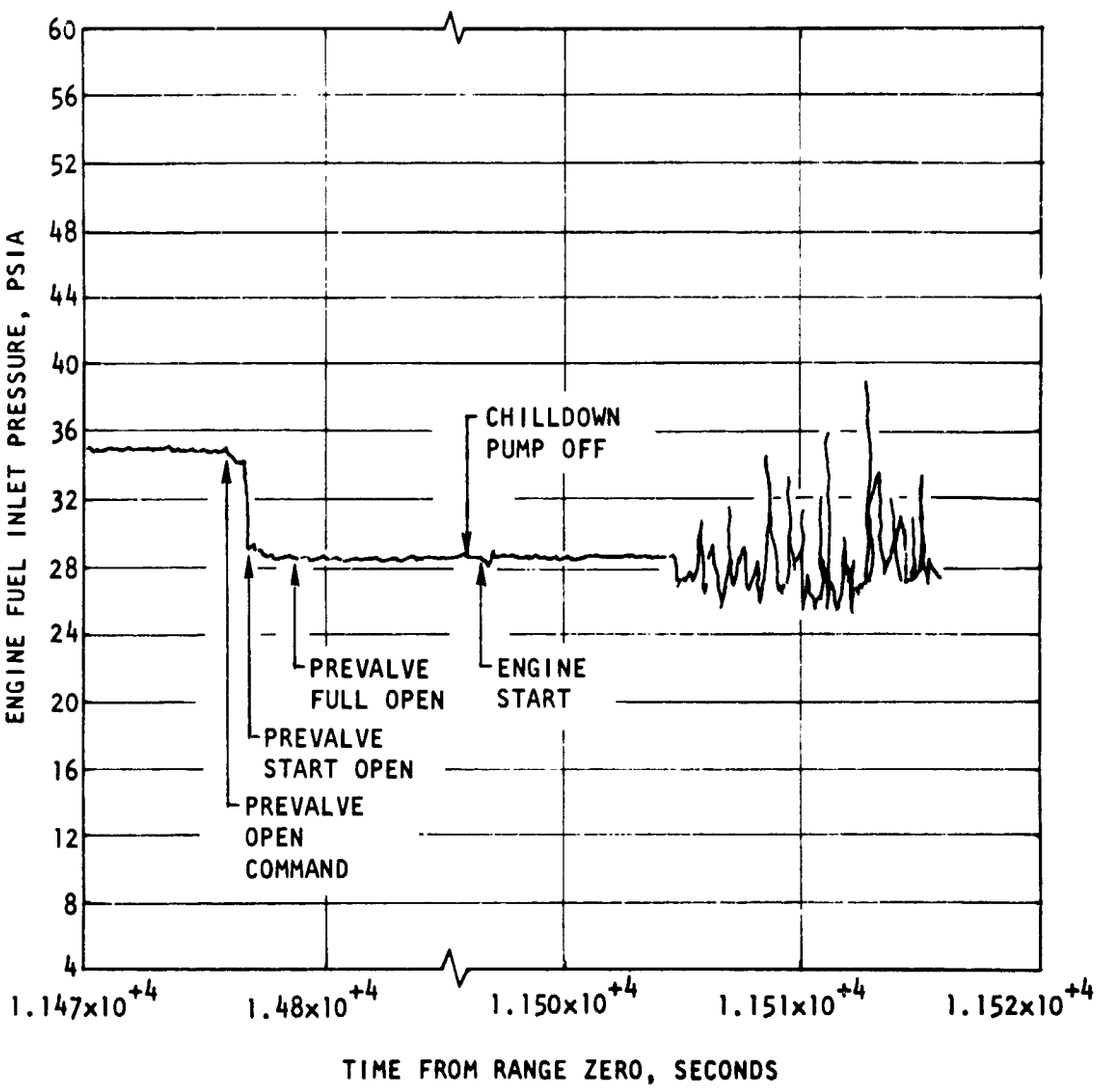

Figure 149. Fuel Pump Inlet Pressure During Second Start Transient

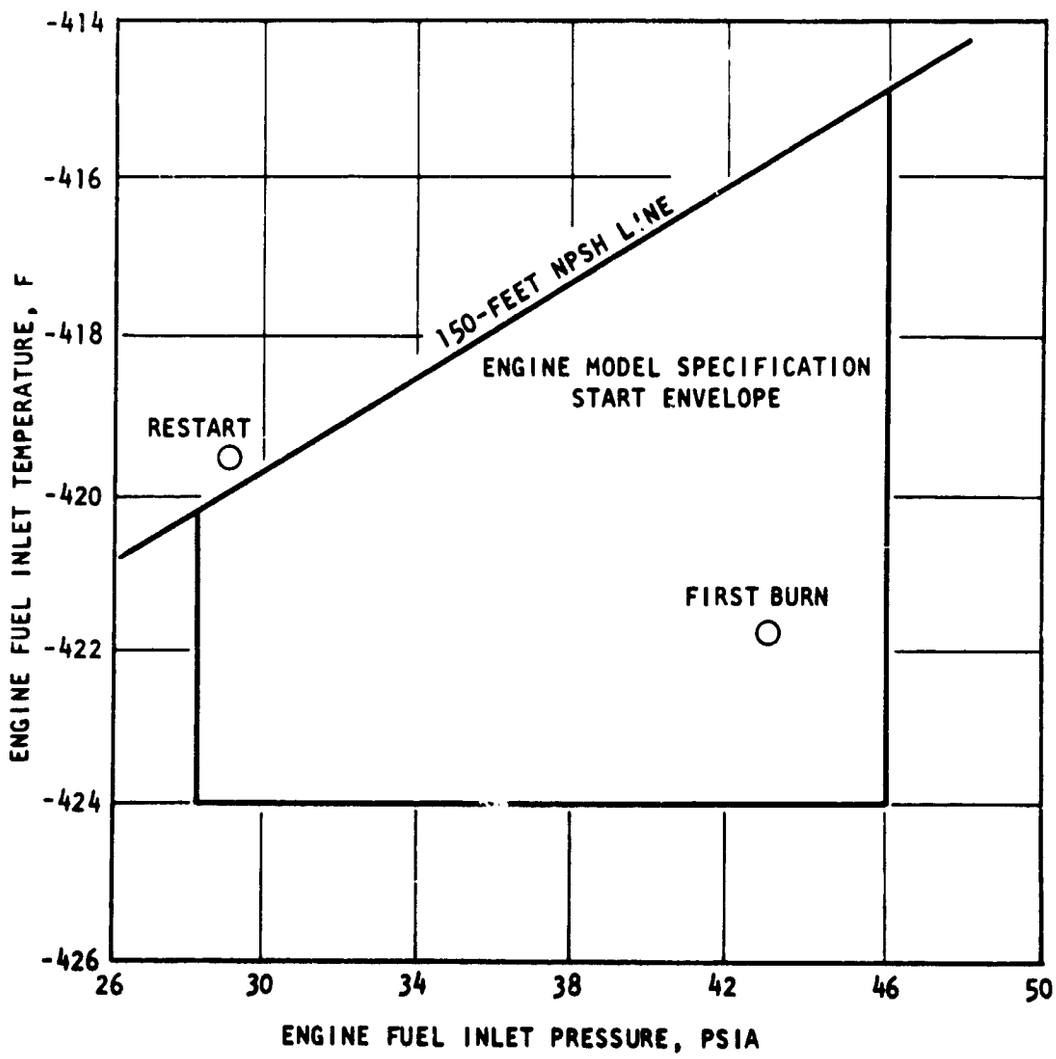

Figure 150. Fuel Inlet Pressure and Temperature at Engine Start

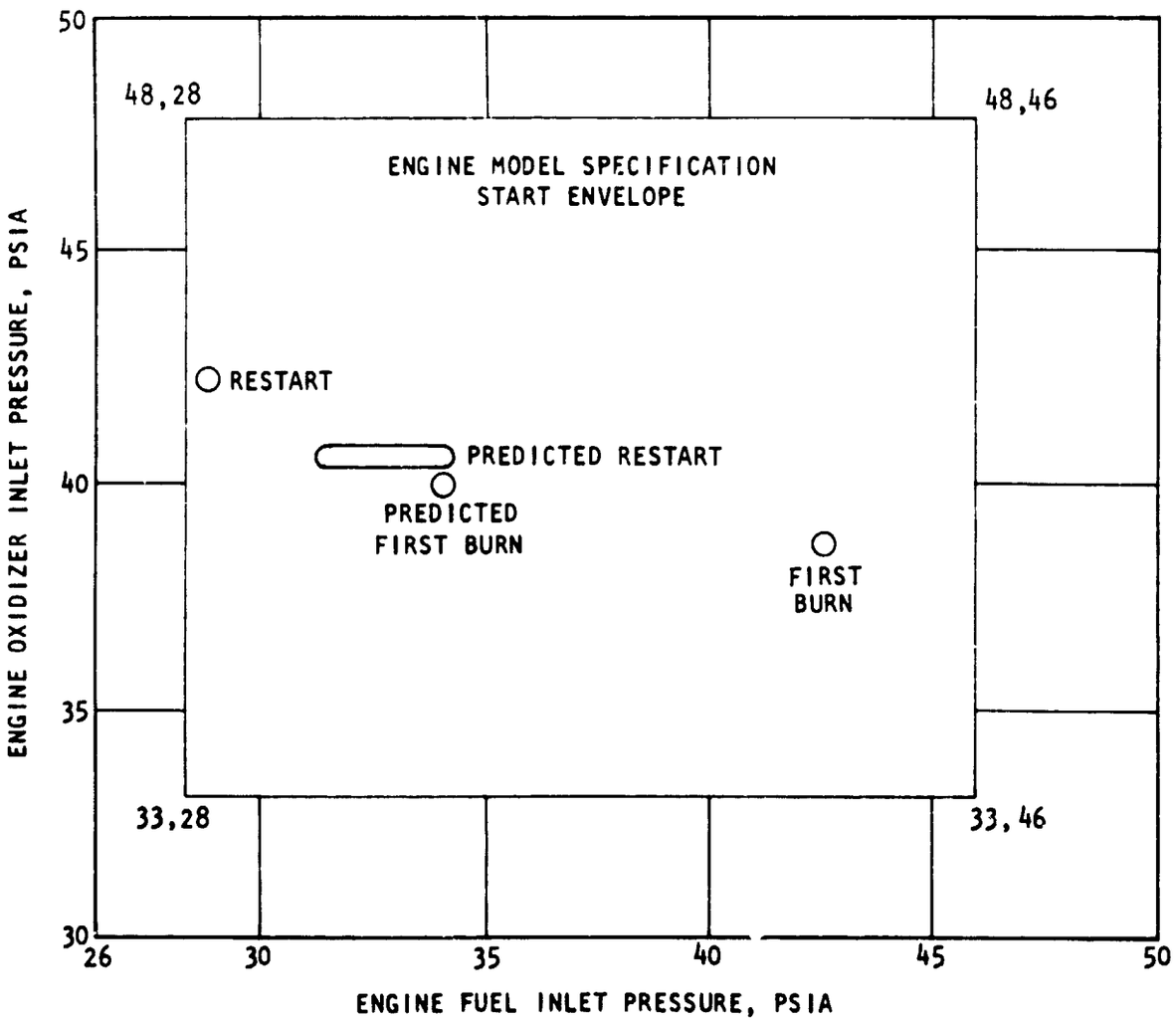

Figure 151. Engine Fuel and Oxidizer Inlet Pressure Start Limits

inlet pressure discrepancy (+8.4 psi) between actual first burn and predicted values is the selecting of engine inlet pressure at ESC rather than at some point beyond ESC where the inlet pressures have reasonably stabilized. By going to the more stabilized region, a pressure value of 36.5 psia was obtained, or 2.5 psi greater than predicted.

The same reasoning was applied to the difference (-1.4 psi) between actual engine oxidizer inlet pressure (first burn) and predicted. By selecting a more stable pressure, a value of 40 psia was obtained which is the same as predicted.

For S-IVB ESC restart, the engine fuel inlet pressure difference (-2.5 psi) between actual and predicted was attributed to the fuel tank repressurization problem. The engine oxidizer pump inlet pressure deviation of 1.8 psi resulted from an unexpected increase in oxidizer tank ullage pressure that took place between S-IVB ECO first burn and S-IVB ESC restart. It is believed the pressure rise was caused by a 5-degree increase in ullage temperature. The temperature rise was perhaps the result of bubbles of gaseous oxygen rising from the bottom of the tank to the ullage. This brought the ullage pressure above the minimum required at repressurization initiation. The helium spheres for repressurization were not needed.

Both the oxidizer and fuel recirculation systems demonstrated satisfactory performance throughout the flight, as evidenced by the adequate propellant inlet temperatures (Table 24) achieved prior to each ESC. Engine fuel inlet temperatures were slightly warmer than predicted prior to S-IVB ESC first burn and restart. A high prelaunch vent stack backpressure caused a higher than predicted fuel bulk temperature. A modification to the facility hydrogen disposal system is expected to reduce the backpressure on future flights. Table 24 summarizes the propellant recirculation system performance at liftoff, S-IVB ESC first burn, and restart.

TABLE 24

STAGE PROPELLANT SYSTEM PARAMETERS

Parameters	Liftoff		Engine Start		Engine Restart	
	Expected or Allowable	Actual	Expected or Allowable	Actual	Expected or Allowable	Actual
Fuel Pump Inlet Pressure (XD002), psia	DNA	44.2	28–46	42.4	28–46	28.5
Fuel Pump Inlet Temperature (XC0003), F	DNA	–421.4	Fig. 7	–421.8	Fig. 7	–419.6
Fuel Bleed Valve Temperature (C0012), F	–	–419.5	–	–420.5	–	–419.0
Fuel Pump Discharge Temperature (C0134), F	–	–415.8	–	–415.8	–	–419.0
Fuel Recirculation Return Pressure (D0062), psia	–	37.3	–	36.7	–	27.7
Fuel Recirculation Pump Outlet Temperature (C0157), F	–	–422.3	–	–421.7	–	–421.3
Fuel Recirculation Return Line Temperature (C0161), F	–	–418.6	–	–420.4	–	–416.0
Fuel Injection Temperature (C0200), F	–	–218	–	–118	–	–150
Fuel Tank Outlet Temperature (C0130), F	–	–422.1	–	–421.5	–	–421.0
Fuel Tank Ullage Pressure (VXD0177), psia	31–37	35.9	34	35.8	31–34	27.8
Fuel Tank Ullage Pressure (VD0178), psia	31–37	36	34	36.0	31–34	27.9

TABLE 24
(Continued)

Parameters	Liftoff		Engine Start		Engine Restart	
	Expected or Allowable	Actual	Expected or Allowable	Actual	Expected or Allowable	Actual
Fuel Recirculation Pump ΔP (D0218), psi	-	-31.5	-	+7.8	-	+3.3
Fuel Recirculation Pump Flow (VXF0005), gpm	-	144	-	140	-	110
Fuel Pump Interstage Pressure (D0224), psia	-	48	-	-	-	120
Oxidizer Pump Inlet Pressure (XD0003), psia	DNA	59.8	33-48	38.7	33-48	42.3
Oxidizer Tank Ullage Temperature (C0135), F	-	-250.0	-	-266.0	-	-297.0
Oxidizer Pump Discharge Temperature (C0133), F	DNA	-293.0	Fig. 4	-294.0	Fig. 4	-292.0
Oxidizer Bleed Valve Temperature (C0013), F	-	-293.5	-	-295.0	-	-292.5
Oxidizer Recirculation Return Line Tank Inlet Temperature (C0159), F	-	-293.0	-	-295.0	-	-294.0
Oxidizer Recirculation Pump Outlet Temperature (C0163), F	-	-295.6	-	-295.6	-	-294.3
Oxidizer Tank Ullage Pressure (VSD0179), psia	-	42.5	40	40.2	40	42.7

TABLE 24
(Concluded)

Parameters	Liftoff		Engine Start		Engine Restart	
	Expected or Allowable	Actual	Expected or Allowable	Actual	Expected or Allowable	Actual
Oxidizer Recirculation Pump Δ P (D0219), psia	-	-31.5	-	0	-	+2.0
Oxidizer Recirculation Return Pressure (D061), psia	-	49	-	40	-	43
Oxidizer Tank Diffuser Inlet Helium Gas Temperature (C0229), F	-	-252.0	-	-264.0	-	-295.0
Oxidizer Pump Inlet Temperature (XC0004), F	-294.	-295.4	Fig. 3	-295.5	Fig. 3	-294.3
Oxidizer Recirculation Pump Flow (VXF0004), gpm	-	37	-	34	-	43
Oxidizer Pump Bearing Cool Temperature (C202), F	-	-292.5	-	-295.8	-	-285.0

START TANK CONDITIONS

The S-IVB start tank pressure and temperature were within the allowable limits at liftoff, first start, and restart as shown in Fig. 152 and 153. The start tank vent and relief valve was operating prior to liftoff and maintained the start tank pressure level of 1290 psia throughout boost and up to engine start. Start tank refill was successful meeting model specification requirements as shown in Fig. 154 with the pressure and temperature at first burn cutoff reaching 1170 psia and 187 R, respectively. During the first orbit, the start tank pressure reached 1290 psia and the vent and relief valve maintained the pressure near that level. Start tank temperature instrumentation indicated temperatures in excess of those possible (based on pressure increase) during the orbit as was also typical on vehicle AS-203. Therefore, it became necessary to calculate a temperature profile for the start tank so that helium tank temperatures, which are also erroneous during orbit, could be obtained.

The calculated temperatures versus time are shown in Fig. 155. Curves numbered 1 through 4 are based on start tank vent and relief valve characteristics and start tank pressure measured during orbit. Curve No. 2 is for a vent and relief valve which has a high mass flowrate for a given pressure (fast valve). Curve No. 4 is based on a valve which has a low mass flowrate for a given pressure (slow valve). The No. 1 curve is based on component checkouts run on the valve installed on engine J2031.

HELIUM TANK

The helium tank pressure and temperatures were satisfactory at liftoff, first engine start, and restart. Helium consumption during engine operation was as expected. However, a pressure rise, which was expected during the orbit, was not realized. A comparison of calculated helium tank pressures and actual flight data during orbit is shown in Fig. 156.

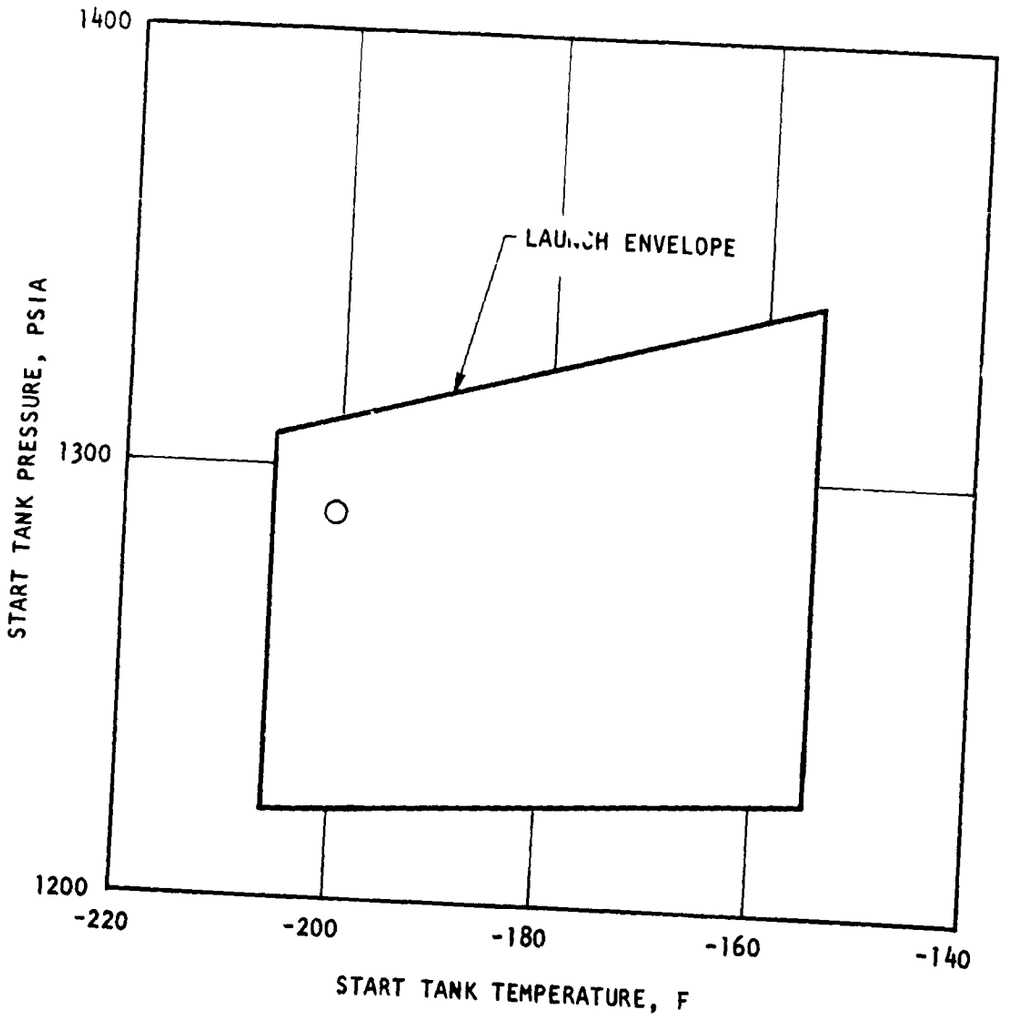

Figure 152. Start Tank Condition (Liftoff -8.9 Seconds)

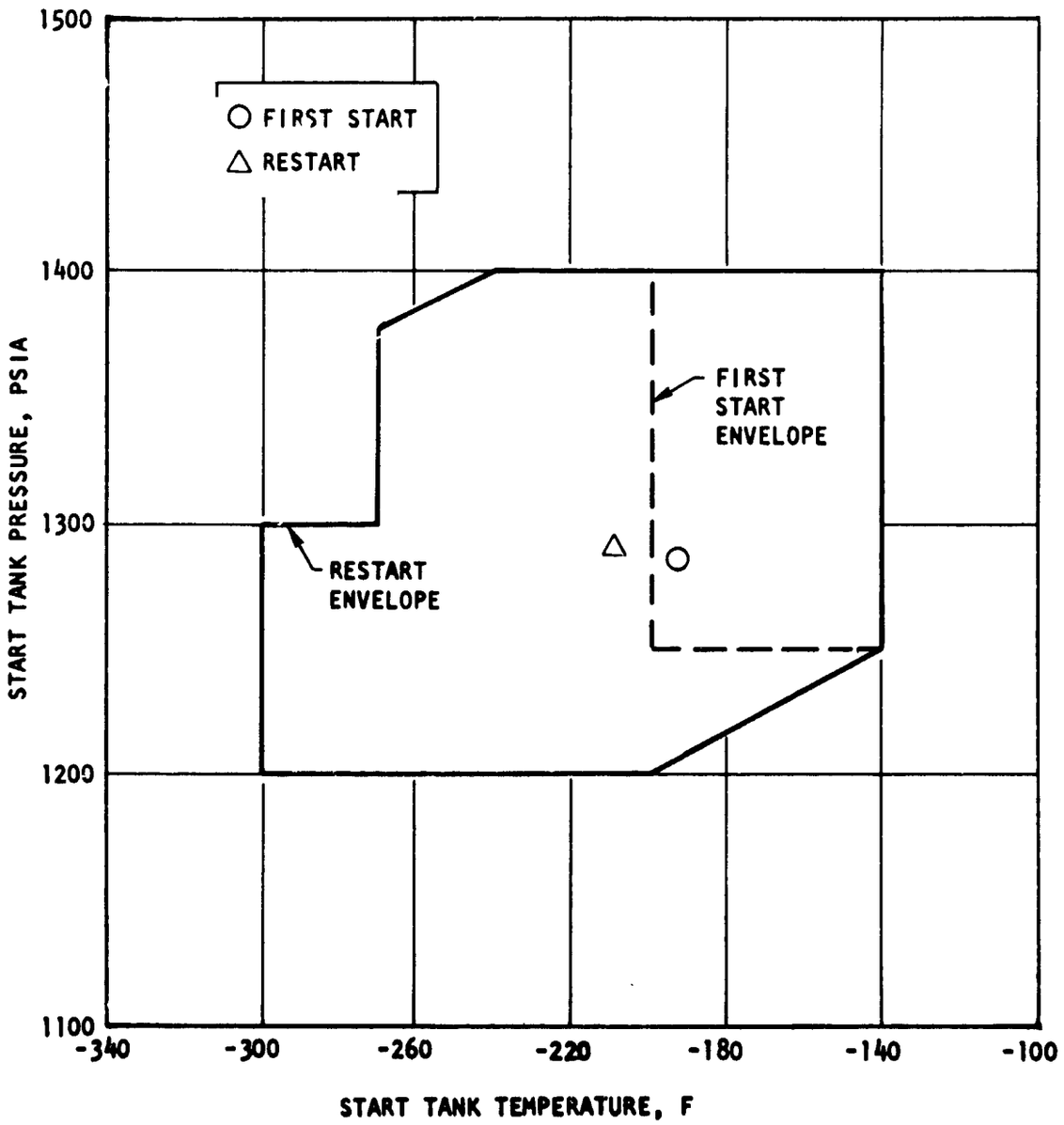

Figure 153. Start Tank Condition at Engine Start

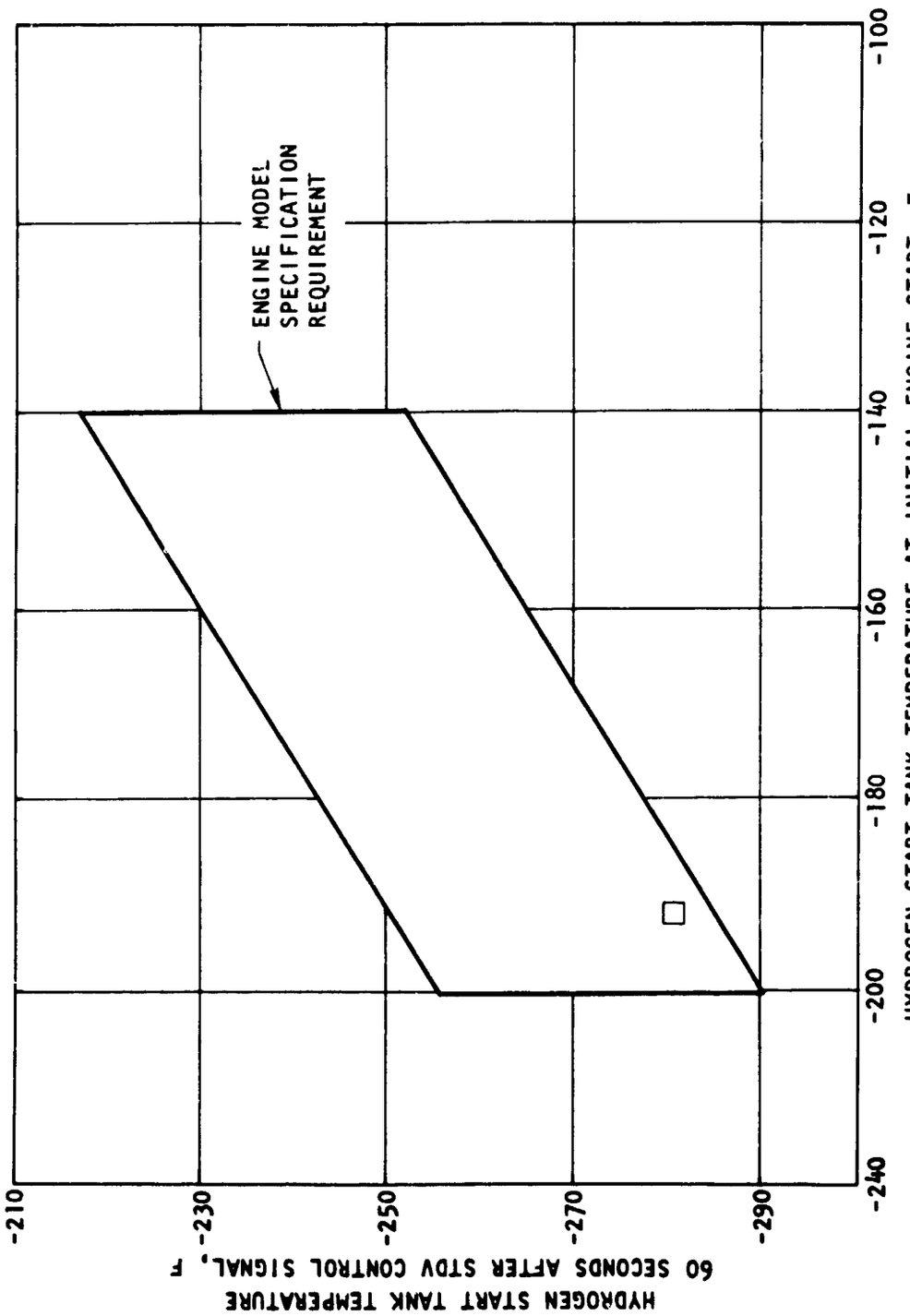

Figure 154. Start Tank Refill Limits

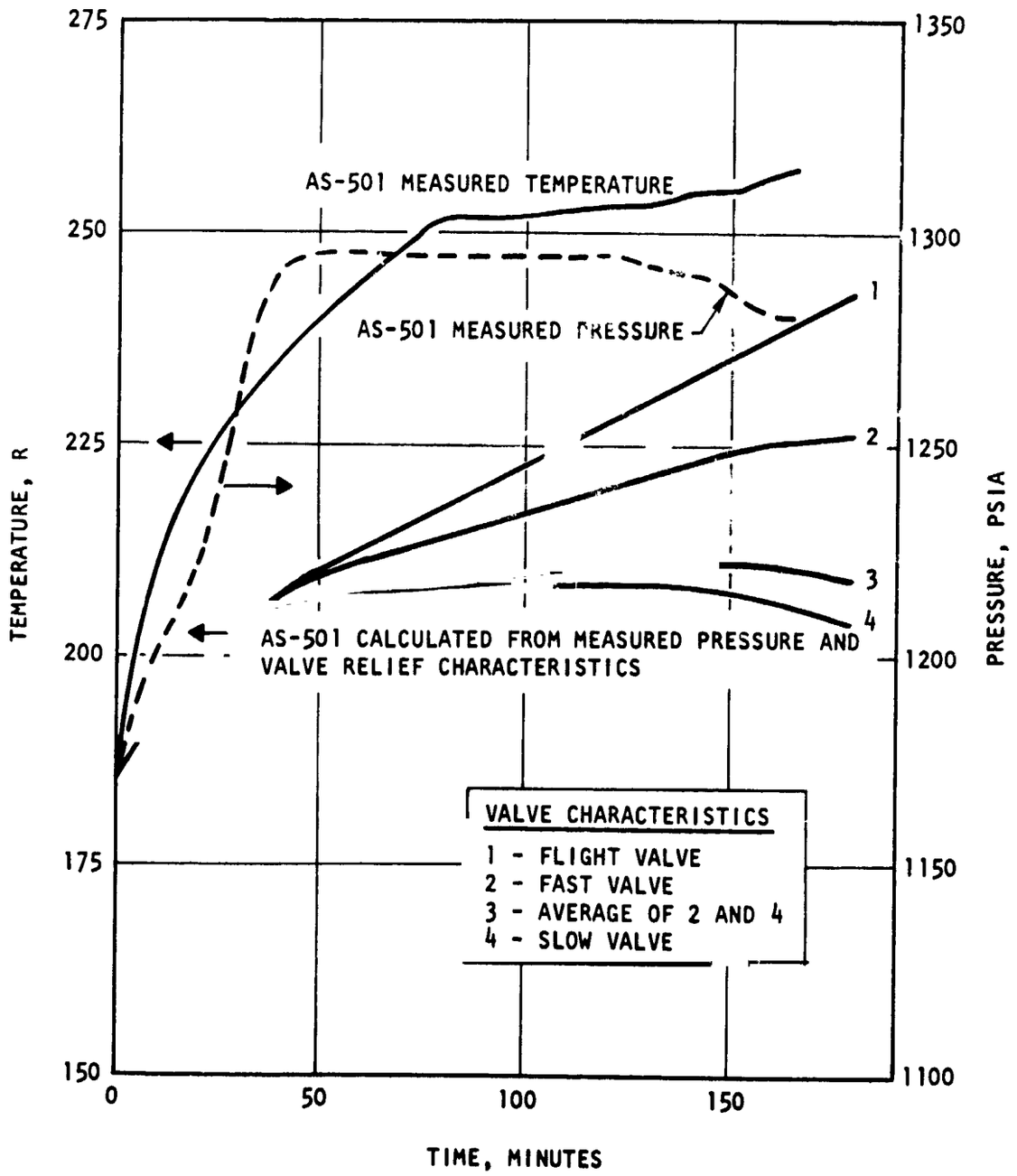

Figure 155. Start Tank Gas State During Earth Orbit

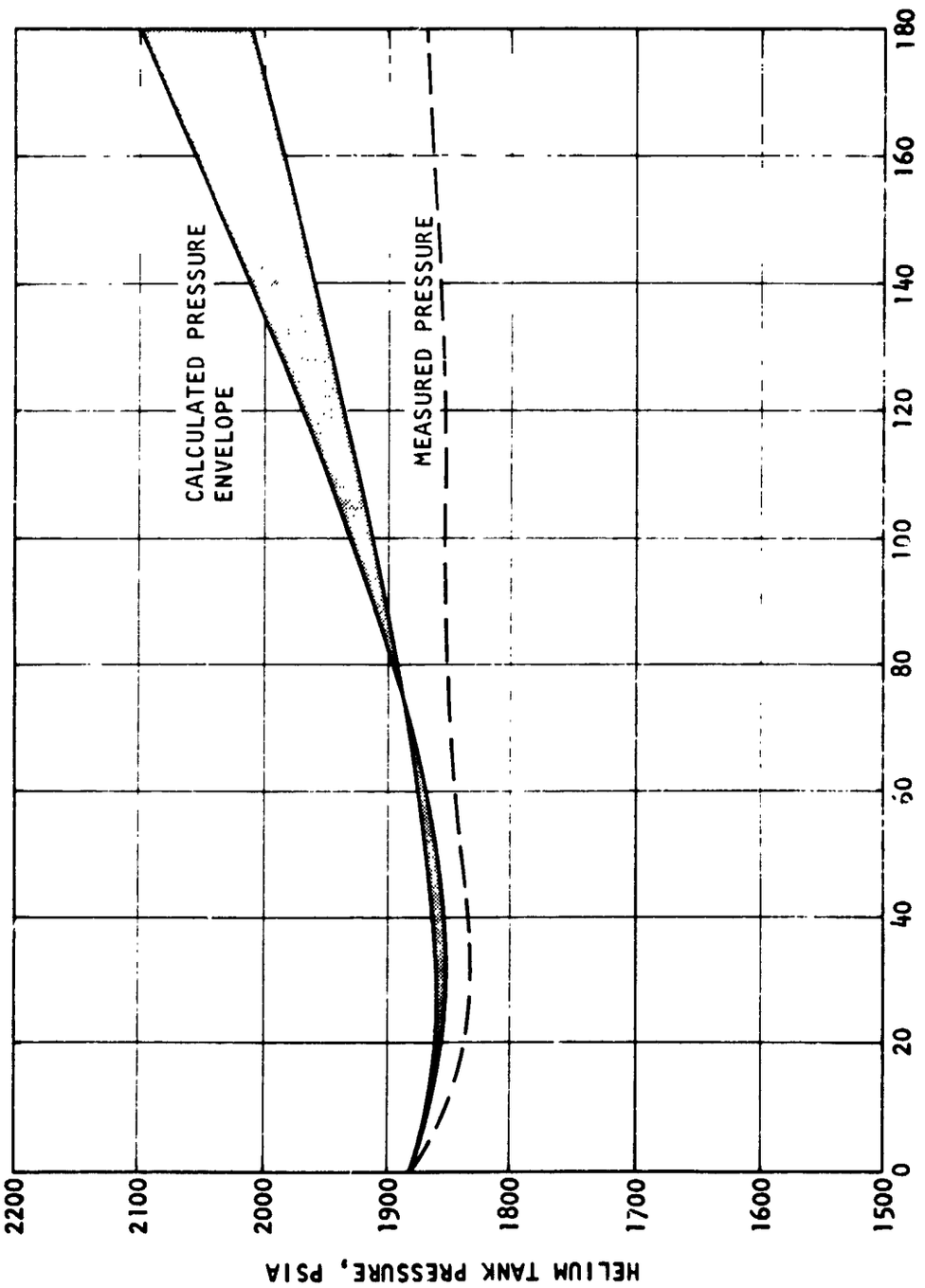

Figure 156. Comparison of Calculated and Actual Helium Tank Pressure

It will be noted that the calculated helium pressure is above that measured. This variation is believed caused by a leak in the helium system during orbit which amounted to a helium mass loss during the 3 hours of 0.13 to 0.22 pounds. These values must be used with caution, because they are based on calculated temperatures which are dependent upon assumed start tank vent and relief valve characteristics as discussed earlier. The maximum helium loss allowed during ground checkout of the S-IVB is 0.036 lb/hr. Areas considered in an attempt to identify the leak path in the helium high-pressure system were: (1) helium regulator; high-pressure relief, helium control solenoid, emergency vent solenoid, main regulator seat, (2) helium fill check valve, (3) weld joints at transducers, helium regulator, and instrumentation line weld sleeves, and (4) seals at helium fill valve, helium regulator, and temperature probe. Available flight instrumentation data were not adequate to conduct a system analyses and no leakage was detected during the preflight helium pressure decay test which might indicate a problem area. Therefore, isolation of a leak path was not possible.

The start tank-integral helium tank and the helium regulator were replaced subsequent to engine delivery. A redundant pressure transducer and connecting tubing were also added on the helium high-pressure system. The change of regulators and addition of instrumentation were not accompanied by a helium mass loss test as specified in the Rocketdyne Manuals. However, the aforementioned pressure decay test was accepted by Rocketdyne as being adequate.

Helium tank pressures and temperatures from liftoff to restart cutoff are shown in Fig. 157. Figure 158 shows that start tank-helium tank differential temperature at engine start was within the model specification allowable of 20 degrees.

The helium regulator operated nominally throughout the flight. The helium regulator outlet pressure transducer had a zero shift of approximately 3 psi, which is within the allowable.

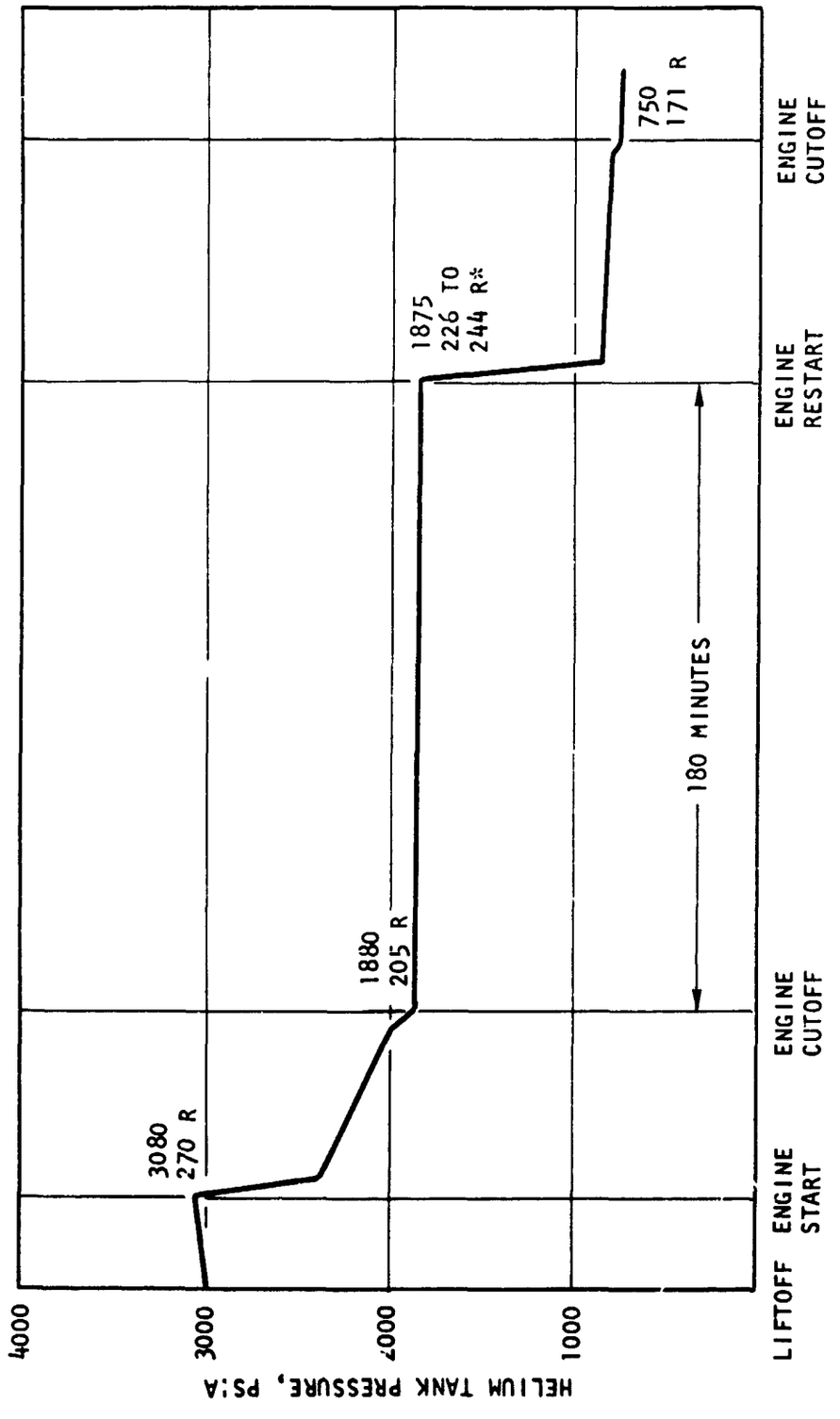

Figure 157. Helium Usage During Flight

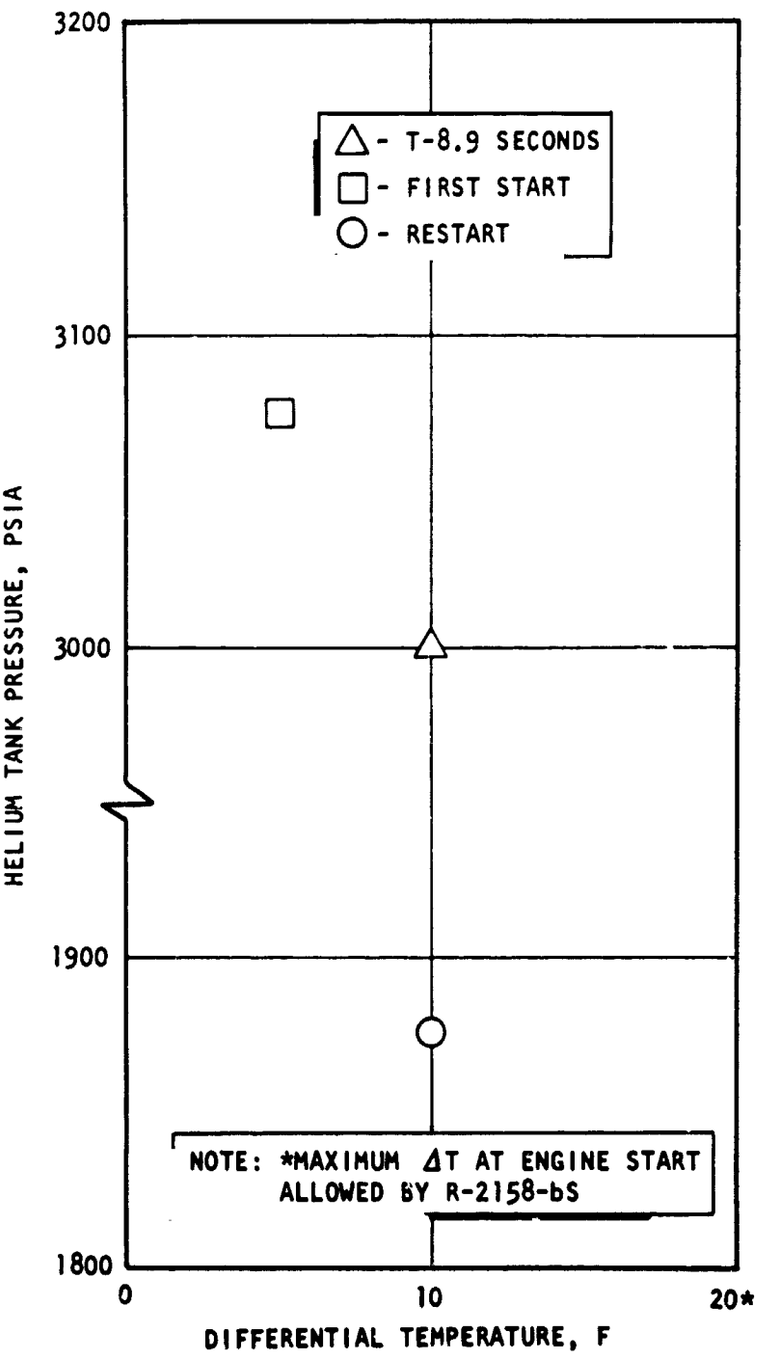

Figure 158. Helium Tank Pressure vs Start Tank Minus Helium Tank Temperature

THRUST INCREASE

The flight thrust buildup curve for the S-IVB initial start is shown in Fig. 159 and for the restart in Fig. 160. Also shown are the respective predicted envelopes from AEDC testing and the allowable thrust buildup limits.

Both curves are within the allowable buildup limits and agree well with the predicted envelopes.

MAINSTAGE PERFORMANCE

The engine mainstage performance for the flight is summarized in Table 27. Included for comparison are the respective values obtained during engine and vehicle acceptance demonstrations, plus those values predicted by Rocketdyne for the flight. While performance was as predicted on the first burn, it was higher in both thrust and mixture ratio during the second burn.

Data Reduction and Evaluation

Mainstage performance of the engine was evaluated using data obtained from the S-IVB stage contractor. The data was recorded on magnetic tape at a frequency of 10 samples per second.

The performance evaluation was made using Rocketdyne's digital computer steady-state data reduction program (PT 641). This program calculates and reduces to standard altitude conditions engine and subsystem performance characteristics. By reducing the data to standard conditions, comparisons may be made between engine and vehicle acceptance and the flight. The standard conditions include engine inlet pressures and temperatures, auxiliary pump power, heat exchanger flowrate, hydrogen tapoff flowrate, and ambient pressure.

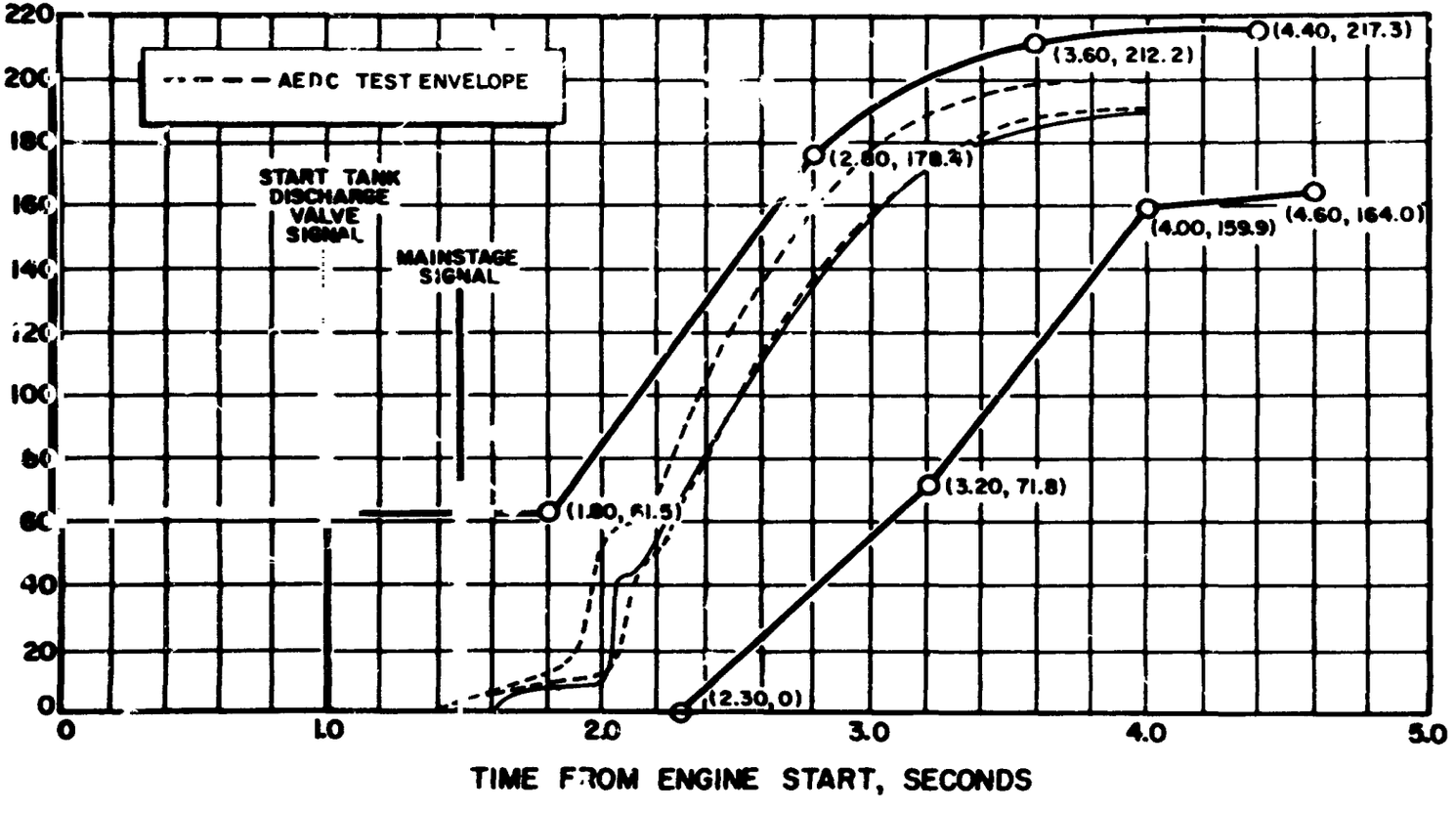

Figure 159. S-IVB First Burn Thrust Increase (PU Valve at Null)

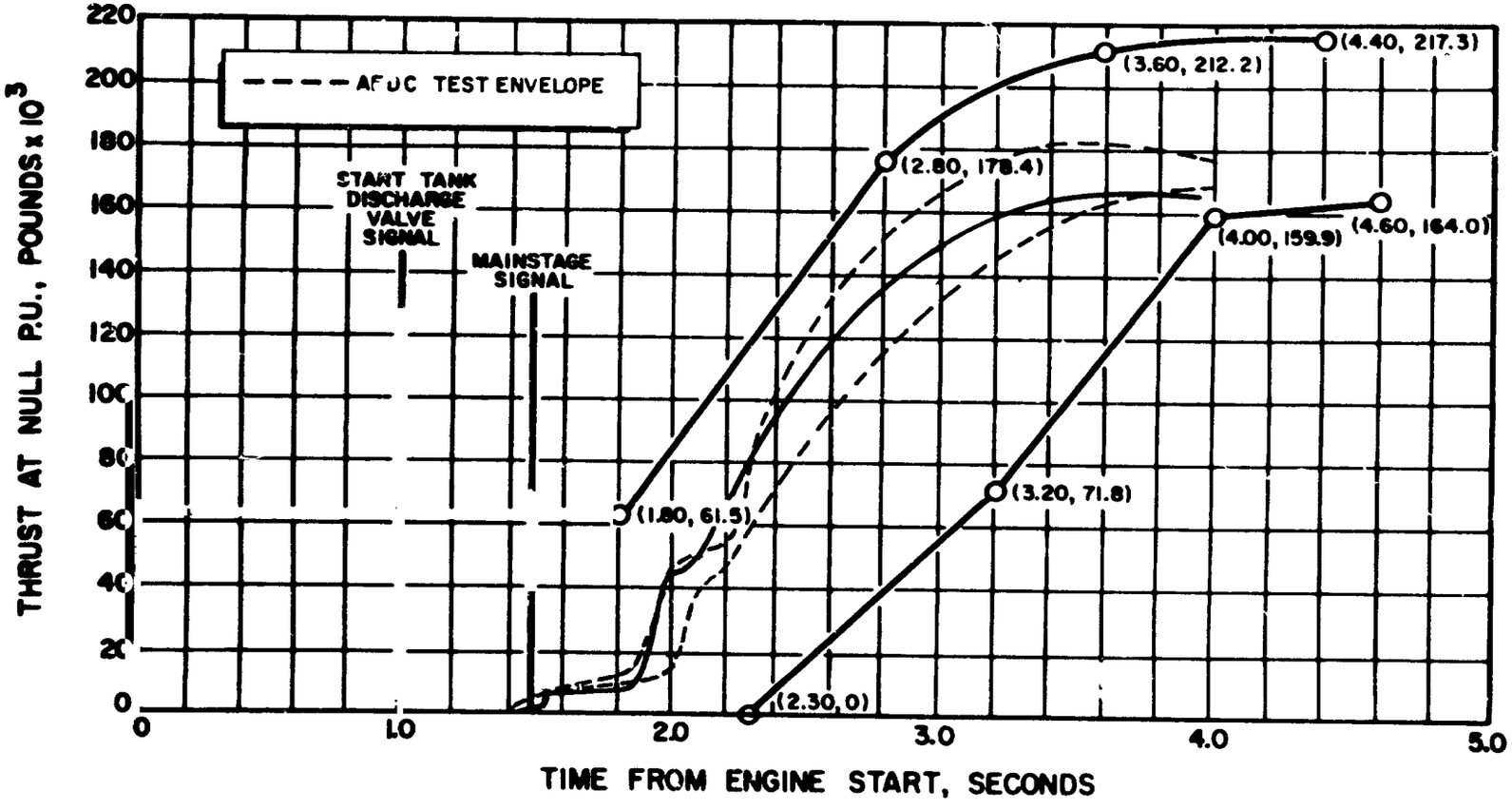

Figure 160. S-IVB Restart Thrust Increase (PU Valve Open)

TABLE 25

MAINSTAGE PERFORMANCE, ENGINE J2031

Parameter	Standard Altitude Conditions				Actual Conditions
	Engine Acceptance	Vehicle Acceptance	Predicted Flight (Tag Values)	Flight	Flight
First Burn					
Thrust, pounds	222,118	229,003	222,118	222,454	224,093
Mixture Ratio	5.506	5.496	5.506	5.480	5.523
Specific Impulse, seconds	423.1	423.5	423.1	423.5	423.2
Second Burn					
Thrust, pounds		226,470	222,118	224,302	225,459
Mixture Ratio		5.572	5.506	5.576	5.639
Specific Impulse, seconds		422.7	423.1	422.7	422.2

All performances given at 60 seconds from STDV signal.

Standard altitude conditions:

Oxidizer Pump Inlet Pressure, psia	39.0
Oxidizer Pump Inlet Density, lb/ft^3	70.79
Fuel Pump Inlet Pressure, psia	30.0
Fuel Pump Inlet Density, lb/ft^3	4.40
Fuel Tank Pressurization Tapoff Flowrate, lb/sec	0.80
Oxidizer Heat Exchanger Flowrate, lb/sec	1.80
Auxiliary Pump Power, horsepower	15
Ambient Pressure, psia	0.0

To obtain more comparable results with engine and vehicle testing, the following procedures were used. All flowmeter and pump speeds were counted from the high-frequency oscillograph to detect and account for any noise or data dropout. All pressure measurements sensing ambient pressure pre-engine start were "zero shift" corrected by noting the differential between the measurement and ambient pressure just prior to engine ignition. Flight thrust and chamber pressure were calculated using specific impulse and thrust coefficients as determined from engine acceptance.

Significant data anomalies encountered were a large apparent zero shift in fuel pump discharge pressure (+25 psi) and a +40 degree shift in fuel turbine inlet temperature. This bias in fuel turbine inlet temperature has been noted on other S-IVB vehicles.

Engine Performance

Table 26 summarizes mainstage performance as determined from engine acceptance, vehicle acceptance, and the flight. Flight performance on the first burn was essentially as predicted. However, on the second burn, following a 3-hour coast, thrust and mixture ratio were higher by +1848 pounds and +0.086 mixture ratio units with respect to the first burn. The shift in mixture ratio was attributed to both a shift in fuel turbine efficiency and a change in operating point of the balance piston system. The turbine efficiency shift was estimated to be approximately -1 percent. The shift in the balance piston system was indicated by a change in the operating pressure of the balance piston system and a change in fuel pump efficiency. The balance piston system bleeds flow from the pump discharge to balance the turbopump's axial thrusts. A change in operating point of this system causes a shift in the bleed flow and subsequently a change in pump delivered flow and engine mixture ratio. The thrust increase between the first and second burn was caused by a decrease in gas generator oxidizer bootstrap system resistance. During vehicle static testing, the high thrusts on both burns and the shift between burns was attributed to resistance shifting of the gas generator oxidizer system.

TABLE 26

MAINSTAGE PERFORMANCE, ENGINE J2031

	Standard Altitude Conditions					Actual Conditions	
		Vehicle Acceptance		Flight		Flight	
	Engine Acceptance	First Burn	Second Burn	First Burn	Second Burn	First Burn	Second Burn
Engine Performance							
Mixture Ratio	5.506	5.496	5.572	5.480	5.576	5.523	5.639
Thrust Chamber Pressure, psia	756.8	777.8	769.4	756.4	762.7	761.6	766.0
Thrust (vehicle and flight from chamber pressure), pounds	222,118	229,003	226,470	222,454	224,302	224,093	225,459
Specific Impulse, seconds	423.1	423.5	422.7	423.5	422.7	423.2	422.2
Engine Oxidizer Flow, lb/sec	444.31	457.50	454.24	444.20	449.94	448.37	453.61
Engine Fuel Flow, lb/sec	80.70	83.24	81.52	81.06	80.69	81.18	80.44
Fuel Tapoff Flow, lb/sec	0.80	0.80	0.80	0.80	0.80	0.80	0.80
Oxidizer Heat Exchanger Flow, lb/sec	1.80	1.80	1.80	1.80	1.80	1.80	1.80
Fuel Turbopump Performance							
Pump Inlet Pressure (total), psia	30.0	30.0	30.0	30.0	30.0	32.3	31.2
Pump Inlet Density, lb/ft^3	4.40	4.40	4.40	4.40	4.40	4.35	4.34
Pump Discharge Pressure (total), psia	1197.6	1243.4	1229.7	1189.3	1208.8	1194.2	1210.9
Pump Speed, rpm	26,202.2	26,732.6	26,461.7	26,362.6	26,469.0	26,568.0	26,667.0
Pump Head, feet	36,704.0	38,096.4	37,679.8	36,452.3	37,047.3	36,937.8	37,521.2
Pump Flow, gpm	8313.3	8572.9	8397.4	8350.4	8312.2	8430.5	8389.6
Turbine Inlet Temperature, F	1166.3	1286.5	1244.2	1231.3	1265.1	1252.6	1286.9
Turbine Inlet Pressure (total), psia	620.4	648.8	633.4	620.0	633.7	623.4	635.9
Oxidizer Turbopump Performance							

Pump Head, feet	36,704.0	38,096.4	37,679.8	36,452.3	37,047.3	36,937.8	37,521.2
Pump Flow, gpm	8313.3	8572.9	8397.4	8350.4	8312.2	8430.5	8389.6
Turbine Inlet Temperature, F	1166.3	1286.5	1244.2	1231.3	1265.1	1252.6	1286.9
Turbine Inlet Pressure (total), psia	620.4	648.8	633.4	620.0	633.7	623.4	635.9
Oxidizer Turbopump Performance							
Pump Inlet Pressure (total), psia	39.0	39.0	39.0	39.0	39.0	41.7	41.9
Pump Inlet Density, lb/ft^3	70.79	70.79	70.79	70.79	70.79	70.88	70.73
Pump Discharge Pressure (total), psia	1059.8	1107.2	1087.3	1054.3	1057.5	1064.6	1065.8
Pump Speed, rpm	8481.1	8658.2	8585.2	8484.4	8557.9	8512.0	8587.0
Pump Head, feet	2072.8	2167.5	2127.1	2062.3	2069.3	2075.2	2082.0
Pump Flow, gpm	2876.2	2960.0	2939.3	2875.6	2912.0	2887.1	2926.6
Turbine Inlet Temperature, F	764.3	837.5	805.8	788.1	819.4	803.3	835.2
Turbine Inlet Pressure (total), psia	83.2	86.5	85.2	84.4	84.7	84.8	85.0
Turbine Outlet Temperature, F	612.8	678.8	651.8	610.4	637.4	623.8	651.3
Auxiliary Pump Power, horsepower	15.0	15.0	15.0	15.0	15.0	5.0	5.0
Gas Generator Performance							
Oxidizer Weight Flow, lb/sec	3.14	3.35	3.25	3.18	3.26	3.20	3.29
Fuel Weight Flow, lb/sec	3.42	3.38	3.37	3.31	3.34	3.30	3.31
Gas Generator Chamber Pressure, psia	647.0	676.5	660.5	646.5	660.8	650.0	663.1

Footnote ... 2

Flight Reconstruction

The mainstage operating characteristics have been reconstructed for engine J2031 as flown on the S-IVB vehicle. The following parameters were reconstructed for both burns and compared to the actual telemetry values: engine mixture ratio, main thrust chamber pressure, oxidizer and fuel flowrates, oxidizer and fuel pump speeds, oxidizer and fuel pump discharge pressures, and gas generator chamber pressure. The reconstructed performance was in good agreement with the actual except in those cases explained by shifts in engine performance and instrumentation shifts.

The reconstructions were made with a linear model using influence coefficients to operate on the predicted "Tag" values. For engine J2031, the predicted values were from engine acceptance performance given in Table 26. The influence coefficients were used with the following independent variables shown in the respective figures. In each case, the two figures for each parameter represent the first and second burns, respectively.

Figures 161 and 162, Heat Exchanger Helium Flowrate
Figures 163 and 164, Fuel Tapoff Flowrate
Figures 165 and 166, Engine Oxidizer Inlet Temperature
Figures 167 and 168, Engine Fuel Inlet Temperature
Figures 169 and 170, Engine Oxidizer Inlet Pressure
Figures 171 and 172, Engine Fuel Inlet Pressure
Figures 173 and 174, PU Valve Position

The plots of heat exchanger helium flowrate and fuel tapoff flowrate are estimates from predicted flight performance by the S-IVB stage contractor. All other plots are from telemetry data. Another independent variable, the auxiliary pump power extraction, was assumed to be a constant 4.0 horsepower throughout both burns.

Figures 175 through 196 show the reconstructed performance as compared to the flight telemetry data, except in the cases of thrust and specific

impulse where only the reconstructed has been calculated. The following figures are included for the respective parameters for first and second burns.

Figures 175 and 176, Engine Thrust
Figures 177 and 178, Engine Specific Impulse
Figures 179 and 180, Engine Mixture Ratio
Figures 181 and 182, Main Thrust Chamber Pressure
Figures 183 and 184, Engine Oxidizer Flowrate
Figures 185 and 186, Engine Fuel Flowrate
Figures 187 and 188, Oxidizer Pump Speed
Figures 189 and 190, Fuel Pump Speed
Figures 191 and 192, Oxidizer Pump Discharge Pressure
Figures 193 and 194, Fuel Pump Discharge Pressure
Figures 195 and 196, Gas Generator Chamber Pressure

The comparisons of actual and reconstructed are in good agreement. On the second burn, several parameters did indicate some differences but this was attributable to the performance shift discussed in the previous section. On both burns, fuel pump discharge pressure was in poor agreement because of a zero shift in the flight measurement.

Table 27 summarizes the comparison between reconstructed and actual performance at the full-closed PU valve position.

Table 28 presents the first and second burn reconstructed average thrust, mixture ratio, and specific impulse; for maximum and null PU operation, and from 90-percent thrust to cutoff signal. These average values permit general comparisons with similar calculations by the stage contractor for preflight predictions and for flight analysis.

TABLE 27

COMPARISON BETWEEN RECONSTRUCTED AND ACTUAL PERFORMANCE
(MAXIMUM PU)

Parameter	First Burn (Actual Minus Reconstructed)	Second Burn (Actual Minus Reconstructed)
Engine Mixture Ratio, o/f	-0.013 (-0.2 percent)	0.10 (2.0 percent)
Thrust Chamber Pressure, psi	-2.2 (-0.3 percent)	3.0 (0.1 percent)
Engine Fuel Flow, lb/sec	0.11 (0.1 percent)	-3.2 (-0.37 percent)
Fuel Pump Speed, rpm	200 (0.75 percent	225 (0.9 percent)
Engine Oxidizer, lb/sec	0.46 (0.1 percent)	7.3 (1.6 percent)
Oxidizer Pump Speed, rpm	-9 (-0.1 percent)	90 (1.0 percent)
Fuel Pump Outlet Pressure, psi	-40 (-3.3 percent)	-25 (-2.1 percent)
Oxidizer Pump Outlet Pressure, psi	30 (0.3 percent)	10 (0.1 percent)
Gas Generator Injector End Pressure, psi	4.0 (0.6 percent)	12 (1.8 percent)
Fuel Turbine Inlet Temperature, R	72 (4.3 percent)	100 (6.0 percent)
Oxidizer Turbine Inlet Temperature, R	28 (2.3 percent)	55 (4.6 percent)
Oxidizer Turbine Outlet Temperature, R	2 (0.2 percent)	27 (2.5 percent)
Oxidizer Turbine Inlet Pressure, psi	0.9 (1.1 percent)	0.3 (0.4 percent)
Oxidizer Turbine Outlet Pressure, psi	0.8 (2.5 percent)	0.5 (1.6 percent)
Thrust Chamber Fuel Injection Pressure, psi	5.0 (0.6 percent)	18 (2.1 percent)
Thrust Chamber Oxidizer Injection Pressure, psi	12 (1.3 percent)	20 (2.1 percent)

TABLE 28

AVERAGE ENGINE RECONSTRUCTED PERFORMANCE

Description of Engine Operation	Average Thrust, pounds	Mixture Ratio, o/f	Specific Impulse, seconds	Propellant Flowrate, lb/sec
High Mixture Ratio Region				
First Burn	223,278	5.5231	423.28	527.83
Second Burn	222,402	5.5291	422.95	525.81
15 Seconds After Mixture Ratio Cutback to Cutoff Signal				
Second Burn	194,595	4.8915	427.12	454.94
90-Percent Thrust to Cutoff Signal				
First Burn	223,278	5.5231	423.28	527.83
Second Burn	202,357	5.0677	425.97	474.73

248

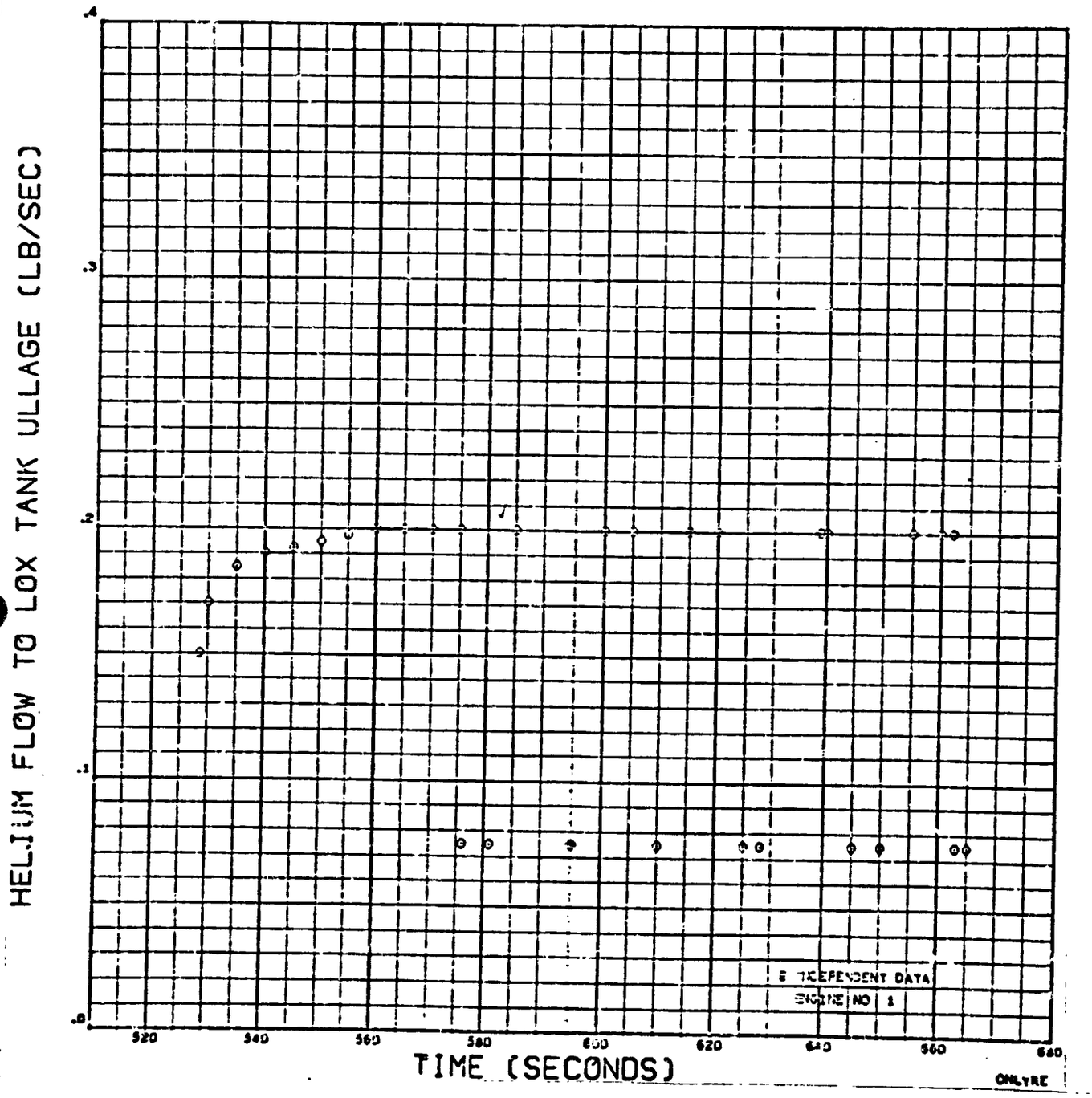

Figure 161. Helium Flow to Oxidizer Tank Ullage (First Burn)

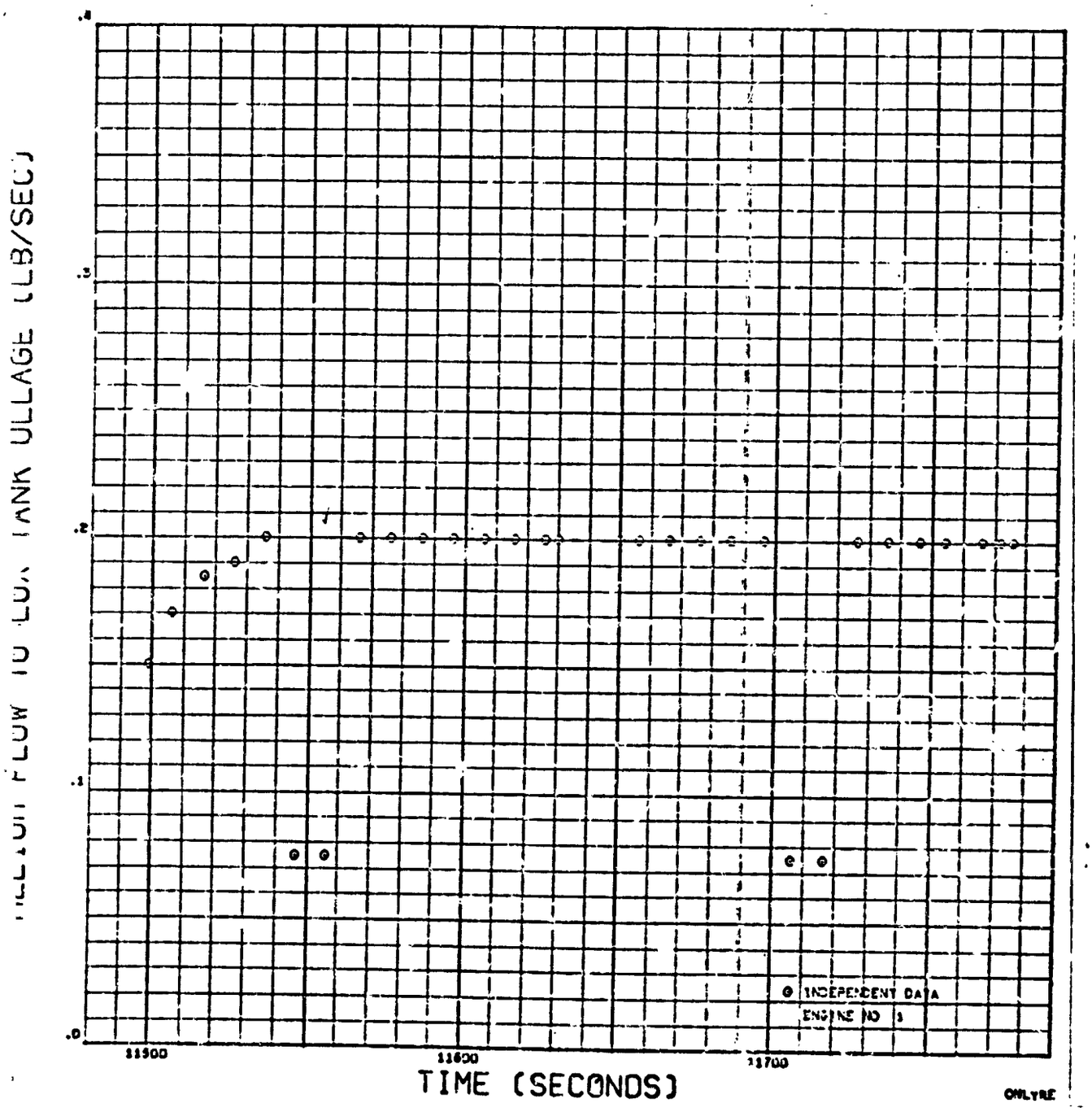

Figure 162. Helium Flow to Oxidizer Tank Ullage (Second Burn)

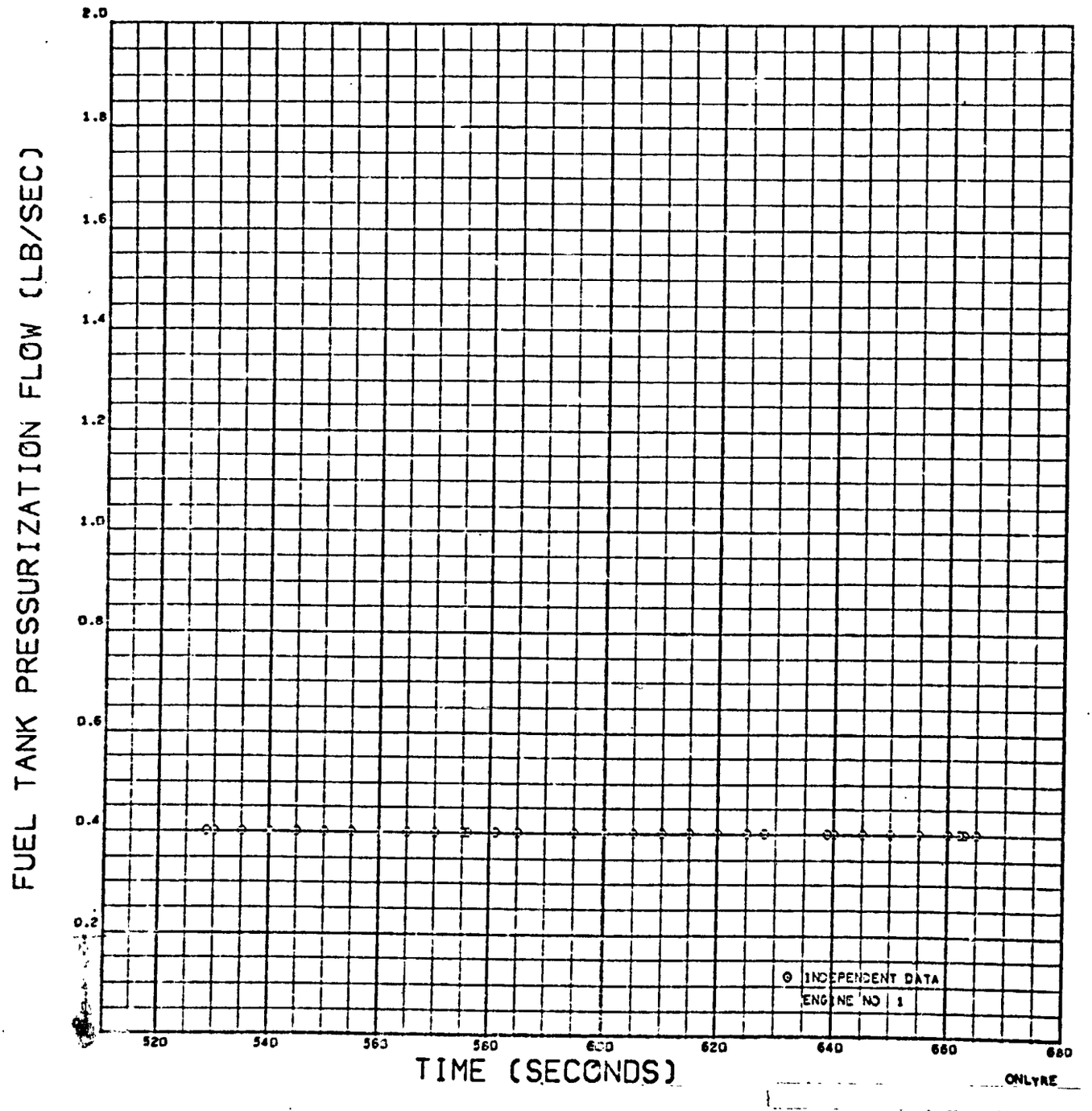

Figure 163. Fuel Tank Pressurization Flow (First Burn)

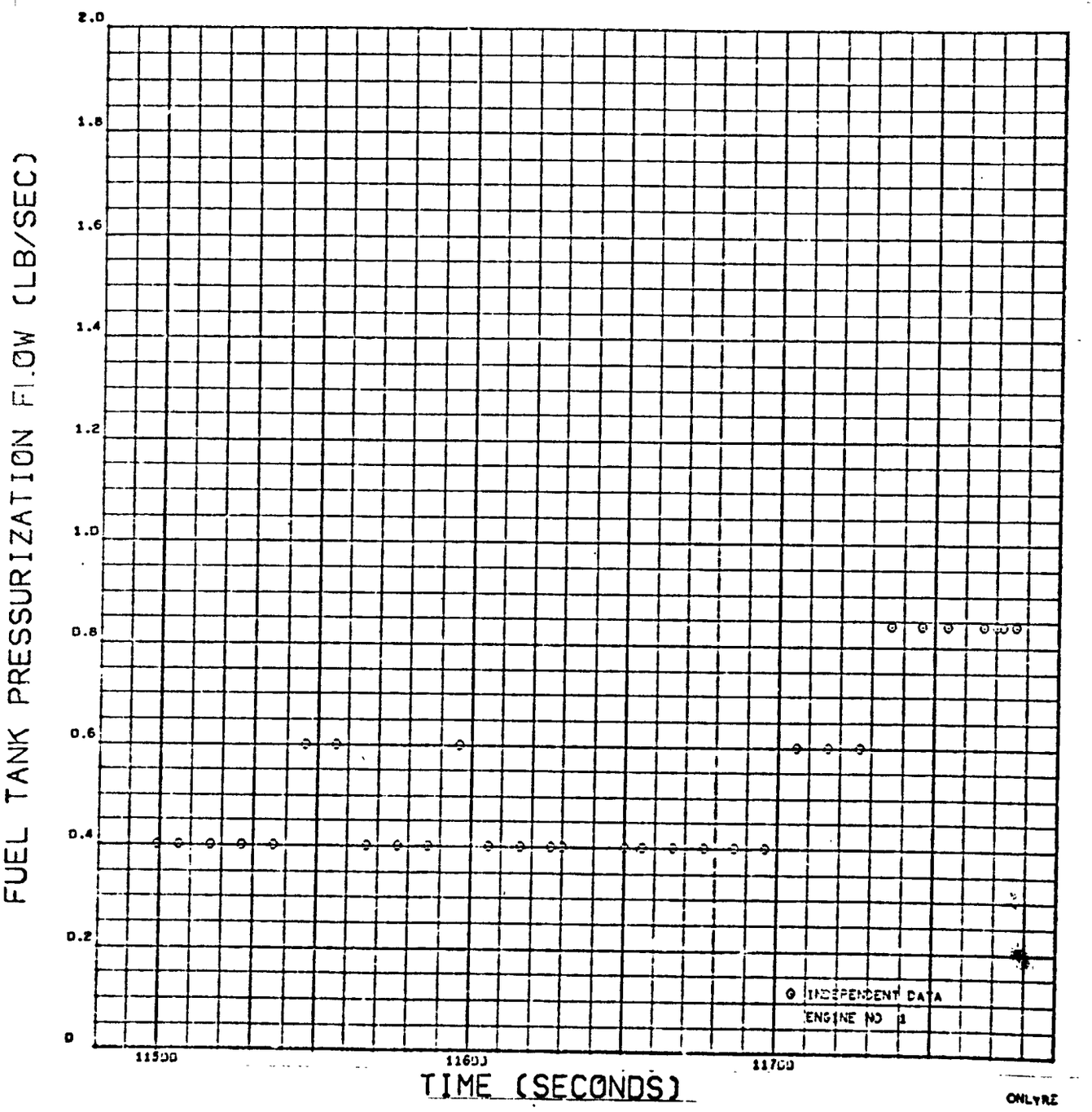

Figure 164. Fuel Tank Pressurization Flow (Second Burn)

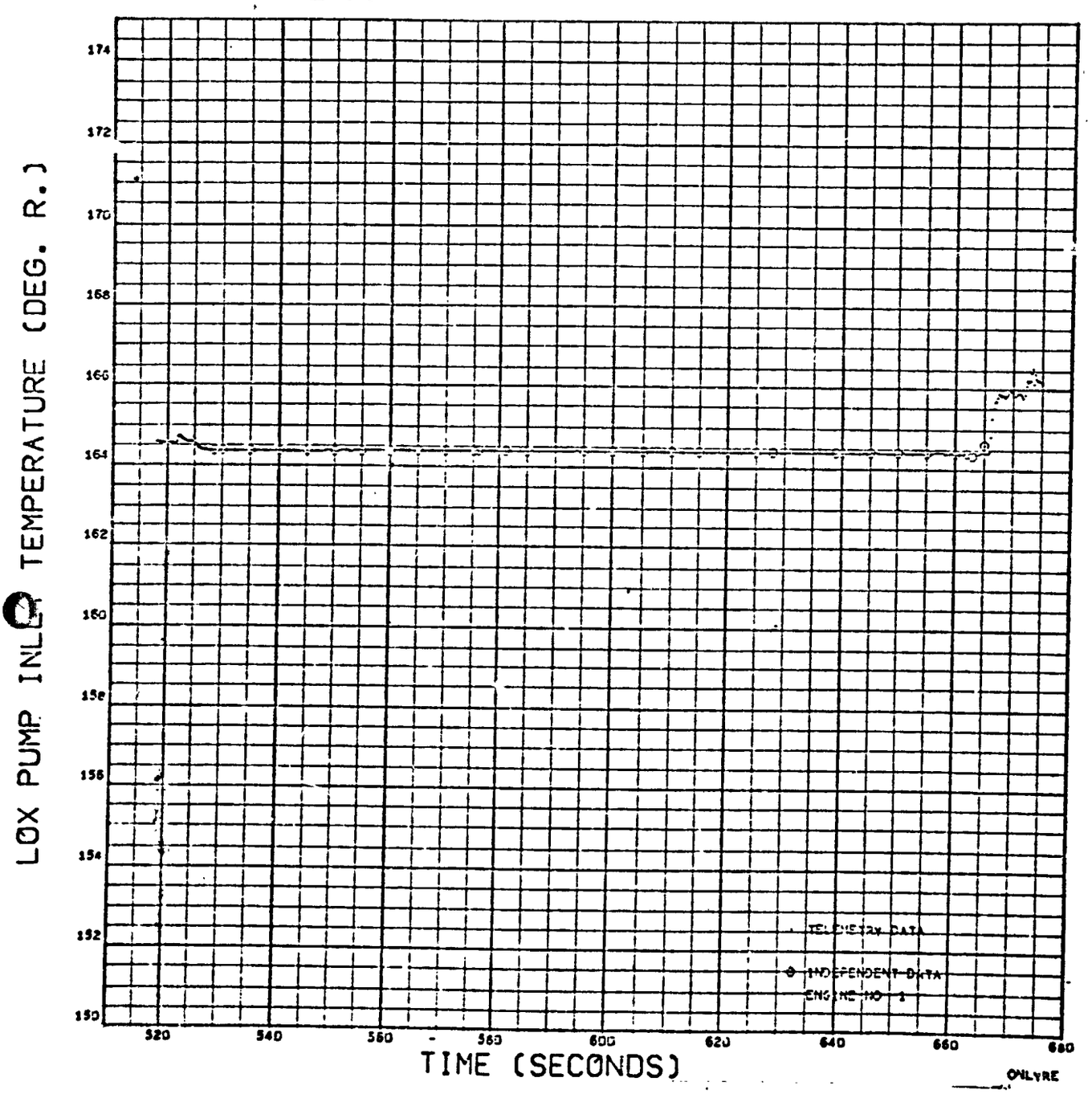

Figure 165. Oxidizer Pump Inlet Temperature (First Burn)

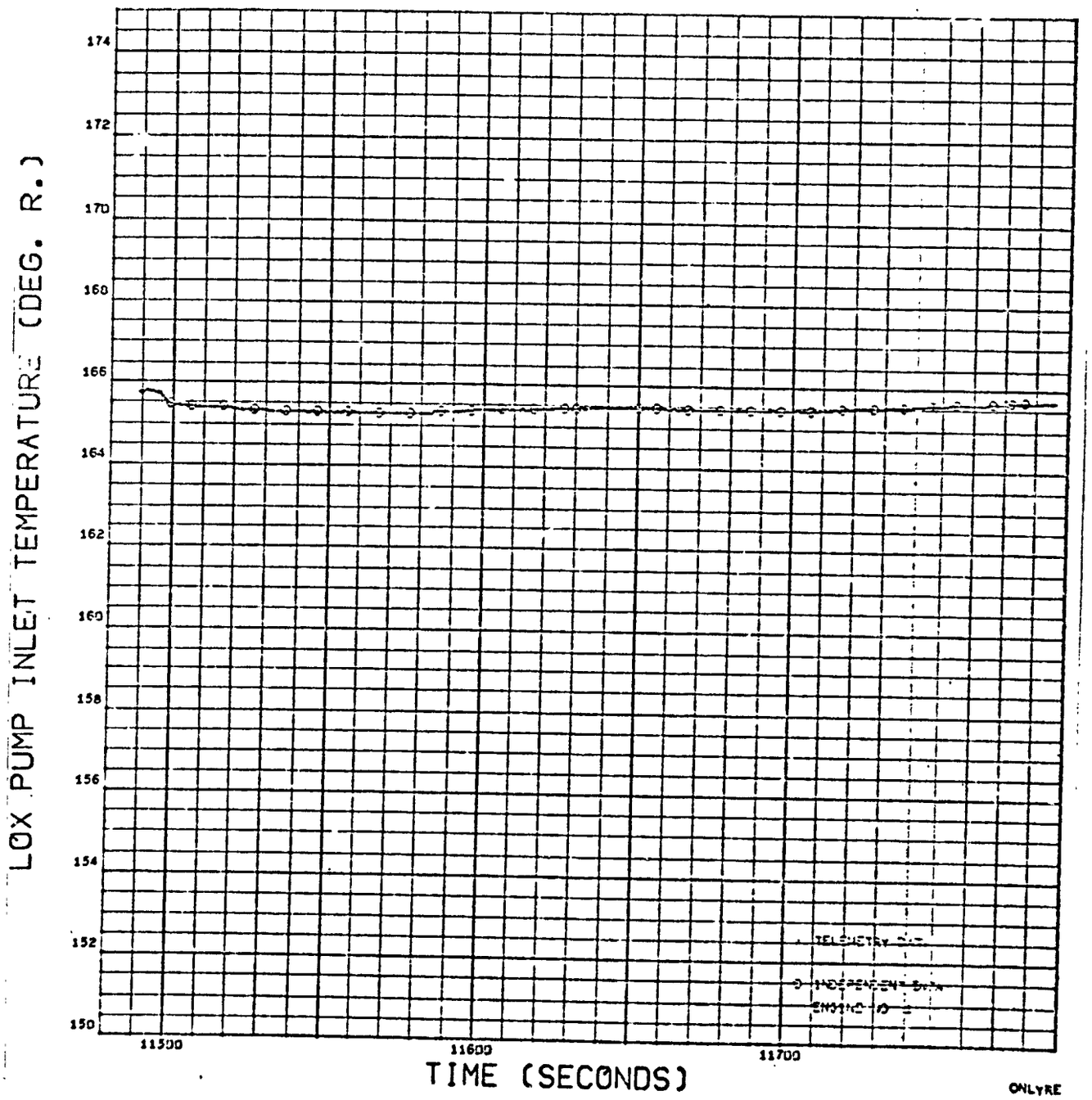

Figure 166. Oxidizer Pump Inlet Temperature (Second Burn)

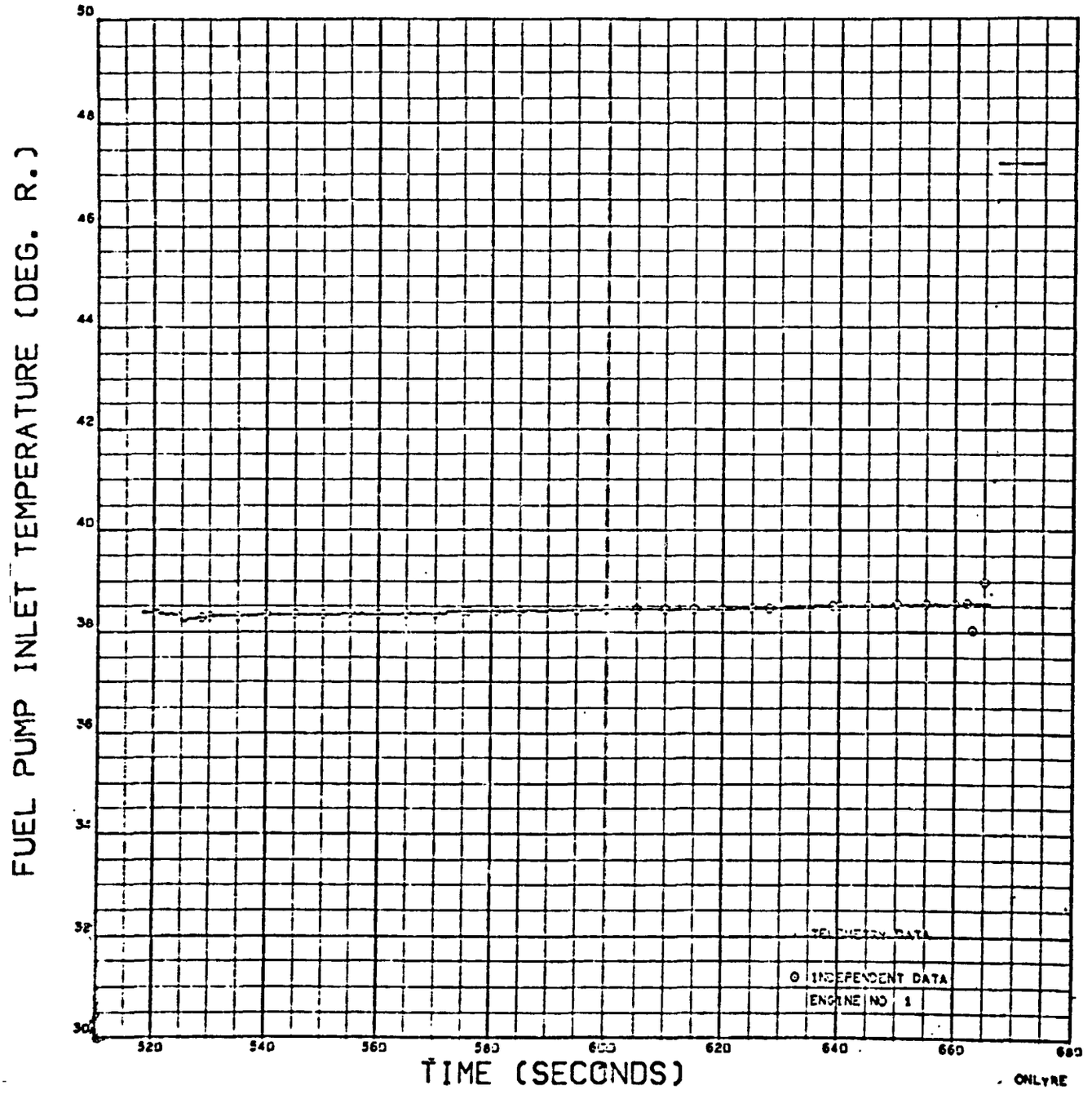

Figure 167. Fuel Pump Inlet Temperature (First Burn)

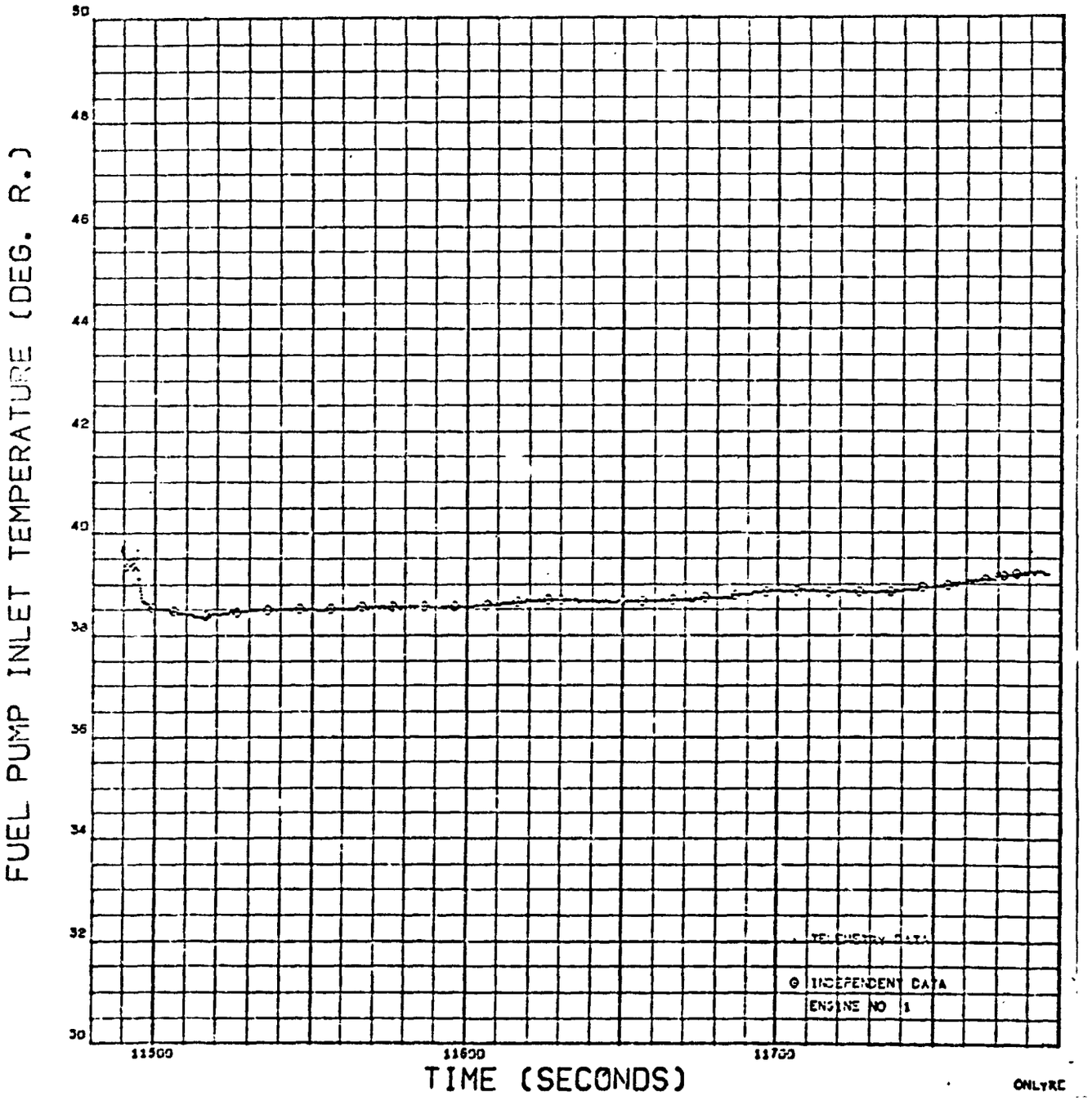

Figure 168. Fuel Pump Inlet Temperature (Second Burn)

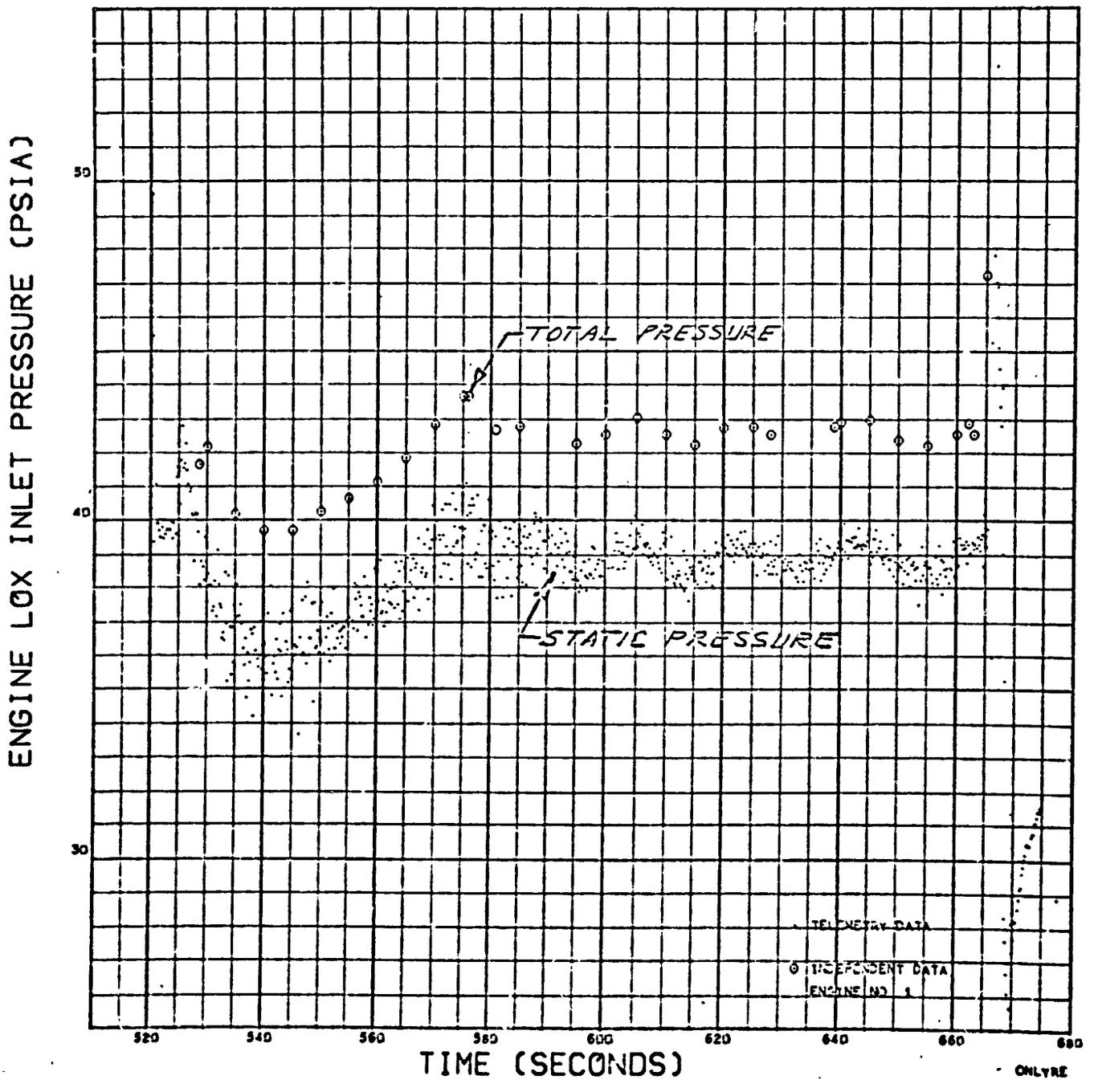

Figure 169. Engine Oxidizer Inlet Pressure (First Burn)

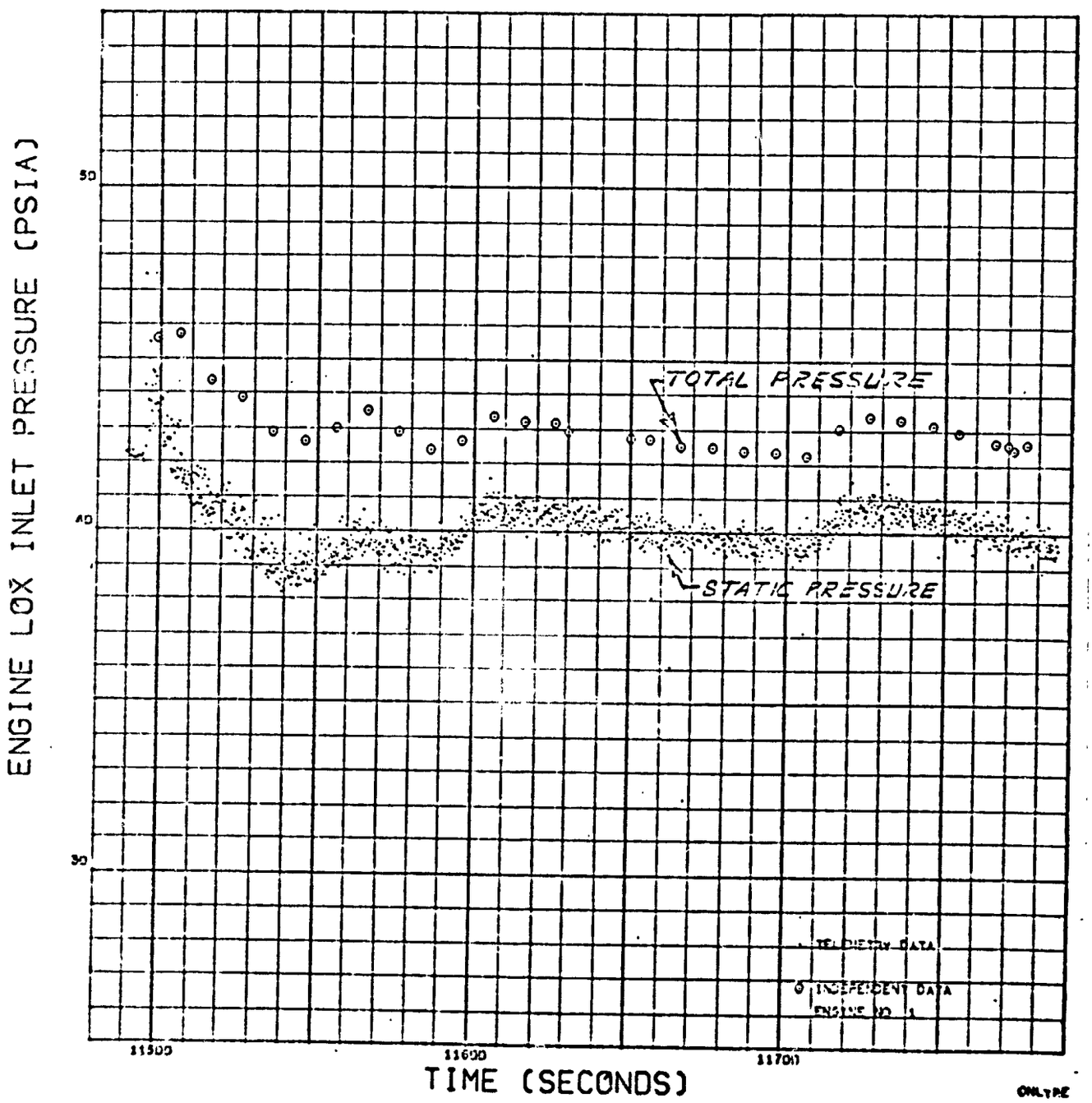

Figure 170. Engine Oxidizer Inlet Pressure (Second Burn)

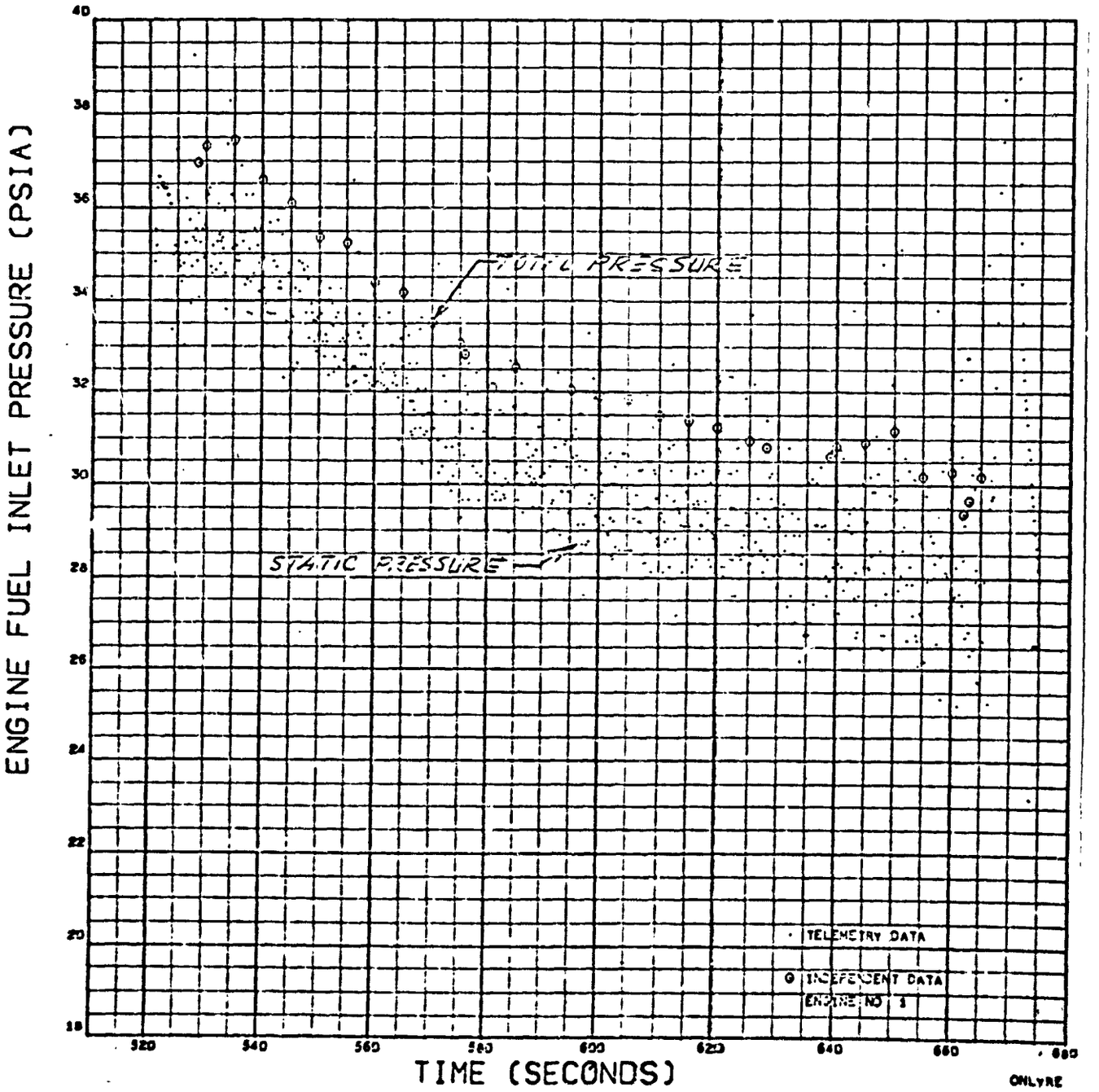

Figure 171. Engine Fuel Inlet Pressure (First Burn)

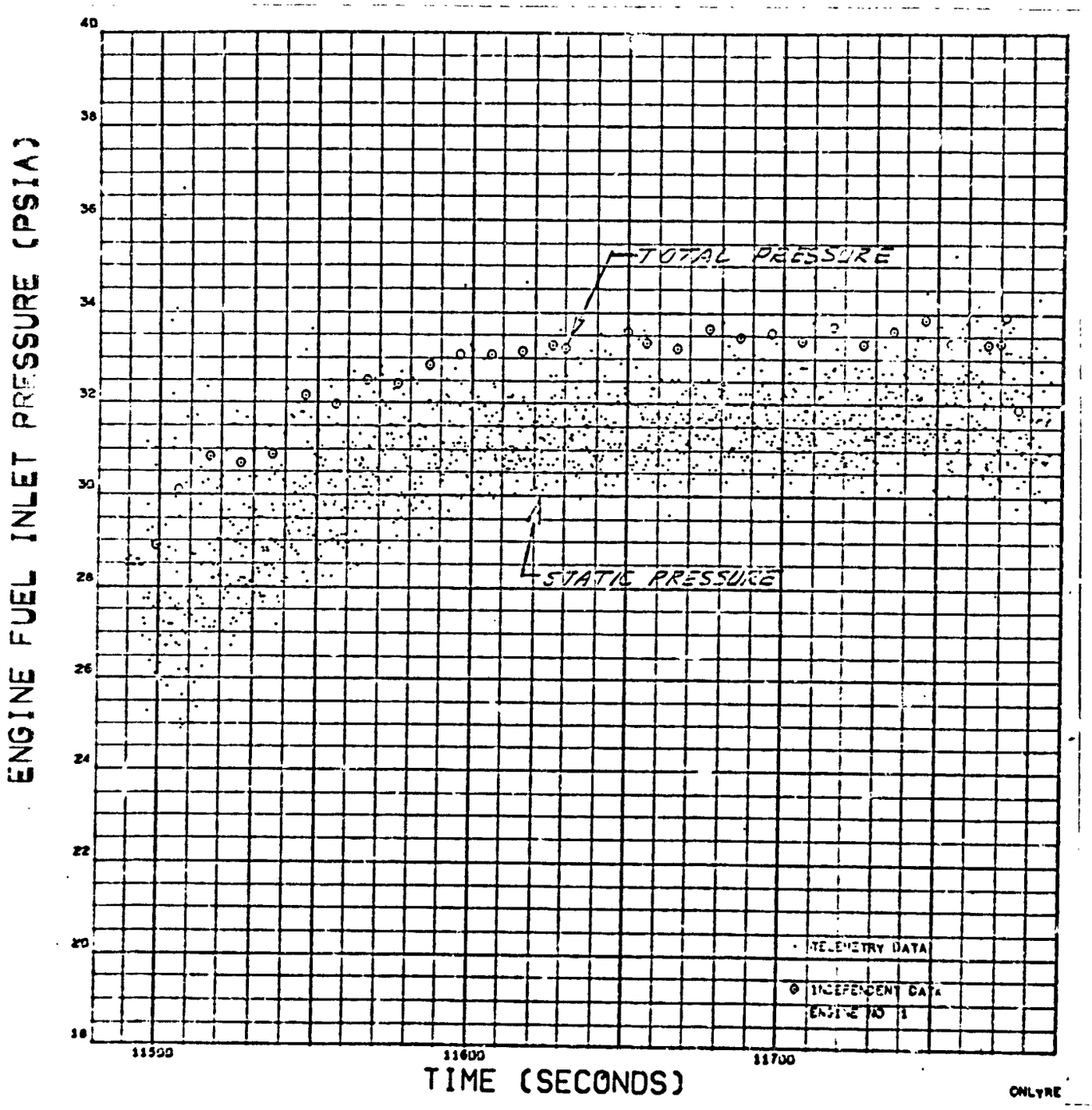

Figure 172. Engine Fuel Inlet Pressure (Second Burn)

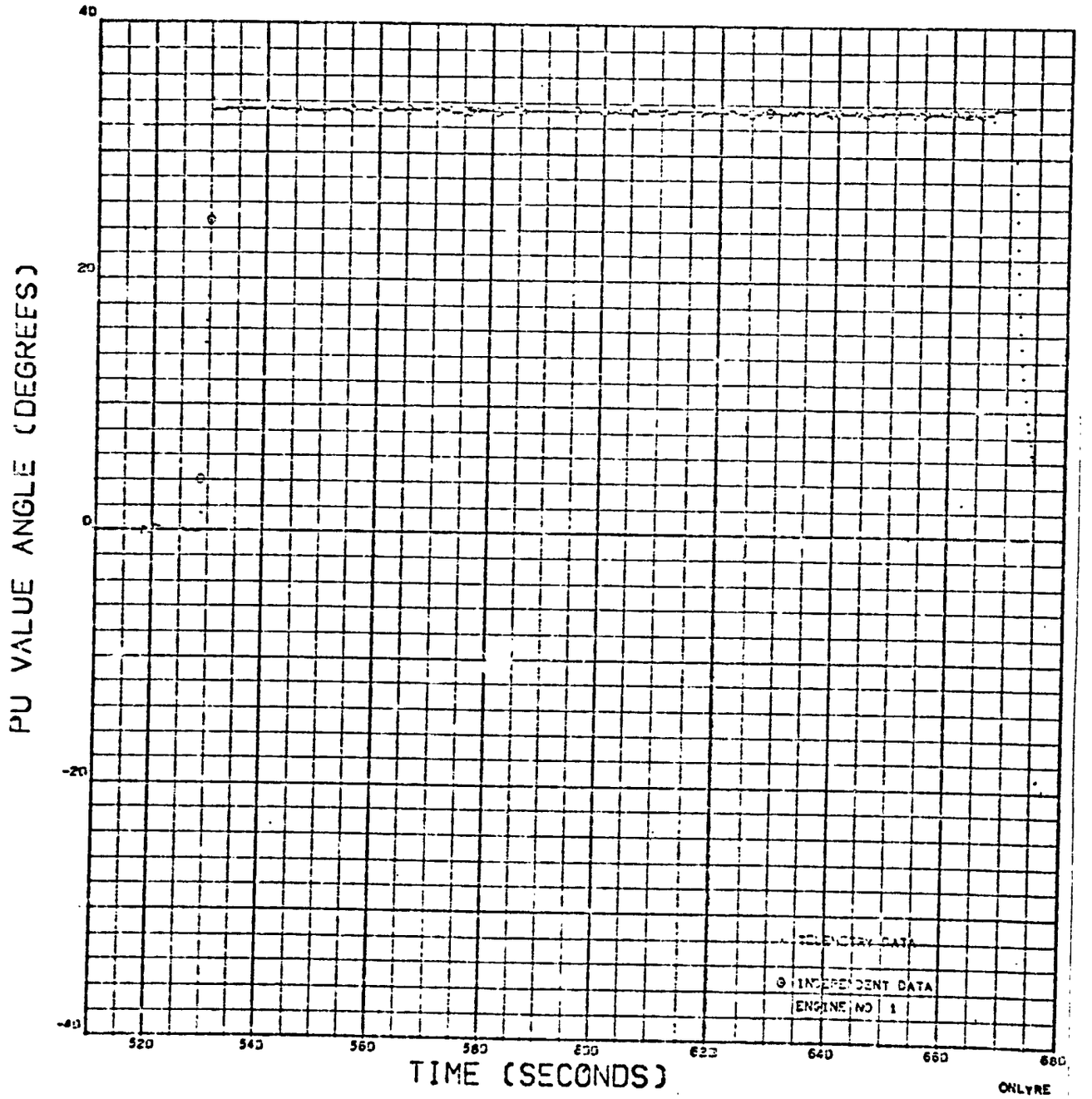

Figure 173. PU Valve Angle (First Burn)

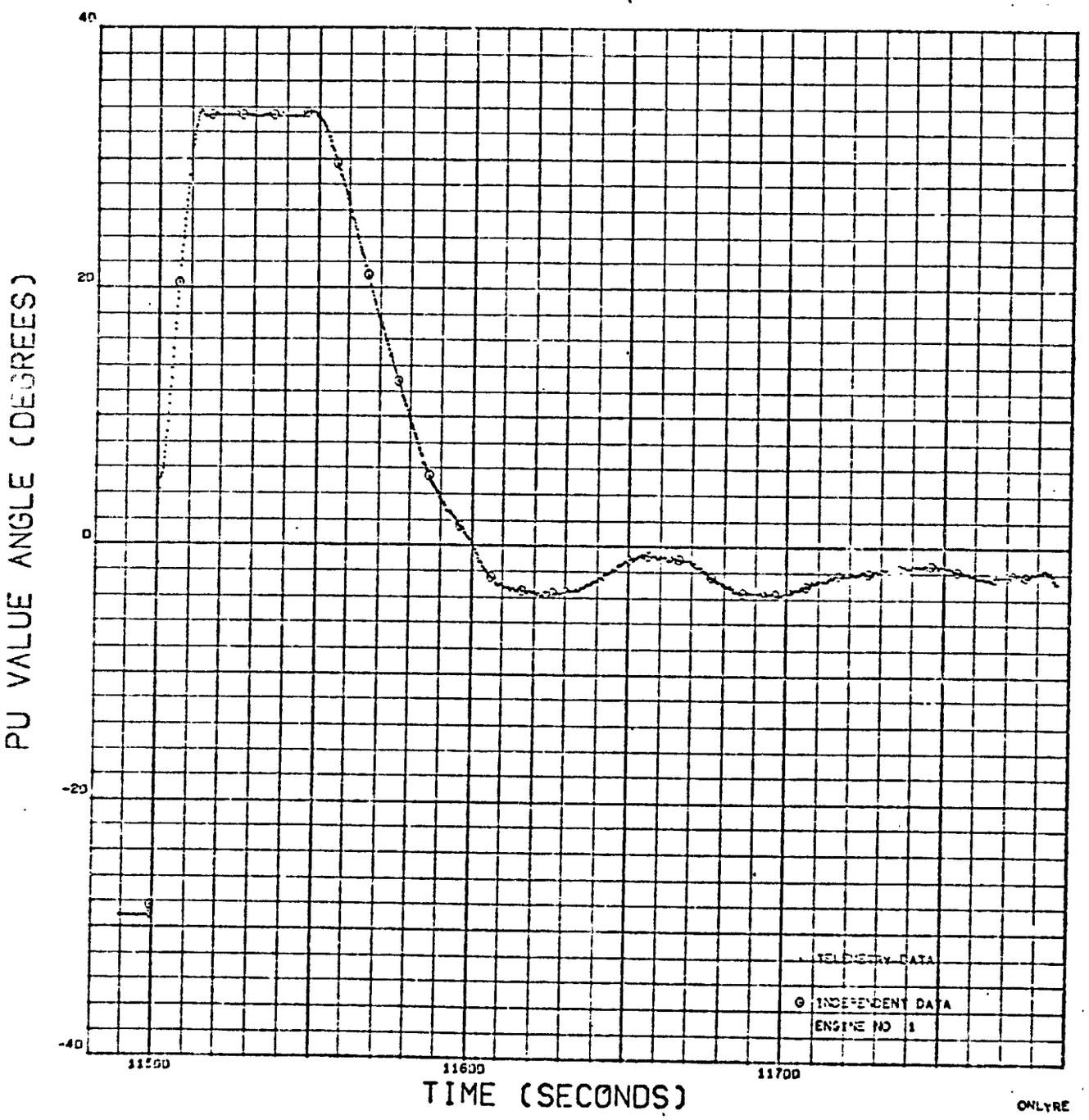

Figure 174. PU Valve Angle (Second Burn)

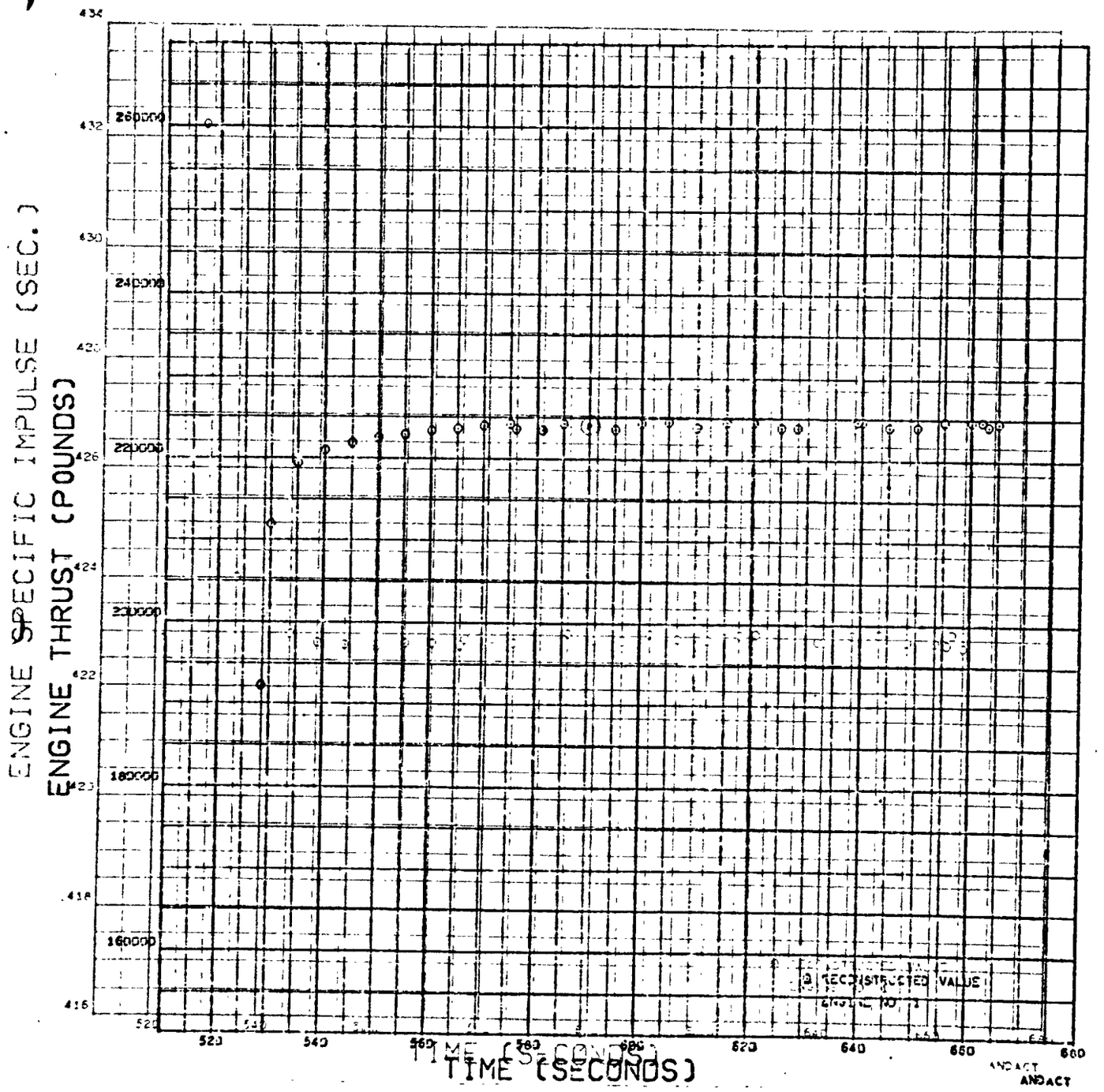

Figure 177. Engine Specific Impulse (First Burn)

Figure 175. Engine Thrust (First Burn)

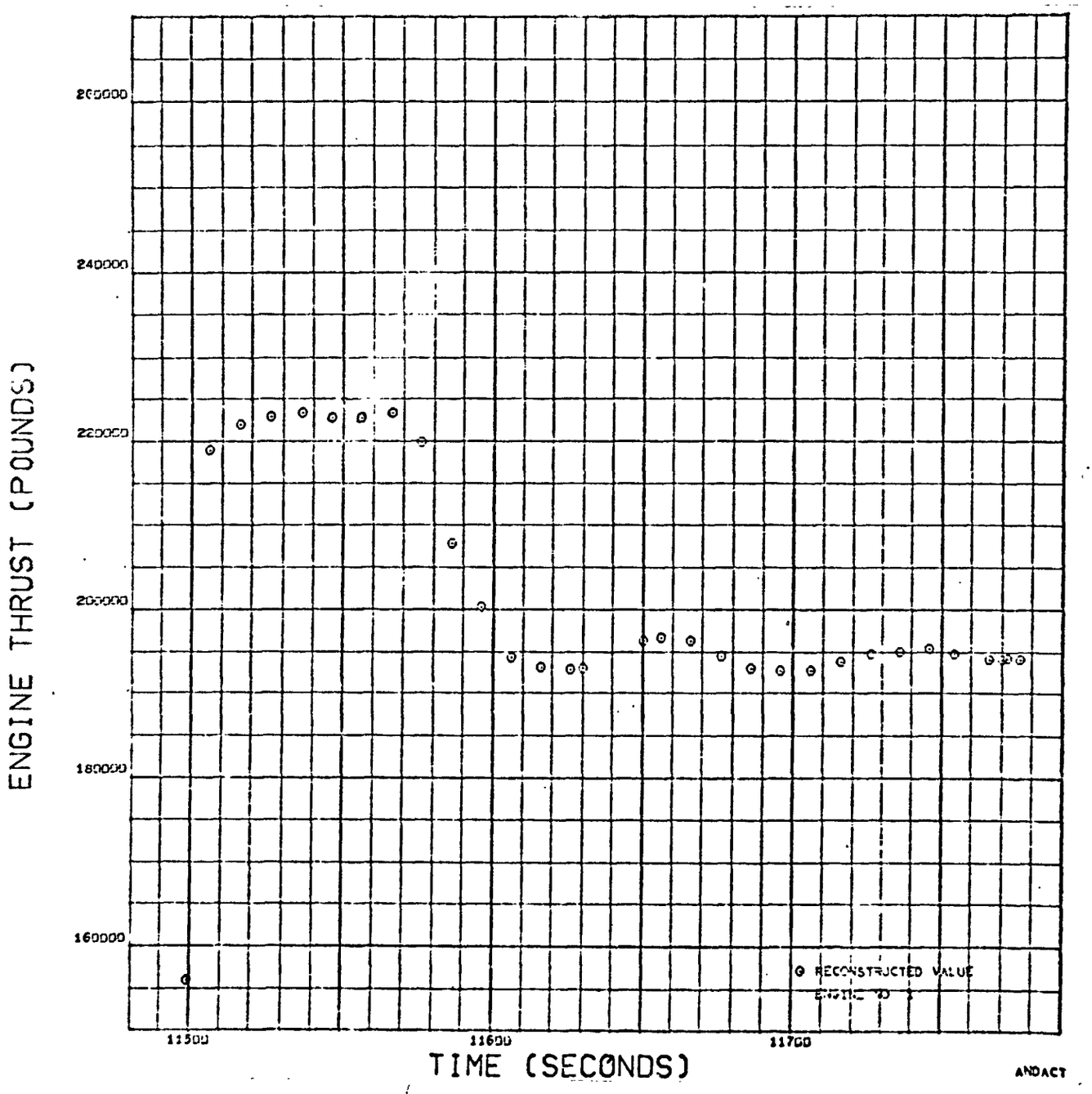

Figure 176. Engine Thrust (Second Burn)

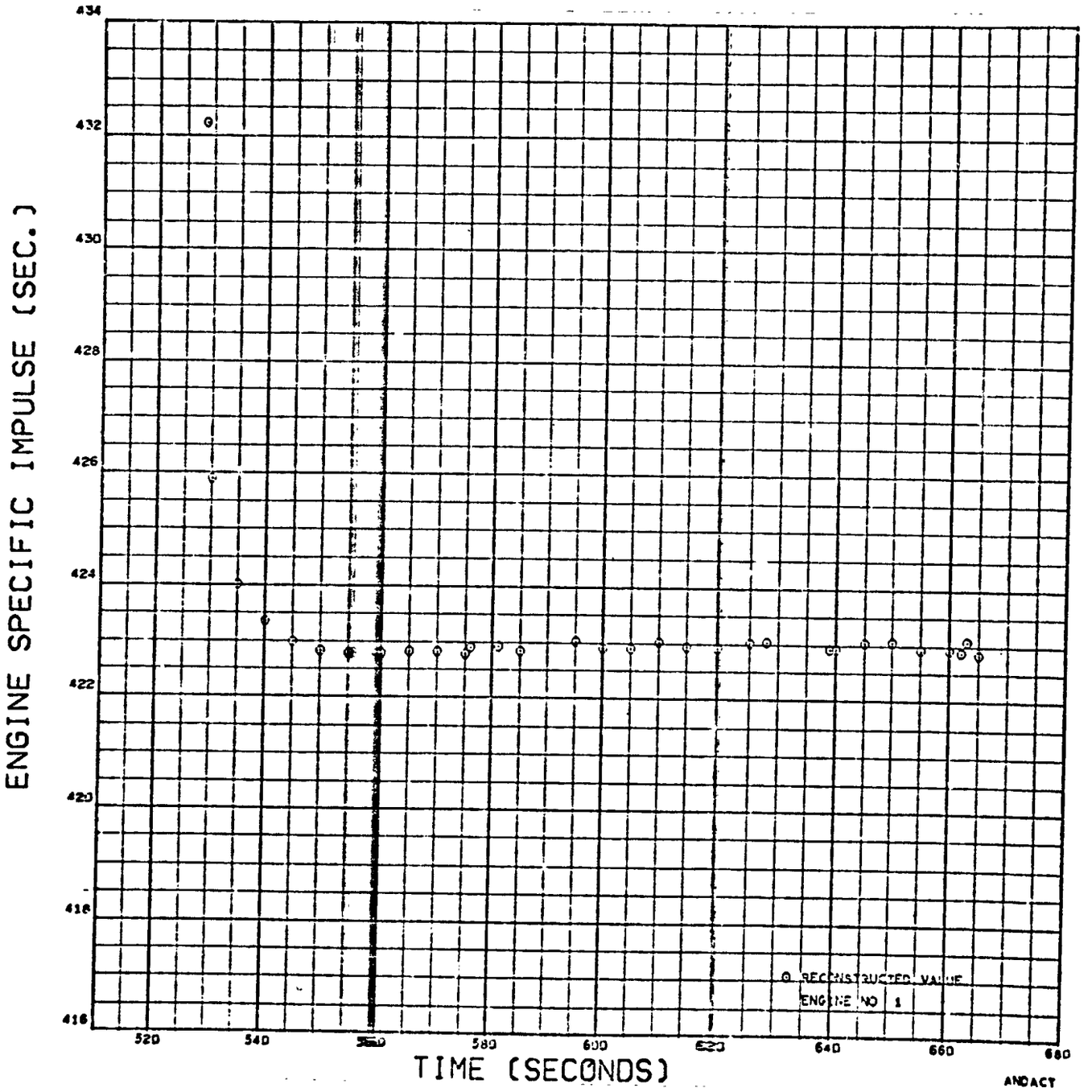

Figure 177. Engine Specific Impulse (First Burn)

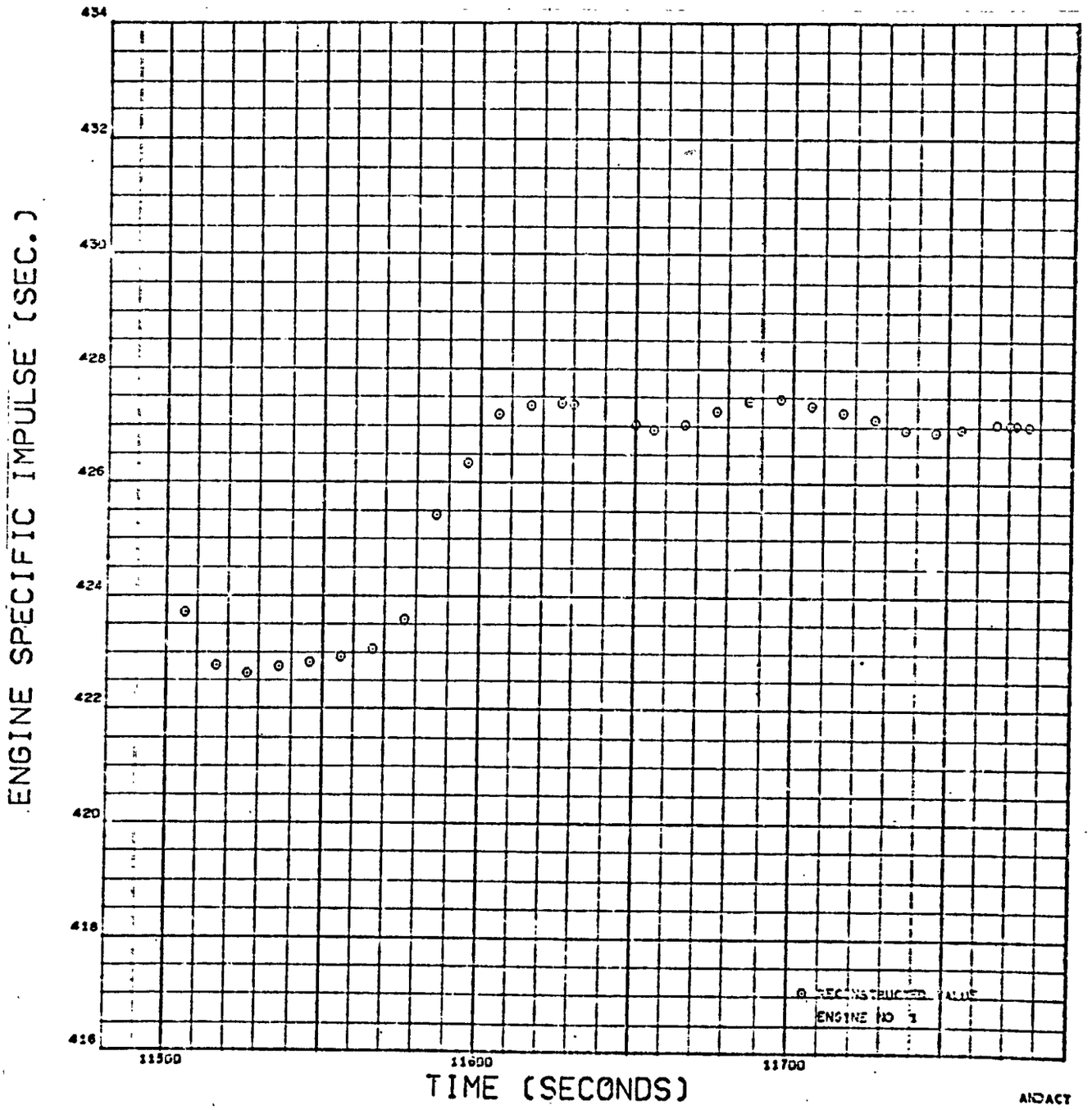

Figure 178. Engine Specific Impulse (Second Burn)

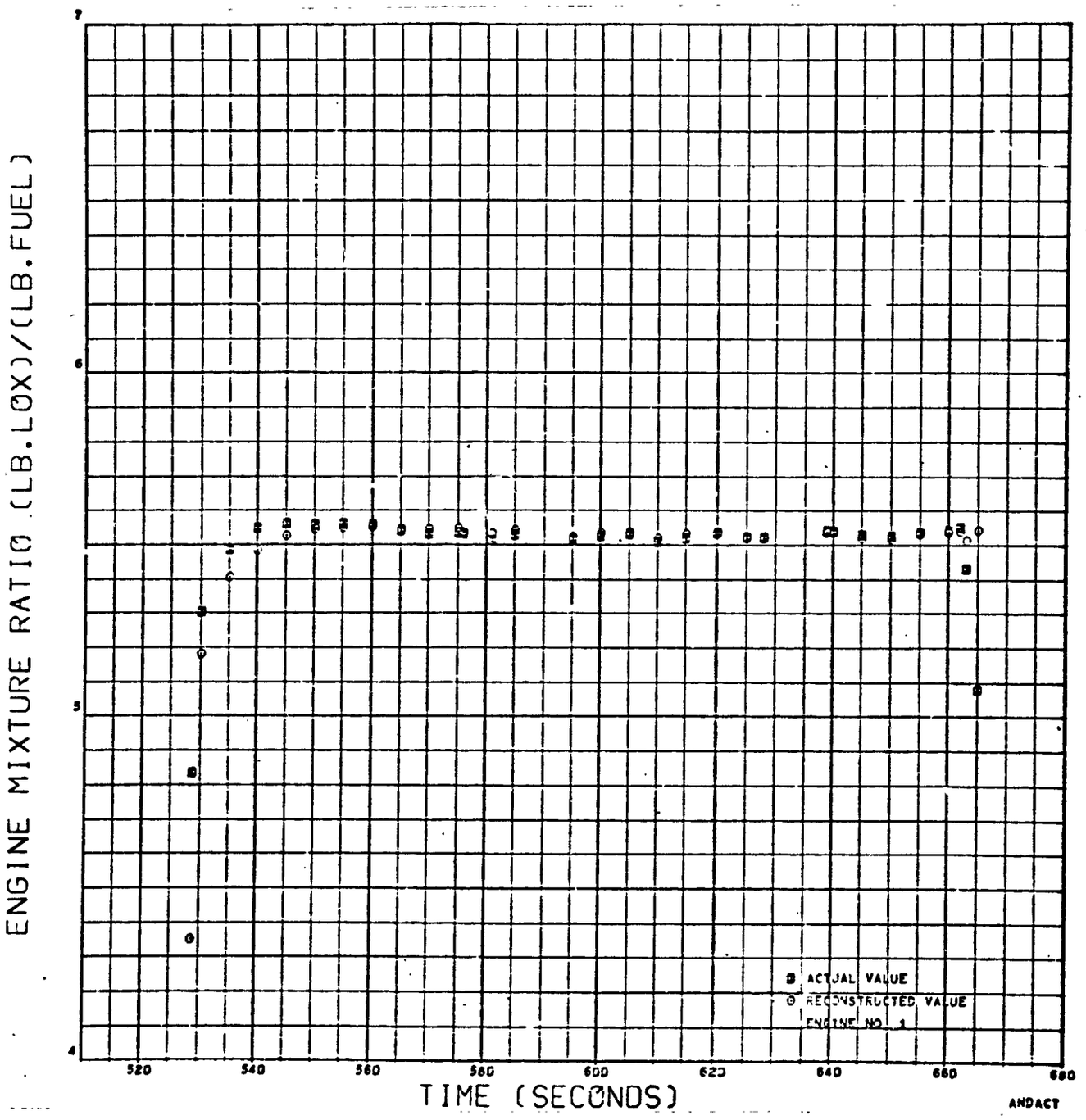

Figure 179. Engine Mixture Ratio (First Burn)

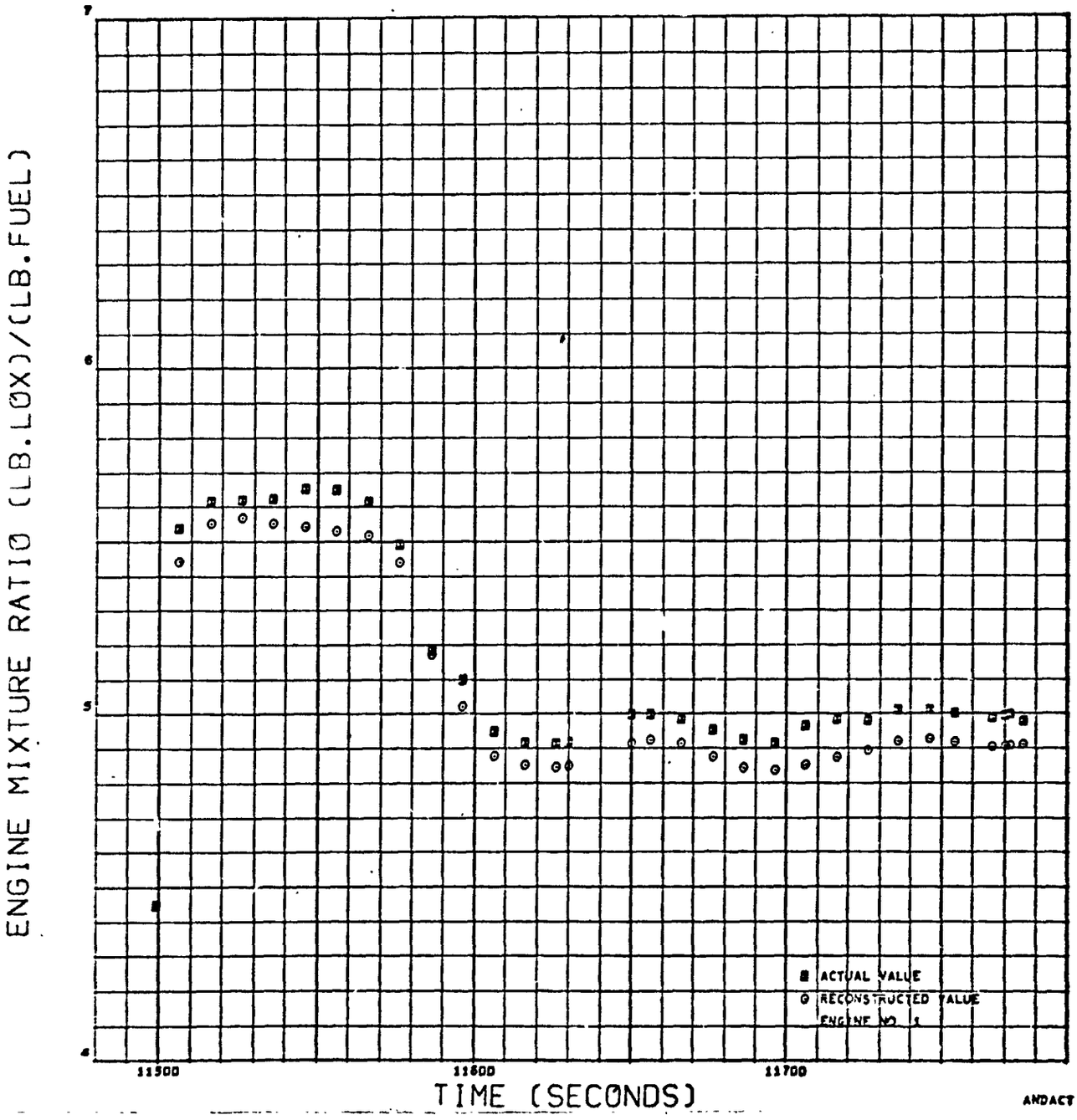

Figure 180. Engine Mixture Ratio (Second Burn)

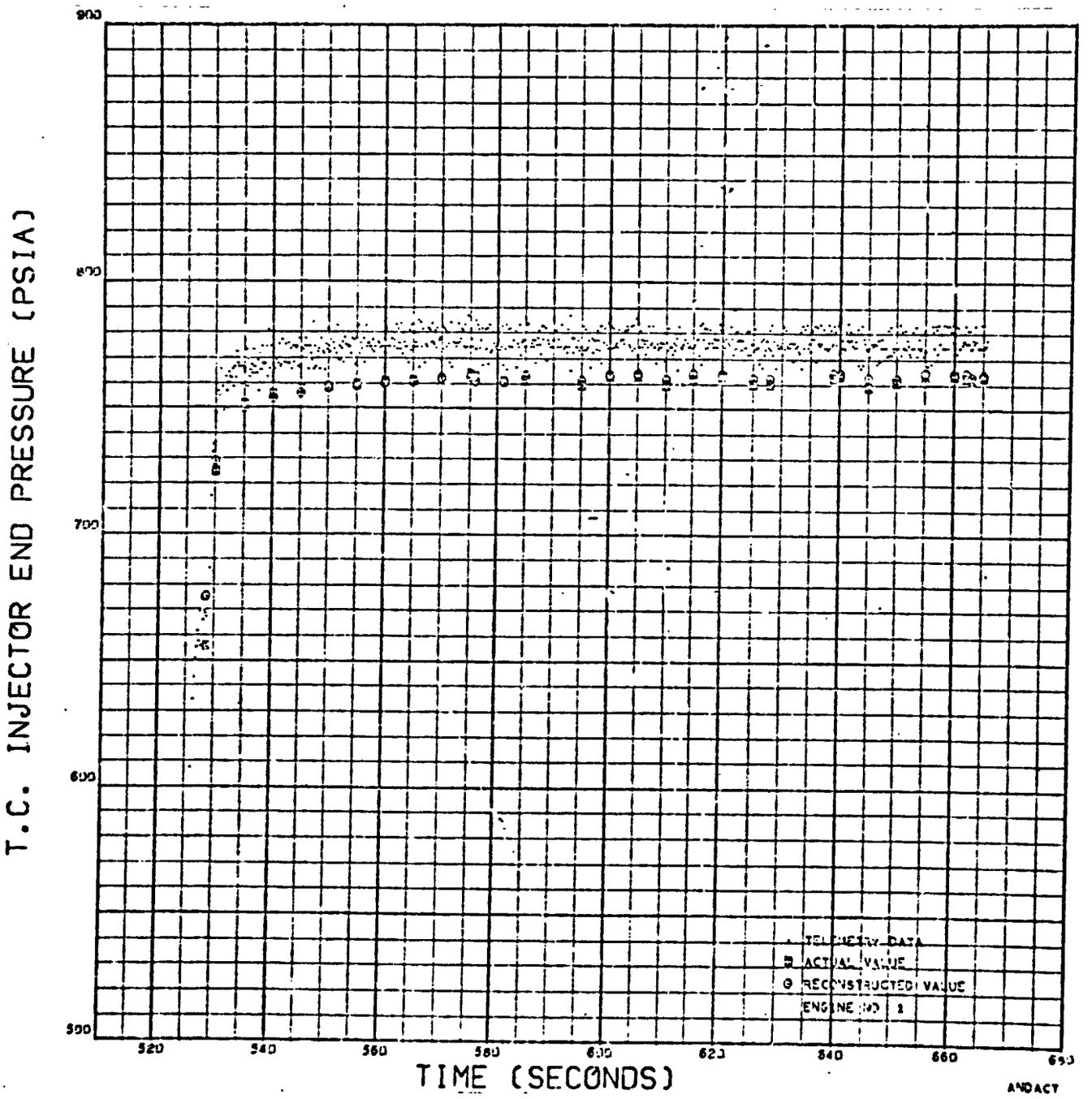

Figure 181. Thrust Chamber Injector End Pressure (First Burn)

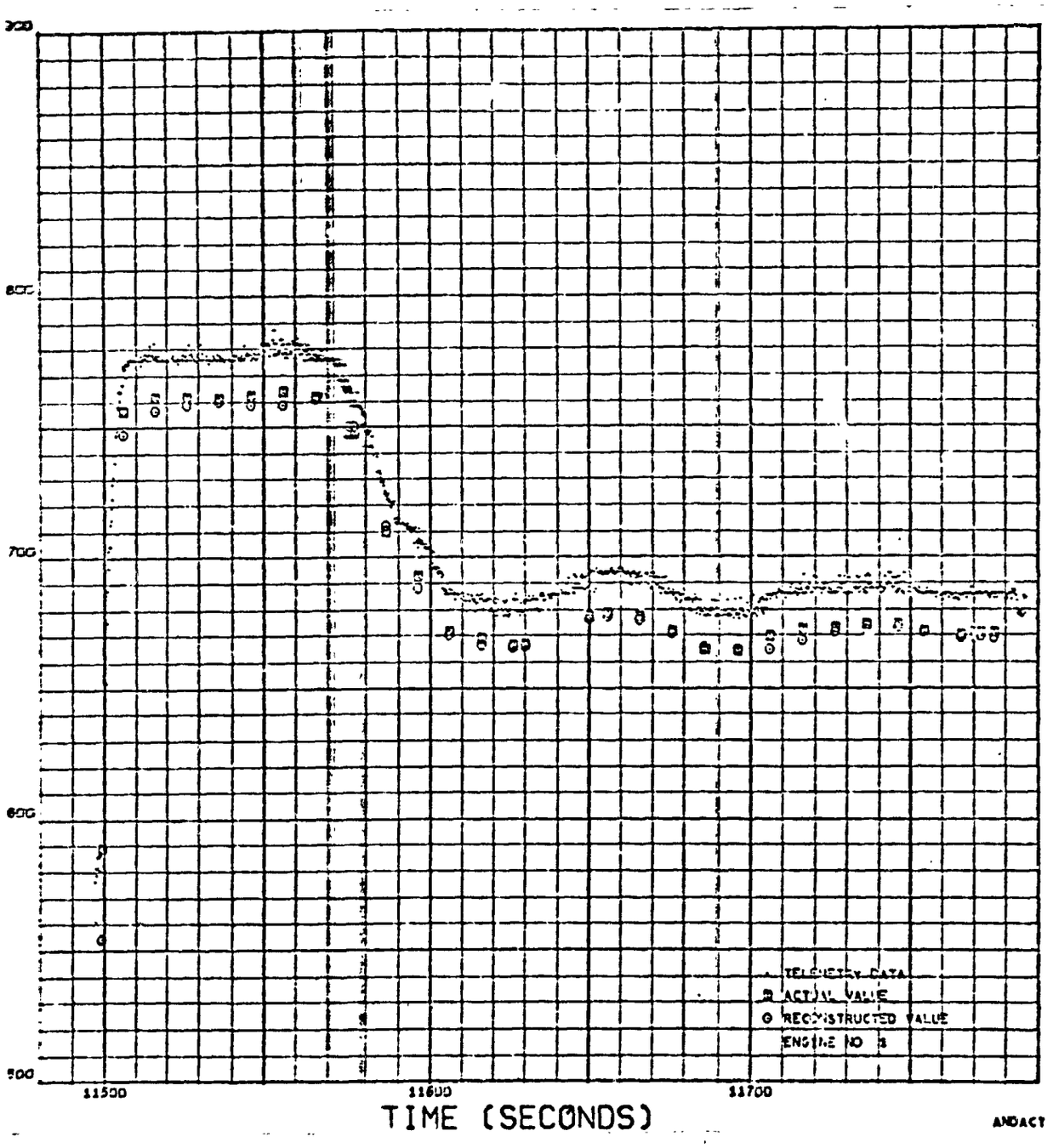

Figure 182. Thrust Chamber Injector End Pressure (Second Burn)

270

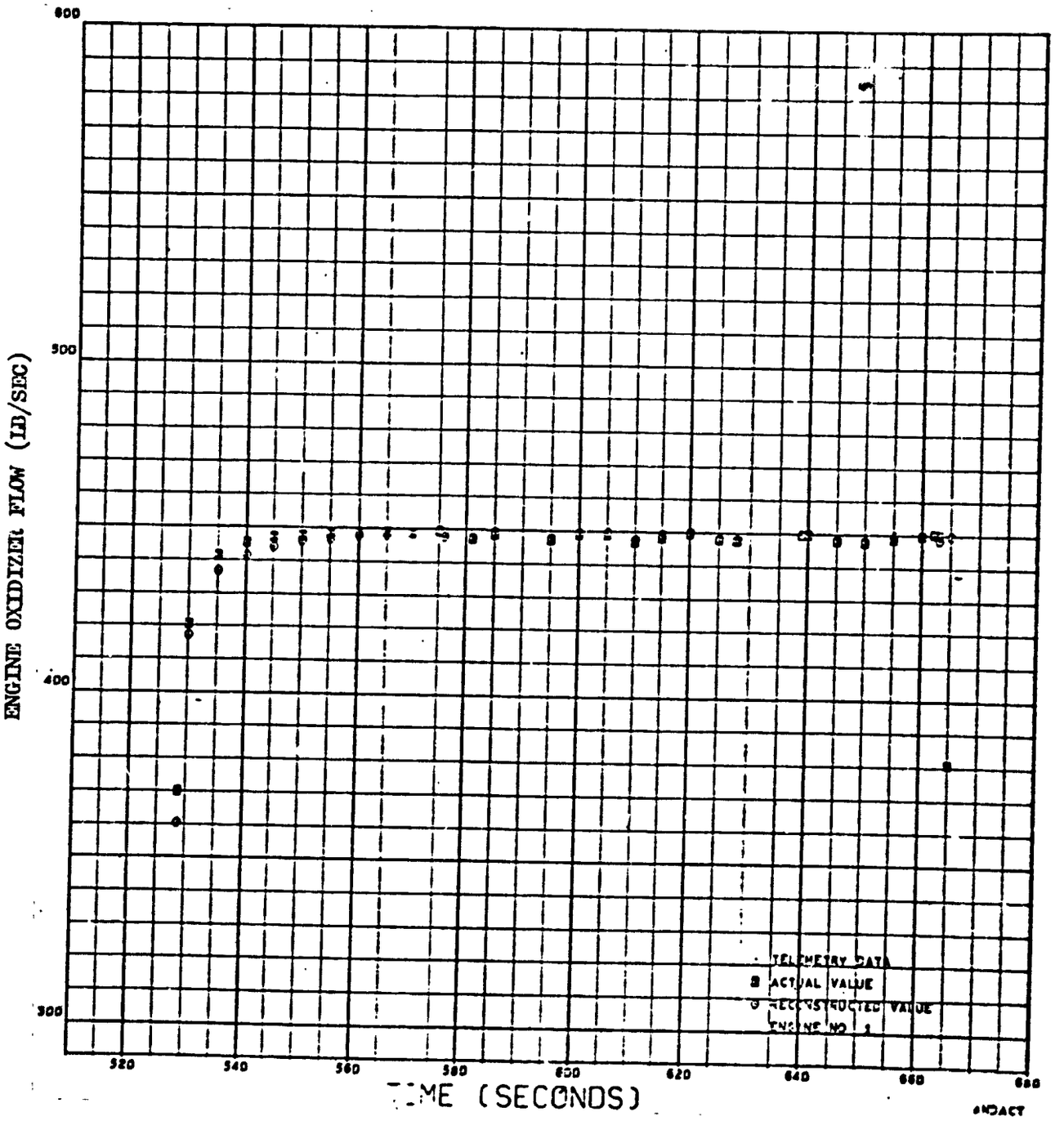

Figure 183. Engine Oxidizer Flow (First Burn)

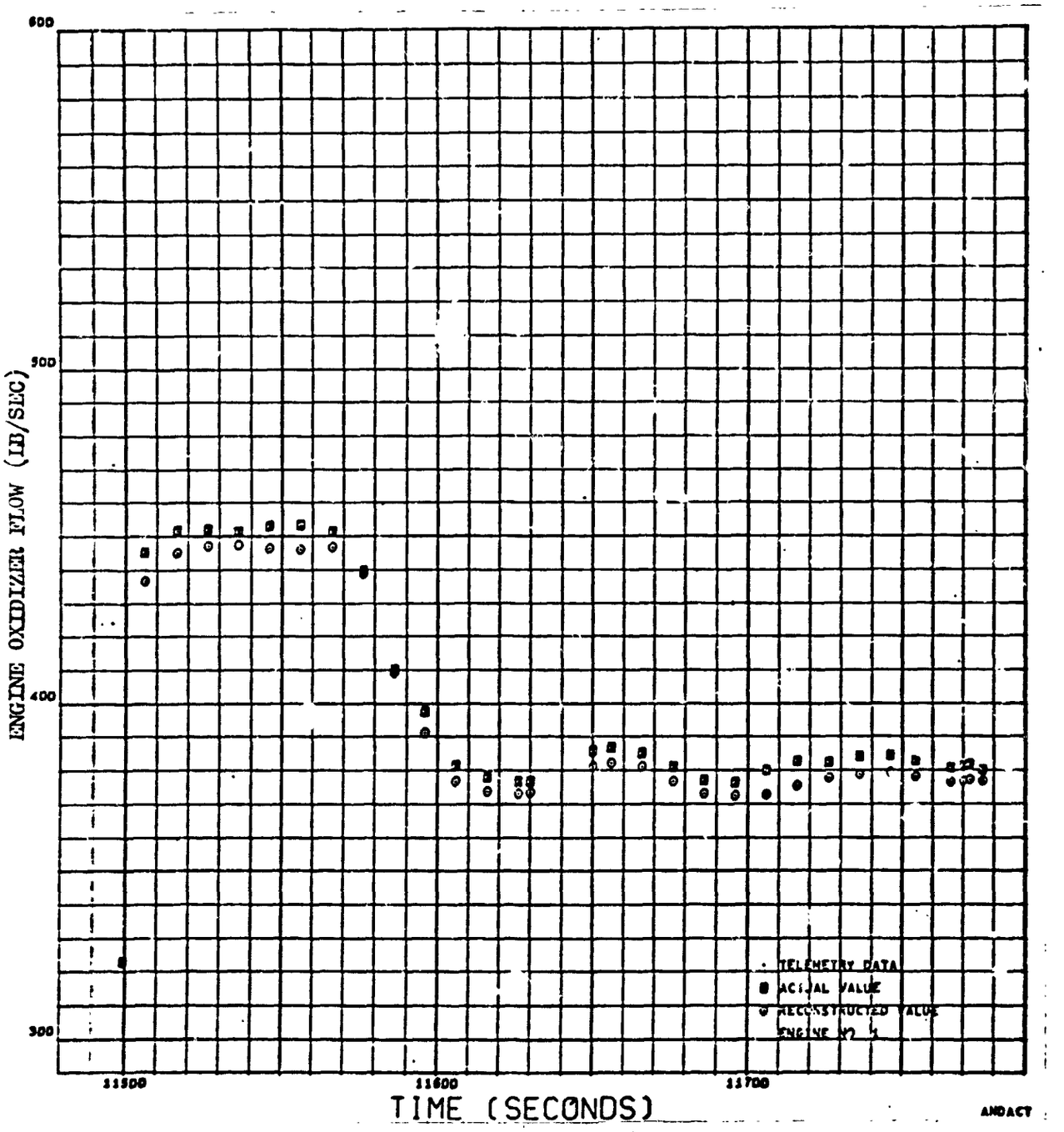

Figure 184. Engine Oxidizer Flow (Second Burn)

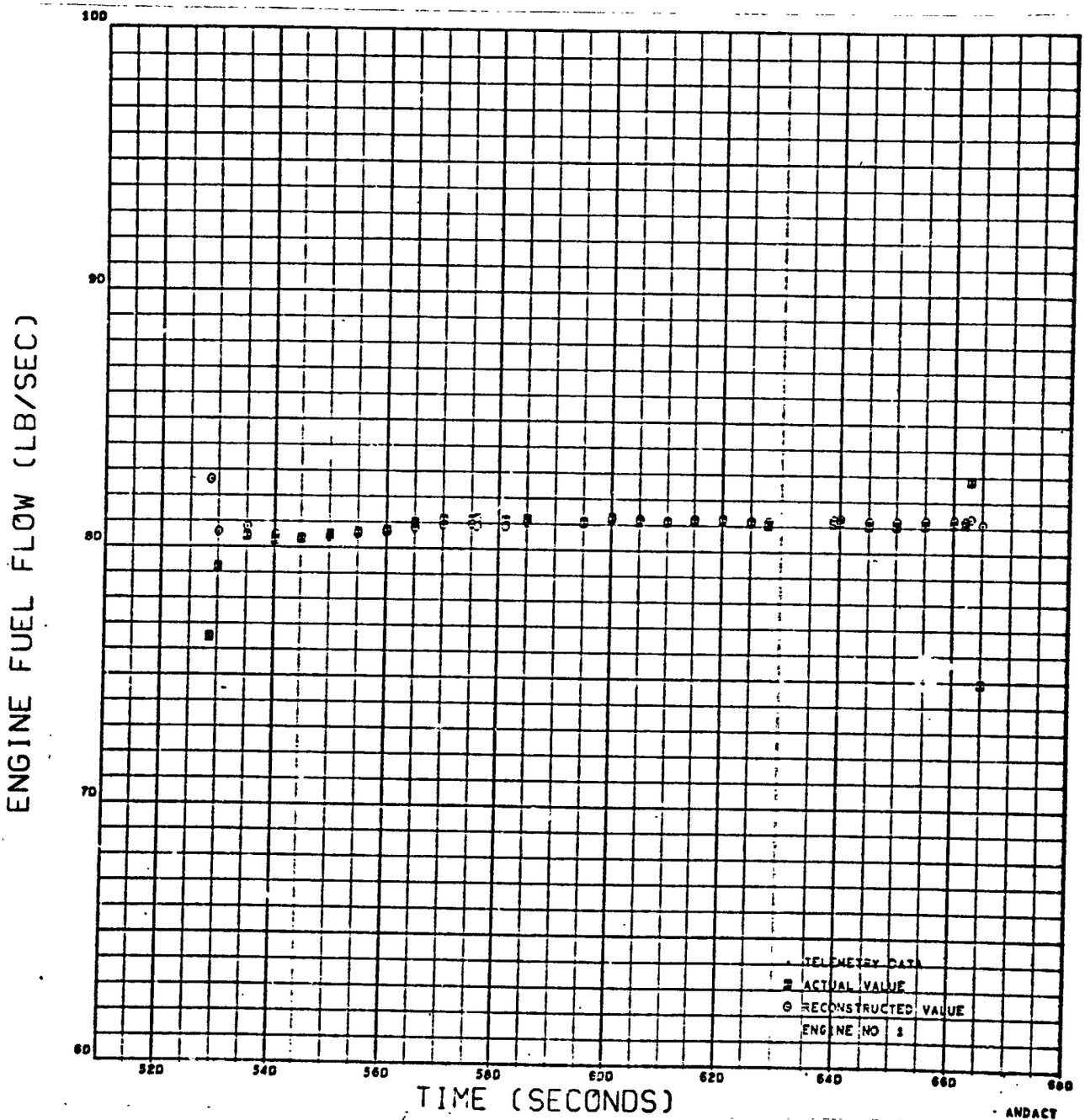

Figure 185. Engine Fuel Flow (First Burn)

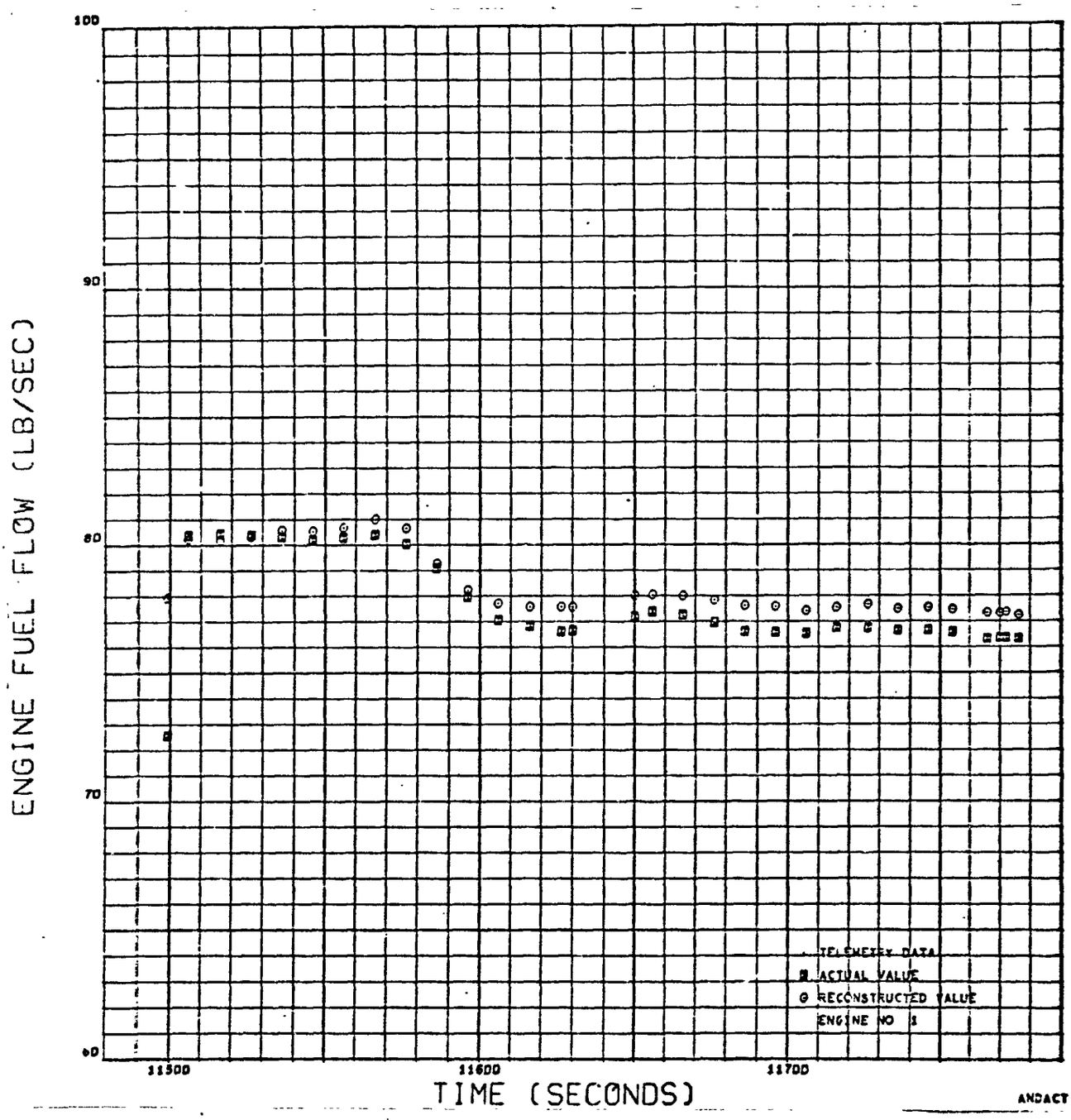

Figure 186. Engine Fuel Flow (Second Burn)

274

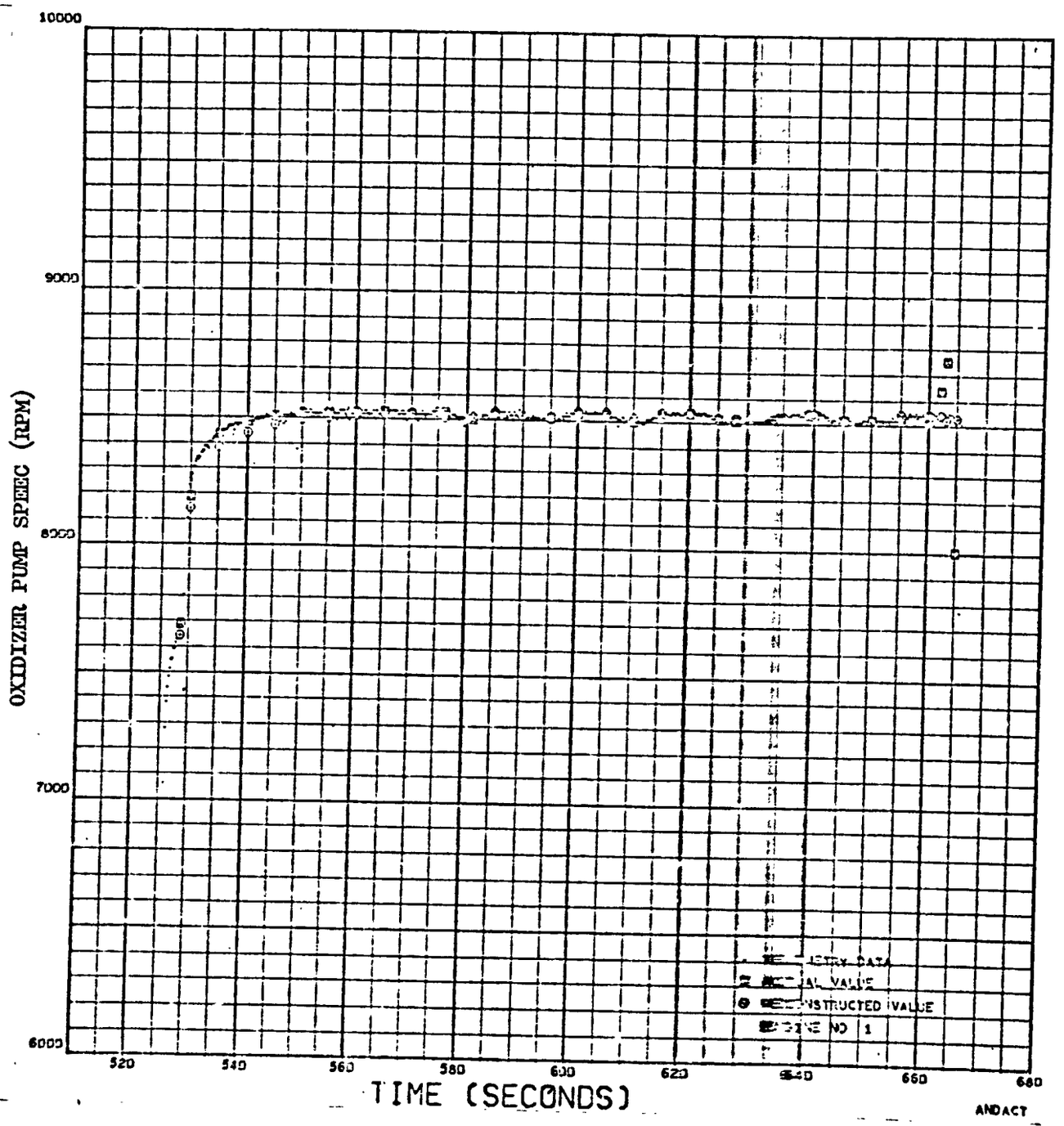

Figure 187. Oxidizer Pump Speed (First Burn)

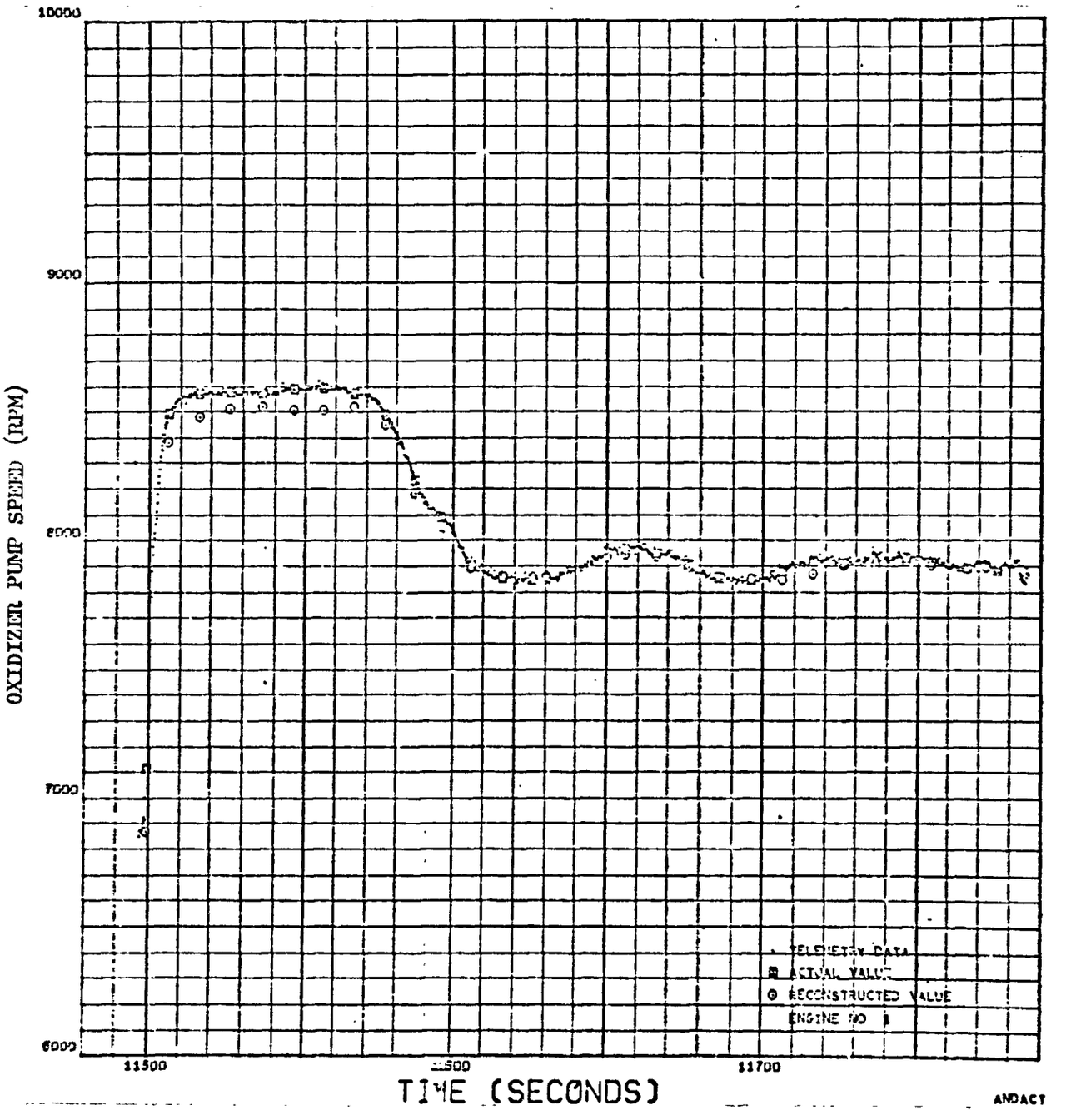

Figure 188. Oxidizer Pump Speed (Second Burn)

276

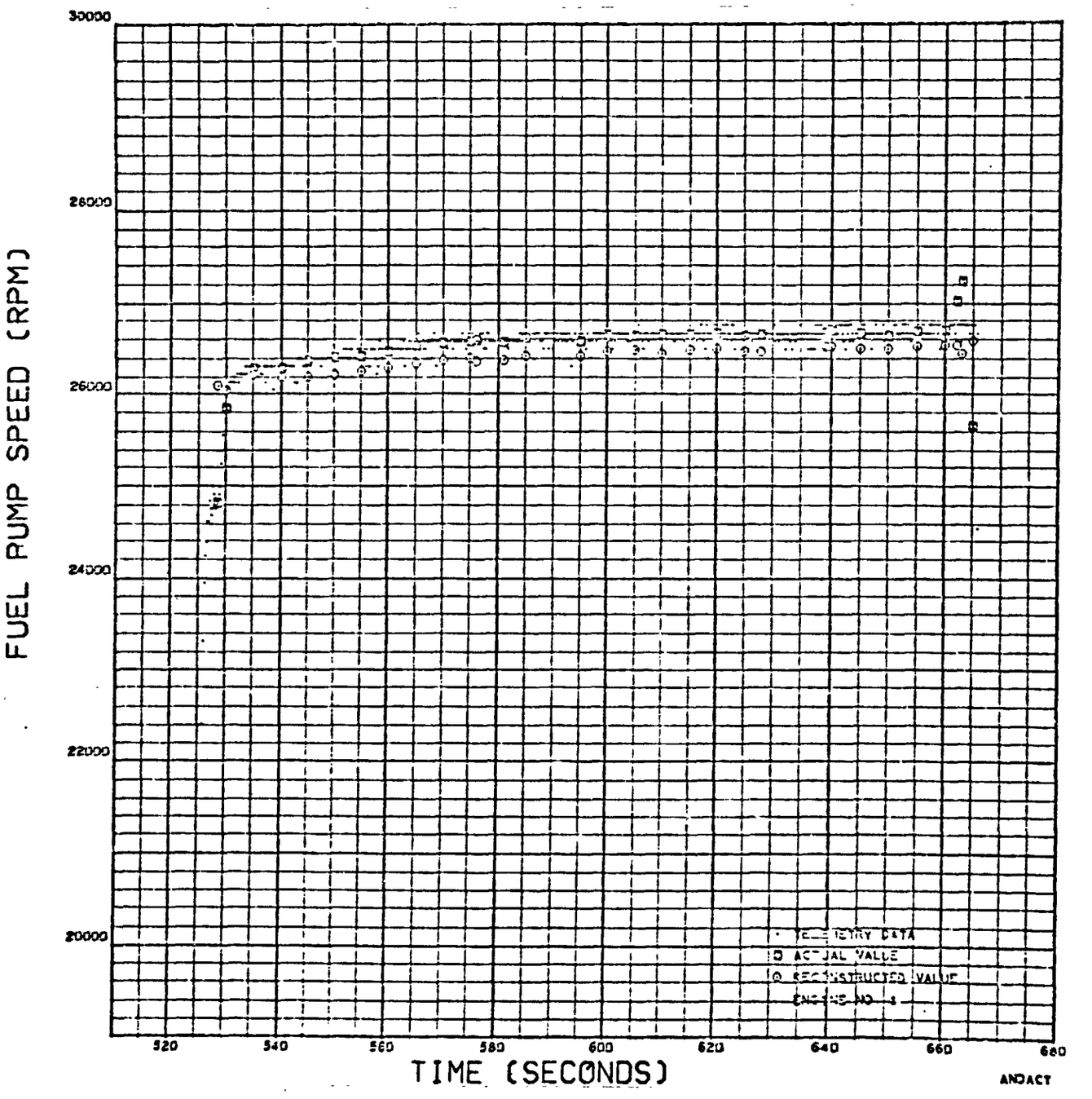

Figure 189. Fuel Pump Speed (First Burn)

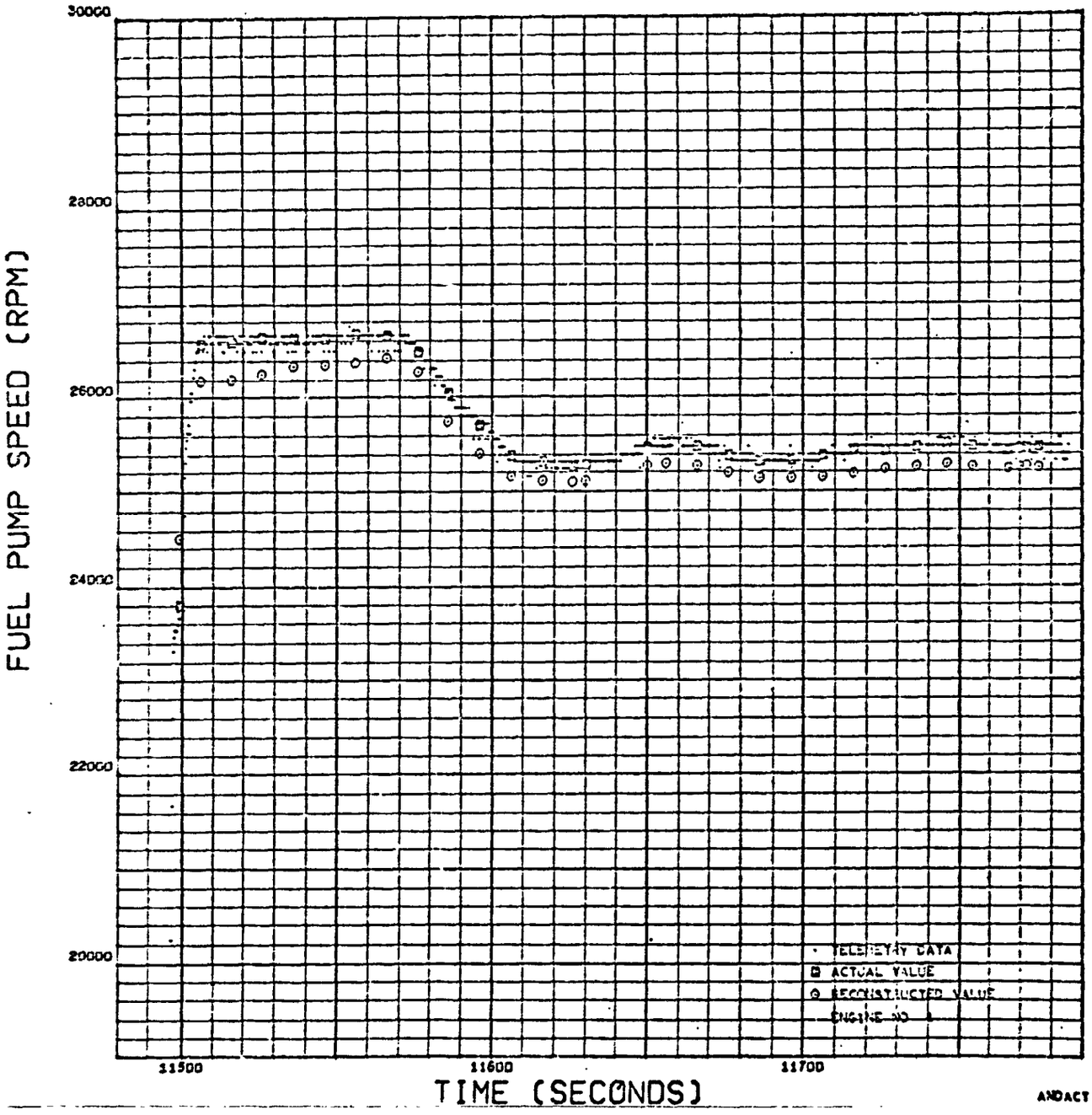

Figure 190. Fuel Pump Speed (Second Burn)

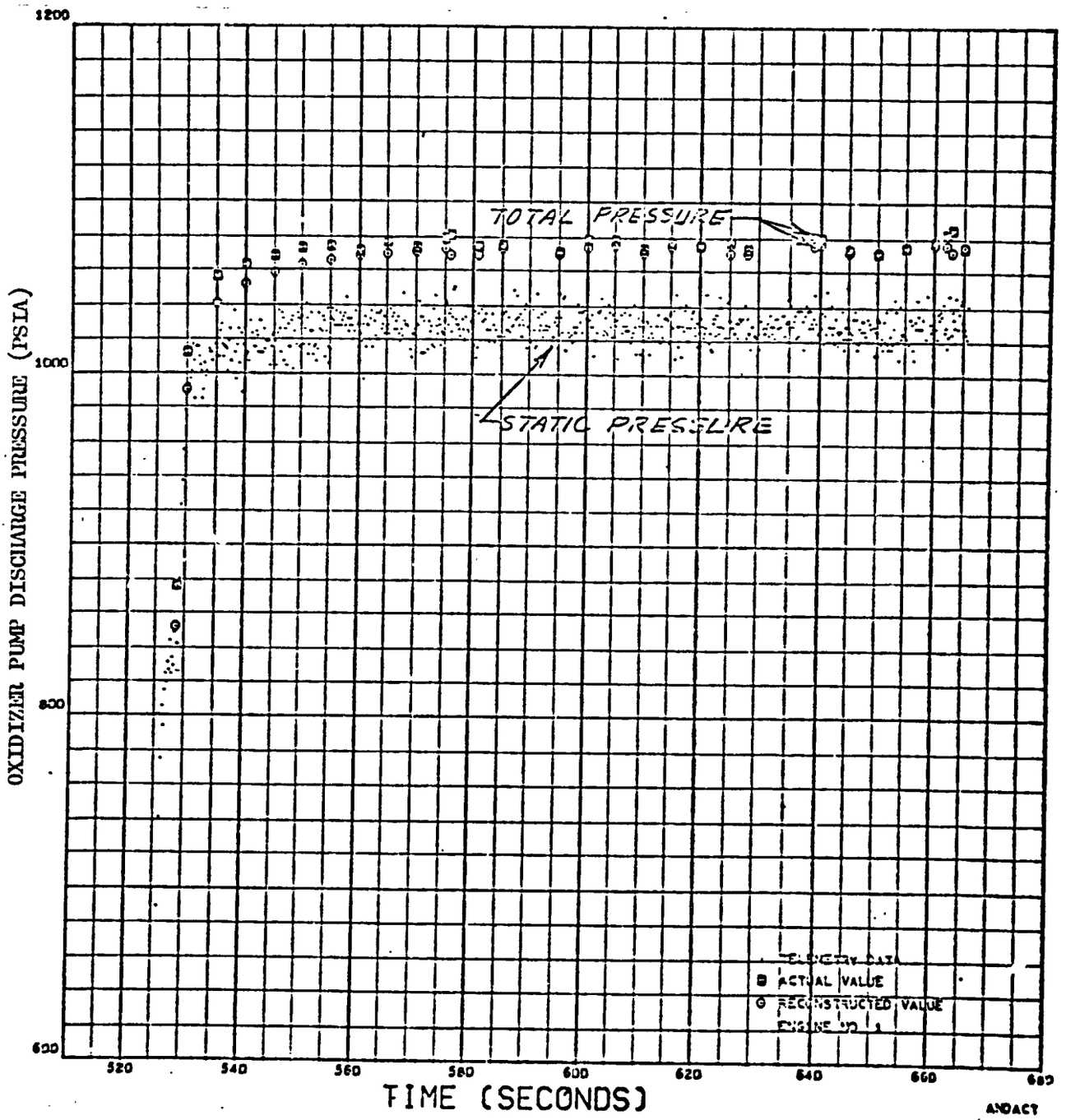

Figure 191. Oxidizer Pump Discharge Pressure (First Burn)

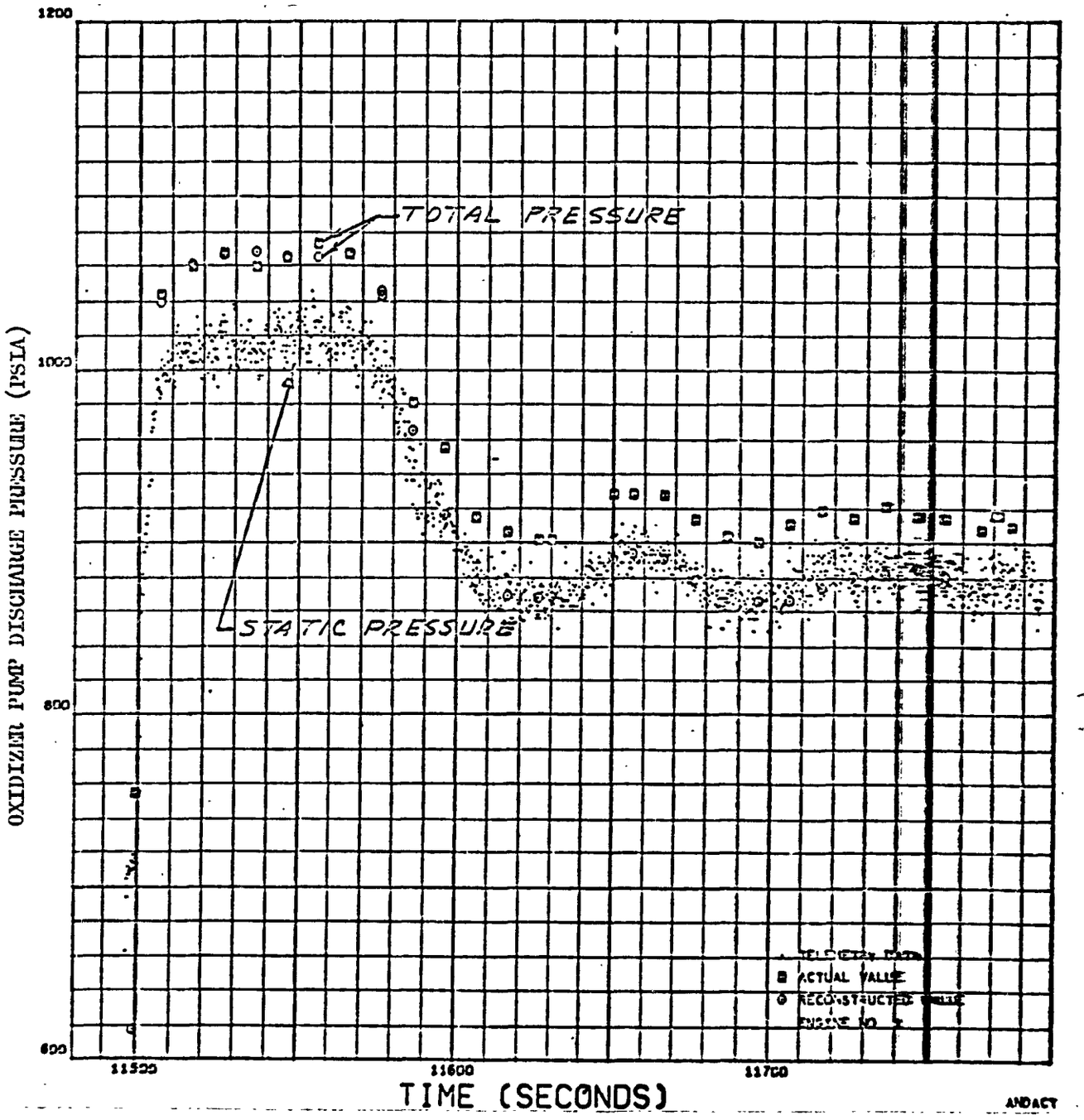

Figure 192. Oxidizer Pump Discharge Pressure (Second Burn)

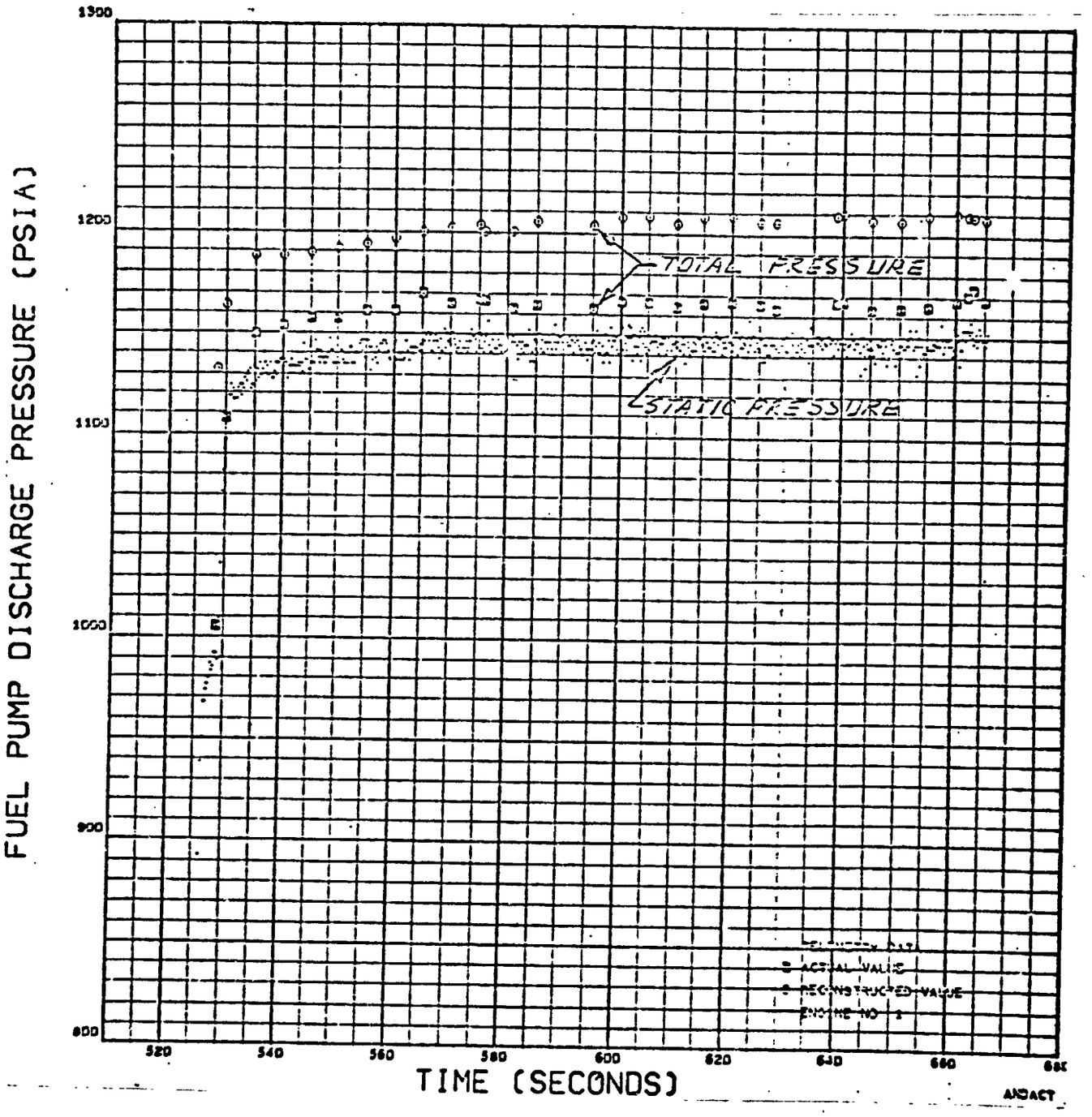

Figure 193. Fuel Pump Discharge Pressure (First Burn)

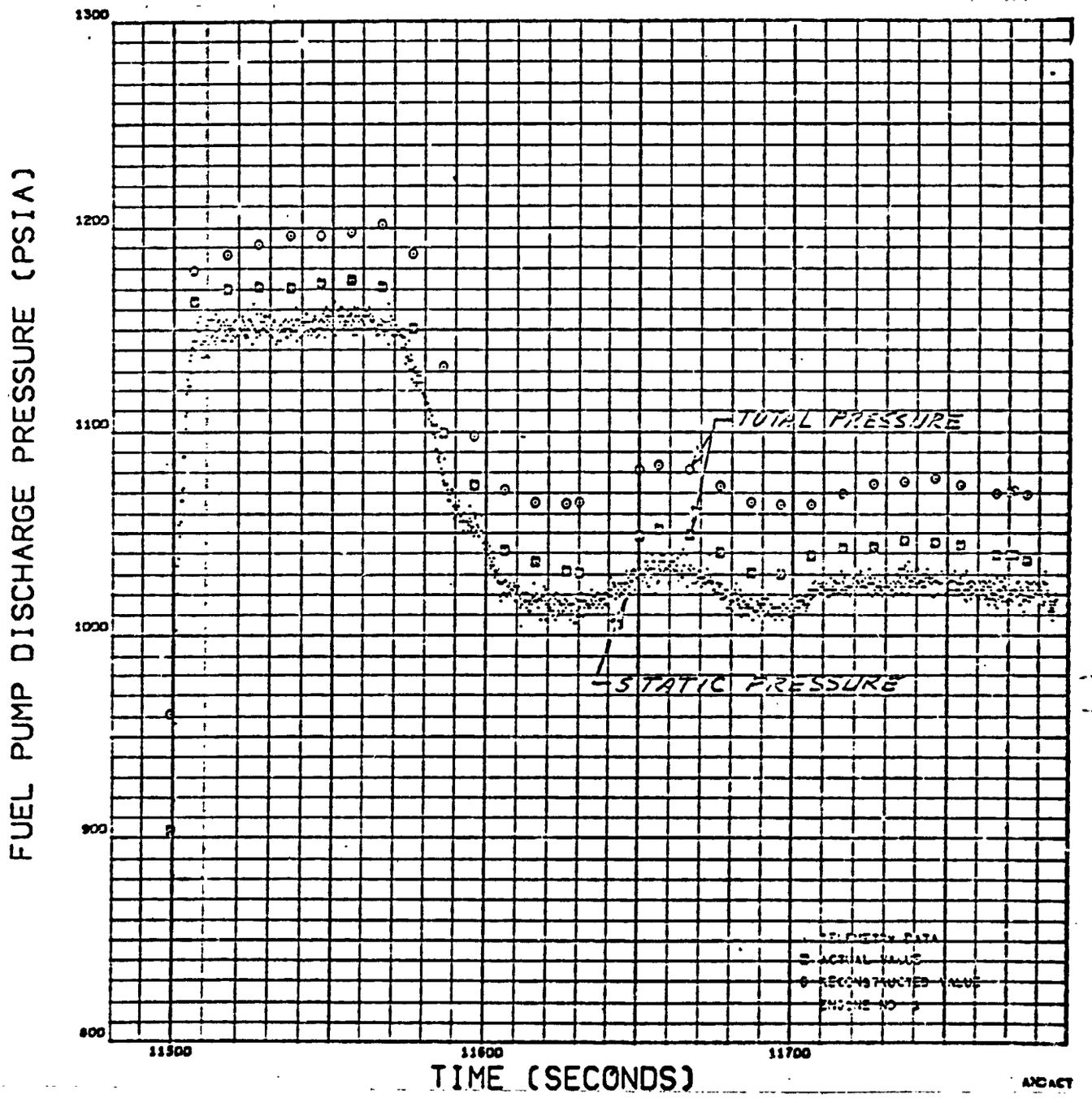

Figure 194. Fuel Pump Discharge Pressure (Second Burn)

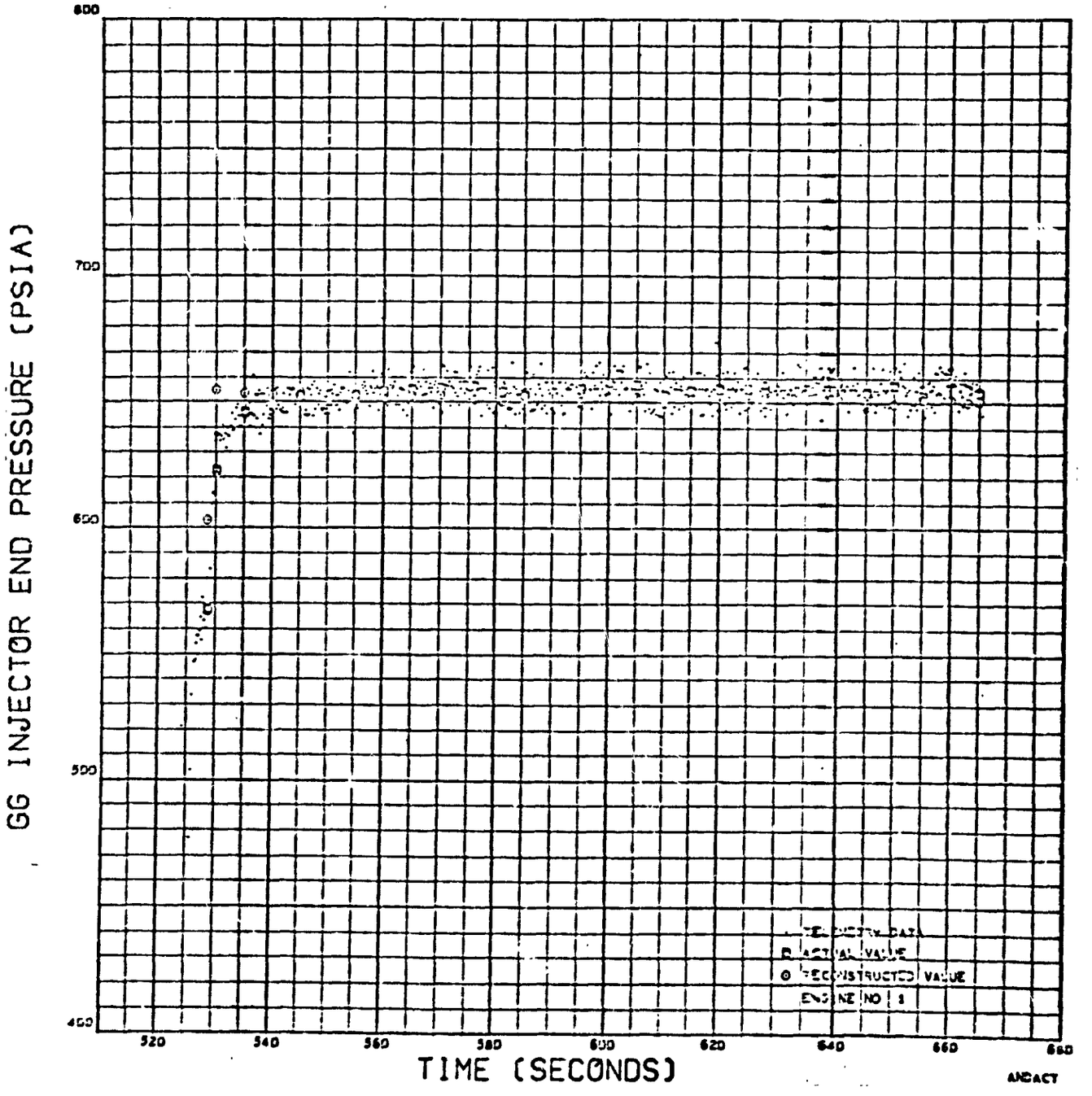

Figure 195. Gas Generator Injector End Pressure (First Burn)

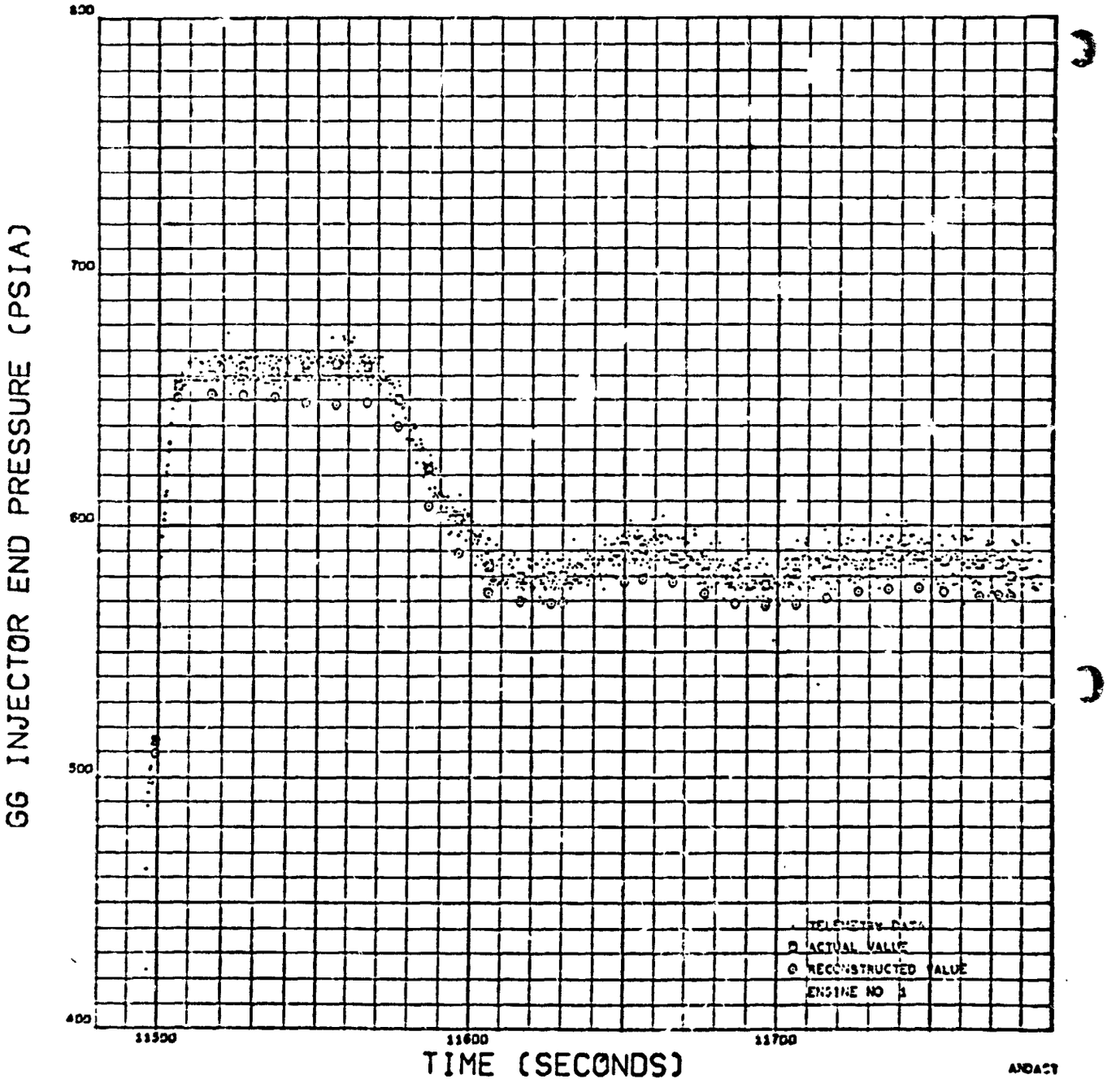

Figure 190. Gas Generator Injector End Pressure (Second Burn)

TANK PRESSURIZATION PERFORMANCE

The fuel tank pressurization performance is presented in Fig. 197 and 198. The values are within the expected operating band and consistent with the data seen on vehicle acceptance testing.

The helium heat exchanger discharge pressure and temperature for flight are shown in Fig. 199 through 202, and a comparison of the values to vehicle acceptance testing is shown in Fig. 203 and 204. The values are in good agreement and within the expected operating bands.

THRUST DECREASE

The thrust decrease summary for the S-IVB stage is shown in Table 29. The actual cutoff impulse values for both the initial start and the restart were higher than the engine acceptance values, mainly because of the colder main oxidizer valve actuator temperature on the flight. The high thrust at cutoff on the initial start also contributed to its high cutoff impulse.

The engine model specification limits on cutoff impulse to 5 percent of rated thrust are 30,000 to 50,000 lb-sec. When the impulse is taken to zero thrust, these limits become 36,400 to 56,400 lb-sec. Both flight cutoff impulse values at standard conditions met the specification requirements. The times from cutoff signal to 5 percent of rated thrust also meet the specification requirements (0.800 seconds maximum).

The thrust decrease traces from both burns are shown in Fig. 205 along with the envelope of engine acceptance testing. The main oxidizer valve actuator temperatures at cutoff were -155 F for the initial start and -151 F for the restart.

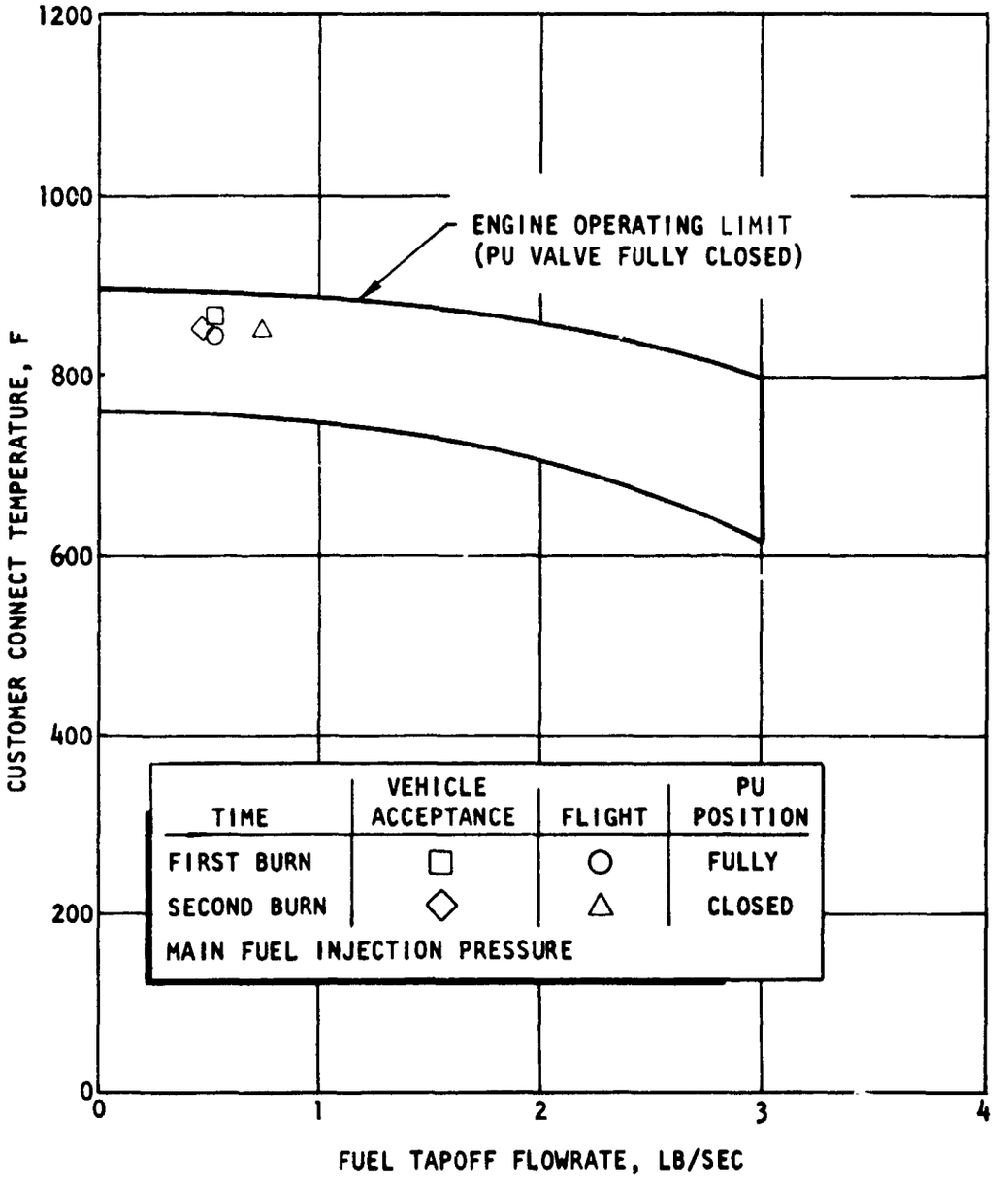

Figure 197. Fuel Tank Pressurization Operating Band

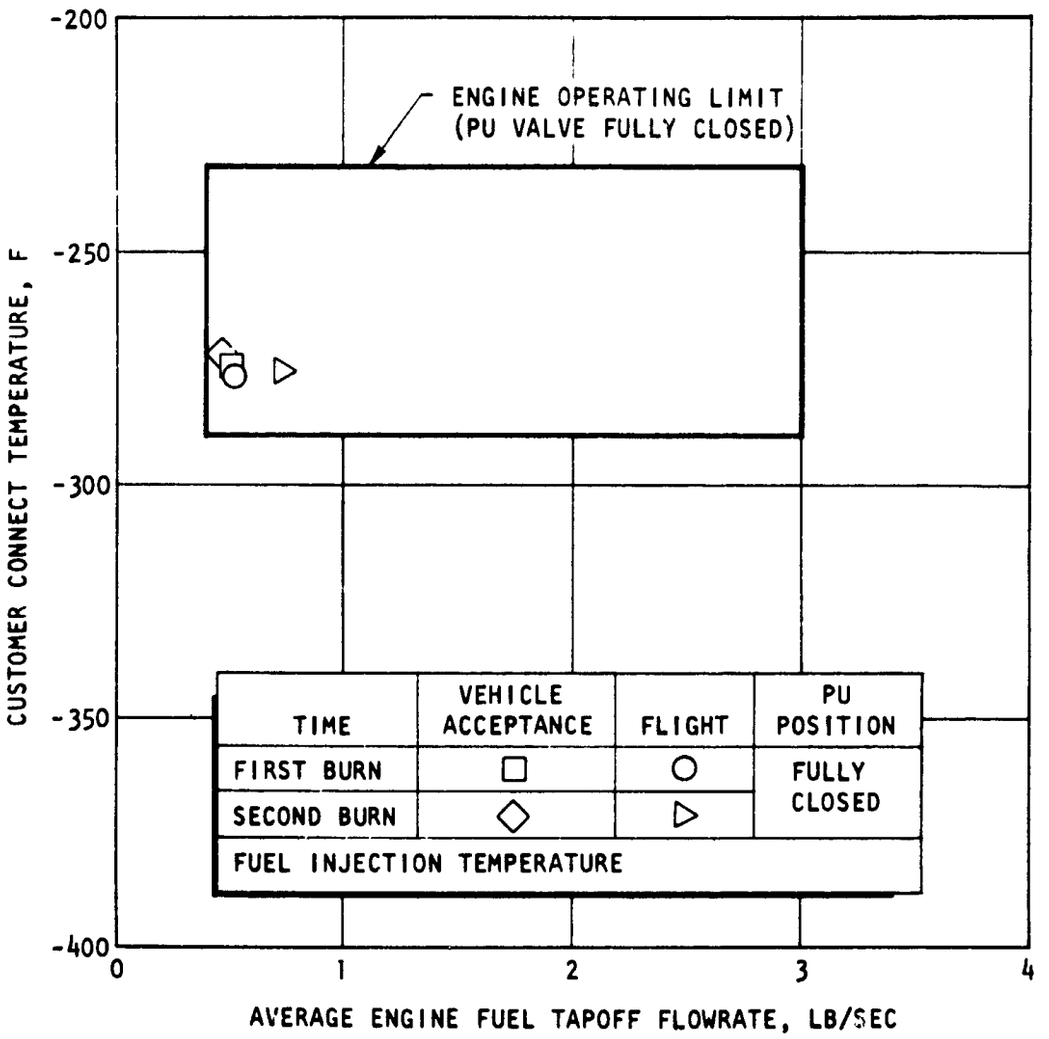

Figure 198. Fuel Tank Pressurization Operating Band

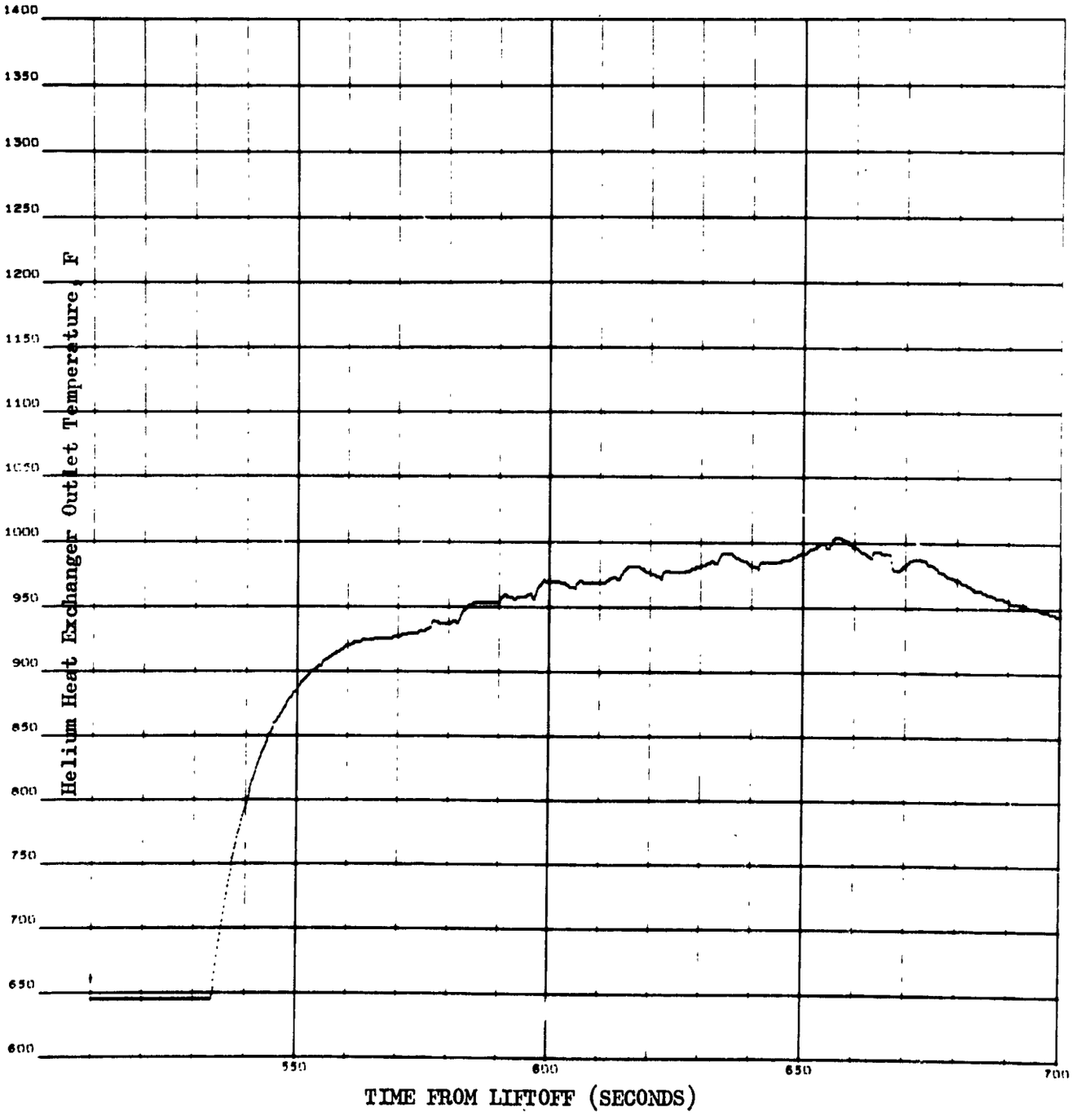

Figure 199. Helium Heat Exchanger Outlet Temperature (First Burn)

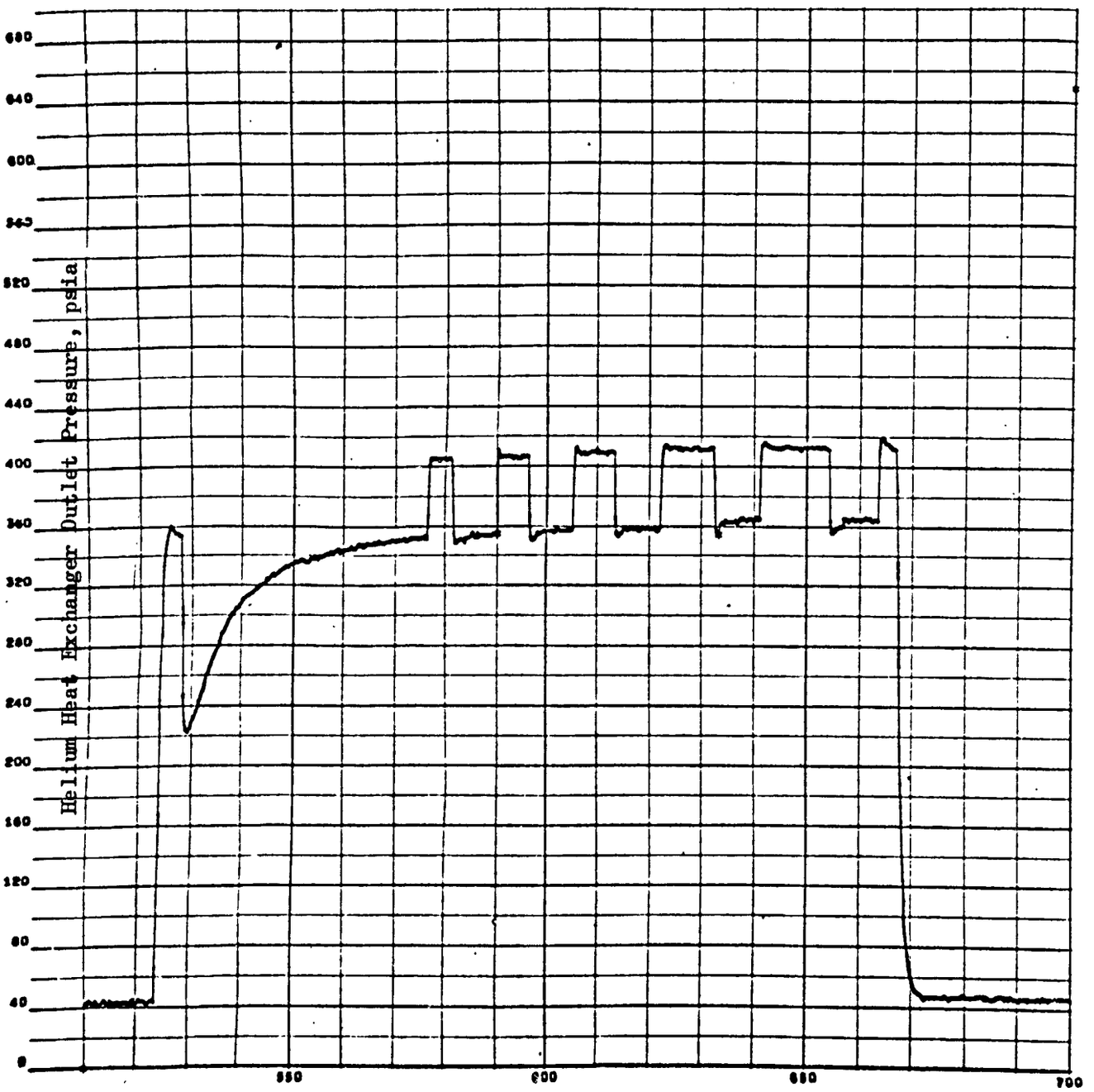

Figure 200. Helium Heat Exchanger Outlet Pressure (First Burn)

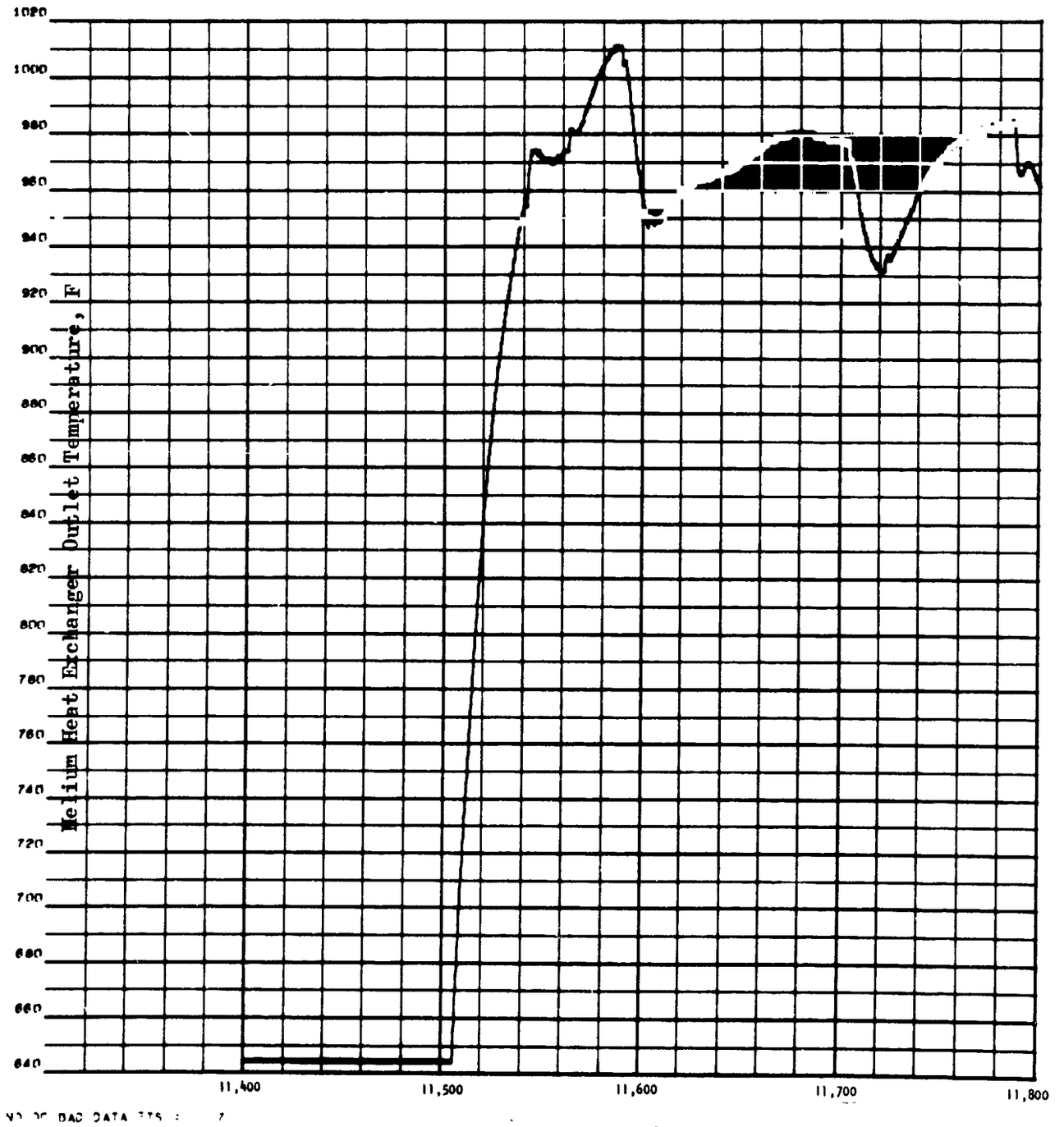

Figure 201. Helium Heat Exchanger Outlet Temperature, Restart

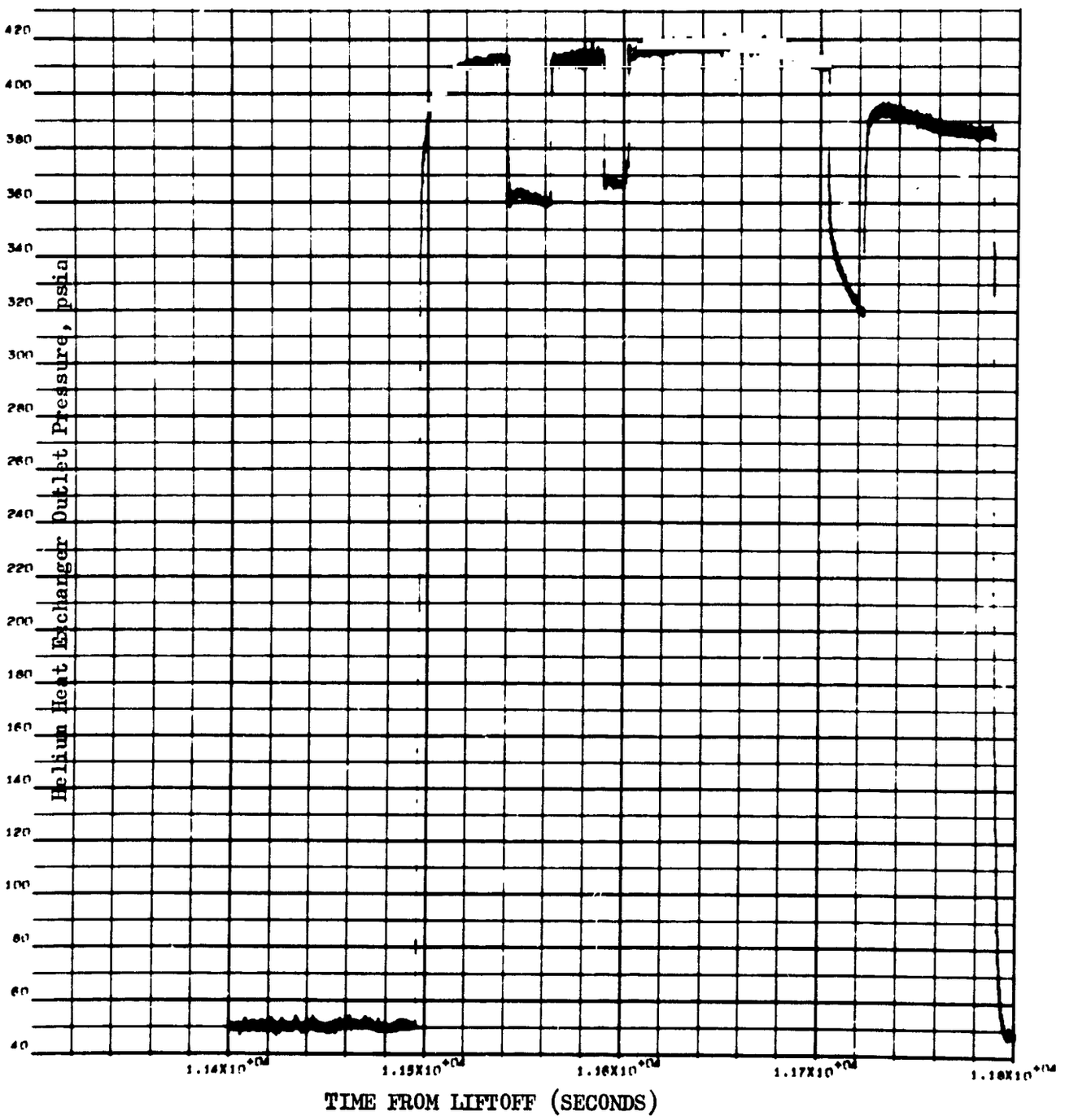

Figure 202. Helium Heat Exchanger Outlet Pressure, Restart

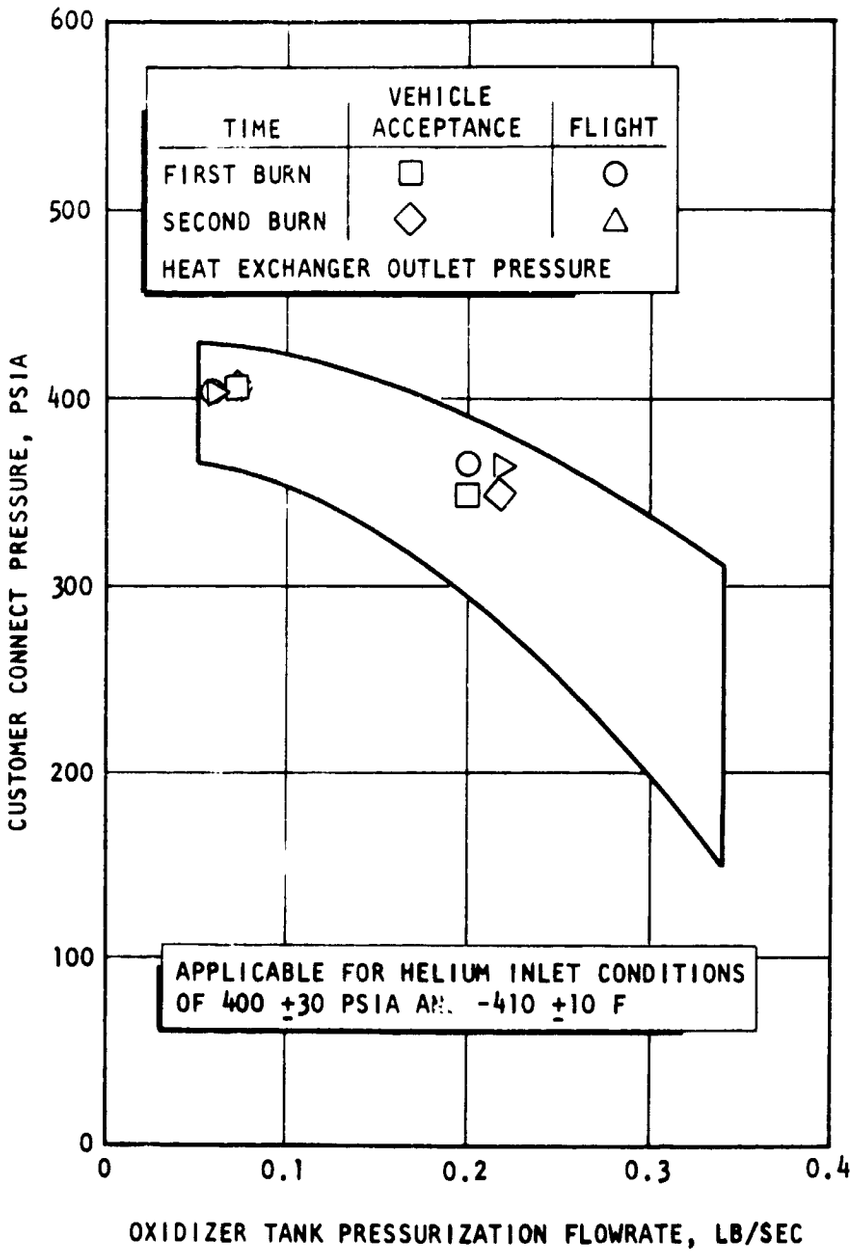

Figure 203. Helium Heat Exchanger Operating Band

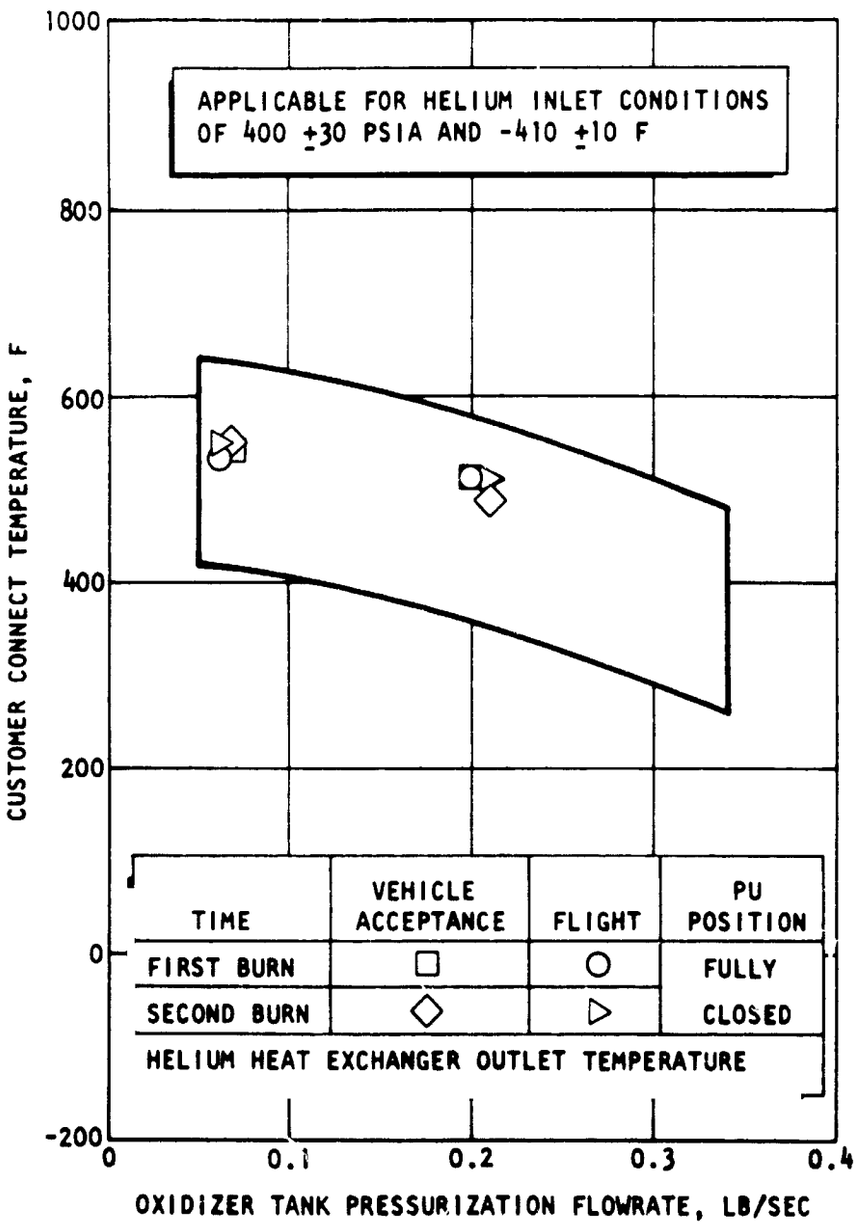

Figure 204. Helium Heat Exchanger Operating Band

TABLE 29

ALTITUDE CUTOFF IMPULSE TO ZERO THRUST

Parameter	Engine Acceptance	Flight	
		Initial Start	Restart
Actual Cutoff Impulse, lb-sec	43,907	52,389	47,318
Cutoff Impulse at Standard Conditions, lb-sec*	43,907	39,065	41,607
Time to 5 Percent of Rated Thrust, second	0.334	0.390	0.340
Thrust at Cutoff, pounds	199,099	224,307	195,079
MOV Actuator Temperature, F	0**	-155	-151
MOV Delay Time, second	0.081		
MOV Travel Time, second	0.175		

*Standard Conditions are: null PU valve position; main oxidizer valve actuator temperature of 0 F at standard inlet conditions, pressurization flowrates, and auxiliary power extraction.

**Assumed, not measured on this engine

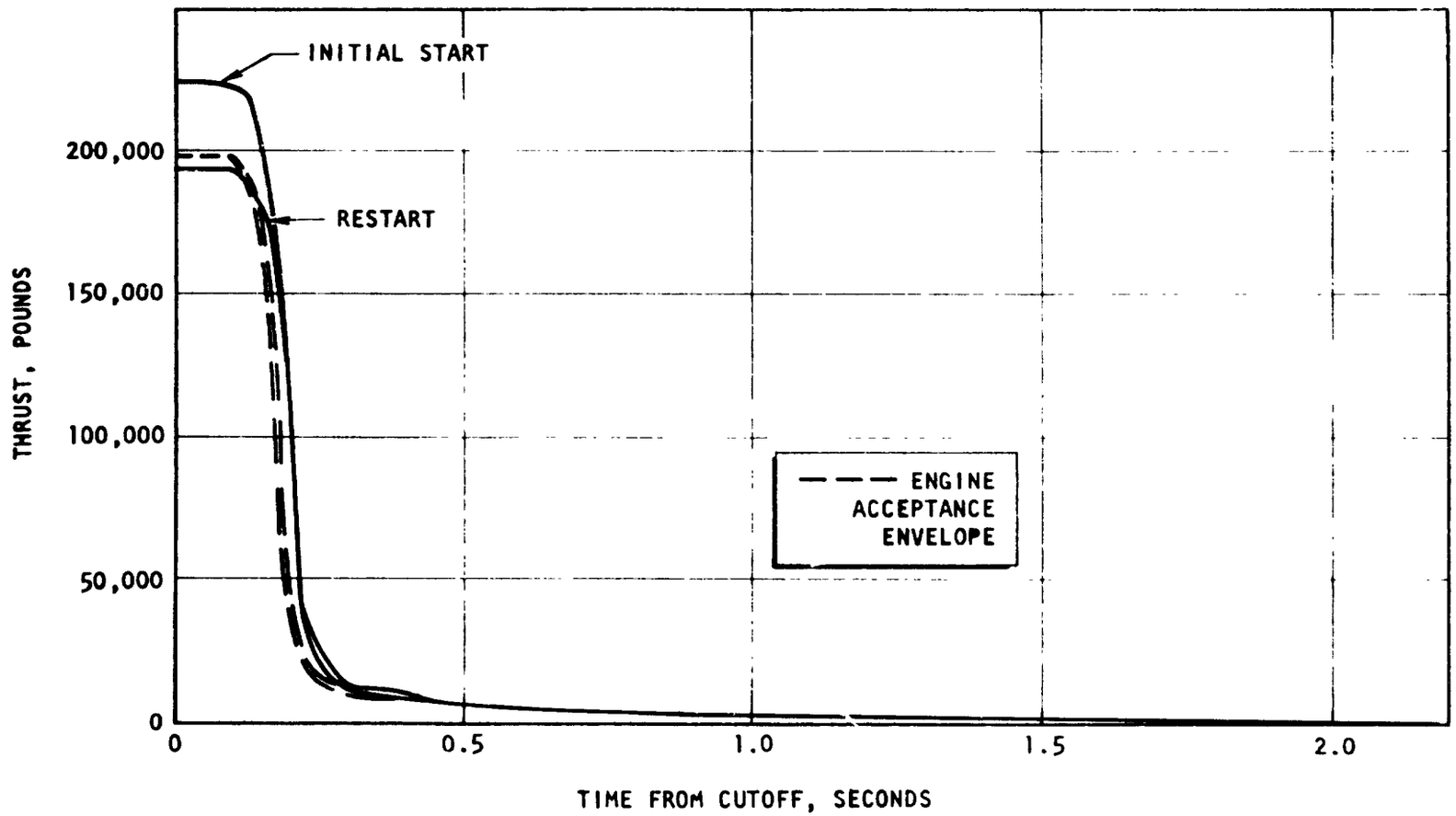

Figure 205. Thrust Decrease Transient

ELECTRICAL SYSTEM

The engine control and ignition voltages (Table 30) for both the initial start and restart are well within the engine model specification operating limits (Table 31). No problem is evident from the data in this system.

TABLE 30

ENGINE VOLTAGES

Parameter No.	Parameter	Liftoff	Engine Start	Engine Cutoff
	Initial Start			
M0006-401	Engine Control Voltage	29.3	27.5	28.6
M007-401	Engine Ignition Voltage	29.3	27.2	28.8
	Restart			
M006-401	Engine Control Voltage	29.3	28.6	29.3
M007-401	Engine Ignition Voltage	29.3	28.8	29.5

TABLE 31

ENGINE LIMITS

Control Power	22 to 31 vdc
Ignition Power	24 to 31 vdc

ENGINE GIMBAL DATA

The engine actuation system on the S-IVB stage performed satisfactorily during both first and second engine burn periods with no anomalies noted. Pertinent engine gimbal data is presented below. The data indicate that engine loads and gimbal displacements were well within the engine structural design limits.

Actuator Position	Peak Actuator Loads, pounds*	Maximum Gimbal Displacement, degrees**
	First Burn	
Pitch	+4,948	+1.2
Yaw	-5,654	-0.9
	Second Burn	
Pitch	+8,246	+1.07
Yaw	-7,068	-1.55

*Actuator Loads: (-) Tension (+) Compression

**Gimbal Displacement: (-) Actuator Retract (+) Actuator Extend for Pitch
(-) Actuator Extend (+) Actuator Retract for Yaw

There are no problems evident in the engine gimbal data.

VIBRATION ANALYSIS

Analysis of the J-2 engine vibration data, supplied by the MSFC facility, from the S-IVB stage of the AS-501 flight produced limited valid results. The S-IVB stage engine vibration data provided valid frequency spectra data for the three engine measurements based on a single time sample analysis for the two-stage operations. However, the composite vibration levels for these data were 50 percent greater than static test results; but preliminary results from the stage contractor (responsible for final stage performance results) showed composite vibration levels which correlated closely with stage and engine static test levels.

Start transient evaluation was seriously impaired by the over-ranging of the vibration measurements which were scaled for the lower mainstage vibration levels. The S-IVB stage, second burn, transient data appeared to be within the measurement range although the flight calibrations were not recorded.

The engine vibration data as supplied by MSFC, from the S-IVB stage during the AS-501 vehicle flight, were analyzed for overall instrumentation performance and response characteristics. A total of four engine associated measurements were recorded: the engine dome, oxidizer pump and fuel pump, and one gimbal pad measurement. All engine measurements appeared operative during their respective stage operation.

The engine vibration data was recorded by commutation of 3-second samples at 12-second intervals. Frequency spectra analysis of the engine vibration data was limited to one sample provided at maximum performance 10 seconds into the first burn. However, there is a discrepancy in the composite g rms energy level reported by MTF and the stage contractor. The S-IVB stage contractor's preliminary results agreed with engine and stage static test levels and the MTF preliminary results were 30 to 50 percent higher.

The S-IVB stage use of 50 g rms measurement range, as compared to the S-II stage use of 35 g rms for the same measurements, was regarded as the major difference of the two recording systems.

Review of the commutated S-IVB stage engine vibration data from the oscillogram records indicated consistent mainstage levels for the first burn duration. These measurements were recorded for only the first 85 percent of the second burn duration. At approximately 85 seconds into mainstage of the second burn, 11,580 seconds flight time, the oxidizer pump data indicated a decrease from maximum engine performance for propellant utilization. Data recording terminated at 11,753 seconds. Failure to record the second burn flight calibration prevented direct comparison of overall levels for the stage's two engine operations.

For the two S-IVB stage engine start transients, only the engine dome measurement was being commutated (switched on) for recording of the engine measurements. The gimbal pad measurement, stage-oriented, was recorded continuously. The first burn ignition transient occured at 525.3 seconds flight time, with a 65 g peak-to-peak level and a duration of 0.13 second. The maximum transient level at 525.8 seconds overdrove the measurement range, similar to the S-II stage engine start characteristic.

This transient duration was estimated at 0.20 second from the MSFC oscillogram data. The high-speed playback record did not agree in transient duration or with the commutation period of the engine dome measurement. The engine dome measurement was commutated off at 526.6 seconds. Cutoff occurred at 660.8 seconds referenced to the decrease of activity on the continuous gimbal pad measurement, because all engine measurements were off at this time.

The second burn engine start transient recorded levels apparently within the engine dome measurement range. Using the first burn flight calibrations, this ignition transient was 75 g peak to peak for 0.03 second at 11,494.53 seconds. The levels and durations indicated good correlation of the MSFC records with the high-speed oscillograms. All recording terminated at 11,753 seconds.

Engine Start Transients

The S-IVB stage engine start transient vibration data were analyzed for determination of levels and duration during the ignition and transition into mainstage periods. These data from the MSFC oscillograms and additional high-speed oscillograms had overdriven or questionable portions during the S-IVB stage, first-burn, engine starts that prevented conclusive results. However, the S-IVB stage, second burn, engine start transient vibration levels appeared to be within the measurement range. Direct comparison of the flight transient data levels with static test results was limited by the telemetry system frequency recording bandwidth

of 50 Hz to 3000 Hz. The major energy content of static test transient data (recorded 10 Hz to 10,000 Hz bandwidth) is in the 2000 Hz to 6000 Hz frequency range.

Analysis of the S-IVB stage J-2 engine vibration data resulted in the following:

1. The maximum J-2 engine vibration level during the S-1C stage operation occurred at liftoff with a value of 1.3 g rms.
2. The S-IVB stage engine vibration data, limited to a single frequency spectra analysis, agreed with stage and engine static test results.

BOATTAIL LEAKAGE

The oxidizer pump seal leakage into the boattail of the S-IVB stage was alleviated by means of a burst diaphragm assembly installed near the exit of the oxidizer pump primary seal cavity drain line. The burst diaphragm survived undamaged during the initial 520 seconds of the vehicle boost with cavity pressure ranging from 3.0 to 3.5 psia. Performance of the diaphragm is tabulated below and also depicted in Fig. 206.

Engine	Diaphragm Rupture		Mean Primary Seal Cavity Pressure	
	Time From Engine Start, seconds	Pressure at Break, psia	During Maximum PU, psia	During Nominal PU, psia
J2031	First Burn			
	50	22	12 to 17	12 to 17
	Second Burn			
	DNA	DNA	12 to 19	11-1/2 to 16

During the initial 50 seconds of the S-IVB stage firing sequence, leakage of liquid oxygen resulted in cycling of the cavity pressure with a progressive pressure buildup which culminated in the diaphragm rupture at approximately 22 psia.

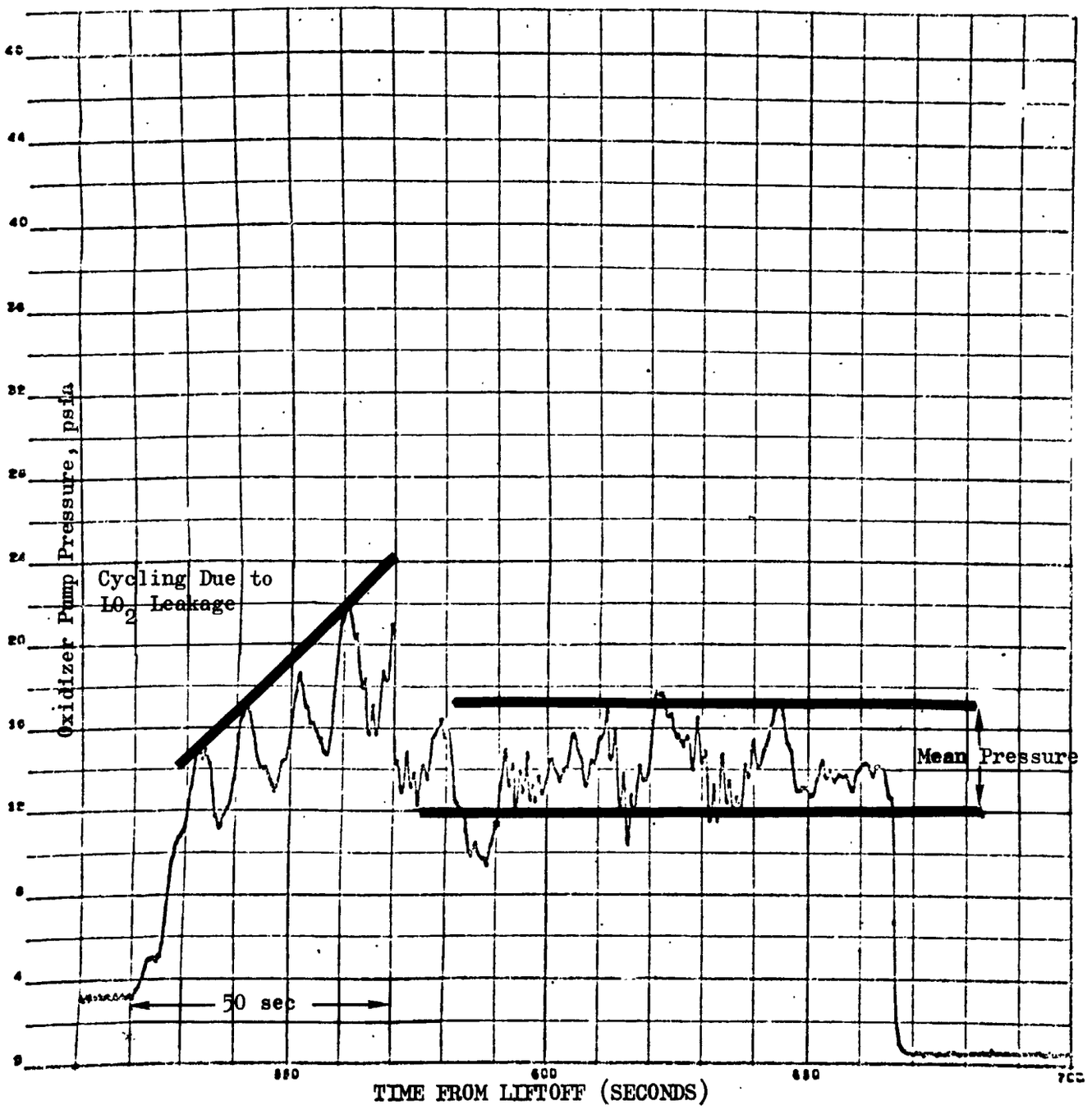

Figure 206. Performance of Burst Diaphragm on J2031 (S-IVB Stage)

This behavior is understandable because engine J2031 was known to have a relatively high leakage rate. The engine, however, did not contribute any oxygen to the boattail environment during the static condition and the gas analyzer failed to register any measurable concentration of oxygen.